Preliminary results of the winter bottom-trawl survey on board the NM Mersey Venture in the Gulf of St. Lawrence, Laurentian Channel and Laurentian Fan in 2022, 2023 and 2024

Manuelle Beaudry-Sylvestre, Jean-Martin Chamberland, Jordan Ouellette-Plante, Mathieu Desgagnés, David Poissant, Caroline Senay, Hugo Bourdages

Institut Maurice-Lamontagne
Pêches et Océans Canada
850 Rte de la Mer
Mont-Joli, QC
G5H 3Z4

2026

Canadian Technical Report of
Fisheries and Aquatic Sciences 3777

Fisheries and Oceans Canada | Pêches et Océans Canada

Canada

Canadian Technical Report of Fisheries and Aquatic Sciences

Technical reports contain scientific and technical information that contributes to existing knowledge but which is not normally appropriate for primary literature. Technical reports are directed primarily toward a worldwide audience and have an international distribution. No restriction is placed on subject matter and the series reflects the broad interests and policies of Fisheries and Oceans Canada, namely, fisheries and aquatic sciences.

Technical reports may be cited as full publications. The correct citation appears above the abstract of each report. Each report is abstracted in the data base *Aquatic Sciences and Fisheries Abstracts*.

Technical reports are produced regionally but are numbered nationally. Requests for individual reports will be filled by the issuing establishment listed on the front cover and title page.

Numbers 1-456 in this series were issued as Technical Reports of the Fisheries Research Board of Canada. Numbers 457-714 were issued as Department of the Environment, Fisheries and Marine Service, Research and Development Directorate Technical Reports. Numbers 715-924 were issued as Department of Fisheries and Environment, Fisheries and Marine Service Technical Reports. The current series name was changed with report number 925.

Rapport technique canadien des sciences halieutiques et aquatiques

Les rapports techniques contiennent des renseignements scientifiques et techniques qui constituent une contribution aux connaissances actuelles, mais qui ne sont pas normalement appropriés pour la publication dans un journal scientifique. Les rapports techniques sont destinés essentiellement à un public international et ils sont distribués à cet échelon. II n'y a aucune restriction quant au sujet; de fait, la série reflète la vaste gamme des intérêts et des politiques de Pêches et Océans Canada, c'est-à-dire les sciences halieutiques et aquatiques.

Les rapports techniques peuvent être cités comme des publications à part entière. Le titre exact figure au-dessus du résumé de chaque rapport. Les rapports techniques sont résumés dans la base de données *Résumés des sciences aquatiques et halieutiques.*

Les rapports techniques sont produits à l'échelon régional, mais numérotés à l'échelon national. Les demandes de rapports seront satisfaites par l'établissement auteur dont le nom figure sur la couverture et la page du titre.

Les numéros 1 à 456 de cette série ont été publiés à titre de Rapports techniques de l'Office des recherches sur les pêcheries du Canada. Les numéros 457 à 714 sont parus à titre de Rapports techniques de la Direction générale de la recherche et du développement, Service des pêches et de la mer, ministère de l'Environnement. Les numéros 715 à 924 ont été publiés à titre de Rapports techniques du Service des pêches et de la mer, ministère des Pêches et de l'Environnement. Le nom actuel de la série a été établi lors de la parution du numéro 925.

Canadian Technical Report of
Fisheries and Aquatic Sciences 3777

2026

Preliminary results of the winter bottom-trawl survey on board the NM Mersey Venture in the Gulf of St. Lawrence, Laurentian Channel and Laurentian Fan in 2022, 2023 and 2024

by

Manuelle Beaudry-Sylvestre, Jean-Martin Chamberland, Jordan Ouellette-Plante, Mathieu Desgagnés, David Poissant, Caroline Senay, Hugo Bourdages

Institut Maurice-Lamontagne
Pêches et Océans Canada
850 Rte de la Mer
Mont-Joli, QC
G5H 3Z4

© His Majesty the King in Right of Canada, as represented by the Minister of the Department of Fisheries and Oceans, 2026

This work is licensed under the Open Government Licence

Cat. No. Fs 97-6/3777E-PDF ISBN 978-1-100-00517-1 ISSN 1488-5379

https://doi.org/10.60825/9jk4-1m50

Correct citation for this publication:

Beaudry-Sylvestre, M., Chamberland, J.-M., Ouellette-Plante, J., Desgagnés, M., Poissant, D., Senay, C., Bourdages, H. 2026. Preliminary results of the winter bottom-trawl survey on board the NM Mersey Venture in the Gulf of St. Lawrence, Laurentian Channel and Laurentian Fan in 2022, 2023 and 2024. Can. Tech. Rep. Fish. Aquat. Sci. 3777: v + 321 p. https://doi.org/10.60825/9jk4-1m50

Aussi disponible en français :

Beaudry-Sylvestre, M., Chamberland, J.-M., Ouellette-Plante, J., Desgagnés, M., Poissant, D., Senay, C., Bourdages, H. 2026. Résultats préliminaires du relevé hivernal au chalut de fond à bord du NM Mersey Venture dans le golfe du Saint-Laurent, le chenal et le cône laurentiens en 2022, 2023 et 2024. Rapp. tech. can. sci. halieut. aquat. 3777 : v + 325 p. https://doi.org/10.60825/cccq-y010

TABLE OF CONTENTS

Abstract iv
Résumé v
1 Introduction 1
2 Methods 2
2.1 Data description and treatment 2
2.1.1 Coverage and sampling plan 2
2.1.2 Treatment of taxonomic codes 4
2.2 Detailed analyzes for common taxa 6
2.2.1 Estimation of biomass and abundance per tow 6
2.2.2 Spatial interpolation with sdmTMB 6
2.2.3 Cumulative distributions of catches as a function of environmental variables 9
2.2.4 Length frequencies and length-weight relationships 10
2.3 Descriptive statistics for common and rare taxa 11
2.4 Other research questions 11
3 Results 11
3.1 Results of detailed analyzes on common fish taxa 12
3.2 Results of detailed analyzes on common invertebrate taxa 18
3.3 Results of summary analyzes on rare taxa 19
4 Discussion 19
Acknowledgements 22
References 23
Tables 27
Figures 39
Appendices 293
Appendix A. Supplemental information on the survey and analyzes 293
Appendix B. Spatial model residuals and diagnostics for common taxa 297
Appendix C. Tagging of Atlantic halibut 317
Appendix D. Other research projects 319
Appendix E. List of participants to the survey 321

ABSTRACT

Beaudry-Sylvestre, M., Chamberland, J.-M., Ouellette-Plante, J., Desgagnés, M., Poissant, D., Senay, C., Bourdages, H. 2026. Preliminary results of the winter bottom-trawl survey on board the NM Mersey Venture in the Gulf of St. Lawrence, Laurentian Channel and Laurentian Fan in 2022, 2023 and 2024. Can. Tech. Rep. Fish. Aquat. Sci. 3777: v + 321 p. https://doi.org/10.60825/9jk4-1m50

Many demersal and benthic species occur in the Laurentian Channel and its associated channels within and outside the Gulf of St. Lawrence (GSL) in winter. However, knowledge of their spatial distribution during this time of year dates back more than 30 years, limiting the capacity to plan for the consequences of specific human activities such as reopening fisheries targeted at redfish (*Sebastes* spp.) in the sector. To overcome these deficiencies, the Canadian Department of Fisheries and Oceans (DFO) conducted a winter bottom-trawl survey on board the Motor Vessel Mersey Venture in 2022, 2023 and 2024 in the deep waters (> 150 m) of the Laurentian Channel, within and outside the GSL (NAFO Divisions 3P4RSTV). The survey employed an unaligned systematic design and led to a total of 413 successful tows. The 88 taxa occurring in 25 tows or more were subjected to (1) a simple visualization of catches in weight and number, (2) spatial interpolations of catches, either with or without an effect of depth, within the sdmTMB framework, (3) analyzes of cumulative distribution curves based on environmental variables (depth, temperature and oxygen) and (4) estimation of length frequencies and length-weight relationships. The 202 taxa present in less than 25 tows were subjected instead to presence-absence maps combining the three survey years. This report employed some of the best available tools to describe the spatial and environmental distribution of fish and invertebrates associated with the Laurentian Channel in winter.

RÉSUMÉ

Beaudry-Sylvestre, M., Chamberland, J.-M., Ouellette-Plante, J., Desgagnés, M., Poissant, D., Senay, C., Bourdages, H. 2026. Preliminary results of the winter bottom-trawl survey on board the NM Mersey Venture in the Gulf of St. Lawrence, Laurentian Channel and Laurentian Fan in 2022, 2023 and 2024. Can. Tech. Rep. Fish. Aquat. Sci. 3777: v + 321 p.
https://doi.org/10.60825/9jk4-1m50

De nombreuses espèces démersales et benthiques fréquentent le chenal Laurentien et ses chenaux associés dans et hors du golfe Saint-Laurent (GSL) en hiver. Cependant, les connaissances disponibles sur leur distribution spatiale durant cette période de l'année remontent à plus de 30 ans, limitant la capacité à prévoir les conséquences d'activités humaines spécifiques comme la réouverture de la pêche au sébaste (*Sebastes* spp.) dans le secteur. Dans le but de pallier ce manque, le Ministère Pêches et Océans Canada (MPO) a réalisé un relevé hivernal au chalut de fond à bord du Navire Marchand Mersey Venture en 2022, 2023 et 2024 dans les eaux profondes (> 150 m) du chenal Laurentien, à l'intérieur et l'extérieur du GSL (divisions OPANO 3P4RSTV). Le relevé était de type systématique non-aligné et a donné lieu à un total de 413 traits réussis. Les 88 taxons présents dans 25 traits et plus ont fait l'objet (1) d'une visualisation simple des captures en poids et en nombre, (2) d'une interpolation spatiale des captures avec ou sans effet de la profondeur dans un cadre sdmTMB, (3) d'une analyse des courbes de distribution cumulative des captures selon des variables environnementales (profondeur, température et oxygène) et (4) de l'estimation des fréquences de longueur et des paramètres de la relation masse-longueur. Les 202 taxons présents dans moins de 25 traits ont plutôt fait l'objet de cartes de présence et absence combinant les trois années du relevé. Ce rapport a utilisé certains des meilleurs outils disponibles pour décrire les distributions spatiale et environnementale des poissons et invertébrés associés au chenal Laurentien en hiver.

1 INTRODUCTION

The Gulf of St. Lawrence (GSL; NAFO[1] Divisions 4RST) is a semi-enclosed sea that undergoes major ecosystem changes throughout the seasons (Galbraith, 2006; Galbraith et al., 2025; Blais et al., 2024). Specimens of several demersal and benthic species from the GSL overwinter in the deep waters of the Laurentian Channel and Cabot Strait (Bowering, 1982; Morin et al., 1994; Swain et al., 1998). However, observations of this phenomenon date back to the early 1990s, a period during which environmental and ecological conditions were very different from those observed today (McCallum and Walsh, 1997; Chouinard and Hurlbut, 2011; Galbraith et al., 2025). The fact that the available knowledge about this environment is not up to date raises uncertainties about the ability to assess the impact of new human pressures, such as the reopening of the commercial fishery for redfish (*Sebastes* spp.) in 2024, an activity which takes place partly in winter, as well as climate change.

The Canadian Department of Fisheries and Oceans (DFO) coordinated a scientific bottom-trawl survey on board the Motor Vessel (MV) Mersey Venture in the anticipated overwintering areas of several groundfish species in 2022, 2023, and 2024. The primary objective of the survey was to quantify the potential impacts of reopening the redfish fishery on other species in the area, particularly in terms of bycatch (e.g., Sutton et al., 2024). The redfish fishery resumed in Management Unit 1 (defined by NAFO Divisions 4RST and, from January to May, Subdivisions 3Pn4Vn) toward the end of 2024 (DFO, 2025b), ending a prolonged period of little to no winter trawling activity targeting groundfish. The resumption of such activity could disrupt the recovery of COSEWIC[2]-designated species, including Atlantic cod (*Gadus morhua*; COSEWIC, 2010a) and white hake (*Urophycis tenuis*; COSEWIC, 2013), which have often been caught as bycatch in the redfish fishery in recent years (e.g., Rolland et al., 2022; Sutton et al., 2024). The sampling also included a portion of Management Unit 2 (defined by NAFO Subdivisions 3Ps4Vs, 4Wfgj and, from June to December, 3Pn4Vn), a redfish management area that has never been under a moratorium but for which other uncertainties exist (DFO, 2025b). The survey carried out with the MV Mersey Venture in 2022-2024 therefore represents the main source of information on these issues and other key questions concerning the state of the ecosystem.

This technical report aims to provide an overview of the data collected during the winter survey on board the MV Mersey Venture in 2022, 2023, and 2024. The taxa observed that were present in a minimum of 25 tows over the three survey years were subjected to detailed statistical analysis, including spatial modeling, cumulative distribution curves based on environmental variables, and data characterization in terms of length and weight. Taxa present in fewer than 25 tows were instead subjected to a basic descriptive analysis applicable to all observed taxa. The results of the main analyzes were then interpreted by taxon or group of taxa, with a particular focus on those most likely to be affected by the redfish fishery and/or with a particular status under COSEWIC.

[1] NAFO : Northwest Atlantic Fisheries Organization
[2] COSEWIC : Committee on the Status of Endangered Wildlife in Canada

2 METHODS

2.1 Data description and treatment

2.1.1 Coverage and sampling plan

The area covered by the survey was defined based on bathymetry (depth > 150 m) and the known distribution ranges of several commercial species such as Atlantic cod, white hake, and redfish within NAFO Divisions 3P4RSTV (**Figure 1**). The survey followed an unaligned systematic sampling plan; that is, the study area was first transformed into a grid with a theoretical spacing of 11 nautical miles (nm) and, then, a station was placed at each grid node. A random component was added along the x-axis for each row and the y-axis for each column, following a uniform distribution bounded from zero to plus or minus half the theoretical sampling step (Ripley, 1981). Station selection was performed using the *spSample* function from the R *sp* library (Pebesma and Bivand, 2005). In order to maximize the spatial extent of the survey, the area covered in 2022 was extended to the southeast in 2023, and again in 2024 (see paragraph below). The survey study area considered in the analyzes was adjusted to exclude planned, but unvisited stations, maintaining an 11 nm margin between stations located at the boundaries of the study area and the polygon defining the study area.

The changes made to the sampling plan in 2024 were intended to address specific gaps in the available knowledge on certain species. In particular, three stations were manually added to the sampling grid within the Cape Breton Basin area and south of it to refine the winter distribution of white hake (shown in yellow in **Figure 1**). Stations were also added outside the initial grid to cover (1) shallower areas east of Anticosti Island and west of Newfoundland Island, to identify potential aggregations of Atlantic cod, (2) Burgeo Bank, in Subdivision 3Ps, and (3) the Laurentian Fan, outside the GSL. Thus, there was a total of 413 successful[3] trawling activities distributed among 219 distinct geographical points (i.e., stations) ranging from the western tip of Anticosti Island to the mouth of the Laurentian Fan. The location of the various channels and other relevant landmarks is shown in **Figure A1**.

The survey took place from February 10 to 26, 2022 (N = 86 successful tows), from January 17 to February 3, 2023 (N = 118 successful tows) and from February 8 to March 8, 2024 (N = 209 successful tows); details of successful and unsuccessful tows are presented in **Table 1**. The vessel employed, the MV Mersey Venture, is a trawler with the same dimensions (length: 63 m; width: 14 m), built in the same year (1988) and at the same shipyard (Tomrefjord, Norway), the Canadian Coast Guard Ship (CCGS) Teleost. The MV Mersey Venture was equipped with the same trawl used during the summer survey of the Estuary and Northern Gulf of St. Lawrence (nGSL) on board the CCGS Teleost, namely a Campelen 1800 with a 12.7 mm mesh liner (Bourdages et al., 2023b; note that this differs from the modified Campelen 1800 trawl employed on board the CCGS John Cabot, see Chamberland et al., 2025). The trawl was equipped with Morgere Oval Cambered Trawl Doors[4] (4 square meters). A standard tow for the MV Mersey Venture was conducted for a duration of 15 minutes and a speed of 3 knots (kn), resulting in a

[3] A tow was considered unsuccessful when there was (1) snagging of the trawl on the bottom; (2) severe damage to the trawl; (3) less than 10 minutes of trawling on the bottom; (4) poor operation of the trawl (e.g., problematic contact with the bottom or geometry of the trawl for the duration of the tow); and/or (5) a large quantity of mud or rocks in the trawl, making it difficult to haul the trawl on board or to process the catch.

[4] Note that trawl doors were similar to those described for the CCGS Teleost (see characteristics in Walsh et al., 2009), but whether they were exactly the same could not be confirmed.

standard tow distance of 0.75 nm. Since the horizontal opening of the trawl (i.e., wing spread) was not recorded in real time, catches were standardized based solely on the trawl distance. All data collected on board were entered into the Andes software (details in Ricard et al., 2024).

At each tow, a Seabird SBE19Plus™ CTD equipped with an Optode probe was deployed to record physicochemical parameters of the environment, including depth, temperature, and bottom dissolved oxygen. However, only the available data associated with successful tows are presented and analyzed in this report (**Figure 2**). Due to equipment failure on February 28, 2024, the original CTD had to be replaced with an equivalent device, but one not equipped with an Optode probe which is used to measure dissolved oxygen (J.-F. Lussier, pers. comm. June 2, 2025). Therefore, no dissolved oxygen data were collected for tows conducted after this date, which all corresponded to the southernmost sector of the study area. To facilitate the interpretation of dissolved oxygen data, values expressed in parts per million (ppm; 1 ppm equals 1 mg L^{-1}) were converted to percentage saturation from associated temperature and salinity values (see Garcia and Gordon, 1992). No other analyzes involving salinity were undertaken in this report.

2.1.1.1 Catch processing on board the vessel

Catches of each successful tow were processed similarly to the August nGSL survey coordinated by DFO Quebec Region (see Chamberland et al., 2025). Briefly, the catch in each tow was first sorted by taxon, i.e., by species, genus, family, order, class, or phylum, depending on the level of detail available and desired at the time of the survey (e.g., Nozères and Archambault, 2014; Nozères, 2018; Isabel et al., 2024). The catch for each taxon was then weighed for a total weight and associated with a number of individuals by direct counting or estimation from a known sample. Counting the catch or a sample of the catch was not possible or reliable for colonial organisms such as most sponges, corals, and hydrozoans; therefore, only the catch weights were analyzed for these organisms. The next step for many taxa was to take a random sample from the total catch to obtain a length frequency (LF), record individual weights, and complete taxon-specific protocols such as otolith sampling and macroscopic determination of sex and maturity stage. When catch for a taxon was very large and exhibited more than one mode in its size distribution, the catch was first separated by size category and, then, the aforementioned protocol was repeated for each category of that tow (e.g., small, medium, large). Standardization of catches based on the sampled fraction was therefore applied to each sorting category and tow.

2.1.1.2 Separation of redfish species

The study area included two redfish species that could not be visually distinguished during the survey: Deepwater redfish (*Sebastes mentella*) and Acadian redfish (*S. fasciatus*). Therefore, redfish catches were initially attributed to the genus *Sebastes* and then separated into these two species in the database. To do this, for each tow and, where applicable, for each sorting category, a random sample of 30 individuals was selected for anal fin ray (AFR) counting. Then, as described by Senay et al. (2022), a chi-square (X^2) function was adjusted with the aim of minimizing the difference between the observed proportions of individuals per AFR class (6, 7, 8, 9, or 10 rays) and those expected for each species and Management Unit based on a genetic study conducted in the mid-1990s (Valentin et al., 2006). The proportions of *S. mentella* and *S. fasciatus*, inferred for each of the subsamples used for AFR counts, were directly applied to the total catch weights and numbers, in addition to being used to weight the individual weight and length observations in the analyzes of biological characteristics (see section 2.2.2.4).

It was not possible to apply the approach described above to a specific sample for which the AFR count was omitted. Specifically, no AFR values were available for redfish in sorting category 1 from station 52 – located within Unit 1 – surveyed in 2022. In this particular case, the expected relationship between the proportion of *S. fasciatus* (SF) and depth (D) was used, namely:

$$prop_{SF} = e^{5.3401-0.0184D}/(1+e^{5.3401-0.0184D}) \quad (1)$$

The robustness of the approach described by Senay et al. (2022) for species separation has been called into question in light of conflicting genetic data (Senay et al., 2026). Nevertheless, in the absence of an alternative approach applicable to all redfish abundance series from Units 1 and 2 (DFO, 2025b), the decision was made to maintain this approach in the present report.

2.1.1.3 Handling of shrimp catches

The protocol for processing the 2022 and 2023 shrimp catches was the same as that used in the DFO August survey in the Estuary and the nGSL (Chamberland et al., 2025). Briefly, the entire shrimp catch of the tow was processed if the total weight was < 3.0 kg, while only a 1.5 to 2.5 kg sample of the catch was retained when the weight exceeded 3.0 kg. This approach aimed to ensure that a minimum of 200 northern shrimp (*Pandalus borealis*) individuals were available for analysis for stock assessment (Bourdages et al., 2023a). For *P. borealis*, the presence and type of parasites, stage of maturity, sex, and cephalothorax length[5] were also recorded for a minimum of 200 individuals. For other shrimp species, observations were limited to the presence of parasites and cephalothorax length, with a maximum of 50 individuals per species.

Shrimp catches in 2024 were processed differently depending on the geographic location of the tow. The protocol applied within the GSL, specifically NAFO Divisions 4RST, was the same as that described for 2022 and 2023. In tows conducted outside the GSL, specifically NAFO Divisions 3P4V, northern shrimp were processed as described for other shrimp species. This difference between the two areas primarily reflected the stock assessment needs of northern shrimp in the Estuary and the GSL, which do not utilize data from outside the GSL (Bourdages et al., 2023a).

2.1.2 Treatment of taxonomic codes

The taxonomic codes used for the survey and this report are those established in the DFO Quebec Region STRAP system (Smith and Somerton, 1981; Miller and Chabot, 2014). The list used for this report has been updated as needed[6] and scientific names have been added as required. The validity of the scientific names on this list is periodically checked against the World Register of Marine Species (https://www.marinespecies.org/). Because some STRAP codes may refer to levels higher than species, the latter are referred to as 'taxon' in this report.

Some taxa have been treated differently due to uncertainties and/or possible differences in the quality of identification of specimens from one tow to another. Among others, validated catches of spotted lanternfish (*Myctophum punctatum*; code 281), glacier lanternfish (*Benthosema glaciale*; code 290), Kroyer's lanternfish (*Notoscopelus kroyeri*; code 275), mirror lanternfish (*Lampadena speculigera*; code 285) and glowingfish (*Neoscopelus macrolepidotus*; code 278), as well as catches identified to the family Myctophidae (code 272), the subfamily Gonostomatidae

[5] Cephalothorax length: For all shrimp taxa, oblique cephalothorax length was always measured from the inside of the eye socket to the central end of the cephalothorax.

[6] Here, the additions were mainly needed for areas outside the area historically covered during the DFO August Estuary and nGSL survey since the list used was based primarily on the taxa present in that survey.

(code 205) or the order Myctophiformes (code 271), were combined with the Myctophiformes code. This grouping reflects the fact that, in several cases, the specimens associated with these taxonomic codes were too damaged to be identified using the resources available on board the vessel (e.g., it was impossible to note the presence of photophores or observe the shape of the otoliths; Nozères et al., 2010) and/or the identification of specimens in the laboratory was based on a sample that was not necessarily representative of the tow catch (P.-M. Scallon-Chouinard, pers. comm. December 1, 2025). It would not have been taxonomically consistent to group them at the level of the family Myctophidae because this code could have included the glowingfish (family: Neoscopelidae) and specimens from the subfamily Gonostomatidae (family: Stomiiformes). Although not ideal, this approach represented the most robust method for conducting the analysis for the taxon Myctophiformes.

Changes were also required for sponges to account for certain constraints associated with working at sea (e.g., the need to examine spicules under a microscope) and a generally less advanced level of knowledge regarding the phylum. Taxonomic analysis was possible for the four species considered most likely to be identified accurately on board the vessel, namely *Polymastia hemisphaerica* (code 1107), *Tentorium semisuberites* (code 1108), *Stylocordyla borealis* (code 1112), and *Asconema foliatum* (code 1120) (J. Paradis-Hautcoeur, pers. comm. June 13, 2025). The other taxa, including those that could be identified through laboratory analysis[7], were grouped under the phylum Porifera (code 1101).

Finally, some taxonomic codes underwent specific corrections to reflect recent changes in available knowledge. The jellyfish *Stephalia corona* was identified as Rhodaliidae in 2022 and 2023, an error that was corrected in 2024 (P-M. Scallon-Chouinard, pers. comm. December 10, 2025). Rhodaliidae catches were therefore reassigned to *Stephalia corona* in the dataset. Due to a taxonomic update, catches associated with the Atlantic spiny lumpsucker (*Eumicrotremus spinosus*; code 844) were reassigned to the Newfoundland spiny lumpsucker (*Eumicrotremus terraenovae*; code 847), a change that affected only one tow.

The observed taxa were separated into two groups according to their number of occurrences in the database (i.e., tows with presence). Those considered rare—defined as present in < 25 of the tows recorded during the three survey years—were subjected to descriptive statistics of catches and a map of the spatial distribution of presences. For more frequently observed taxa (≥ 25 occurrences), the results presented included, depending on data availability, (a) a map of the spatial distribution and range of standardized catch weights and numbers per station and year; (b) spatial interpolation maps of catches and the shape of the smoothing function for depth when retained as a covariate; (c) the cumulative distribution of catches as a function of depth, temperature, and bottom dissolved oxygen; and (d) the annual LF and the estimated length-weight relationship for the three combined survey years. Finally, following a preliminary exploration of the data, it was decided to exclude taxa that could not be identified at a taxonomic level relevant to the analyzes presented in this report (details in **Table A1**).

[7] It is important to note that at the time of analyzing the survey data, laboratory analyzes were still in progress to clarify the taxonomic identification of certain sponges attributed to Porifera (e.g., observation of spicules).

2.2 Detailed analyzes for common taxa

All analyzes were performed using R software version 4.4.1 (R Core Team, 2024). The equations that follow have been applied to each taxon separately, but the taxon is not shown as an index to variables for clarity.

2.2.1 Estimation of biomass and abundance per tow

Total catch weights and numbers per tow were estimated for each year and common taxon. To this end, the weights or numbers caught X of each sorting category c (c = 1, 2, ..., C) were summed by tow j (j = 1, 2, ..., J) and year y (y = 1, 2, ..., Y), then scaled to a standard distance of 0.75 nm:

$$X_{std_{yj}} = \frac{0.75}{b_{yj}} \sum_{c=1}^{C} X_{yjc} \quad (2)$$

where $X_{std_{yj}}$ is the standardized weight or number per tow, depending on the analysis, X_{yjc} is the corresponding 'raw' observed value and b_{yj} is the observed tow distance based on the speed and duration of trawling, in nm.

The results of this analysis were represented as bubbles of varying sizes (presences) and crosses (absences) on a map of the study area. Specifically, values of $X_{std_{yj}}$ ≥ 99.5th percentile were represented by bubbles of the same size, the largest of which is shown in the legend. Similarly, the scale for bubble size was determined from the 0th, 50th, 75th, and 100th percentiles of the distribution of catches truncated at the 99.5th percentile (including zero catches). In some cases, however, the values representing 0, 50, 75, and 100 % of the 99.5th percentile were shown in the legend (these cases are identified in the legend title).

To facilitate comparison of observed values with those predicted by spatial interpolation (see section 2.2.2), the values per tow entered in each legend were accompanied by their equivalent per 0.25 km^2 cell in parentheses. A conversion of values was necessary for a fair comparison given that a standard tow had an anticipated area of 0.0235 km^2, an area smaller than that of a bathymetric grid cell by a factor of slightly more than 10.

2.2.2 Spatial interpolation with sdmTMB

Spatial interpolation maps were generated using the mixed model from the *sdmTMB* library (Anderson et al., 2024). The number of survey years and the spatial overlap of the study areas from one year to the next were deemed insufficient to include a temporal component in the model. The covariate chosen for spatial interpolation was depth, given its role in the distribution of several taxa and the ease with which it can be obtained (e.g., see Johnson et al., 2019). The depth data for the study area originate from the General Bathymetric Chart of the Oceans (GEBCO Bathymetric Compilation Group, 2020; available at https://www.gebco.net/), where the resolution of one cell s was 0.5 by 0.5 km (number S of cells for the study area: 499,164; see the outline of the area in **Figure A1**). Thus, for each taxon, the modeling was applied to the catches from the 413 successful tows during the three survey years.

2.2.2.1 Estimation of dependent variables

The sdmTMB modeling algorithm requires, among other things, providing an object of type *sdmTMBmesh* or Delaunay triangulation (Anderson et al., 2024). This object was defined using the *make_mesh* function based on the average coordinates of the survey tows taken at each station and projected in NAD83 Quebec Lambert (EPSG: 32198) on a scale expressed in kilometers. The minimum distance between adjacent points of the triangulation (*cutoff* argument) was set to 10 nm (18.52 km) to reflect the approximate distance between the theoretical coordinates of the stations (see **Figure A2**). No correlation barriers were applied for this triangulation.

Since the spatial resolution of the bathymetric grid was 0.5 by 0.5 km, the dependent variable of the models was the density of the taxon within a square cell s with an area of 0.25 km^2, $dens_s$:

$$dens_s = \frac{0.25 \sum_{c=1}^{C} X_{yjc}}{b_{yj} \cdot 1.852 \cdot 0.01694} \tag{3}$$

where the variables X_{yjc} and b_{yj} are defined as in Equation 2, the constant value of 1.852 represents nm per km and the constant value of 0.01694 represents the mean horizontal opening, in km, of the Campelen 1800 trawl as part of the August Estuary and nGSL survey on board the CCGS Teleost (Bourdages et al., 2007). In this report, the choice of a constant value of 0.01694 km was arbitrary and served only to represent the model predictions on the correct scale in a map (annotated figures b). The value itself had no impact on the results.

2.2.2.2 Model specification and fitting

The sdmTMB models applied to weight and number densities were specified with a spatial random field on the intercept (spatial argument = '*on*'), but without a spatiotemporal effect (spatiotemporal argument = '*off*'). Since year-to-year variations were not considered in this analysis, all observations of $dens_s$ were assigned the same level of a year factor (*time* argument referring to a constant value). Furthermore, to allow for better consistency between the input data and the predictions, the depth variable used was that from the GEBCO bathymetric grid and not that recorded by the echosounder at each tow.

The catches of a majority of taxa covered sufficiently large ranges of values to anticipate overdispersion in the input data. Thus, the weight densities of each cell s (s = 1, 2, ..., S), $dens_weight_s$, were modeled assuming a Tweedie distribution with a log link function and an effect of depth D in meters:

$$\begin{gathered} dens_weight_s \sim Tweedie(\mu_s, \varphi, \tau) \\ E[dens_weight_s] = \mu_s = \exp(\boldsymbol{X_0} + f(D_s) + \omega_s) \\ \omega_s \sim MVN(0, \Sigma_\omega) \\ Var[dens_weight_s] = \varphi(\mu_s)^\tau \end{gathered} \tag{4}$$

where μ_s is the expected number density within cell s, $f(D_s)$ is a smoothing function of depth specified with a maximum of 5 basis dimensions ($k = 5$) and as thin plate regression spline, $\boldsymbol{X_0}$ is the intercept fixed effect and ω_s corresponds to spatial random effects which follow a multivariate normal (MVN) distribution with a mean of zero and Matérn covariance matrix Σ_ω

developed from the *sdmTMBmesh* object. In the Tweedie distribution, φ is the dispersion parameter and τ is a power parameter restricted to the interval $1 < \tau < 2$.

For densities expressed in number per cell, $dens_number_s$, the dependent variable followed a type II negative binomial distribution (*nbinom2;* Hilbe, 2011) with a log link function :

$$\begin{gathered} dens_number_s \sim nbinom2(\mu_s, k) \\ E[dens_number_s] = \mu_s = \exp(\boldsymbol{X_0} + f(D_s) + \omega_s) \\ \omega_s \sim MVN(0, \Sigma_\omega) \\ Var[dens_number_s] = \frac{\mu_s}{1+\mu_s/k} \end{gathered} \quad (5)$$

where μ_s is the expected density in number within cell s, k is the distribution's overdispersion parameter and the other parameters and symbols are as defined in Equation 4.

Some taxa in the analysis were present in such small quantities per tow (~10 individuals or fewer) that a model based on a Tweedie (weight) or negative binomial (number) distribution was neither appropriate nor even possible. Modeling catches in weight was not deemed relevant for these taxa given the expected similarity to the patterns of variation in catch numbers. Since overdispersion was not expected, these catch numbers were instead modeled by assuming a Poisson distribution with a log link function:

$$\begin{gathered} dens_number_s \sim Poisson(\mu_s) \\ E[dens_number_s] = \mu_s = \exp(\boldsymbol{X_0} + f(D_s) + \omega_s) \\ \omega_s \sim MVN(0, \Sigma_\omega) \\ Var[dens_number_s] = \mu_s \end{gathered} \quad (6)$$

The taxa concerned by this simplified analysis and for which the Poisson distribution model has converged are, in the order of appearance of the figures, the fish *Alosa pseudoharengus*, *Helicolenus dactylopterus*, *Artediellus atlanticus*, *Paraliparis copei*, *Hippoglossus hippoglossus* and *Lophius americanus*, as well as the invertebrates *Ptychogena lactea*, Scyphozoa, *Cuspidaria glacialis*, *Stoloteuthis leucoptera*, *Bathypolypus bairdii*, *Laetmonice filicornis*, *Aega psora*, *Munidopsis curvirostra*, *Hippasteria phrygiana*, *Pseudarchaster parelii* and the genus *Henricia*.

2.2.2.3 Comparison of models with a variant without a depth effect and validation

The influence of depth on the observed density per cell was assessed by comparing the models of Equations 4, 5, and 6 with equivalent variants without the effect of depth. A depth effect was considered relevant when the difference in the Akaike Information Criterion (AIC) between the two variants was greater than 2 units (i.e., AIC of the model with depth < AIC of the model without depth + 2). Otherwise, or in cases of non-convergence of the model with depth, the model without the effect of depth was retained for the taxon.

The goodness of fit of the selected model for catch weights and the selected model for catch numbers was first assessed using 'mle-mvn' residuals (maximum likelihood estimate – multivariate normal; Thygesen et al., 2017) and Q-Q normal plots generated with a modified version of the *qqPlot* function from the *car* library in R (Fox and Weisberg, 2019). The models selected for each analysis were also subjected to a basic diagnostic using the *sanity* function of *sdmTMB*. The residuals for each taxon and details of the diagnostics for models with certain problems are presented in the figures in Appendix B. Finally, the ability of each model to

reproduce the input data—a quality not necessarily apparent in the residuals—was assessed using the Pearson correlation coefficient (*r*) between observed and predicted values.

2.2.2.4 Spatial predictions and estimation of global means

The densities of each taxon per 0.25 km^2 cell of the GEBCO grid were predicted from selected models for visualization on a map. In cases where the selected model included a depth effect, the fit and uncertainty of the depth smoothing function were also shown; otherwise, only the prediction map was displayed. It is important to remember that the depths used in the adjustment of the mixed model were those of GEBCO (obtained by a spatial join with the coordinates of the tows) since these differed from those recorded during the trawling operations.

The average catches per tow of each taxon were averaged over the entire study area using a post-stratification scheme and the standard weighted average estimator. Specifically, Voronoi polygons were generated around the theoretical coordinates of each of the stations using the *st_voronoi* function from the *sf* library in R, with a NAD 83 Quebec Lambert projection (Pebesma, 2018; illustrated in **Figure A3**). The area occupied by each polygon h (h = 1, 2, …, H), denoted A_h, was obtained with the *st_area* function and used to weight the calculation:

$$\overline{X_{std}} = \frac{\sum_{h=1}^{H}\left(\overline{X_{std_h}} \cdot A_h\right)}{\sum_{h=1}^{H} A_h} \tag{7}$$

where $\overline{X_{std}}$ represents the taxon's mean catch weight or number in the whole survey and $\overline{X_{std_h}}$ is the average standardized catch in tows completed within each polygon h. As an alternative calculation method, it would have been possible to apply the *get_index* function from the *sdmTMB* library to the values predicted by the models. However, the reliability of the results obtained in an exploratory analysis varied widely between taxa, depending, among other things, on the extent of the depths in which the taxon was present relative to that of the predicted bathymetric grid.

2.2.3 Cumulative distributions of catches as a function of environmental variables

Empirical cumulative catch distributions according to tow depth (m), temperature (°C) and bottom dissolved oxygen (% saturation) were generated for the standardized catches per tow ($X_{std_{yj}}$ of Equation 2) of each common taxon. Given the changes in survey coverage between years, the Voronoi polygons defined in Equation 7 were used in a post-stratification scheme for the calculation.

In accordance with the method described by Perry and Smith (1994), the cumulative distribution function $f(t)$ was estimated for each environmental variable E, excluding tows for which E was not available:

$$f(t) = \sum_{h=1}^{H}\sum_{j=1}^{J} \frac{W_h}{n_h}\, I(E_{hj}) \tag{8}$$

where t is a vector of length 100 covering the range of values observed for the environmental variable E, W_h is the proportion of the study area occupied by each stratum h (here, the Voronoi polygon) and n_h is the number of tows j realized within each of these strata. The values J and H represent, respectively, the numbers of tows and of strata for which the environmental variable was available.

In Equation 8, the indicator function I serves to determine whether or not E_{hj} exceeds a value of t in order to perform a cumulative sum:

$$I(E_{hj}) = \begin{cases} 1 \; if \; E_{hj} \; \leq t \\ 0 \; if \; E_{hj} > t \end{cases} \tag{9}$$

The interpretation of the results for each environmental variable depended in part on data availability (see **Figure 2**). In particular, the interruption of data collection for quantifying dissolved oxygen from February 28, 2024, meant that catches made after that date were not included in the calculation for this purpose. The analyzes based on depth measured by the trawl probes, temperature, and dissolved oxygen were possible for 413, 394, and 332 observations, respectively.

The distribution of catches according to the environmental conditions of each tow was described as :

$$g(t) = \sum_{h=1}^{H} \sum_{j=1}^{J} \frac{W_h}{n_h} \frac{X_{std_{hj}}}{\overline{X_{std}}} \; I(E_{hj}) \tag{10}$$

where $X_{std_{hj}}$ corresponds to the catch weight or number in stratum h and tow j, $\overline{X_{std}}$ is the mean that was estimated in Equation 7, and W_h and n_h are defined as in Equation 8. The sum of $g(t)$ over the 100 values of t employed in the calculation equaled 1.

The standardized weight and number values corresponding to the 1st, 25th, 50th, 75th, and 99th percentiles of the cumulative environmental distributions were calculated by linear interpolation. Specifically, if y is the percentile value of interest for X_{std}, the associated environmental value x should be:

$$x = \frac{(y - y_1)(x_2 - x_1)}{(y_2 - y_1)} + x_1 \tag{11}$$

where x_1 and y_1 correspond to the coordinates of the last point preceding the percentile of interest y (i.e., the maximum cumulative percentage not exceeding the targeted percentage), and x_2 and y_2 are the coordinates of the first point following the percentile of interest y (i.e., the minimum cumulative percentage among the values exceeding the targeted percentile).

2.2.4 Length frequencies and length-weight relationships

The LFs by taxon were generated for the entire study area and by year for visual comparisons over time, as well as for a general idea of the range of observed lengths. First, the number of individuals per year y, tow j and length class i (i = 1, 2, ..., I; intervals of 1 cm or 1 mm, depending on the taxon) in a total catch, N_{yji}, was estimated as :

$$N_{yji} = \frac{0.75}{b_{yj}} \sum_{c=1}^{C} \frac{n_{yjci} \cdot \; P_{yjc}}{p_{yjc}} \tag{12}$$

where b_{yj} is the observed tow distance based on the speed and duration of trawling in nm, n_{yjci} is the number of individuals in the LF sample, by sorting category c if applicable, p_{yjc} is the weight of this sample and P_{yjc} is the total weight of the corresponding catch.

The mean numbers per year and length class, $\overline{N_{y\iota}}$, were then estimated as:

$$\overline{N_{y\iota}} = \frac{\sum_{j=1}^{J_y} N_{yji}}{J_y} \quad (13)$$

where J_y is the number of successful trawling activities in year y, regardless of whether the taxon was observed or not.

The relationship between the log of weight (kg) and the log of length (cm) for individuals for which both pieces of information were available was quantified using a single linear model. However, the model input data were color-coded by year to highlight potential interannual variations in the figure (note that the survey area varied between years). The models assumed that each observation corresponded to one individual, regardless of sampling effort or sample fraction. However, for both redfish species, the proportion of individuals of each species was used as a weighting argument in the regression.

2.3 Descriptive statistics for common and rare taxa

The analyzes presented in this section were applied to all taxa observed in the survey. However, these constituted the only presented analyzes for those considered rare (< 25 occurrences over the three survey years).

First, the total catch weights and numbers were standardized as in Equation 2, then summed over all successful tows for each taxon.

Secondly, a summary of the data available for length and weight measurements was produced for each taxon, in number of individuals observed. Specific characteristics of the observed size distribution are also presented, including minimum, maximum and specific percentile values.

Finally, for rare taxa only, presence and absence maps were generated to give a general idea of their spatial distribution in winter. These maps differed from those produced for common taxa in that all catches were represented by a circle of the same size and within the same panel, regardless of the year.

2.4 Other research questions

Various research protocols were integrated into the survey to further understanding of biodiversity (e.g., gorgonocephalian taxonomy), interactions between taxa (e.g., stomach contents), and life histories (e.g., gonad collection). In 2024, for example, Atlantic halibut (*Hippoglossus hippoglossus*) were tagged with satellite transmitters to estimate the degree to which specimens belonged to the GSL stock (NAFO Divisions 4RST) and the Scotian Shelf and southern Grand Banks stock (SSSGB; NAFO Divisions 3NOPs4VWX5Zc); details and results of this experiment are presented in Appendix C. A brief description of the other projects is presented in Appendix D.

3 RESULTS

A total of 290 taxa were considered in this analysis. **Table 2** presents the STRAP code, the scientific and English names of each taxon, the number of occurrences (i.e., the number of tows with presence), the total and mean catches expressed in weight and number, and the figure numbers in which the results of the analyzes described in sections 2.2 and 2.3 of the Methods

are presented. **Table 3** presents, for each taxon subjected to biological sampling, the number of specimens with a weight and/or length measurement, as well as descriptive length statistics. The results in the tables and figures are presented in the same order: first, by type of analysis (common or rare taxon), then in ascending order of the STRAP code, and finally by phylogenetic group.

Figures 3 to **90** present the results of detailed analyzes on common (≥ 25 occurrences) fish (section 3.1) and invertebrate (section 3.2) taxa. Each set of figures includes (a) a map of the spatial distribution of catches in weight and number per survey year, (b) the results of selected spatial interpolation models in the weight-based and number-based analyzes, with the depth smoothing function where relevant, (c) the cumulative proportions of catches in weight and number according to depth, temperature, and bottom dissolved oxygen and, where available, (d) the annual LF and overall length-weight relationship based on the three combined survey years for each taxon with individual measurements. To limit redundancy, a detailed legend is provided for the first set of figures only, that is, below **Figure 3**. The model diagnostics for the sdmTMB analyzes are presented in Appendix B.

Figures 91 to **95** present distribution maps of the presence and absence of taxa considered rare over the three years of the survey. Each panel indicates the STRAP code of a taxon, but the order of some of them has been revised so that the results for taxa of the same phylogenetic group are consecutive.

The bottom trawl used and the spatial coverage of the survey were not adequate for all taxa present in the environment. Indeed, it is likely that catches of taxa associated with depths, habitats, and/or regions less well covered by the survey are not representative of actual spatial distribution. Furthermore, some taxa likely had variable catchability from year to year and/or from one tow to the next. Also, organisms such as sea pens and certain sponges could remain attached to the trawl and contaminate catches from subsequent tows. The results concerning these taxa should therefore be interpreted with caution, and future analyzes should take these uncertainties into account.

3.1 Results of detailed analyzes on common fish taxa

The majority of analyzes applied to common fish taxa were deemed of sufficient quality to be retained and interpreted. In the following section, the number of occurrences in **Table 2** and the four sets of figures are presented for each taxon separately, with a mention of the COSEWIC status where applicable.

The mud hagfish (*Myxine limosa*) was present in slightly more than half of the 413 successful tows in the survey (N = 232), with a maximum catch of 53 individuals during a single tow in 2024 (**Figure 3a**). Spatial interpolation maps encompassing the three survey years suggested a particularly high presence of mud hagfish in the vicinity of Cabot Strait, although the species was present throughout the Laurentian Channel (**Figure 3b**). Half of the catch biomass was located at depths between 341 and 432 m and at temperatures between 6.0 and 6.6 °C (**Figure 3c**). Catches were dominated by lengths from 20 to 50 cm (**Figure 3d**).

Black dogfish (*Centroscyllium fabricii*) was present in a total of 198 tows, most of which were located in the Laurentian Channel within the GSL (**Figure 4a**). A probable effect of depth was detected on the interpolated catches in weight and number in space, although the uncertainty associated with the depth smoothing functions increased rapidly from ~500 m (**Figure 4b**). The

majority of individuals caught originated from the greatest depths and highest temperatures recorded in the survey (**Figure 4c**). The catches also represented a wide range of lengths, from less than 10 cm to almost 70 cm (**Figure 4d**).

The thorny skate (*Amblyraja radiata*), which has been designated as a species of special concern by COSEWIC (2012a), was present in a very large number of tows (N = 335), but the largest catches originated outside the GSL (**Figure 5a**). The role of depth in its distribution was not entirely clear; the weight-based interpolation model suggested an improved model fit with the inclusion of a depth effect, while the number-based model did not suggest a depth effect (**Figure 5b**). The cumulative catch distributions according to the three environmental variables reflected fairly well the conditions sampled during the survey (**Figure 5**c). Annual LFs had a fairly wide range, from approximately 10 cm to over 80 cm (**Figure 5d**).

The smooth skate (*Malacoraja senta*), another species of special concern in the study area (COSEWIC, 2012e), was present in fewer tows (N = 197) and in smaller quantities than the thorny skate (**Figure 6a**). Depth appeared to affect the distribution of catch weights, but this effect could not be tested for catches by number as the model did not converge (**Figure 6b**). There was no marked difference between the cumulative distribution curves of catches and the values recorded at tows (**Figure 6c**), nor was there any particular pattern in the LF for this species (**Figure 6d**).

The results applicable to Atlantic herring (*Clupea harengus*) should be interpreted with caution given the lower probability of this species being caught by bottom trawling in the study area (e.g., pelagic species). The species was particularly abundant in the northeastern part of the GSL and near Anticosti Island, but almost absent from the Laurentian Channel (**Figure 7a**). Other analyzes indicated a clear predominance of Atlantic herring at depths around 200 m and at length classes from 25 to 35 cm (**Figure 7b,c,d**).

The alewife (*Alosa pseudoharengus*), another species to consider with caution, was recorded 45 times during the three years of the survey; this species was observed primarily along the south side of the Laurentian Channel (**Figure 8a,b**). Half of the alewife biomass was located at depths between 257 and 324 m, at temperatures between 5.7 and 7.3 °C, and oxygen saturation levels between 35.3 and 48.8 % (**Figure 8c**). Length observations were deemed insufficient for a detailed interpretation of annual LFs of this species (**Figure 8d**).

The exposure and catchability of capelin (*Mallotus villosus*) in the winter survey were also deemed uncertain (see also Chamberland et al., 2022). Nevertheless, it was still caught in the northeastern part of the GSL, in addition to observations near Anticosti Island and off Cape Breton (**Figure 9a**). The interpolation model applied to catch weights and the cumulative curves based on environmental variables indicated larger catches at depths around 200 m, but these predictions were less clearly defined than for Atlantic herring, and there was no convergence of the models based on numbers (**Figure 9b,c**). The majority of measured individuals belonged to the 10 to 15 cm length classes (**Figure 9d**).

The Atlantic argentine (*Argentina silus*) was present within the GSL, but the largest catches were made south of Newfoundland, within NAFO Division 3P (**Figure 10a**). Spatial interpolation models suggested uncertain effects of depth on catch weights and numbers (**Figure 10b**), while cumulative distribution curves identified a greater presence of the species at temperatures and oxygen levels higher than those recorded on average during the survey (**Figure 10c**). Annual LFs for the species showed more or less defined peaks around 17 cm and between 25 and 30 cm (**Figure 10d**).

Fish of the order Myctophiformes were almost exclusively caught in the easternmost section of the Laurentian Channel (**Figure 11a**). Spatial interpolation models suggested an increase in catches beyond approximately 400 m, an effect that was, however, associated with very wide confidence intervals (**Figure 11b**). Given the ecological diversity of the species considered in this taxonomic group, the patterns described above as well as those observed in the cumulative curves (**Figure 11c**) and the annual LFs (**Figure 11d**) should be interpreted with particular caution.

The white barracudina (*Arctozenus risso*) is another species whose catchability by trawl may have varied among tows. Nevertheless, it was very common in the survey catches, with a total of 300 occurrences across the study area (**Figure 12a**). The largest catch weights and numbers were associated with depths of 300 to 400 m according to interpolation models and cumulative distribution curves as a function of depth (**Figure 12b,c**). The LFs for the species showed slightly different modes in 2022, 2023, and 2024, but all were within the 20–25 cm length range (**Figure 12d**).

The northern cutthroat eel (*Synaphobranchus kaupii*) was observed in 30 of the 413 successful tows in the survey, mostly outside the GSL (**Figure 13a**). Models fitted to catch weights or numbers did not converge. Half of the species' biomass was found at depths between 457 and 523 m, at temperatures between 4.3 and 5.4 °C and oxygen saturation levels between 27.8 and 52.1 % (**Figure 13b**). The LF for 2024 indicated a mode at almost 35 cm, while the 2022 and 2023 values were not interpreted due to an insufficient number of observations (**Figure 13c**).

The threespine stickleback (*Gasterosteus aculeatus*), a species that may have been less well represented in the survey, was observed in only 40 tows. Observations appeared to be largely concentrated in the southwest and east of Anticosti Island (**Figure 14a**). The interpolation model used for catch weights did not suggest an effect of depth, although the agreement between observed and predicted values was considered limited for this species (Pearson's *r* of 0.5) and there was no convergence for the number-based model (**Figure 14b**). Half of the threespine stickleback biomass occupied depths of 259 to 361 m, temperatures of 6.3 to 6.9 °C, and oxygen saturation levels of 19.7 to 34.5 % (**Figure 14c**). Annual LFs were generally dominated by length classes of 5 to 7 cm (**Figure 14d**).

The Atlantic cod stocks of the nGSL (NAFO Divisions 3Pn4RS), southern Newfoundland (3Ps), and sGSL (4T + 4Vn [November to April]) are considered endangered by COSEWIC (2010a) and are the subject of separate recovery plans (DFO, 2024d; 2024c; 2024b). Similarly to the results of a survey conducted in January from 1994 to 1997 (Chouinard and Hurlbut, 2011), the largest Atlantic cod catches were from the north and south sides of the Laurentian Channel within the GSL (**Figure 15a**). The depth smoothing functions exhibited a bell shape, with a fairly well-defined mode around 200 m (**Figure 15b**). Half of the Atlantic cod biomass was located at depths between 232 and 358 m, at temperatures between 6.0 and 6.8 °C and oxygen saturation levels of 27.7 to 42.8 % (**Figure 15c**). Atlantic cod LFs were dominated by the 20–40 cm length classes (**Figure 15d**).

The pollock (*Pollachius virens*) was observed in 26 of the 413 successful survey tows, mostly in those conducted in 2024 and outside the GSL (**Figure 16a**). The species was particularly abundant south of Newfoundland and on the Laurentian Fan, a pattern not associated with a depth effect for catch weights (**Figure 16b**). Cumulative distribution curves suggested pollock were found in shallower, warmer, and more oxygenated waters than observed on averages

(**Figure 16c**). The majority of individuals measured in 2024 were in length classes from 60 to 70 cm, while observations from 2022 and 2023 were deemed insufficient for a robust interpretation (**Figure 16d**).

Longfin hake (*Physis chesteri*) was recorded 213 times, with a clear association to the Laurentian Channel (**Figure 17a**). Depth influenced catch weights, with a mode of smoothing between 400 and 600 m, in addition to a less pronounced effect on catch numbers (**Figure 17b**). Longfin hake was generally present at greater depths and dissolved oxygen levels than the average of the tows covered by the survey (**Figure 17c**). Annual LFs were dominated by length classes of 20 to 40 cm (**Figure 17d**).

White hake, a species designated as threatened in the survey area (COSEWIC, 2013), was observed primarily along the south side of the Laurentian Channel and on the Laurentian Fan (**Figure 18a**). The spatial interpolation model used for catch weights, as well as the cumulative distribution curves, suggested a predominance of the species at depths of approximately 250 to 400 m (**Figure 18b,c**). Annual LFs were dominated by values associated with a juvenile or presumed immature status, i.e., < 45 cm (Rolland et al., 2022; **Figure 18d**).

The silver hake (*Merluccius bilinearis*) was also strongly associated with the Laurentian Channel during the survey (**Figure 19a**). The spatial interpolation models indicated depth effects on catch weights and numbers, with the mode of the smoothing functions located around 300 m (**Figure 19b**). Silver hake occurred in slightly warmer and significantly more oxygenated waters than the average of the tows conducted in the survey (**Figure 19c**). The catches were mainly represented by individuals of 25 to 30 cm (**Figure 19d**).

The fourbeard rockling (*Enchelyopus cimbrius*), another species whose vulnerability to trawling may have varied among tows, was generally present in small numbers and mostly near Anticosti Island (**Figure 20a**). The weight-based model indicated a gradual increase, with a wide confidence interval, in catch values with depth, while the number-based model did not converge (**Figure 20b**). The depths occupied by the species differed little from those recorded by trawling during the survey; however, observations originated from areas that were slightly less oxygenated than average (**Figure 20c**). Annual LFs were dominated by length classes of 15 to 20 cm (**Figure 20d**).

The common grenadier (*Nezumia bairdii*) was observed in a significant number of successful tows (N = 336) and exhibited a very wide distribution within the study area (**Figure 21a**). Spatial interpolation models predicted an increase in catch weight and number with depth, an effect that became less certain beyond 500 m (**Figure 21b**). Common grenadier also appeared to occur in deeper, warmer, and less oxygenated areas than most survey tows (**Figure 21c**). The LFs for all three years showed a mode at approximately 25 cm (**Figure 21d**).

Atlantic wolffish (*Anarhichas lupus*), a species of special concern according to COSEWIC (2012b), was generally associated with the west coast of Newfoundland and, to a lesser extent, east of Cape Breton (**Figure 22a**). This pattern was well represented in the spatial interpolation model predictions for weight, while the model for number did not converge (**Figure 22b**). Half of the Atlantic wolffish catches in weight were associated with depths of 143–186 m, temperatures of 2.0–5.3 °C, and oxygen saturations of 61.4–78.1 % (**Figure 22c**). Annual LFs ranged from 7.5 to 88.5 cm, but the majority of observations were associated with length classes < 50 cm (**Figure 22d**).

The Atlantic soft pout (*Melanostigma atlanticum*) was present in 115 tows, the majority of which were located along the Laurentian Channel and on the Laurentian Fan (**Figure 23a**). The spatial interpolation model used for catch weights suggested a positive effect of depth, but with greater uncertainty beyond 400 m, while the model applied to catch numbers did not converge (**Figure 23b**). Half of the Atlantic soft pout biomass occupied depths of 349–420 m, temperatures of 6.2–6.7 °C, and oxygen saturation levels of 16.2–40.7 % (**Figure 23c**). Annual LFs had modes between 10 and 12 cm (**Figure 23d**).

Fish of the genus *Sebastes* were observed in almost all the survey tows (N = 408) and constituted 51 % of the total biomass trawled during the three years of the survey (**Table 2**). The results for this group presented below account for the separation of data between the two main species.

The deepwater redfish (*S. mentella*) was particularly abundant along the Laurentian Channel and southwest of Newfoundland (**Figure 24a**). The predictive power of the weight- and number-based models was generally limited, with Pearson correlation coefficients of 0.39 and 0.46, respectively (**Figure 24b**). These low *r* values may reflect the difficulty the model has in predicting very large catches and/or accounting for depths beyond those observed. Half of the deepwater redfish biomass was observed at depths between 331 and 430 m, temperatures between 5.7 and 6.9 °C, and oxygen levels of 28.2 to 55.3 % (**Figure 24**c). Annual LFs were dominated by length classes of 20 to 25 cm (**Figure 24d**), values associated with the large cohorts of 2011, 2012, and 2013 (DFO, 2025b).

Consistent with other data sources (e.g., DFO, 2025b), the Acadian redfish (*S. fasciatus*) was less abundant than deepwater redfish during the survey (**Figure 25a**). The predictive power of the models was also considered low for this species, with correlation coefficients of 0.31 and 0.38 for catches by weight and number, respectively (**Figure 25b**). Half of the Acadian redfish biomass was found at depths of 233 to 267 m, temperatures of 5.7 to 7.2 °C, and oxygen saturations of 27.6 to 40.6 % (**Figure 25c**). As with deepwater redfish, the LFs were dominated by length classes of 20 to 25 cm (**Figure 25d**).

The blackbelly rosefish (*Helicolenus dactylopterus*) was less abundant inside than outside the GSL (**Figure 26a**). The Poisson distribution model used for the analysis of catch numbers indicated a probable effect of depth, but the shape of this effect suggested uncertainty (**Figure 26b**). The species generally occupied more oxygenated waters than the average of survey tows (**Figure 26c**). The mode of the 2024 LF for blackbelly rosefish was between 15 and 17 cm, while the 2022 and 2023 observations were deemed insufficient for a robust interpretation (**Figure 26d**).

The Atlantic hookear sculpin (*Artediellus atlanticus*) was observed in low numbers in 36 tows, mostly associated with shallower areas of the GSL (**Figure 27a**). The Poisson distribution model selected for the species suggested a depth effect on catch numbers, but this effect was uncertain (**Figure 27b**). In addition to occurring within the shallowest waters of the survey, the Atlantic hookear sculpin was also found in colder and more oxygenated areas than the average of tows (**Figure 27c**). Individuals retained for the LFs generally measured 4 to 9 cm (**Figure 27d**).

The blacksnout seasnail (*Paraliparis copei*) was present in 41 tows, with a maximum catch of 4 individuals reported in 2022 (**Figure 28a**). This species was primarily associated with the deep waters of the Laurentian Channel, a pattern that was well detected by a Poisson distribution model (**Figure 28b**). Half of the species' biomass was located at depths between 423 and 488 m, at temperatures between 6.0 and 6.2 °C, and at oxygen saturation levels between 43.1 and 47.8 % (**Figure 28c**). Annual LFs ranged from 1 to 15 cm (**Figure 28d**).

The lowfin snailfish (*P. calidus*), another species associated with the Laurentian Channel, was observed in low abundance in 30 tows (**Figure 29a**). The species was generally more prevalent in the Cabot Strait and outside the GSL, but none of the Poisson distribution models converged for catch numbers. Half of the lowfin snailfish biomass was located at depths between 384 and 433 m, at temperatures between 4.9 and 6.3 °C, and at dissolved oxygen saturation levels between 39.7 and 56.6 % (**Figure 29b**). Annual LFs were dominated by length classes of 10–12 cm, but this pattern was informed by relatively few individuals (**Figure 29c**).

The American plaice (*Hippoglossoides platessoides*) is a species that, within the sGSL (NAFO Division 4T), is designated as threatened by COSEWIC (2009) and has been the subject of a recovery plan since 2024 (DFO, 2024e). The species was present in 342 tows, mostly on the south slope of the Laurentian Channel (**Figure 30a**). The model used for catch weights did not include a depth effect, while the model based on numbers indicated a gradual decline, but with wide confidence intervals for catches with depth (**Figure 30b**). The depths and temperatures at which the species was caught were representative of those covered by the survey tows, but the oxygen saturation levels occupied were slightly lower than those available (**Figure 30c**). The LFs had a mode around 20 cm, a value significantly lower than that reported for the species in 1971–1995 (~26 cm; **Figure 30d**; DFO, 2016).

The witch flounder (*Glyptocephalus cynoglossus*) was recorded in 349 survey tows and appeared to be more prevalent outside than inside the GSL (**Figure 31a**). Spatial interpolation models suggested a depth effect on both catch weights and numbers, with a mode between 400 and 500 m (**Figure 31b**). Witch flounder tended to frequent slightly deeper waters than the average of the survey tows; half of the recorded biomass occupied depths of 343 to 490 m, temperatures of 5.8 to 6.3 °C, and oxygen saturation levels of 39.1 to 46.7 % (**Figure 31c**). Most of the measured individuals were in length classes from 30 to 40 cm (**Figure 31d**).

Greenland halibut was observed in 252 tows, with the largest catches observed in the portion of the Laurentian Channel located within the GSL (**Figure 32a**). In 2023, the species was particularly abundant upstream of the Laurentian Channel, an area not covered by the survey in other years. The presence of Greenland halibut in this region could reflect that the survey took place a few weeks earlier than in 2022 and 2024, possibly before the spawning season. Depth appeared to affect catches expressed in weight and number, but the uncertainty associated with this effect increased rapidly beyond 400 m (**Figure 32b**). Half of the biomass of this species was found at depths of 379–492 m, temperatures of 6.0–6.6 °C, and oxygen saturation levels of 27.2–47.5 % (**Figure 32c**). Annual LFs had a dominant mode between 35 and 40 cm (**Figure 32d**).

Atlantic halibut catches were fairly well distributed throughout the study area, with a total of 115 occurrences over the three survey years (**Figure 33a**). The selected Poisson distribution model for catch numbers indicated an uncertain effect of depth for the species (**Figure 33b**). Half of the Atlantic halibut biomass originated from depths between 316 and 423 m, temperatures between 6.0 and 6.8 °C, and oxygen saturation levels between 23.6 and 45.1 % (**Figure 33c**). Annual LFs ranged from 7.5 to 175.5 cm, but no particular pattern was detected across the three survey years (**Figure 33d**).

The monkfish (*Lophius americanus*) was present in 49 tows, with a maximum of 5 individuals per tow (**Figure 34a**). The Poisson distribution model used for this species suggested a depth effect on catch numbers, with peak catches on the north slope of the Laurentian Channel, outside the GSL (**Figure 34b**). Half of the monkfish catches in weight were associated with depths of 306–

390 m, temperatures of 5.9–6.8 °C, and oxygen saturation levels of 43.7–55.2 % (**Figure 34c**). No particular pattern was observed in the species' LFs, a result that may reflect the limited number of length observations available (**Figure 34d**).

3.2 Results of detailed analyzes on common invertebrate taxa

For common invertebrates, it was more frequent for models to converge for only one of the two catch parameters, either catch weight or number. Given the large number of results presented and the major differences in trawl vulnerability among taxa, only the results applicable to certain key taxa are detailed in this section.

The pink glass shrimp (*Pasiphaea multidentata*) was observed in 266 tows which generally were located along the Laurentian Channel (**Figure 70a**). Spatial interpolation models for both weight and number predicted an increase in catches with depth beyond 400 m, but this effect was uncertain and associated with a Pearson $r < 0.65$ (**Figure 70b**). The presence of the pink glass shrimp at greater depths was supported by the cumulative distribution curves, with half of the biomass caught between 412 and 486 m (**Figure 70c**). Annual LFs exhibited a mode between 25 and 27 mm, depending on the year (**Figure 70d**).

Northern shrimp were most abundant in the GSL and near Cape Breton (**Figure 73a**). This pattern was well detected by weight and number models, with depth-smoothing functions showing a mode between 200 and 300 m (**Figure 73b**). Half of the captured biomass was found at depths of 205 to 277 m, temperatures of 5.4 to 6.9 °C, and oxygen saturation levels of 20.7 to 34.6 % (**Figure 73c**). Annual LFs of northern shrimp were characterized by a mode between 15 and 25 mm (**Figure 73d**).

The striped pink shrimp (*Pandalus montagui*) was present in 54 tows, with an apparent concentration of catches toward the central west coast of Newfoundland (**Figure 74a**). The spatial interpolation model for catch weights indicated a rapid decline with depth, while the model based on catch numbers did not converge (**Figure 74b**). In addition to being found at the shallowest depths sampled in the survey, the striped pink shrimp also occupied much colder and more oxygenated waters than the average across tows (**Figure 74c**). The 2024 LF was dominated by length classes around 15 mm, while the 2022 and 2023 observations were deemed insufficient for reliable interpretation (**Figure 74d**).

The Norwegian shrimp *Pontophilus norvegicus* was the most frequently recorded species among the common invertebrates in the survey, with nearly three-quarters of successful tows reporting its presence (N = 310; **Table 2**). The largest recorded catch for a tow was estimated at 92 individuals, but observations generally suggested a wide distribution within the study area (**Figure 77a**). Spatial interpolation of catch weights indicated a likely increase in values with depth, while the analysis of catch numbers did not show convergence (**Figure 77b**). Half of the *Pontophilus norvegicus* biomass was found at depths of 316–451 m, temperatures of 5.6–6.7 °C, and dissolved oxygen saturation levels of 21.5–48.6 % (**Figure 77c**). The LFs appeared to be dominated by individuals of 12 to 14 mm (**Figure 77d**).

The Norway king crab (*Lithodes maja*) was widely distributed in the study area, with a total of 219 occurrences (**Figure 79a**). None of the spatial interpolation models applied to the species converged. However, catches appeared to originate from areas slightly deeper than the average for the tows (**Figure 79b**). Catches made in 2022 were dominated by specimens smaller than 15

mm (shell width), while the 2023 and 2024 observations did not show a well-defined pattern (**Figure 79c**).

The survey appears to have covered areas at the margin of the expected winter distribution of snow crab (*Chionoecetes opilio*) in the GSL (S. Loboda and T. Bermingham, pers. comm. May 14, 2026). The species was captured in a total of 60 tows, with a maximum of 16 individuals per tow in 2024 (**Figure 80a**). The spatial interpolation model used for catch weights showed no effect of depth, while the model used for catch numbers did not converge (**Figure 80b**). Half of the snow crab biomass was found at depths of 155 to 282 m, temperatures of 4.8 to 6.7 °C, and oxygen saturation levels of 29.3 to 42.1 % (**Figure 80c**). Finally, catches were represented by sizes ranging from 2 to 134 mm (**Figure 80d**).

3.3 Results of summary analyzes on rare taxa

As in the previous section, only results specific to certain major rare taxa are described in the following section due to highly variable catchability among taxa and the large number of observations. The names of taxa corresponding to the STRAP codes for each panel can be found in **Table 2**.

Figure 91 shows the distribution of rare taxa belonging to the phylum Chordata. The spiny dogfish (*Squalus acanthias*; code 24), which was designated as a species of special concern in the GSL (COSEWIC, 2010b), was observed only at the GSL entrance and outside the GSL. The Winter skate (*Leucoraja ocellata*; code 100), which is considered endangered (COSEWIC, 2015), was recorded 12 times west of Newfoundland, north of Cape Breton, and near the Laurentian Fan. There were a few occurrences of the Northern wolffish (*Anarhichas denticulatus*; code 699) and the spotted wolffish (*A. minor*; code 701) near Newfoundland and on the Laurentian Fan; these two species were designated as threatened by COSEWIC (2012d, 2012c). Finally, the lumpfish (*Cyclopterus lumpus*; code 849), which was designated as threatened in the study area (COSEWIC, 2017), was recorded 8 times near Anticosti Island and south of Newfoundland.

Figures 92, **93**, **94**, and **95** present the results relating to phyla and classes other than Chordata. A complete description of the observed patterns is not provided here.

4 DISCUSSION

The objective of this technical report was to present the summary results of the winter survey conducted on board the MV Mersey Venture in 2022, 2023, and 2024. This survey was the first source of independent fisheries information on taxa present in the Laurentian Channel, both inside and outside the GSL, since the 1990s—a period markedly different in terms of physical (e.g., temperature and oxygen) and biological (e.g., fish communities) environmental conditions. The results of this report provide a recent overview of the spatial distribution of fish communities encountered in winter in the area, and also cover a portion of the Esquiman and Anticosti Channels. The data obtained could inform stock and ecosystem assessment models, as well as help anticipate the consequences of specific human activities such as the recent reopening of the Unit 1 redfish fishery during this time of year and formulate scientific recommendations to reduce catches of non-target organisms. The main results and their interpretation are briefly discussed in the following paragraphs.

The spatial distribution maps of catch weights and numbers showed several key differences compared to the results of previous winter surveys (McCallum and Walsh, 1997; Chouinard and

Hurlbut, 2011). As expected, redfish was much more abundant and more widely distributed than during the winters of 1978–1994 and 1994–1997; this difference largely reflects the arrival of the 2011, 2012, and 2013 cohorts in stocks from Units 1 and 2 (Senay et al., 2026). Conversely, Atlantic cod catches in the Cabot Strait and south of Burgeo Bank were lower than at the same time of year in 1994–1997 (Campana et al., 1999), despite little change in stock biomass (DFO, 2024a, 2025a). This distributional shift could reflect the decline in ice cover in the GSL since the 1990s (Galbraith et al., 2025), one of the main factors cited to explain cod migration out of the GSL at that time (e.g., Fréchet, 1990; Le Bris et al., 2013). Although comparisons over time were not possible for each taxon, it is interesting to note that the spatial distribution of several of them appears to have changed little over time; this is particularly true for Greenland halibut (Chamberland et al., 2026), American plaice (Swain et al., 1998), and white hake (Rolland et al., 2022). In general, the results presented in the spatial distribution maps support several of the concerns raised regarding the resumption of directed redfish fishing in the deep channels of the study area since the winter of 2024. Indeed, given the wide distribution of both redfish species, it could be difficult to avoid all other commercial stocks and populations with special status during the trawling activities in question.

The sdmTMB analytical framework proved particularly useful for estimating the spatial distribution of common taxa in winter. A depth effect was detected in 51 of the 64 common taxa for which the analysis of catch weights converged and in 47 of the 55 taxa of the analysis of catch numbers. A depth effect applied to only one of the two catch variables (weight or number) in 5 of the 37 common taxa for which both types of analysis were possible. Such a difference could indicate effects of body size on the spatial distribution as a function of depth in winter, a hypothesis considered in the analysis of data from the 1994–1997 winter survey (Chouinard and Hurlbut, 2011). An anticipated result of the analysis was that using a single approach—except for 20 taxa for which only a Poisson distribution model was specified— might lead to lower-quality fits or predictions for some taxa. Another possible drawback is that the survey mainly targeted the deep waters of the area of interest (≥ 150 m); therefore, effects of depth on catches may not have been detected or adequately predicted for taxa whose range of depths occupied within the survey did not allow for the identification of contrasts. Finally, despite the limit imposed on the effect of depth in the model (maximum of 5 basis dimensions), some effects that improved the model fit according to the AICs did not follow a well-defined shape or were associated with very high uncertainty at the extremes of the prediction range (e.g., Greenland halibut, **Figure 32b**). More complex analyzes or analyzes that are more sensitive to the realities of each taxon could be considered to improve the predictive capacity of the analysis, for example, models integrating additional environmental variables and/or considering the temporal variability of the data.

The survey sampling design was particularly well-suited to spatial interpolations without temporal effects. One advantage of the spatial model implemented in sdmTMB compared to classical geostatistical approaches such as linear interpolation (e.g., inverse distance-weighted interpolation; IDW) and kriging was the ability to use reference distributions more appropriate for the nature and variability of the data, as well as to account for both spatial variation and specific environmental effects on catches (Anderson et al., 2024). Indeed, the latter approaches were considered less suitable for accounting for the overdispersion of catch data; these could also have predicted catches in implausible locations, for example, due to unfavorable depths for certain taxa, which would probably have led to less accurate predictions in cross-validation. The choice of depth as the explanatory variable for all taxa was supported by a substantial body of literature on groundfish (Johnson et al., 2019; Ward et al., 2022). An apparent weakness of the sdmTMB

models for certain taxa was the tendency to overestimate catches at the edge or outside the observed depth range. This issue could have been better addressed by restricting the spatial interpolation area to the sampled depths rather than the polygon defining the study area for station selection. However, given that the objective of the analysis was to develop a global overview of the distribution of numerous taxa and their presence in the study area during winter, such an alternative was not explored. Overall, the use of sdmTMB proved to be an excellent choice, offering greater flexibility and more integrated validation and diagnostic capabilities than many other available approaches.

The cumulative distribution curves of Perry and Smith (1994) were designed to identify associations between the distribution of certain taxa and their environment. These curves allow, among other things, the comparison of environmental conditions in which the biomass of different populations is found within the same survey and, thus, inform fisheries management on concrete issues such as the risks of bycatch. A recent analysis of the same dataset (winter survey of 2022–2024) suggested that 69 % of the Greenland halibut biomass was found at depths greater than 400 m, while 67 % of the biomass of the two redfish species was found at shallower depths; this result suggests that the spatial overlap between these two taxa may be limited (Chamberland et al., 2026). A key aspect of the interpretation of results is that several taxa, such as Atlantic cod, exhibit reduced activity levels during the winter (e.g., Dutil et al., 2003). Their exposure to stresses such as warming waters and hypoxia—as suggested in some figures—could therefore have less of an impact on their metabolism in winter than exposure to similar stresses in summer. The strength of the conclusions that can be drawn from the analysis of the cumulative curves depends largely on the sampling method used. Therefore, it is likely that the dissolved oxygen-dependent curves are less reliable for taxa observed outside the GSL after February 28, 2024, the date on which the original CTD was replaced with a device not equipped with an Optode probe (e.g., squat lobster, **Figure 78c**).

Analyzes of LFs and length-weight relationships were possible for most taxa targeted by a commercial fishery. Comparing the LF of a taxon among years should be done with caution given the changes in spatial coverage over the survey period (i.e., combined effects of time and space). Similarly, the length-weight relationship parameters in this report did not account for the expected spatiotemporal variability in explanatory processes such as growth, feeding, and mortality (e.g., see Yin et al., 2022; Odell et al., 2025).

Overall, this report provides a fairly comprehensive overview of the status of stocks and unexploited populations in the deep waters associated with the GSL in 2022, 2023, and 2024. This work is particularly important in the context of climate change and the return of the winter redfish fishery to Unit 1 since the end of 2024. The data collected in this survey can also address specific stock assessment needs and inform more advanced analyzes on certain taxa affected by particular management issues.

ACKNOWLEDGEMENTS

We wish to thank all those who made the winter survey possible, including the crew members of the MV Mersey Venture and the scientific staff on board the vessel (Appendix E). Special thanks are addressed to François Turcotte (DFO Gulf Region) and Jean-François Lussier (DFO Quebec Region) for their involvement as mission leaders in 2022 and 2023-2024, respectively. This report also benefited from the support of Hugues Benoît for the selection of analyzes, Caroline Vanier for data access and management, and Pierre-Marc Scallon-Chouinard for taxonomy-related questions. We thank our editor Aurélie Chagnon-Lafortune and our colleagues Mathieu Boudreau and Pierre-Marc Scallon-Chouinard for reviewing this technical report.

REFERENCES

Anderson, S. C., Ward, E. J., English, P. A., Barnett, L. A. K., and Thorson, J. T. 2024. sdmTMB: an R package for fast, flexible, and user-friendly generalized linear mixed effects models with spatial and spatiotemporal random fields. bioRxiv, 2022.03.24.485545.

Blais, M., Galbraith, P. S., Lizotte, M., Clay, S. A., and Starr, M. 2024. Chemical and Biological Oceanographic Conditions in the Estuary and Gulf of St. Lawrence During 2023. Can. Tech. Rep. Hydrogr. Ocean Sci. 385: v + 84 p.

Bourdages, H., Bourret, A., and Parent, G. J. 2023a. Delineation of stock assessment units for northern shrimp in the Estuary and northern Gulf of St. Lawrence. DFO Can. Sci. Advis. Sec. Res. Doc. 2023/082. vi + 30 p.

Bourdages, H., Chamberland, J.-M., Desgagnés, M., Galbraith, P., Isabel, L., Ouellette-Plante, J., Roux, M.-J., and Senay, C. 2023b. Preliminary results from the ecosystemic survey in August 2022 in the Estuary and northern Gulf of St. Lawrence. DFO Can. Sci. Advis. Sec. Res. Doc. 2023/074. iv + 100 p.

Bourdages, H., Savard, L., Archambault, D., and Valois, S. 2007. Results from the August 2004 and 2005 comparative fishing experiments in the northern Gulf of St. Lawrence between the CCGS Alfred Needler and the CCGS Teleost. Can. Tech. Rep. Fish. Aquat. Sci. 2750: ix + 57 p.

Bowering, W. R. 1982. Population dynamics of Greenland halibut in the Gulf of St. Lawrence. J. Northwest Atl. Fish. Sci., 3: 141-147.

Campana, S. E., Chouinard, G. A., Hanson, J. M., and Fréchet, A. 1999. Mixing and migration of overwintering Atlantic cod (*Gadus morhua*) stocks near the mouth of the Gulf of St. Lawrence. Can. J. Fish. Aquat. Sci., 56: 1873-1881.

Chamberland, J.-M., Bourdages, H., Desgagnés, M., Galbraith, P., Isabel, L., Ouellette-Plante, J., Roux, M.-J., Scallon-Chouinard, P.-M., and Senay, C. 2025. Preliminary Results from the 2024 August Ecosystemic Survey in the Estuary and Northern Gulf of St. Lawrence. DFO Can. Sci. Advis. Sec. Res. Doc. 2025/032. iv + 101 p.

Chamberland, J.-M., Isabel, L., and Benoît, H. 2026. Gulf of St. Lawrence (4RST) Greenland Halibut Stock Status in 2024. DFO Can. Sci. Advis. Sec. Res. Doc. 2026/033. v + 141 p.

Chamberland, J.-M., Plourde, S., and Benoît, H. B. 2022. Biological characteristics, factors affecting catchability, and abundance indices of capelin in the southern and northern Gulf of St. Lawrence multi species bottom trawl surveys. DFO Can. Sci. Advis. Sec. Res. Doc. 2021/077. iv + 41 p.

Chouinard, G. A., and Hurlbut, T. R. 2011. An atlas of the January distribution of selected marine fish species in the Cabot Strait from 1994 to 1997. Can. Tech. Rep. Fish. Aquat. Sci. 2967: viii + 94 p.

COSEWIC. 2009. COSEWIC assessment and status report on the American Plaice *Hippoglossoides platessoides*, Maritime population, Newfoundland and Labrador population and Arctic population, in Canada. Committee on the Status of Endangered Wildlife in Canada. Ottawa. x + 74 pp.

COSEWIC. 2010a. COSEWIC assessment and status report on the Atlantic Cod *Gadus morhua* in Canada. The Committee on the status of endangered wildlife in Canada. Ottawa. xi+76 p.

COSEWIC. 2010b. COSEWIC assessment and status report on the Spiny Dogfish *Squalus acanthias*, Atlantic population, in Canada. Committee on the Status of Endangered Wildlife in Canada. Ottawa. vii + 50 pp.

COSEWIC. 2012a. COSEWIC assessment and status report on the Thorny Skate *Amblyraja radiata* in Canada. Committee on the Status of Endangered Wildlife in Canada. Ottawa. ix + 75 pp.

COSEWIC. 2012b. COSEWIC assessment and status report on the Atlantic Wolffish *Anarhichas lupus* in Canada. Committee on the Status of Endangered Wildlife in Canada. Ottawa. ix + 56 pp.
COSEWIC. 2012c. COSEWIC assessment and status report on the Spotted Wolffish *Anarhichas minor* in Canada. Committee on the Status of Endangered Wildlife in Canada. Ottawa. x + 44 pp.
COSEWIC. 2012d. COSEWIC assessment and status report on the Northern Wolffish *Anarhichas denticulatus* in Canada. Committee on the Status of Endangered Wildlife in Canada. Ottawa. x + 41 pp.
COSEWIC. 2012e. COSEWIC assessment and status report on the Smooth Skate *Malacoraja senta* in Canada. Committee on the Status of Endangered Wildlife in Canada. Ottawa. xix + 77 pp.
COSEWIC. 2013. COSEWIC assessment and status report on the White Hake *Urophycis tenuis* in Canada. Committee on the Status of Endangered Wildlife in Canada. Ottawa. xiii + 45 pp.
COSEWIC. 2015. COSEWIC assessment and status report on the Winter Skate *Leucoraja ocellata*, Gulf of St. Lawrence population, Eastern Scotian Shelf - Newfoundland population and Western Scotian Shelf - Georges Bank population in Canada. Committee on the Status of Endangered Wildlife in Canada. Ottawa. xviii + 46 pp.
COSEWIC. 2017. COSEWIC assessment and status report on the Lumpfish *Cyclopterus lumpus* in Canada. Committee on the Status of Endangered Wildlife in Canada. Ottawa. xi + 78 pp.
DFO. 2016. Stock assessment of American Plaice (*Hippoglossoides platessoides*) of the southern Gulf of St. Lawrence (NAFO Div. 4T) to 2015. DFO Can. Sci. Advis. Sec. Sci. Advis. Rep. 2016/031.
DFO. 2024a. Southern Gulf of St. Lawrence, NAFO Division 4T-4VN (November-April), Atlantic Cod (*Gadus morhua*) Stock Assessment to 2023. DFO Can. Sci. Advis. Sec. Sci. Advis. Rep. 2024/026.
DFO 2024b. Rebuilding Plan for Atlantic Cod (*Gadus morhua*) NAFO Sub-division 3Ps Newfoundland and Labrador Region. Available at: https://www.dfo-mpo.gc.ca/fisheries-peches/ifmp-gmp/cod-morue/2024/cod-atl-morue-2024-eng.html.
DFO 2024c. Rebuilding plan: Atlantic cod (*Gadus morhua*) - NAFO Divisions 4T and 4Vn. Available at: https://www.dfo-mpo.gc.ca/fisheries-peches/ifmp-gmp/cod-morue/2024/cod-4TVn-morue-eng.html.
DFO 2024d. Rebuilding plan: Atlantic Cod, *Gadus morhua* - NAFO Subdivision 3Pn and Divisions 4RS. Available at: https://www.dfo-mpo.gc.ca/fisheries-peches/ifmp-gmp/cod-morue/2024/cod-3Pn4RS-morue-eng.html.
DFO 2024e. Rebuilding plan: American plaice (*Hippoglossoides platessoides*) - NAFO Division 4T. Available at: https://www.dfo-mpo.gc.ca/fisheries-peches/ifmp-gmp/groundfish-poisson-fond/american-plaice-plie-canadienne-eng.html.
DFO. 2025a. Northern Gulf of St. Lawrence (3Pn, 4RS) Atlantic Cod (*Gadus morhua*) Stock Assessment in 2024. DFO Can. Sci. Advis. Sec. Sci. Advis. Rep. 2025/011.
DFO. 2025b. Units 1 and 2 Redfish (*Sebastes mentella* and *Sebastes fasciatus*) Stocks Assessment in 2024. DFO Can. Sci. Advis. Sec. Sci. Advis. Rep. 2025/014.
Dutil, J.-D., Lambert, Y., and Chabot, D. 2003. Winter and spring changes in condition factor and energy reserves of wild cod compared with changes observed during food-deprivation in the laboratory. ICES J. Mar. Sci., 60: 780-786.
Fox, J., and Weisberg, S. 2019. An *R* Companion to Applied Regression, Sage, Thousand Oaks, CA.
Fréchet, A. 1990. Catchability variations of cod in the marginal ice zone. Can. J. Fish. Aquat. Sci., 47: 1678-1683.

Galbraith, P. S. 2006. Winter water masses in the Gulf of St. Lawrence. J. Geophys. Res. Oceans, 111.
Galbraith, P. S., Chassé, J., Shaw, J.-L., Lefaivre, D., and Bourassa, M.-N. 2025. Physical Oceanographic Conditions in the Gulf of St. Lawrence during 2024. Can. Tech. Rep. Hydrogr. Ocean Sci. 397: v + 95 p. https://doi.org/10.60825/eznq-0815.
Garcia, H. E., and Gordon, L. I. 1992. Oxygen solubility in seawater: Better fitting equations. Limnol. Oceanogr., 37: 1307-1312.
GEBCO Bathymetric Compilation Group 2020. The GEBCO_2020 Grid Collection - a continuous terrain model of the global oceans and land. Ed. by N. B. O. D. Centre.
Hilbe, J. M. 2011. Negative Binomial Regression, Cambridge University Press, Cambridge.
Isabel, L., Bourdages, H., and Nozères, C. 2024. Guide d'identification des macroinvertébrés du relevé multidisciplinaire annuel dans l'estuaire et le nord du golfe du Saint-Laurent (NGCC Teleost 2004 - 2022). Rapp. manus. can. sci. halieut. aquat. 3277 : iv + 326 p.
Johnson, K. F., Thorson, J. T., and Punt, A. E. 2019. Investigating the value of including depth during spatiotemporal index standardization. Fish. Res., 216: 126-137.
Le Bris, A., Fréchet, A., Galbraith, P. S., and Wroblewski, J. S. 2013. Evidence for alternative migratory behaviours in the northern Gulf of St Lawrence population of Atlantic cod (*Gadus morhua* L.). ICES J. Mar. Sci., 70: 793-804.
McCallum, B. R., and Walsh, S. J. 1997. Groundfish survey trawls used at the Northwest Atlantic Fisheries Centre, 1971 to present. NAFO Sci. Coun. Studies, 29: 93-104.
Miller, R., and Chabot, D. 2014. Code List of Marine Plants, Invertebrates and Vertebrates Used by the Quebec Region of DFO. Can. Data Rep. Fish. Aquat. Sci. 1254: iv + 115 p.
Morin, B., Power, D., and Gagnon, P. 1994. Distribution of redfish (*Sebastes* spp.) in the Gulf of St. Lawrence and in the Laurentian Channel based on RV surveys and commercial fishery catch rates. DFO Atl. Fish. Res. Doc. 94/91: 52 p.
Nozères, C. 2018. Poissons marins du Saint-Laurent : un photoguide / Marine fishes of the St. Lawrence: a photoguide. Version 2018-04-15. 176 p.
Nozères, C., and Archambault, D. 2014. Portfolio pour l'identification rapide d'invertébrés capturés au chalut dans l'estuaire et le nord du golfe du Saint-Laurent. Rapp. manus. can. sci. halieut. aquat. 3033 : iv + 30 p.
Nozères, C., Archambault, D., Chouinard, P.-M., Gauthier, J., Miller, R., Parent, E., Schwab, P., Savard, L., and Dutil, J.-D. 2010. Identification guide for marine fishes of the estuary and northern Gulf of St. Lawrence and sampling protocols used during trawl surveys between 2004 and 2008. Can. Tech. Rep. Fish. Aquat. Sci. 2866: xi + 243 p.
Odell, A. N., Marshall, K. N., Ward, E. J., Johnson, K. F., and Baskett, M. L. 2025. Spatiotemporal models reveal dynamic growth patterns in U.S. West Coast groundfish. Trans. Am. Fish. Soc., 155: 76-89.
Pebesma, E. 2018. Simple Features for R: Standardized Support for Spatial Vector Data. The R Journal, 10: 439-446.
Pebesma, E. J., and Bivand, R. S. 2005. Classes and methods for spatial data in R. R News, 5: 9-13.
Perry, R. I., and Smith, S. J. 1994. Identifying habitat associations of marine fishes using survey data: an application to the Northwest Atlantic. Can. J. Fish. Aquat. Sci., 51: 589-602.
R Core Team 2024. R: A language and environment for statistical computing. 4.4.1 edn. R Foundation for Statistical Computing, Vienna, Austria.
Ricard, D., Fishman, D., Beazley, L., Boivin, B., Emberley, J., Martin, R., Rolland, N., Sean-Fortin, D., Stoyel, Q., and Vergara, P. 2024. Design goals, technical implementation and practical use of Another data entry system (Andes). Can. Tech. Rep. Fish. Aquat. Sci. 3621: vi + 48 p.
Ripley, B. D. 1981. Spatial Sampling. *In* Spatial Statistics, pp. 19-27.

Rolland, N., McDermid, J. L., Swain, D. P., and Senay, C. 2022. Impact of an expanding Redfish (*Sebastes* spp.) fishery on southern Gulf of St. Lawrence White Hake (*Urophycis tenuis*). DFO Can. Sci. Advis. Sec. Res. Doc. 2022/005. viii + 69 p. .

Senay, C., Bermingham, T., Parent, G. J., Benoît, H. P., Parent, E., and Bourret, A. 2022. Identifying two Redfish species, *Sebastes mentella* and *S. fasciatus,* in fishery and survey catches using anal fin ray count in Units 1 and 2. Can. Tech. Rep. Fish. Aquat. Sci. 3445: viii + 46 p.

Senay, C., Poissant, D., Chavarria, C., Benoît, H. P., Bourdages, H., Blais, M., Bourret, A., and Parent, G. J. 2026. Units 1 and 2 Redfish (*Sebastes mentella* and *Sebastes fasciatus*) Stock Status in 2024. DFO Can. Sci. Advis. Sec. Res. Doc. 2026/037. xvii + 174 p.

Smith, S. J., and Somerton, G. D. 1981. STRAP: a user-oriented computer analysis system for groundfish research trawl survey data. Can. Tech. Rep. Fish. Aquat. Sci., 1030: iv + 66 p.

Sutton, J. T., McDermid, J. L., Landry, L., and Turcotte, F. 2024. Spatiotemporal analysis provides solutions to mitigate bycatch of southern Gulf of St. Lawrence Atlantic Cod in an expanding Redfish fishery. Fish. Res., 276: 107038.

Swain, D. P., Chouinard, G. A., Morin, R., and Drinkwater, K. F. 1998. Seasonal variation in the habitat associations of Atlantic cod (*Gadus morhua*) and American plaice (*Hippoglossoides platessoides*) from the southern Gulf of St. Lawrence. Can. J. Fish. Aquat. Sci., 55: 2548-2561.

Thygesen, U. H., Albertsen, C. M., Berg, C. W., Kristensen, K., and Nielsen, A. 2017. Validation of ecological state space models using the Laplace approximation. Environ. Ecol. Stat., 24: 317-339.

Valentin, A., Sévigny, J.-M., Morin, B., Power, D., and Branton, R. M. 2006. Extensive sampling and concomitant use of meristic characteristics and variation at the MDH-A * locus reveal new information on Redfish species distribution and spatial pattern of introgressive hybridization in the Northwest Atlantic. J. Northwest Atl. Fish. Sci., 36: 65-80.

Walsh, S. J., Hickey, W. H., Porter, J., Delouche, H., and McCallum, B. R. 2009. NAFC Survey Trawl Operations Manual: Version 1.0. Fisheries and Oceans, Northwest Atlantic Fisheries Centre, Newfoundland Region, St. John's. .

Ward, E. J., Barnett, L. A. K., Anderson, S. C., Commander, C. J. C., and Essington, T. E. 2022. Incorporating non-stationary spatial variability into dynamic species distribution models. ICES J. Mar. Sci., 79: 2422-2429.

Yin, Y., Sameoto, J. A., Keith, D. M., and Flemming, J. M. 2022. Improving estimation of length–weight relationships using spatiotemporal models. Can. J. Fish. Aquat. Sci., 79: 1896-1910.

TABLES

Table 1. Number of successful and failed tows per combination of year and NAFO Division or Subdivision in the winter survey in 2022, 2023 and 2024.

Year	NAFO	Number of successful tows	Number of failed tows
2022	3Pn	12	0
	3Ps	8	1
	4R	10	0
	4S	26	6
	4T	11	1
	4Vn	19	2
Total 2022		**86**	**10**
2023	3Pn	9	0
	3Ps	4	0
	4R	18	1
	4S	56	5
	4T	18	2
	4Vn	13	2
Total 2023		**118**	**10**
2024	3Pn	11	1
	3Ps	51	1
	4R	30	0
	4S	43	5
	4T	18	1
	4Vn	34	4
	4Vs	22	1
Total 2024		**209**	**13**
Total		**413**	**33**

Table 2. List of taxonomic codes used in the analysis for the winter survey in 2022, 2023, and 2024, along with their scientific and English correspondences. Taxa present in 25 tows or more are presented first, followed by taxa with fewer occurrences. The information provided for each taxon includes the total number of occurrences (number of tows with presence, maximum = 413), the total standardized catches in weight and number, and the overall means per tow calculated with post-stratification. The column Fig No indicates the figure number in which the results for the taxon are presented, and the columns Res., Val-W, and Val-N provide, respectively, the figure numbers in Appendix B where the residuals and model validations in weight and number of the selected models are shown.

Code	Scientific name	English name	Occ.	Std. total		Std. mean		Fig No	Appendix B		
				Weight	Number	Weight	Number		Res.	Val-W	Val-N
13	*Myxine limosa*	Mud hagfish	232	66.07	1316	0,17	3.32	3	B1	-	-
27	*Centroscyllium fabricii*	Black dogfish	198	1956	5638	4,8	12.88	4	B1	-	-
90	*Amblyraja radiata*	Thorny skate	335	2226	2470	5,83	5.92	5	B1	-	-
91	*Malacoraja senta*	Smooth skate	197	112.9	493.2	0,29	1.25	6	B1	-	B20
150	*Clupea harengus*	Atlantic herring	203	3094	16184	6,66	35.78	7	B1	-	-
151	*Alosa pseudoharengus*	Alewife	45	15.73	103	0,04	0.24	8	B2	-	B20
187	*Mallotus villosus*	Capelin	102	6.16	648.6	0,02	1.94	9	B2	-	-
193	*Argentina silus*	Atlantic argentine	157	940.9	7128	1,86	12.94	10	B2	-	-
271	Myctophiformes	Deepwater fishes	178	10.6	3088	0,03	8.75	11	B2	B19	B20
320	*Arctozenus risso*	White barracudina	300	21.81	1562	0,01	0.92	12	B2	-	-
373	*Synaphobranchus kaupii*	Northern cutthroat eel	30	10.39	308.6	0,03	0.72	13	B3	-	-
426	*Gasterosteus aculeatus*	Threespine stickleback	40	0.18	75.92	< 0.01	0.18	14	B3	-	-
438	*Gadus morhua*	Atlantic cod	314	8117	24440	3,28	13.15	15	B3	-	-
443	*Pollachius virens*	Pollock	26	331.7	146	0,93	0.42	16	B3	-	-
444	*Phycis chesteri*	Longfin hake	213	390.1	3479	0,22	3.65	17	B3	-	-
447	*Urophycis tenuis*	White hake	270	1340	3181	2,85	5.69	18	B4	-	-
449	*Merluccius bilinearis*	Silver hake	326	6086	40064	4,13	30.06	19	B4	-	-
461	*Enchelyopus cimbrius*	Fourbeard rockling	218	16.74	542.1	0,04	1.41	20	B4	B19	B20
478	*Nezumia bairdii*	Common grenadier	336	336.8	8217	0,19	5.06	21	B4	-	-
700	*Anarhichas lupus*	Atlantic wolffish	49	34.58	157.3	0,07	0.31	22	B4	-	-
745	*Melanostigma atlanticum*	Atlantic soft pout	115	2.18	447.5	< 0.01	1.36	23	B5	B19	-
794	*Sebastes mentella*	Deepwater redfish	408	27134	123283	19,95	88.33	24	B5	-	-
796	*Sebastes fasciatus*	Acadian redfish	408	11323	55056	7,76	32.59	25	B5	-	-
797	*Helicolenus dactylopterus*	Blackbelly rosefish	25	6.77	84.77	0,01	0.18	26	B5	-	-
811	*Artediellus atlanticus*	Atlantic hookear sculpin	36	0.31	92.04	< 0.01	0.25	27	B5	-	-
856	*Paraliparis copei*	Blacksnout seasnail, Blacksnout snailfish	41	0.6	55.84	< 0.01	0.12	28	B6	-	-
874	*Paraliparis calidus*	Lowfin snailfish	30	0.36	39.69	< 0.01	0.12	29	B6	-	-
889	*Hippoglossoides platessoides*	American plaice	342	1288	12856	0,56	7.81	30	B6	-	B20
890	*Glyptocephalus cynoglossus*	Witch flounder	349	2608	12814	1,2	7.57	31	B6	-	-
892	*Reinhardtius hippoglossoides*	Greenland halibut	252	1514	3181	13,74	3.32	32	B6	B19	-
893	*Hippoglossus hippoglossus*	Atlantic halibut	115	2296	236.6	5,37	0.53	33	B7	-	-
966	*Lophius americanus*	Monkfish	49	357.6	64.26	0,88	0.16	34	B7	-	-

Table 2 (continued).

Code	Scientific name	English name	Occ.	Std. total		Std. mean		Fig No	Appendix B		
				Weight	Number	Weight	Number		Res.	Val-W	Val-N
1101	Porifera	Sponges	205	87.34	1188	0,03	-	35	B7	B19	-
1107	*Polymastia hemisphaerica*	Sponge	47	1.43	254.4	< 0.01	-	36	B7	-	-
1353	*Ptychogena lactea*	Jellyfish	34	0.4	91.11	< 0.01	0.27	37	B7	-	-
1381	*Stephalia corona*	Jellyfish	78	0.85	313.8	< 0.01	0.84	38	B8	-	-
2040	Scyphozoa	Scyphozoans	38	0.56	53.86	< 0.01	0.14	39	B8	-	-
2080	*Cyanea capillata*	Lion's mane	30	36.75	34.55	0,09	0.08	40	B8	-	-
2096	*Periphylla periphylla*	Crown jellyfish	219	477.1	606.2	0,31	0.4	41	B8	-	-
2097	*Atolla wyvillei*	Jellyfish	35	5.39	89.62	0,02	0.33	42	B8	B19	-
2158	*Bolocera tuediae*	Sea anemone	140	25.23	503.3	0,01	-	43	B9	-	-
2159	*Stephanauge nexilis*	Sea anemone	25	1.04	145.6	< 0.01	-	44	B9	-	-
2162	*Actinostola callosa*	Sea anemone	83	65.98	470.1	0,2	1.48	45	B9	B19	-
2165	Actiniaria	Sea anemones	55	2.29	183.3	< 0.01	0.42	46	B9	-	-
2182	*Actinauge cristata*	Sea anemone	81	76.93	6972	0,21	16.31	47	B9	-	-
2207	*Liponema multicorne*	Sea anemone	26	6.33	64.53	0,02	0.17	48	B10	B19	B20
2183	*Duva florida*	Sea cauliflower	41	1.02	37.71	< 0.01	0.09	49	B10	-	-
2203	*Pennatula aculeata*	Sea pen	201	7.65	2576	0,02	8.42	50	B10	-	-
2210	*Ptilella grandis*	Sea pen	37	38.15	965	0,14	3.52	51	B10	-	-
2217	*Halipteris finmarchica*	Sea pen	33	39.6	577.6	0,11	2.94	52	B10	-	-
2218	*Anthoptilum grandiflorum*	Sea pen	127	27.21	3219	0,06	6.45	53	B11	B19	B20
2224	*Flabellum (Ulocyathus) alabastrum*	Cup coral	73	6.37	697.9	0,02	2.03	54	B11	-	B20
2255	*Pleurobrachia pileus*	Sea gooseberry	145	8.19	2523	0,02	7.72	55	B11	-	-
3418	*Arrhoges occidentalis*	American pelicanfoot	73	10.39	1025	0,04	3.71	56	B11	B19	B20
3715	*Scaphander punctostriatus*	Giant canoe bubble	67	0.7	234.6	< 0.01	0.83	57	B11	-	-
4025	*Megayoldia thraciaeformis*	Broad yoldia	83	13.72	1288	0,05	4.45	58	B12	-	B20
4526	*Cuspidaria glacialis*	Glacial dipperclam	29	0.07	50.99	< 0.01	0.12	59	B12	-	-
4557	*Rossia* spp.	Bobtails	35	0.46	36.5	< 0.01	0.08	60	B12	-	-
4587	*Stoloteuthis leucoptera*	Butterfly squid	41	0.32	69.4	< 0.01	0.18	61	B12	-	-
4904	*Bathypolypus bairdii*	North Atlantic octopus	98	5.76	172.4	0,01	0.37	62	B12	-	-
4950	Polychaeta	Polychaetes	107	4.82	1110	0,01	1.92	63	B13	-	-
5003	*Laetmonice filicornis*	Seaworm	59	0.1	79.87	< 0.01	0.21	64	B13	-	-
6771	*Aega psora*	Isopod	33	0.14	48.89	< 0.01	0.15	65	B13	-	-
6791	*Syscenus infelix*	Isopod	224	1.3	764.7	< 0.01	1.89	66	B13	-	B20
7383	*Epimeria loricata*	Gammarid	35	0.03	93.68	< 0.01	0.16	67	B13	-	-
8033	*Eusergestes arcticus*	Shrimp	163	7.28	6106	0,03	27.16	68	B14	-	-
8056	*Pasiphaea tarda*	Crimson pasiphaeid	26	1.04	104.5	< 0.01	0.33	69	B14	B19	-
8057	*Pasiphaea multidentata*	Pink glass shrimp	266	117.9	36850	0,23	71.52	70	B14	B19	-
8087	*Spirontocaris liljeborgii*	Friendly blade shrimp	69	0.26	199.8	< 0.01	0.41	71	B14	B19	-
8093	*Lebbeus polaris*	Polar lebbeid	103	0.52	411.8	< 0.01	1.02	72	B14	B19	B20

Table 2 (continued).

Code	Scientific name	English name	Occ.	Std. total		Std. mean		Fig No	Appendix B		
				Weight	Number	Weight	Number		Res.	Val-W	Val-N
8111	*Pandalus borealis*	Northern shrimp	309	396.8	61025	0,96	144.4	73	B15	-	-
8112	*Pandalus montagui*	Striped pink shrimp	54	13.41	5609	0,07	28.33	74	B15	-	-
8113	*Atlantopandalus propinqvus*	Shrimp	184	6.31	1689	0,01	3.71	75	B15	-	-
8129	*Sabinea sarsii*	Sars shrimp	25	0.17	105.3	< 0.01	0.21	76	B15	B19	-
8135	*Pontophilus norvegicus*	Norwegian shrimp	310	6.04	3257	0,02	8.01	77	B15	-	-
8164	*Munidopsis curvirostra*	Squat lobster	37	0.11	87.06	< 0.01	0.29	78	B16	-	-
8196	*Lithodes maja*	Norway king crab	217	221.7	594.7	0,51	1.37	79	B16	-	-
8213	*Chionoecetes opilio*	Snow crab	60	30.77	169.3	0,05	0.43	80	B16	-	-
8378	*Brisaster fragilis*	Heart urchin	213	162.9	26114	0,46	77.22	81	B16	-	B20
8407	*Ctenodiscus crispatus*	Mud star	182	173.7	44623	0,44	105.8	82	B16	-	-
8429	*Ceramaster granularis*	Sea star	72	1.97	175.5	< 0.01	0.35	83	B17	B19	-
8431	*Hippasteria phrygiana*	Sea star	66	19.1	89.04	0,06	0.24	84	B17	-	B20
8433	*Pseudarchaster parelii*	Sea star	57	1.01	80.78	< 0.01	0.2	85	B17	-	-
8483	*Henricia* spp.	Sea stars	79	1.02	147.3	< 0.01	0.32	86	B17	-	-
8520	*Psilaster andromeda*	Sea star	171	84.98	15704	0,23	35.09	87	B17	-	B20
8553	*Ophiura sarsii*	Brittle star	58	1.76	989.2	< 0.01	3.52	88	B18	B19	-
8583	*Ophiopholis aculeata*	Daisy brittle star	42	0.26	231.9	< 0.01	0.78	89	B18	-	B20
8742	*Ascidia* spp.	Sea squirts	118	7.92	2197	0,02	5.1	90	B18	-	B20
24	*Squalus acanthias*	Spiny dogfish	20	117.3	62.35	0,43	0.23	91	-	-	-
94	*Rajella fyllae*	Round skate	7	3.74	10.69	< 0.01	0.02	91	-	-	-
100	*Leucoraja ocellata*	Winter skate	12	90.27	25.52	0,34	0.09	91	-	-	-
102	*Bathyraja spinicauda*	Spinytail skate	7	47.23	6.95	0,08	0.01	91	-	-	-
8680	Ascidiacea	Ascidians, Sessile tunicates	15	0.12	27.51	< 0.01	0.06	91	-	-	-
8778	*Eudistoma vitreum*	Tunicate	17	0.29	73.01	< 0.01	0.26	91	-	-	-
8783	*Polycarpa fibrosa*	Tunicate	15	0.08	65.93	< 0.01	0.18	91	-	-	-
8792	*Boltenia ovifera*	Sea potato	8	1.16	21.09	< 0.01	0.05	91	-	-	-
8793	*Boltenia echinata*	Cactus sea squirt	2	0.03	15	< 0.01	0.04	91	-	-	-
152	*Alosa sapidissima*	American shad	3	0.54	8.24	< 0.01	0.02	91	-	-	-
208	*Cyclothone microdon*	Veiled anglemouth	2	< 0.01	4.58	< 0.01	< 0.01	91	-	-	-
219	*Serrivomer* spp.	Serrivomer unidentified	1	0.02	1.01	< 0.01	< 0.01	91	-	-	-
220	Sternoptychidae	Hatchetfishes	2	< 0.01	1.91	< 0.01	< 0.01	91	-	-	-
222	*Polyipnus clarus*	Slope hatchetfish	2	< 0.01	1.9	< 0.01	< 0.01	91	-	-	-
225	*Argyropelecus gigas*	Greater silver hatchetfish	1	< 0.01	0.91	< 0.01	< 0.01	91	-	-	-
227	*Chauliodus sloani*	Sloane's viperfish	23	0.56	28.19	< 0.01	0.08	91	-	-	-
230	*Stomias boa boa*	Boa dragonfish	7	0.15	9.52	< 0.01	0.03	91	-	-	-
244	*Polymetme thaeocoryla*	Lightfishes	1	< 0.01	0.99	< 0.01	< 0.01	91	-	-	-
359	*Simenchelys parasitica*	Subnose eel	1	1.06	0	< 0.01	0	91	-	-	-
368	*Nemichthys scolopaceus*	Atlantic snipe eel	19	0.28	22.63	< 0.01	0.08	91	-	-	-

Table 2 (continued).

Code	Scientific name	English name	Occ.	Std. total		Std. mean		Fig No	Appendix B		
				Weight	Number	Weight	Number		Res.	Val-W	Val-N
369	*Serrivomer beanii*	Stout sawpalate	14	0.65	18.16	< 0.01	0.06	91	-	-	-
372	Synaphobranchidae	Cutthroat eels	1	0.07	0.94	< 0.01	< 0.01	91	-	-	-
375	*Polyipnus* spp.	Polyipnus unidentified	2	< 0.01	1	< 0.01	< 0.01	91	-	-	-
418	*Syngnathus fuscus*	Northern pipefish	1	< 0.01	1	< 0.01	< 0.01	91	-	-	-
436	Gadidae	Codfishes	4	0.08	4.8	< 0.01	0.01	91	-	-	-
440	*Micromesistius poutassou*	Blue whiting	1	0.17	0.97	< 0.01	< 0.01	91	-	-	-
441	*Melanogrammus aeglefinus*	Haddock	22	940.3	939	2,36	2	91	-	-	-
451	*Boreogadus saida*	Arctic cod	1	< 0.01	0.89	< 0.01	< 0.01	91	-	-	-
454	*Gaidropsarus ensis*	Threebeard rockling	2	0.04	1.87	< 0.01	< 0.01	91	-	-	-
518	*Hoplosthetus atlanticus*	Orange roughy	1	0.02	1.01	< 0.01	< 0.01	91	-	-	-
527	*Hoplostethus mediterraneus mediterraneus*	Rosy soldierfish	2	0.05	1.9	< 0.01	< 0.01	91	-	-	-
572	*Scomber scombrus*	Atlantic mackerel	5	1.07	4.82	< 0.01	< 0.01	91	-	-	-
618	*Epigonus pandionis*	Big eye	5	0.31	13.57	< 0.01	0.05	91	-	-	-
699	*Anarhichas denticulatus*	Northern wolffish	2	1.85	1.88	< 0.01	< 0.01	91	-	-	-
701	*Anarhichas minor*	Spotted wolffish	3	5.75	2.9	0,01	< 0.01	91	-	-	-
711	*Eumesogrammus praecisus*	Fourline snakeblenny	7	1.39	54.96	< 0.01	0.3	91	-	-	-
716	*Lumpenus lampretaeformis*	Snakeblenny	7	0.22	11.63	< 0.01	0.05	91	-	-	-
717	*Leptoclinus maculatus*	Daubed shanny	11	0.39	82.9	< 0.01	0.39	91	-	-	-
721	*Cryptacanthodes maculatus*	Wrymouth	16	3.66	24.5	0,01	0.07	91	-	-	-
725	Zoarcidae	Eelpouts, Pouts, Wolf eels	1	0.04	0.97	< 0.01	< 0.01	91	-	-	-
726	*Lycodes* spp.	Eelpouts	1	< 0.01	0.96	< 0.01	< 0.01	91	-	-	-
727	*Lycodes esmarkii*	Esmark's eelpout	20	5.05	21.99	0,01	0.04	91	-	-	-
728	*Lycodes lavalaei*	Newfoundland eelpout	5	2.03	40.78	0,01	0.22	91	-	-	-
730	*Lycodes vahlii*	Vahl's eelpout	15	1.24	29.95	< 0.01	0.07	91	-	-	-
734	*Lycodes terraenovae*	Atlantic eelpout	2	0.22	1.91	< 0.01	< 0.01	91	-	-	-
746	*Gymnelus viridis*	Fish doctor	1	< 0.01	0.99	< 0.01	< 0.01	91	-	-	-
750	*Lycenchelys paxillus*	Common wolf eel	6	0.12	6.5	< 0.01	0.02	91	-	-	-
752	*Lycenchelys verrillii*	Wolf eelpout	4	0.01	3.7	< 0.01	0.01	91	-	-	-
783	*Peprilus triacanthus*	Butterfish	2	0.19	1.96	< 0.01	< 0.01	91	-	-	-
809	*Hemitripterus americanus*	Sea sculpin	23	24.64	37.01	0,06	0.09	91	-	-	-
810	*Artediellus* spp.	Hookear sculpins	10	0.03	15.25	< 0.01	0.03	91	-	-	-
812	*Artediellus uncinatus*	Arctic hookear sculpin	6	1.88	13.74	< 0.01	0.06	91	-	-	-
814	*Triglops murrayi*	Moustache sculpin	22	0.67	79.49	< 0.01	0.32	91	-	-	-
819	*Myoxocephalus scorpius*	Shorthorn sculpin	13	10.42	26.24	0,05	0.11	91	-	-	-
820	*Myoxocephalus octodecemspinosus*	Longhorn sculpin, Gray sculpin	14	9.65	35.79	0,03	0.09	91	-	-	-
829	*Cottunculus microps*	Polar sculpin	1	0.01	0.95	< 0.01	< 0.01	91	-	-	-
832	*Icelus spatula*	Spatulate sculpin	1	< 0.01	0.95	< 0.01	< 0.01	91	-	-	-
836	*Leptagonus decagonus*	Atlantic poacher	1	0.03	1	< 0.01	< 0.01	91	-	-	-

Table 2 (continued).

Code	Scientific name	English name	Occ.	Std. total		Std. mean		Fig No	Appendix B		
				Weight	Number	Weight	Number		Res.	Val-W	Val-N
837	*Aspidophoroides olrikii*	Arctic alligatorfish	1	< 0.01	0.97	< 0.01	< 0.01	91	-	-	-
838	*Aspidophoroides monopterygius*	Alligatorfish	9	0.07	17.11	< 0.01	0.04	91	-	-	-
847	*Eumicrotremus terraenovae*	Newfoundland spiny lumpsucker	14	1.05	173.8	< 0.01	0.73	91	-	-	-
849	*Cyclopterus lumpus*	Lumpfish	8	7.45	9.42	< 0.01	0.02	91	-	-	-
865	*Careproctus reinhardti*	Sea tadpole	3	0.09	5.69	< 0.01	0.01	91	-	-	-
868	*Liparis bathyarcticus*	Nebulous snailfish	1	< 0.01	2	< 0.01	< 0.01	91	-	-	-
882	Pleuronectiformes	Flatfish	3	< 0.01	5	< 0.01	< 0.01	91	-	-	-
891	*Limanda ferruginea*	Yellowtail flounder	18	140.9	428.1	0,34	0.91	91	-	-	-
895	*Pseudopleuronectes americanus*	Winter flounder	2	2.09	4.91	0,01	0.03	91	-	-	-
907	*Scophthalmus aquosus*	Spotted flounder	15	5.48	37.6	< 0.01	0.06	91	-	-	-
982	*Cryptopsaras couesii*	Triplewart seadevil, Warted seadevil	6	0.87	5.75	< 0.01	0.02	91	-	-	-
1112	*Stylocordyla borealis*	Sponge	3	< 0.01	2.85	< 0.01	0.01	92	-	-	-
1116	*Phakellia* spp.	Sponges	2	3.05	0	< 0.01	0	92	-	-	-
1120	*Asconema foliatum*	Sponge	18	11.47	0.96	0,02	< 0.01	92	-	-	-
1341	Hydrozoa	Hydrozoans	2	< 0.01	0	< 0.01	0	92	-	-	-
1357	*Thuiaria thuja*	Bottlebrush hydroid	1	< 0.01	0.96	< 0.01	< 0.01	92	-	-	-
2050	*Lucernaria quadricornis*	Horned stalked jellyfish	1	0.02	0.99	< 0.01	< 0.01	92	-	-	-
2150	*Hormathia digitata*	Sea anemone	9	0.17	38.85	< 0.01	0.14	92	-	-	-
2152	*Urticina crassicornis*	Sea anemone	5	0.61	6.69	< 0.01	0.01	92	-	-	-
2153	*Ptychodactis patula*	Anemone	1	0.02	0.96	< 0.01	< 0.01	92	-	-	-
2156	*Epizoanthus erdmanni*	Zoanthid	17	0.02	82.81	< 0.01	0.28	92	-	-	-
2157	*Epizoanthus* spp.	Sea anemone	3	< 0.01	13.5	< 0.01	0.03	92	-	-	-
2167	*Hormathia nodosa*	Rugose anemone	5	0.55	18.1	< 0.01	0.04	92	-	-	-
2171	*Metridium senile*	Clonal plumose anemone	1	0.03	15	< 0.01	0.03	92	-	-	-
2173	*Stomphia coccinea*	Sea anemone	2	0.07	1.87	< 0.01	< 0.01	92	-	-	-
2184	*Gersemia rubiformis*	Sea strawberry	5	< 0.01	8.93	< 0.01	0.03	92	-	-	-
2191	*Drifa glomerata*	Soft coral	5	0.05	7.61	< 0.01	0.04	92	-	-	-
2201	Pennatulacea	Sea pens	8	0.26	120.5	< 0.01	0.21	92	-	-	-
2212	*Gersemia fruticosa*	Hedge carnation coral	9	0.98	7.69	< 0.01	0.03	92	-	-	-
2213	*Kophobelemnon stelliferum*	Sea pen	21	2.76	126.4	< 0.01	0.46	92	-	-	-
2219	Nephtheidae	Soft corals	2	0.01	2.89	< 0.01	< 0.01	92	-	-	-
2222	*Heteropolypus* spp.	Soft coral	3	< 0.01	1.9	< 0.01	< 0.01	92	-	-	-
2250	Ctenophora	Comb-jellies	9	0.26	98.62	< 0.01	0.16	92	-	-	-
2295	Fecampiidae	Flatworms	13	< 0.01	17.81	< 0.01	0.04	92	-	-	-
2670	Bryozoa	Bryozoans	5	0.06	3.85	< 0.01	0.01	92	-	-	-
2675	*Alcyonidium* spp.	Bryozoan	2	0.02	0	< 0.01	0	92	-	-	-
2679	*Securiflustra securifrons*	Marine bryozoans	5	0.06	0.96	< 0.01	< 0.01	92	-	-	-
4955	*Phyllodoce groenlandica*	Paddle worm	1	< 0.01	1	< 0.01	< 0.01	92	-	-	-

Table 2 (continued).

Code	Scientific name	English name	Occ.	Std. total		Std. mean		Fig No	Appendix B		
				Weight	Number	Weight	Number		Res.	Val-W	Val-N
5002	*Aphrodita hastata*	Sea mouse	16	0.27	18.12	< 0.01	0.05	92	-	-	-
5007	Polynoidae	Fifteen-scaled worm	15	0.03	21.96	< 0.01	0.07	92	-	-	-
5264	*Polyphysia crassa*	Sea worm	2	0.01	2.84	< 0.01	< 0.01	92	-	-	-
5755	*Brada inhabilis*	Flabelligerid worm	3	< 0.01	4.86	< 0.01	0.02	92	-	-	-
5930	Echiura	Echiurids	1	0.51	13.64	< 0.01	0.03	92	-	-	-
5902	*Golfingia (golfingia) margaritacea*	Sipunculid	1	< 0.01	0.89	< 0.01	< 0.01	92	-	-	-
5907	*Phascolion (Phascolion) strombus strombus*	Hermit sipunculid	3	< 0.01	2.91	< 0.01	< 0.01	92	-	-	-
2585	Nematoda	Nematode	3	< 0.01	2.77	< 0.01	< 0.01	93	-	-	-
3101	*Terebratulina septentrionalis*	Northern lamp shell	17	0.05	29.37	< 0.01	0.1	93	-	-	-
3141	*Hanleya hanleyi*	Chiton	1	< 0.01	0.95	< 0.01	< 0.01	93	-	-	-
3216	*Margarites groenlandicus*	Greenland margarite	1	< 0.01	0.97	< 0.01	< 0.01	93	-	-	-
3219	*Margarites costalis*	Boreal rosy margarite	2	< 0.01	1.91	< 0.01	< 0.01	93	-	-	-
3422	*Cryptonatica affinis*	Arctic moonsnail	4	0.01	4.62	< 0.01	0.01	93	-	-	-
3437	*Euspira pallida*	Pale moonsnail	4	< 0.01	5.87	< 0.01	0.02	93	-	-	-
3491	*Scabrotrophon fabricii*	Murex	1	< 0.01	0.96	< 0.01	< 0.01	93	-	-	-
3516	*Buccinum* spp.	Whelk	17	0.49	25.73	< 0.01	0.09	93	-	-	-
3517	*Buccinum undatum*	Waved whelk	2	0.02	1.93	< 0.01	< 0.01	93	-	-	-
3523	*Buccinum scalariforme*	Ladder whelk	1	< 0.01	0.97	< 0.01	< 0.01	93	-	-	-
3575	*Colus* spp.	Whelks	1	< 0.01	1	< 0.01	< 0.01	93	-	-	-
3576	*Colus stimpsoni*	Whelk	2	0.04	2.05	< 0.01	< 0.01	93	-	-	-
3577	*Colus pubescens*	Hairy whelk	7	0.08	7.44	< 0.01	0.02	93	-	-	-
3908	*Colga villosa*	Nudibranch	6	0.01	8.9	< 0.01	0.04	93	-	-	-
3964	*Heterodoris robusta*	Nudibranch	4	0.03	3.82	< 0.01	0.02	93	-	-	-
3965	*Doridoxa walteri*	Nudibranch	3	< 0.01	2.82	< 0.01	0.01	93	-	-	-
3978	*Antalis occidentalis*	Occidental tuskshell	5	< 0.01	26.92	< 0.01	0.06	93	-	-	-
3995	Bivalvia	Bivalves	3	0.9	40.8	< 0.01	0.07	93	-	-	-
4019	*Nuculana* spp.	Nutclams	1	< 0.01	0.97	< 0.01	< 0.01	93	-	-	-
4121	*Mytilus* spp.	Mussels	1	< 0.01	1	< 0.01	< 0.01	93	-	-	-
4167	*Chlamys islandica*	Iceland scallop	6	0.17	40.42	< 0.01	0.19	93	-	-	-
4218	Anomiidae	Scallop	1	< 0.01	0.96	< 0.01	< 0.01	93	-	-	-
4227	*Astarte* spp.	Astartes	20	0.05	28.73	< 0.01	0.07	93	-	-	-
4231	*Astarte borealis*	Boreal astarte	1	< 0.01	0.94	< 0.01	< 0.01	93	-	-	-
4301	*Thyasira* spp.	Cleftclam	1	< 0.01	0.95	< 0.01	< 0.01	93	-	-	-
4352	*Serripes groenlandicus*	Greenland smoothcockle	1	< 0.01	0.95	< 0.01	< 0.01	93	-	-	-
4451	*Xylophaga atlantica*	Atlantic woodeater	4	0.04	0.96	< 0.01	< 0.01	93	-	-	-
4498	*Teredo navalis*	Naval shipworm	1	0.05	0.88	< 0.01	< 0.01	93	-	-	-
4545	Cephalopoda	Cephalopods	7	0.62	6.67	< 0.01	0.02	93	-	-	-
4753	*Illex illecebrosus*	Northern shortfin squid	11	1.26	10.48	< 0.01	0.03	93	-	-	-

Table 2 (continued).

Code	Scientific name	English name	Occ.	Std. total		Std. mean		Fig No	Appendix B		
				Weight	Number	Weight	Number		Res.	Val-W	Val-N
4853	*Stauroteuthis syrtensis*	Octopus	2	1.71	4.05	< 0.01	0.02	93	-	-	-
5951	Pycnogonida	Sea spiders	1	< 0.01	0.97	< 0.01	< 0.01	94	-	-	-
5961	*Nymphon* spp.	Sea spiders	7	< 0.01	11.25	< 0.01	0.03	94	-	-	-
6593	*Chirona hameri*	Turban barnacle	3	1.17	0.97	< 0.01	< 0.01	94	-	-	-
6594	*Arcoscalpellum michelottianum*	Barnacle	4	0.09	9.56	< 0.01	0.03	94	-	-	-
6930	Amphipoda	Amphipods	5	< 0.01	17.54	< 0.01	0.04	94	-	-	-
6972	*Themisto libellula*	Hyperiid	8	< 0.01	10.47	< 0.01	0.02	94	-	-	-
7195	*Eusirus cuspidatus*	Gammarid	1	< 0.01	0.97	< 0.01	< 0.01	94	-	-	-
7211	*Rhachotropis aculeata*	Gammarid	6	0.03	56.62	< 0.01	0.18	94	-	-	-
7389	*Anonyx* spp.	Gammarids	2	< 0.01	3.04	< 0.01	0.02	94	-	-	-
7586	*Paramphithoe hystrix*	Gammarid	1	< 0.01	1.01	< 0.01	< 0.01	94	-	-	-
7750	*Stegocephalus inflatus*	Gammarid	5	< 0.01	5.61	< 0.01	0.02	94	-	-	-
7927	*Gnathophausia* spp.	Mysid	1	< 0.01	0.96	< 0.01	< 0.01	94	-	-	-
7999	*Bentheuphausia amblyops*	Shrimp	4	< 0.01	3.88	< 0.01	0.02	94	-	-	-
8024	*Aristaeopsis edwardsiana*	Scarlet shrimp	4	0.2	7.74	< 0.01	0.02	94	-	-	-
8026	*Gennadas* spp.	Shrimp	3	0.01	0	< 0.01	0	94	-	-	-
8028	*Hymenopenaeus debilis*	Shrimp	7	0.02	14.81	< 0.01	0.05	94	-	-	-
8035	*Sergia robusta*	Scarlet sergestid	11	0.04	27.41	< 0.01	0.1	94	-	-	-
8036	Benthesicymidae	Shrimp	7	0.01	1.87	< 0.01	< 0.01	94	-	-	-
8039	*Acanthephyra* spp.	Shrimp	1	< 0.01	0	< 0.01	0	94	-	-	-
8040	*Acanthephyra pelagica*	Shrimp	14	0.17	29	< 0.01	0.1	94	-	-	-
8052	*Nematocarcinus rotundus*	Rotund shrimp	2	0.02	2.96	< 0.01	0.01	94	-	-	-
8074	*Eualus* spp.	Eualid	1	< 0.01	1.01	< 0.01	< 0.01	94	-	-	-
8075	*Eualus fabricii*	Arctic eualid	2	< 0.01	1.99	< 0.01	0.01	94	-	-	-
8077	*Eualus macilentus*	Greenland shrimp	2	< 0.01	9.04	< 0.01	0.06	94	-	-	-
8079	*Eualus gaimardii*	Circumpolar eualid	2	< 0.01	1.99	< 0.01	< 0.01	94	-	-	-
8084	*Spirontocaris* spp.	Blade shrimp	11	0.03	21.85	< 0.01	0.05	94	-	-	-
8085	*Spirontocaris spinus*	Parrot shrimp	5	0.01	6.91	< 0.01	0.04	94	-	-	-
8095	*Lebbeus microceros*	Shrimp	1	< 0.01	2.03	< 0.01	0.01	94	-	-	-
8108	*Dichelopandalus leptocerus*	Bristled longbeak shrimp	12	0.16	33	< 0.01	0.07	94	-	-	-
8114	*Plesionika martia*	Golden shrimp	2	< 0.01	1.85	< 0.01	< 0.01	94	-	-	-
8128	*Sabinea septemcarinata*	Sevenline shrimp	11	0.12	79.68	< 0.01	0.41	94	-	-	-
8138	*Argis dentata*	Arctic argid	17	0.59	299.5	< 0.01	1.53	94	-	-	-
8145	*Stereomastis sculpta*	Flatback blind lobster	2	0.78	19.48	< 0.01	0.05	94	-	-	-
8154	*Homarus americanus*	American lobster	13	26.68	32.93	0,04	0.05	94	-	-	-
8173	*Calocaris templemani*	Lobster shrimp	6	< 0.01	7.2	< 0.01	0.02	94	-	-	-
8178	*Pagurus* spp.	Hermit crab	13	3.75	19.19	< 0.01	0.06	94	-	-	-
8217	*Hyas araneus*	Atlantic lyre crab	5	0.15	5.15	< 0.01	0.02	94	-	-	-

Table 2 (continued).

Code	Scientific name	English name	Occ.	Std. total		Std. mean		Fig No	Appendix B		
				Weight	Number	Weight	Number		Res.	Val-W	Val-N
8219	*Hyas alutaceus*	Arctic lyre crab	13	0.23	19.21	< 0.01	0.08	94	-	-	-
8263	*Heliometra glacialis*	Feather star	4	0.27	98.41	< 0.01	0.22	95	-	-	-
8290	Holothuroidea	Sea cucumbers	7	0.03	7.47	< 0.01	0.02	95	-	-	-
8294	*Psolus phantapus*	Sea cucumber	3	0.02	2.76	< 0.01	< 0.01	95	-	-	-
8312	*Cucumaria frondosa*	Orange-footed sea cucumber	3	0.73	14.5	< 0.01	0.04	95	-	-	-
8316	*Ekmania barthii*	Sea cucumber	1	< 0.01	0.95	< 0.01	< 0.01	95	-	-	-
8322	*Molpadia oolitica*	Sea cucumber	4	4.53	15.28	0,02	0.03	95	-	-	-
8363	*Strongylocentrotus* spp.	Sea urchins	22	1.06	508.4	< 0.01	1.87	95	-	-	-
8373	*Echinarachnius parma*	Common sand dollar	2	0.01	1.94	< 0.01	< 0.01	95	-	-	-
8390	Asteroidea	Sea stars	1	< 0.01	0.96	< 0.01	< 0.01	95	-	-	-
8396	*Asterias rubens*	Purple seastar	1	< 0.01	1.23	< 0.01	< 0.01	95	-	-	-
8408	*Diplopteraster multipes*	Sea star	3	0.13	2.97	< 0.01	< 0.01	95	-	-	-
8410	*Pteraster militaris*	Sea star	5	0.25	13.23	< 0.01	0.03	95	-	-	-
8411	*Pteraster pulvillus*	Sea star	10	0.05	15.19	< 0.01	0.04	95	-	-	-
8435	*Poraniomorpha* spp.	Sea star	14	0.4	24.83	< 0.01	0.08	95	-	-	-
8445	*Solaster endeca*	Purple sunstar	2	< 0.01	1.99	< 0.01	< 0.01	95	-	-	-
8446	*Tremaster mirabilis*	Sea star	3	0.12	2.79	< 0.01	< 0.01	95	-	-	-
8447	*Crossaster papposus*	Spiny sun star	2	< 0.01	1.99	< 0.01	< 0.01	95	-	-	-
8448	*Novodinia americana*	Sea star	11	35.83	0	0,09	0	95	-	-	-
8511	*Leptasterias (Hexasterias) polaris*	Polar sea star	1	< 0.01	1.25	< 0.01	< 0.01	95	-	-	-
8513	*Leptasterias groenlandica*	Greenland sea star	5	< 0.01	6.66	< 0.01	0.03	95	-	-	-
8515	*Stephanasterias albula*	Sea star	2	< 0.01	2.21	< 0.01	< 0.01	95	-	-	-
8521	*Leptychaster arcticus*	Sea star	4	< 0.01	3.84	< 0.01	< 0.01	95	-	-	-
8530	Ophiuroidea	Brittle stars	9	< 0.01	13	< 0.01	0.02	95	-	-	-
8540	*Gorgonocephalus* spp.	Basket stars	8	1.12	9.71	< 0.01	0.03	95	-	-	-
8541	*Gorgonocephalus arcticus*	Northern basket star	1	< 0.01	0.93	< 0.01	< 0.01	95	-	-	-
8551	*Ophiura* spp.	Brittle stars	1	< 0.01	8.65	< 0.01	0.02	95	-	-	-
8552	*Ophiura robusta*	Brittle star	1	< 0.01	0.97	< 0.01	< 0.01	95	-	-	-
8585	*Ophioscolex glacialis*	Brittle star	17	0.02	24.83	< 0.01	0.06	95	-	-	-
8593	*Amphiura* spp.	Brittle star	15	0.18	198.6	< 0.01	0.41	95	-	-	-

Table 3. Number of specimens per taxon which were individually measured and weighted, with descriptive statistics of length in mm (min=minimum; P1=1st percentile; P50=50st percentile; P99=99th percentile; max=maximum) in the winter survey in 2022, 2023 et 2024.

Code	Scientific name	Number measured		Desc. length stat. (mm)				
		Length	Weight	Min.	P1	P50	P99	Max.
13	*Myxine limosa*	1317	856	77	220	350	467	650
27	*Centroscyllium fabricii*	4375	1202	131	150	387	620	688
90	*Amblyraja radiata*	1993	1181	87	117	380	810	930
91	*Malacoraja senta*	517	429	83	90	323	565	601
150	*Clupea harengus*	6819	1837	83	169	303	382	400
151	*Alosa pseudoharengus*	107	77	95	106	270	312	316
187	*Mallotus villosus*	613	317	66	100	130	159	181
193	*Argentina silus*	3638	1956	58	74	219	365	415
271	Myctophiformes	43	31	59	60	91	186	202
320	*Arctozenus risso*	1587	976	113	154	221	261	274
373	*Synaphobranchus kaupii*	181	80	198	217	346	523	540
426	*Gasterosteus aculeatus*	82	61	33	38	61	80	80
438	*Gadus morhua*	9994	4357	45	170	318	618	1020
443	*Pollachius virens*	135	68	210	227	624	848	860
444	*Phycis chesteri*	3080	952	93	120	257	384	482
447	*Urophycis tenuis*	2246	1838	80	161	366	760	1064
449	*Merluccius bilinearis*	10748	4744	50	130	284	394	612
461	*Enchelyopus cimbrius*	560	453	73	98	190	277	287
478	*Nezumia bairdii*	6184	2138	20	110	242	324	388
700	*Anarhichas lupus*	166	131	70	81	233	655	880
745	*Melanostigma atlanticum*	462	315	60	86	118	147	158
794	*Sebastes mentella*	23798	6275	42	68	243	345	600
796	*Sebastes fasciatus*	7830	3180	42	68	243	345	600
797	*Helicolenus dactylopterus*	88	58	29	74	167	249	251
811	*Artediellus atlanticus*	94	87	44	46	65	96	97
856	*Paraliparis copei*	59	20	10	10	107	134	134
874	*Paraliparis calidus*	42	40	54	56	107	117	119
889	*Hippoglossoides platessoides*	7888	3851	36	94	216	433	592
890	*Glyptocephalus cynoglossus*	8937	5212	42	76	302	451	537
892	*Reinhardtius hippoglossoides*	3010	2210	91	113	381	564	817
893	*Hippoglossus hippoglossus*	244	244	76	226	734	1714	1756
966	*Lophius americanus*	68	68	90	123	638	1144	1210
8033	*Eusergestes arcticus*	1264	0	0	10	16	21	23
8056	*Pasiphaea tarda*	102	0	18	20	33	49	50
8057	*Pasiphaea multidentata*	8374	0	8	14	24	31	34
8087	*Spirontocaris liljeborgii*	175	0	8	8	11	14	15
8093	*Lebbeus polaris*	369	0	6	7	10	14	16
8111	*Pandalus borealis*	17031	0	7	12	21	27	31
8112	*Pandalus montagui*	948	0	8	9	14	21	26
8113	*Atlantopandalus propinqvus*	1201	0	9	10	16	23	24
8129	*Sabinea sarsii*	99	0	7	7	11	14	14
8135	*Pontophilus norvegicus*	2688	0	7	8	13	16	19
8196	*Lithodes maja*	612	0	1	4	74	119	139
8213	*Chionoecetes opilio*	177	0	2	8	23	129	134
24	*Squalus acanthias*	66	41	633	654	775	924	960
94	*Rajella fyllae*	11	11	96	97	443	504	506
100	*Leucoraja ocellata*	27	25	130	203	761	913	915
102	*Bathyraja spinicauda*	7	4	317	317	1310	12599	12600
152	*Alosa sapidissima*	9	9	105	106	146	307	309
219	*Serrivomer* spp.	1	0	38	38	38	38	38
220	Sternoptychidae	1	1	42	42	42	42	42
225	*Argyropelecus gigas*	1	1	80	80	80	80	80
227	*Chauliodus sloani*	13	13	120	122	220	259	261
230	*Stomias boa boa*	5	5	191	192	211	243	243
244	*Polymetme thaeocoryla*	1	1	115	115	115	115	115

Table 3 (continued).

Code	Scientific name	Number measured		Desc. length stat. (mm)				
		Length	Weight	Min.	P1	P50	P99	Max.
368	*Nemichthys scolopaceus*	16	15	284	284	560	969	974
369	*Serrivomer beanii*	18	18	336	337	445	600	602
372	Synaphobranchidae	1	0	420	420	420	420	420
375	*Polyipnus* spp.	1	0	42	42	42	42	42
418	*Syngnathus fuscus*	1	0	212	212	212	212	212
436	Gadidae	0	2	-	-	-	-	-
440	*Micromesistius poutassou*	1	1	297	297	297	297	297
441	*Melanogrammus aeglefinus*	486	205	150	178	434	676	779
451	*Boreogadus saida*	1	1	79	79	79	79	79
454	*Gaidropsarus ensis*	2	2	118	119	148	178	179
518	*Hoplosthetus atlanticus*	1	0	112	112	112	112	112
527	*Hoplostethus mediterraneus mediterraneus*	2	1	92	93	118	143	144
572	*Scomber scombrus*	5	5	180	180	329	340	340
618	*Epigonus pandionis*	14	2	79	82	132	164	165
699	*Anarhichas denticulatus*	2	2	280	282	381	480	482
701	*Anarhichas minor*	3	3	119	125	409	784	792
711	*Eumesogrammus praecisus*	56	21	103	108	150	183	186
716	*Lumpenus lampretaeformis*	12	12	207	208	288	407	408
717	*Leptoclinus maculatus*	85	37	86	87	120	153	154
721	*Cryptacanthodes maculatus*	25	23	238	238	356	658	675
725	Zoarcidae	1	1	230	230	230	230	230
727	*Lycodes esmarkii*	23	23	240	244	339	581	590
728	*Lycodes lavalaei*	42	23	69	69	125	380	380
730	*Lycodes vahlii*	31	31	80	83	221	336	340
734	*Lycodes terraenovae*	2	2	300	300	310	321	321
746	*Gymnelus viridis*	1	1	144	144	144	144	144
750	*Lycenchelys paxillus*	7	7	160	162	222	266	266
752	*Lycenchelys verrillii*	4	4	100	100	120	150	150
783	*Peprilus triacanthus*	2	2	194	194	203	212	212
809	*Hemitripterus americanus*	37	34	251	256	320	486	500
810	*Artediellus* spp.	15	15	46	46	59	69	70
812	*Artediellus uncinatus*	14	11	50	50	60	70	70
814	*Triglops murrayi*	81	52	59	66	110	137	140
819	*Myoxocephalus scorpius*	27	26	41	43	310	428	440
820	*Myoxocephalus octodecemspinosus*	38	34	220	227	289	358	360
829	*Cottunculus microps*	1	1	90	90	90	90	90
832	*Icelus spatula*	1	1	89	89	89	89	89
836	*Leptagonus decagonus*	1	1	202	202	202	202	202
837	*Aspidophoroides olrikii*	1	1	64	64	64	64	64
838	*Aspidophoroides monopterygius*	18	13	103	103	134	147	147
847	*Eumicrotremus terraenovae*	177	40	22	24	42	87	128
849	*Cyclopterus lumpus*	10	10	35	44	203	388	390
865	*Careproctus reinhardti*	6	6	40	40	60	154	155
868	*Liparis bathyarcticus*	2	2	44	44	64	84	84
882	Pleuronectiformes	5	0	38	38	50	62	62
891	*Limanda ferruginea*	248	115	183	209	346	476	515
895	*Pseudopleuronectes americanus*	5	5	285	286	329	350	351
907	*Scophthalmus aquosus*	40	28	170	170	226	295	295
982	*Cryptopsaras couesii*	6	5	48	48	148	325	333
4545	Cephalopoda	1	1	110	110	110	110	110
4753	*Illex illecebrosus*	10	10	10	11	64	215	216
7927	*Gnathophausia* spp.	1	0	21	21	21	21	21
7999	*Bentheuphausia amblyops*	4	0	11	11	12	15	15
8024	*Aristaeopsis edwardsiana*	8	0	28	28	33	66	66
8028	*Hymenopenaeus debilis*	11	0	12	13	15	19	19
8035	*Sergia robusta*	26	0	11	11	18	24	24
8036	Benthesicymidae	2	0	10	10	10	11	11

Table 3 (continued).

Code	Scientific name	Number measured		Desc. length stat. (mm)				
		Length	Weight	Min.	P1	P50	P99	Max.
8040	*Acanthephyra pelagica*	30	0	10	10	18	24	24
8052	*Nematocarcinus rotundus*	3	0	19	19	19	25	25
8074	*Eualus* spp.	1	0	7	7	7	7	7
8075	*Eualus fabricii*	2	0	8	8	8	8	8
8077	*Eualus macilentus*	7	0	8	8	10	11	11
8079	*Eualus gaimardii*	2	0	8	8	9	10	10
8084	*Spirontocaris* spp.	20	0	8	9	11	14	14
8085	*Spirontocaris spinus*	7	0	9	9	11	13	13
8095	*Lebbeus microceros*	2	0	11	11	12	12	12
8108	*Dichelopandalus leptocerus*	33	0	12	12	18	21	22
8114	*Plesionika martia*	2	0	18	18	20	22	22
8128	*Sabinea septemcarinata*	70	0	6	7	11	14	14
8138	*Argis dentata*	214	0	8	8	13	18	20
8154	*Homarus americanus*	35	0	73	76	98	140	141
8217	*Hyas araneus*	5	0	9	9	15	63	65
8219	*Hyas alutaceus*	19	0	8	9	17	56	63

FIGURES

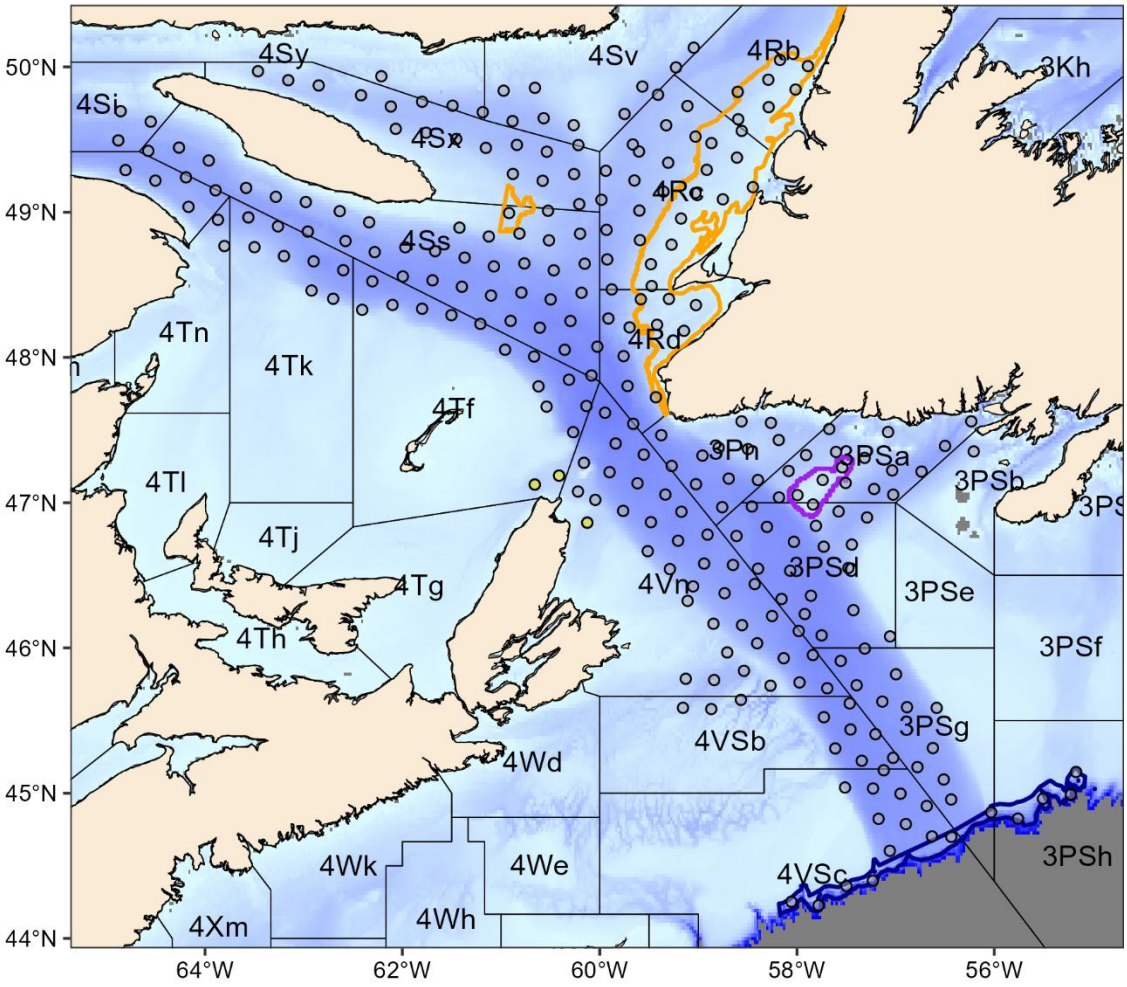


Figure 1. Description of the winter survey area on board the MV Mersey Venture, with shades of blue reflecting bathymetry and black lines delineating NAFO Subdivisions and Unit Areas. Gray and yellow circles identify stations that were part of the initial combined three-year survey plan and hand-selected for white hake, respectively. Colored polygons indicate portions of the study area added in 2024 to address targeted questions on Atlantic cod (orange), Burgeo Bank (purple), and the Laurentian Fan (dark blue).

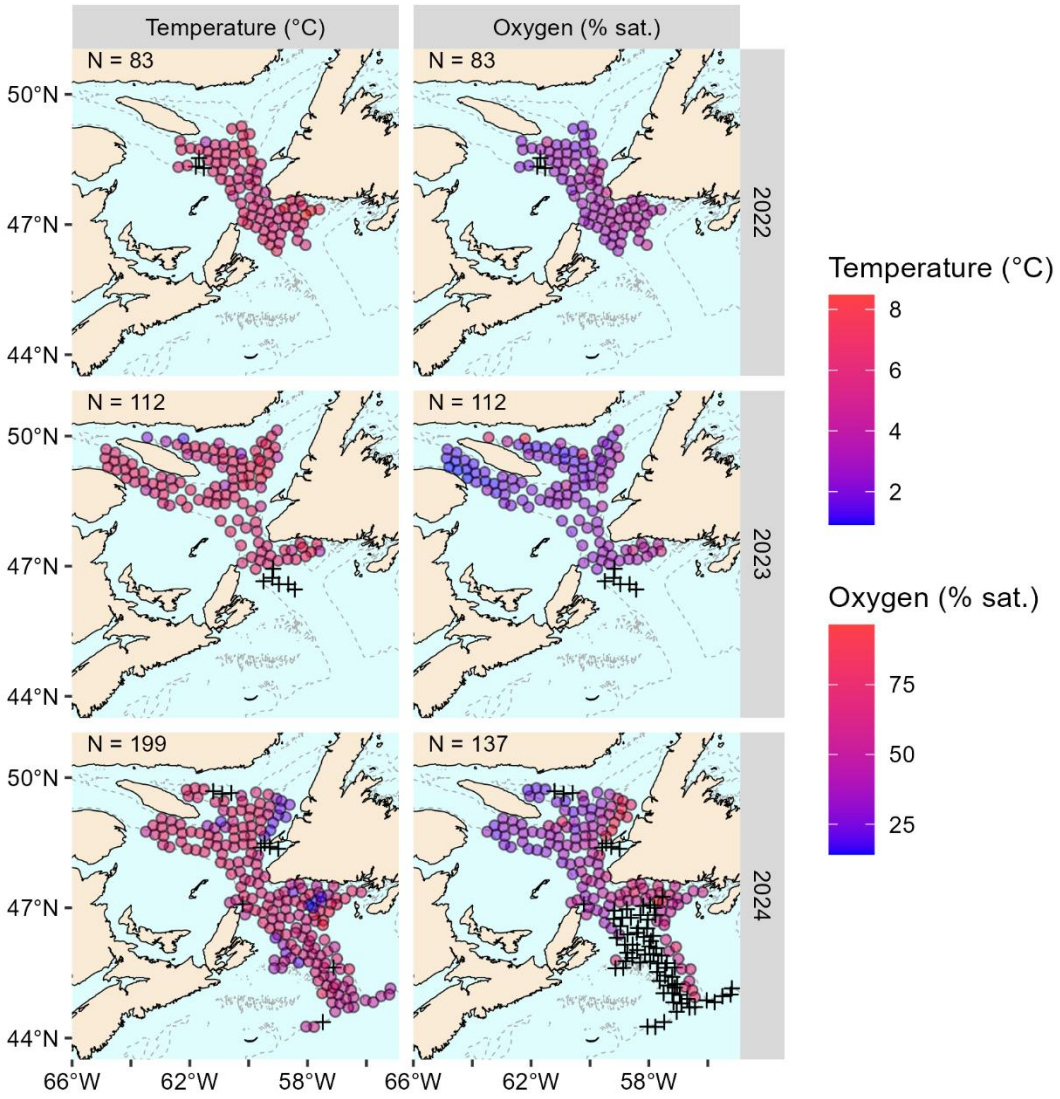


Figure 2. Bottom temperature and dissolved oxygen saturation values observed during the winter survey by year (panels). Stations for which a value was available in 2022, 2023, and 2024 are represented by colored circles according to the corresponding scales, and those for which no value was available are identified by a black cross. The number of tows for which a value was available is given in the upper left corner of each panel. The gray dashed lines in each panel indicate the 200 m isobath.

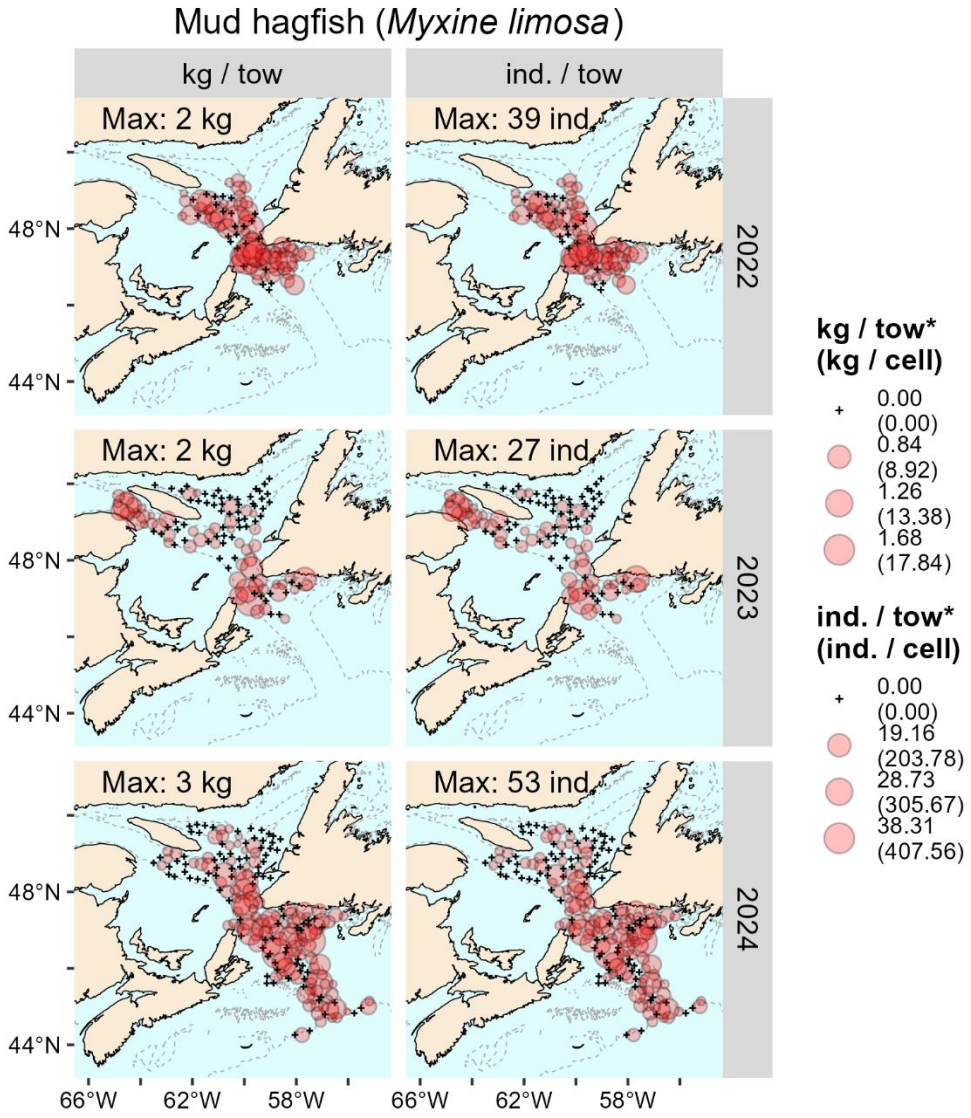


Figure 3a. Standardized catches by weight and/or number (colored bubbles) and cases of absence (black crosses) for the mud hagfish in the winter surveys of 2022, 2023, and 2024. Maximum observed values are indicated in the upper left corner of each panel, and the 200 m isobath is represented by a gray dashed line. As mentioned in Methods (section 2.2.1), where the legend title is marked with an asterisk, the values shown in the legend correspond to specific percentages (0, 50, 75, and 100 %) of the catch distribution truncated at the 99.5th percentile, with their equivalences per 0.25 km^2 cell in parentheses. In other cases, the bubble diameters correspond to the 0th, 50th, 75th, and 100th percentiles of the untruncated standardized catch distribution per tow. Missing observations of standardized catch numbers are not represented.

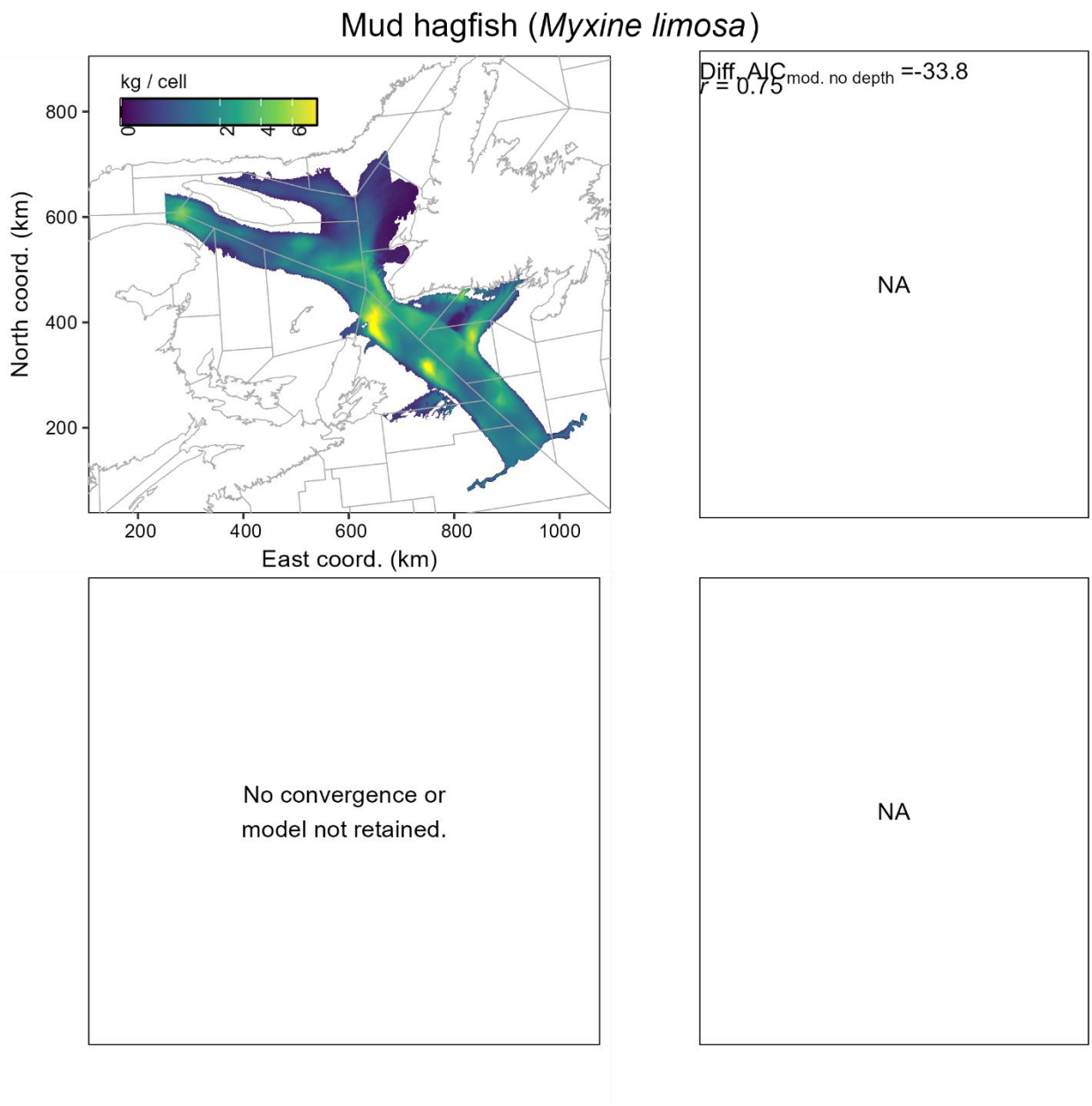


Figure 3b. Predicted weight (upper panels) and number (lower panels) values per 0.25 km^2 cell according to the selected spatial interpolation models for the mud hagfish in the 2022, 2023, and 2024 winter survey. The right-hand panels show, where available, the depth smoothing functions (black lines) and associated 95 % confidence intervals (gray shaded areas) and indicate 'NA' (not available) where a model without a depth effect or that did not converge was favored by AIC. The values in the upper left of these panels are the differences in AIC between the models with and without a depth effect and the Pearson correlation coefficient (*r*) between the observed and predicted density values per cell.

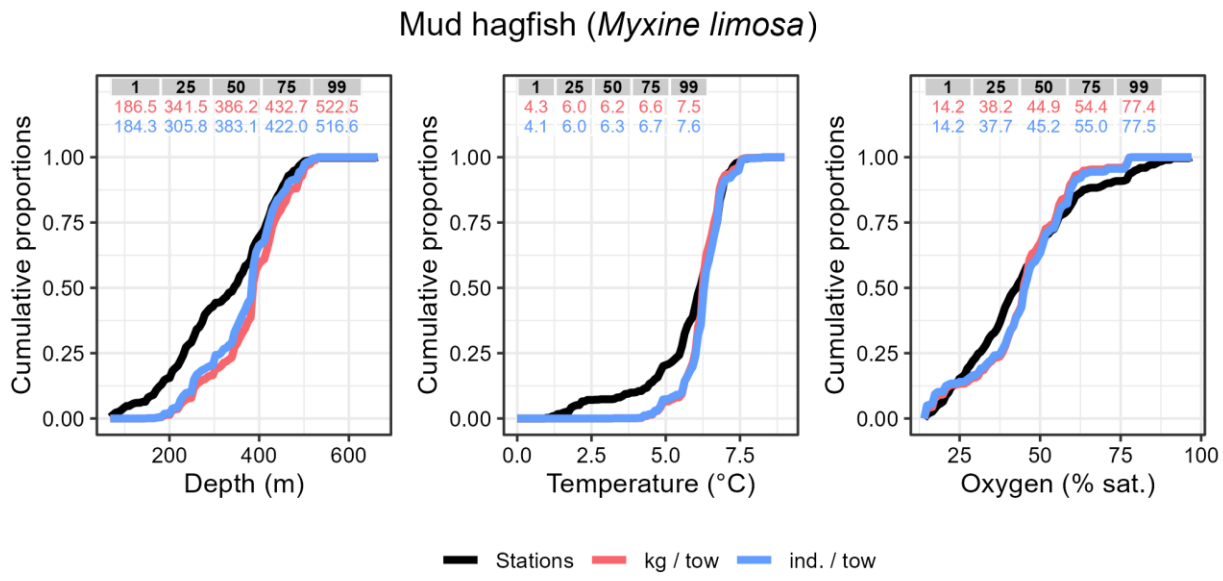


Figure 3c. Cumulative proportions of available values of depth, temperature and dissolved oxygen and standardized catches per tow for the mud hagfish in the winter survey in 2022, 2023 and 2024. The inserted tables give the weights and numbers associated with the 1st, 25th, 50th, 75th and 99th percentiles of each distribution, using the same color scheme as the lines.

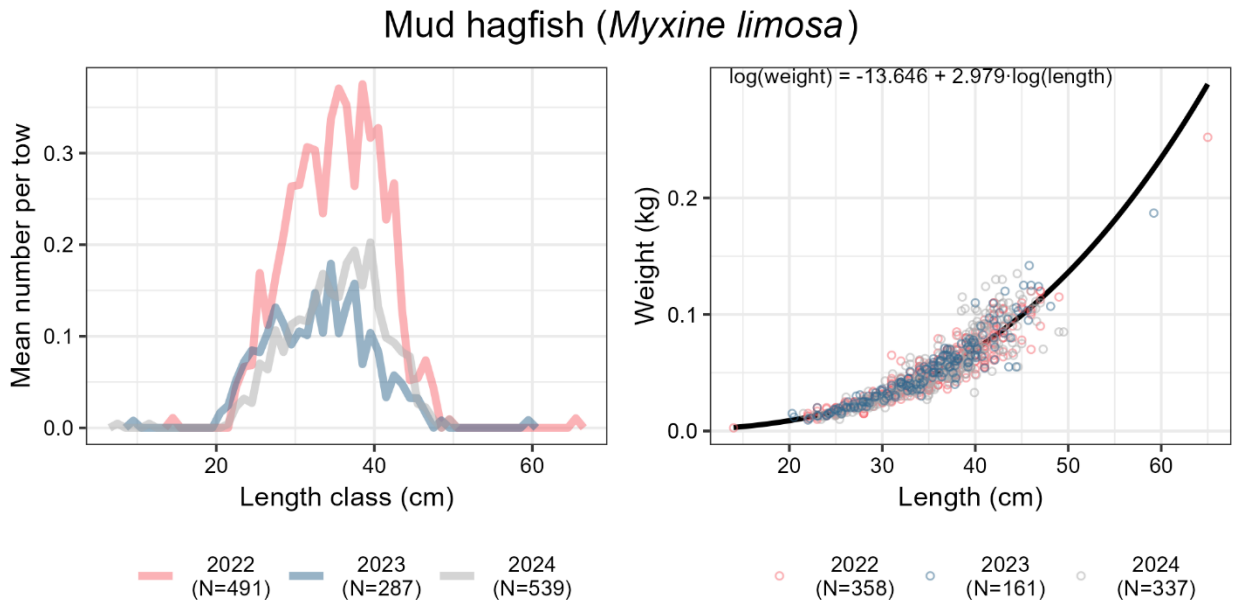


Figure 3d. Annual length frequencies (left panel) and length-weight observations with the global relationship prediction (right panel) for the mud hagfish in the winter survey in 2022, 2023 and 2024. The N values below the legends correspond to the number of individuals in each analysis.

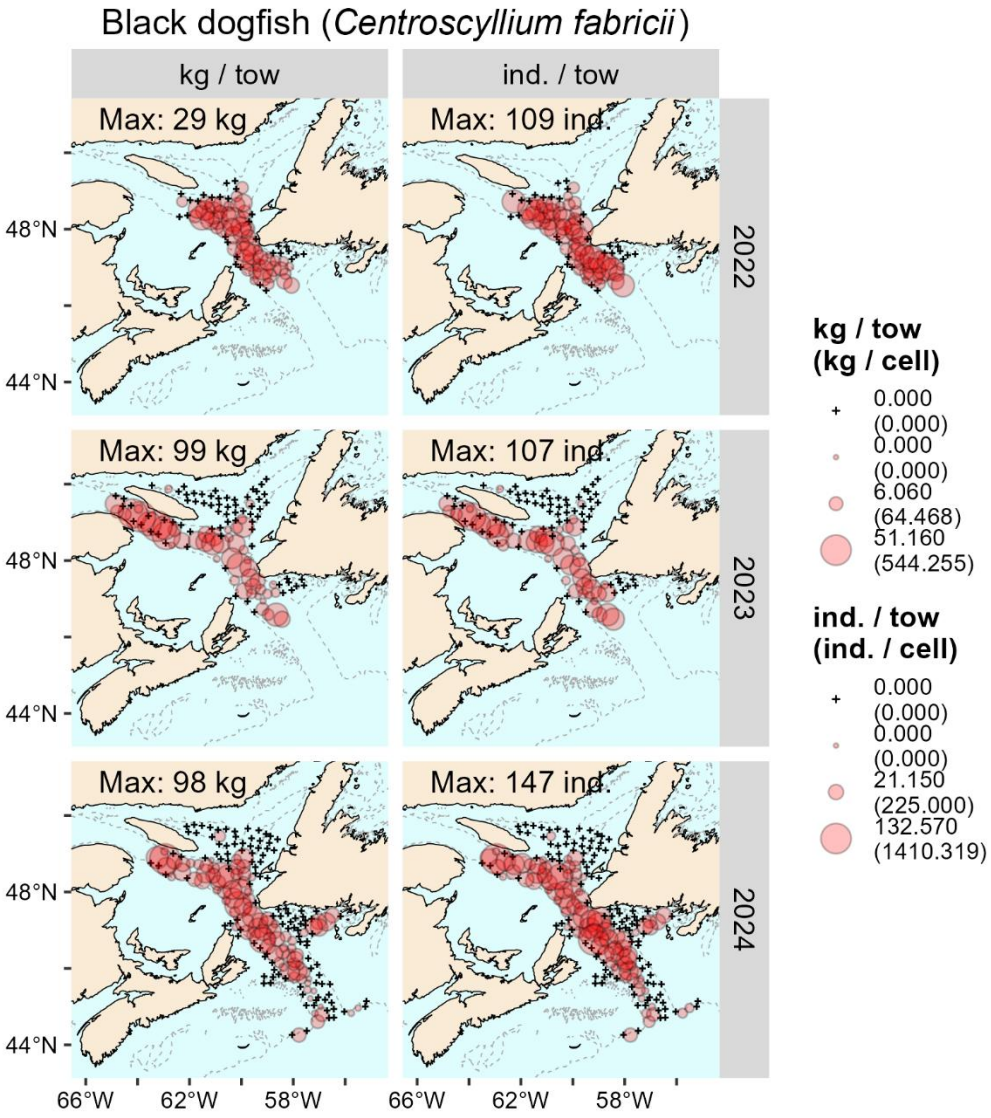


Figure 4a. Standardized catches by weight and/or number (colored bubbles) and cases of absence (black crosses) for the black dogfish in the winter survey in 2022, 2023 and 2024.

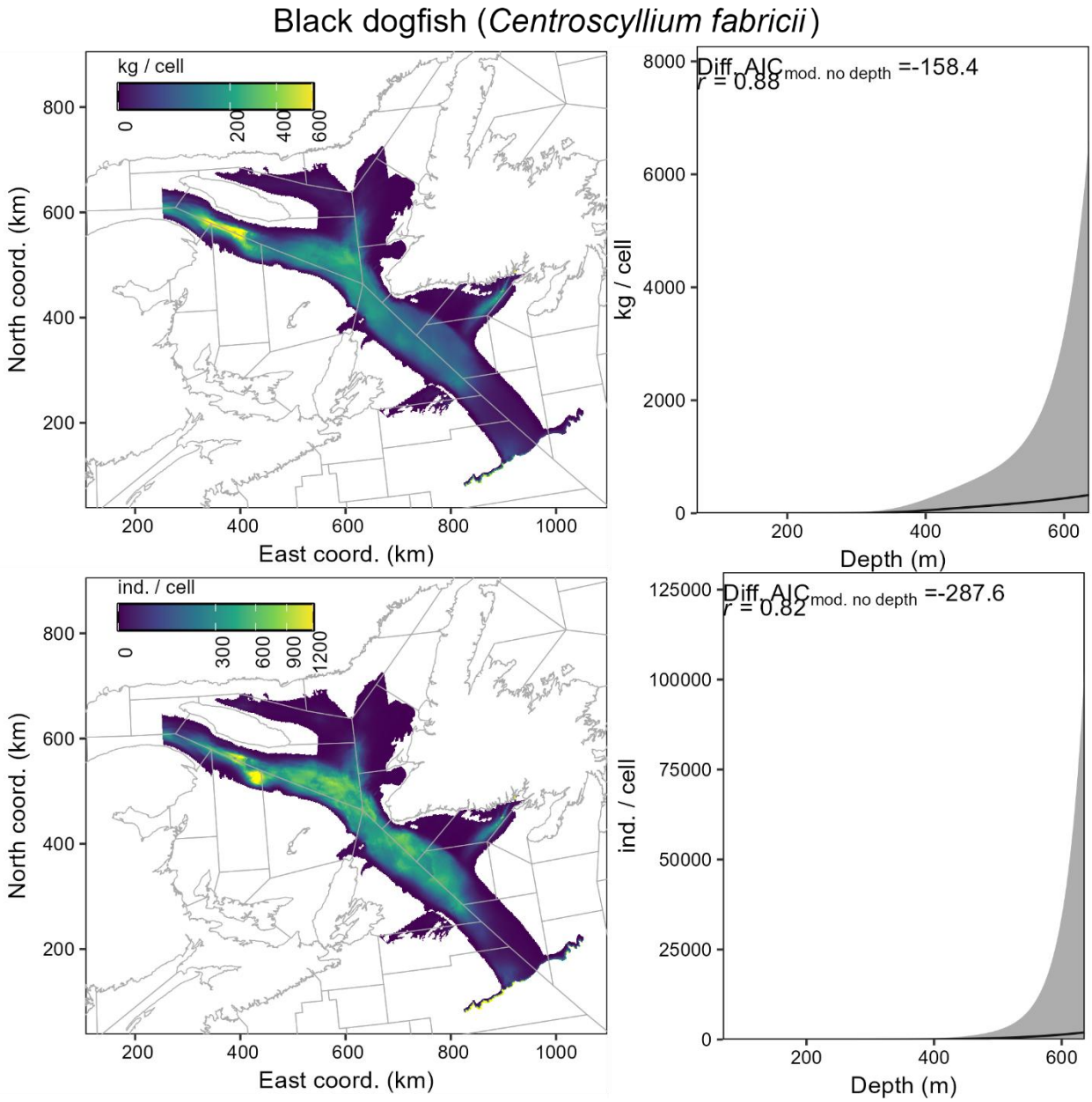


Figure 4b. Predicted weight (upper panels) and number (lower panels) values per 0.25 km^2 cell according to the selected spatial interpolation models for black dogfish in the 2022, 2023, and 2024 winter survey.

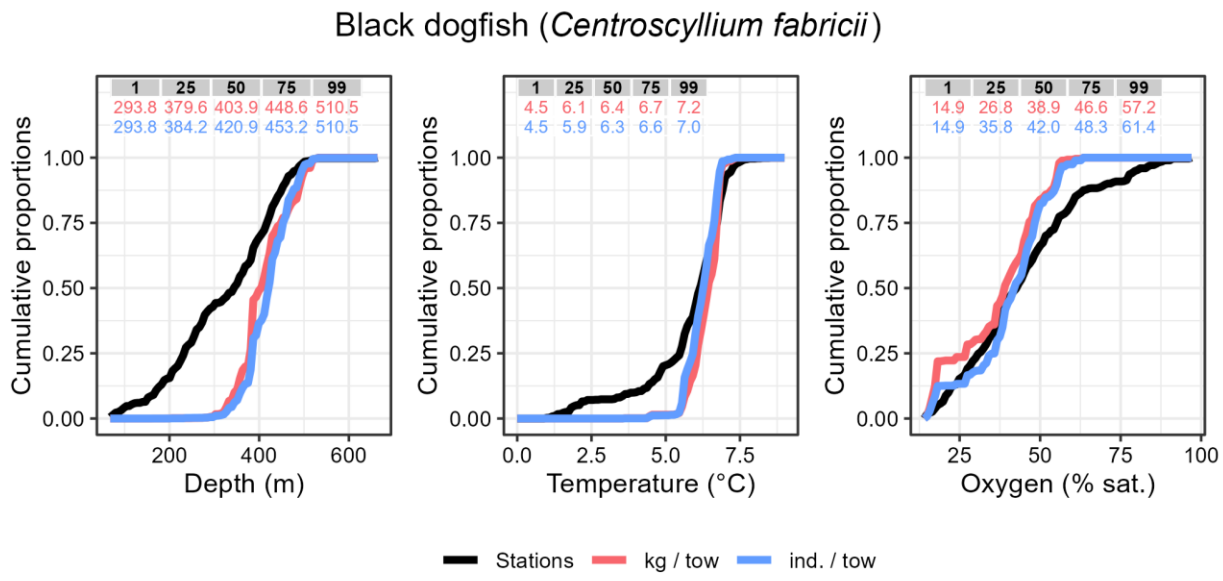


Figure 4c. Cumulative proportions of available values of depth, temperature and dissolved oxygen and standardized catches per tow for the black dogfish in the winter survey in 2022, 2023 and 2024.

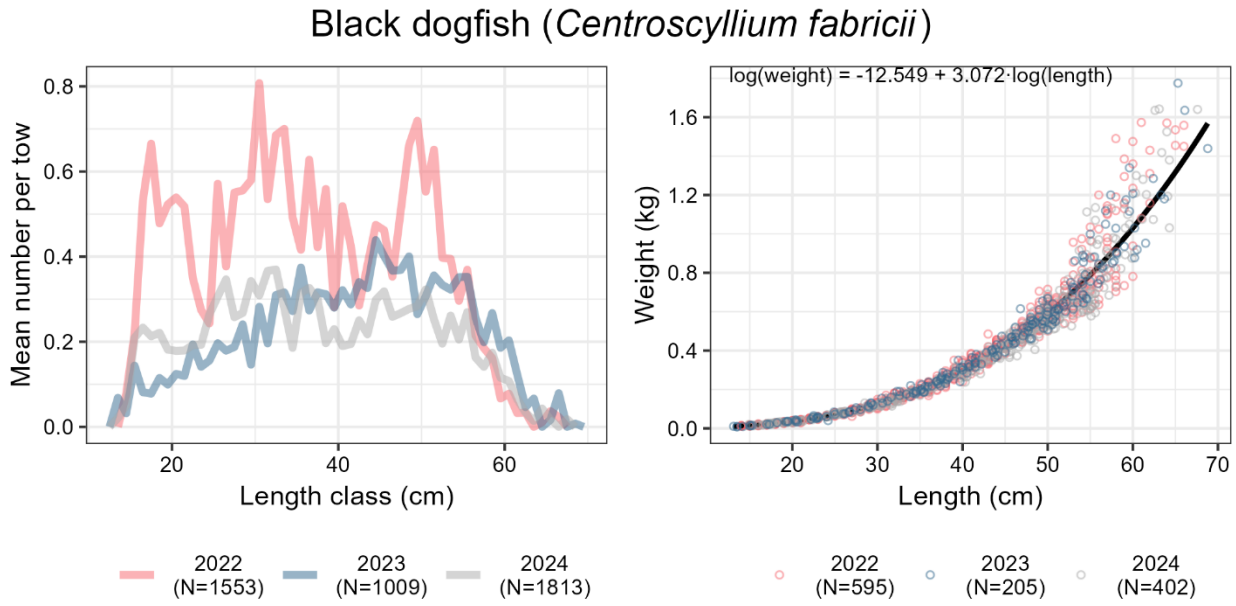


Figure 4d. Annual length frequencies (left panel) and length-weight observations with the global relationship prediction (right panel) for the black dogfish in the winter survey in 2022, 2023 and 2024.

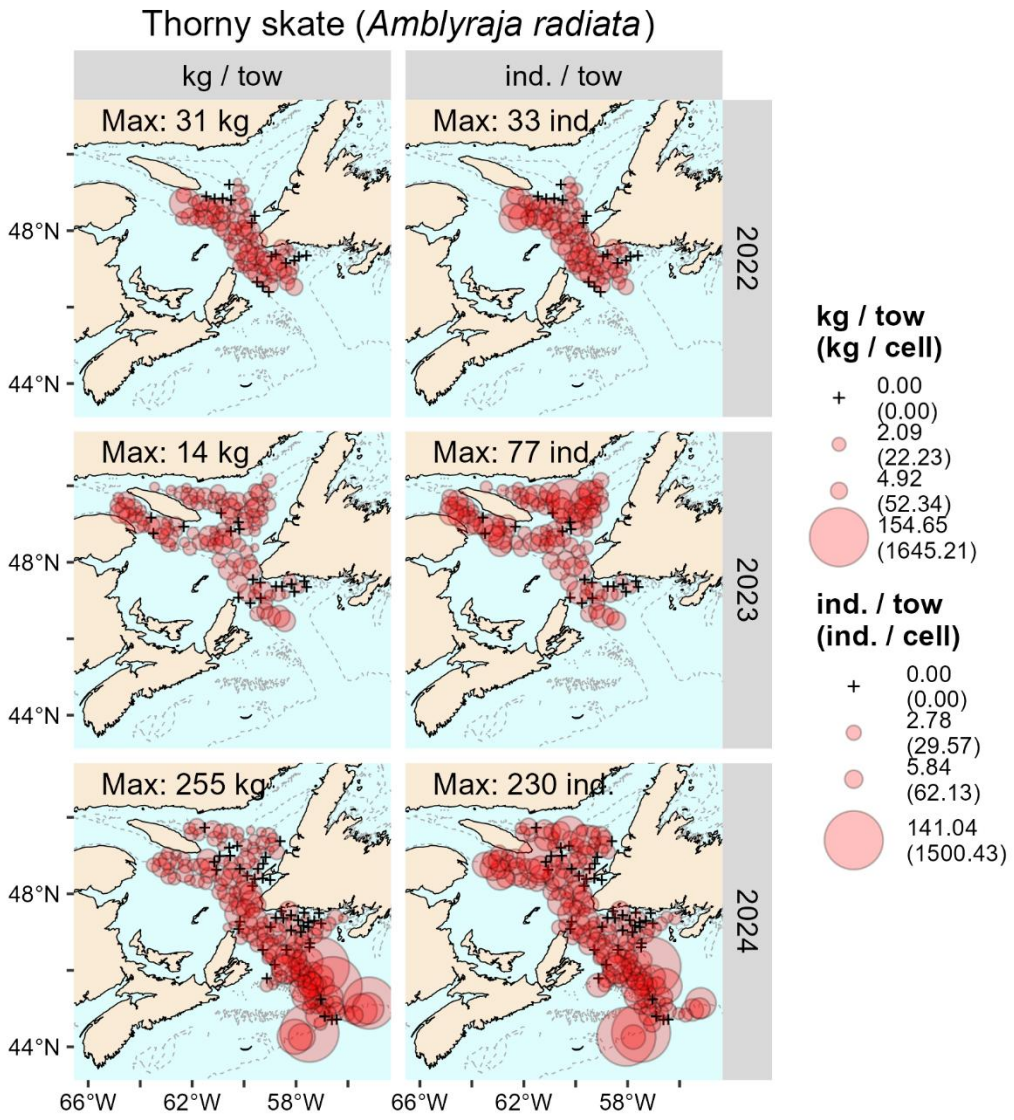


Figure 5a. Standardized catches by weight and/or number (colored bubbles) and cases of absence (black crosses) for the thorny skate in the winter surveys of 2022, 2023, and 2024.

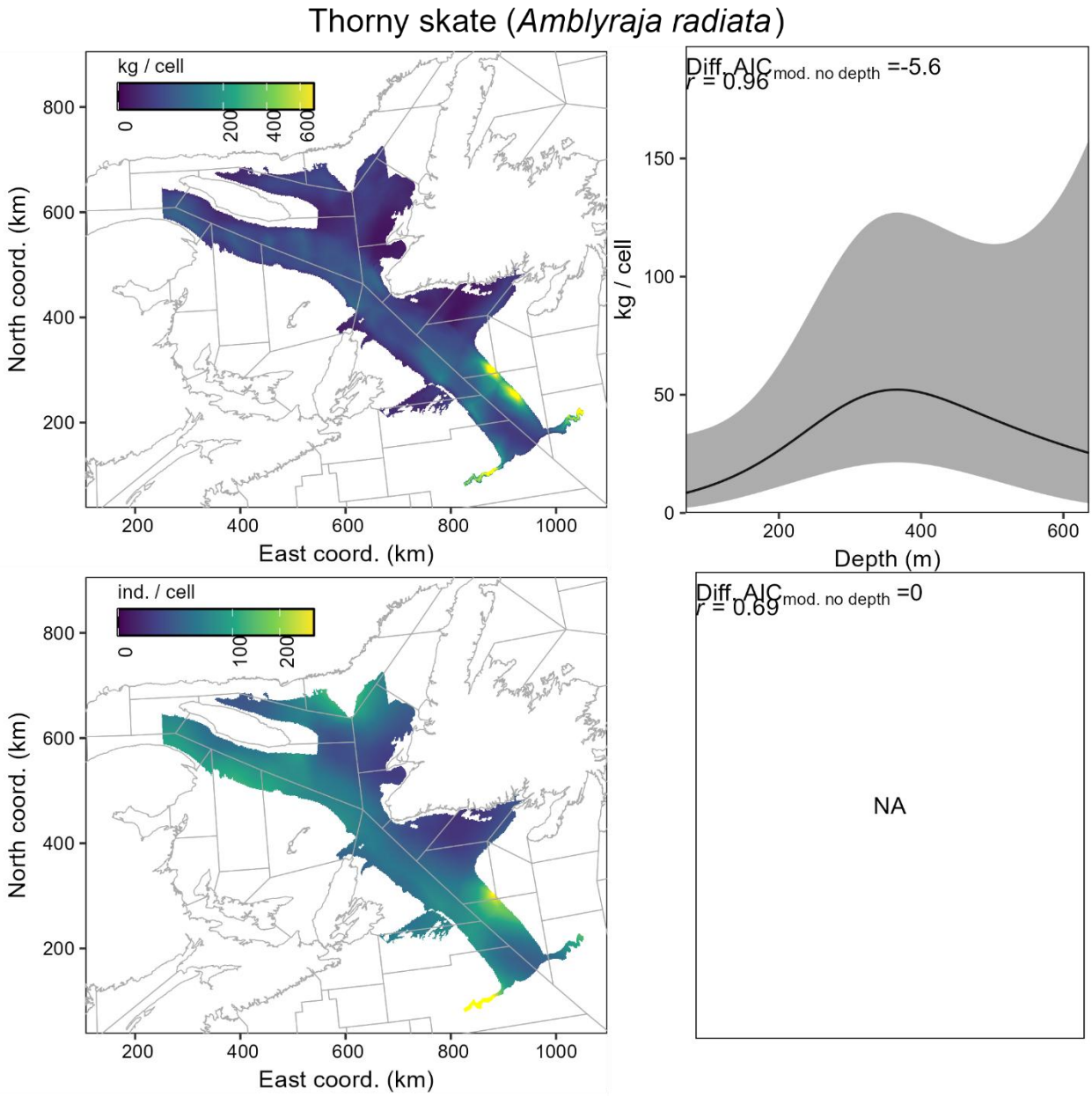


Figure 5b. Predicted weight (upper panels) and number (lower panels) values per 0.25 km^2 cell according to the selected spatial interpolation models for the thorny skate in the 2022, 2023, and 2024 winter survey.

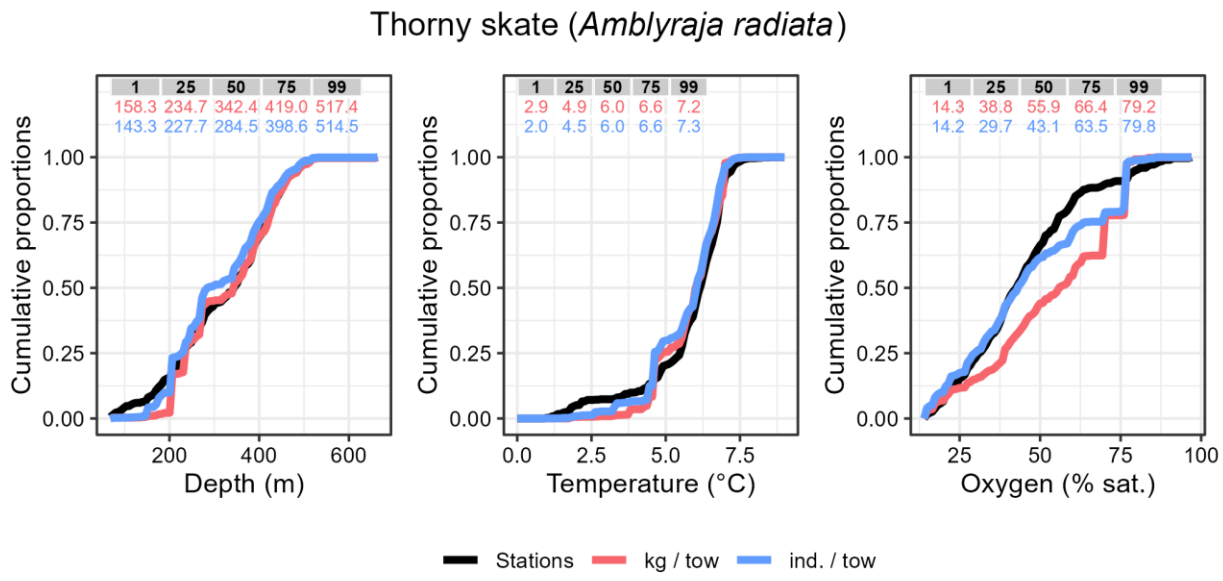


Figure 5c. Cumulative proportions of available values of depth, temperature and dissolved oxygen and standardized catches per tow for the thorny skate in the winter survey in 2022, 2023 and 2024.

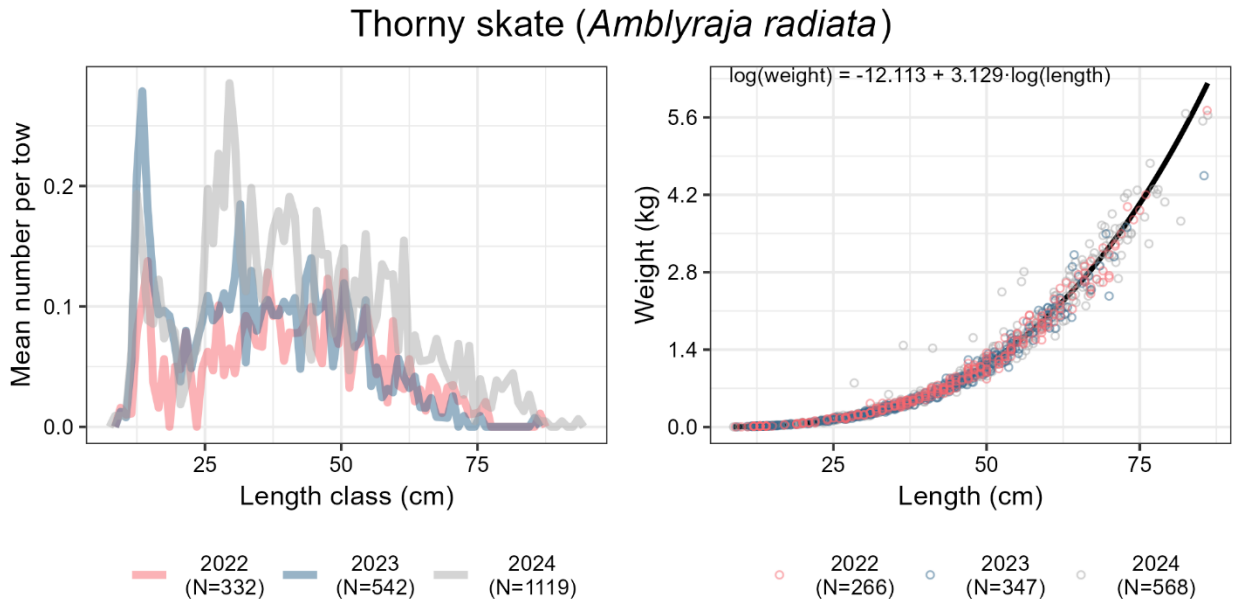


Figure 5d. Annual length frequencies (left panel) and length-weight observations with the global relationship prediction (right panel) for the thorny skate in the winter survey in 2022, 2023 and 2024.

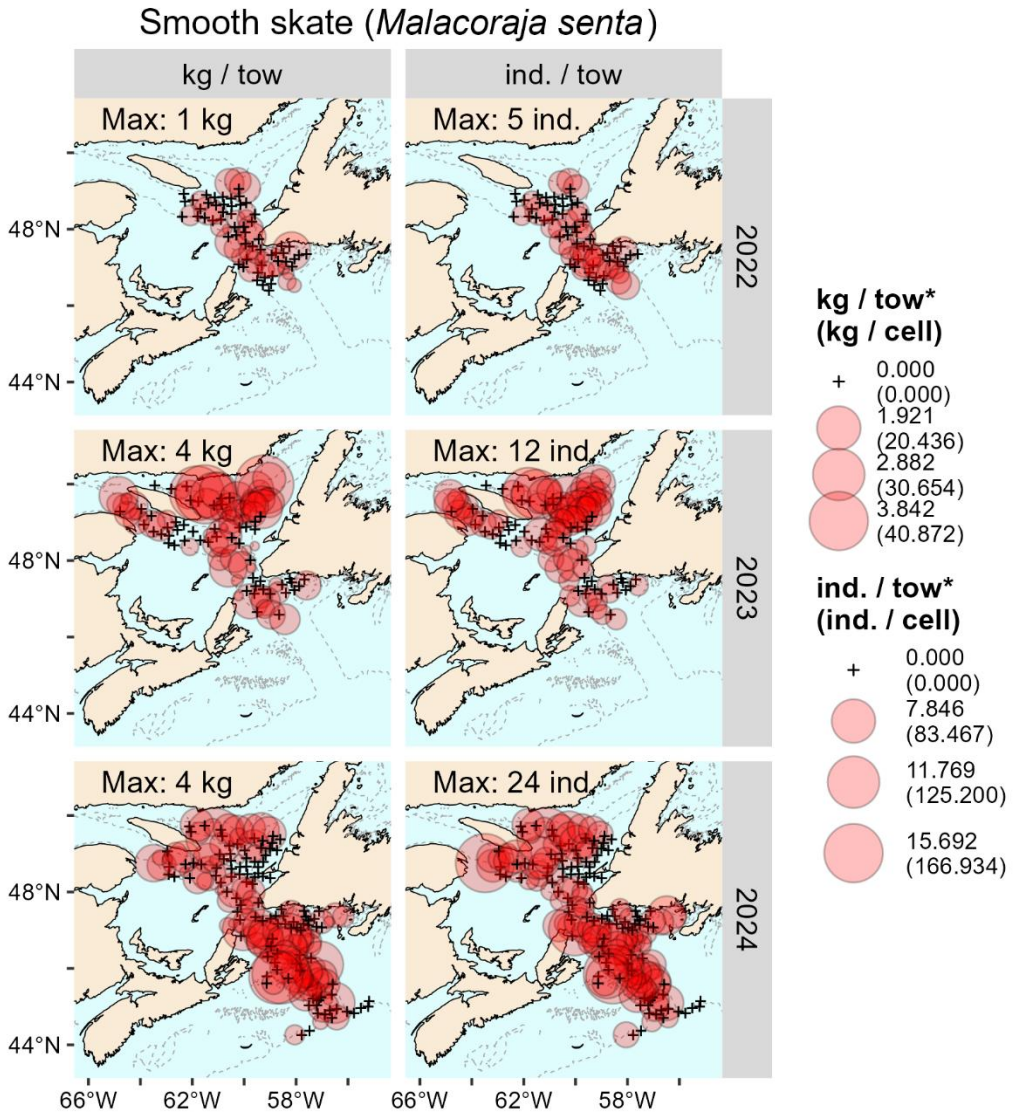


Figure 6a. Standardized catches by weight and/or number (colored bubbles) and cases of absence (black crosses) for the smooth skate in the winter surveys of 2022, 2023, and 2024.

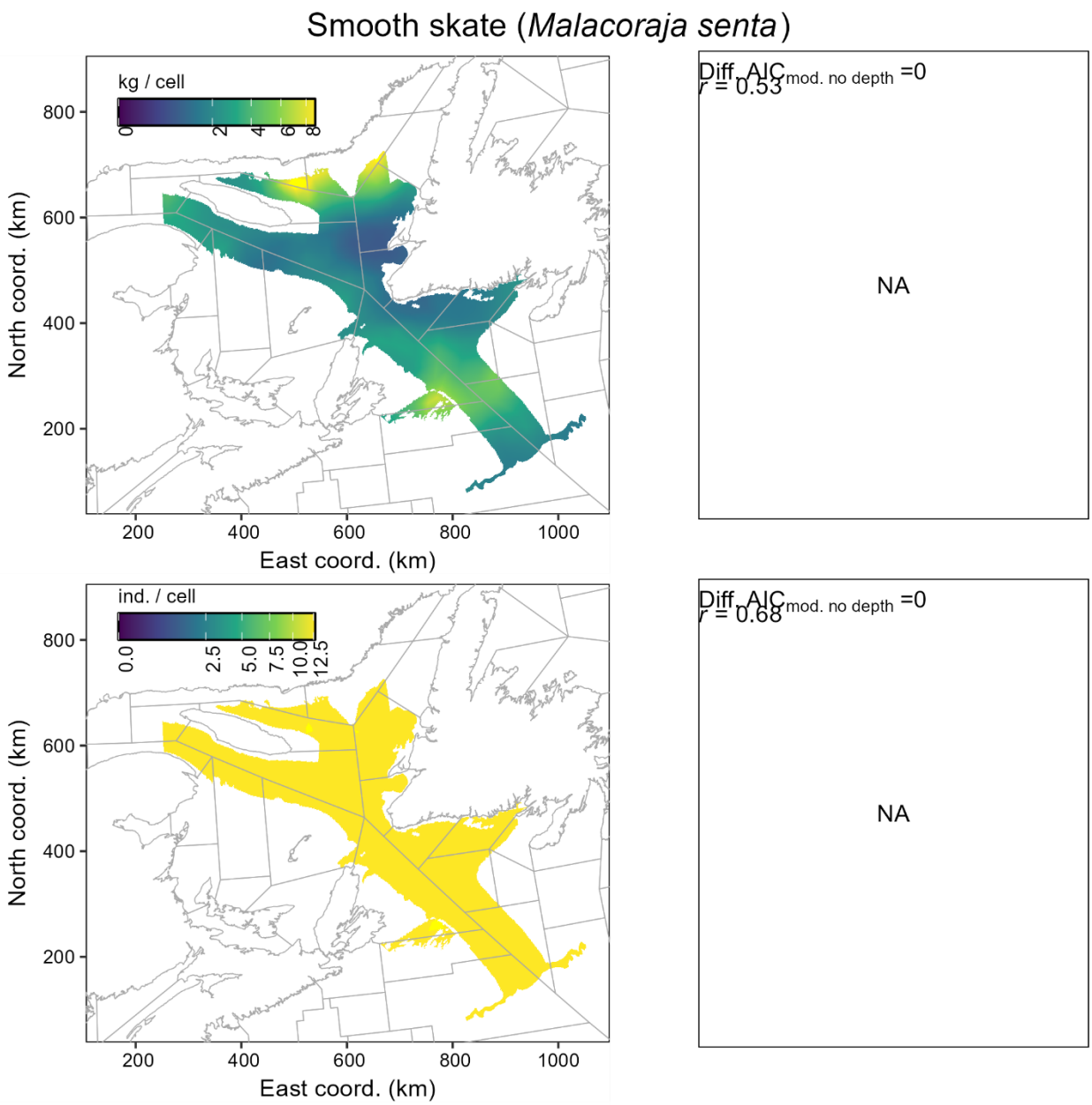


Figure 6b. Predicted weight (upper panels) and number (lower panels) values per 0.25 km^2 cell according to the selected spatial interpolation models for the smooth skate in the 2022, 2023, and 2024 winter survey.

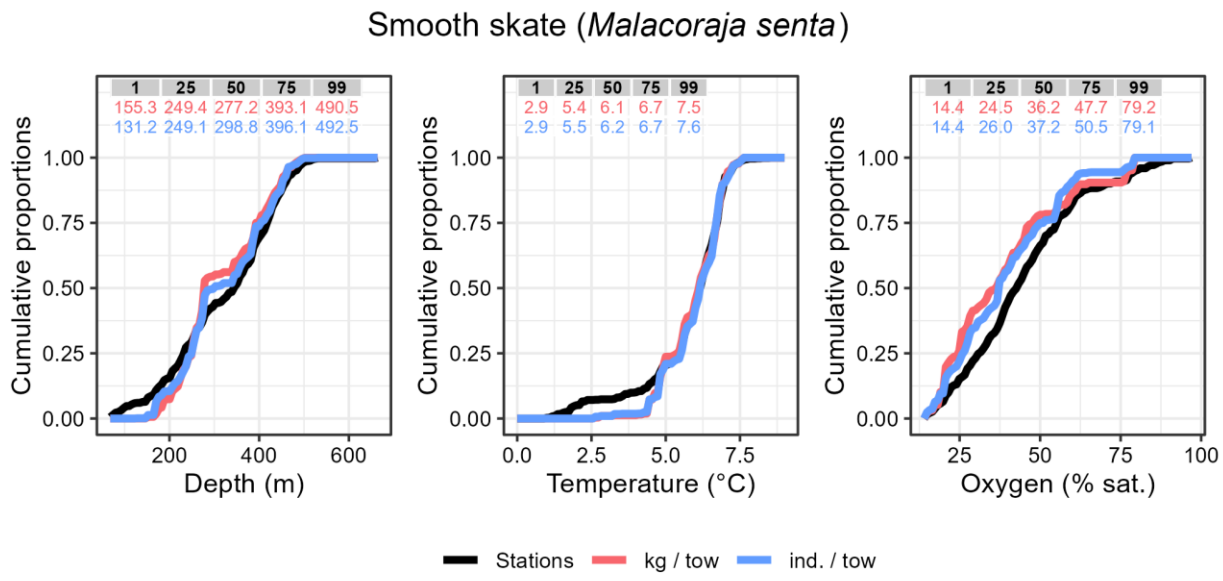


Figure 6c. Cumulative proportions of available values of depth, temperature and dissolved oxygen and standardized catches per tow for the smooth skate in the winter survey in 2022, 2023 and 2024.

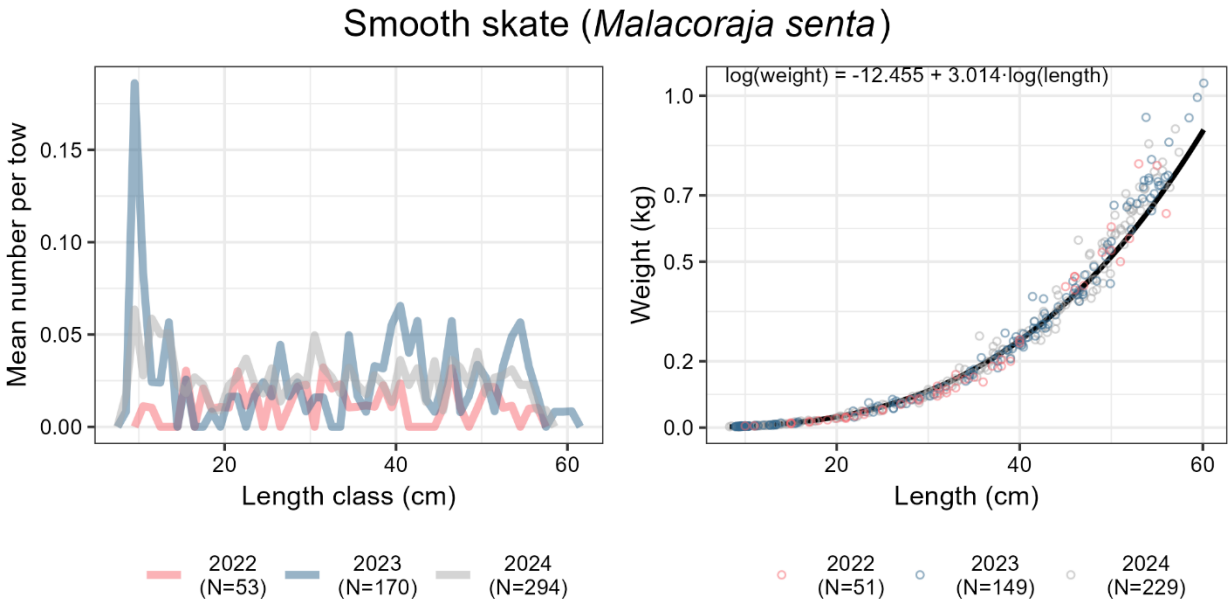


Figure 6d. Annual length frequencies (left panel) and length-weight observations with the global relationship prediction (right panel) for the smooth skate in the winter survey in 2022, 2023 and 2024.

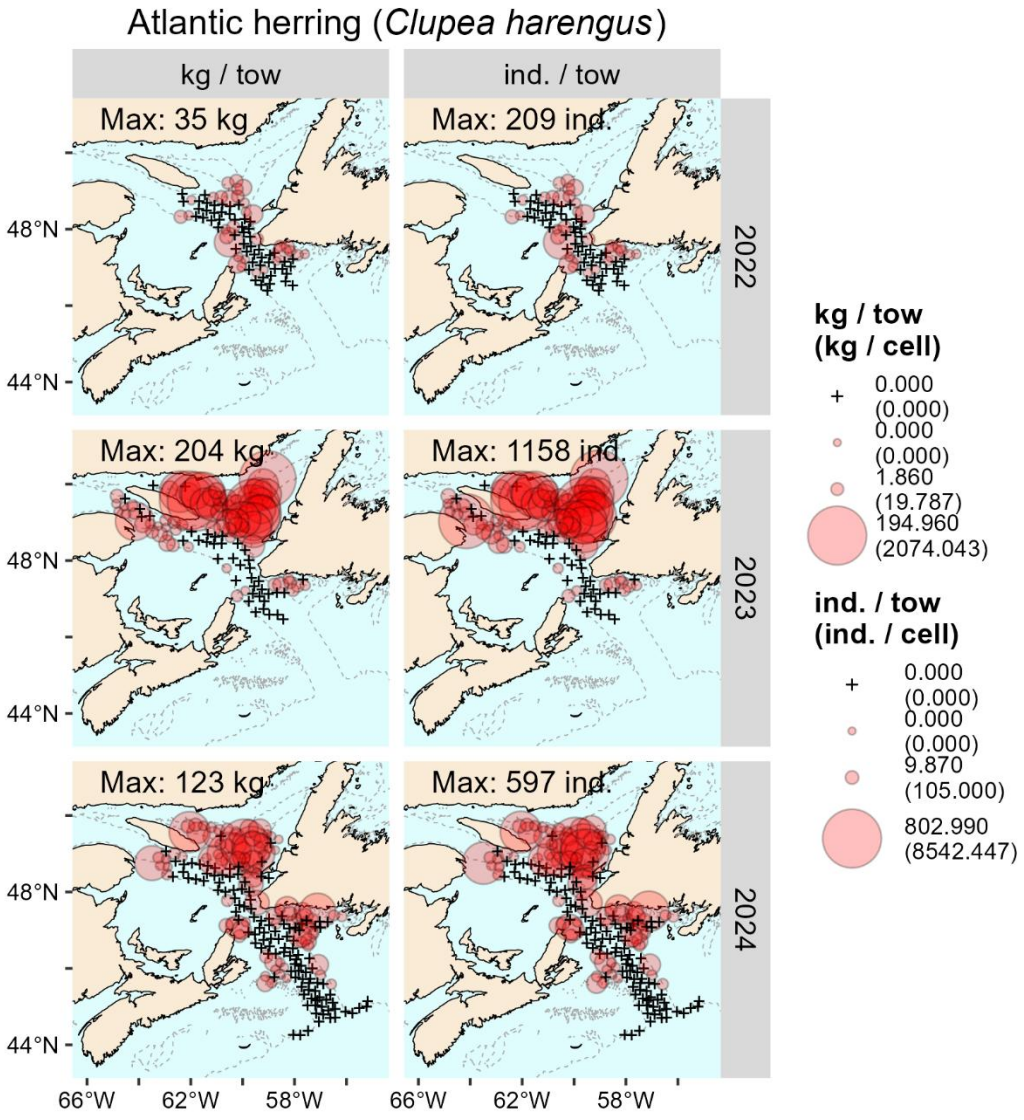


Figure 7a. Standardized catches by weight and/or number (colored bubbles) and cases of absence (black crosses) for the Atlantic herring in the winter surveys of 2022, 2023, and 2024.

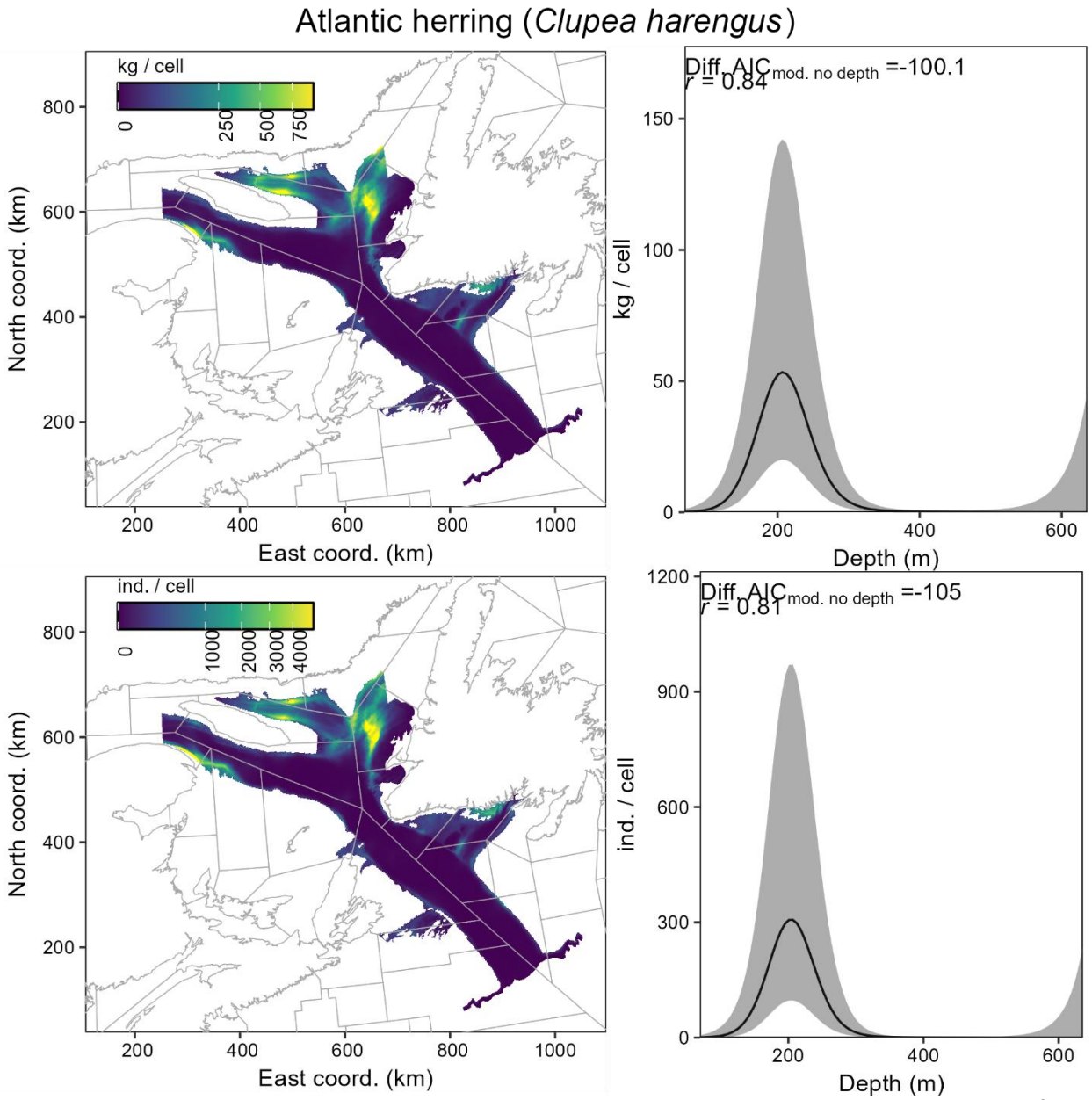


Figure 7b. Predicted weight (upper panels) and number (lower panels) values per 0.25 km^2 cell according to the selected spatial interpolation models for the Atlantic herring in the 2022, 2023, and 2024 winter survey.

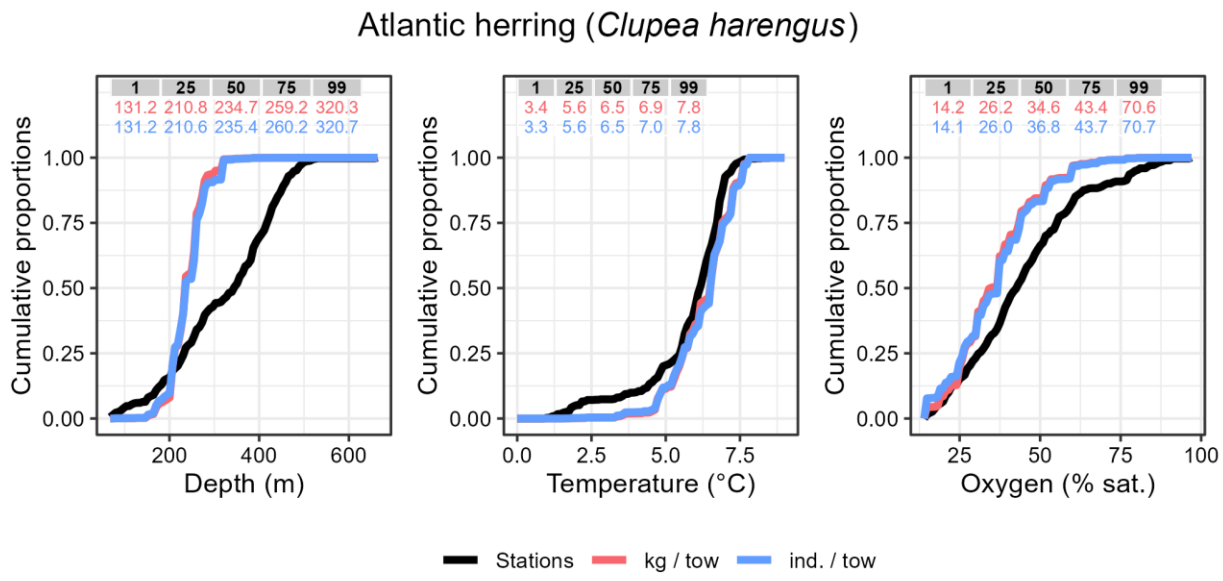


Figure 7c. Cumulative proportions of available values of depth, temperature and dissolved oxygen and standardized catches per tow for the Atlantic herring in the winter survey in 2022, 2023 and 2024.

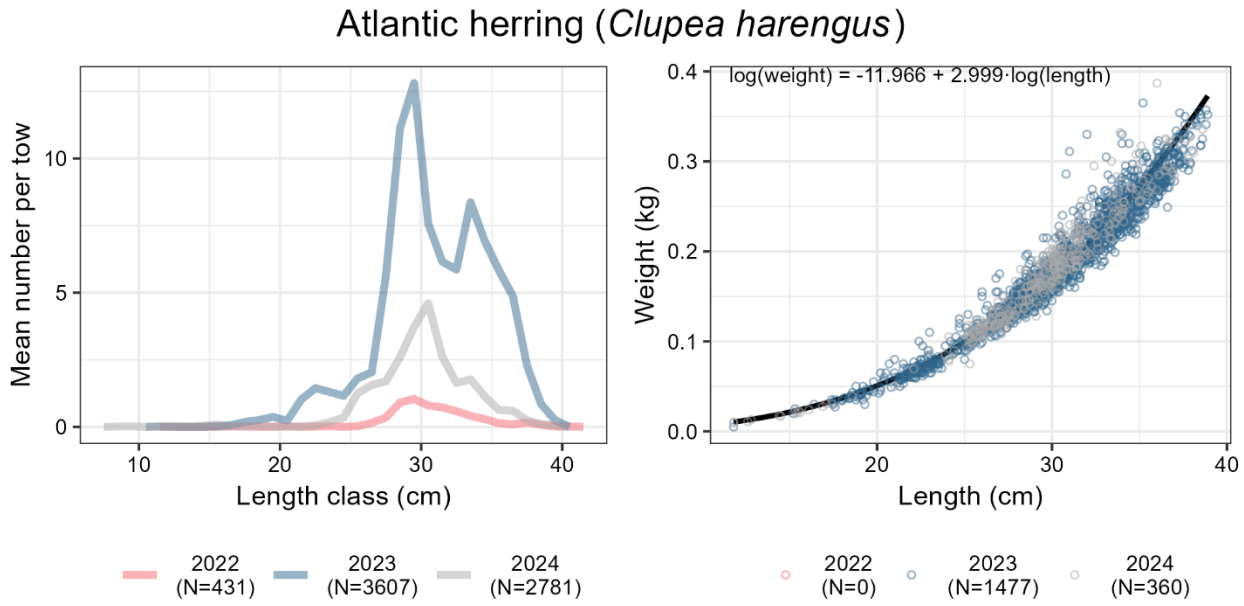


Figure 7d. Annual length frequencies (left panel) and length-weight observations with the global relationship prediction (right panel) for the Atlantic herring in the winter survey in 2022, 2023 and 2024.

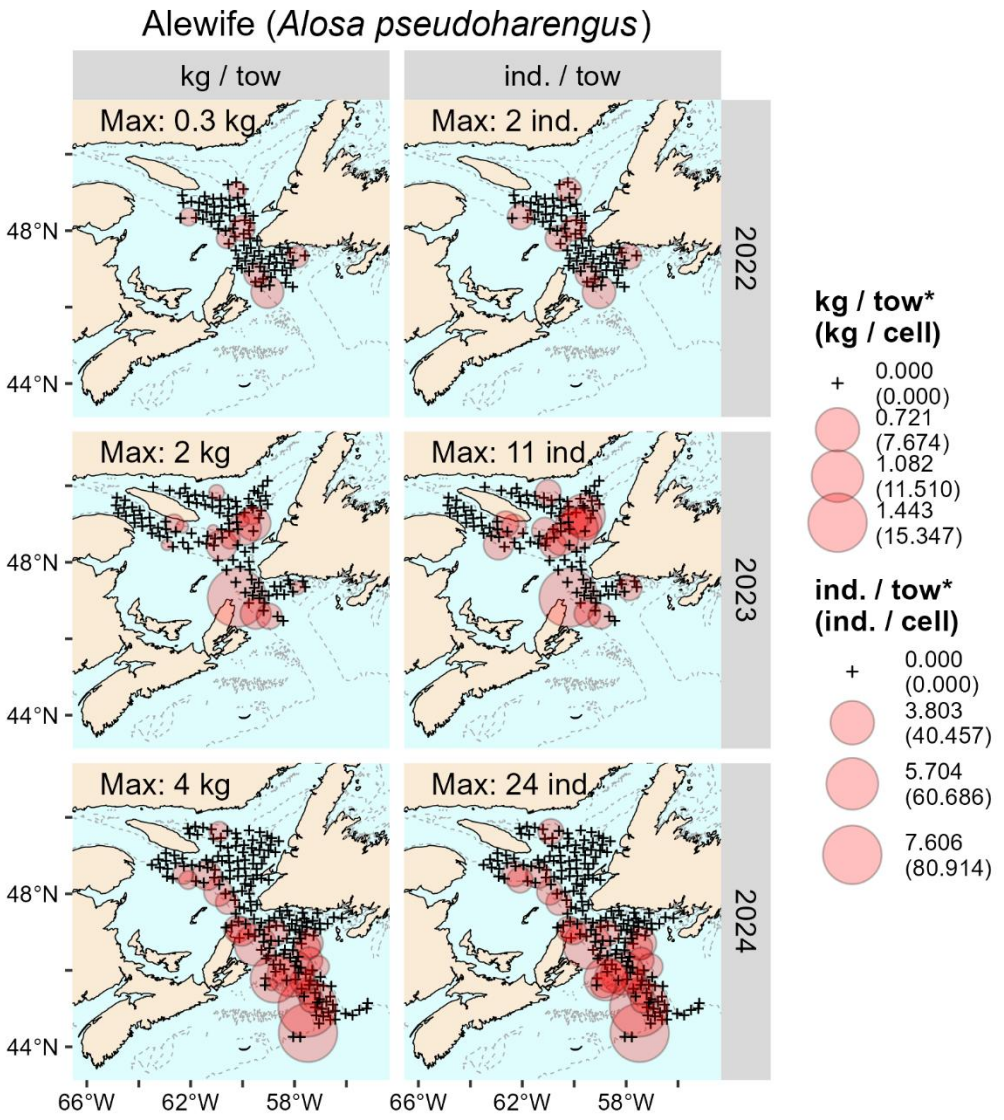


Figure 8a. Standardized catches by weight and/or number (colored bubbles) and cases of absence (black crosses) for the alewife in the winter surveys of 2022, 2023, and 2024.

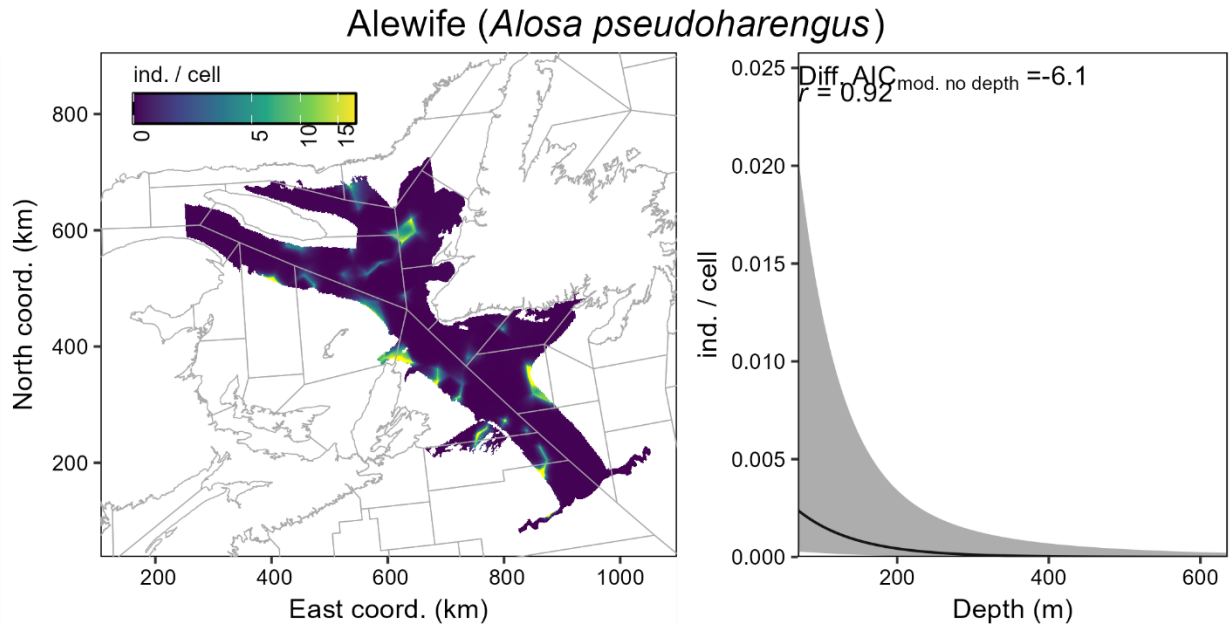


Figure 8b. Predicted number values per 0.25 km^2 cell according to the selected spatial interpolation model for the alewife in the 2022, 2023, and 2024 winter survey.

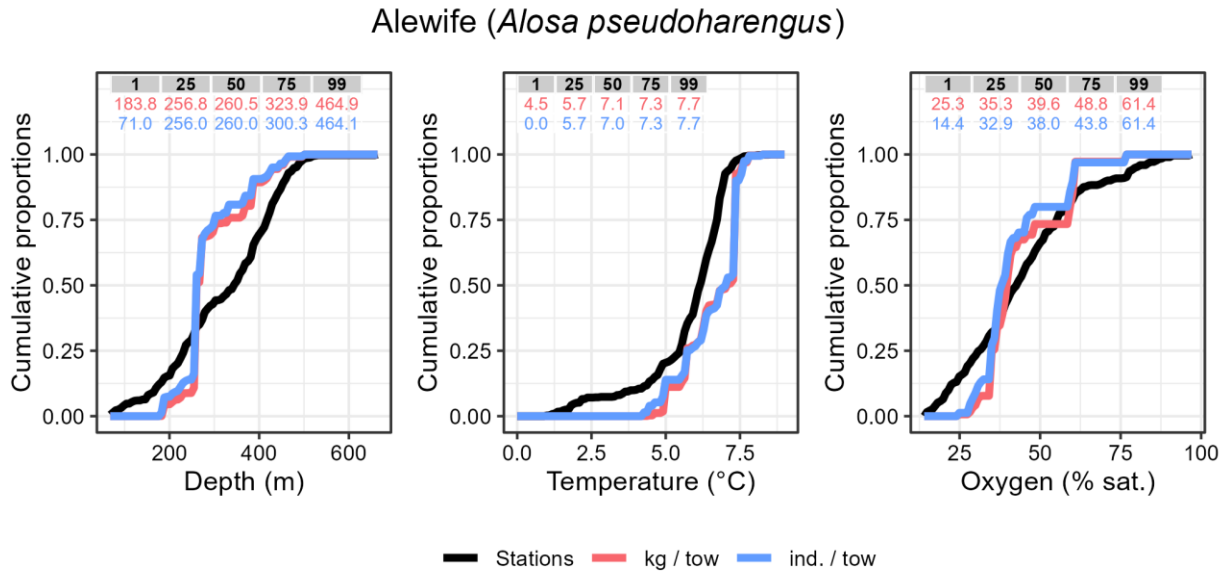


Figure 8c. Cumulative proportions of available values of depth, temperature and dissolved oxygen and standardized catches per tow for the alewife in the winter survey in 2022, 2023 and 2024.

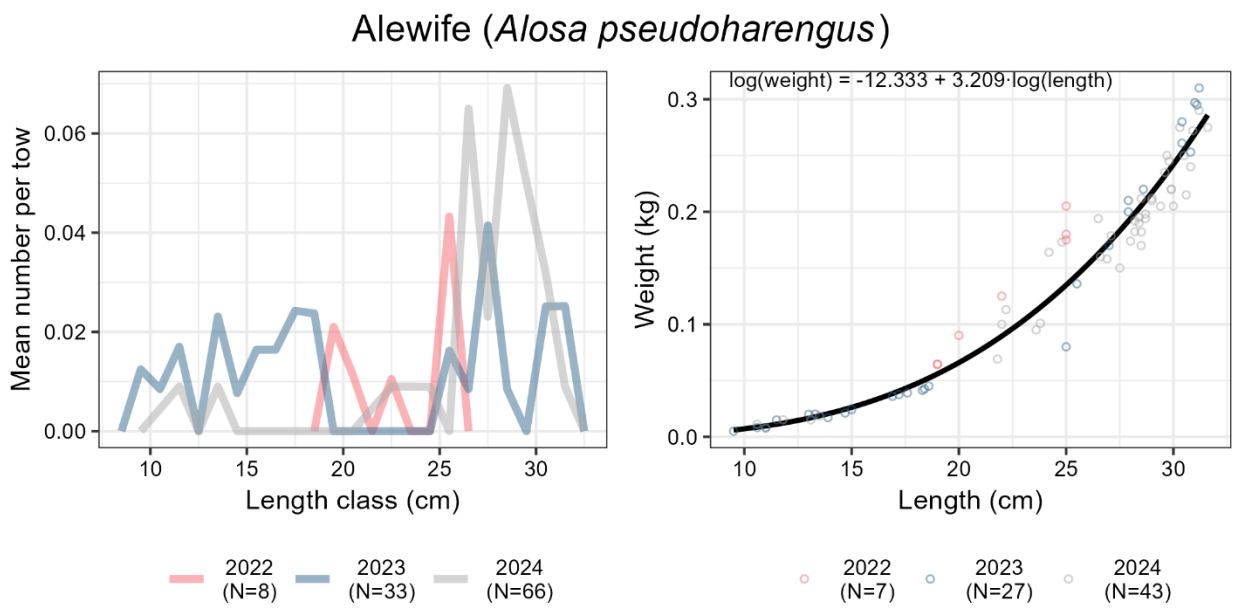


Figure 8d. Annual length frequencies (left panel) and length-weight observations with the global relationship prediction (right panel) for the alewife in the winter survey in 2022, 2023 and 2024.

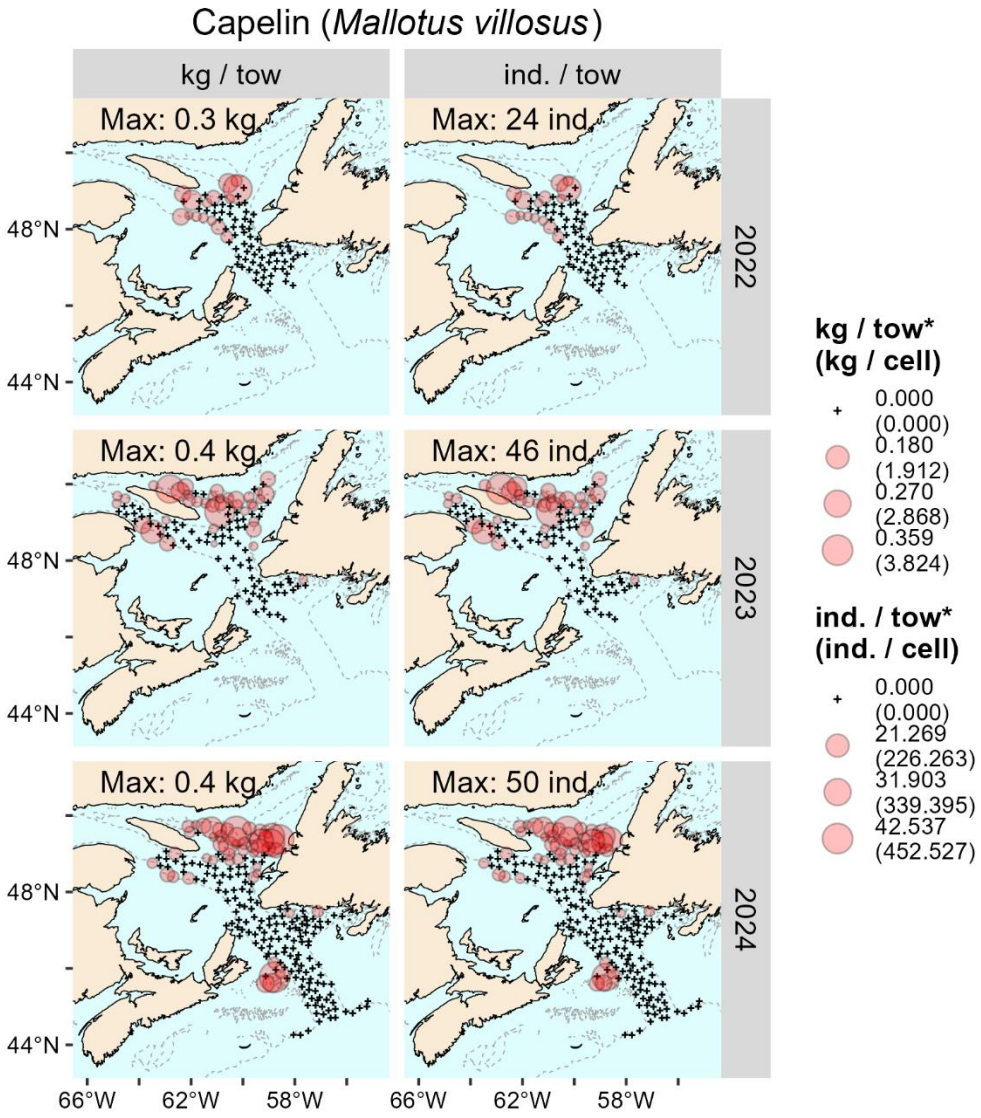


Figure 9a. Standardized catches by weight and/or number (colored bubbles) and cases of absence (black crosses) for the capelin in the winter surveys of 2022, 2023, and 2024.

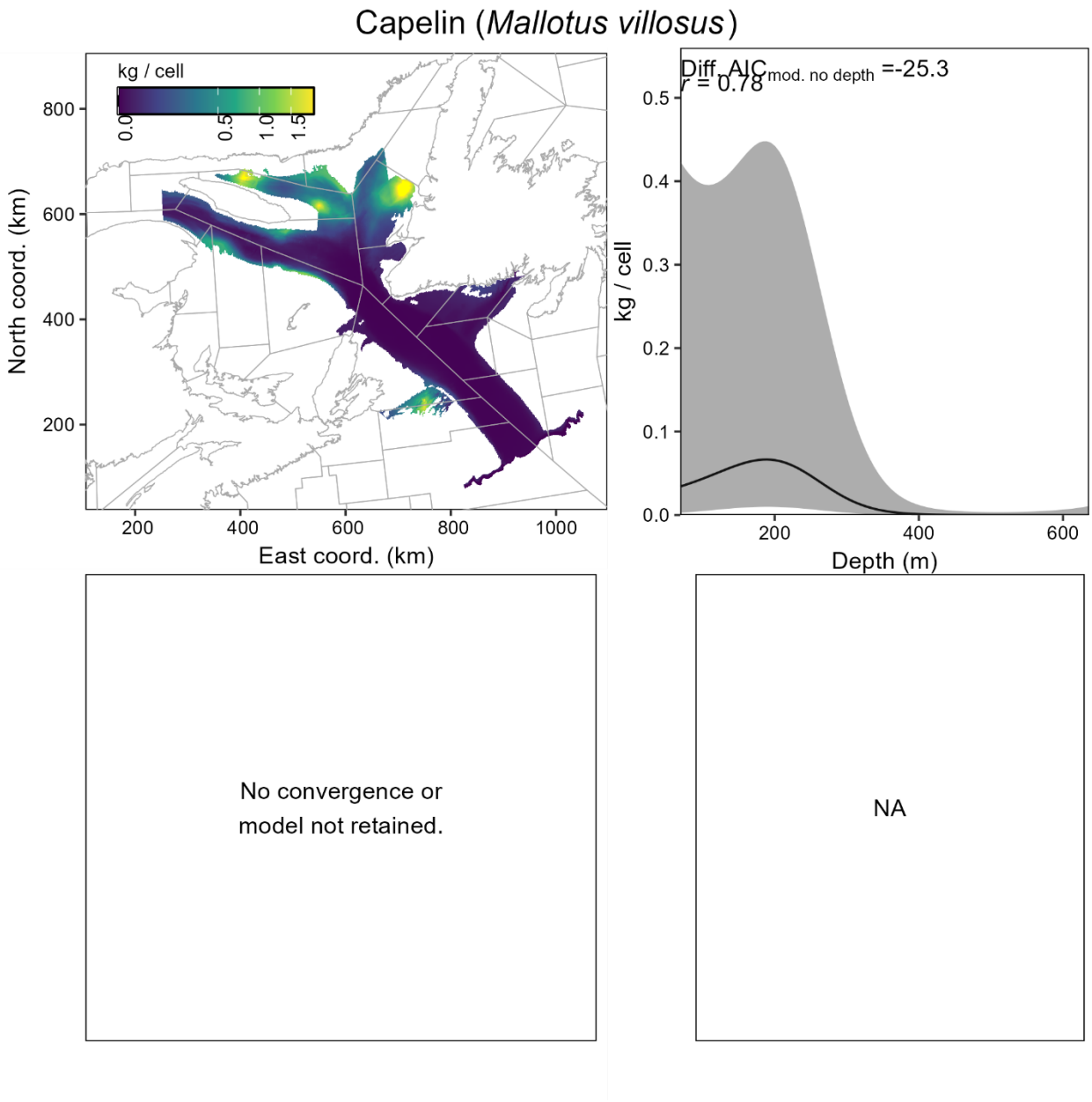


Figure 9b. Predicted weight (upper panels) and number (lower panels) values per 0.25 km^2 cell according to the selected spatial interpolation models for the capelin in the 2022, 2023, and 2024 winter survey.

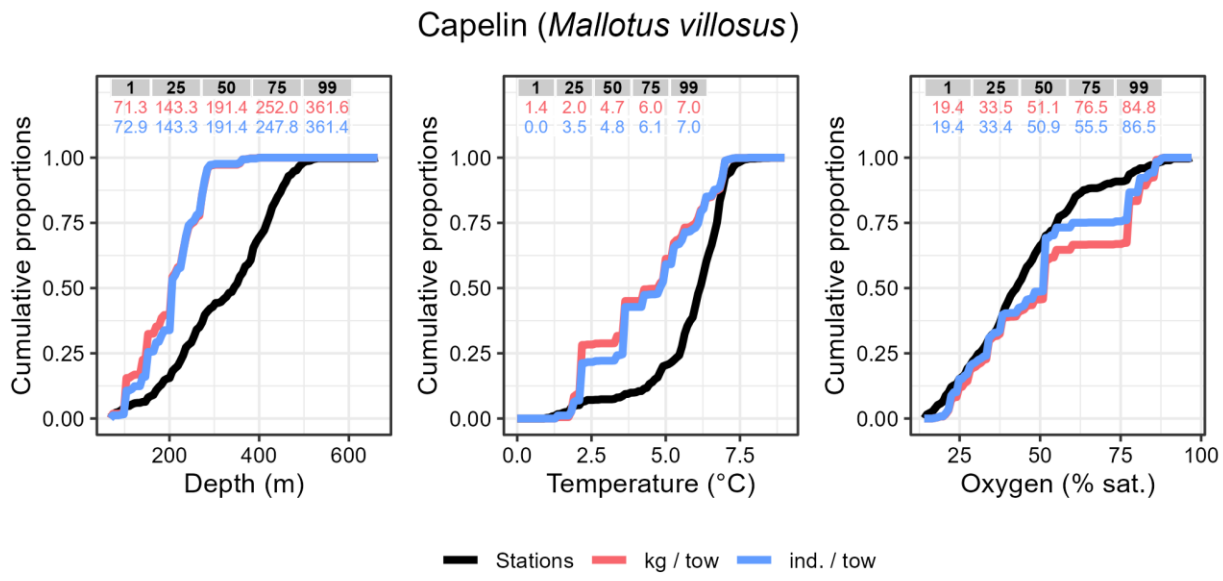


Figure 9c. Cumulative proportions of available values of depth, temperature and dissolved oxygen and standardized catches per tow for the capelin in the winter survey in 2022, 2023 and 2024.

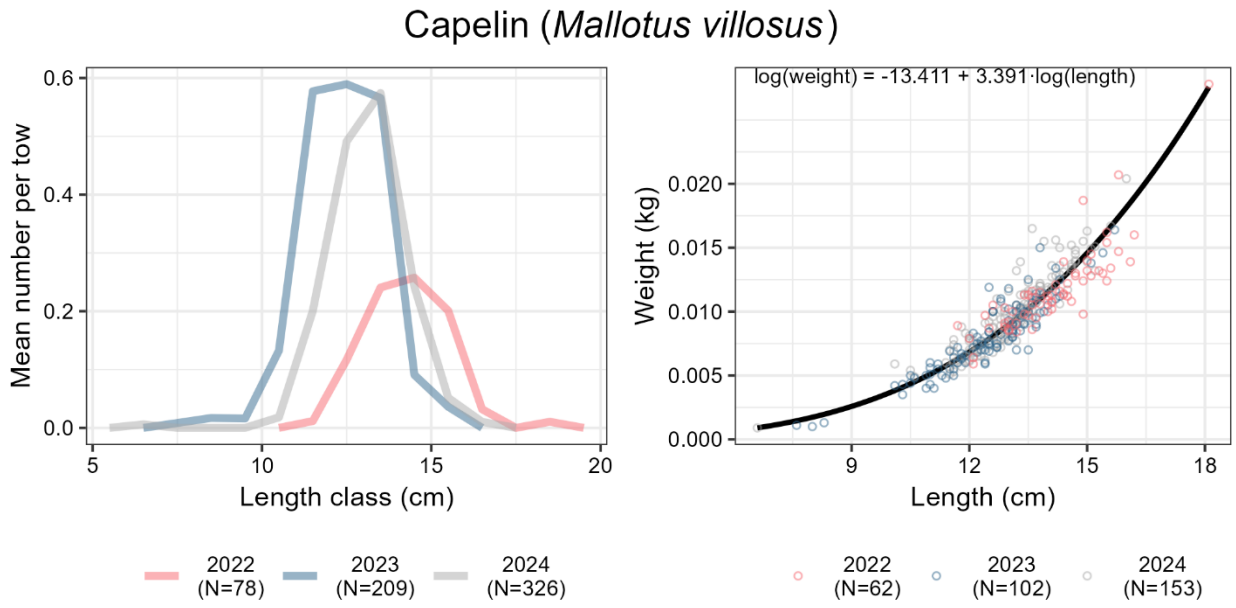


Figure 9d. Annual length frequencies (left panel) and length-weight observations with the global relationship prediction (right panel) for the capelin in the winter survey in 2022, 2023 and 2024.

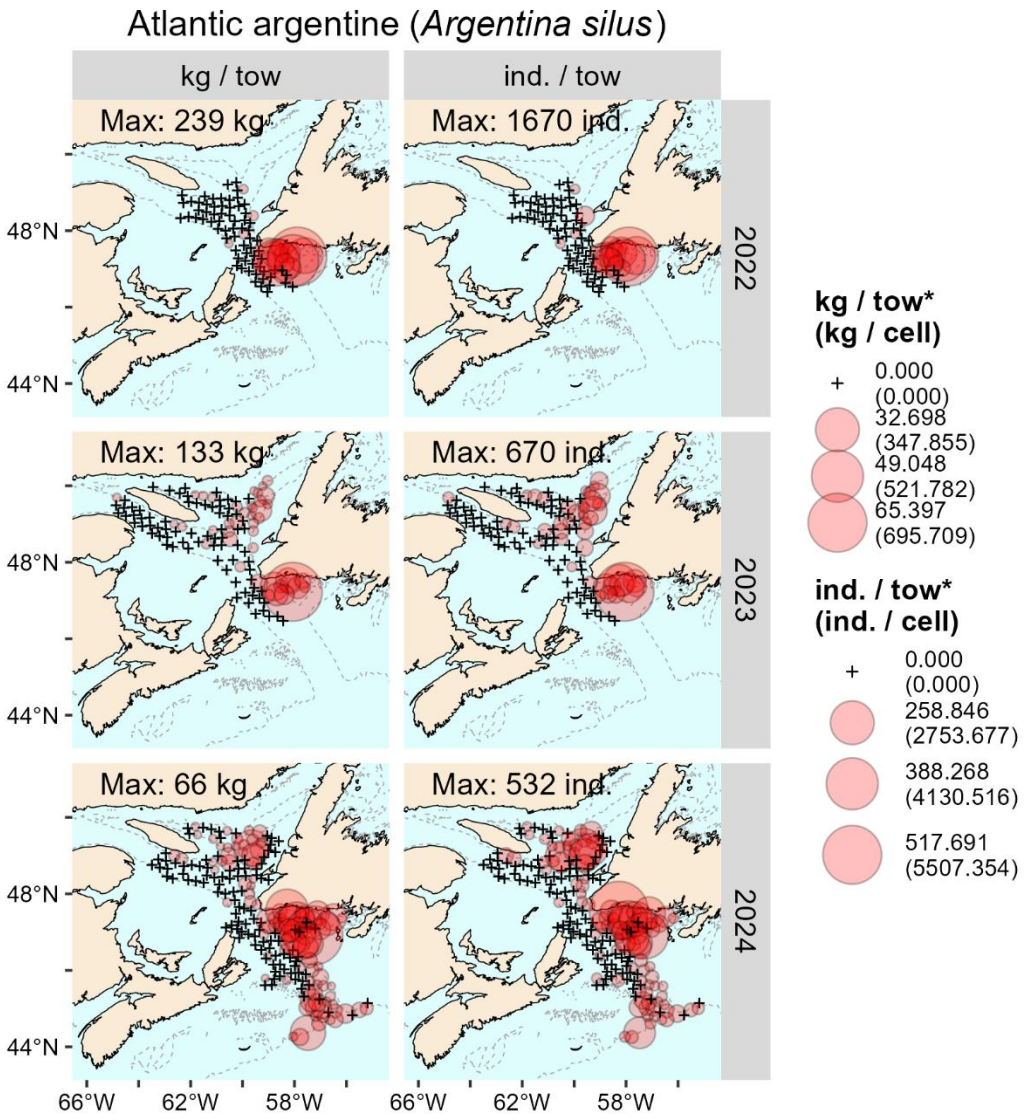


Figure 10a. Standardized catches by weight and/or number (colored bubbles) and cases of absence (black crosses) for the Atlantic argentine in the winter surveys of 2022, 2023, and 2024.

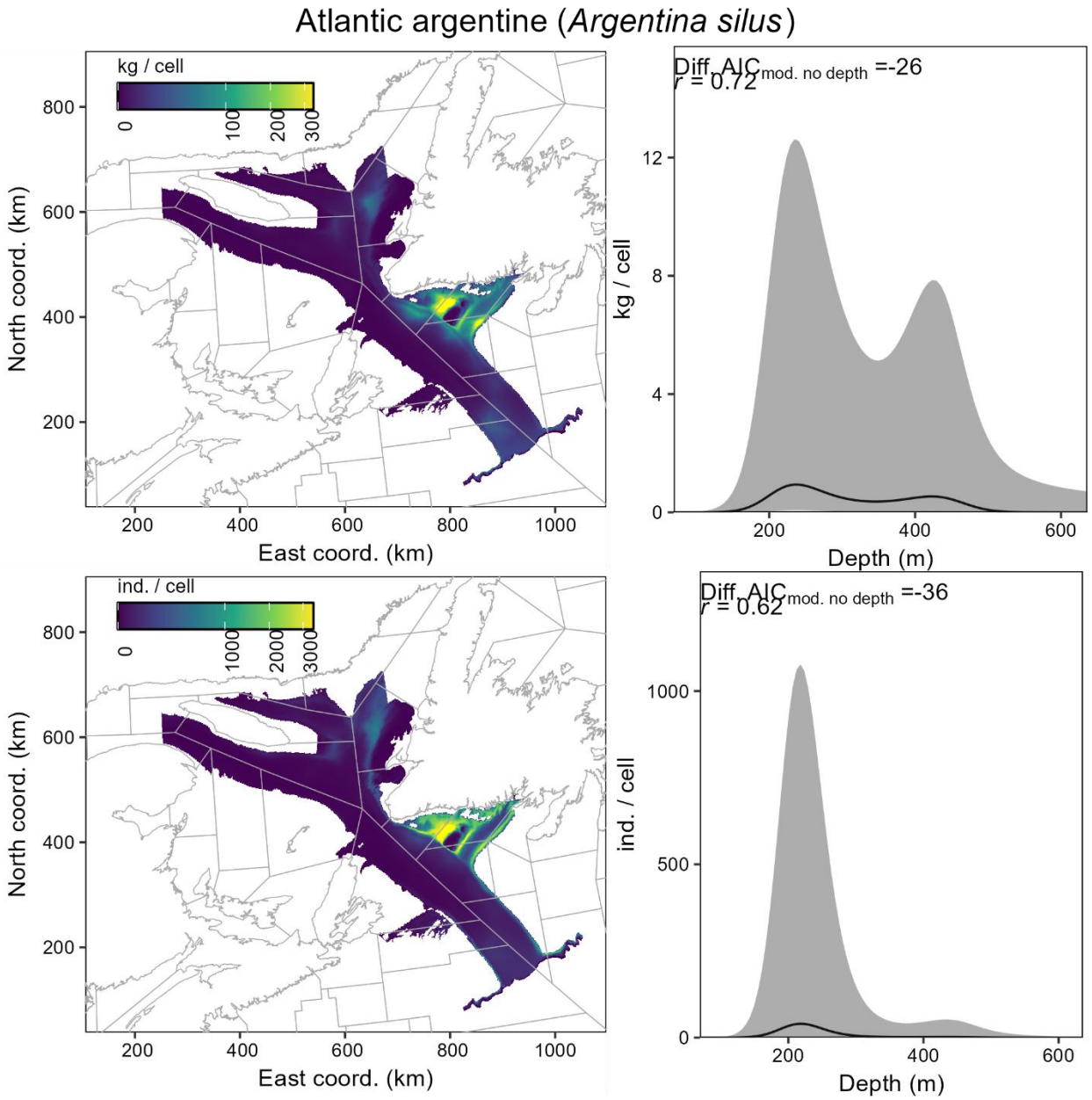


Figure 10b. Predicted weight (upper panels) and number (lower panels) values per 0.25 km^2 cell according to the selected spatial interpolation models for the Atlantic argentine in the 2022, 2023, and 2024 winter survey.

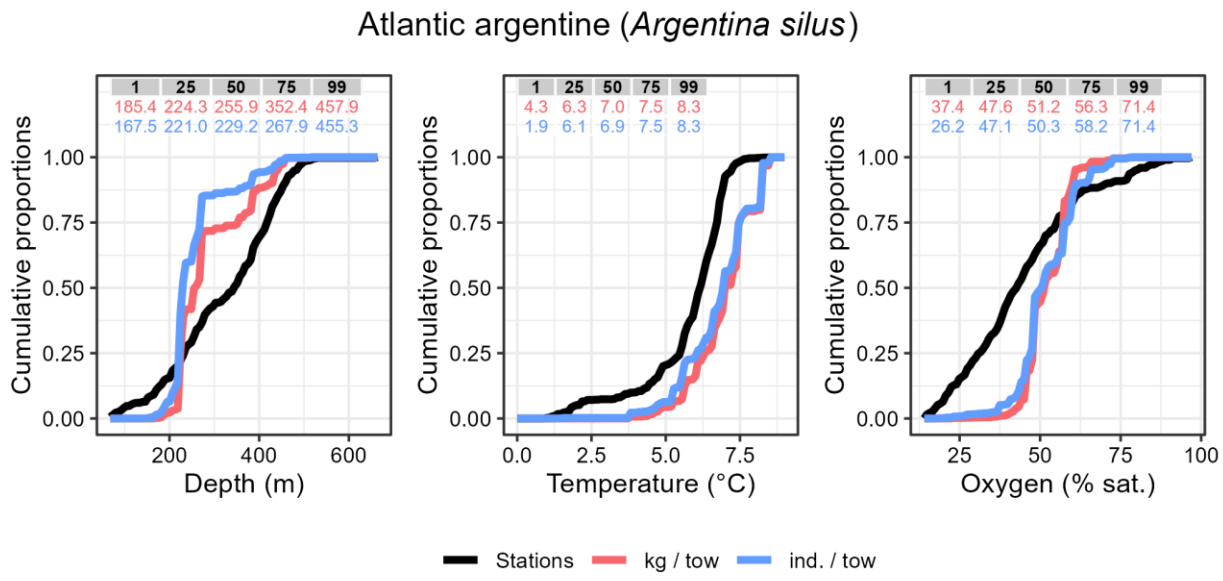


Figure 10c. Cumulative proportions of available values of depth, temperature and dissolved oxygen and standardized catches per tow for the Atlantic argentine in the winter survey in 2022, 2023 and 2024.

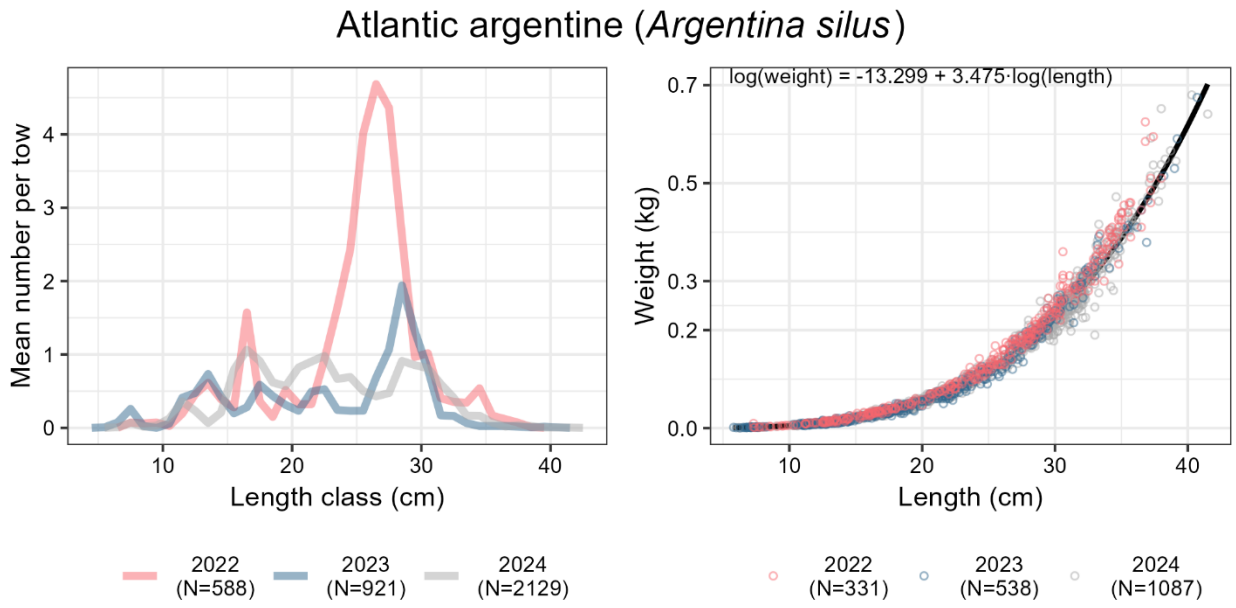


Figure 10d. Annual length frequencies (left panel) and length-weight observations with the global relationship prediction (right panel) for the Atlantic argentine in the winter survey in 2022, 2023 and 2024.

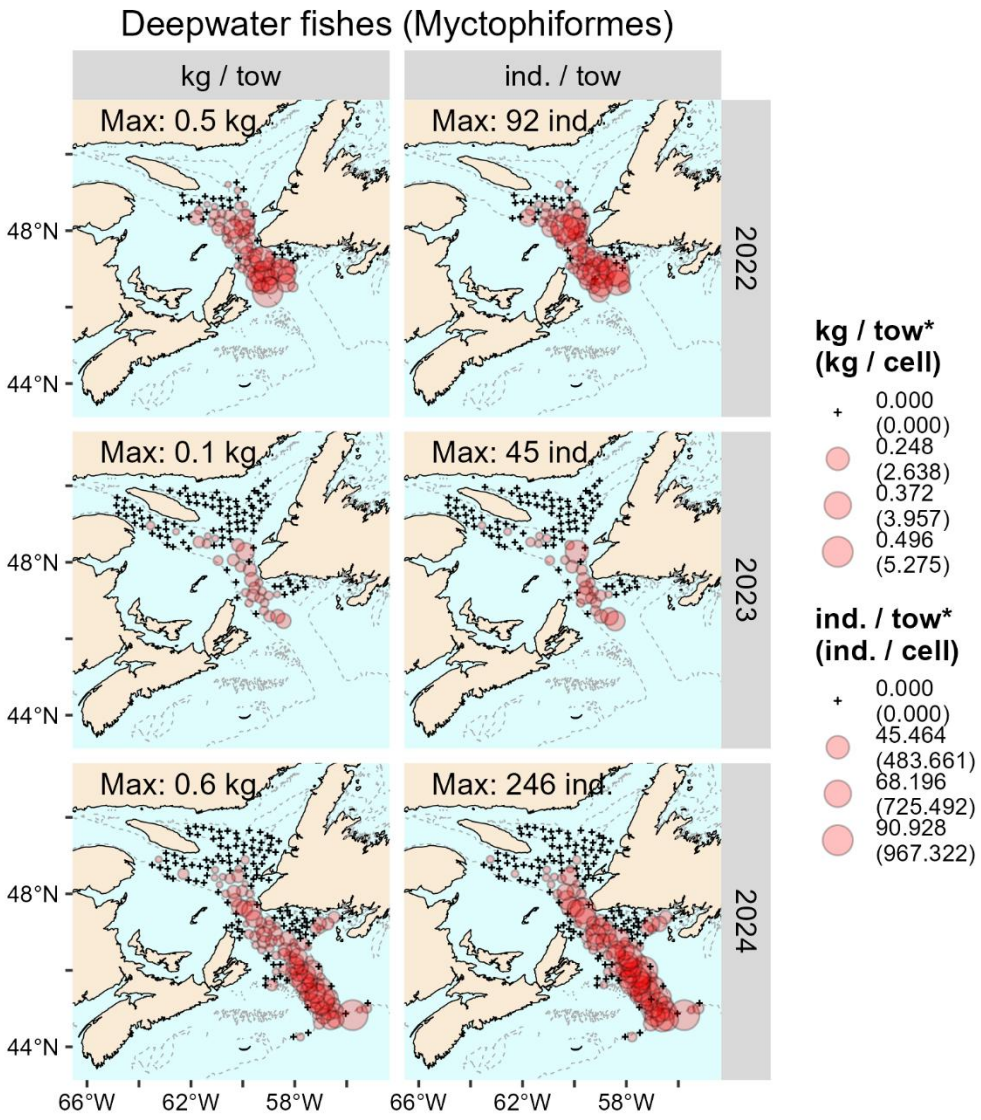


Figure 11a. Standardized catches by weight and/or number (colored bubbles) and cases of absence (black crosses) for deepwater fishes (Myctophiformes) in the winter surveys of 2022, 2023, and 2024.

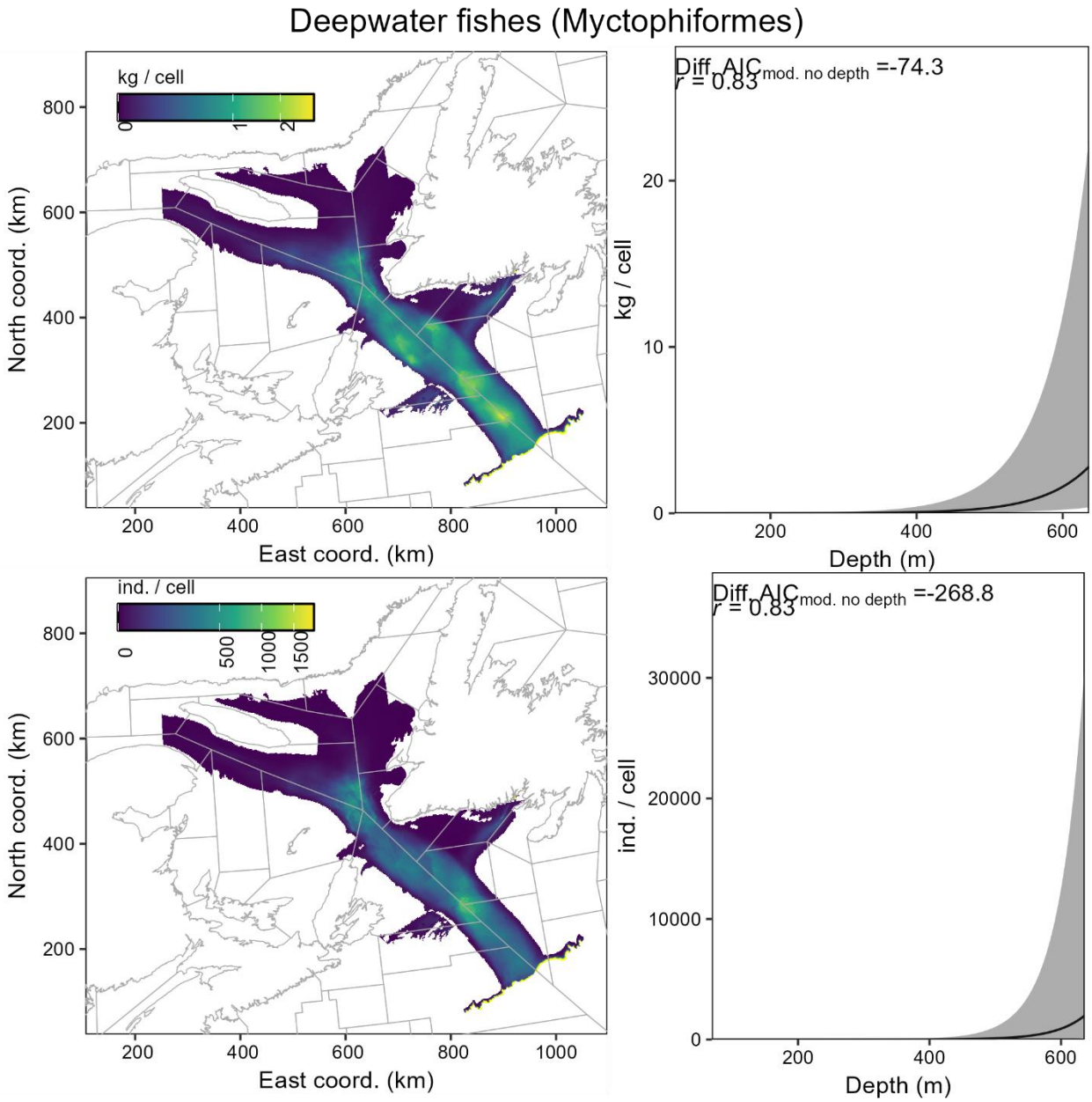


Figure 11b. Predicted weight (upper panels) and number (lower panels) values per 0.25 km^2 cell according to the selected spatial interpolation models for deepwater fishes (Myctophiformes) in the 2022, 2023, and 2024 winter survey.

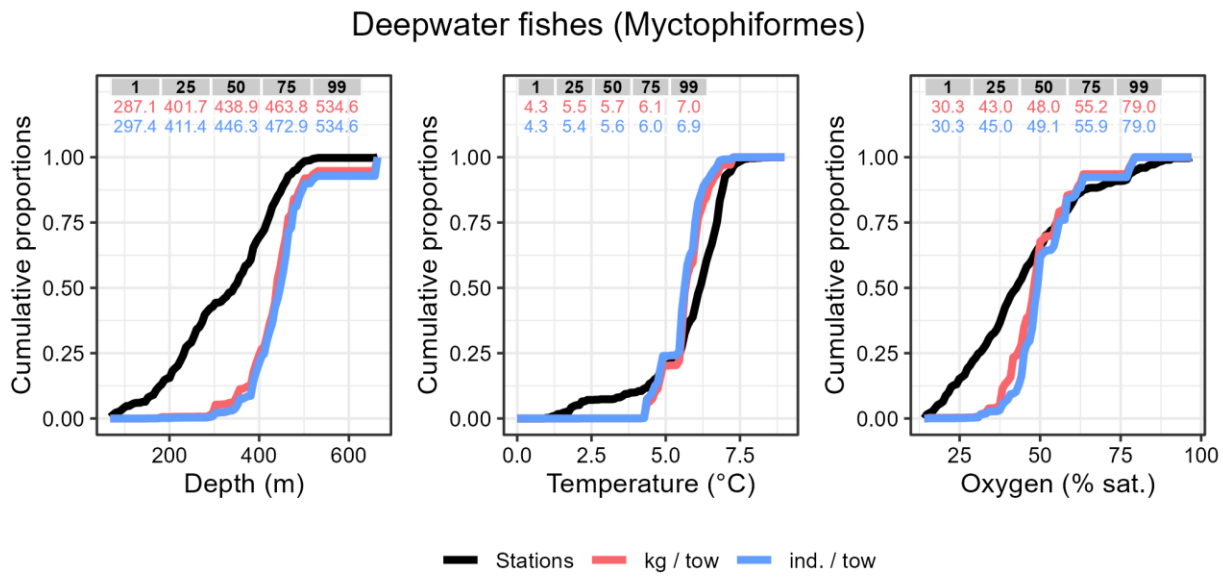


Figure 11c. Cumulative proportions of available values of depth, temperature and dissolved oxygen and standardized catches per tow for deepwater fishes (Myctophiformes) in the winter survey in 2022, 2023 and 2024.

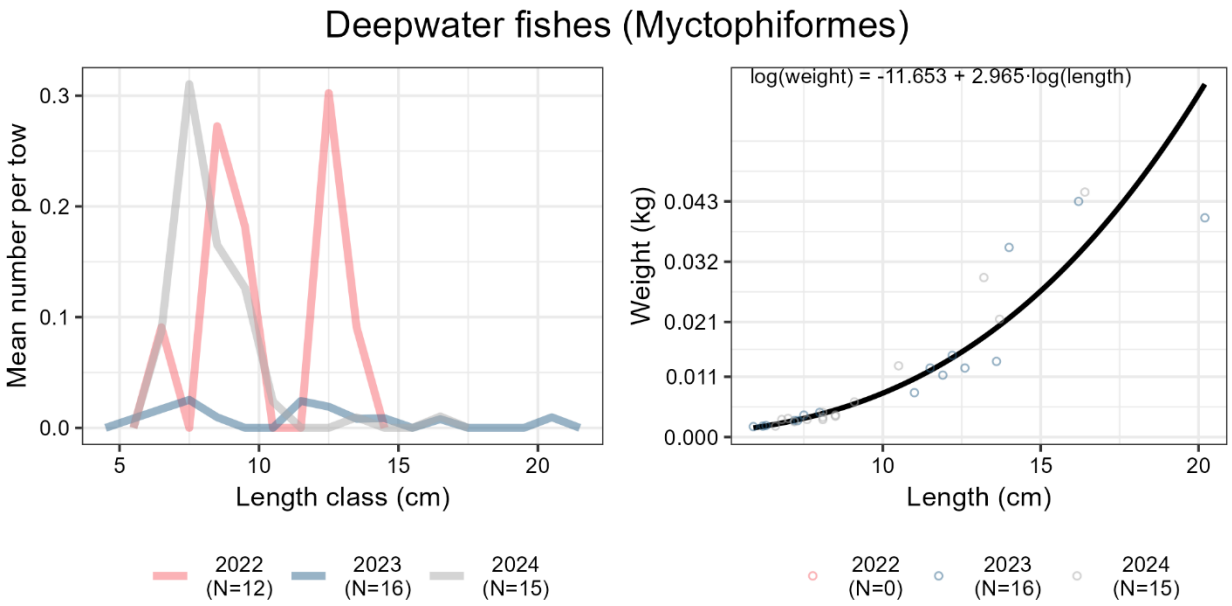


Figure 11d. Annual length frequencies (left panel) and length-weight observations with the global relationship prediction (right panel) for deepwater fishes (Myctophiformes) in the winter survey in 2022, 2023 and 2024.

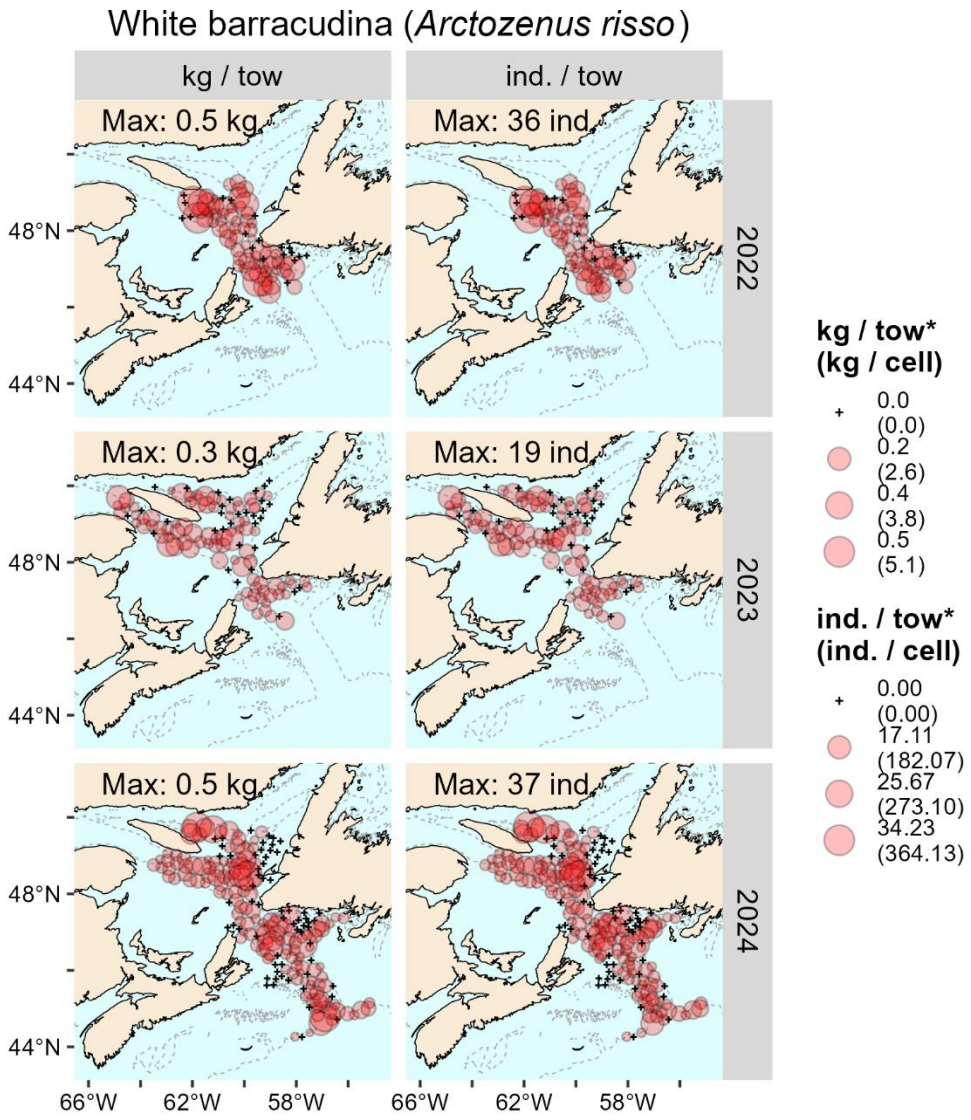


Figure 12a. Standardized catches by weight and/or number (colored bubbles) and cases of absence (black crosses) for the white barracudina in the winter surveys of 2022, 2023, and 2024.

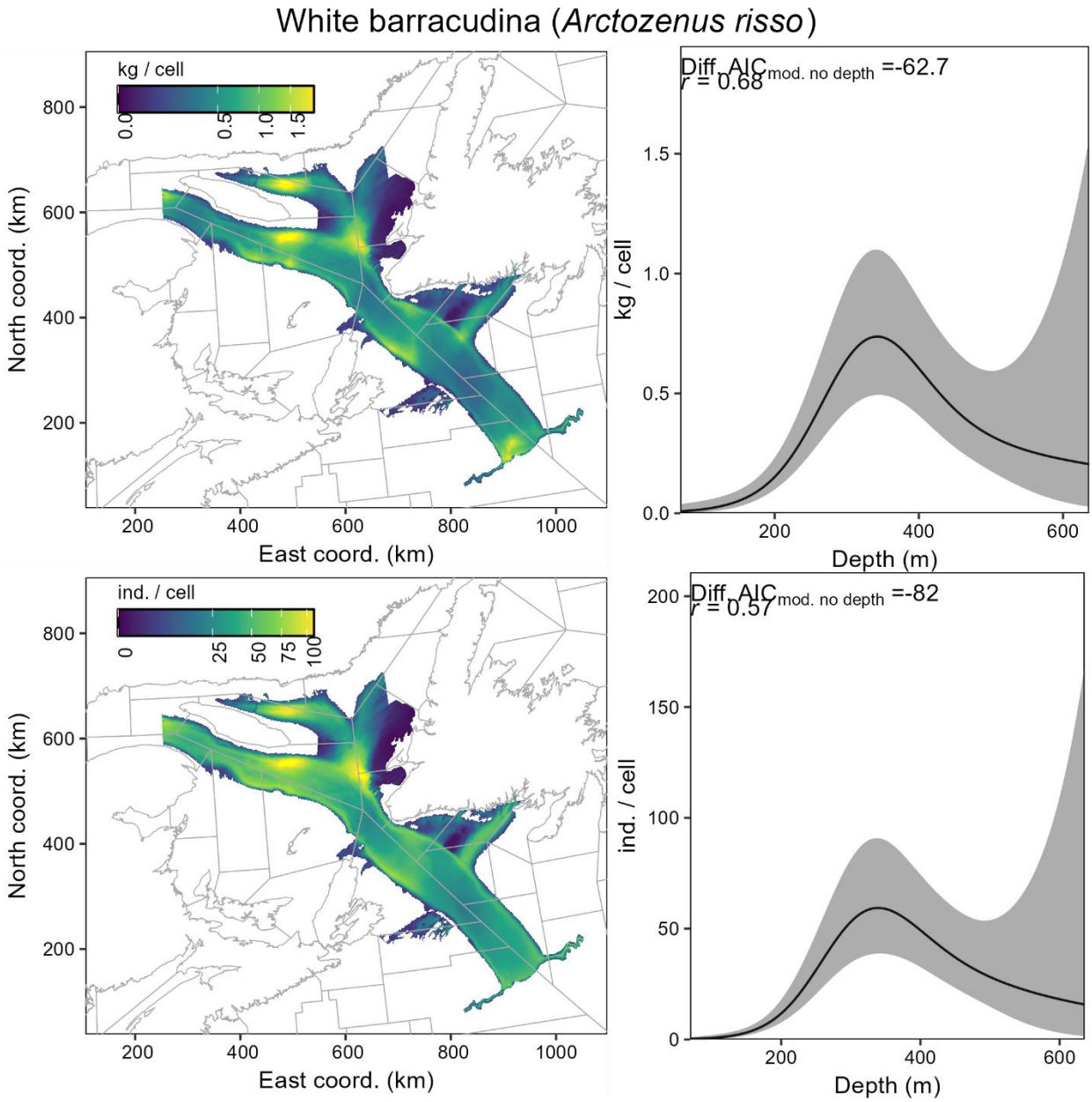


Figure 12b. Predicted weight (upper panels) and number (lower panels) values per 0.25 km^2 cell according to the selected spatial interpolation models for the white barracudina in the 2022, 2023, and 2024 winter survey.

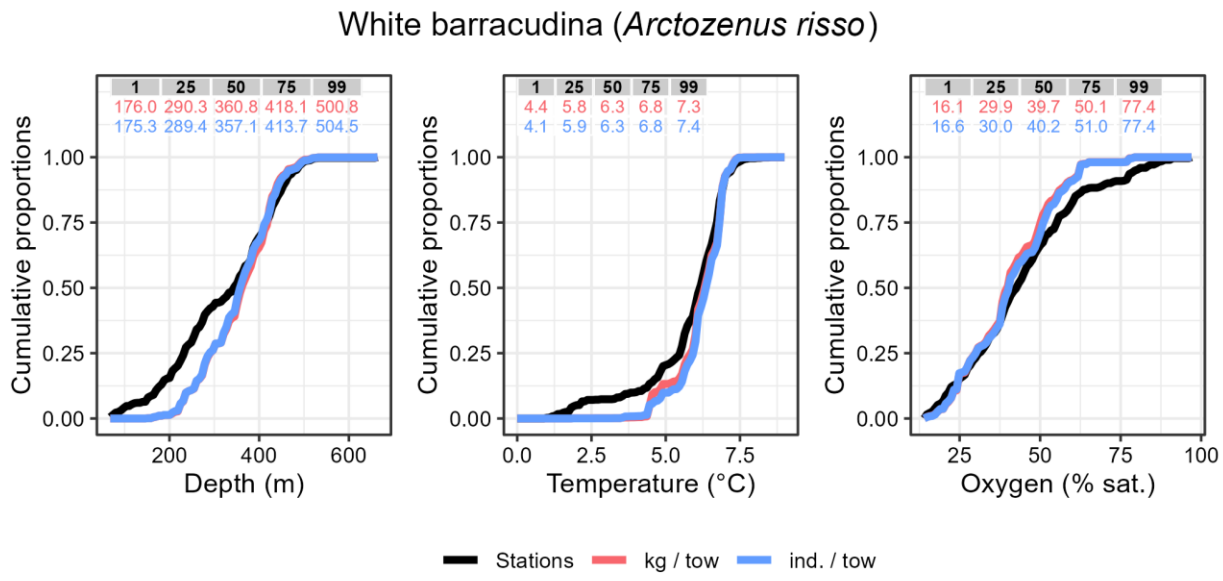


Figure 12c. Cumulative proportions of available values of depth, temperature and dissolved oxygen and standardized catches per tow for the white barracudina in the winter survey in 2022, 2023 and 2024.

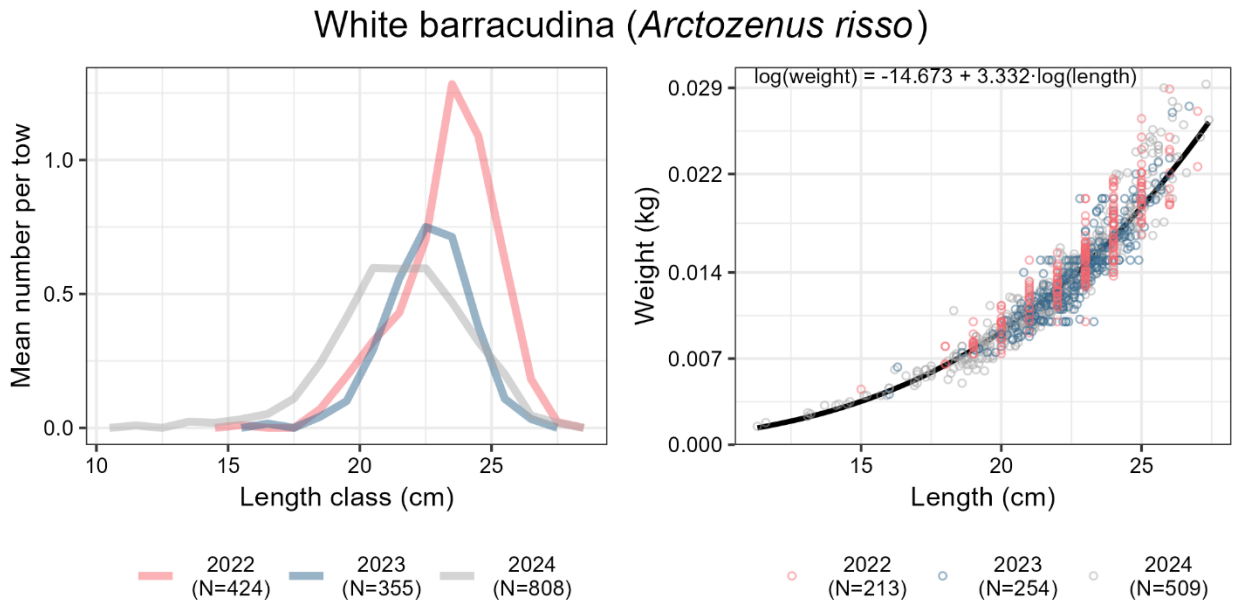


Figure 12d. Annual length frequencies (left panel) and length-weight observations with the global relationship prediction (right panel) for the white barracudina in the winter survey in 2022, 2023 and 2024.

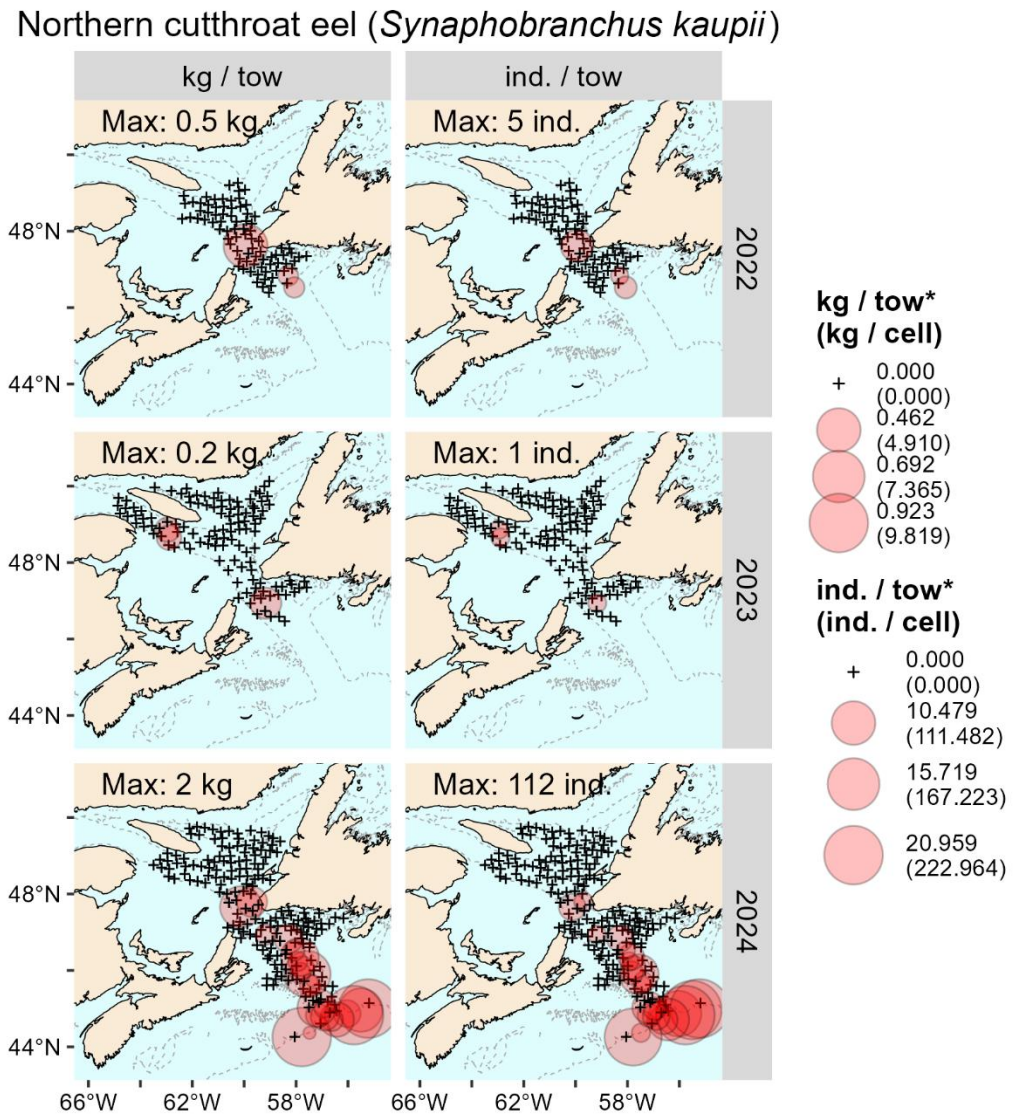


Figure 13a. Standardized catches by weight and/or number (colored bubbles) and cases of absence (black crosses) for the Northern cutthroat eel in the winter surveys of 2022, 2023, and 2024.

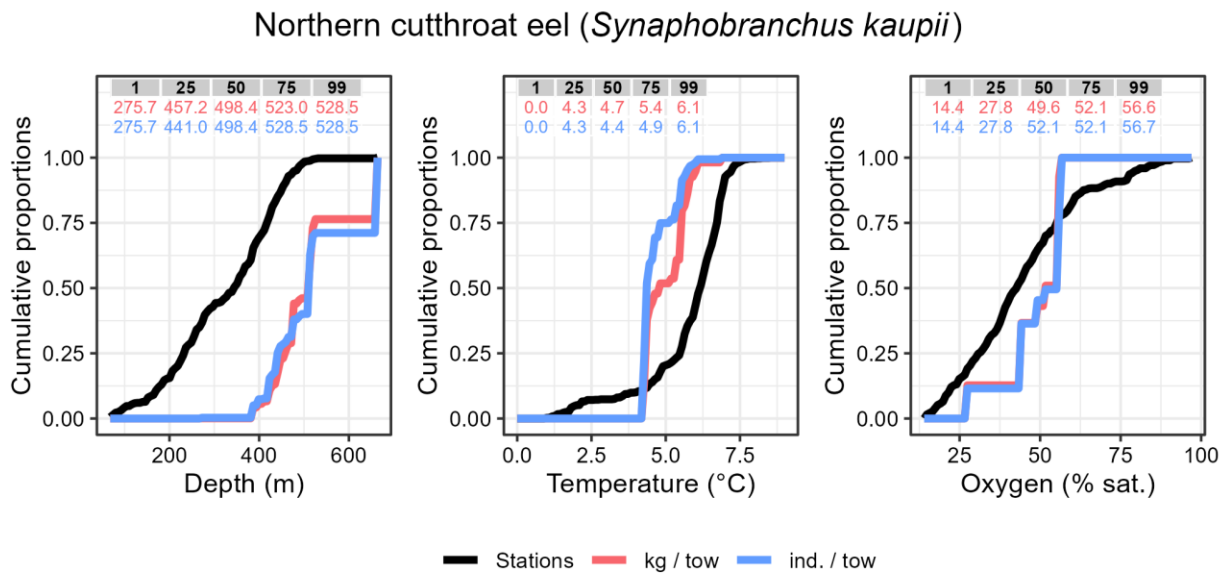


Figure 13b. Cumulative proportions of available values of depth, temperature and dissolved oxygen and standardized catches per tow for the Northern cutthroat eel in the winter survey in 2022, 2023 and 2024.

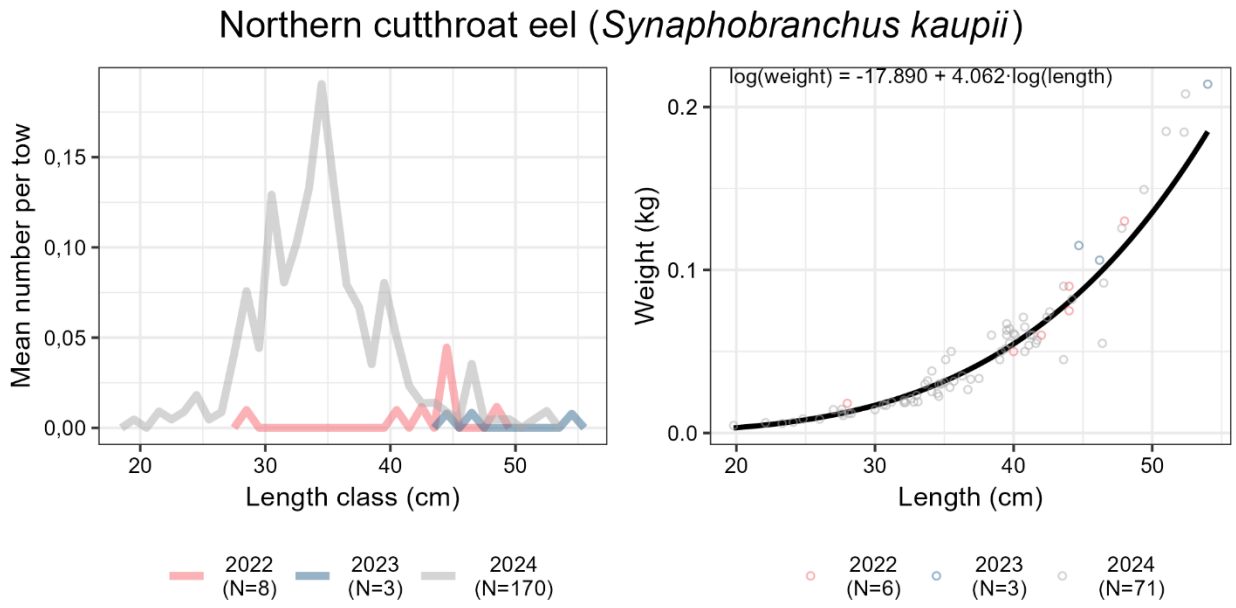


Figure 13c. Annual length frequencies (left panel) and length-weight observations with the global relationship prediction (right panel) for the Northern cutthroat eel in the winter survey in 2022, 2023 and 2024.

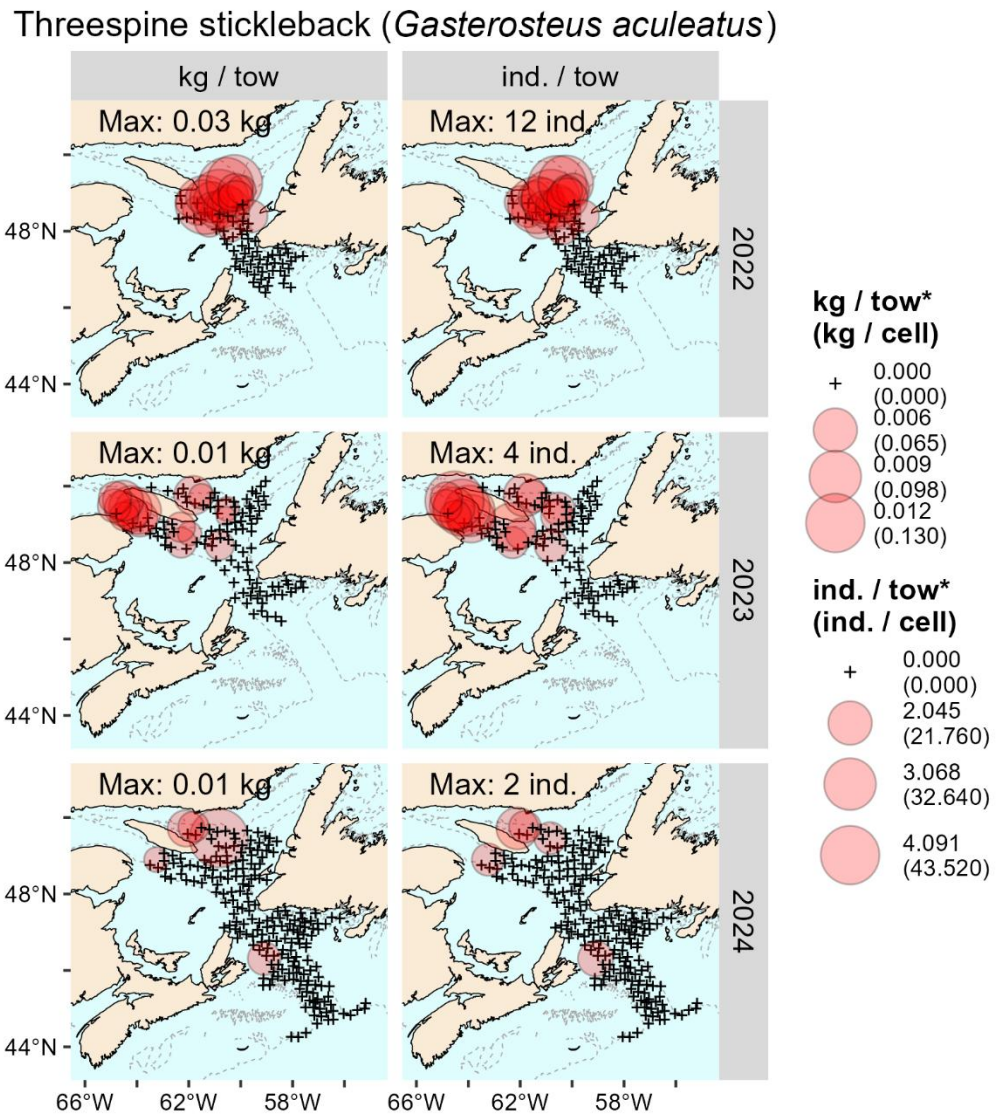


Figure 14a. Standardized catches by weight and/or number (colored bubbles) and cases of absence (black crosses) for the threespine stickleback in the winter surveys of 2022, 2023, and 2024.

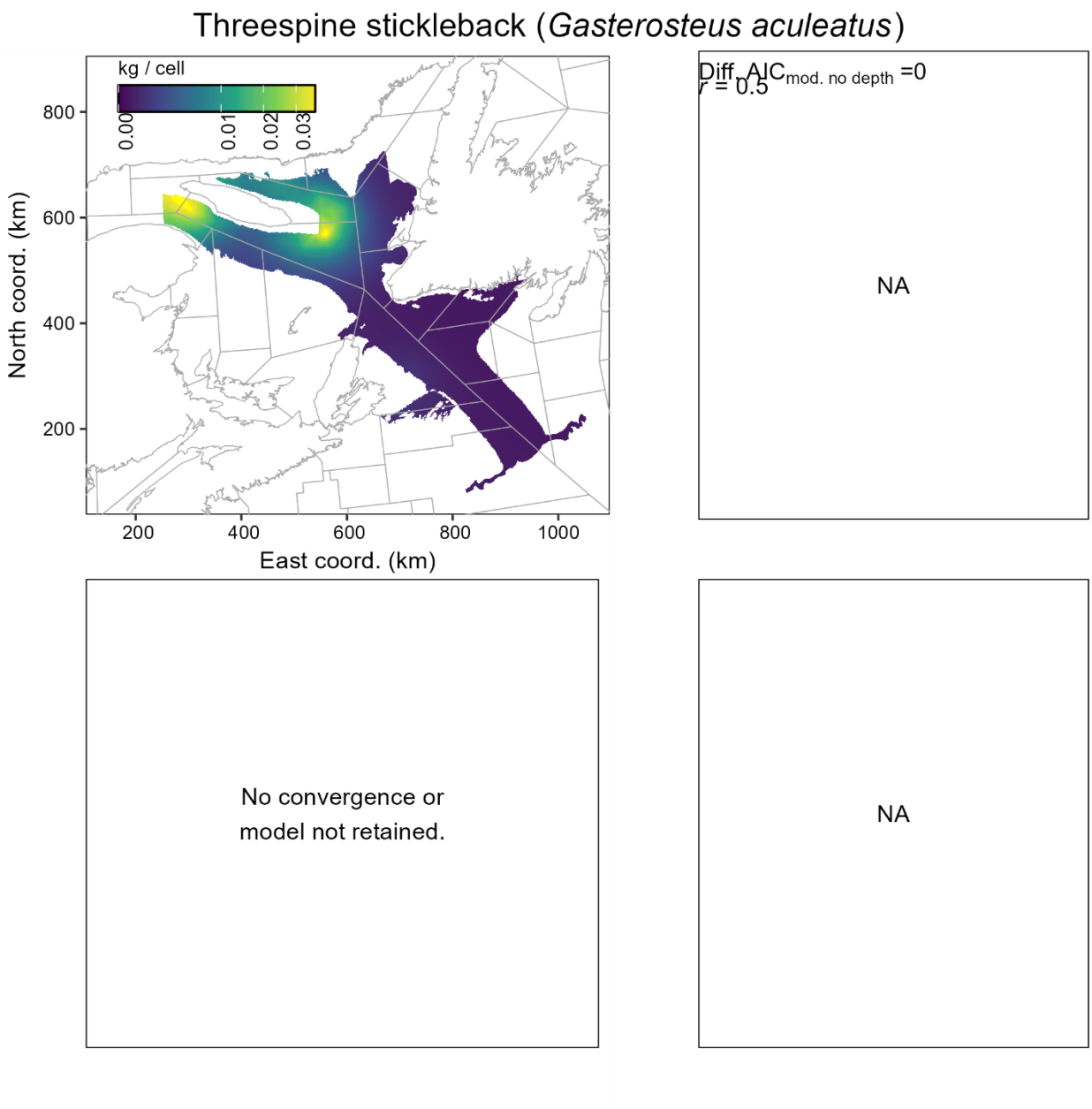


Figure 14b. Predicted weight (upper panels) and number (lower panels) values per 0.25 km^2 cell according to the selected spatial interpolation models for the threespine stickleback in the 2022, 2023, and 2024 winter survey.

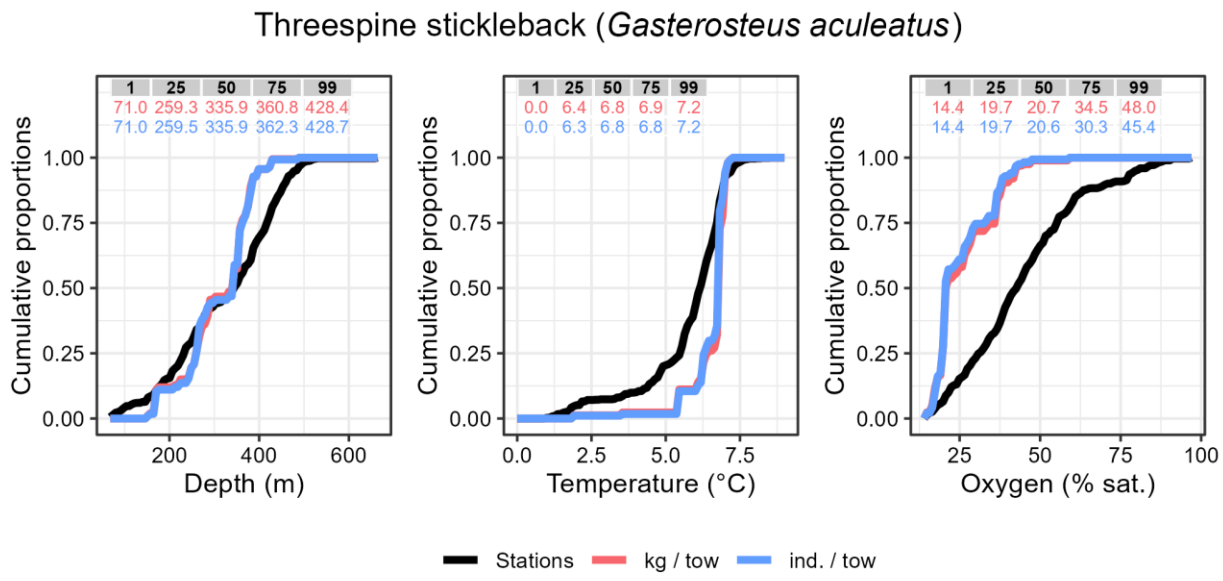


Figure 14c. Cumulative proportions of available values of depth, temperature and dissolved oxygen and standardized catches per tow for the threespine stickleback in the winter survey in 2022, 2023 and 2024.

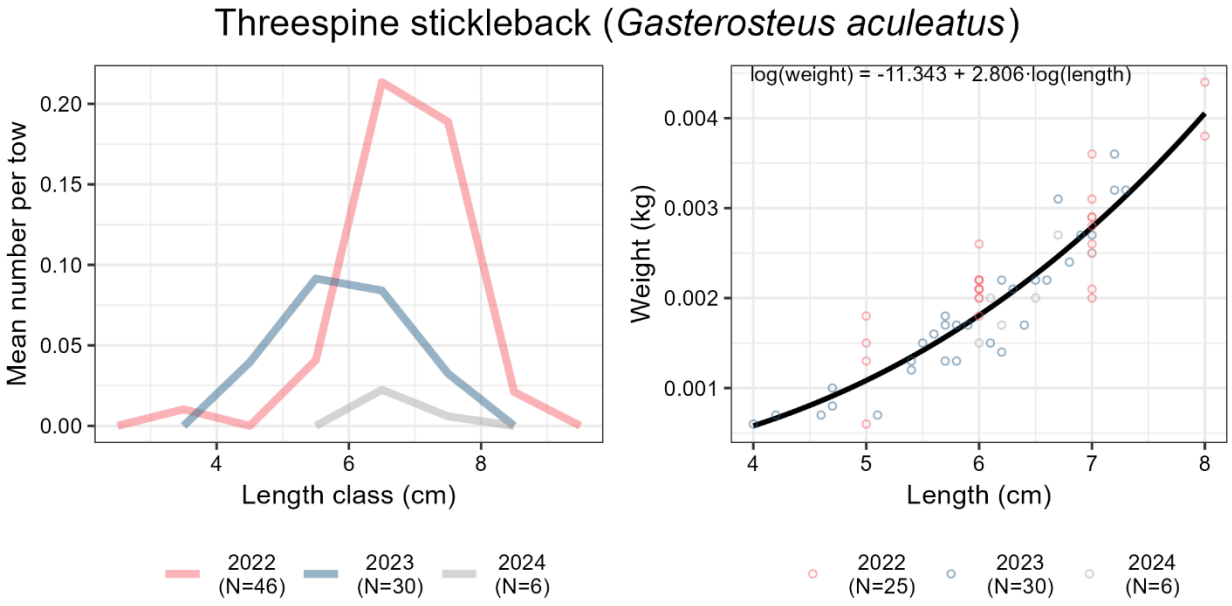


Figure 14d. Annual length frequencies (left panel) and length-weight observations with the global relationship prediction (right panel) for the threespine stickleback in the winter survey in 2022, 2023 and 2024.

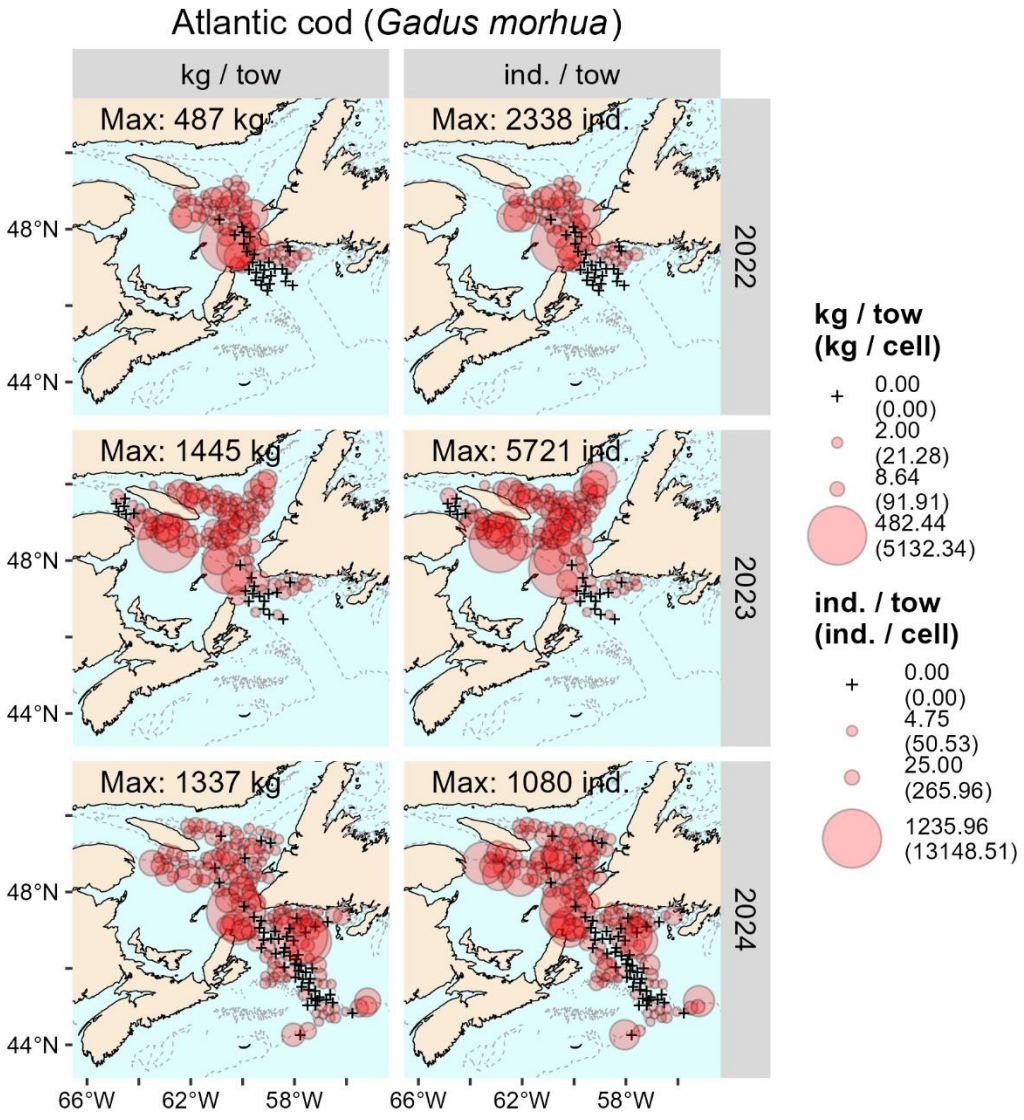


Figure 15a. Standardized catches by weight and/or number (colored bubbles) and cases of absence (black crosses) for the Atlantic cod in the winter surveys of 2022, 2023, and 2024.

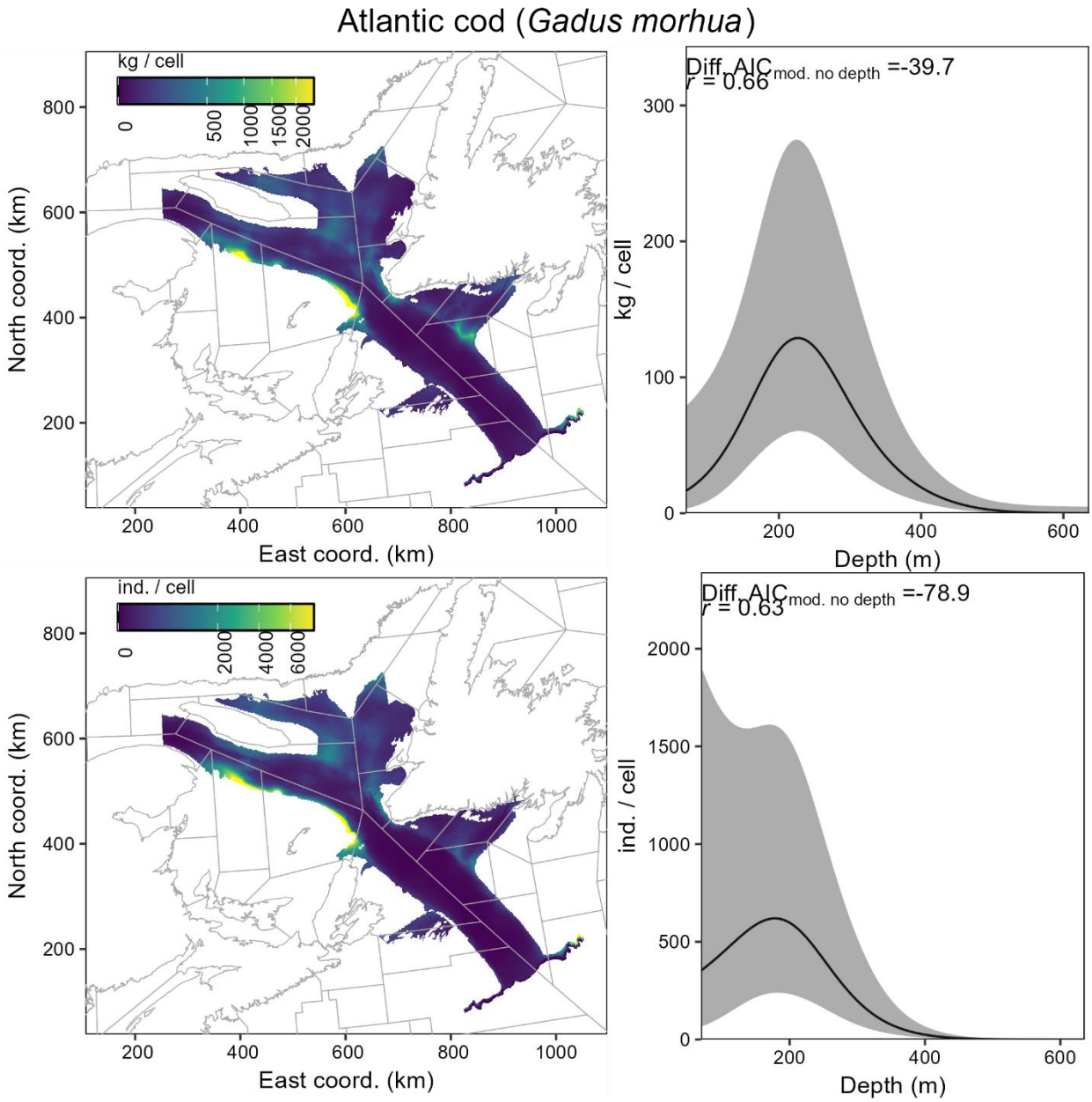


Figure 15b. Predicted weight (upper panels) and number (lower panels) values per 0.25 km^2 cell according to the selected spatial interpolation models for the Atlantic cod in the 2022, 2023, and 2024 winter survey.

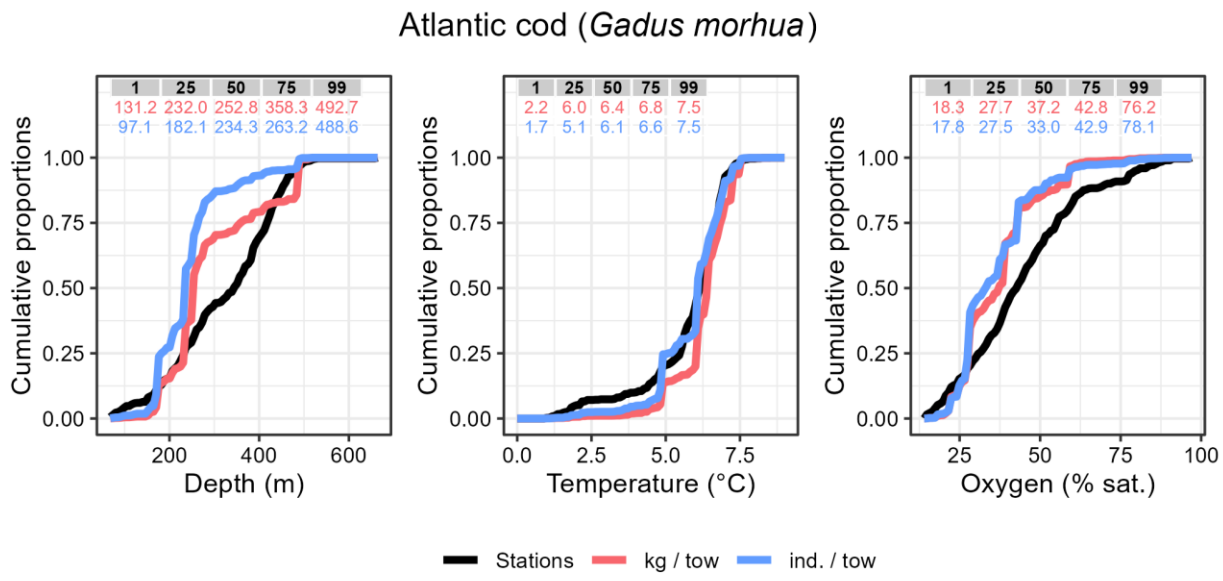


Figure 15c. Cumulative proportions of available values of depth, temperature and dissolved oxygen and standardized catches per tow for the Atlantic cod in the winter survey in 2022, 2023 and 2024.

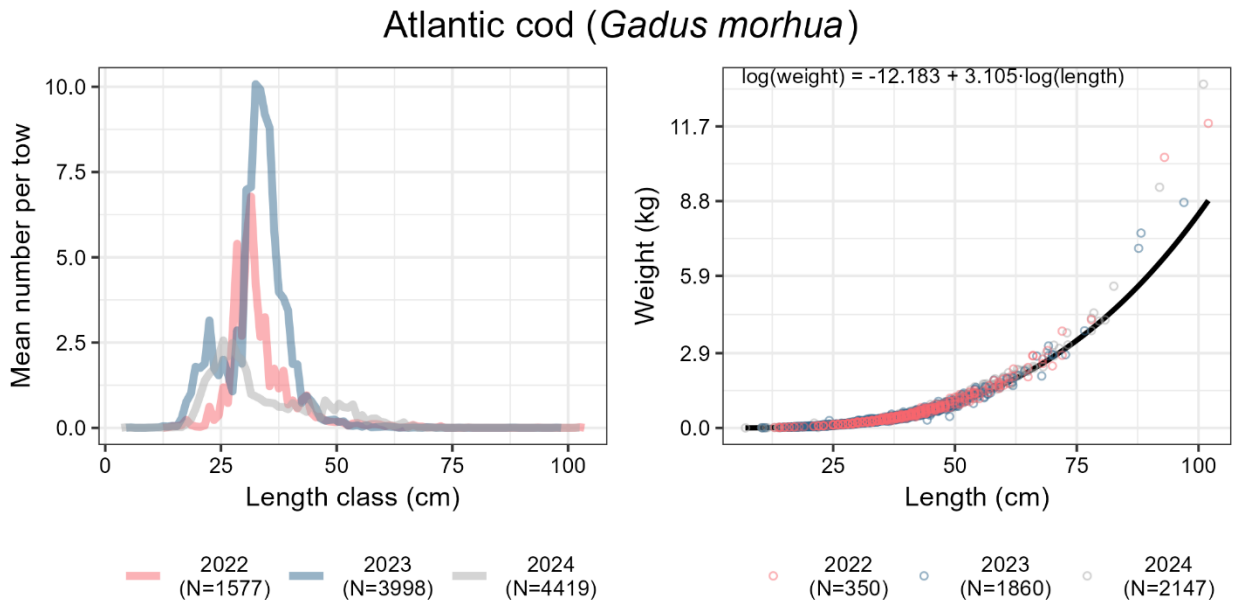


Figure 15d. Annual length frequencies (left panel) and length-weight observations with the global relationship prediction (right panel) for the Atlantic cod in the winter survey in 2022, 2023 and 2024.

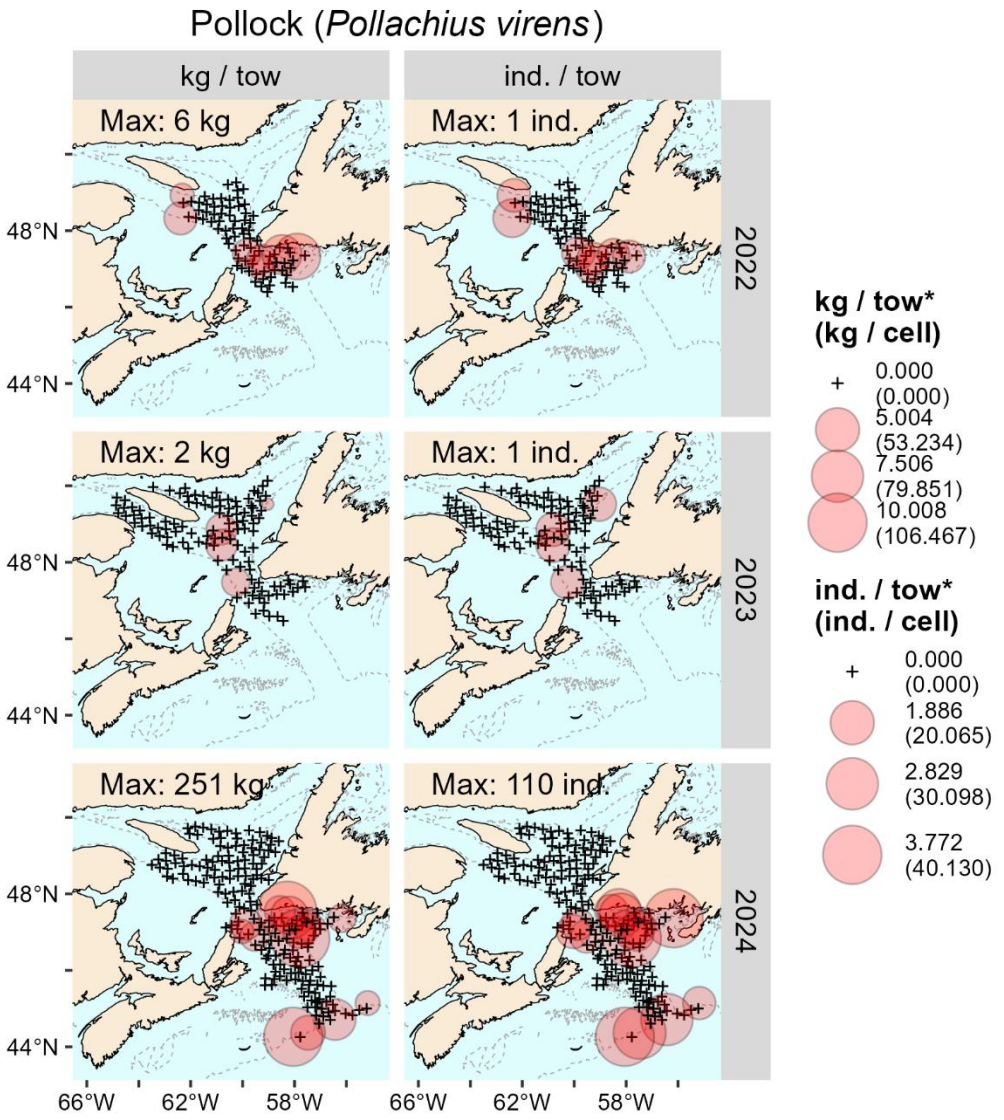


Figure 16a. Standardized catches by weight and/or number (colored bubbles) and cases of absence (black crosses) for pollock in the winter surveys of 2022, 2023, and 2024.

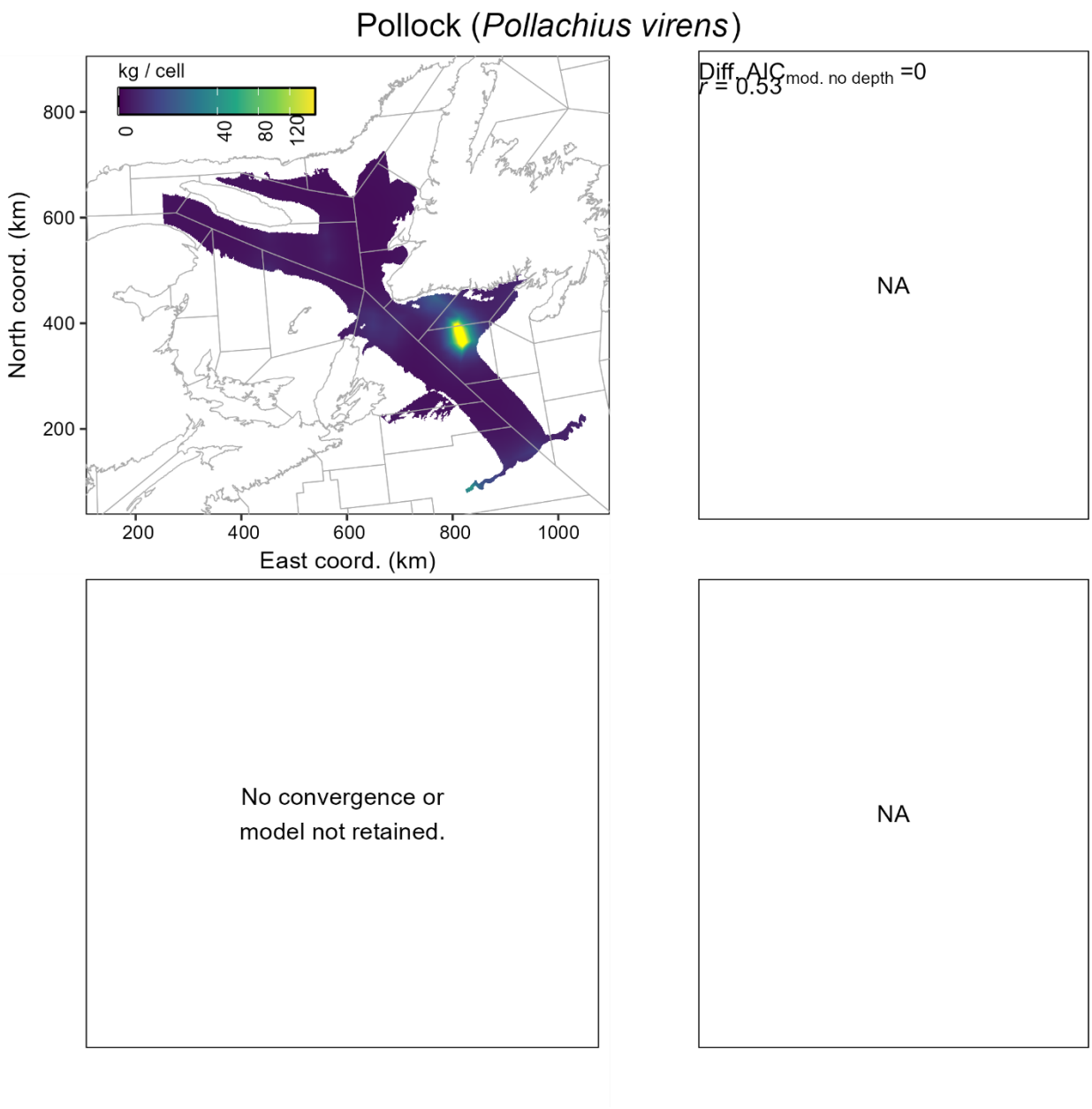


Figure 16b. Predicted weight (upper panels) and number (lower panels) values per 0.25 km^2 cell according to the selected spatial interpolation models for the pollock in the 2022, 2023, and 2024 winter survey.

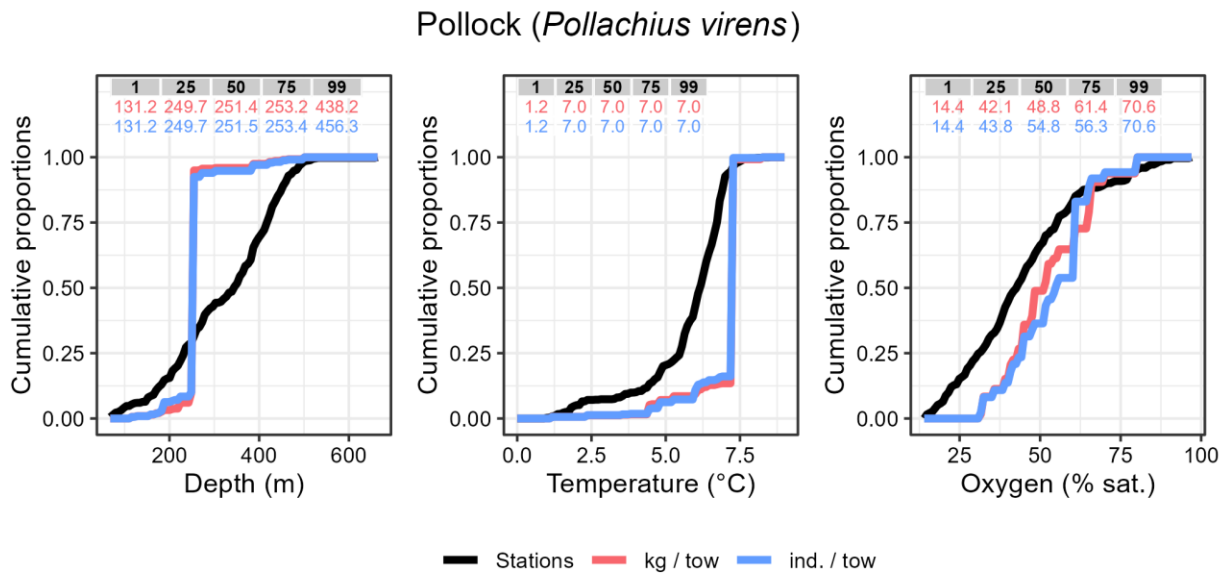


Figure 16c. Cumulative proportions of available values of depth, temperature and dissolved oxygen and standardized catches per tow for the pollock in the winter survey in 2022, 2023 and 2024.

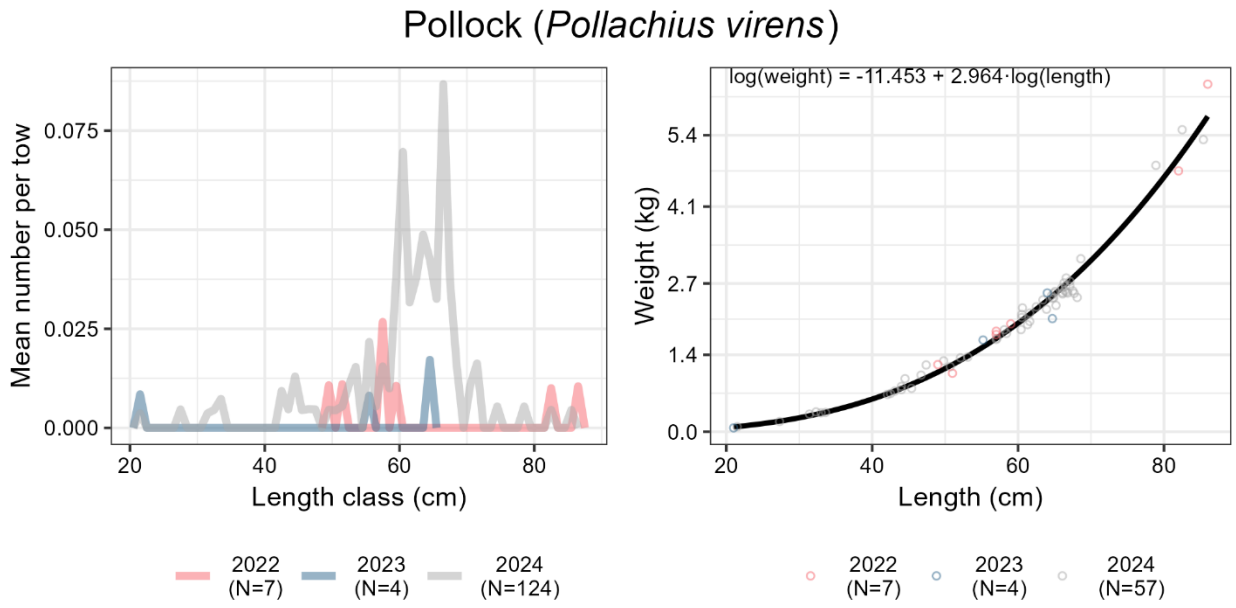


Figure 16d. Annual length frequencies (left panel) and length-weight observations with the global relationship prediction (right panel) for the pollock in the winter survey in 2022, 2023 and 2024.

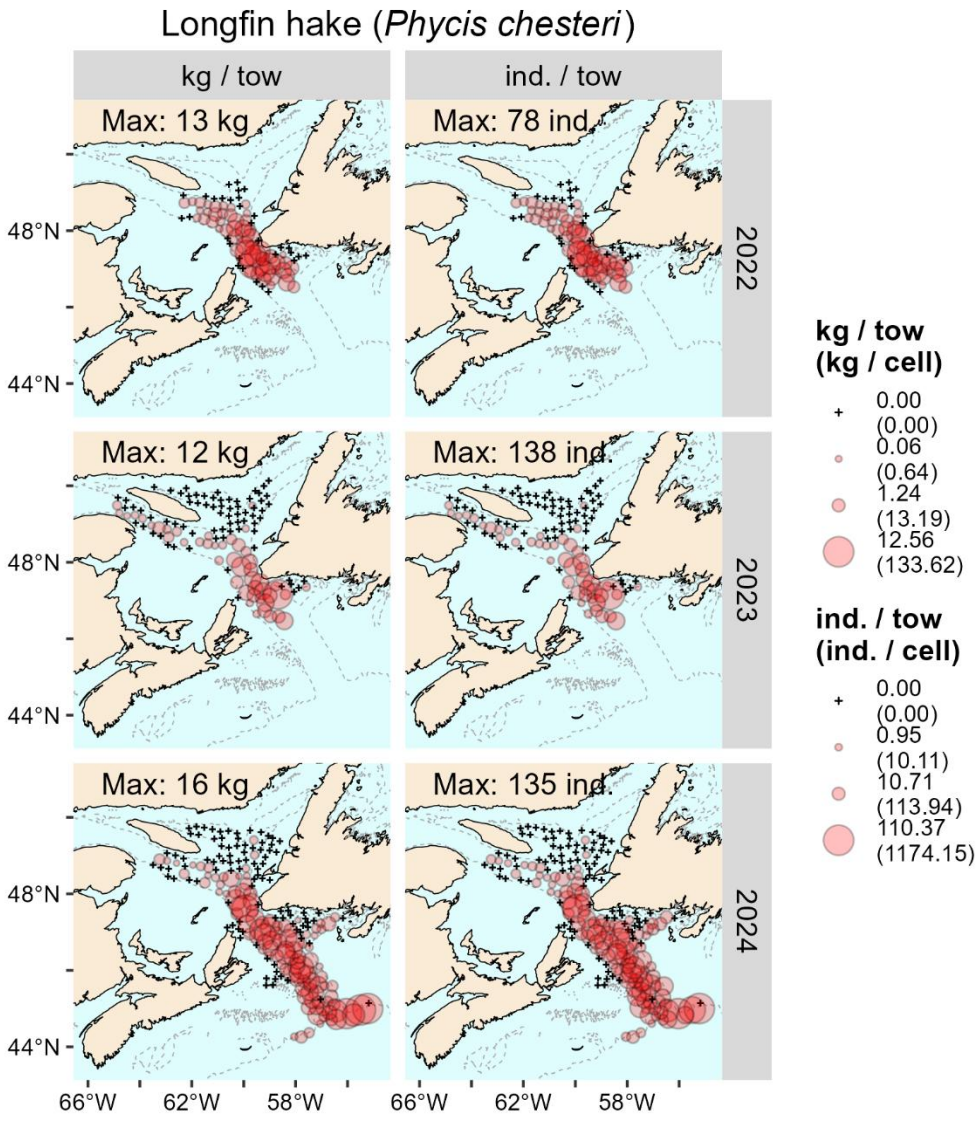


Figure 17a. Standardized catches by weight and/or number (colored bubbles) and cases of absence (black crosses) for the longfin hake in the winter surveys of 2022, 2023, and 2024.

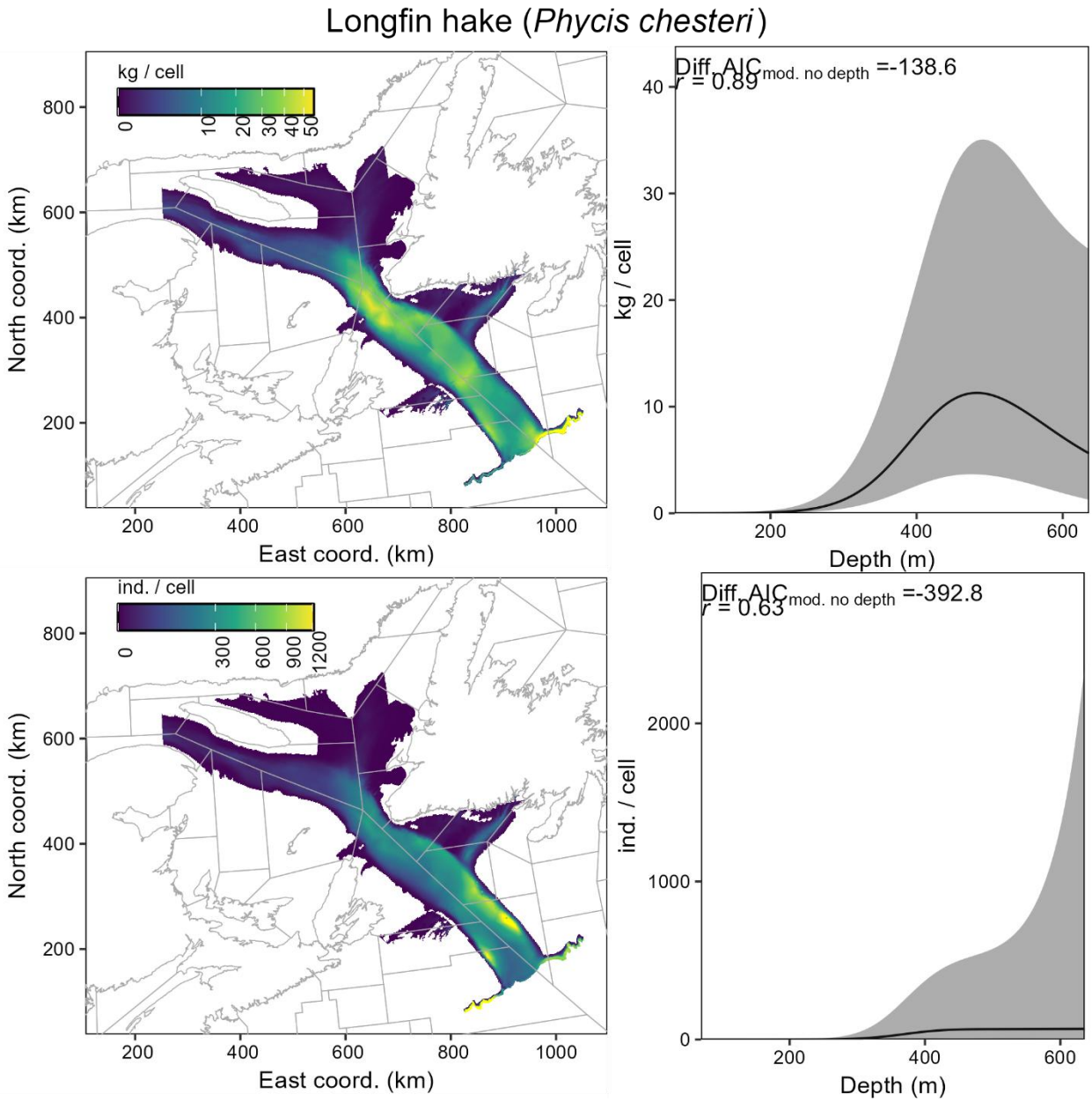


Figure 17b. Predicted weight (upper panels) and number (lower panels) values per 0.25 km^2 cell according to the selected spatial interpolation models for the longfin hake in the 2022, 2023, and 2024 winter survey.

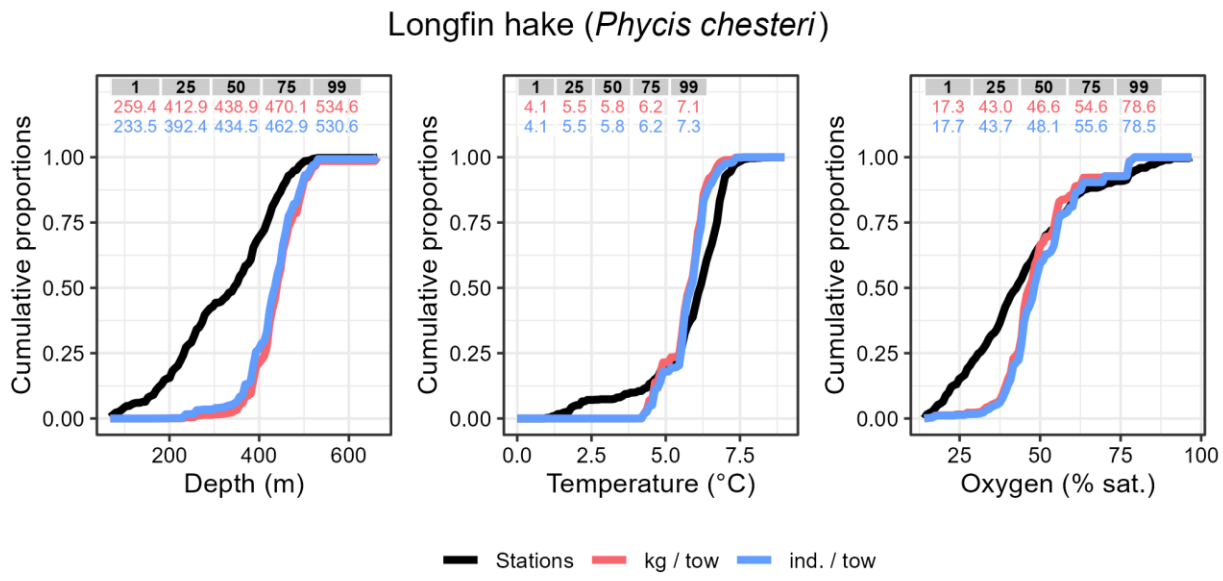


Figure 17c. Cumulative proportions of available values of depth, temperature and dissolved oxygen and standardized catches per tow for the longfin hake in the winter survey in 2022, 2023 and 2024.

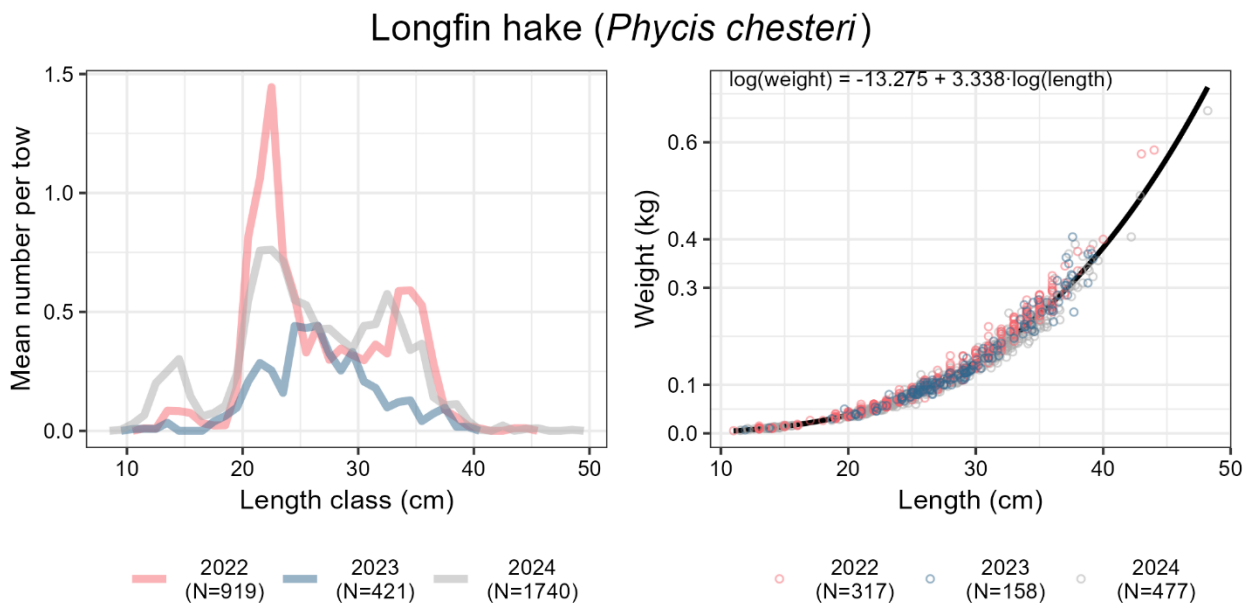


Figure 17d. Annual length frequencies (left panel) and length-weight observations with the global relationship prediction (right panel) for the longfin hake in the winter survey in 2022, 2023 and 2024.

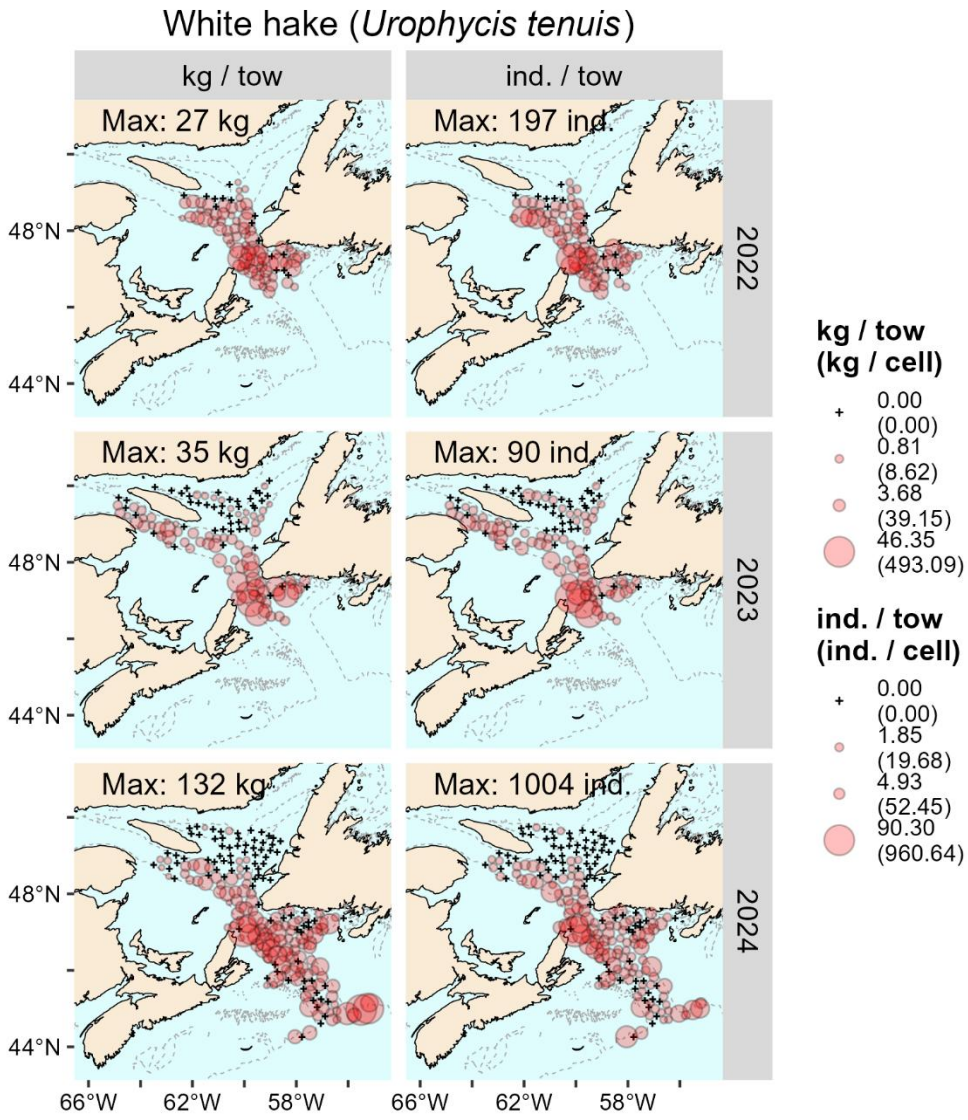


Figure 18a. Standardized catches by weight and/or number (colored bubbles) and cases of absence (black crosses) for the white hake in the winter surveys of 2022, 2023, and 2024.

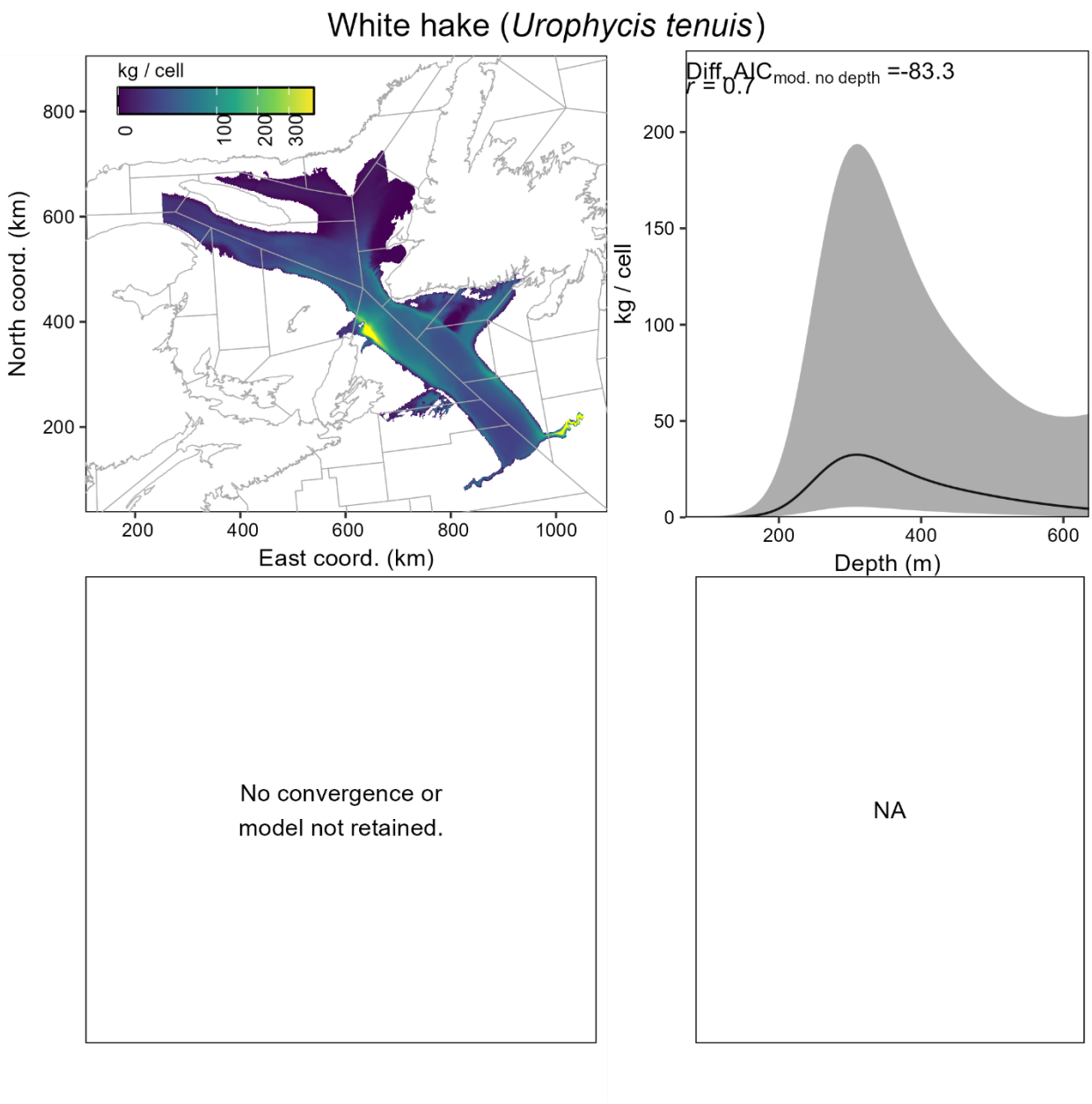


Figure 18b. Predicted weight (upper panels) and number (lower panels) values per 0.25 km^2 cell according to the selected spatial interpolation models for the white hake in the 2022, 2023, and 2024 winter survey.

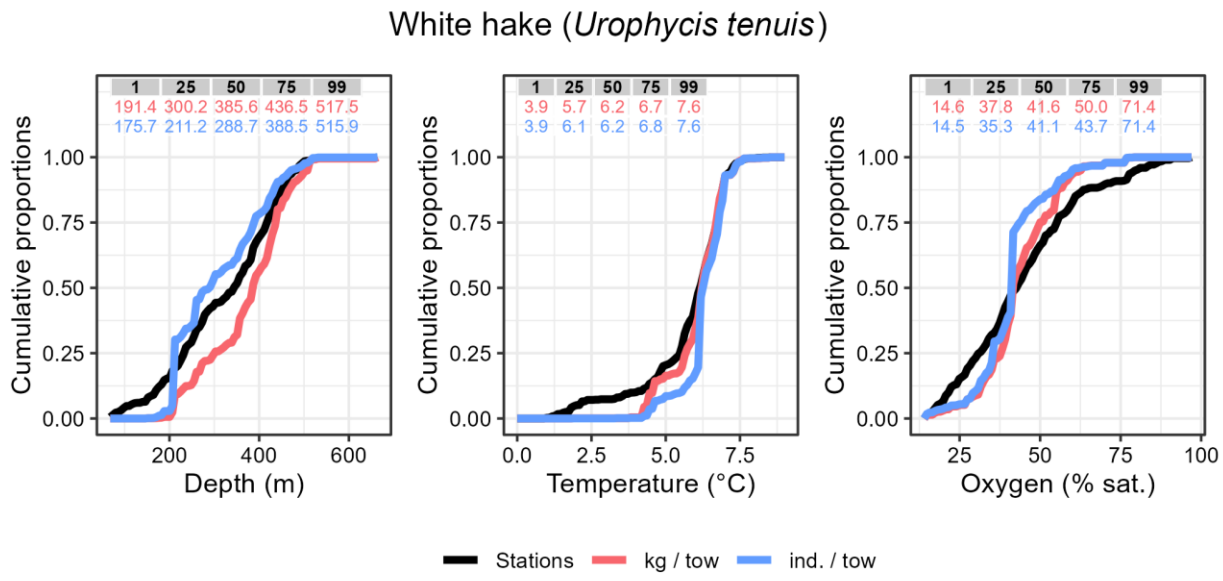


Figure 18c. Cumulative proportions of available values of depth, temperature and dissolved oxygen and standardized catches per tow for the white hake in the winter survey in 2022, 2023 and 2024.

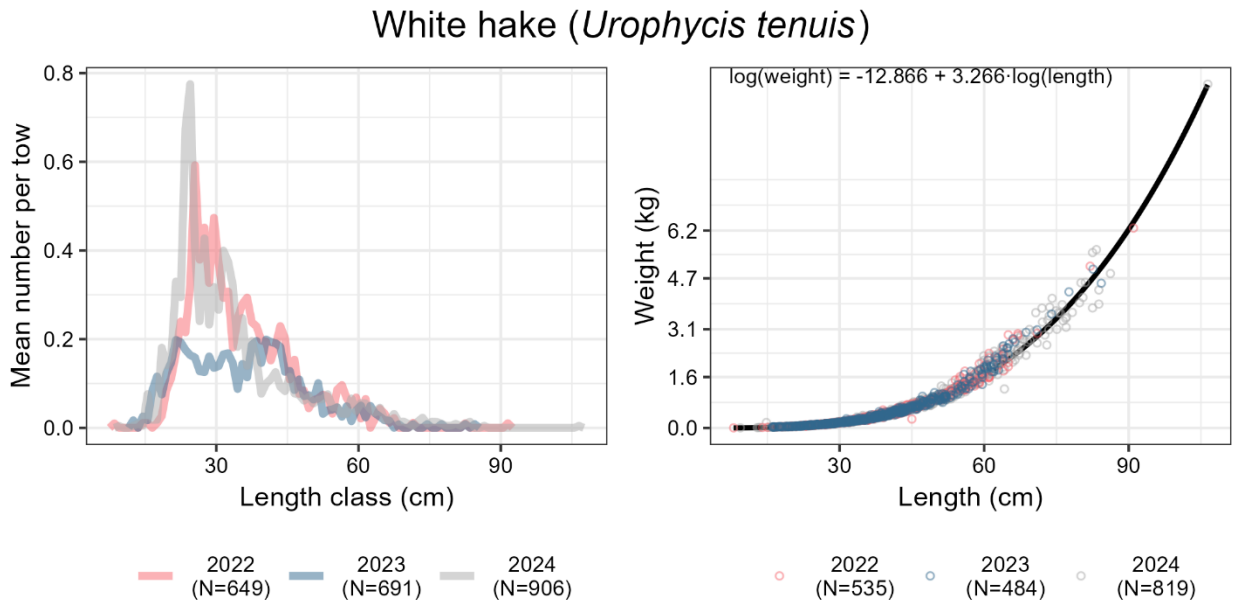


Figure 18d. Annual length frequencies (left panel) and length-weight observations with the global relationship prediction (right panel) for the white hake in the winter survey in 2022, 2023 and 2024.

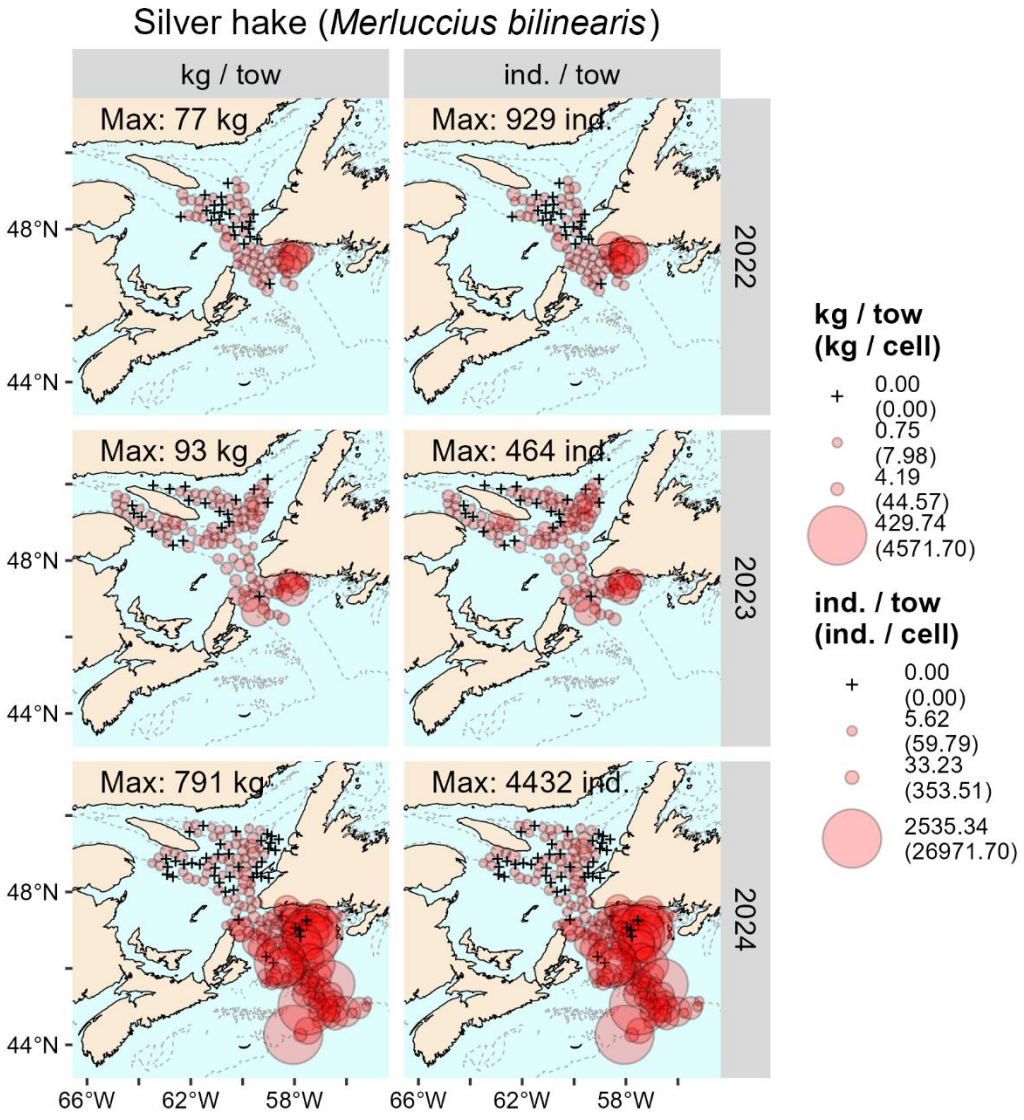


Figure 19a. Standardized catches by weight and/or number (colored bubbles) and cases of absence (black crosses) for the silver hake in the winter surveys of 2022, 2023, and 2024.

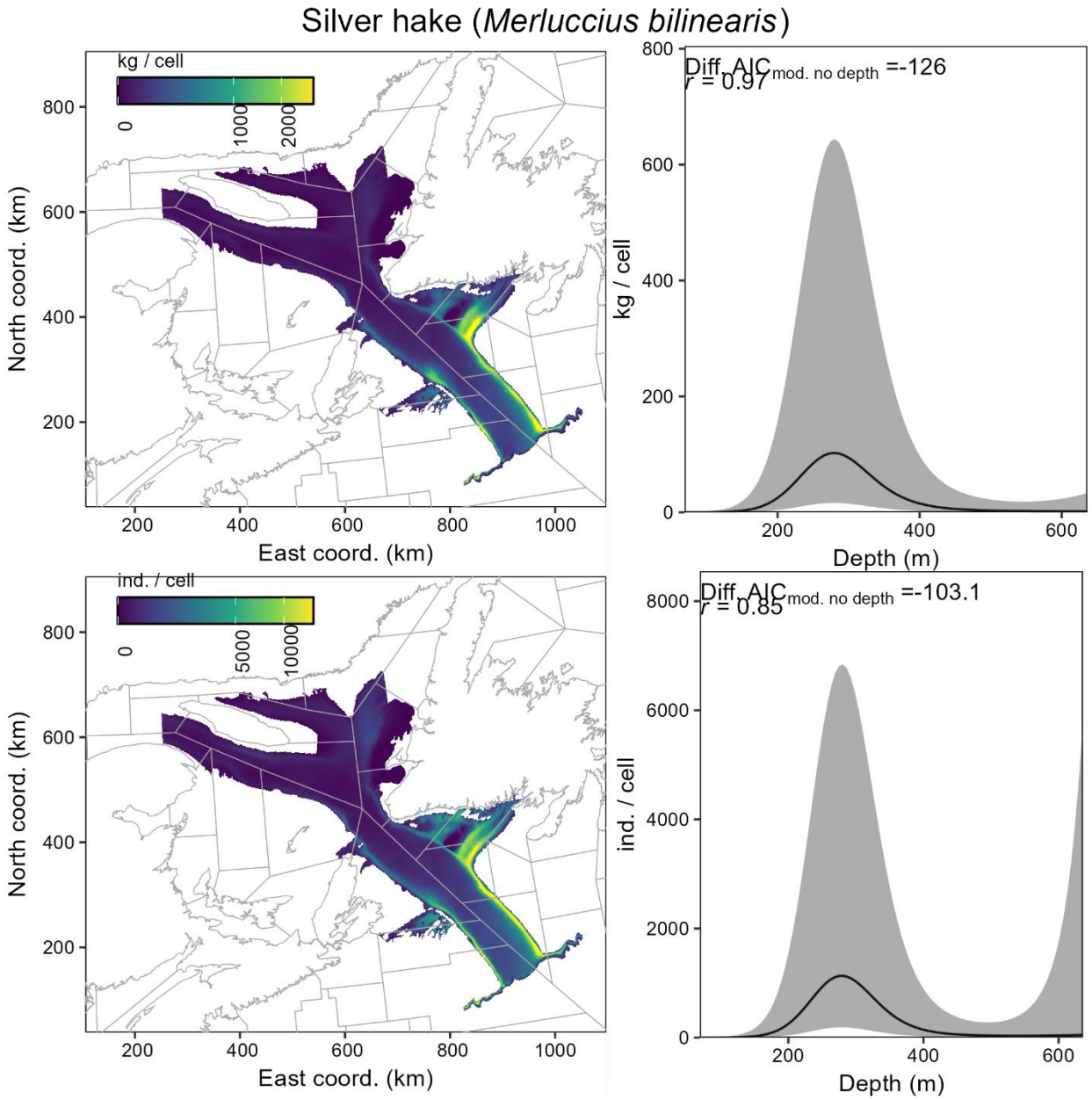


Figure 19b. Predicted weight (upper panels) and number (lower panels) values per 0.25 km^2 cell according to the selected spatial interpolation models for the silver hake in the 2022, 2023, and 2024 winter survey.

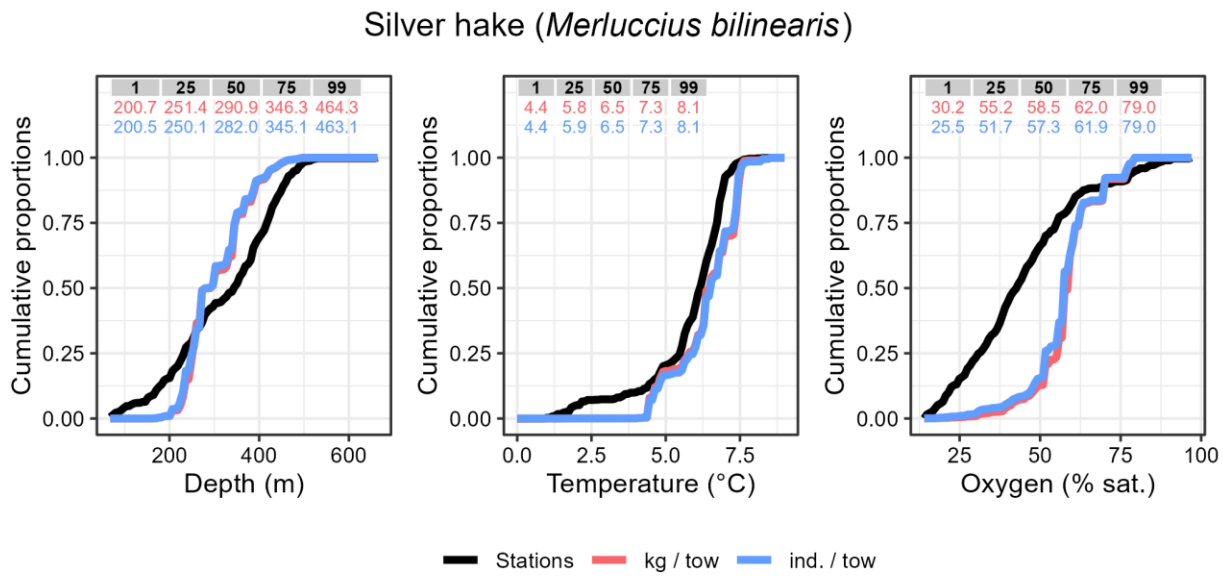


Figure 19c. Cumulative proportions of available values of depth, temperature and dissolved oxygen and standardized catches per tow for the silver hake in the winter survey in 2022, 2023 and 2024.

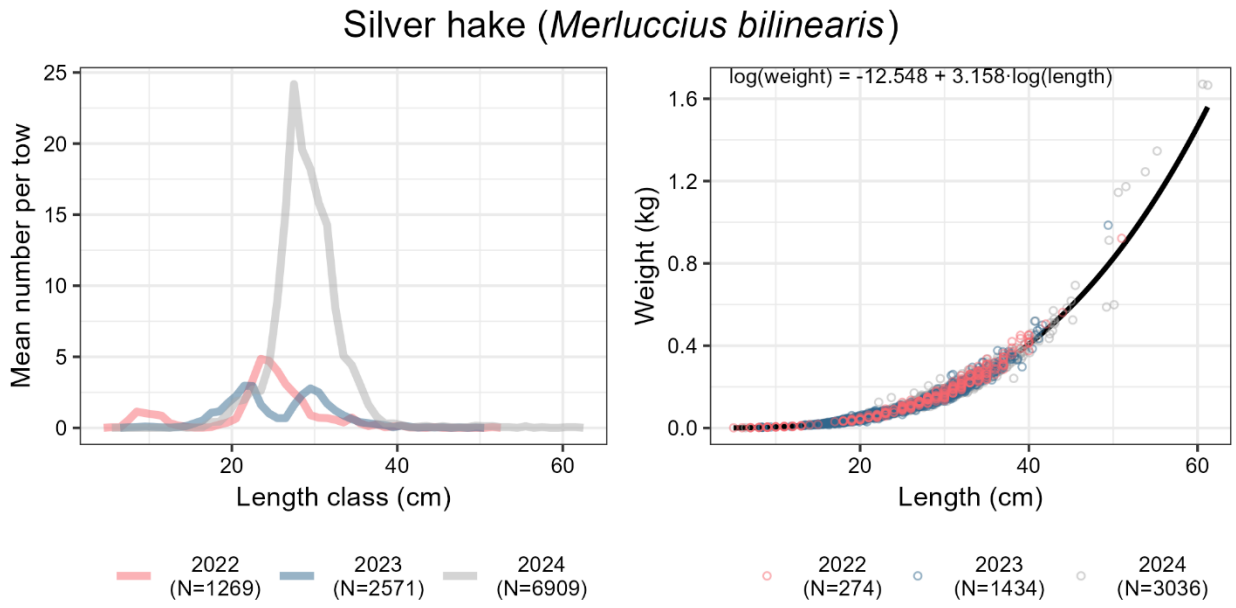


Figure 19d. Annual length frequencies (left panel) and length-weight observations with the global relationship prediction (right panel) for the silver hake in the winter survey in 2022, 2023 and 2024.

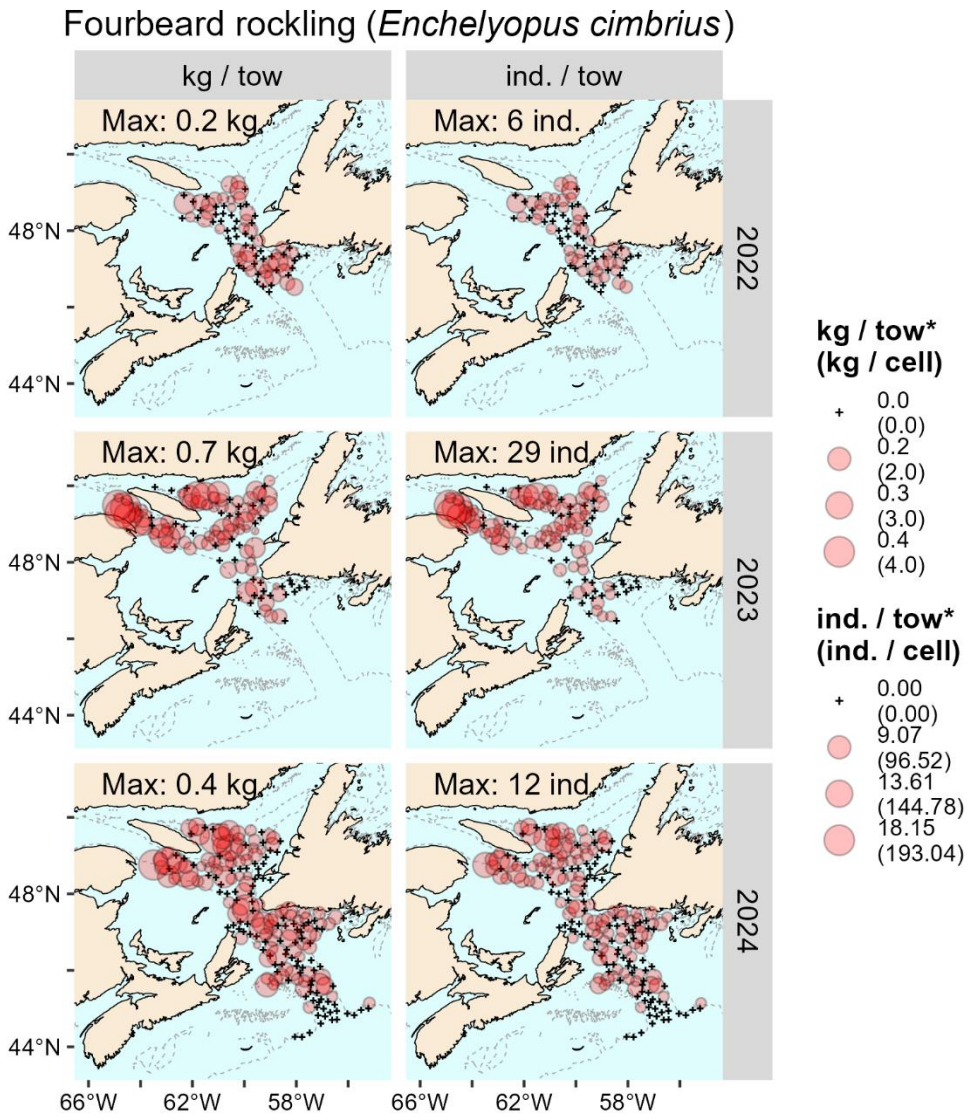


Figure 20a. Standardized catches by weight and/or number (colored bubbles) and cases of absence (black crosses) for the fourbeard rockling in the winter surveys of 2022, 2023, and 2024.

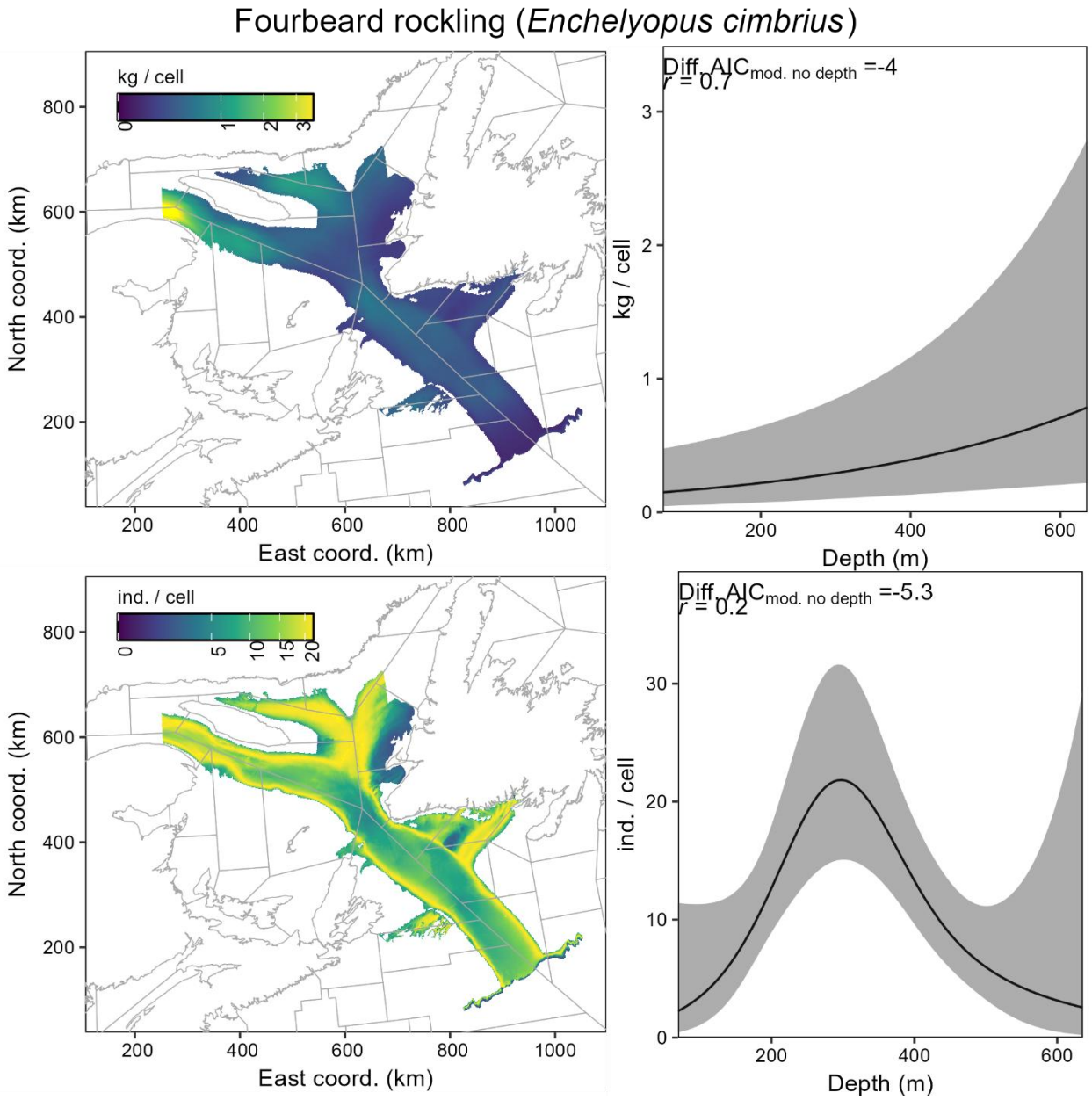


Figure 20b. Predicted weight (upper panels) and number (lower panels) values per 0.25 km^2 cell according to the selected spatial interpolation models for the fourbeard rockling in the 2022, 2023, and 2024 winter survey.

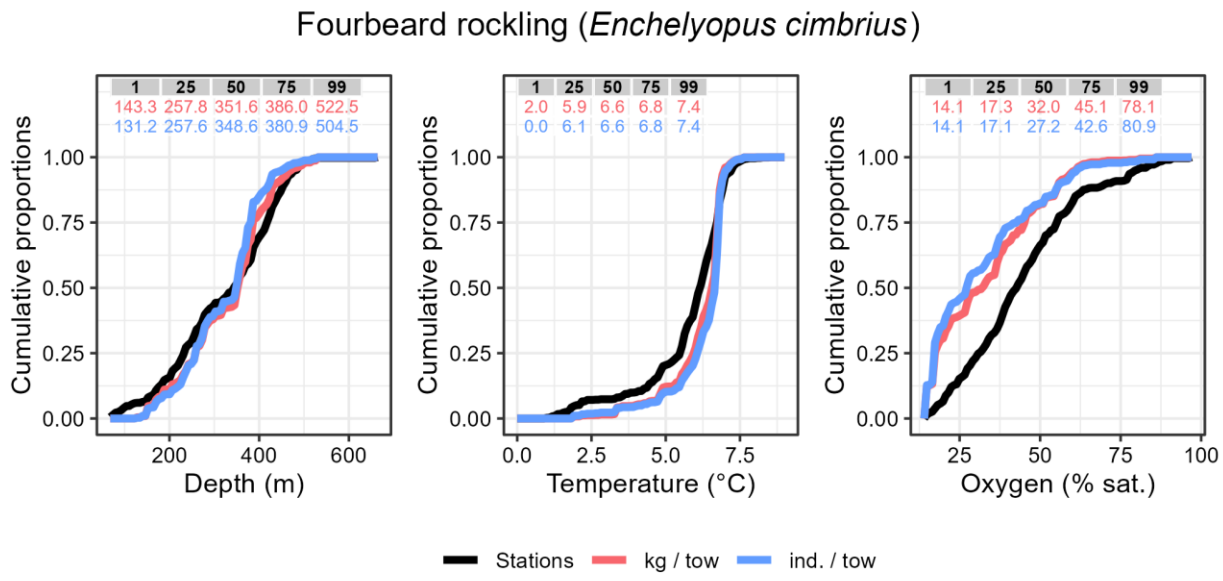


Figure 20c. Cumulative proportions of available values of depth, temperature and dissolved oxygen and standardized catches per tow for the fourbeard rockling in the winter survey in 2022, 2023 and 2024.

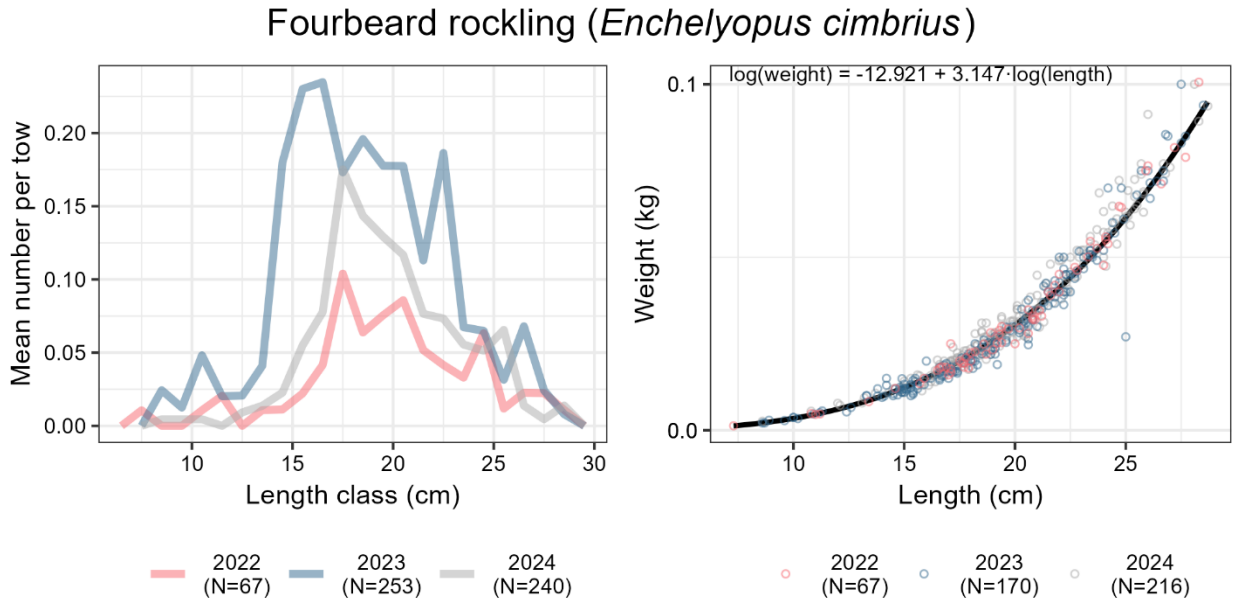


Figure 20d. Annual length frequencies (left panel) and length-weight observations with the global relationship prediction (right panel) for the fourbeard rockling in the winter survey in 2022, 2023 and 2024.

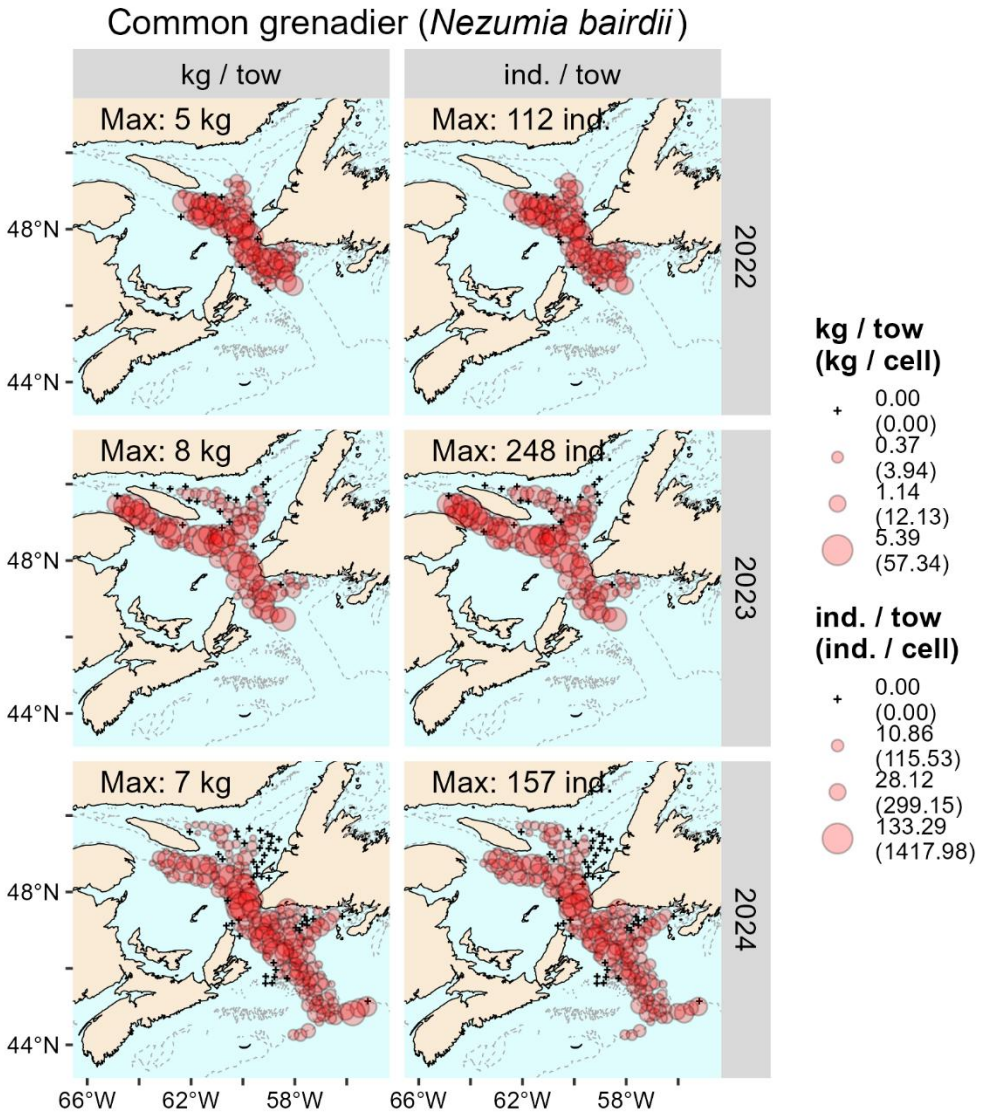


Figure 21a. Standardized catches by weight and/or number (colored bubbles) and cases of absence (black crosses) for the common grenadier in the winter surveys of 2022, 2023, and 2024.

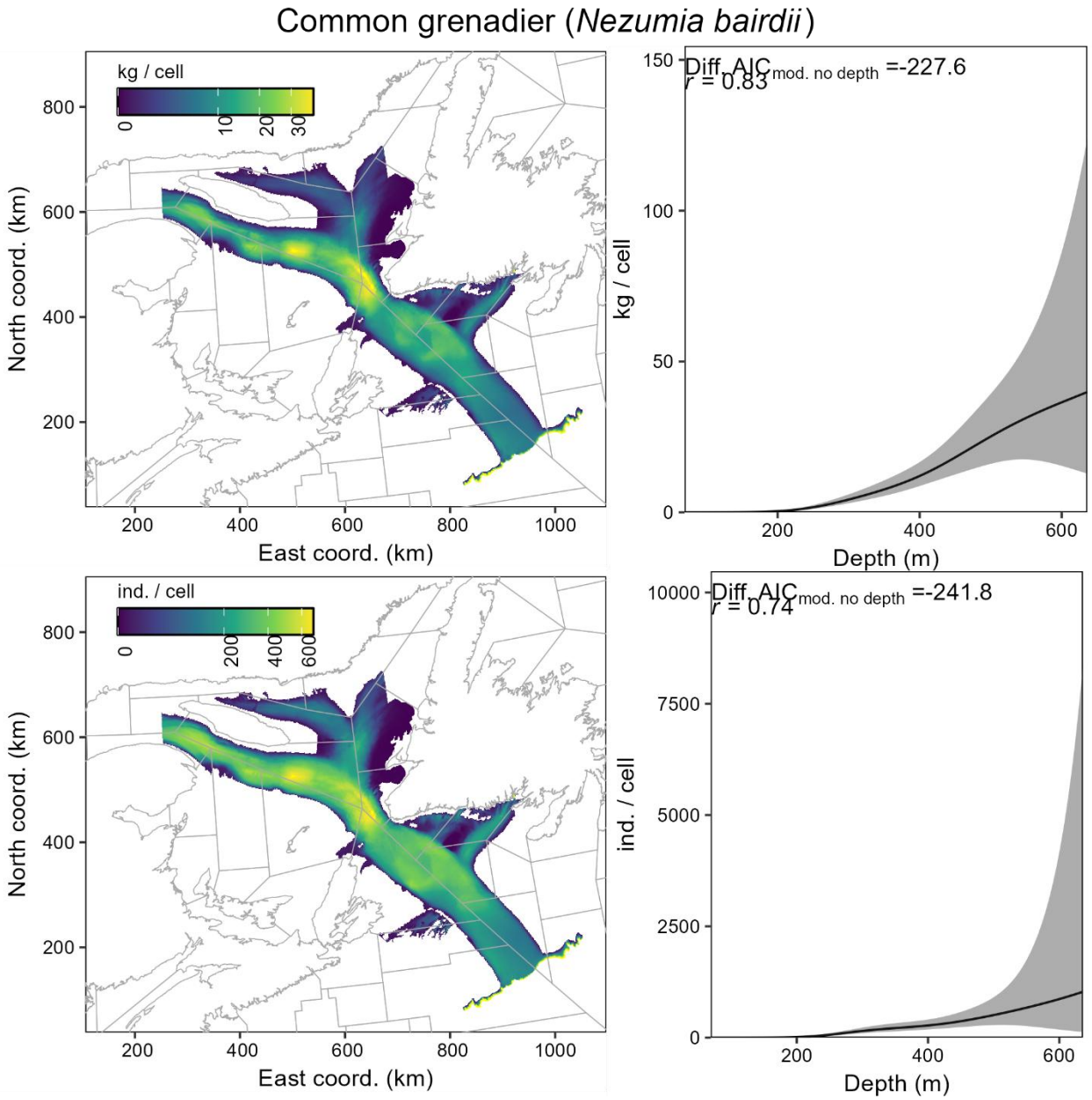


Figure 21b. Predicted weight (upper panels) and number (lower panels) values per 0.25 km^2 cell according to the selected spatial interpolation models for the common grenadier in the 2022, 2023, and 2024 winter survey.

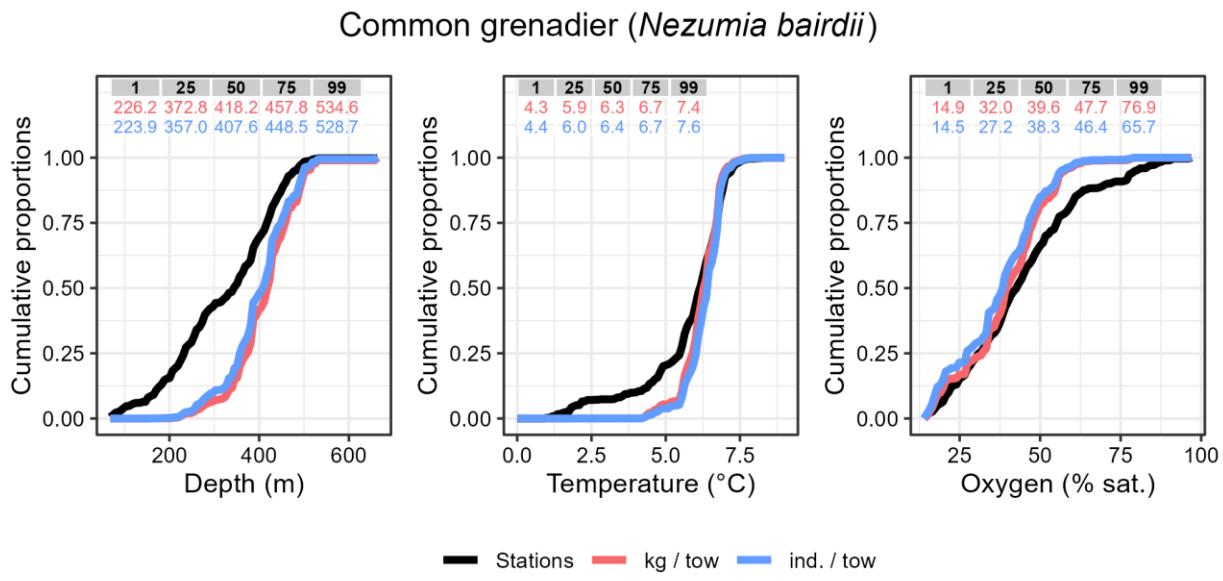


Figure 21c. Cumulative proportions of available values of depth, temperature and dissolved oxygen and standardized catches per tow for the common grenadier in the winter survey in 2022, 2023 and 2024.

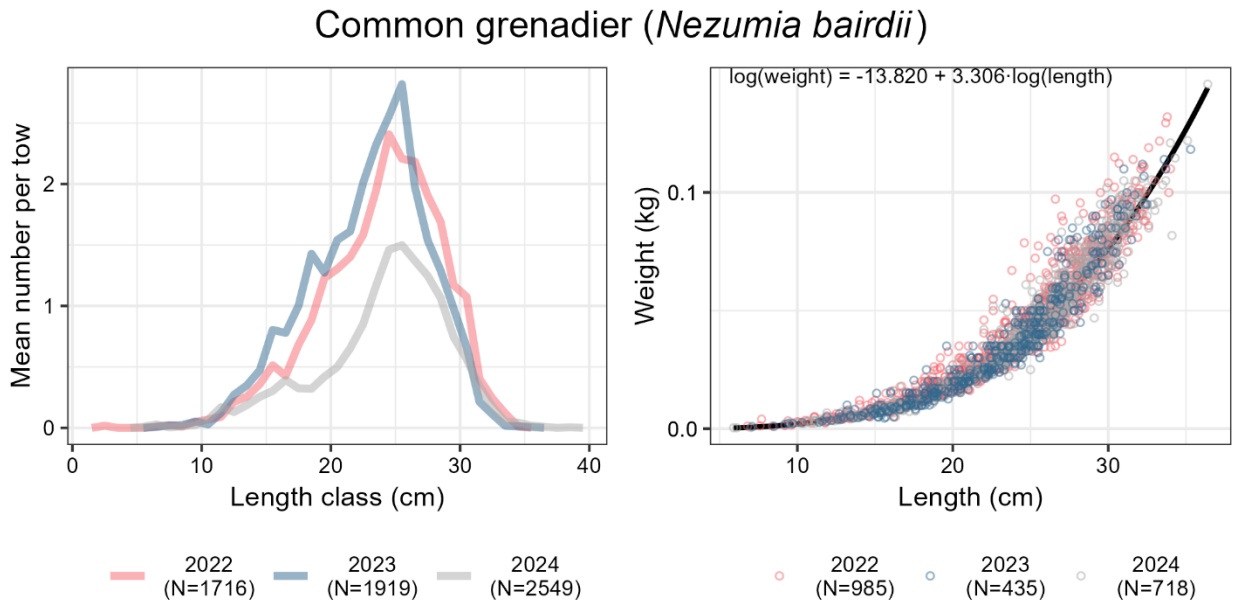


Figure 21d. Annual length frequencies (left panel) and length-weight observations with the global relationship prediction (right panel) for the common grenadier in the winter survey in 2022, 2023 and 2024.

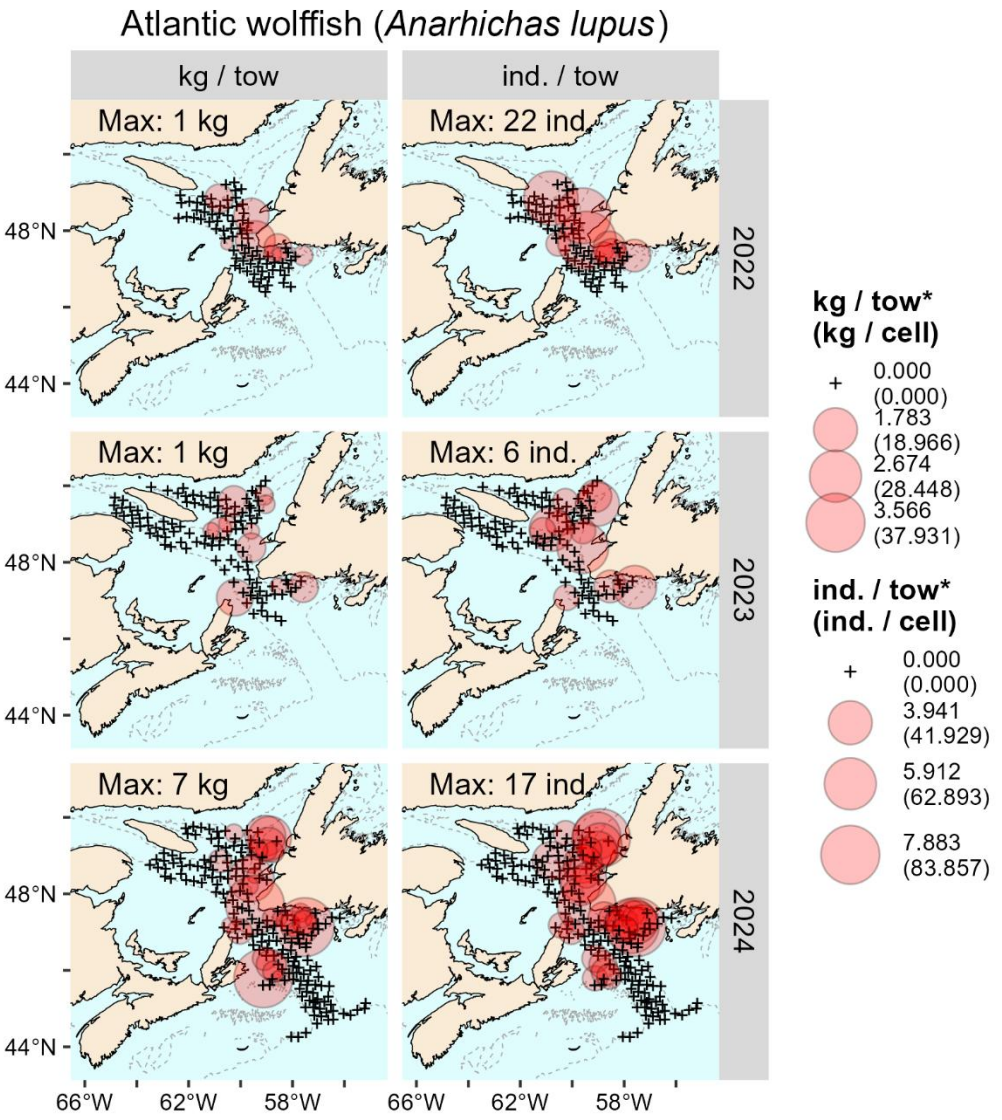


Figure 22a. Standardized catches by weight and/or number (colored bubbles) and cases of absence (black crosses) for the Atlantic wolffish in the winter surveys of 2022, 2023, and 2024.

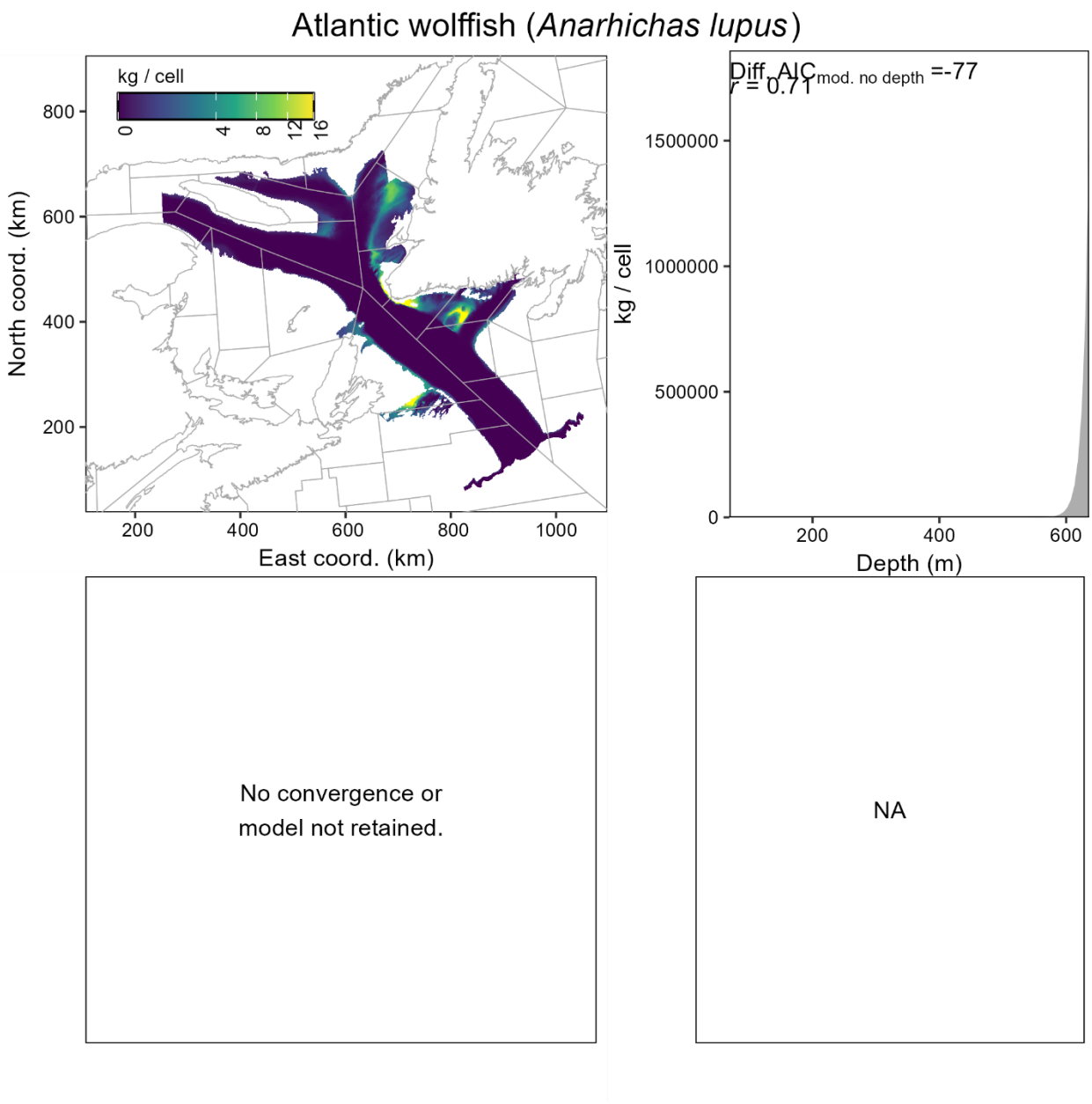


Figure 22b. Predicted weight (upper panels) and number (lower panels) values per 0.25 km^2 cell according to the selected spatial interpolation models for the Atlantic wolffish in the 2022, 2023, and 2024 winter survey.

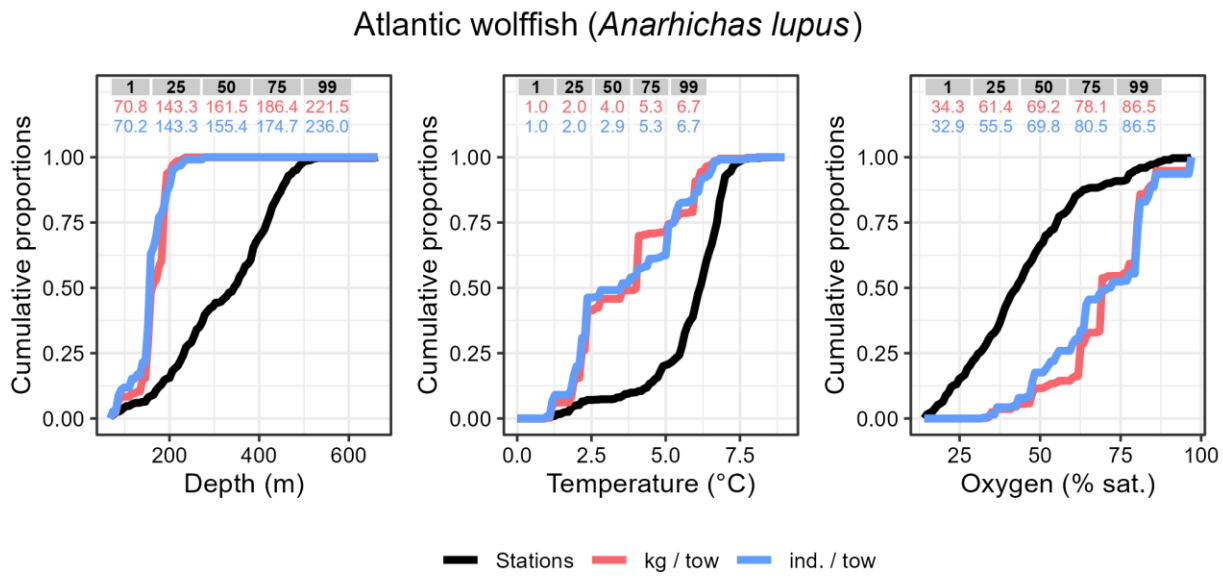


Figure 22c. Cumulative proportions of available values of depth, temperature and dissolved oxygen and standardized catches per tow for the Atlantic wolffish in the winter survey in 2022, 2023 and 2024.

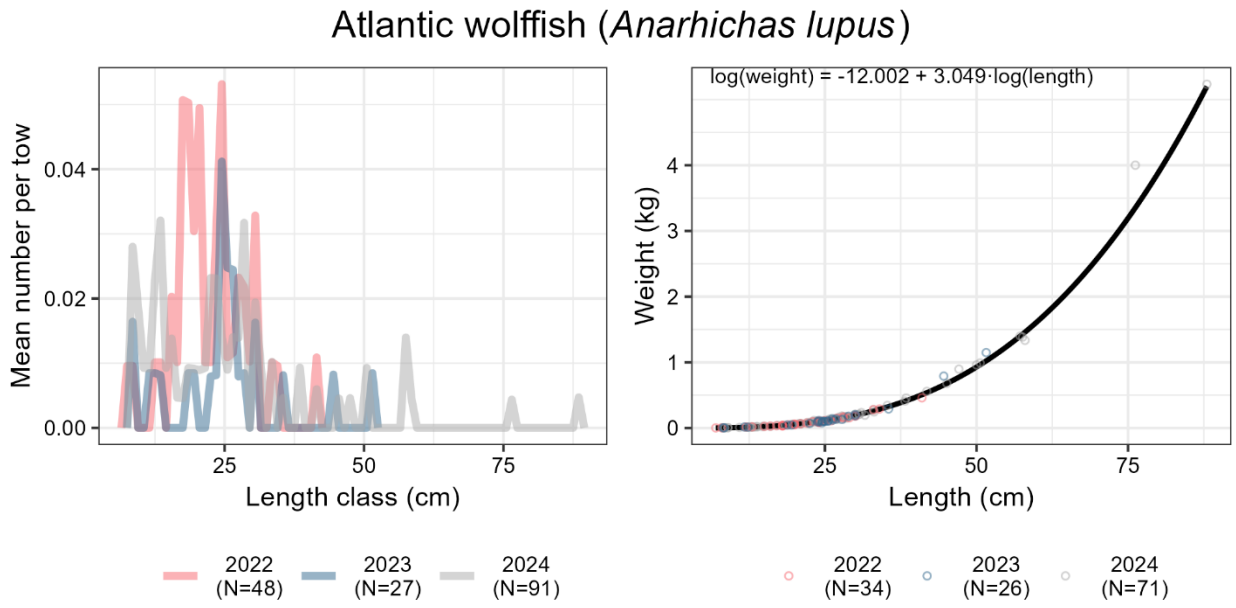


Figure 22d. Annual length frequencies (left panel) and length-weight observations with the global relationship prediction (right panel) for the Atlantic wolffish in the winter survey in 2022, 2023 and 2024.

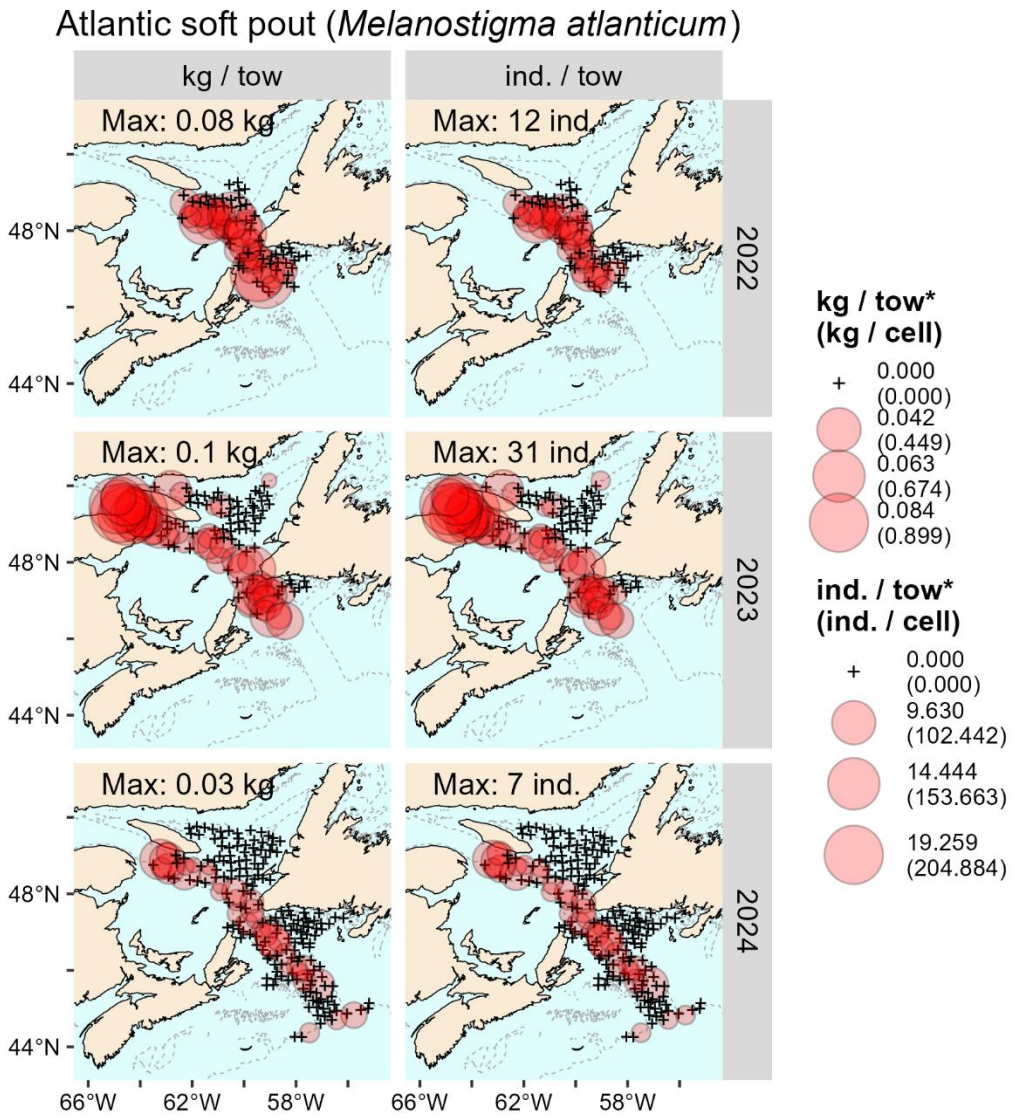


Figure 23a. Standardized catches by weight and/or number (colored bubbles) and cases of absence (black crosses) for the Atlantic soft pout in the winter surveys of 2022, 2023, and 2024.

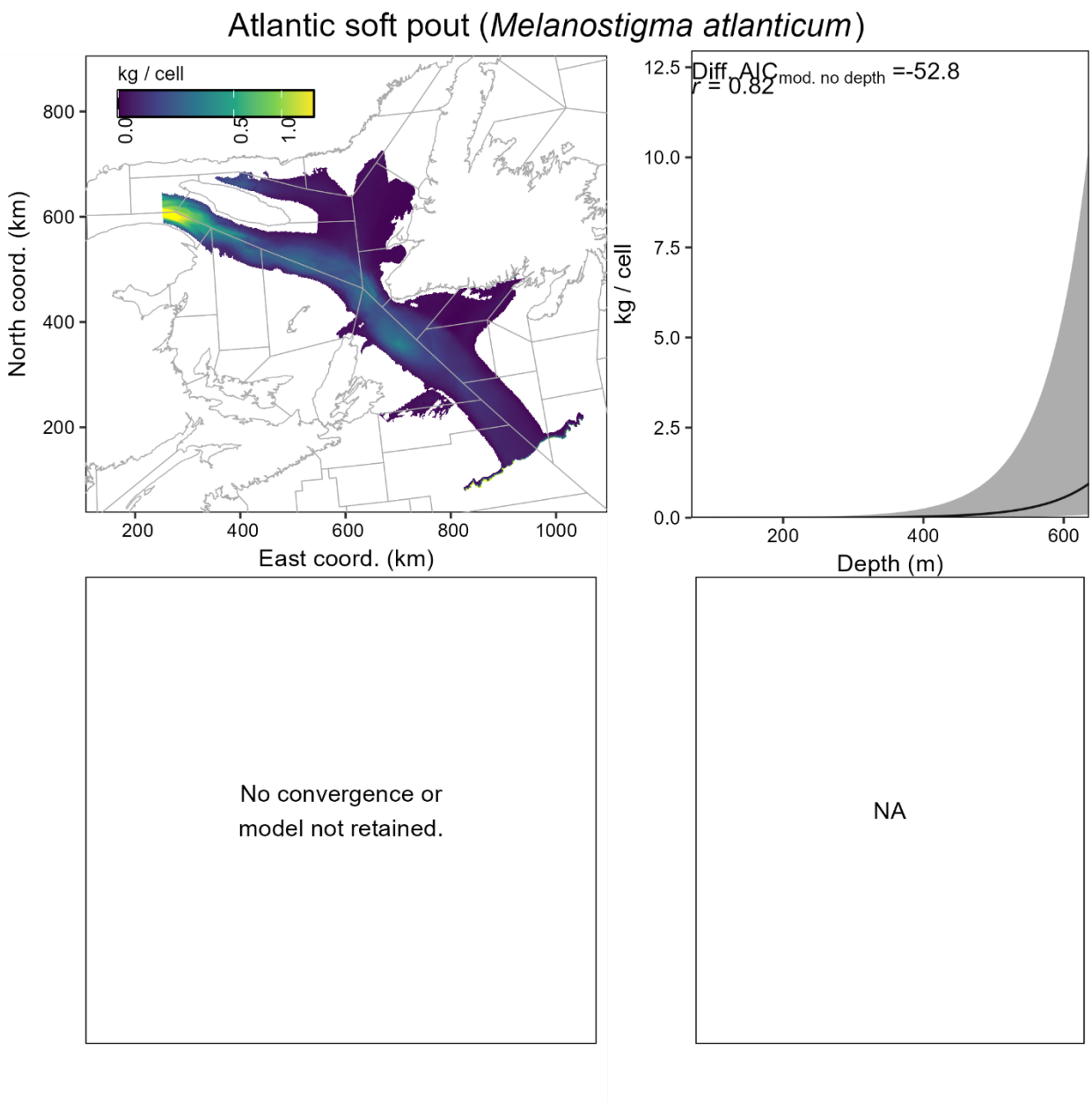


Figure 23b. Predicted weight (upper panels) and number (lower panels) values per 0.25 km^2 cell according to the selected spatial interpolation models for the Atlantic soft pout in the 2022, 2023, and 2024 winter survey.

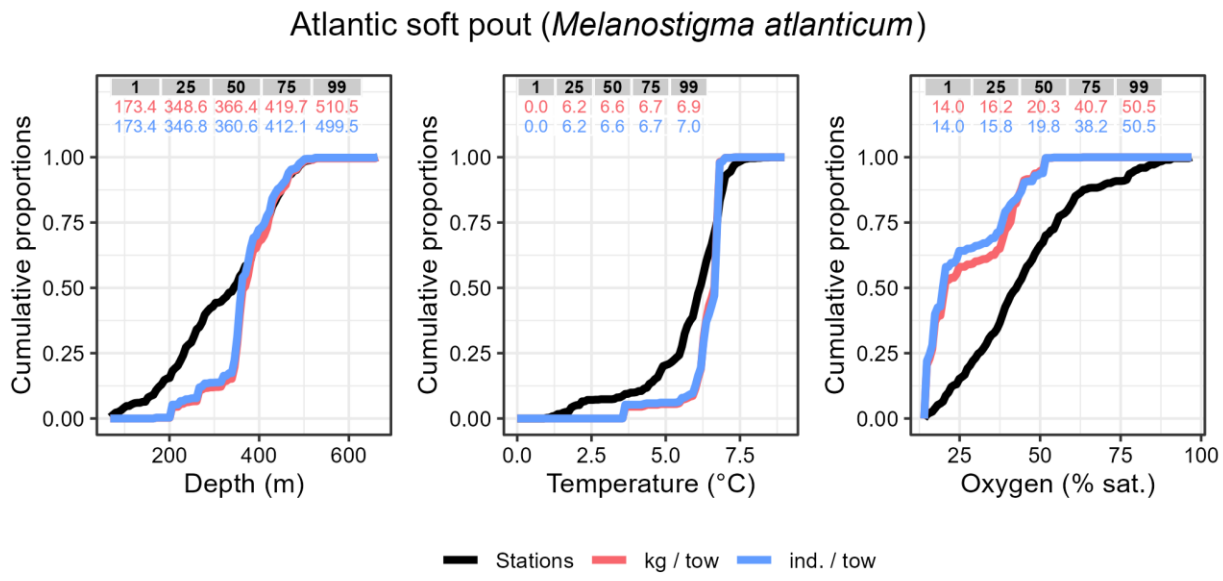


Figure 23c. Cumulative proportions of available values of depth, temperature and dissolved oxygen and standardized catches per tow for the Atlantic soft pout in the winter survey in 2022, 2023 and 2024.

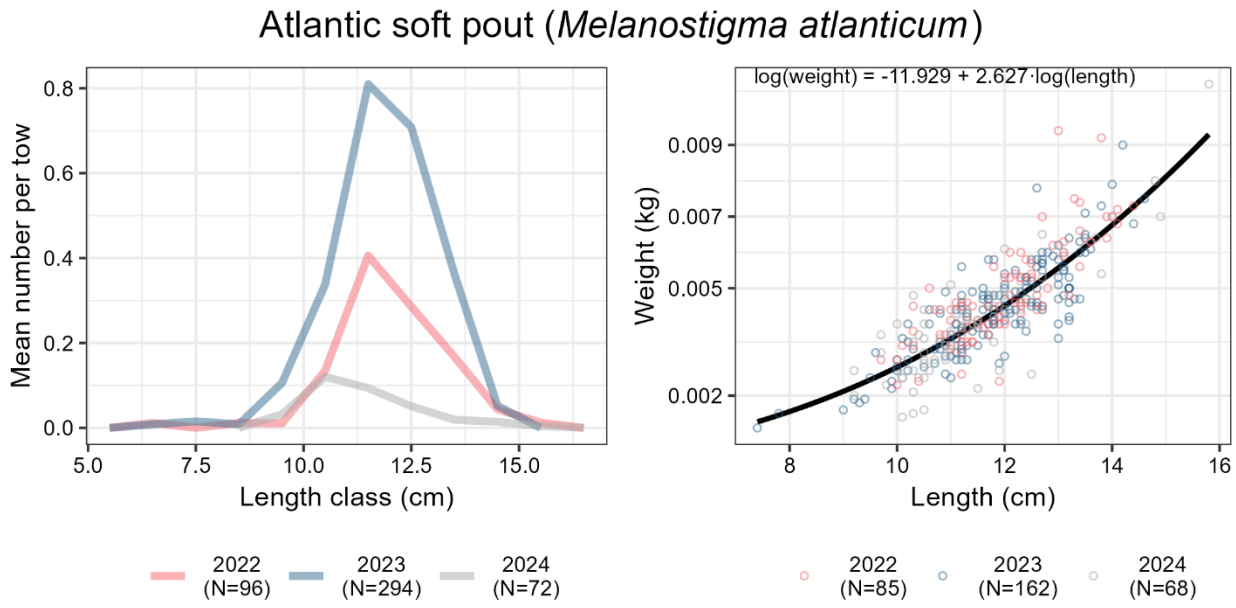


Figure 23d. Annual length frequencies (left panel) and length-weight observations with the global relationship prediction (right panel) for the Atlantic soft pout in the winter survey in 2022, 2023 and 2024.

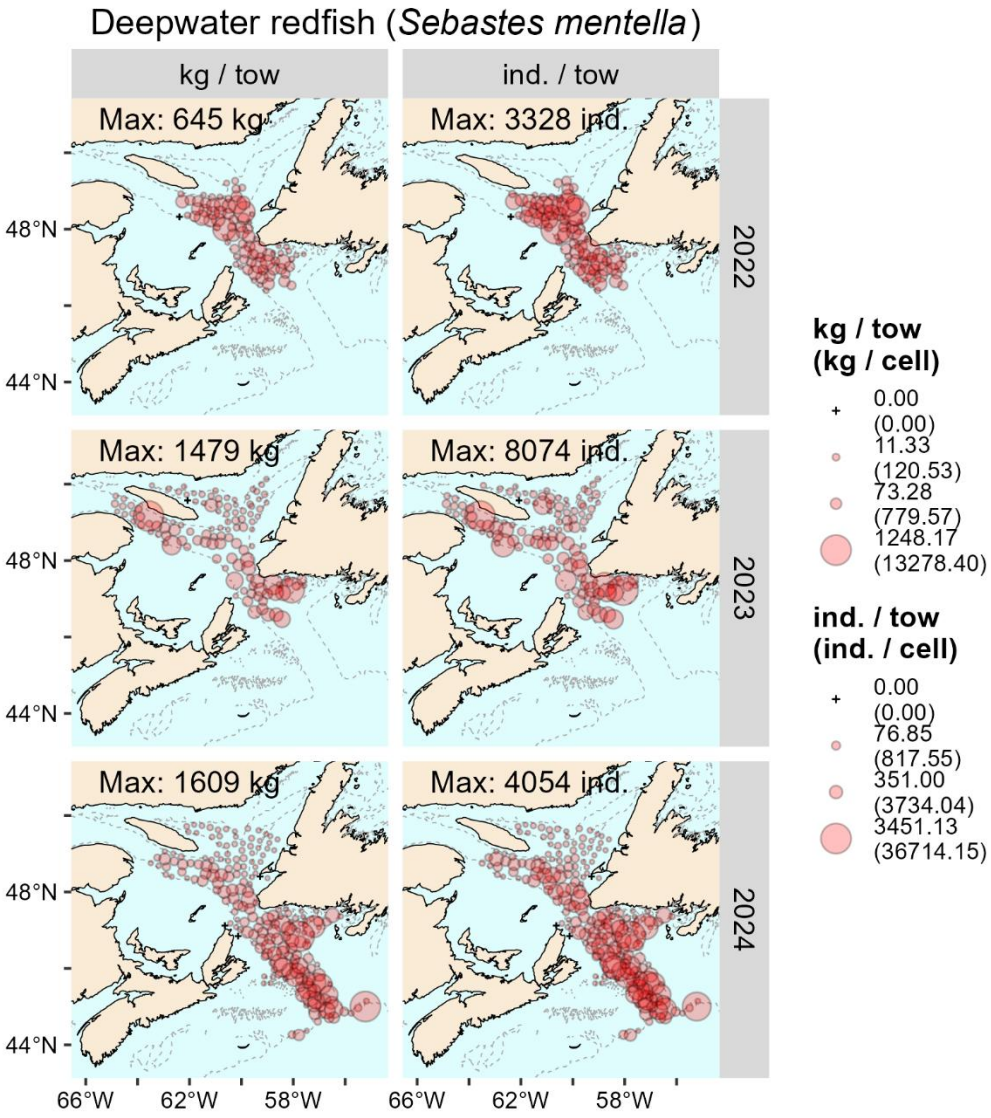


Figure 24a. Standardized catches by weight and/or number (colored bubbles) and cases of absence (black crosses) for the deepwater redfish in the winter surveys of 2022, 2023, and 2024.

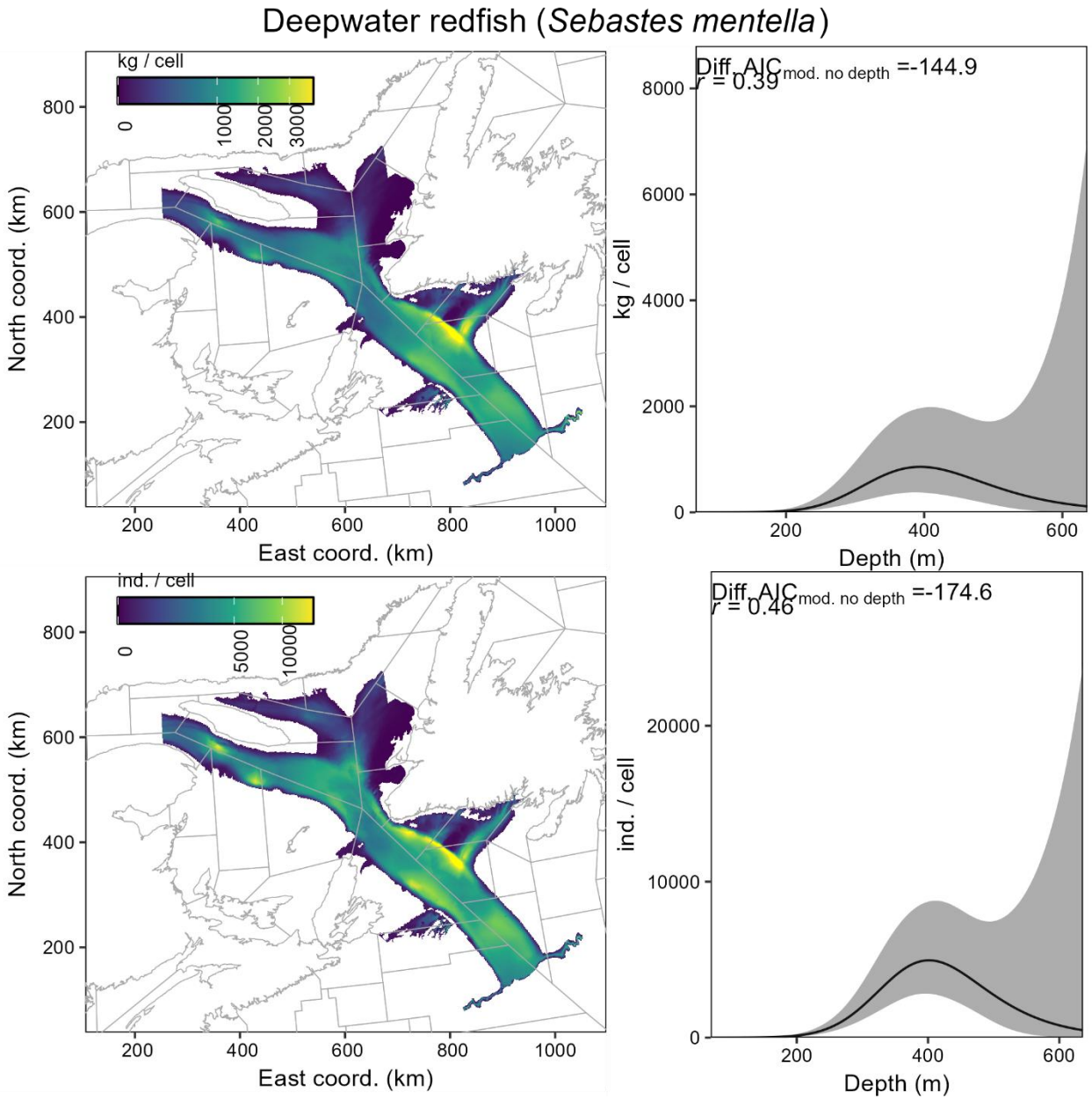


Figure 24b. Predicted weight (upper panels) and number (lower panels) values per 0.25 km^2 cell according to the selected spatial interpolation models for the deepwater redfish in the 2022, 2023, and 2024 winter survey.

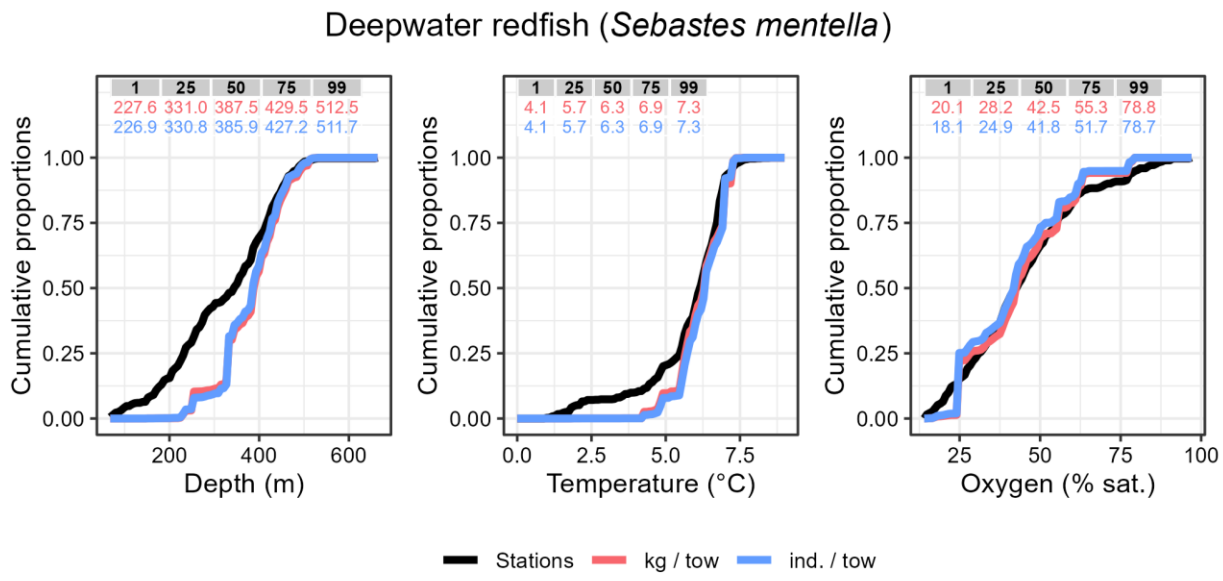


Figure 24c. Cumulative proportions of available values of depth, temperature and dissolved oxygen and standardized catches per tow for the deepwater redfish in the winter survey in 2022, 2023 and 2024.

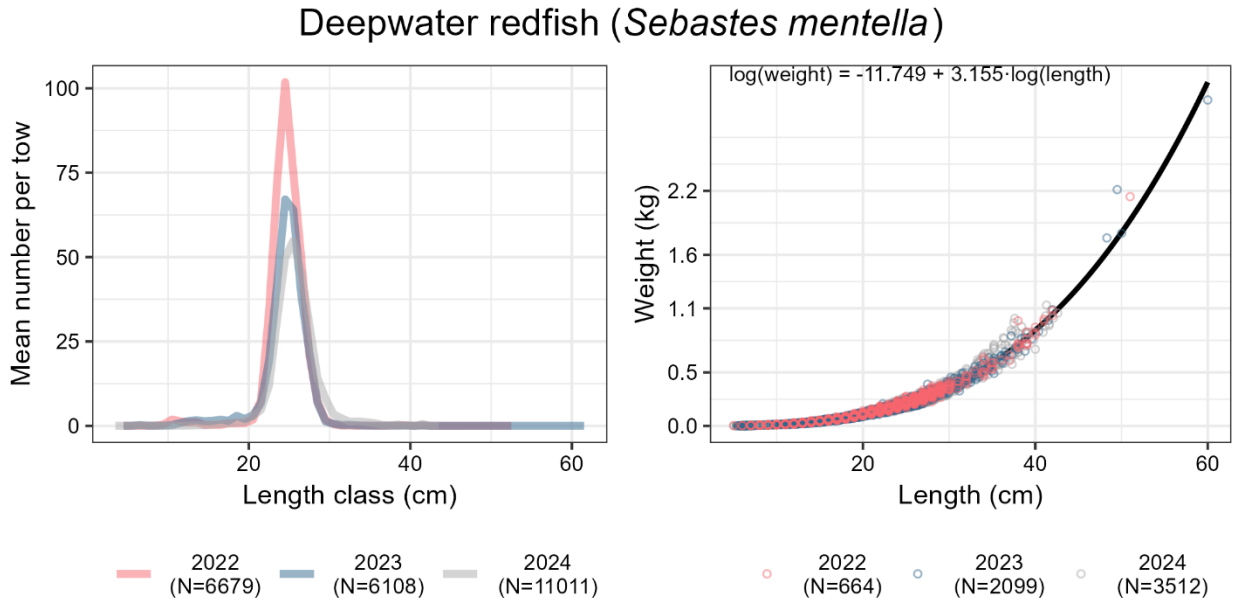


Figure 24d. Annual length frequencies (left panel) and length-weight observations with the global relationship prediction (right panel) for the deepwater redfish in the winter survey in 2022, 2023 and 2024.

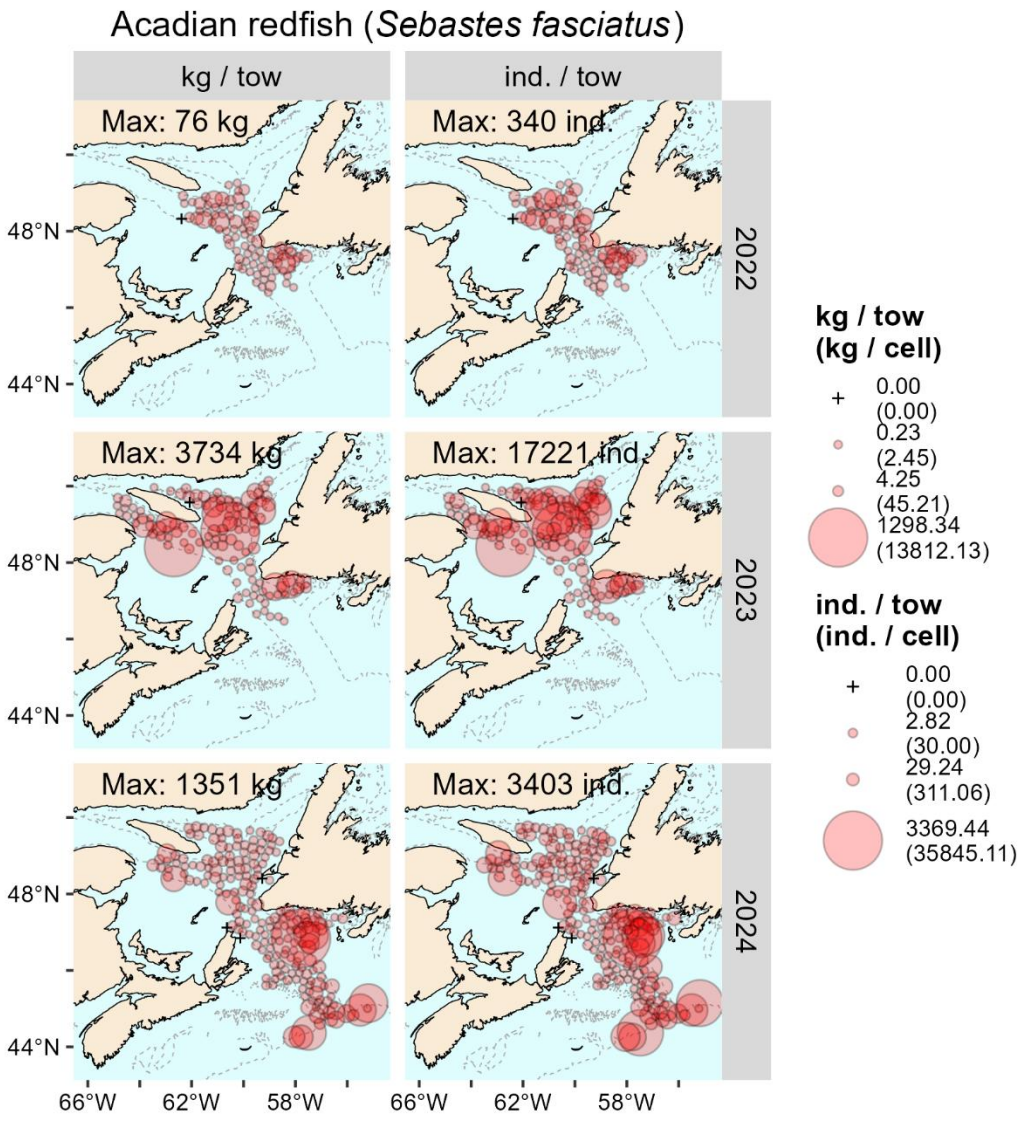


Figure 25a. Standardized catches by weight and/or number (colored bubbles) and cases of absence (black crosses) for the Acadian redfish in the winter surveys of 2022, 2023, and 2024.

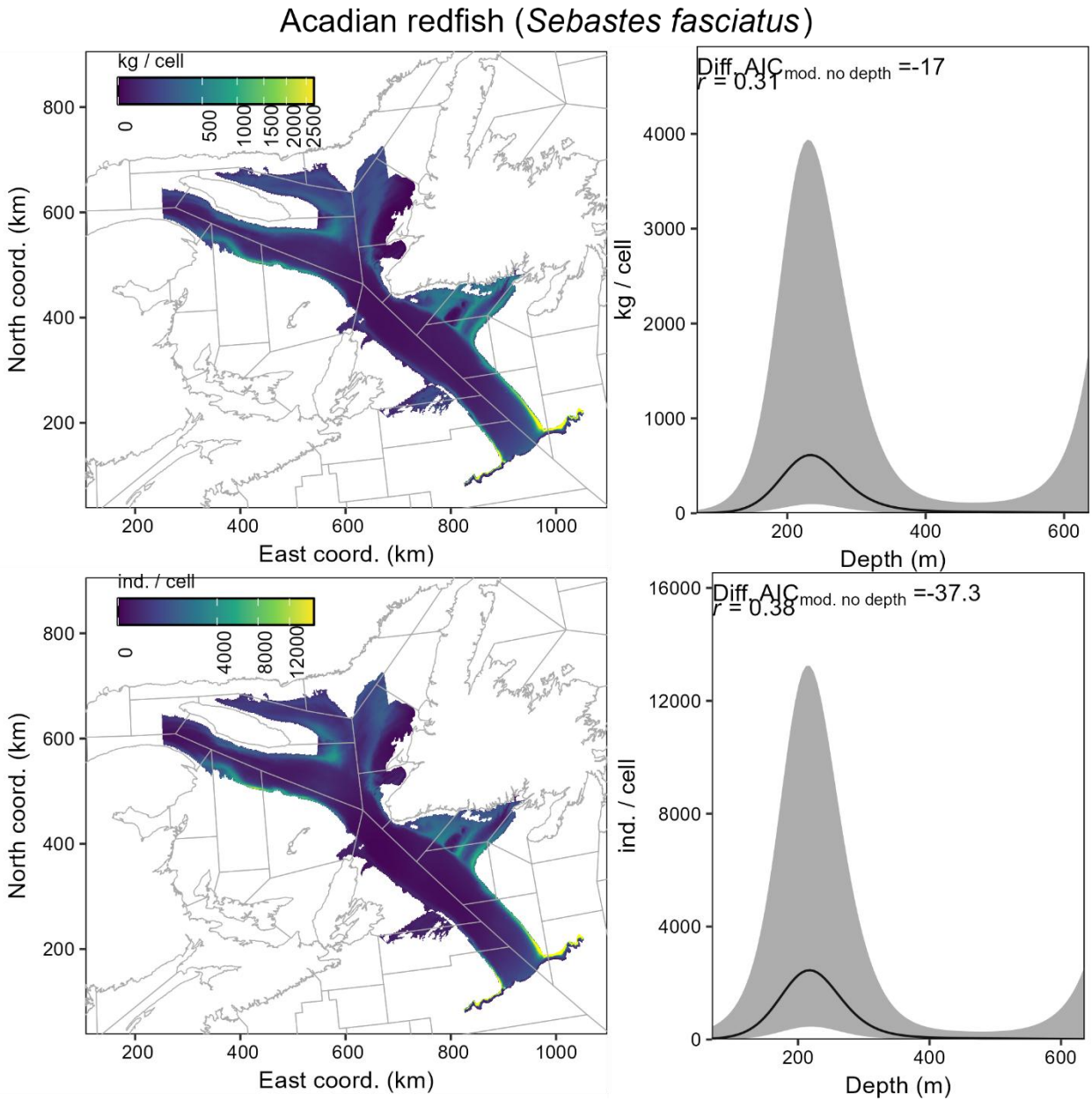


Figure 25b. Predicted weight (upper panels) and number (lower panels) values per 0.25 km^2 cell according to the selected spatial interpolation models for the Acadian redfish in the 2022, 2023, and 2024 winter survey.

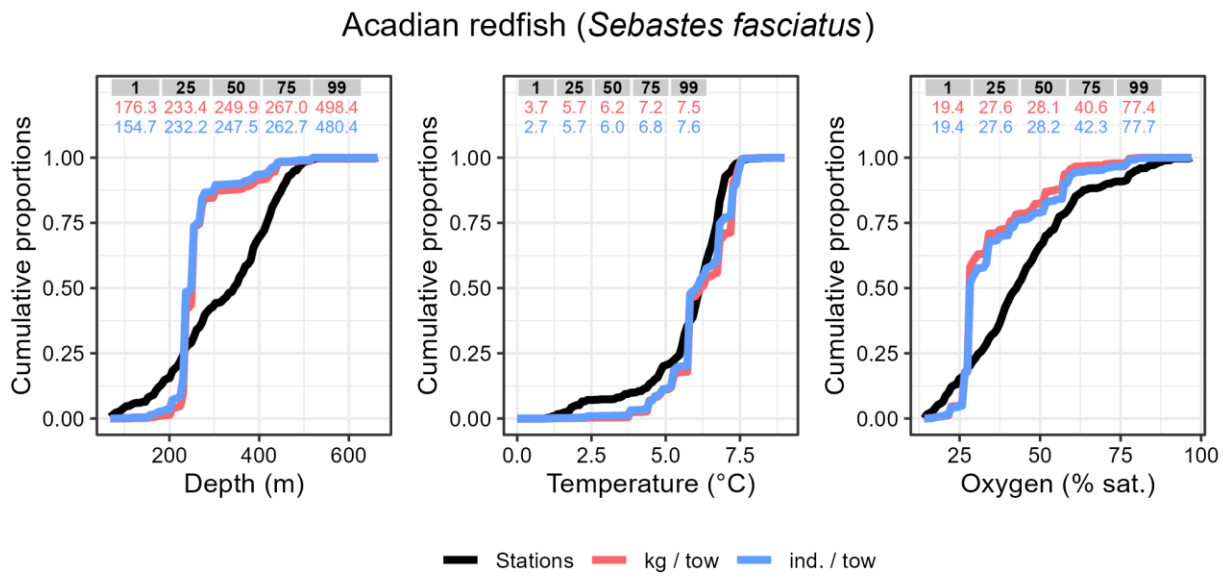


Figure 25c. Cumulative proportions of available values of depth, temperature and dissolved oxygen and standardized catches per tow for the Acadian redfish in the winter survey in 2022, 2023 and 2024.

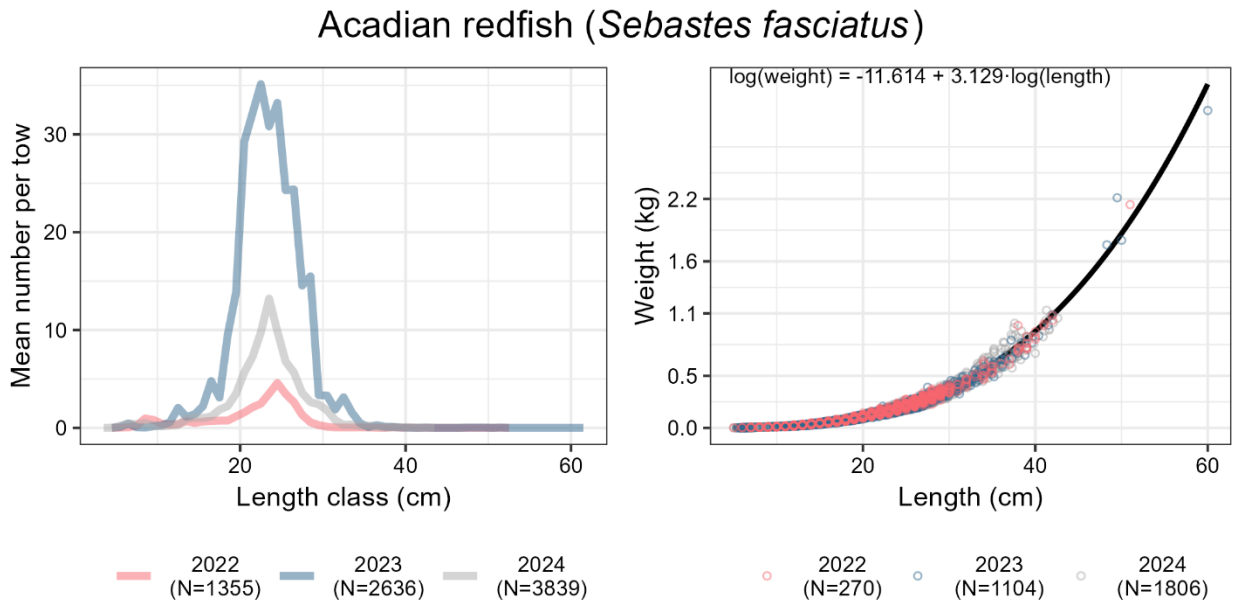


Figure 25d. Annual length frequencies (left panel) and length-weight observations with the global relationship prediction (right panel) for the Acadian redfish in the winter survey in 2022, 2023 and 2024.

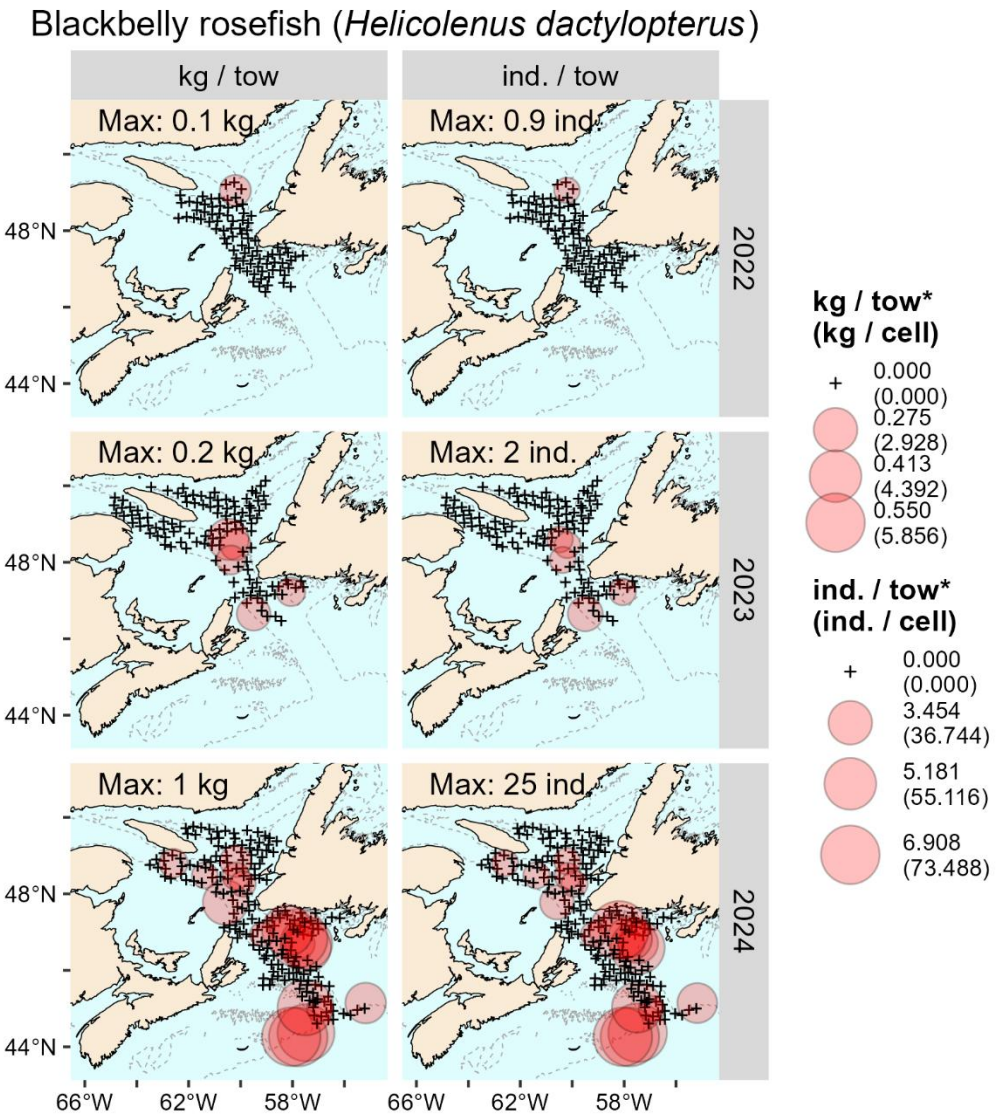


Figure 26a. Standardized catches by weight and/or number (colored bubbles) and cases of absence (black crosses) for the blackbelly rosefish in the winter surveys of 2022, 2023, and 2024.

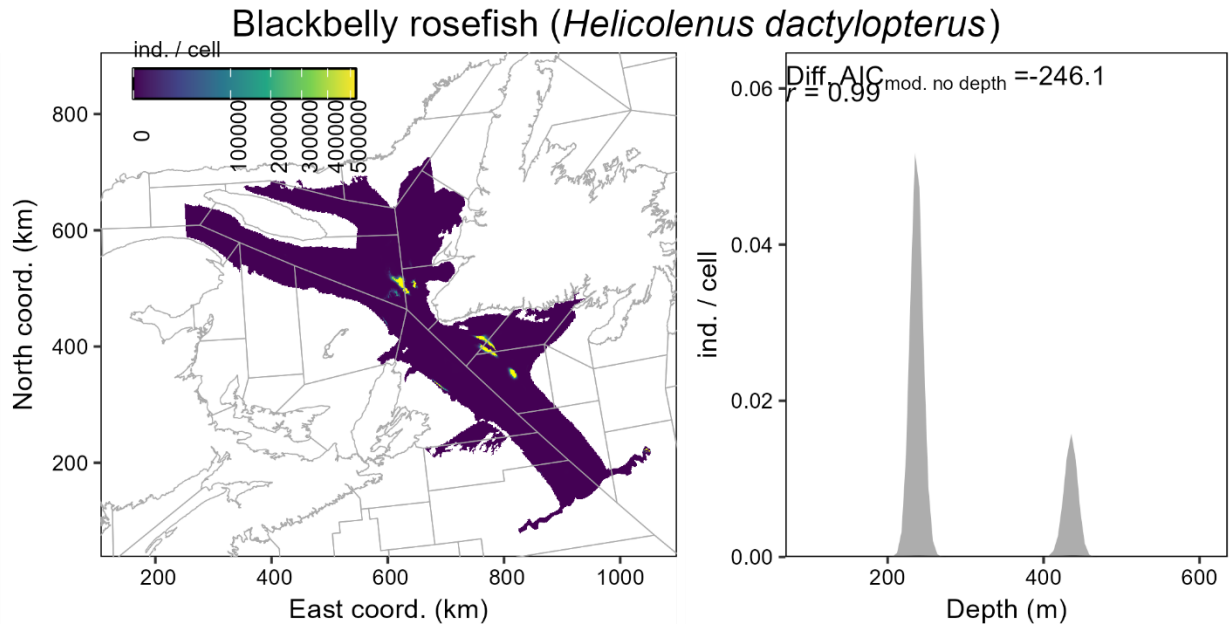


Figure 26b. Predicted number values per 0.25 km^2 cell according to the selected spatial interpolation model for the blackbelly rosefish in the 2022, 2023, and 2024 winter survey.

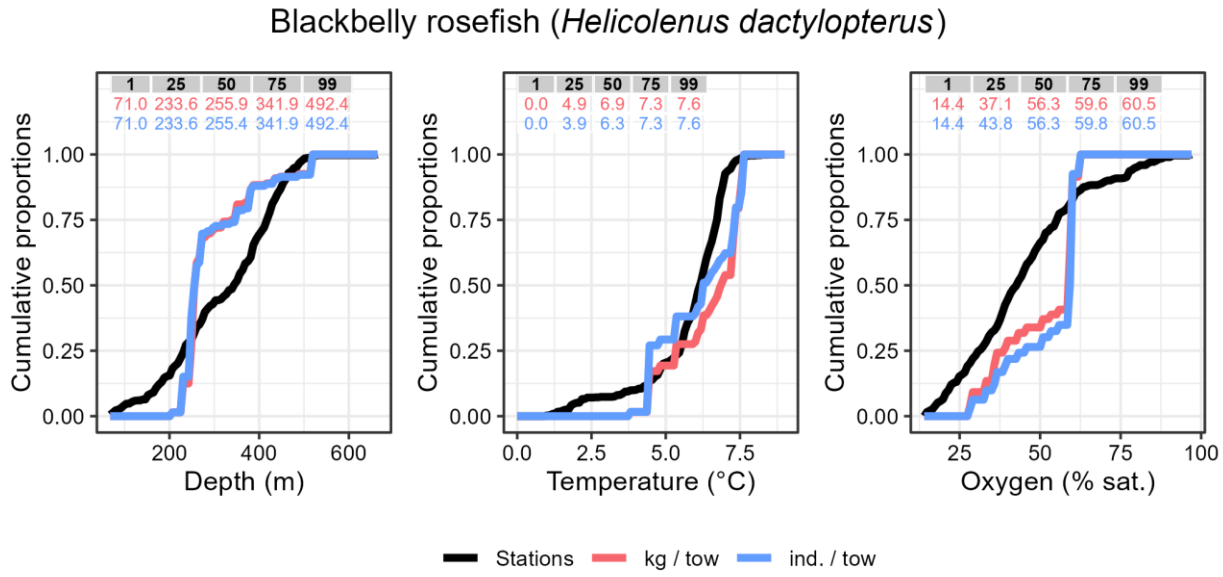


Figure 26c. Cumulative proportions of available values of depth, temperature and dissolved oxygen and standardized catches per tow for the blackbelly rosefish in the winter survey in 2022, 2023 and 2024.

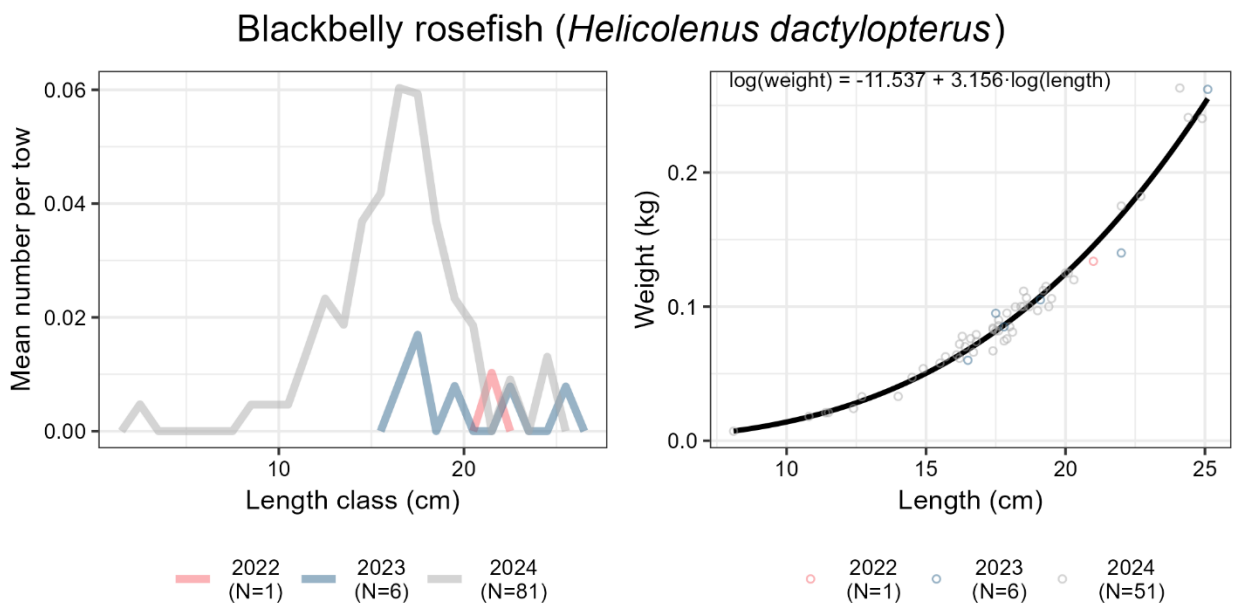


Figure 26d. Annual length frequencies (left panel) and length-weight observations with the global relationship prediction (right panel) for the blackbelly rosefish in the winter survey in 2022, 2023 and 2024.

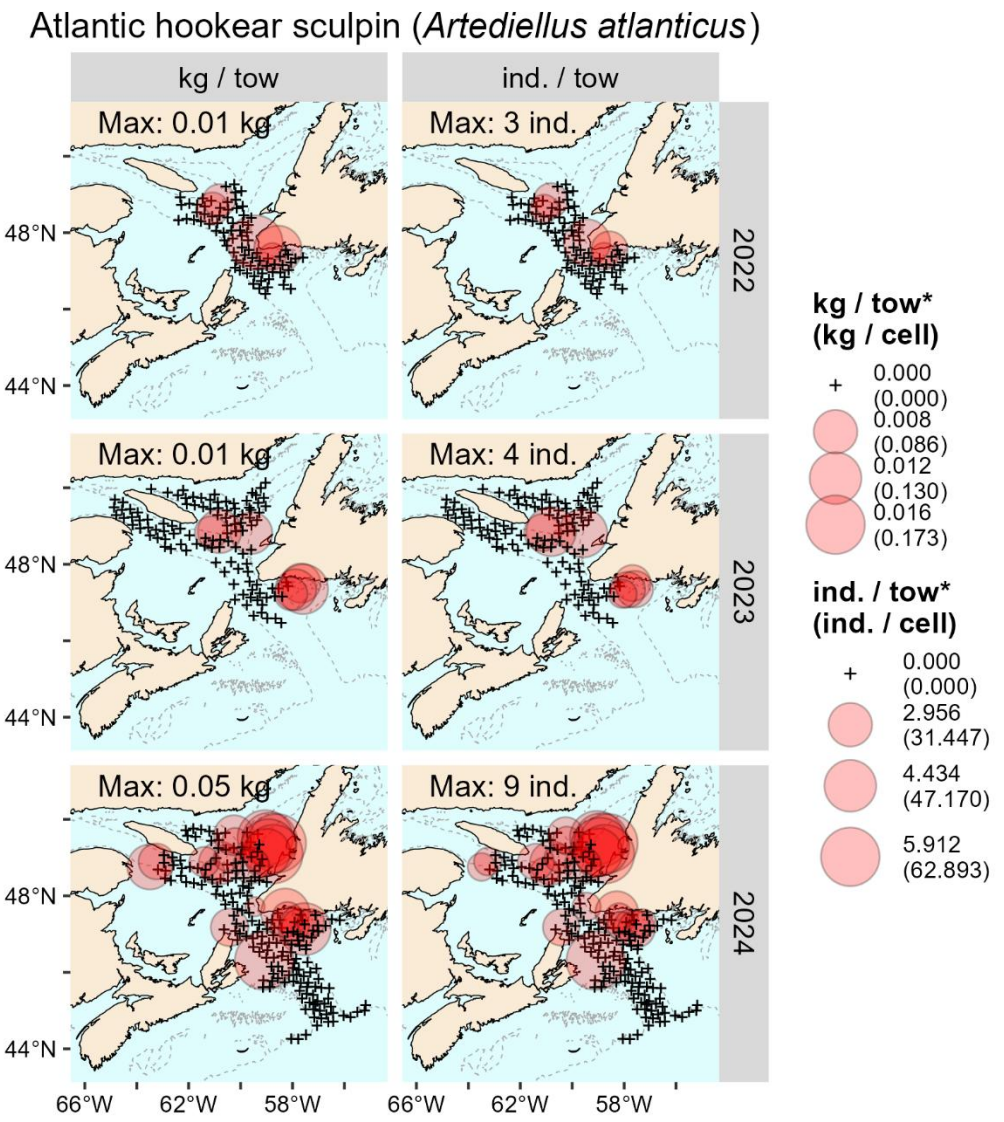


Figure 27a. Standardized catches by weight and/or number (colored bubbles) and cases of absence (black crosses) for the Atlantic hookear sculpin in the winter surveys of 2022, 2023, and 2024.

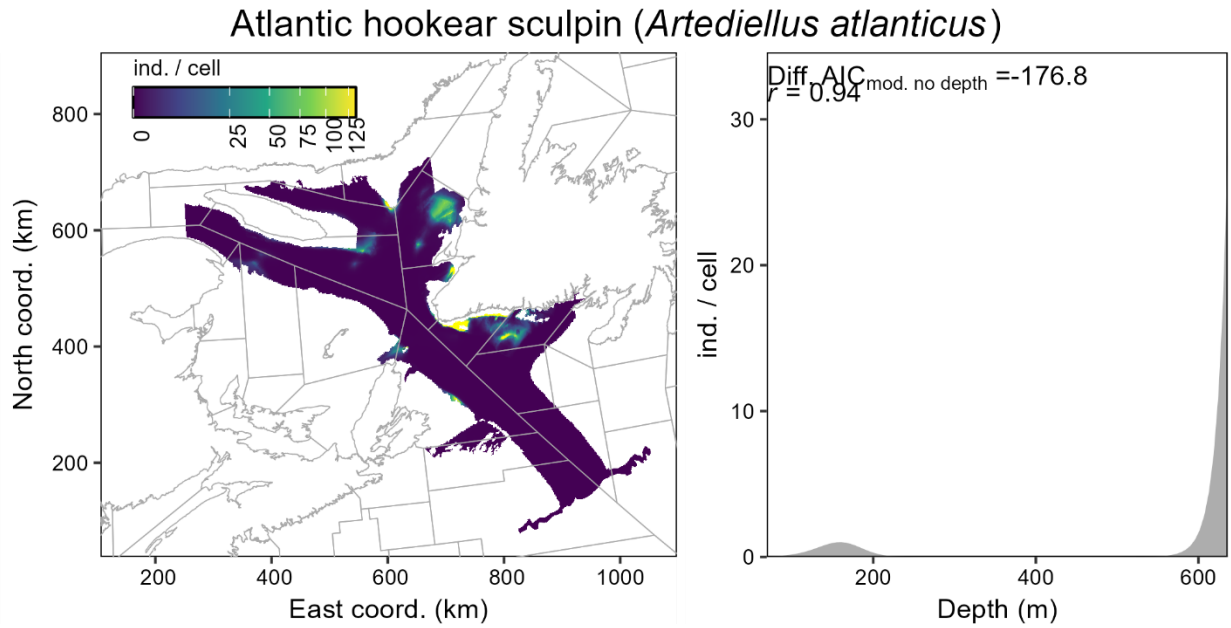


Figure 27b. Predicted number values per 0.25 km^2 cell according to the selected spatial interpolation model for the Atlantic hookear sculpin in the 2022, 2023, and 2024 winter survey.

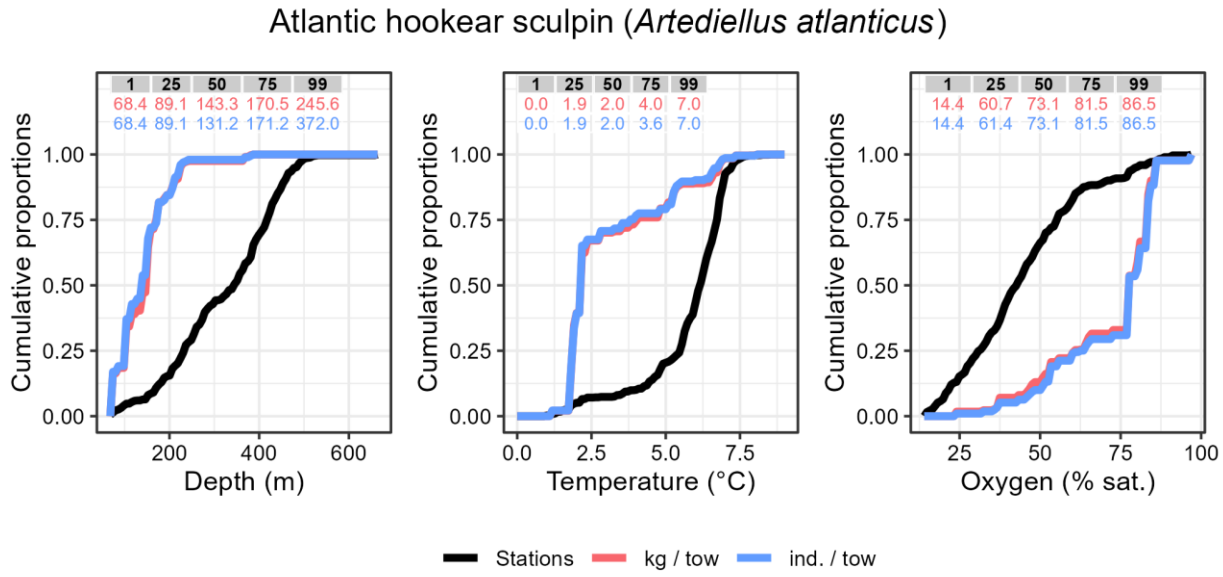


Figure 27c. Cumulative proportions of available values of depth, temperature and dissolved oxygen and standardized catches per tow for the Atlantic hookear sculpin in the winter survey in 2022, 2023 and 2024.

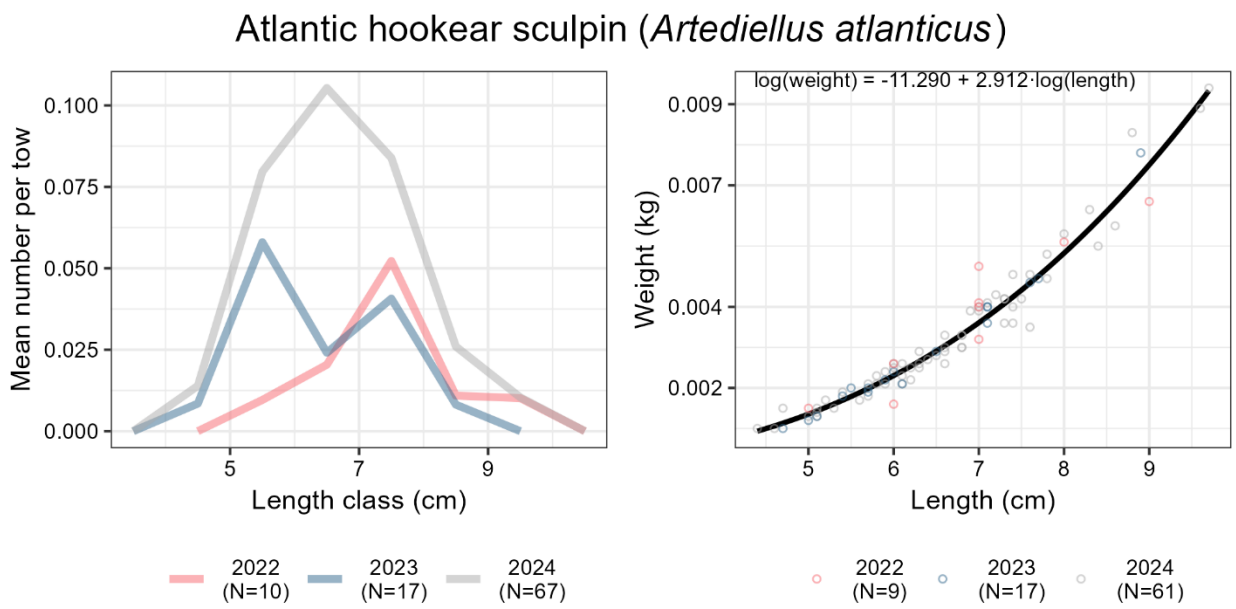


Figure 27d. Annual length frequencies (left panel) and length-weight observations with the global relationship prediction (right panel) for the Atlantic hookear sculpin in the winter survey in 2022, 2023 and 2024.

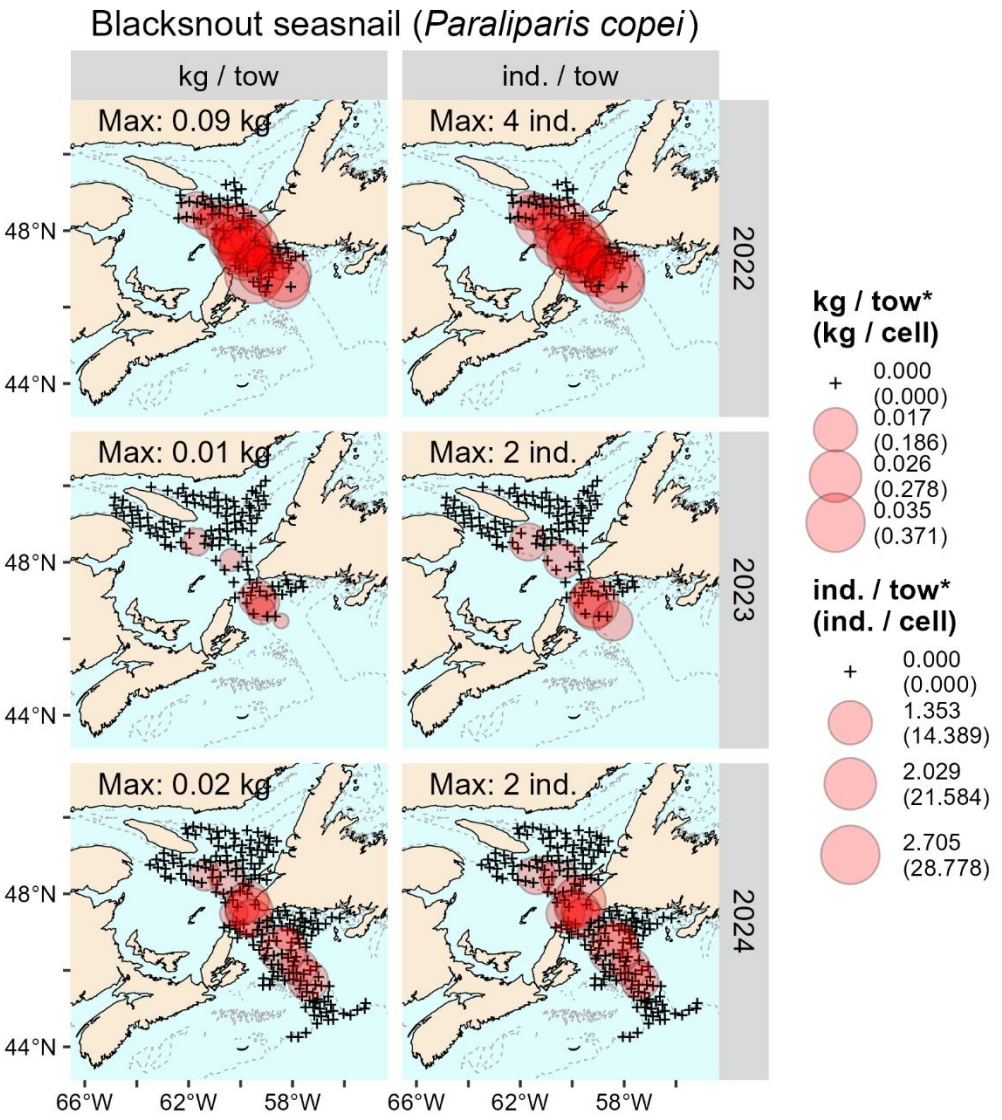


Figure 28a. Standardized catches by weight and/or number (colored bubbles) and cases of absence (black crosses) for the blacksnout seasnail in the winter surveys of 2022, 2023, and 2024.

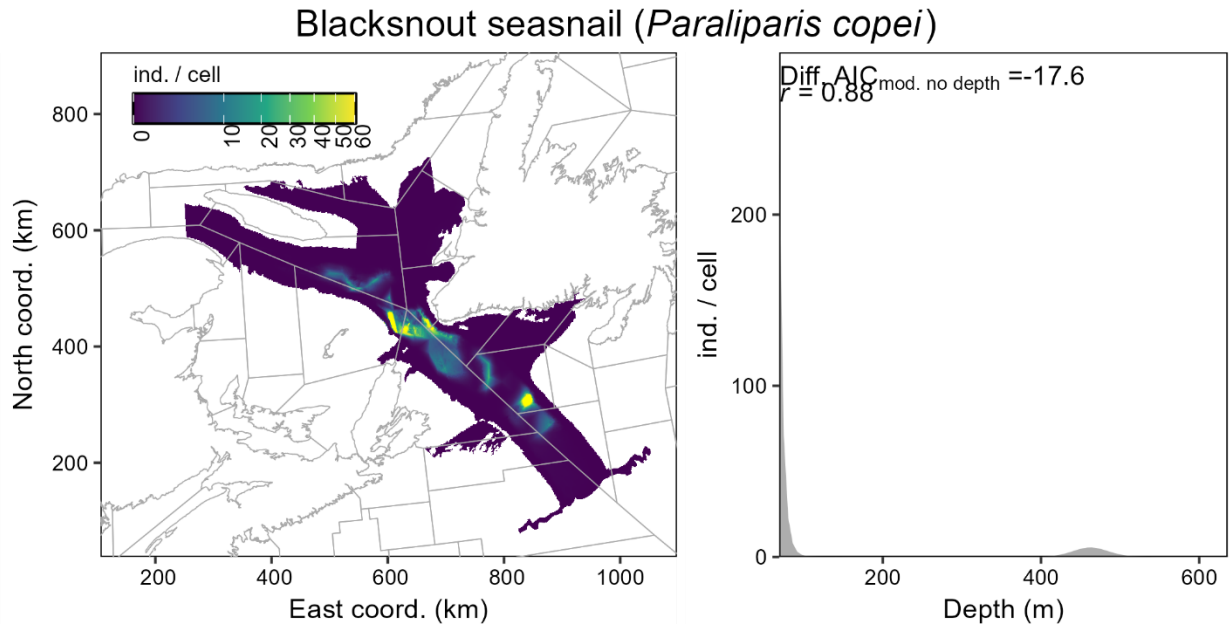


Figure 28b. Predicted number values per 0.25 km^2 cell according to the selected spatial interpolation model for the blacksnout seasnail in the 2022, 2023, and 2024 winter survey.

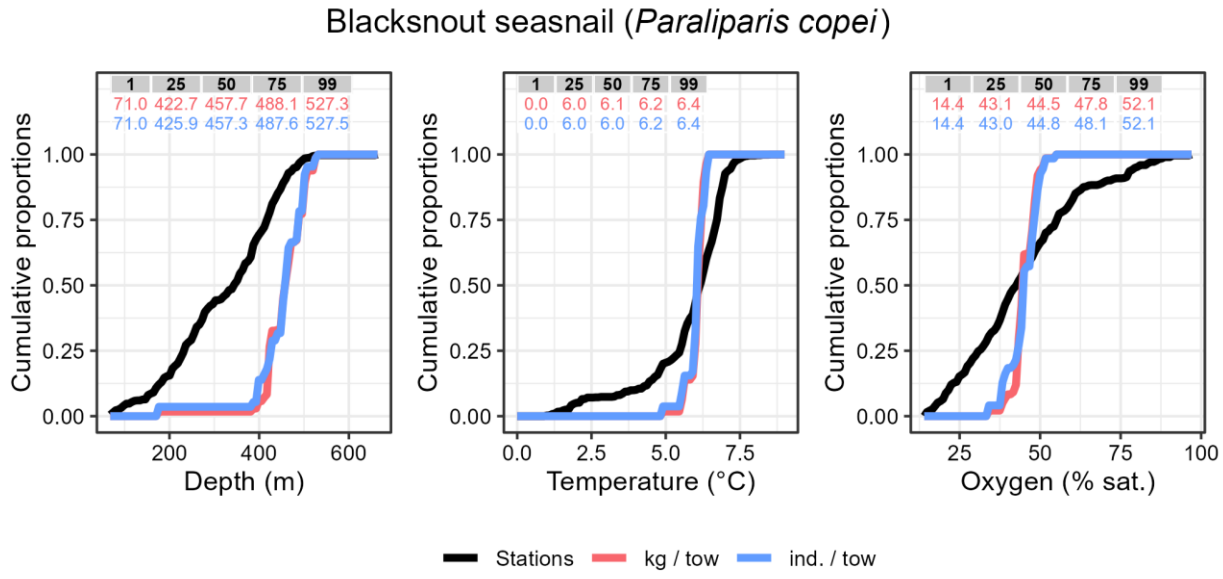


Figure 28c. Cumulative proportions of available values of depth, temperature and dissolved oxygen and standardized catches per tow for the blacksnout seasnail in the winter survey in 2022, 2023 and 2024.

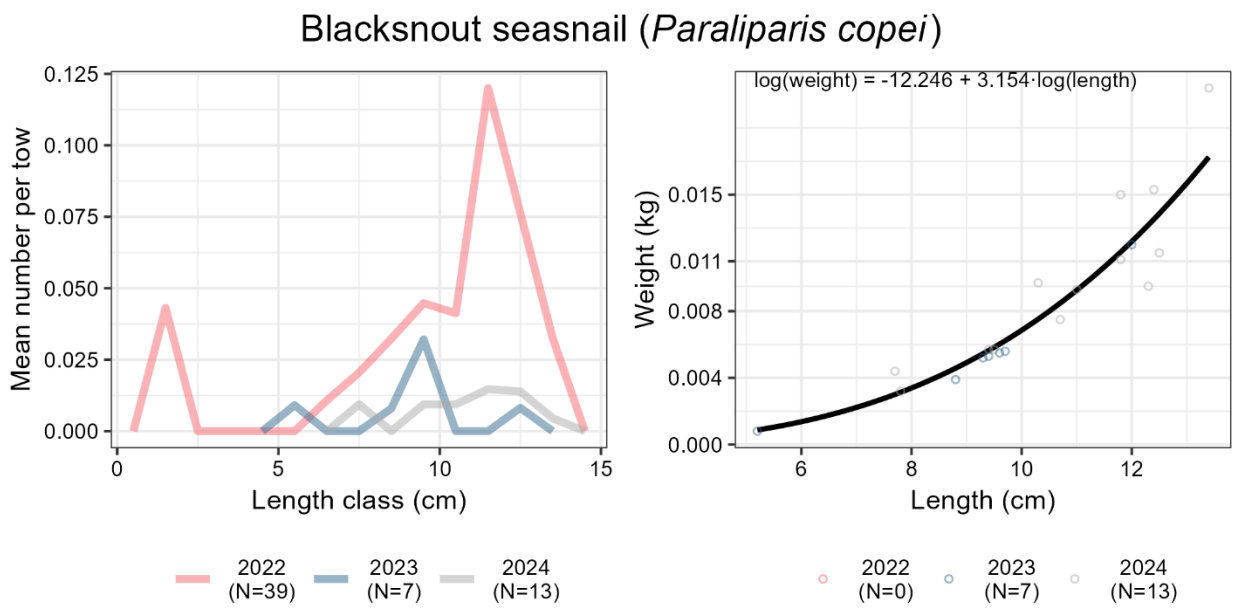


Figure 28d. Annual length frequencies (left panel) and length-weight observations with the global relationship prediction (right panel) for the blacksnout seasnail in the winter survey in 2022, 2023 and 2024.

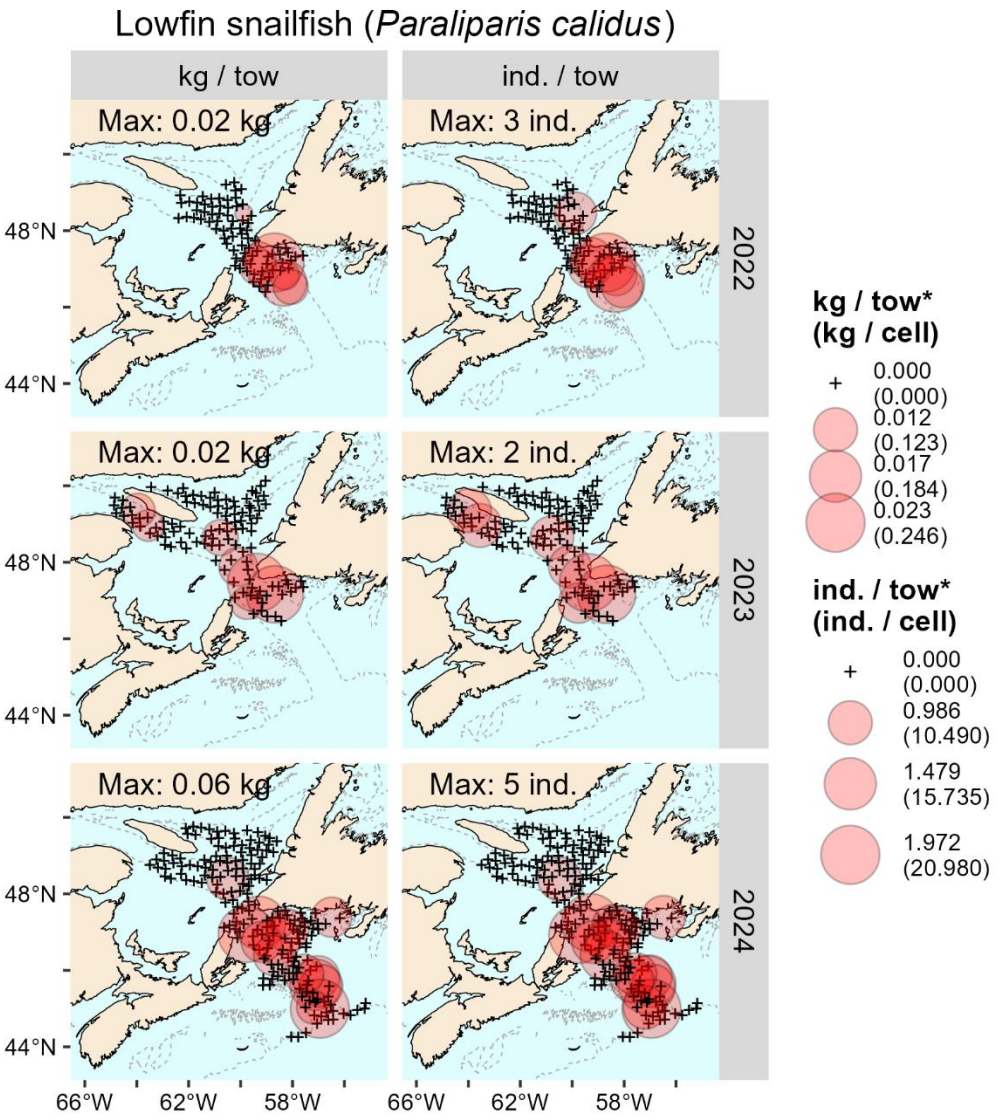


Figure 29a. Standardized catches by weight and/or number (colored bubbles) and cases of absence (black crosses) for the lowfin snailfish in the winter surveys of 2022, 2023, and 2024.

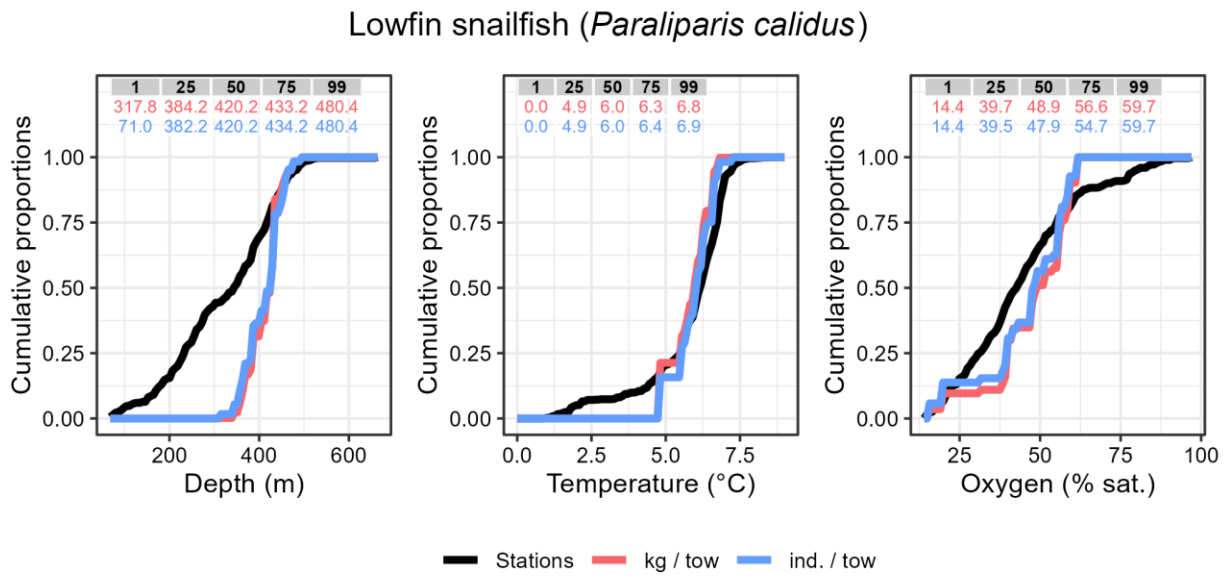


Figure 29b. Cumulative proportions of available values of depth, temperature and dissolved oxygen and standardized catches per tow for the lowfin snailfish in the winter survey in 2022, 2023 and 2024.

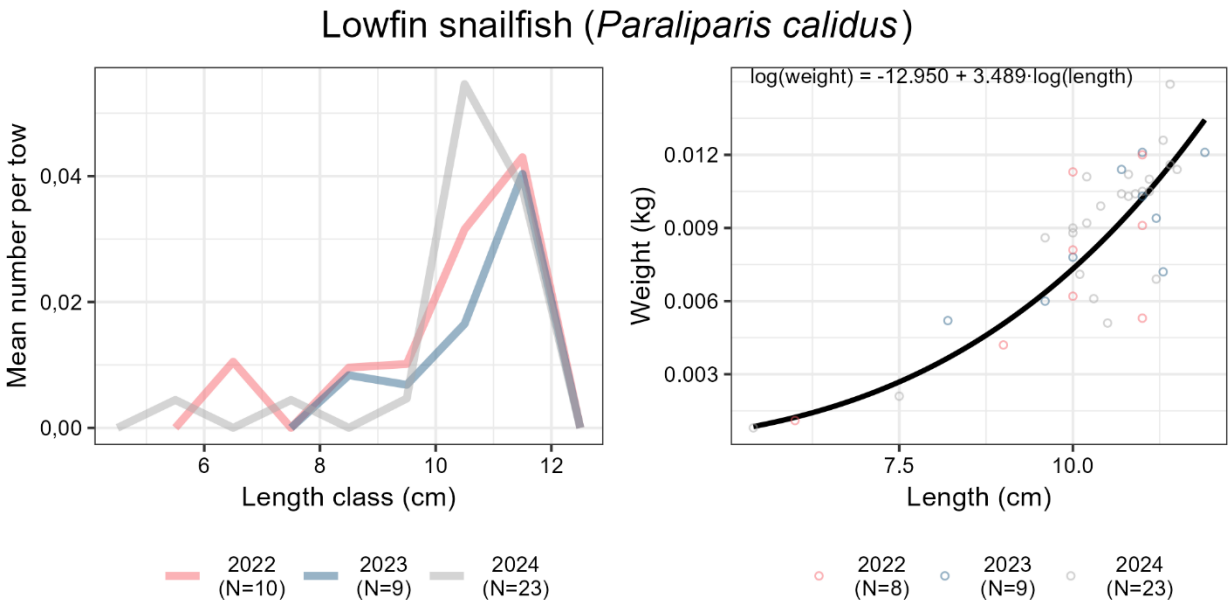


Figure 29c. Annual length frequencies (left panel) and length-weight observations with the global relationship prediction (right panel) for the lowfin snailfish in the winter survey in 2022, 2023 and 2024.

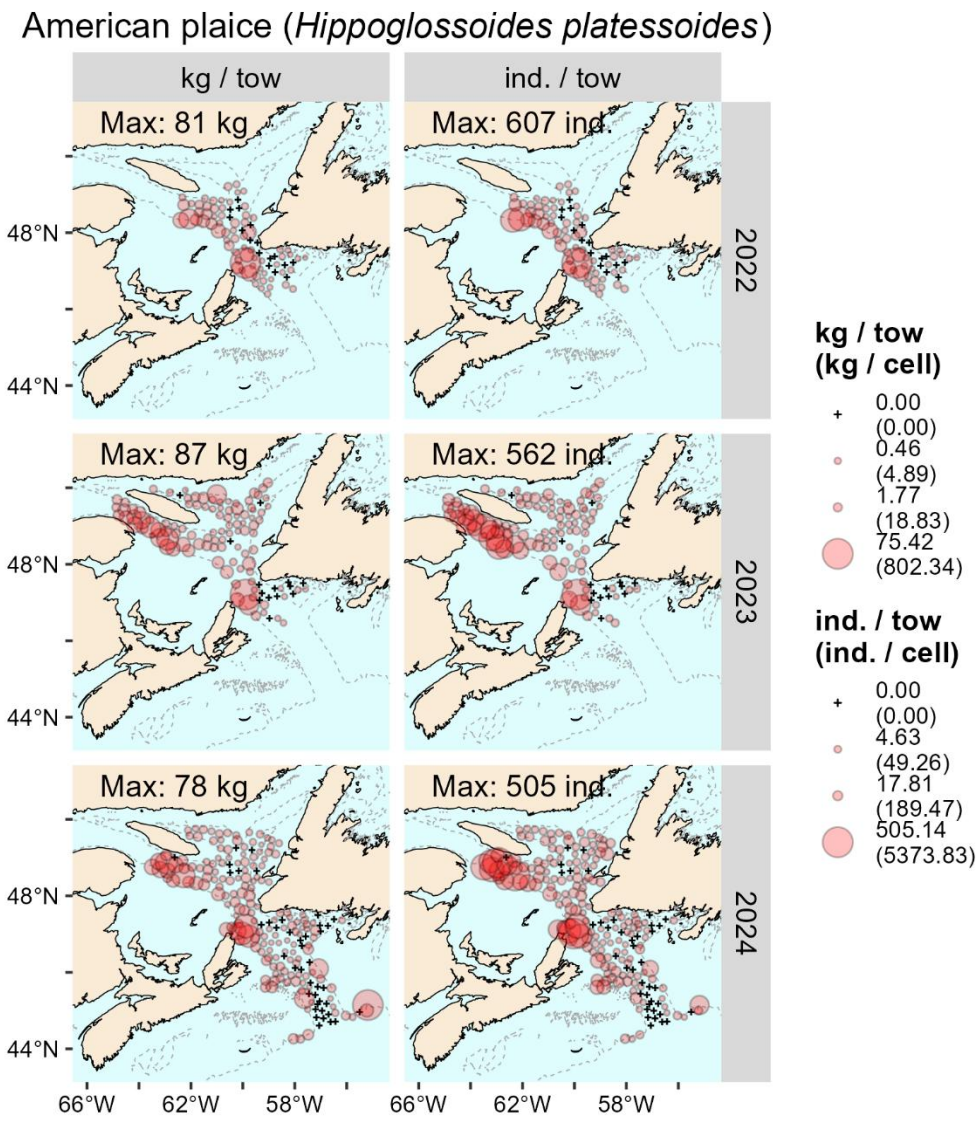


Figure 30a. Standardized catches by weight and/or number (colored bubbles) and cases of absence (black crosses) for the American plaice in the winter surveys of 2022, 2023, and 2024.

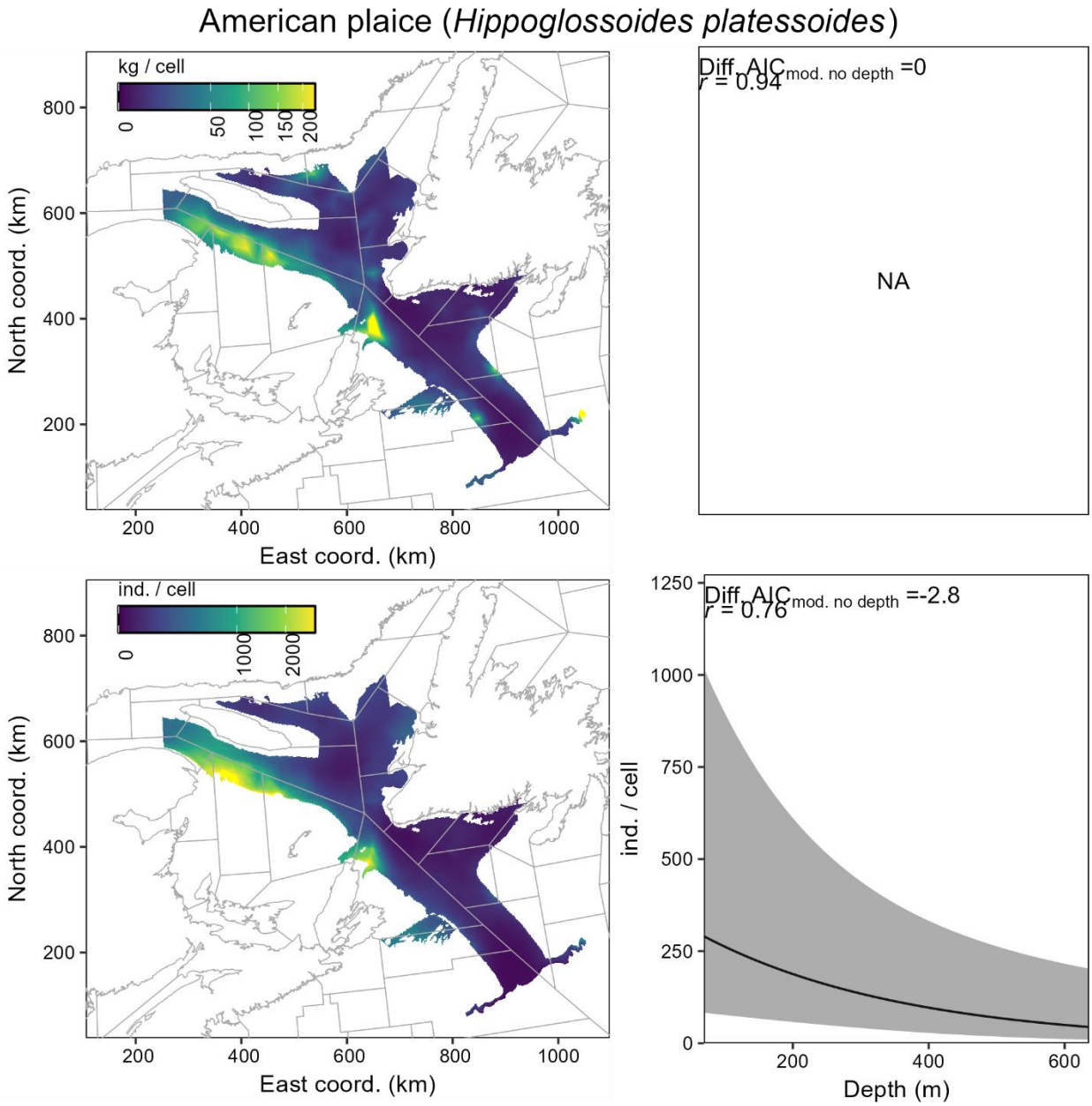


Figure 30b. Predicted weight (upper panels) and number (lower panels) values per 0.25 km^2 cell according to the selected spatial interpolation models for the American plaice in the 2022, 2023, and 2024 winter survey.

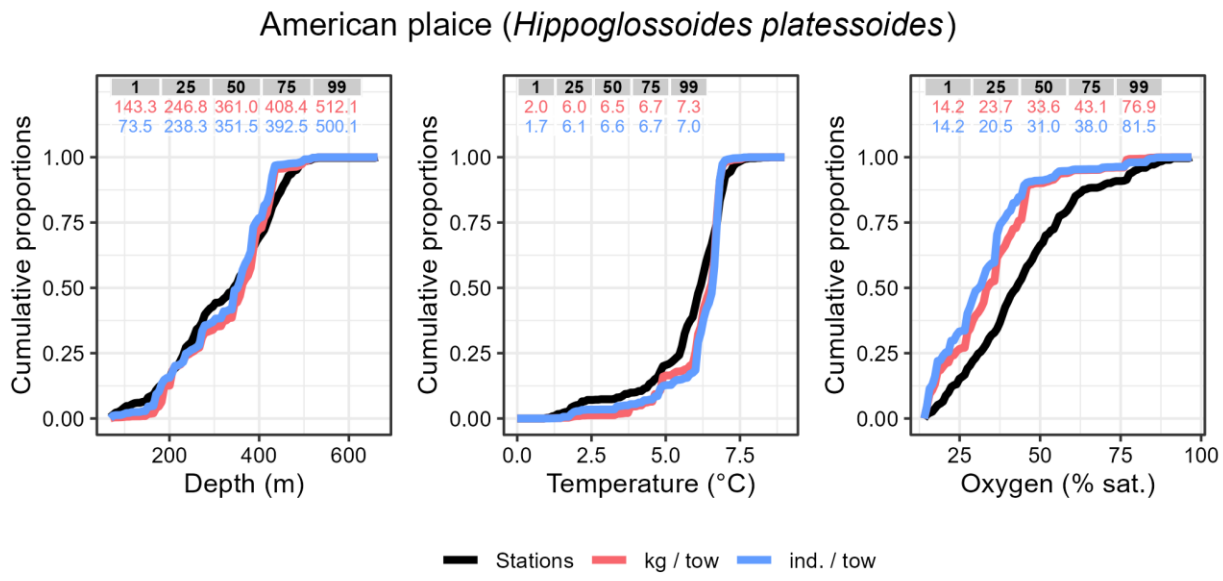


Figure 30c. Cumulative proportions of available values of depth, temperature and dissolved oxygen and standardized catches per tow for the American plaice in the winter survey in 2022, 2023 and 2024.

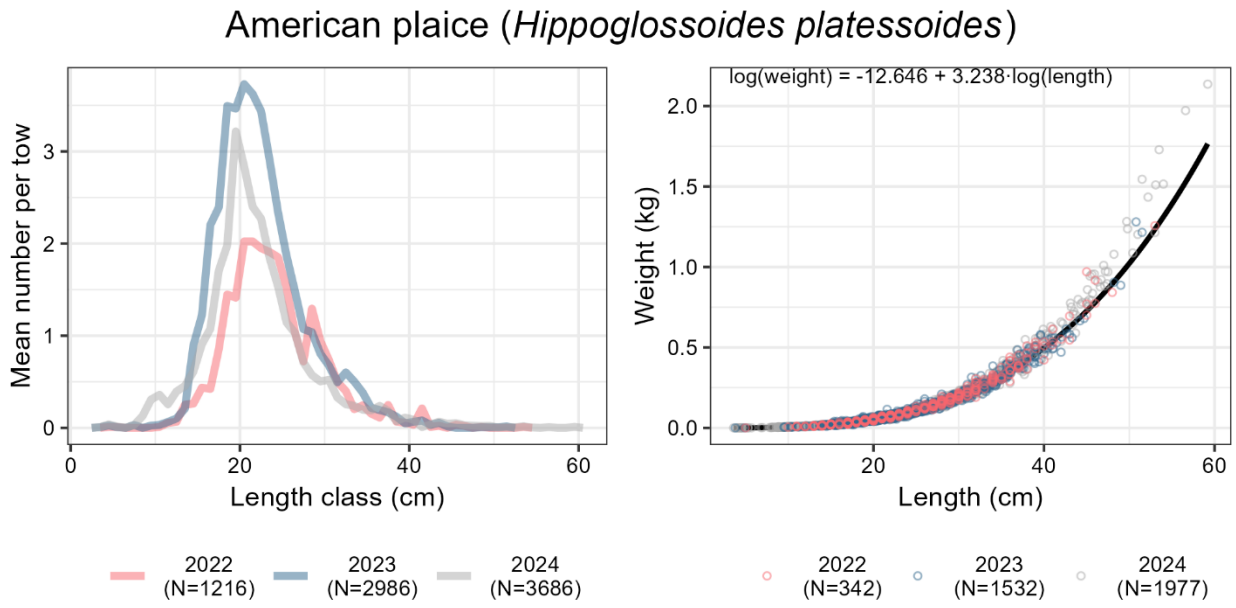


Figure 30d. Annual length frequencies (left panel) and length-weight observations with the global relationship prediction (right panel) for the American plaice in the winter survey in 2022, 2023 and 2024.

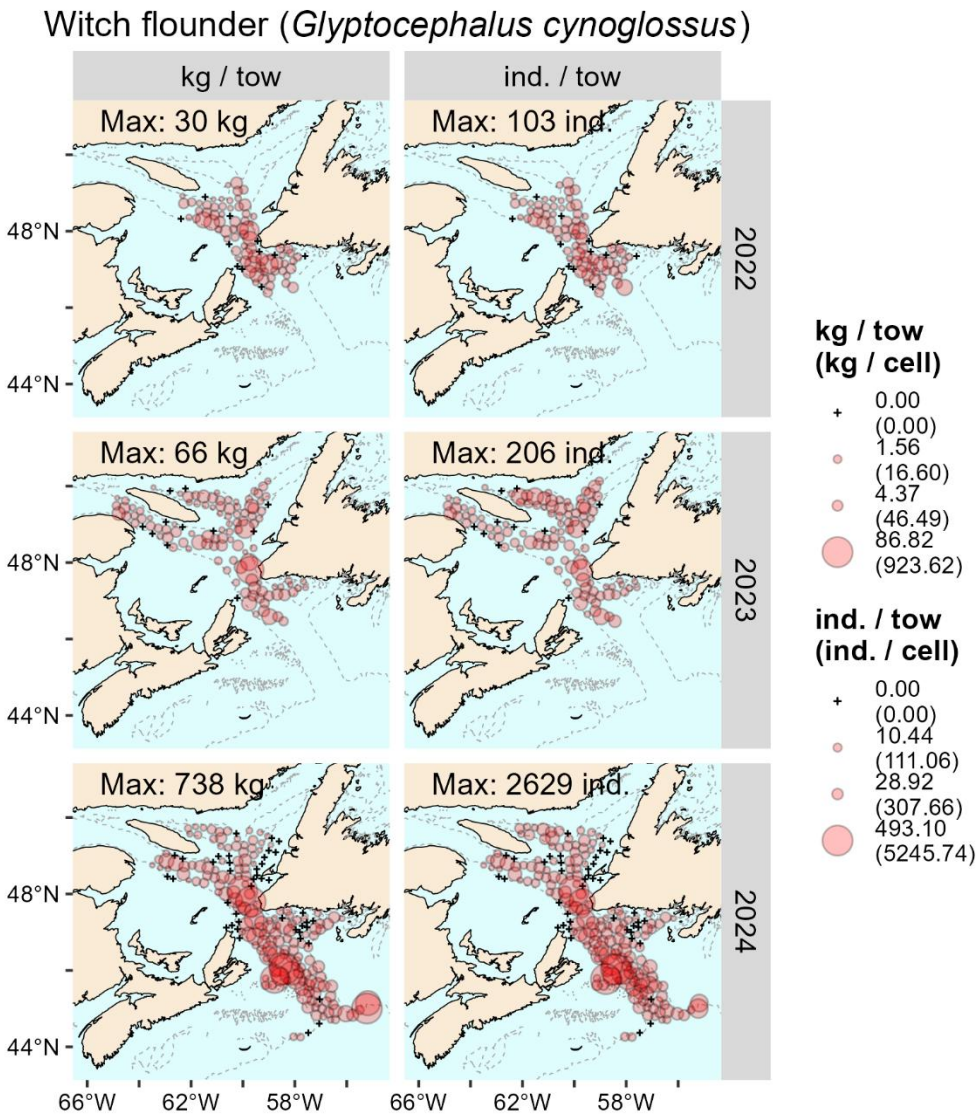


Figure 31a. Standardized catches by weight and/or number (colored bubbles) and cases of absence (black crosses) for the witch flounder in the winter surveys of 2022, 2023, and 2024.

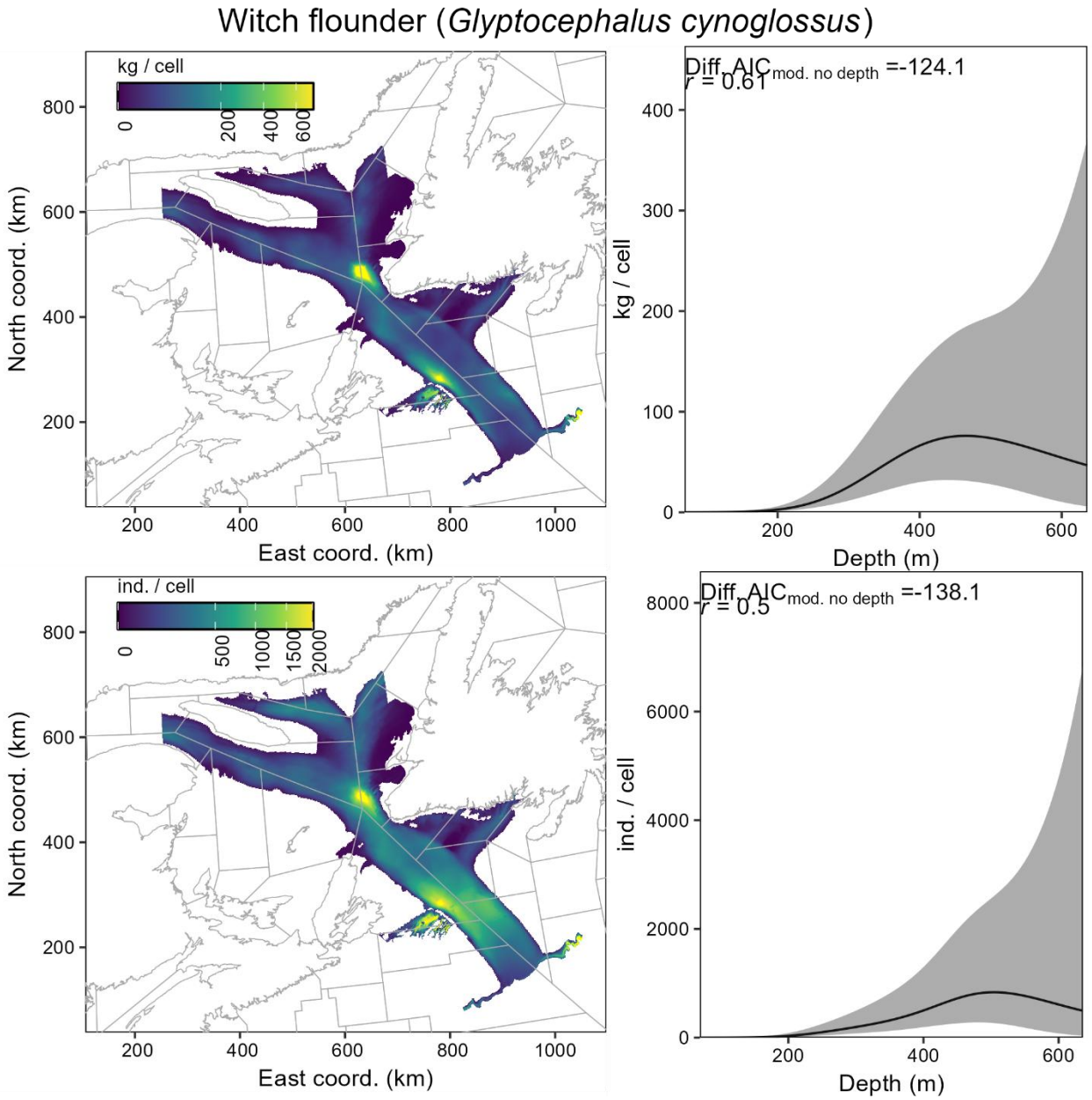


Figure 31b. Predicted weight (upper panels) and number (lower panels) values per 0.25 km^2 cell according to the selected spatial interpolation models for the witch flounder in the 2022, 2023, and 2024 winter survey.

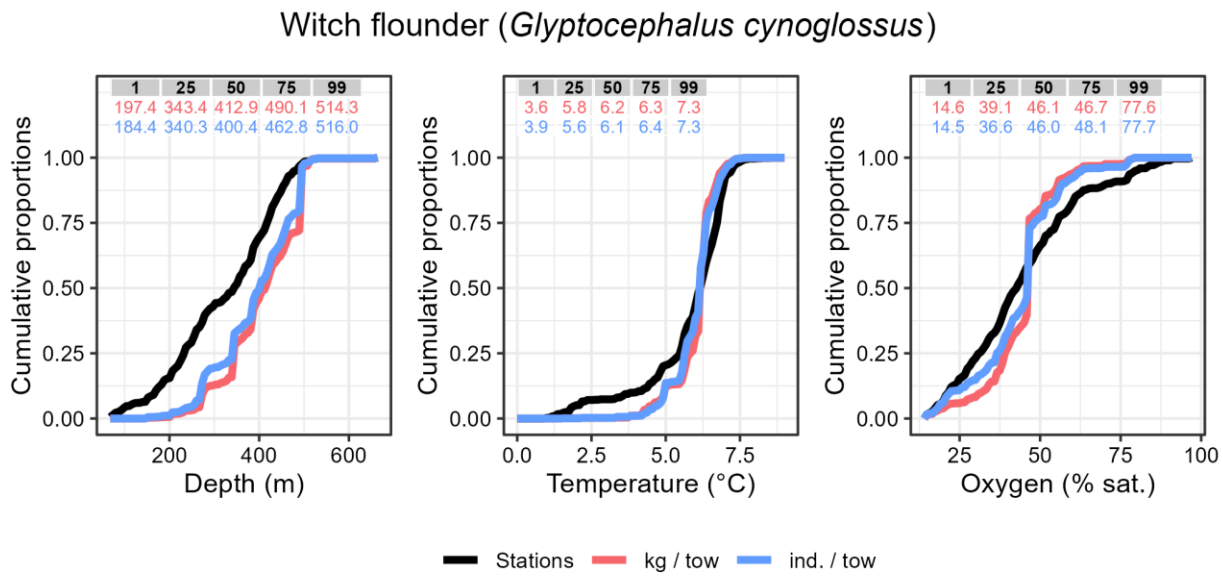


Figure 31c. Cumulative proportions of available values of depth, temperature and dissolved oxygen and standardized catches per tow for the witch flounder in the winter survey in 2022, 2023 and 2024.

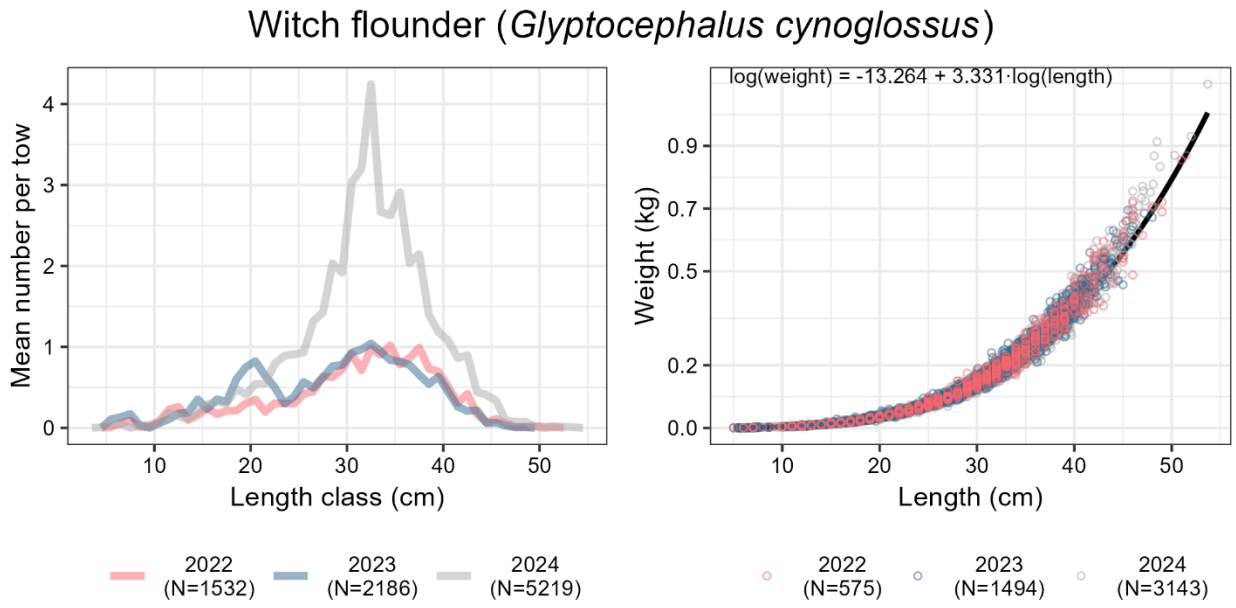


Figure 31d. Annual length frequencies (left panel) and length-weight observations with the global relationship prediction (right panel) for the witch flounder in the winter survey in 2022, 2023 and 2024.

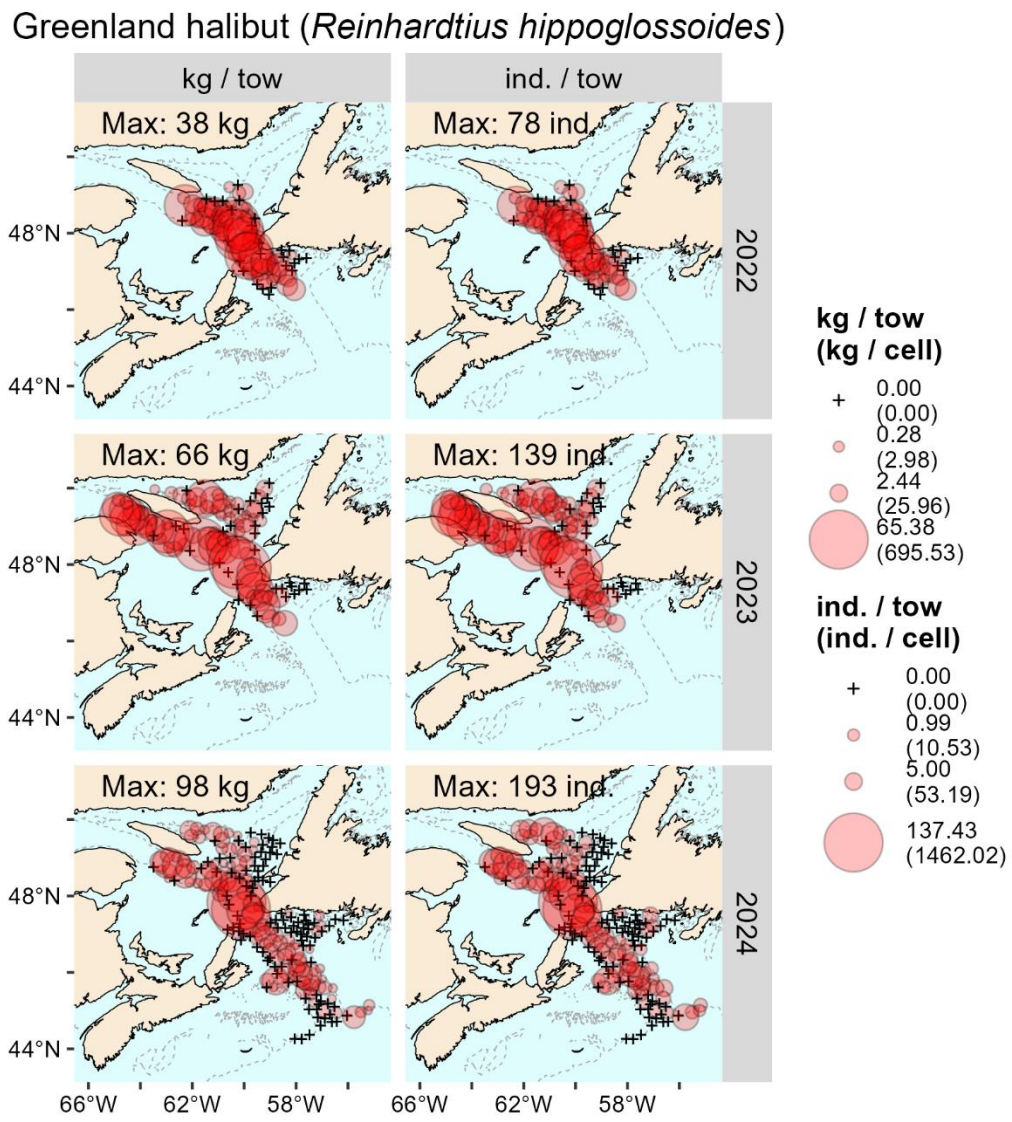


Figure 32a. Standardized catches by weight and/or number (colored bubbles) and cases of absence (black crosses) for the Greenland halibut in the winter surveys of 2022, 2023, and 2024.

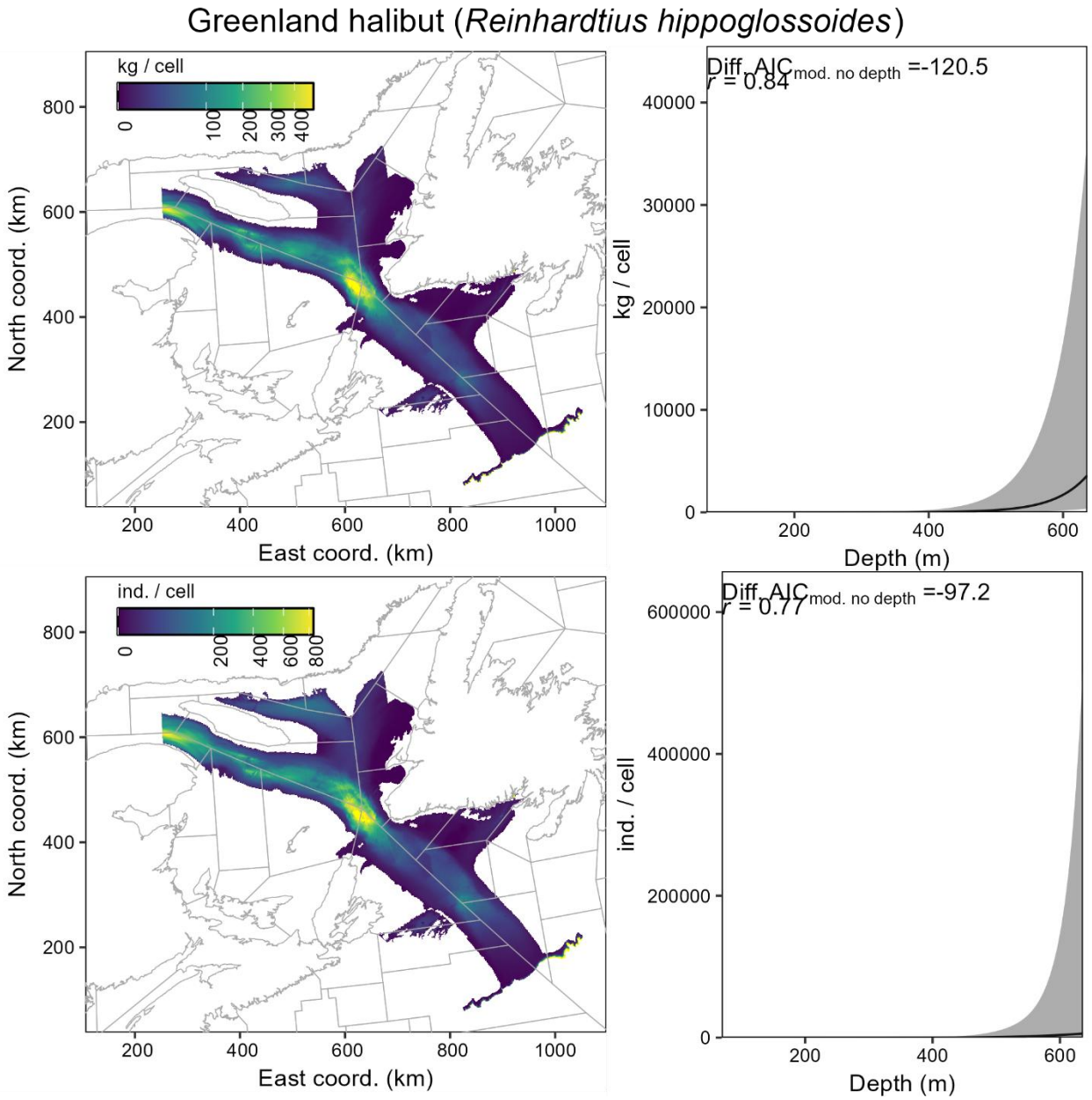


Figure 32b. Predicted weight (upper panels) and number (lower panels) values per 0.25 km^2 cell according to the selected spatial interpolation models for the Greenland halibut in the 2022, 2023, and 2024 winter survey.

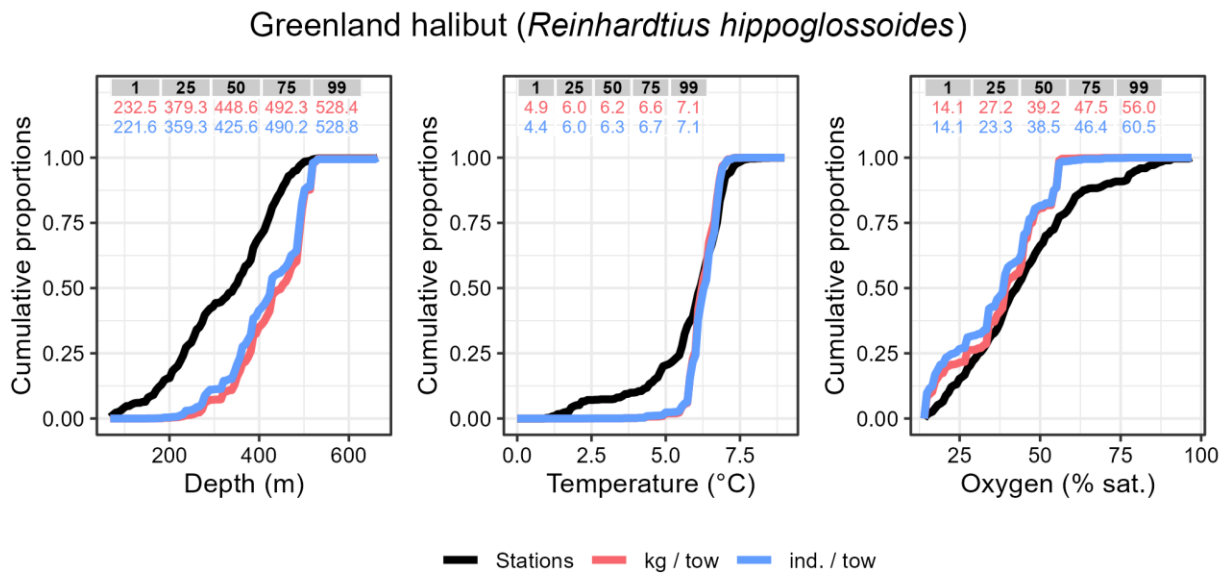


Figure 32c. Cumulative proportions of available values of depth, temperature and dissolved oxygen and standardized catches per tow for the Greenland halibut in the winter survey in 2022, 2023 and 2024.

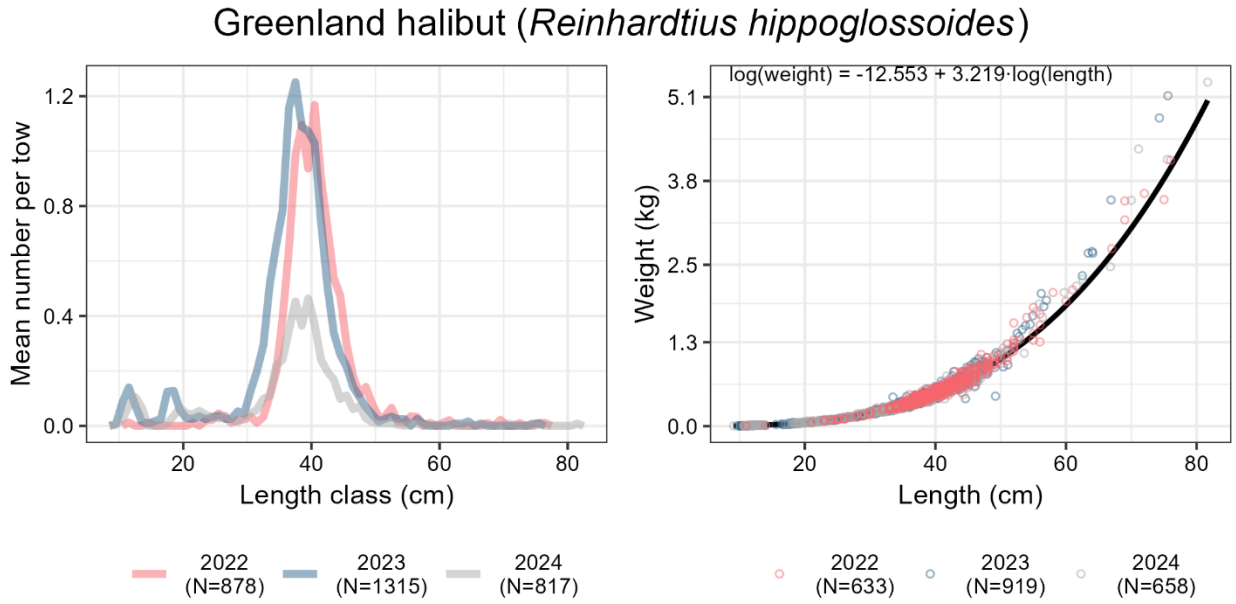


Figure 32d. Annual length frequencies (left panel) and length-weight observations with the global relationship prediction (right panel) for the Greenland halibut in the winter survey in 2022, 2023 and 2024.

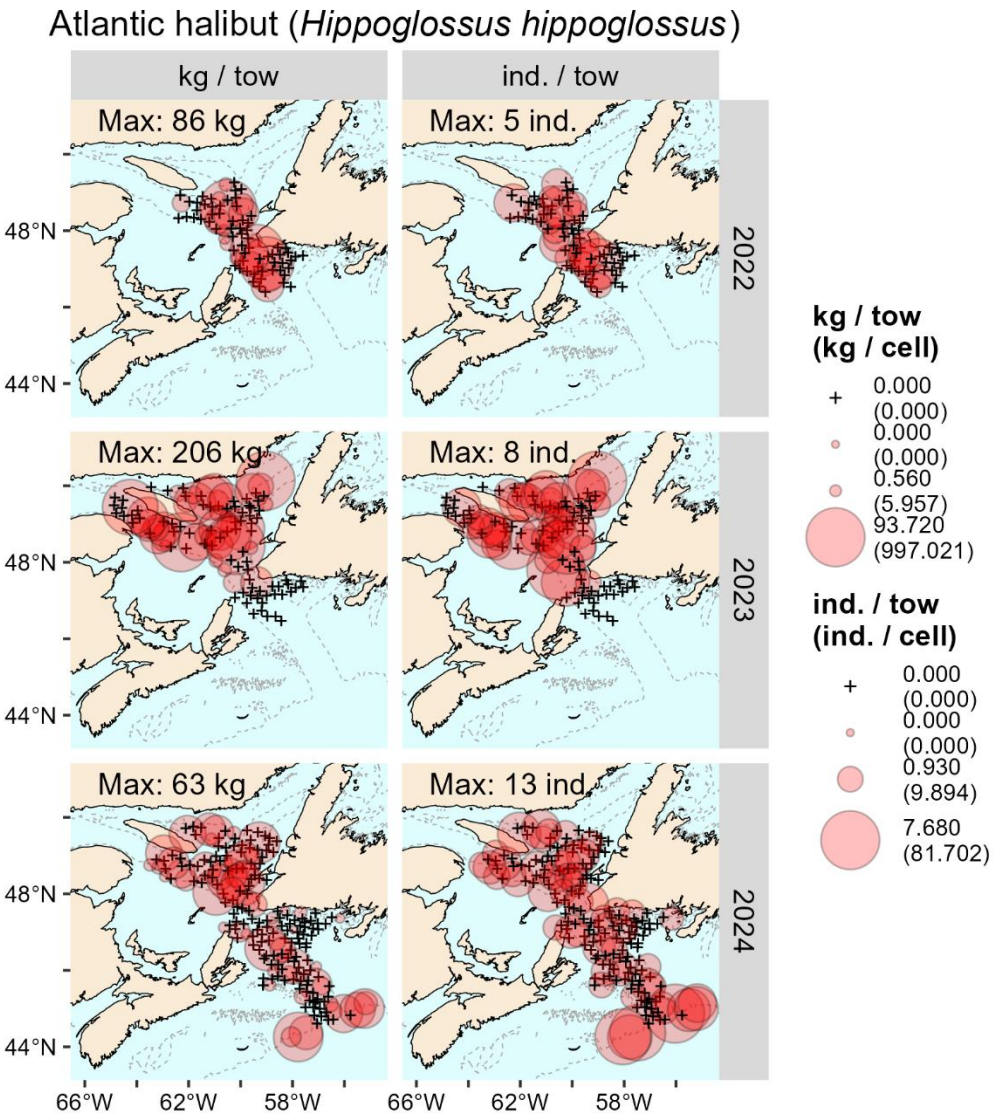


Figure 33a. Standardized catches by weight and/or number (colored bubbles) and cases of absence (black crosses) for the Atlantic halibut in the winter surveys of 2022, 2023, and 2024.

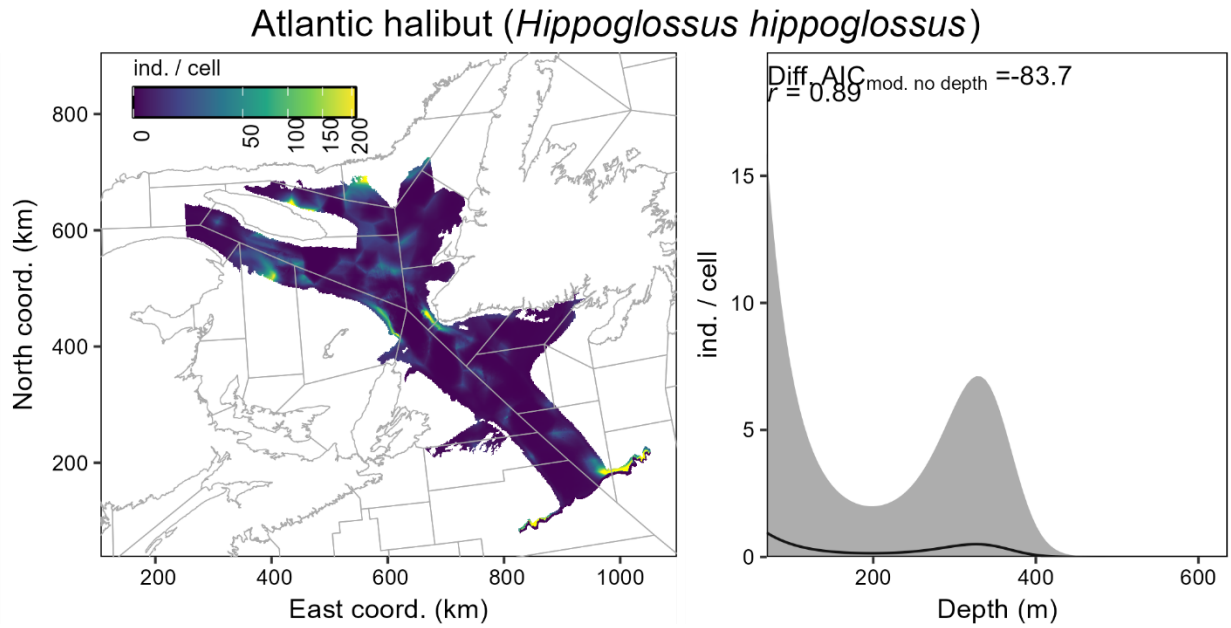


Figure 33b. Predicted number values per 0.25 km^2 cell according to the selected spatial interpolation model for the Atlantic halibut in the 2022, 2023, and 2024 winter survey.

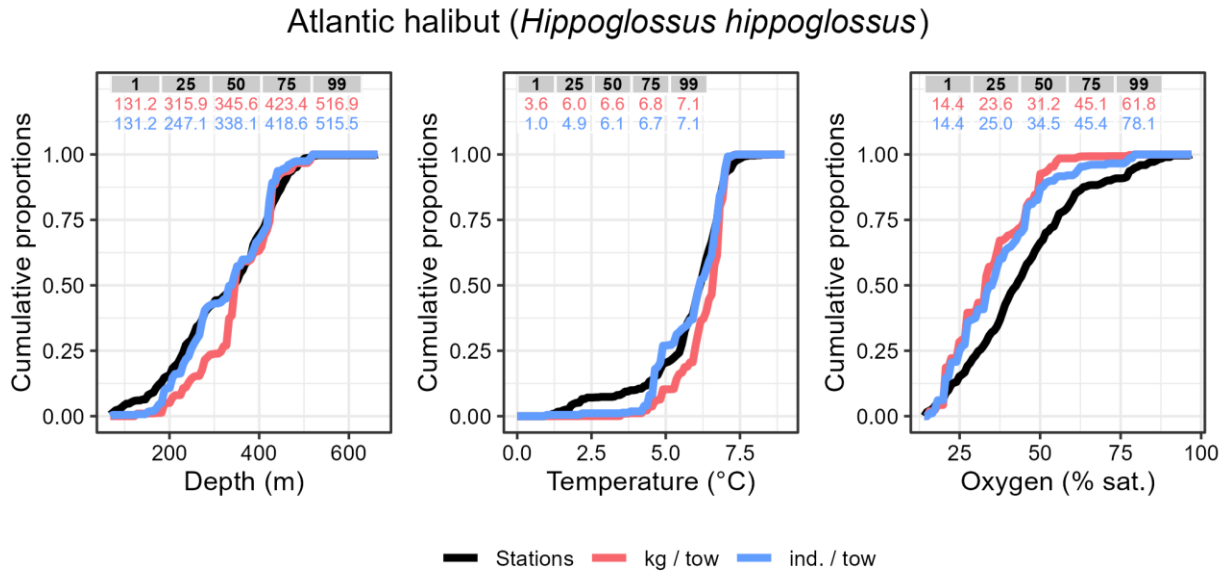


Figure 33c. Cumulative proportions of available values of depth, temperature and dissolved oxygen and standardized catches per tow for the Atlantic halibut in the winter survey in 2022, 2023 and 2024.

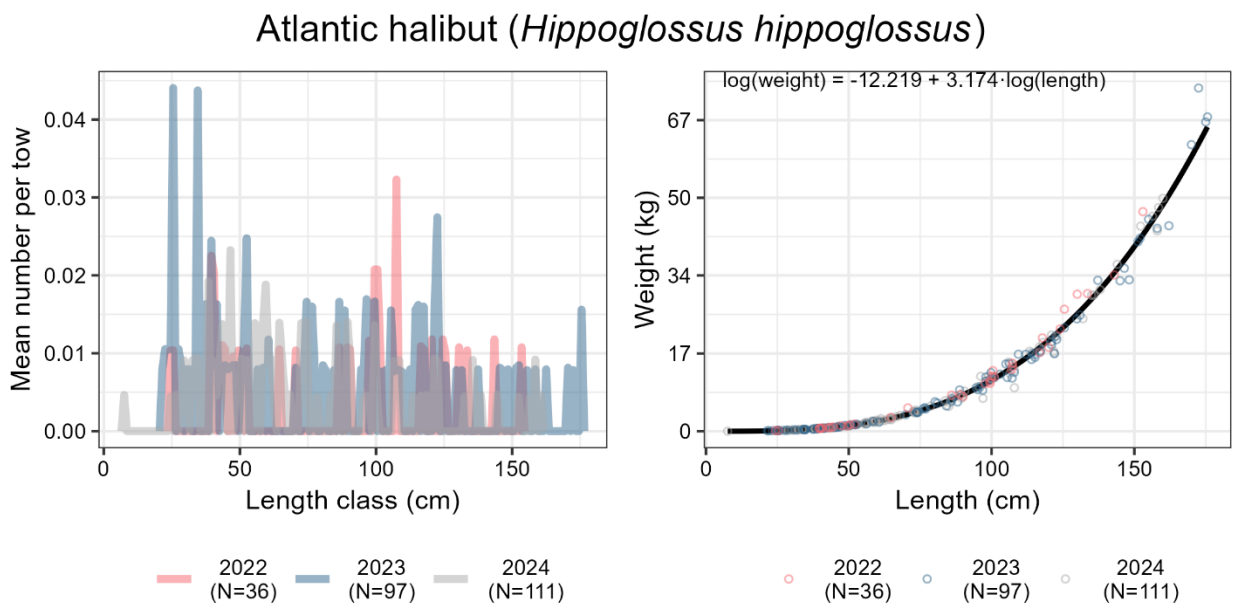


Figure 33d. Annual length frequencies (left panel) and length-weight observations with the global relationship prediction (right panel) for the Atlantic halibut in the winter survey in 2022, 2023 and 2024.

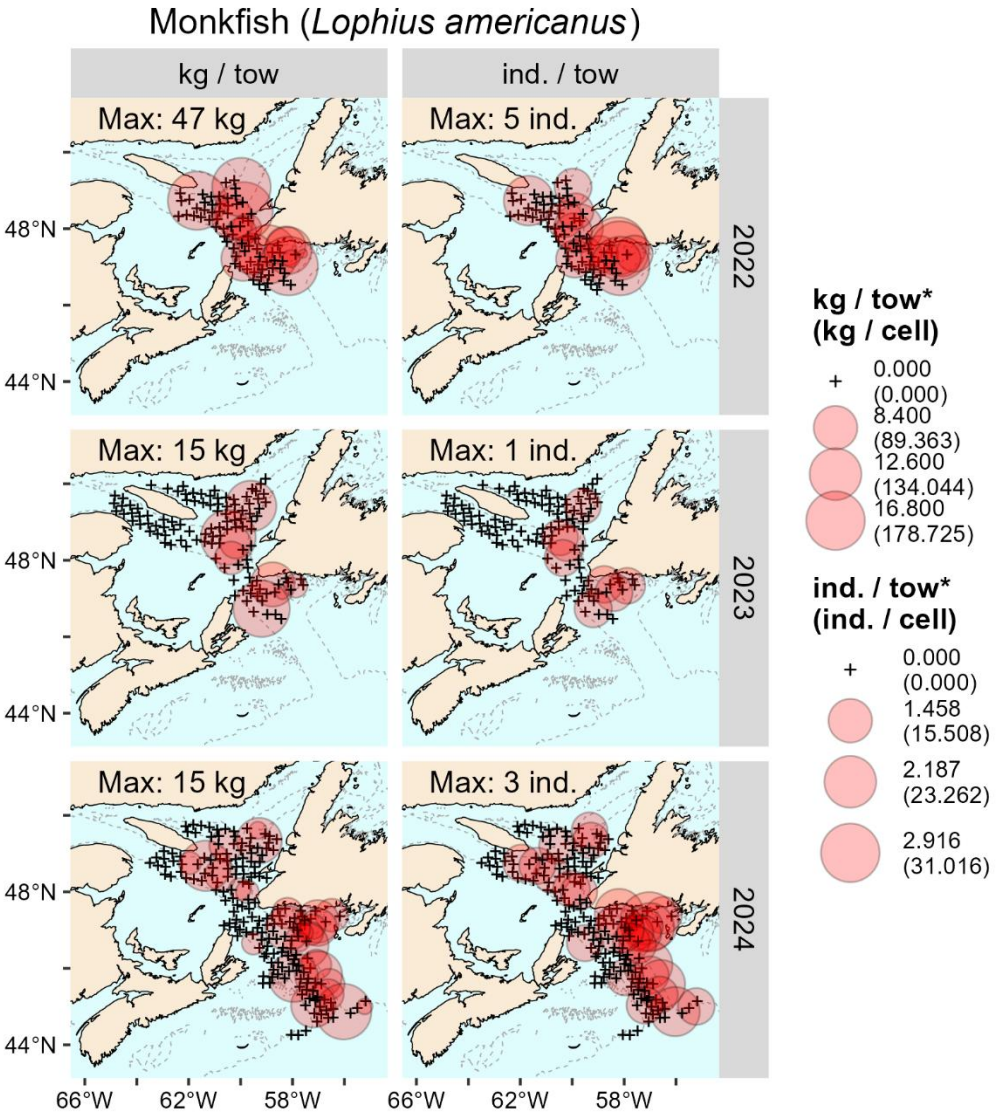


Figure 34a. Standardized catches by weight and/or number (colored bubbles) and cases of absence (black crosses) for the monkfish in the winter surveys of 2022, 2023, and 2024.

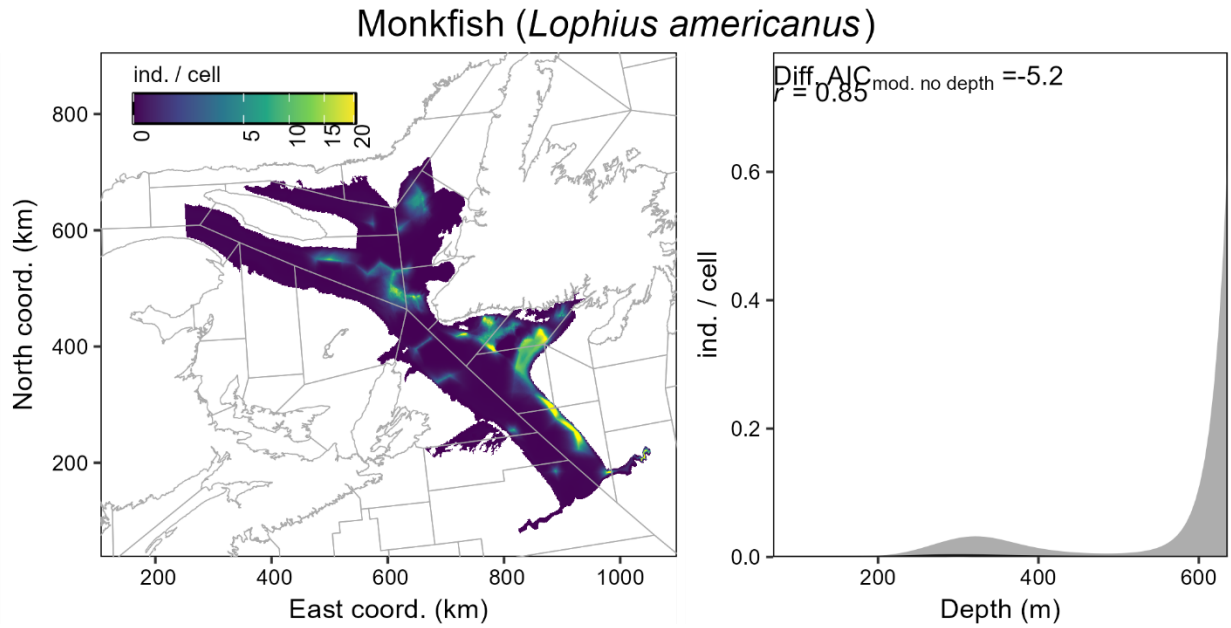


Figure 34b. Predicted number values per 0.25 km^2 cell according to the selected spatial interpolation model for the monkfish in the 2022, 2023, and 2024 winter survey.

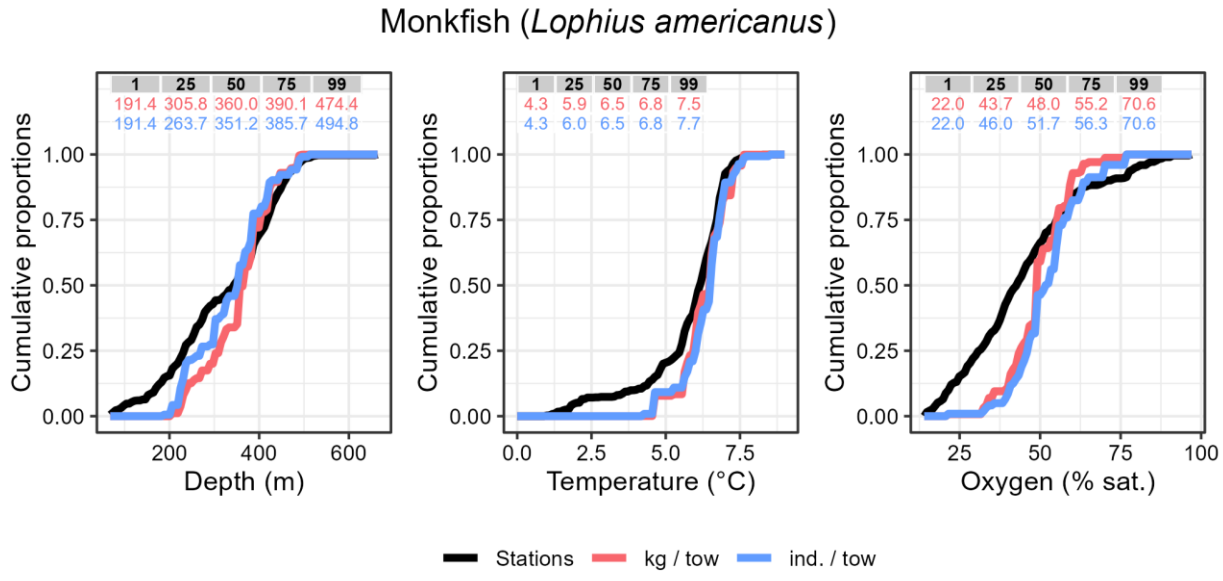


Figure 34c. Cumulative proportions of available values of depth, temperature and dissolved oxygen and standardized catches per tow for the monkfish in the winter survey in 2022, 2023 and 2024.

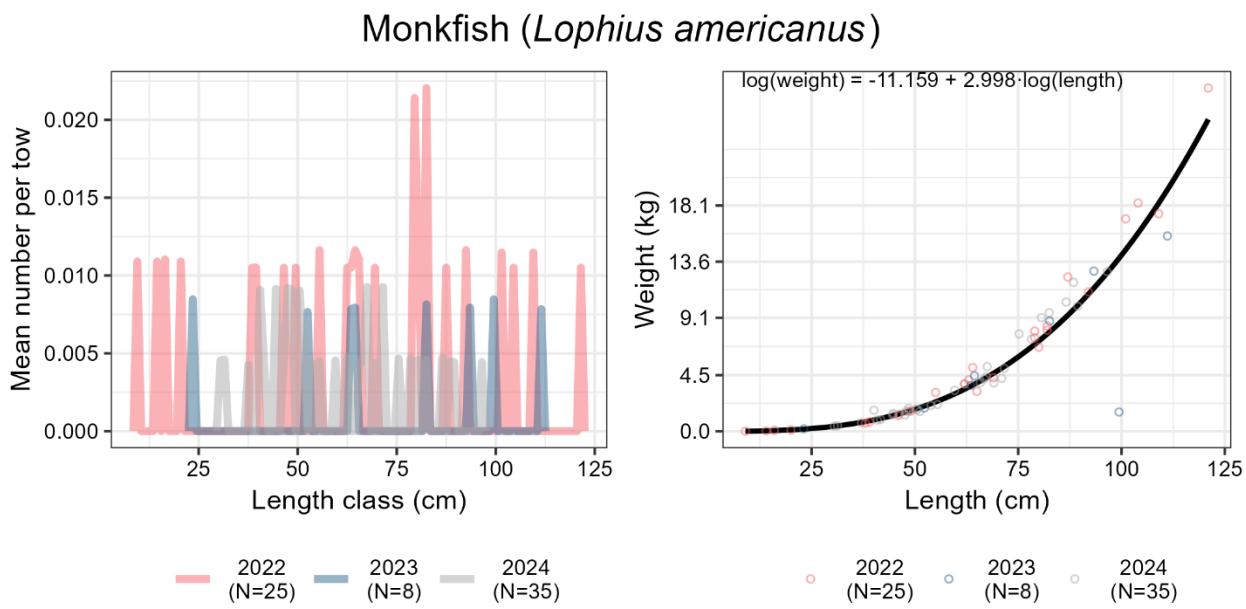


Figure 34d. Annual length frequencies (left panel) and length-weight observations with the global relationship prediction (right panel) for the monkfish in the winter survey in 2022, 2023 and 2024.

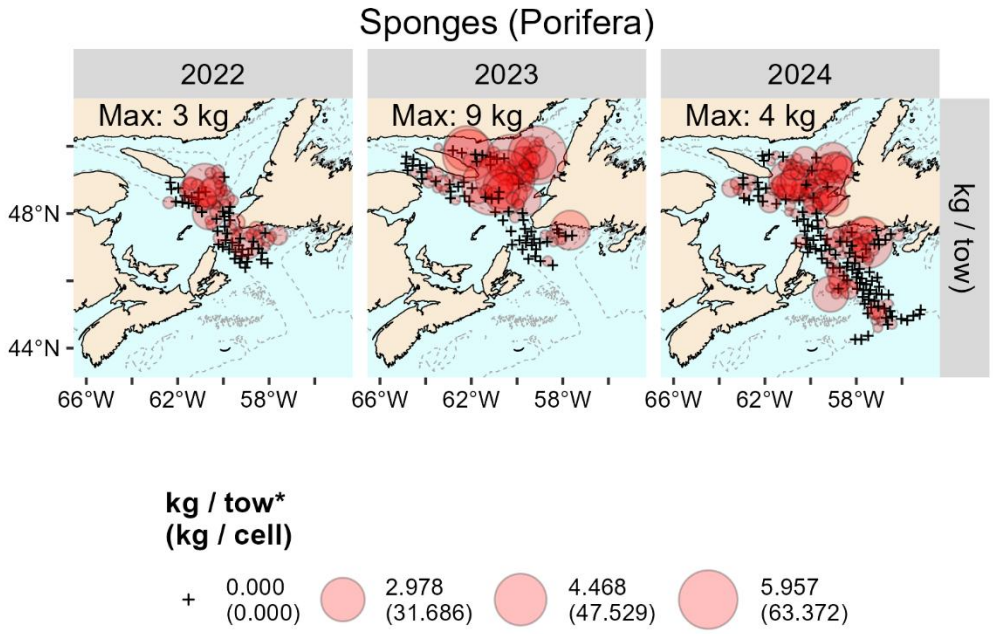


Figure 35a. Standardized catches by weight (colored bubbles) and cases of absence (black crosses) for sponges identified to the phylum Porifera in the winter surveys of 2022, 2023, and 2024.

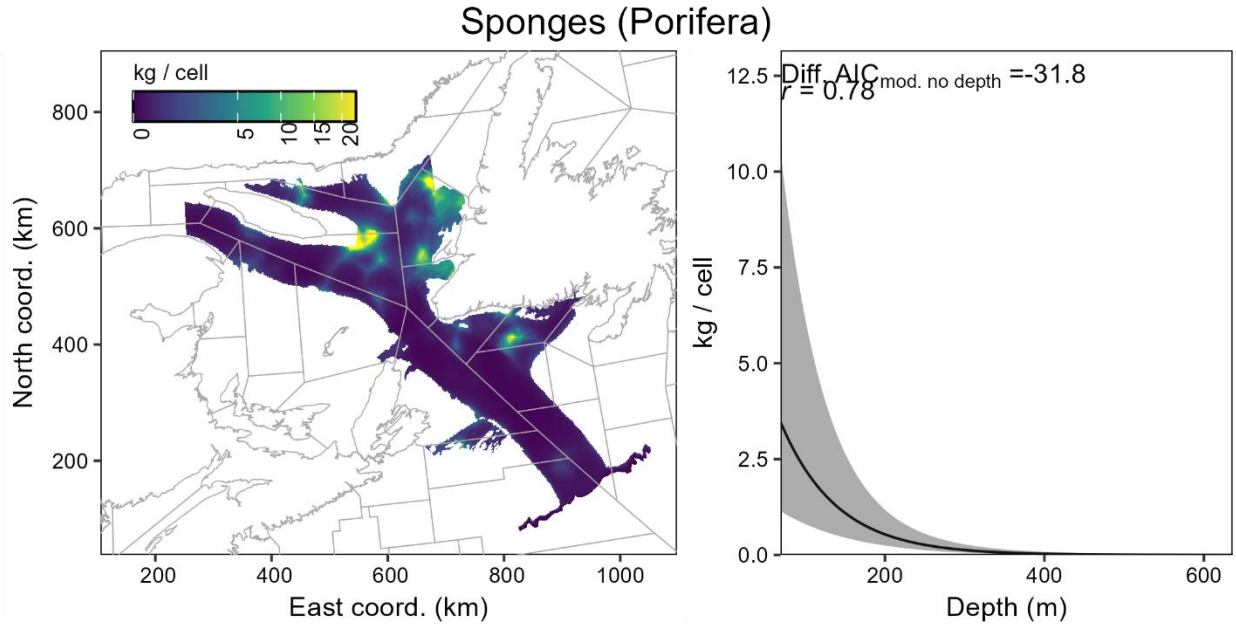


Figure 35b. Predicted weight values per 0.25 km^2 cell according to the selected spatial interpolation model for sponges identified to the phylum Porifera in the 2022, 2023, and 2024 winter survey.

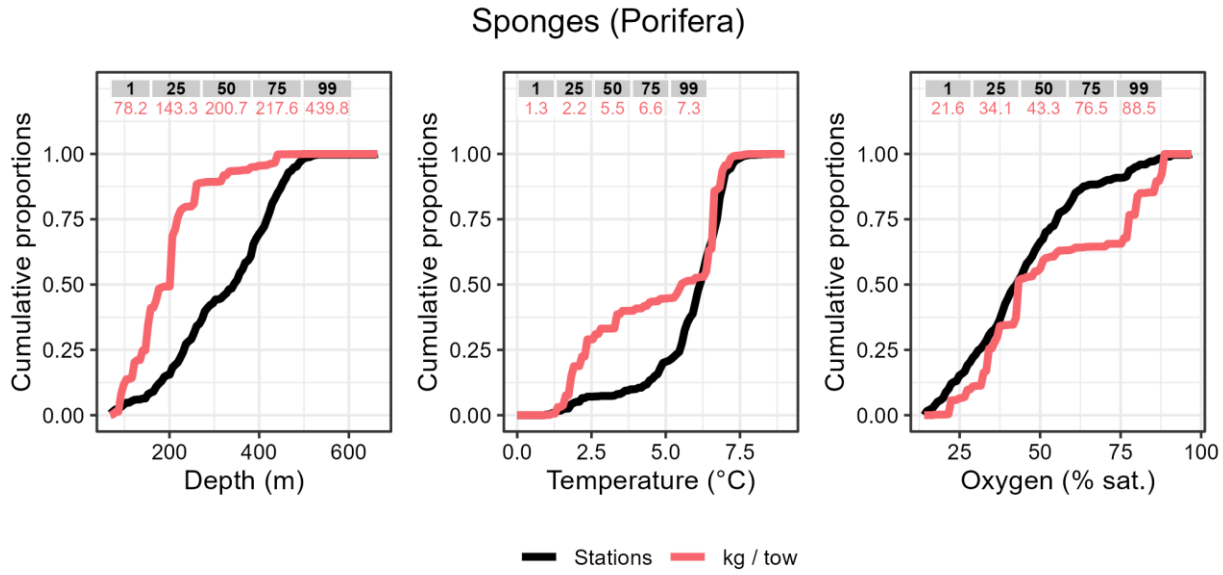


Figure 35c. Cumulative proportions of available values of depth, temperature and dissolved oxygen and standardized catches per tow for sponges identified to the phylum Porifera in the winter survey in 2022, 2023 and 2024.

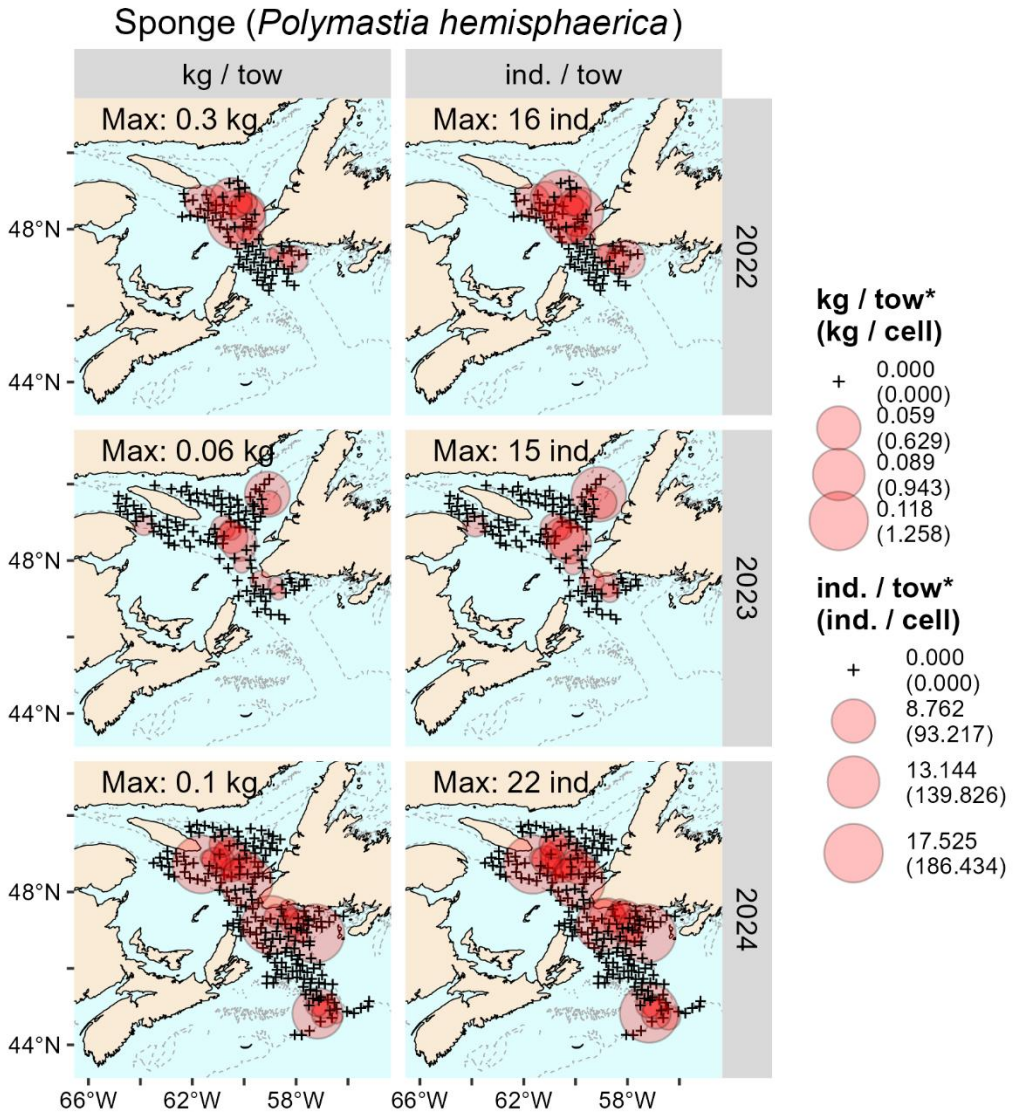


Figure 36a. Standardized catches by weight and/or number (colored bubbles) and cases of absence (black crosses) for the sponge *Polymastia hemisphaerica* in the winter surveys of 2022, 2023, and 2024.

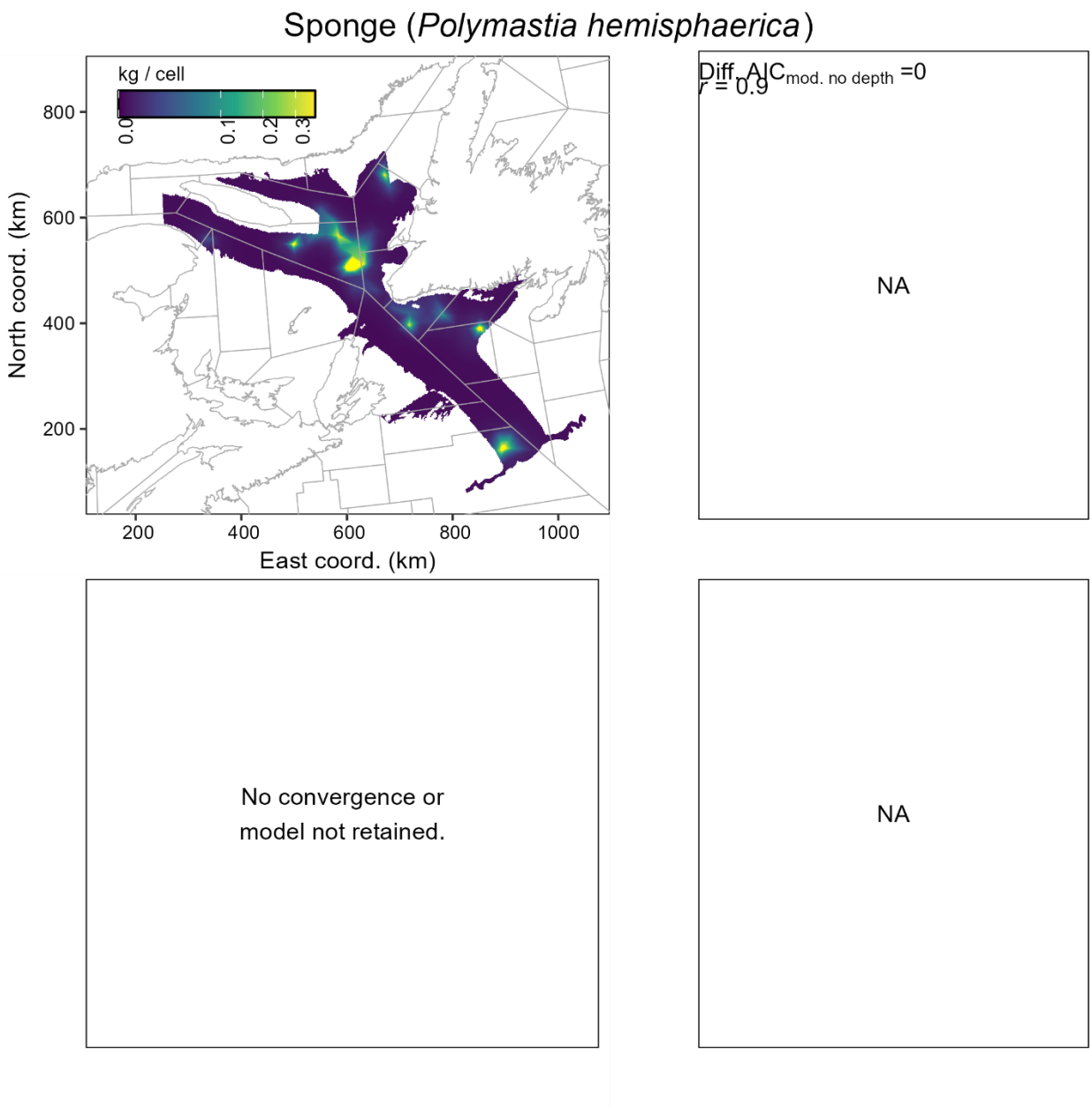


Figure 36b. Predicted weight (upper panels) and number (lower panels) values per 0.25 km^2 cell according to the selected spatial interpolation models for the sponge *Polymastia hemisphaerica* in the 2022, 2023, and 2024 winter survey.

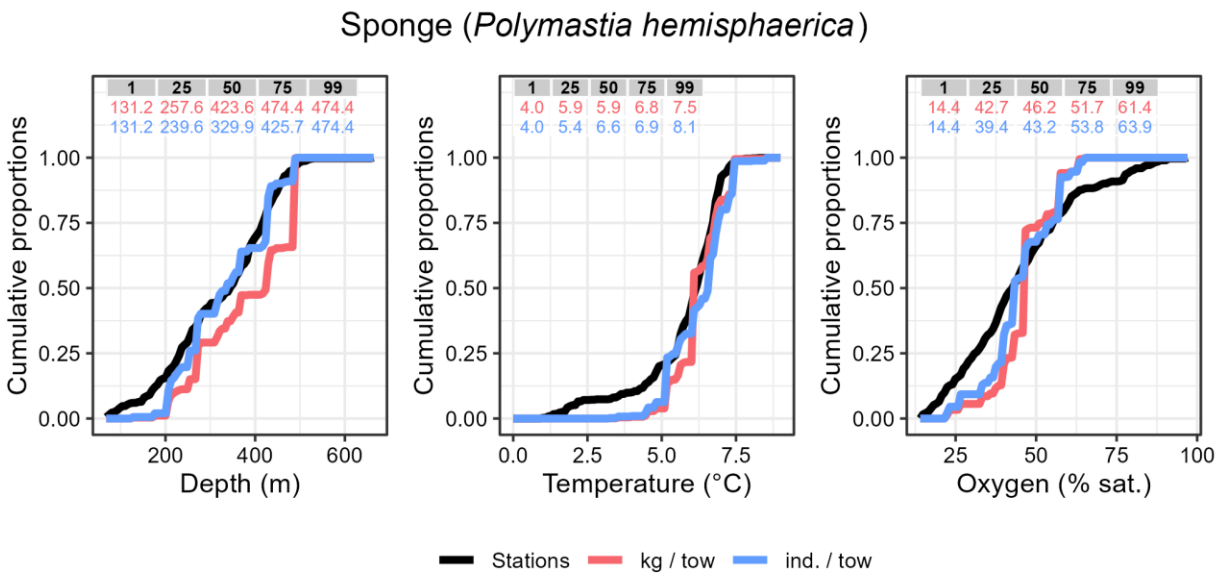


Figure 36c. Cumulative proportions of available values of depth, temperature and dissolved oxygen and standardized catches per tow for the sponge *Polymastia hemisphaerica* in the winter survey in 2022, 2023 and 2024.

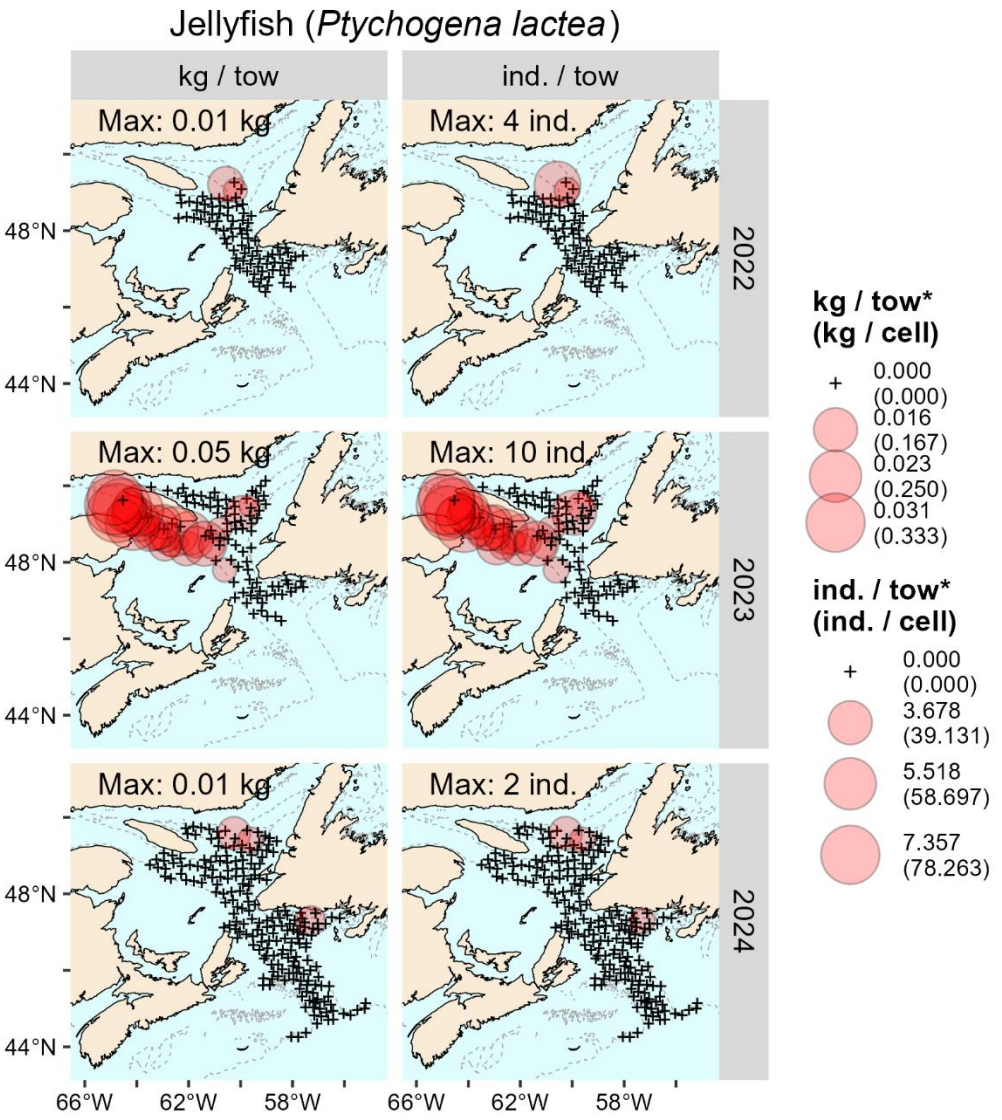


Figure 37a. Standardized catches by weight and/or number (colored bubbles) and cases of absence (black crosses) for the jellyfish *Ptychogena lactea* in the winter surveys of 2022, 2023, and 2024.

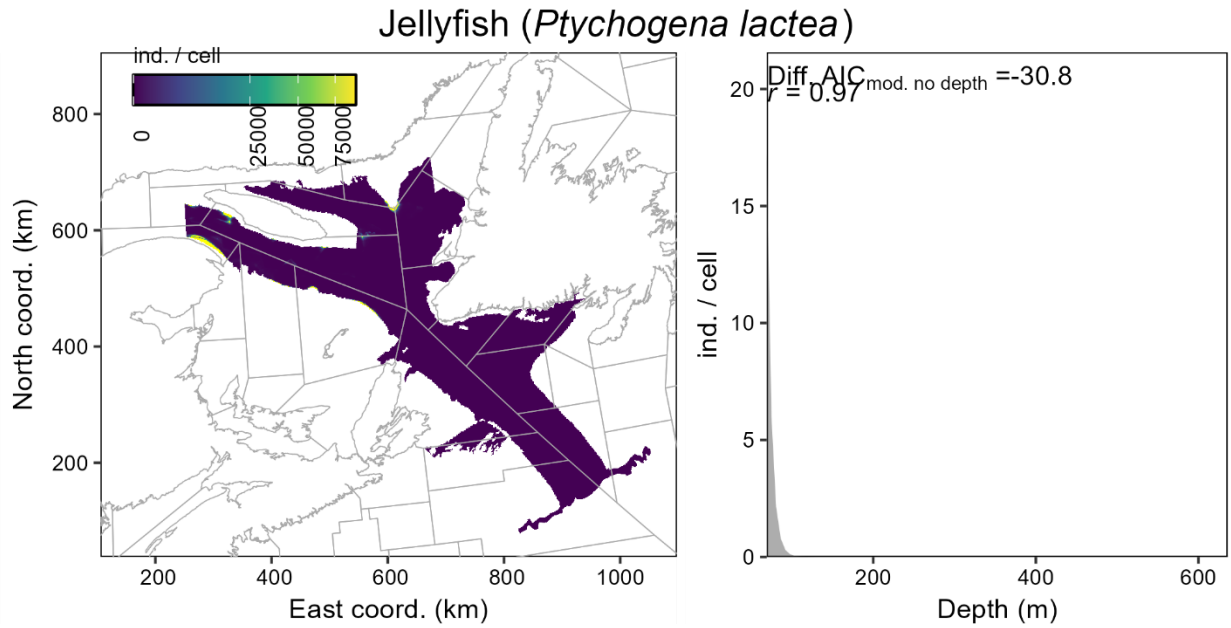


Figure 37b. Predicted number values per 0.25 km^2 cell according to the selected spatial interpolation model for the jellyfish *Ptychogena lactea* in the 2022, 2023, and 2024 winter survey.

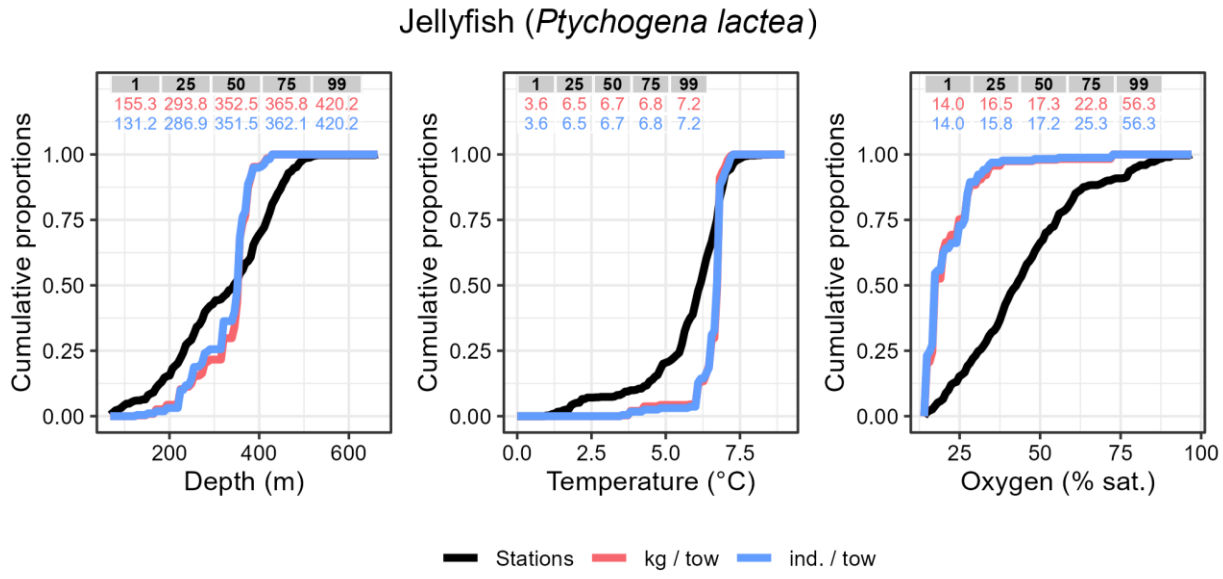


Figure 37c. Cumulative proportions of available values of depth, temperature and dissolved oxygen and standardized catches per tow for the jellyfish *Ptychogena lactea* in the winter survey in 2022, 2023 and 2024.

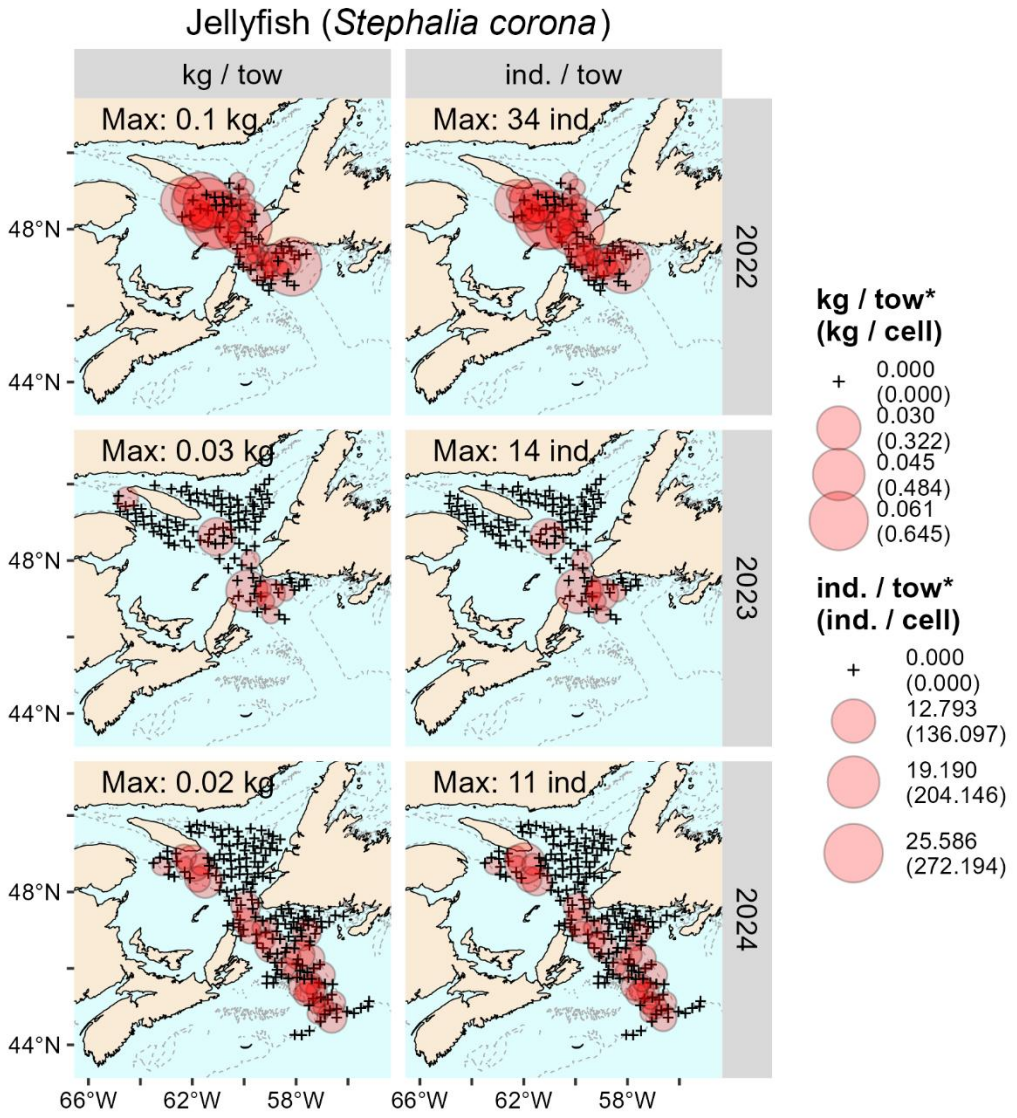


Figure 38a. Standardized catches by weight and/or number (colored bubbles) and cases of absence (black crosses) for the jellyfish *Stephalia corona* in the winter surveys of 2022, 2023, and 2024.

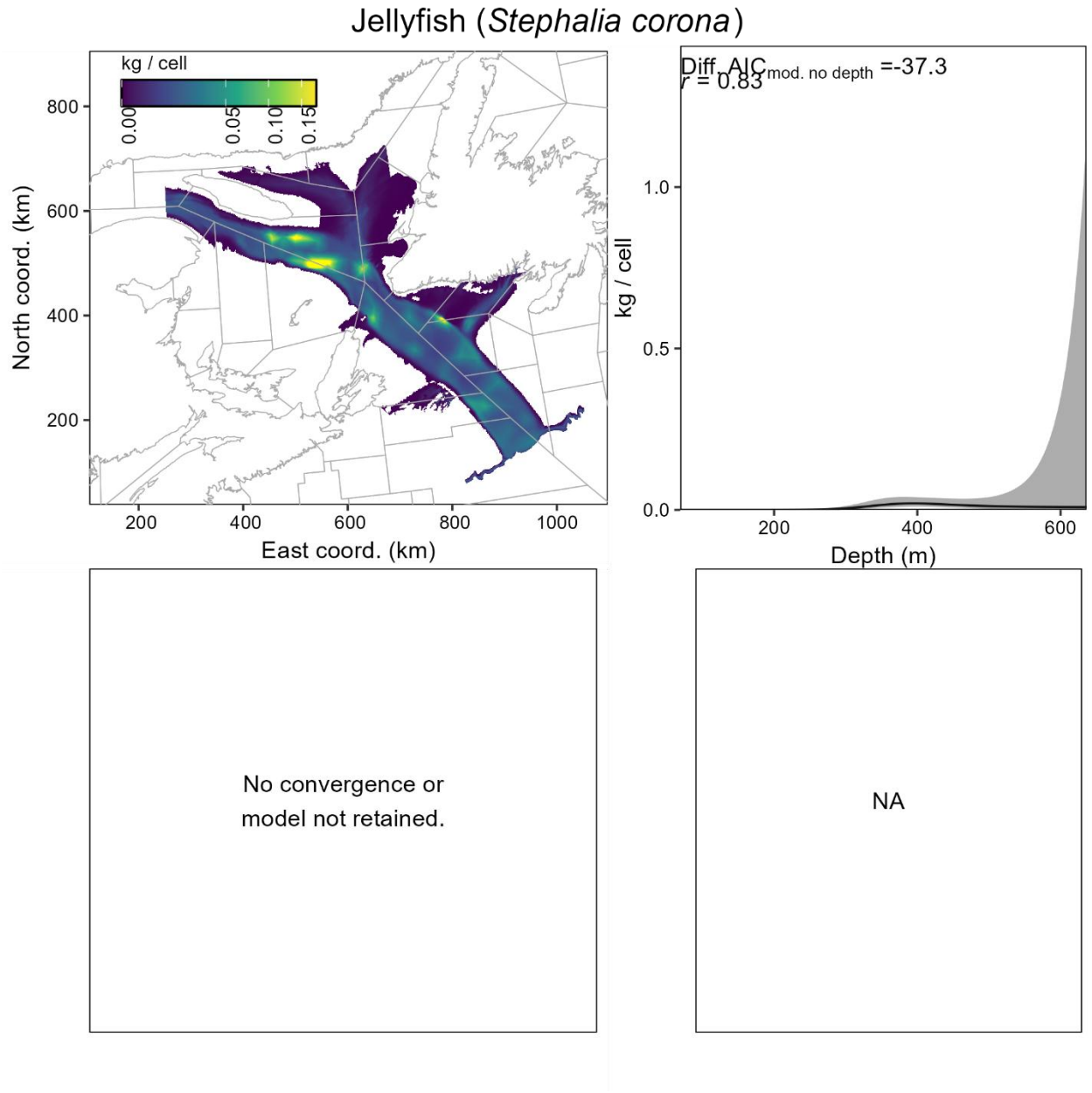


Figure 38b. Predicted weight (upper panels) and number (lower panels) values per 0.25 km^2 cell according to the selected spatial interpolation models for the jellyfish *Stephalia corona* in the 2022, 2023, and 2024 winter survey.

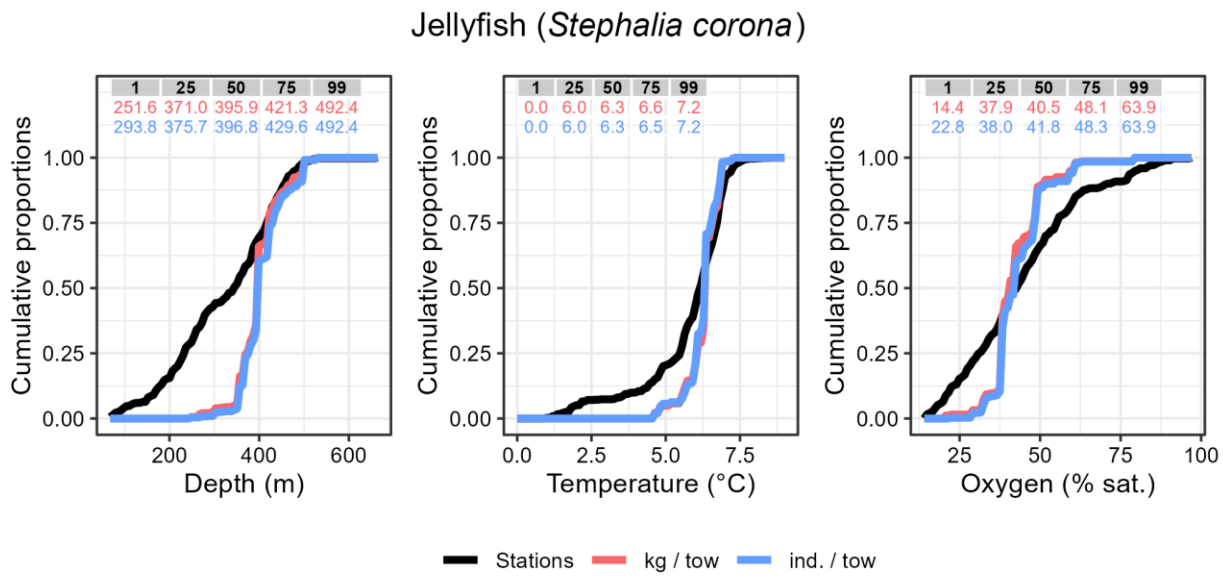


Figure 38c. Cumulative proportions of available values of depth, temperature and dissolved oxygen and standardized catches per tow for the jellyfish *Stephalia corona* in the winter survey in 2022, 2023 and 2024.

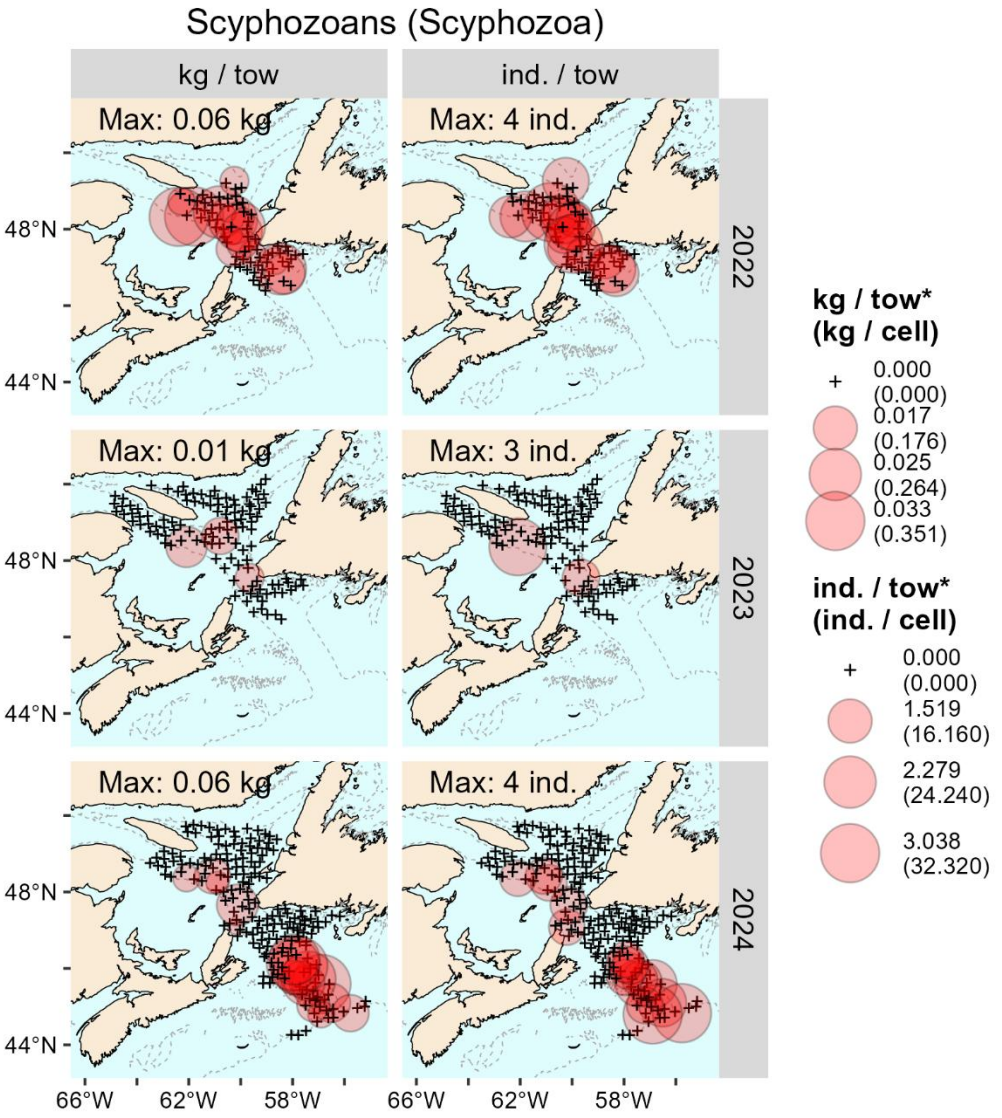


Figure 39a. Standardized catches by weight and/or number (colored bubbles) and cases of absence (black crosses) for specimens whose identification could not be more precise than the class of Scyphozoans (may include taxa 2040, 2080, 2096 and 2097) in the winter surveys of 2022, 2023, and 2024.

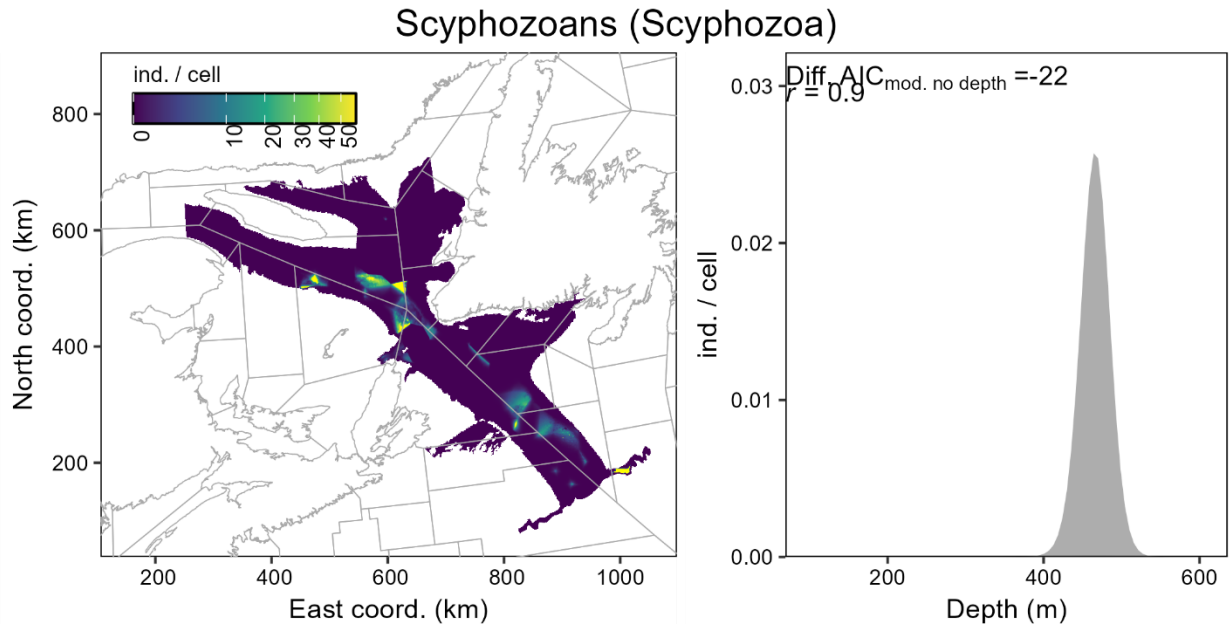


Figure 39b. Predicted number values per 0.25 km^2 cell according to the selected spatial interpolation model for specimens whose identification could not be more precise than the class of Scyphozoans (may include taxa 2040, 2080, 2096 and 2097) in the 2022, 2023, and 2024 winter survey.

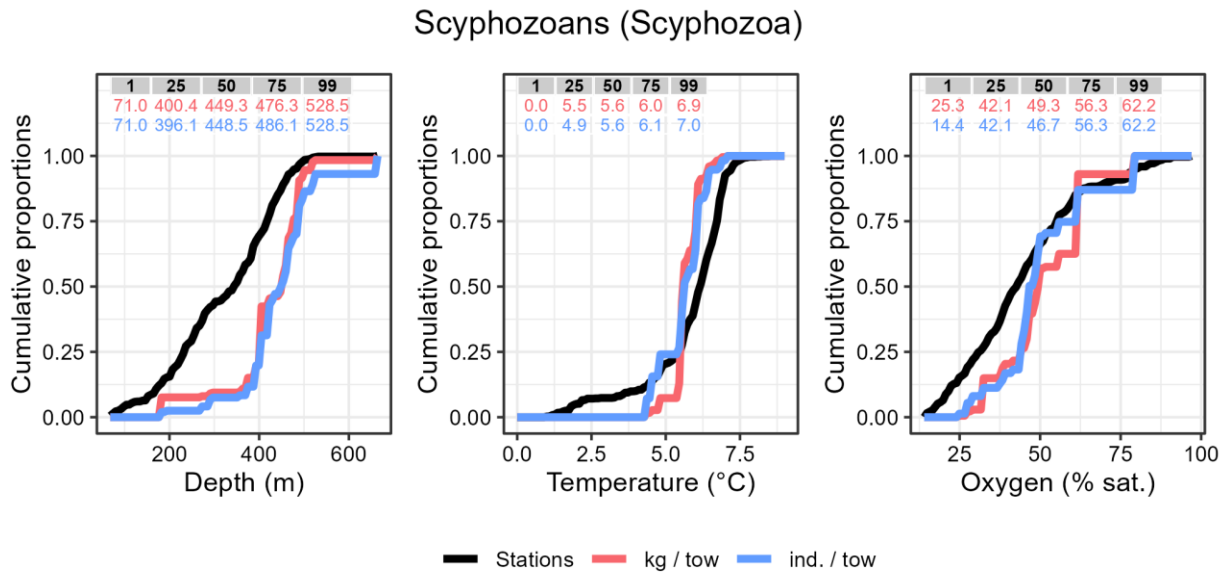


Figure 39c. Cumulative proportions of available values of depth, temperature and dissolved oxygen and standardized catches per tow for specimens whose identification could not be more precise than the class of Scyphozoans (may include taxa 2040, 2080, 2096 and 2097) in the winter survey in 2022, 2023 and 2024.

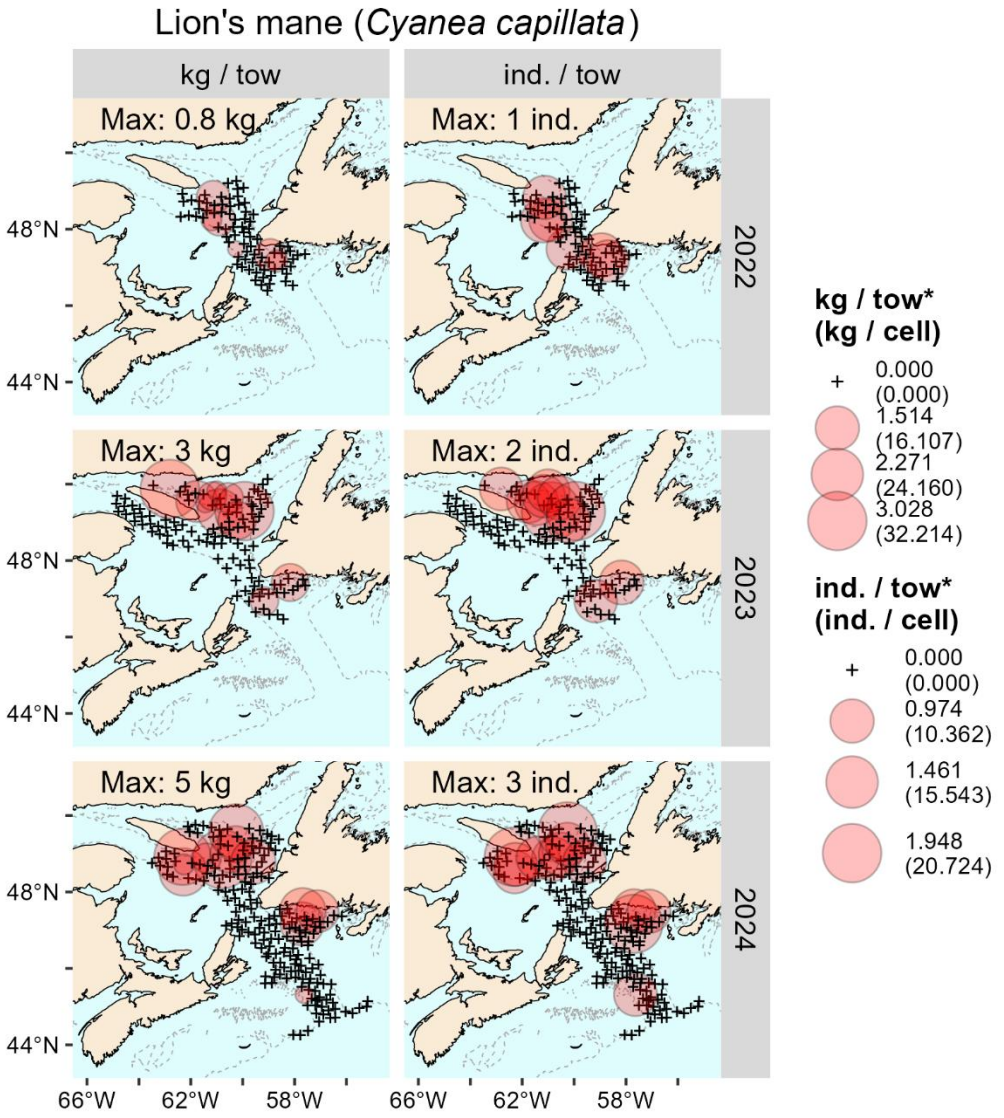


Figure 40a. Standardized catches by weight and/or number (colored bubbles) and cases of absence (black crosses) for the lion's mane in the winter surveys of 2022, 2023, and 2024.

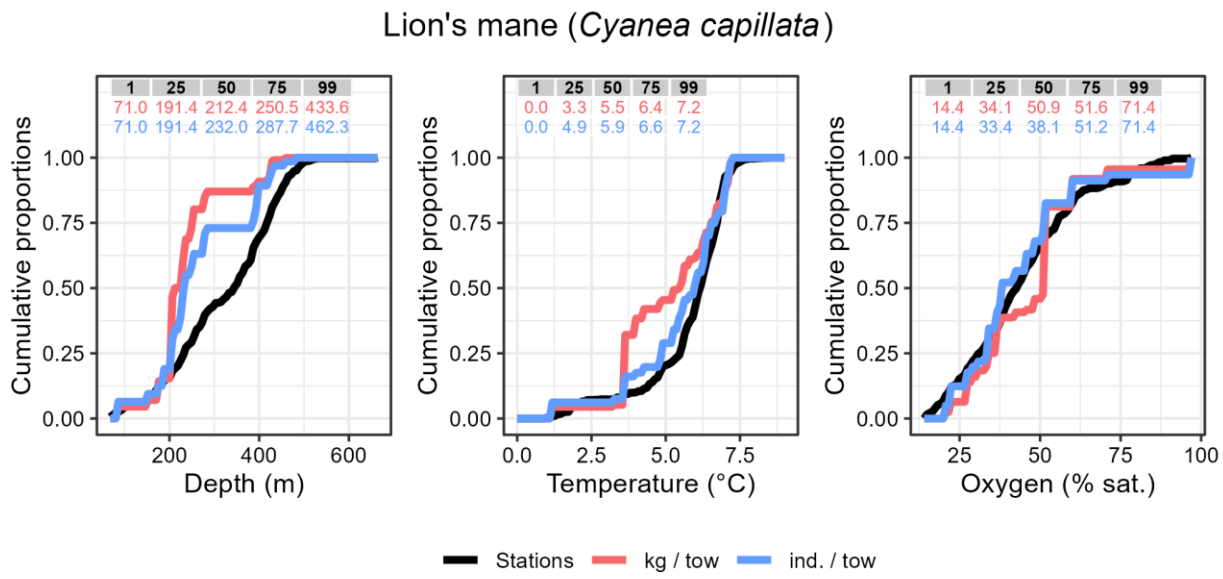


Figure 40b. Cumulative proportions of available values of depth, temperature and dissolved oxygen and standardized catches per tow for the lion's mane in the winter survey in 2022, 2023 and 2024.

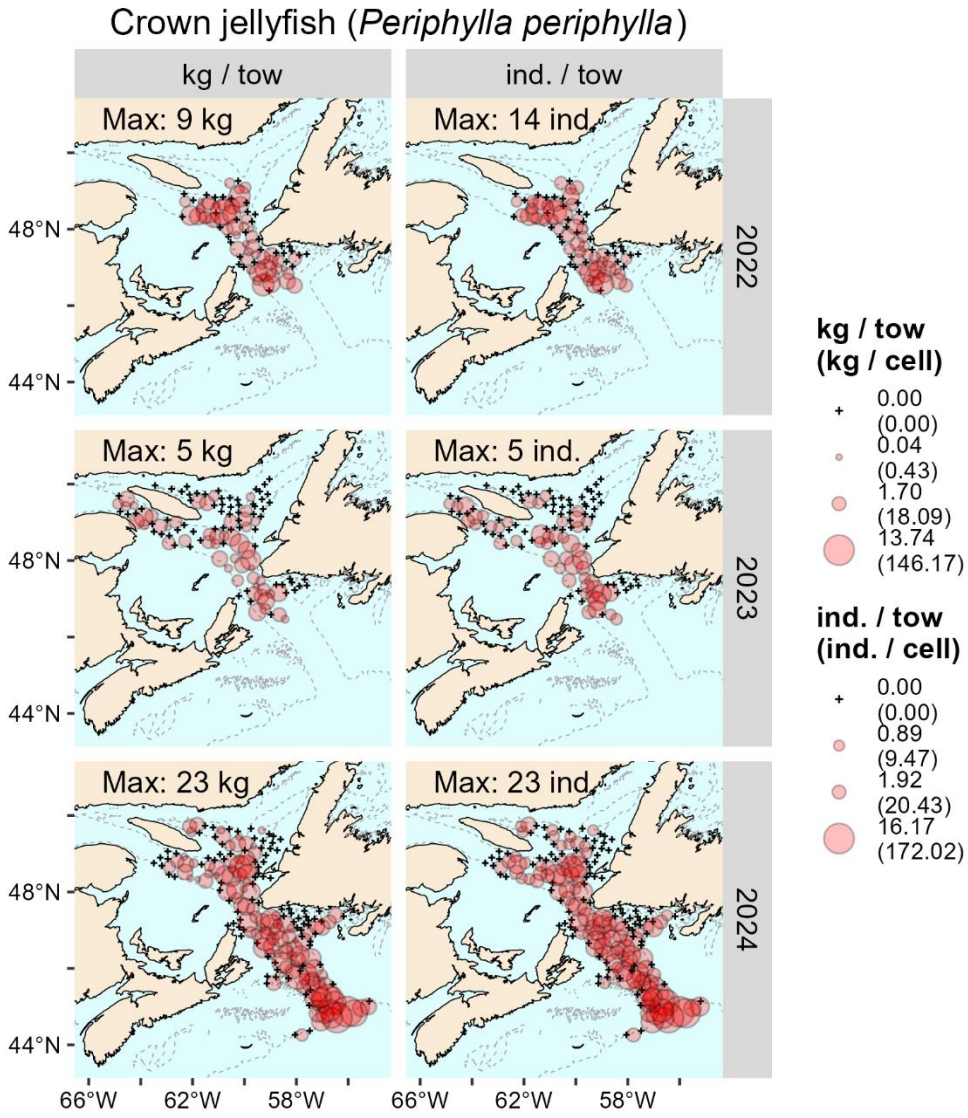


Figure 41a. Standardized catches by weight and/or number (colored bubbles) and cases of absence (black crosses) for the crown jellyfish in the winter surveys of 2022, 2023, and 2024.

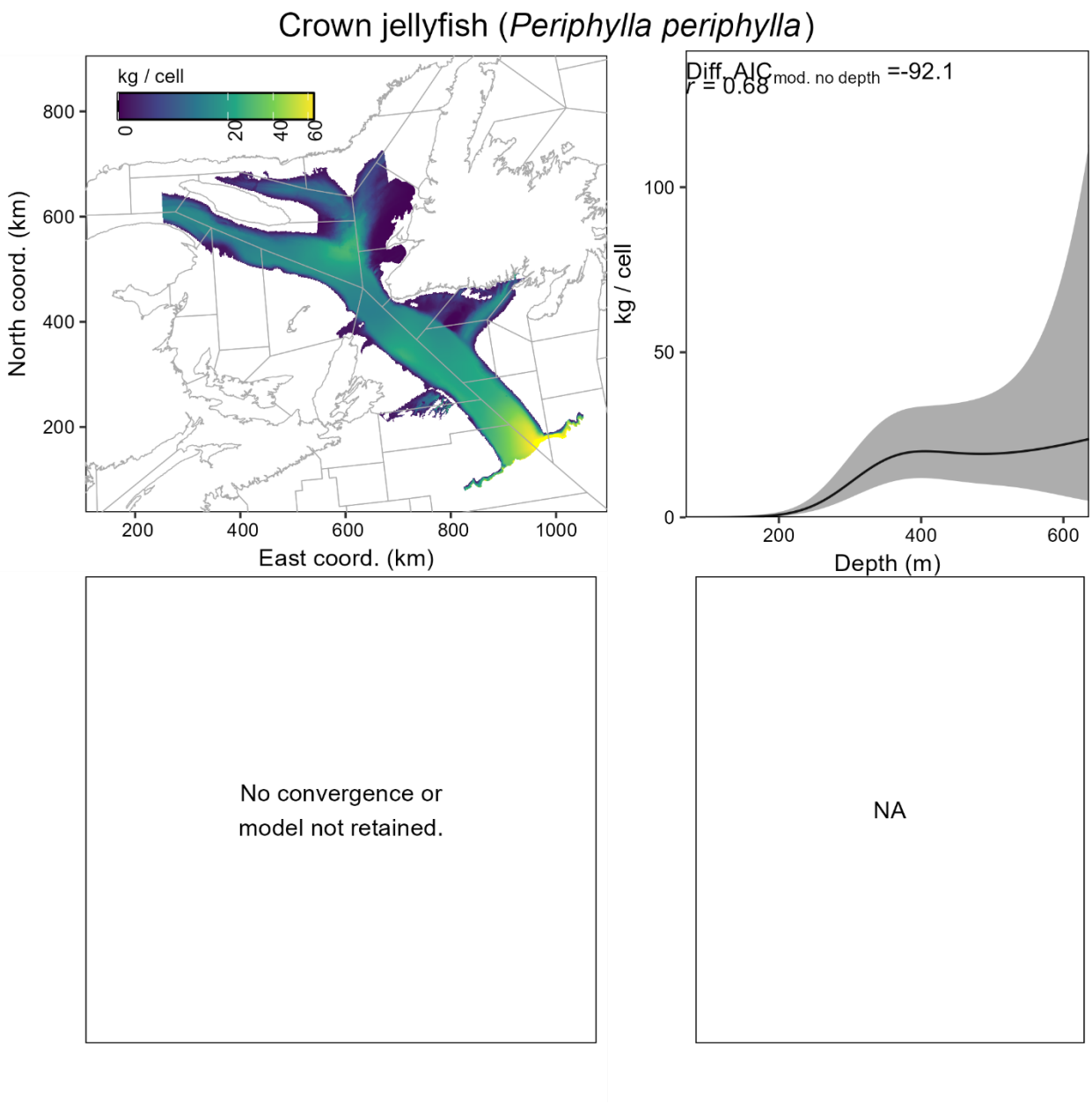


Figure 41b. Predicted weight (upper panels) and number (lower panels) values per 0.25 km^2 cell according to the selected spatial interpolation models for the crown jellyfish in the 2022, 2023, and 2024 winter survey.

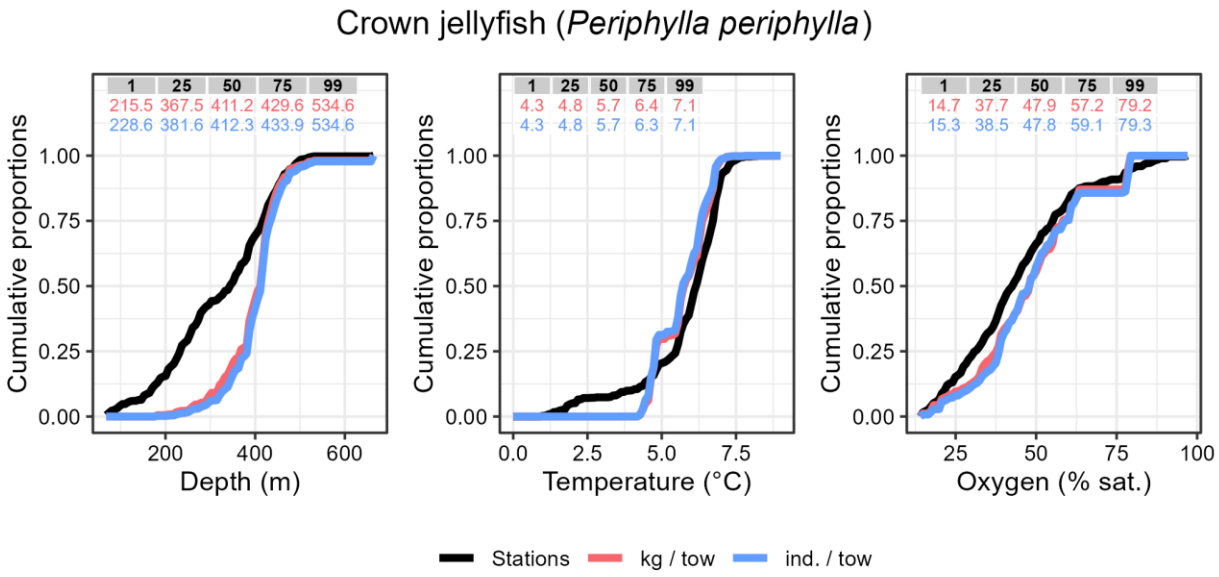


Figure 41c. Cumulative proportions of available values of depth, temperature and dissolved oxygen and standardized catches per tow for the crown jellyfish in the winter survey in 2022, 2023 and 2024.

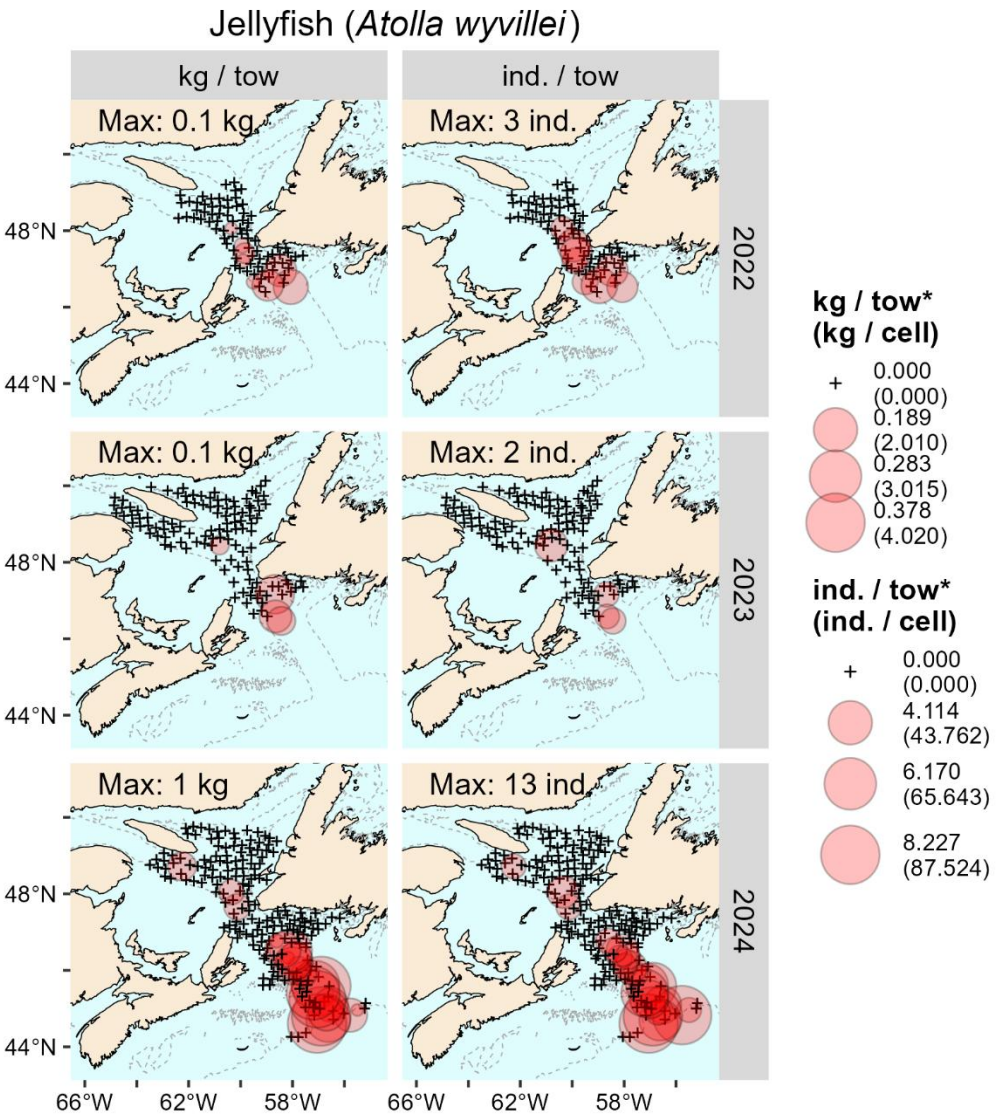


Figure 42a. Standardized catches by weight and/or number (colored bubbles) and cases of absence (black crosses) for the jellyfish *Atolla wyvillei* in the winter surveys of 2022, 2023, and 2024.

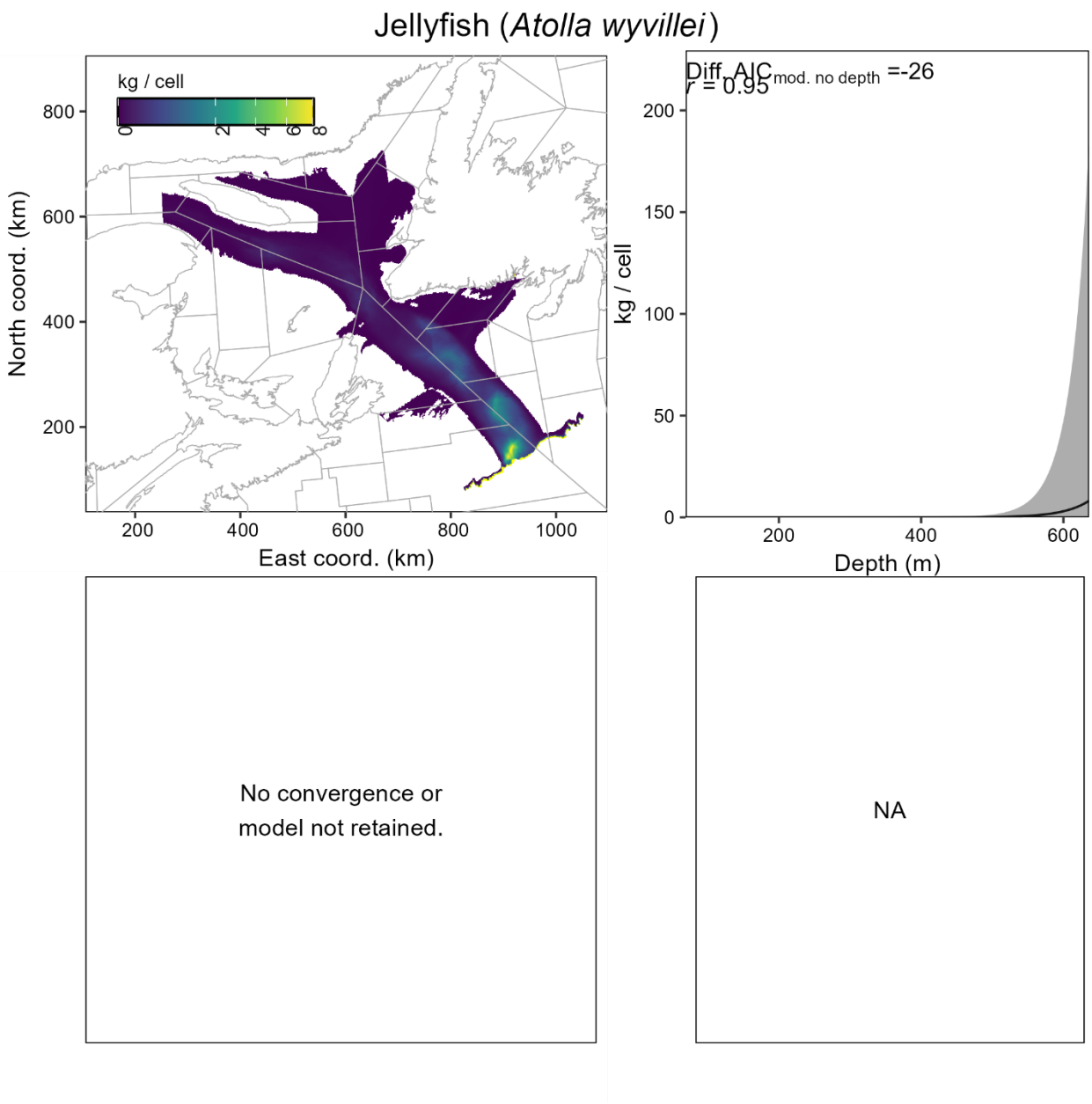


Figure 42b. Predicted weight (upper panels) and number (lower panels) values per 0.25 km^2 cell according to the selected spatial interpolation models for the jellyfish *Atolla wyvillei* in the 2022, 2023, and 2024 winter survey.

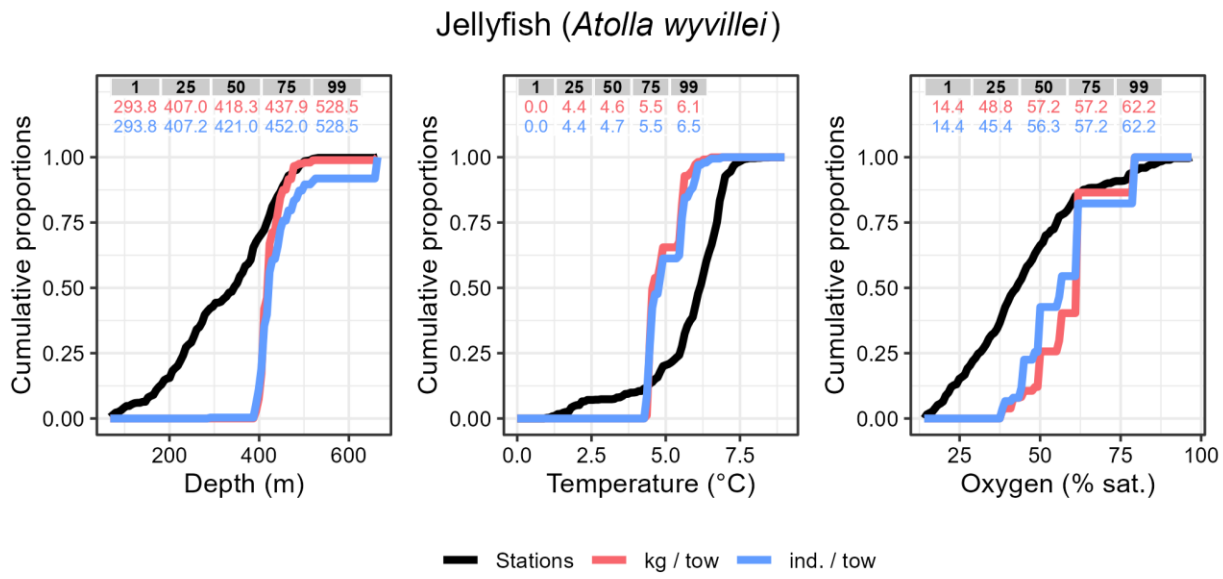


Figure 42c. Cumulative proportions of available values of depth, temperature and dissolved oxygen and standardized catches per tow for the jellyfish *Atolla wyvillei* in the winter survey in 2022, 2023 and 2024.

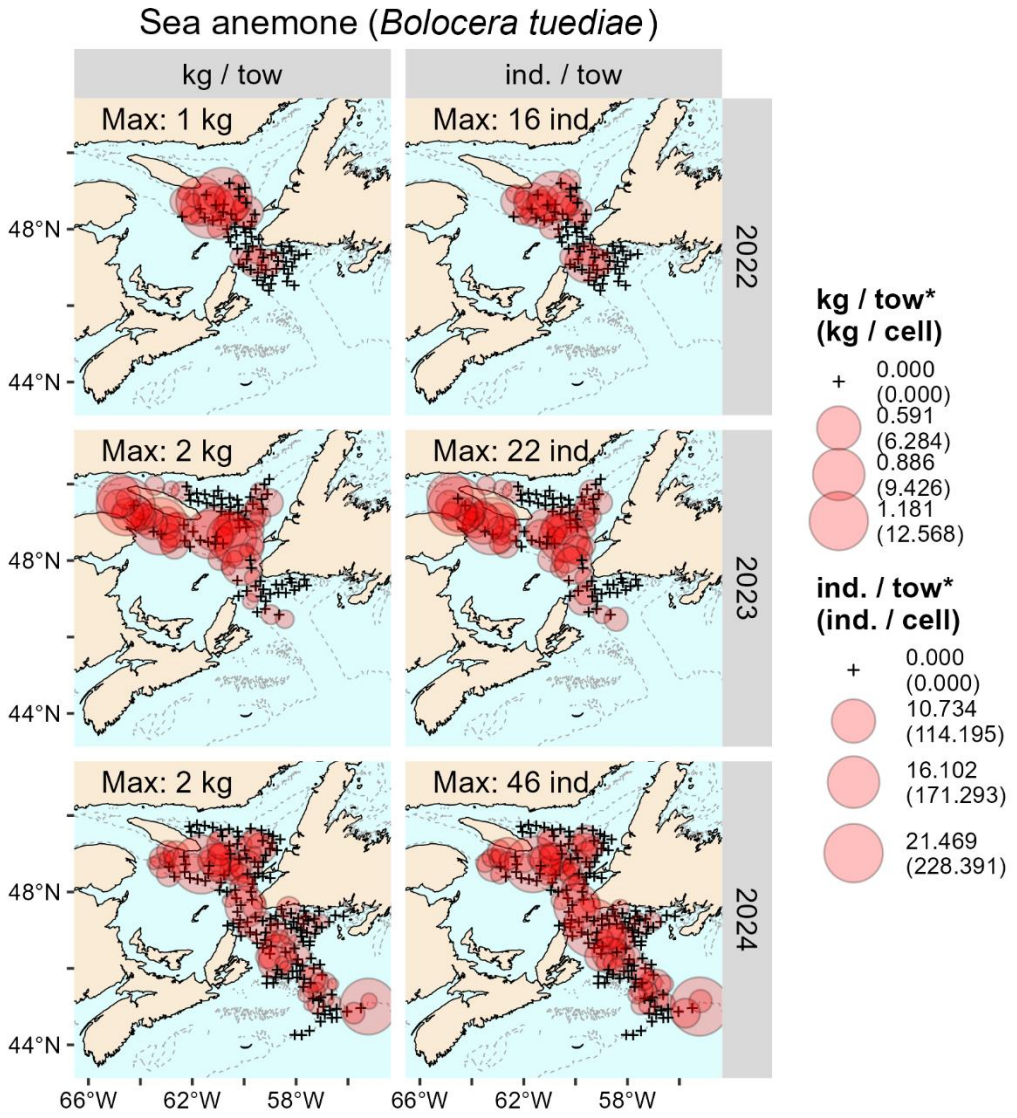


Figure 43a. Standardized catches by weight and/or number (colored bubbles) and cases of absence (black crosses) for the sea anemone *Bolocera tuediae* in the winter surveys of 2022, 2023, and 2024.

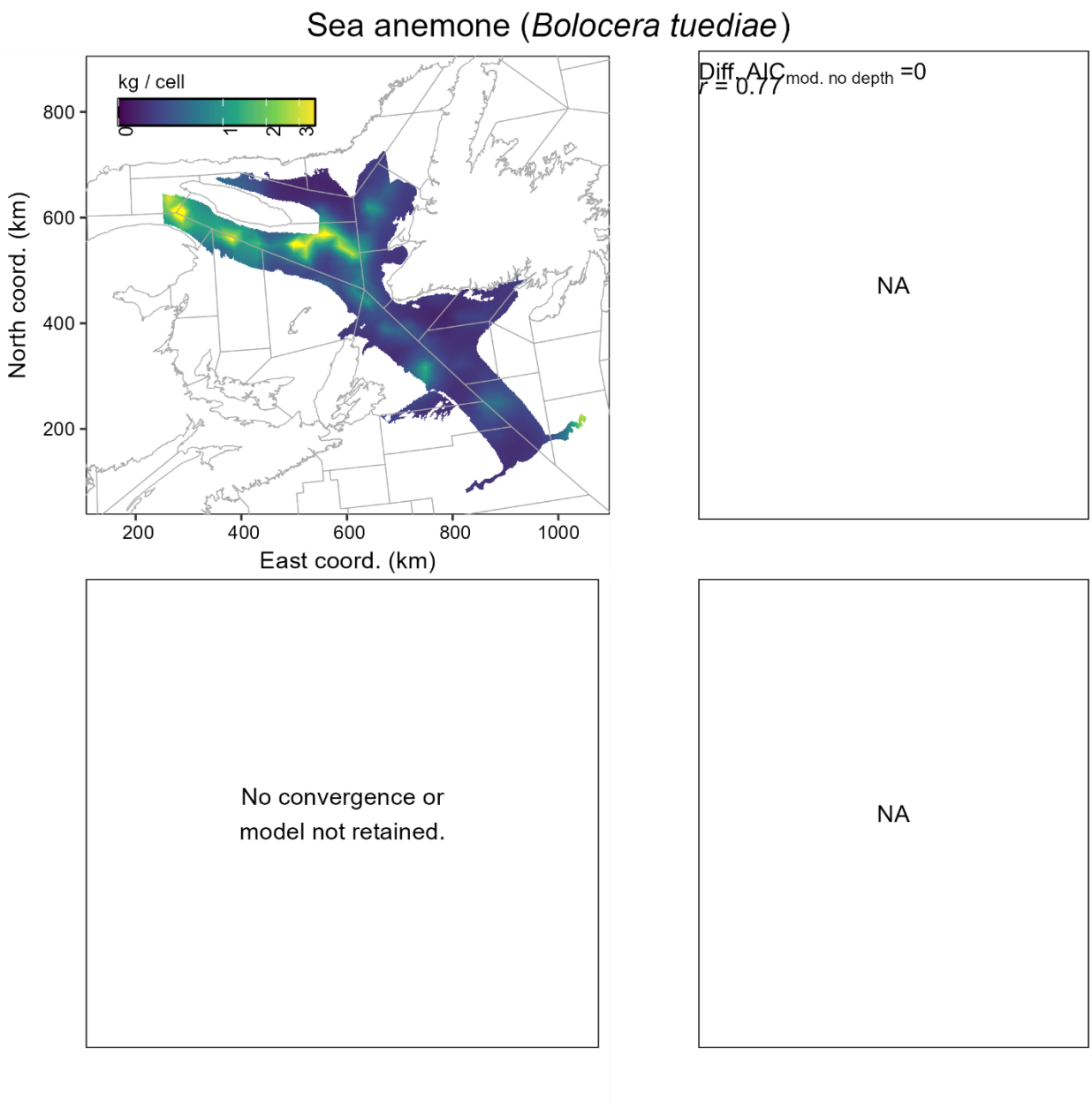


Figure 43b. Predicted weight (upper panels) and number (lower panels) values per 0.25 km^2 cell according to the selected spatial interpolation models for the sea anemone *Bolocera tuediae* in the 2022, 2023, and 2024 winter survey.

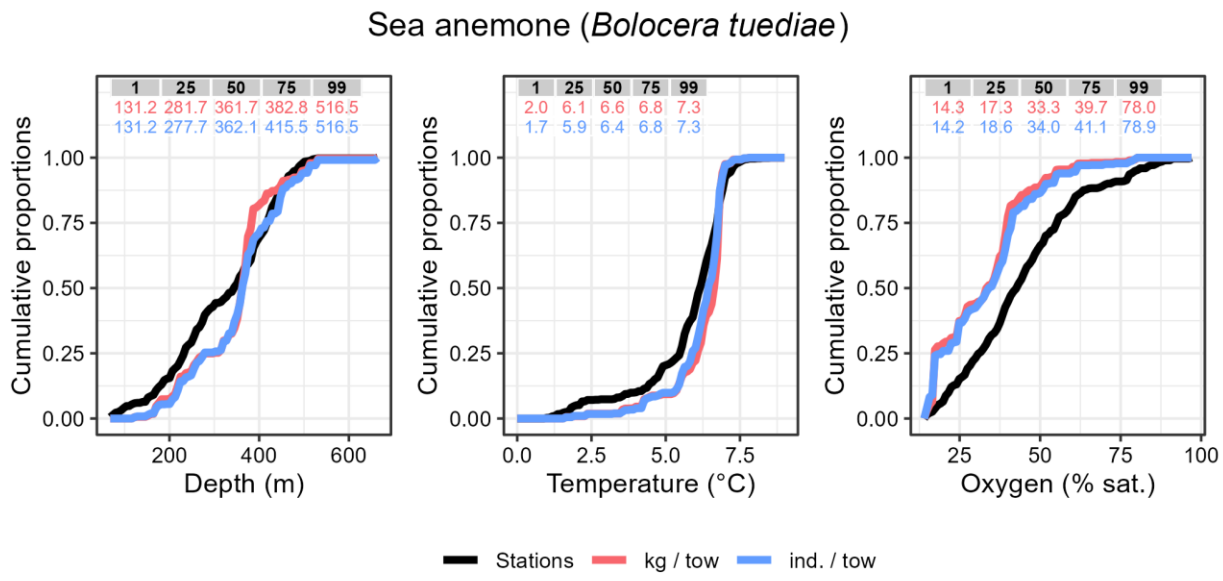


Figure 43c. Cumulative proportions of available values of depth, temperature and dissolved oxygen and standardized catches per tow for the sea anemone *Bolocera tuediae* in the winter survey in 2022, 2023 and 2024.

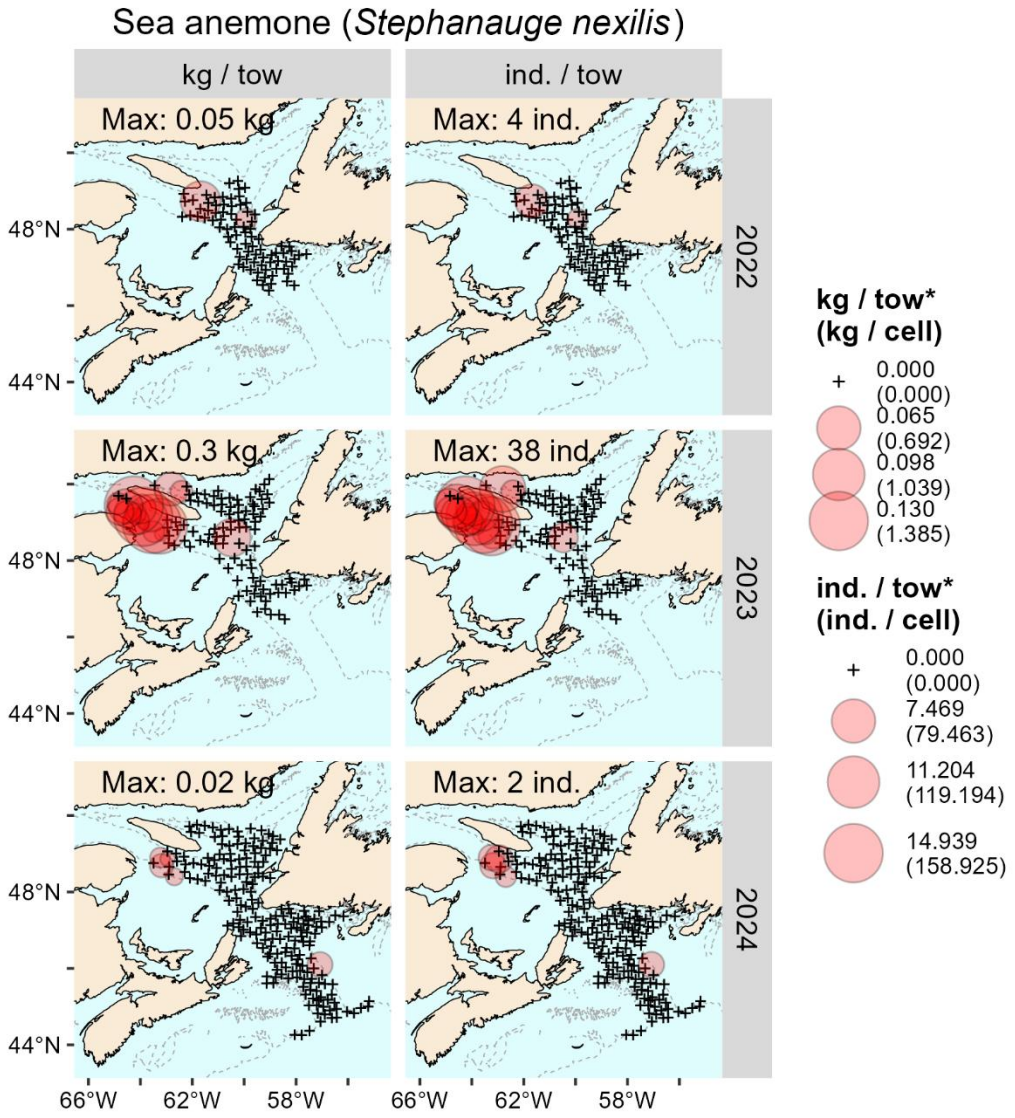


Figure 44a. Standardized catches by weight and/or number (colored bubbles) and cases of absence (black crosses) for the sea anemone *Stephanauge nexilis* in the winter surveys of 2022, 2023, and 2024.

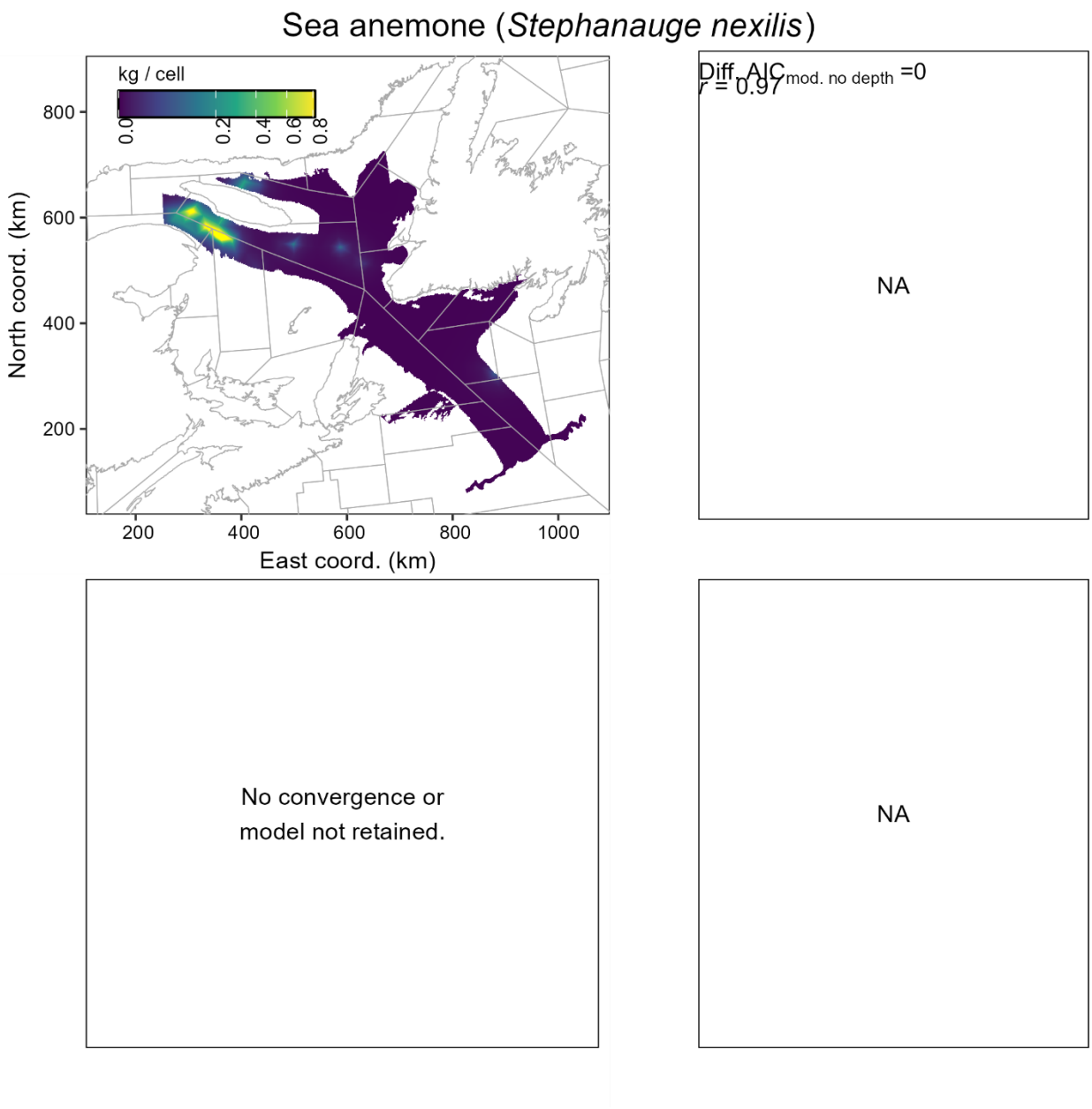


Figure 44b. Predicted weight (upper panels) and number (lower panels) values per 0.25 km^2 cell according to the selected spatial interpolation models for the sea anemone *Stephanauge nexilis* in the 2022, 2023, and 2024 winter survey.

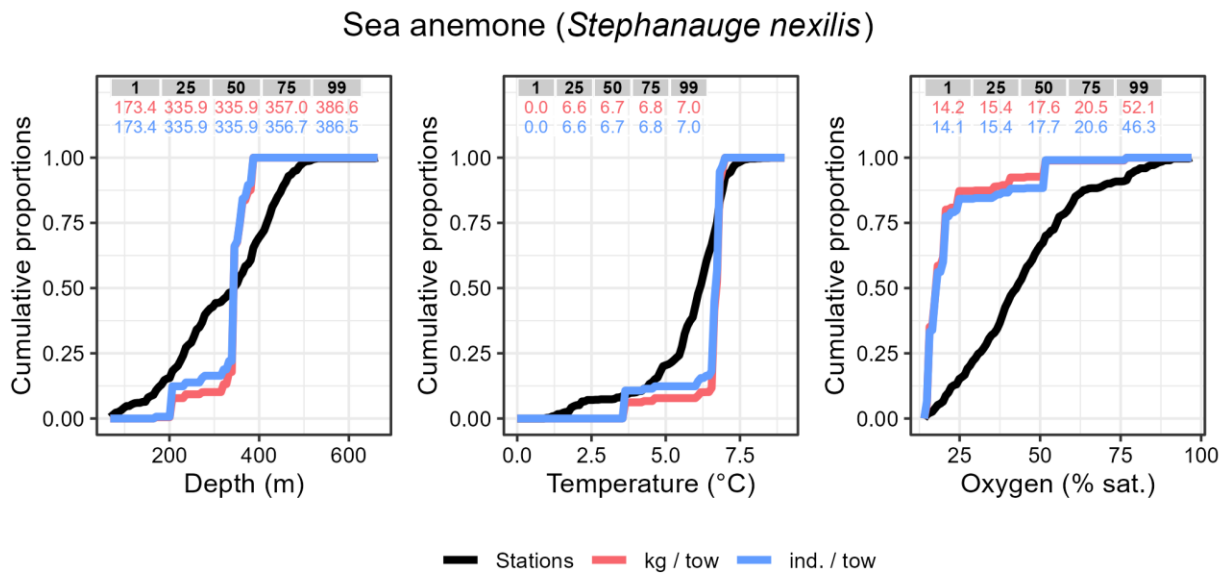


Figure 44c. Cumulative proportions of available values of depth, temperature and dissolved oxygen and standardized catches per tow for the sea anemone *Stephanauge nexilis* in the winter survey in 2022, 2023 and 2024.

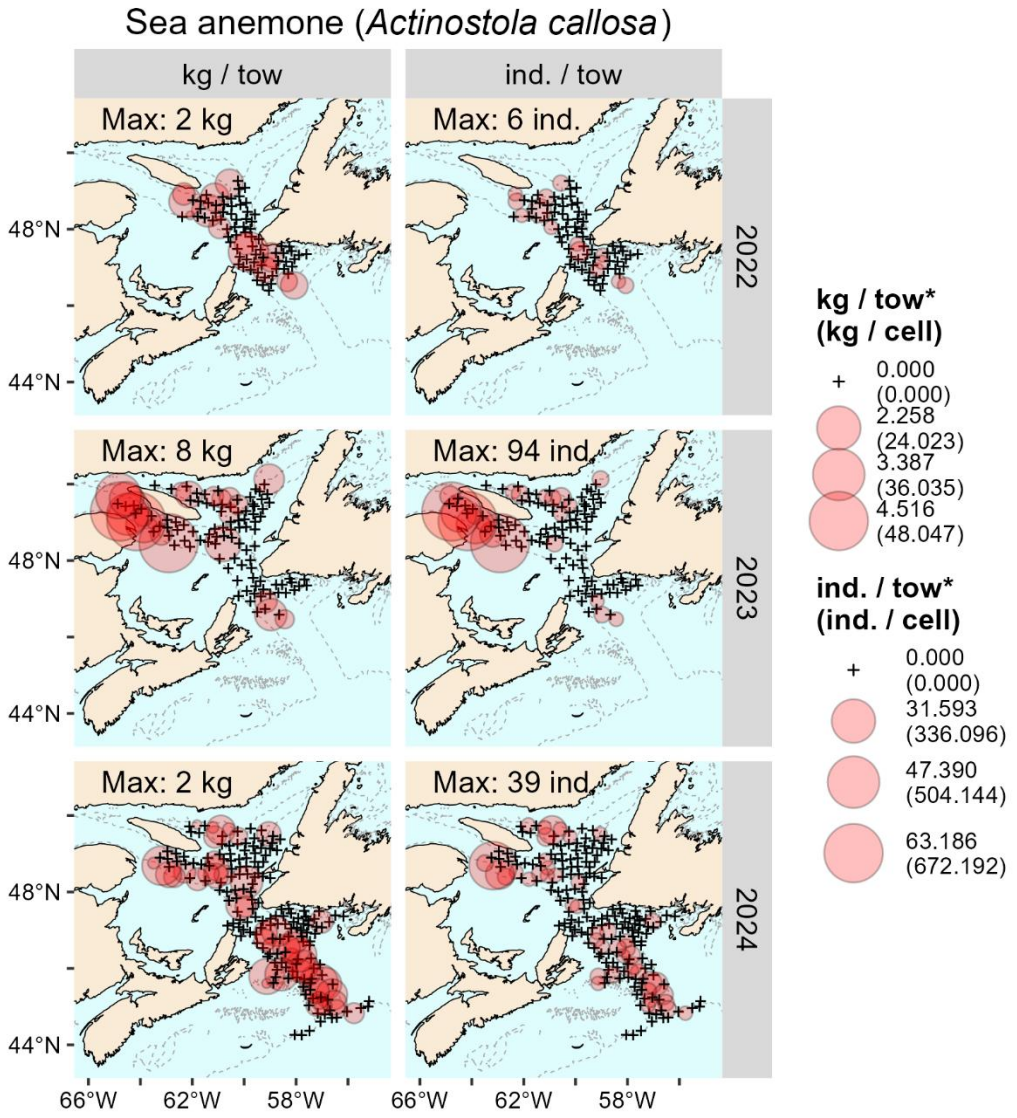


Figure 45a. Standardized catches by weight and/or number (colored bubbles) and cases of absence (black crosses) for the sea anemone *Actinostola callosa* in the winter surveys of 2022, 2023, and 2024.

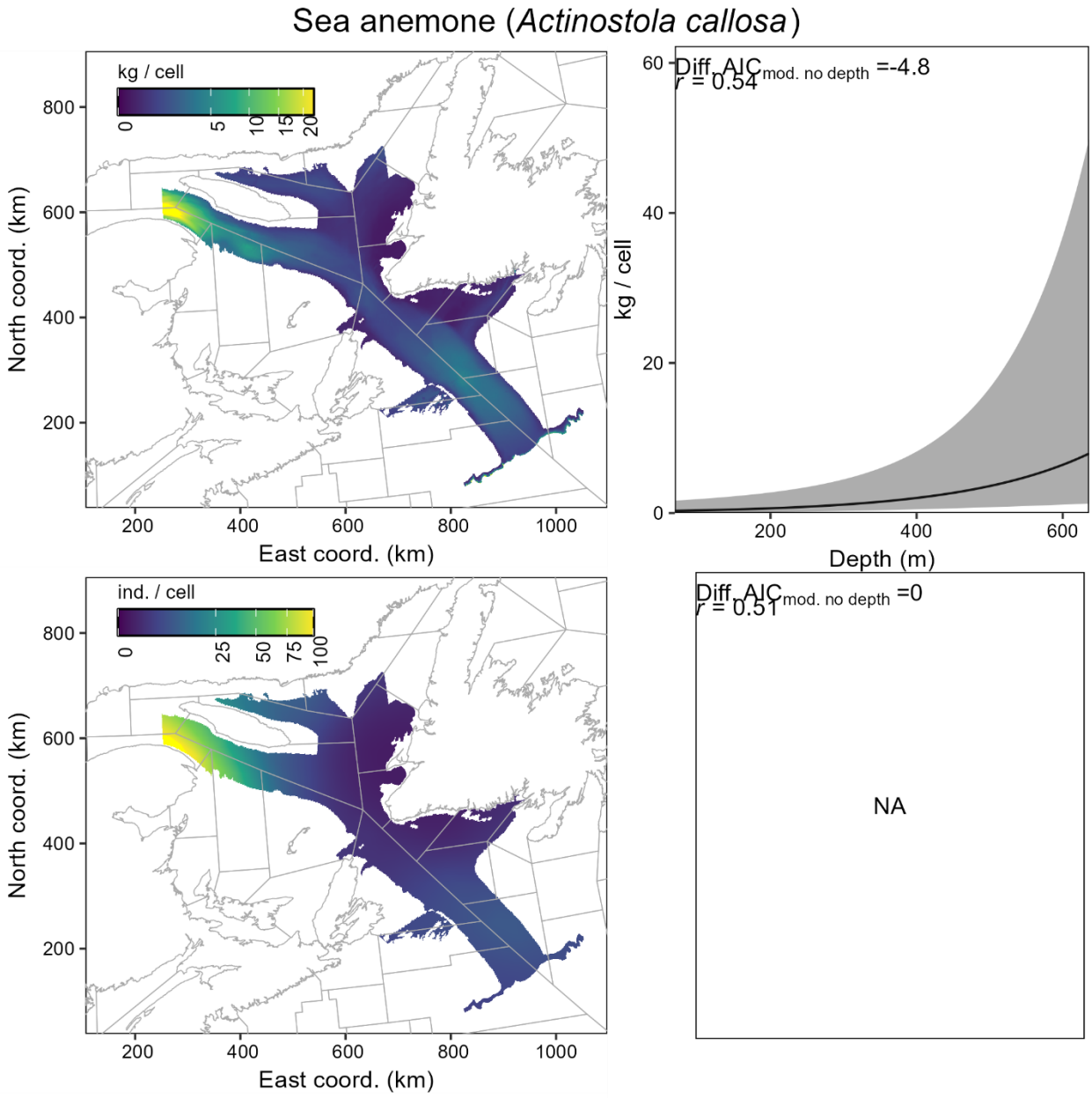


Figure 45b. Predicted weight (upper panels) and number (lower panels) values per 0.25 km^2 cell according to the selected spatial interpolation models for the sea anemone *Actinostola callosa* in the 2022, 2023, and 2024 winter survey.

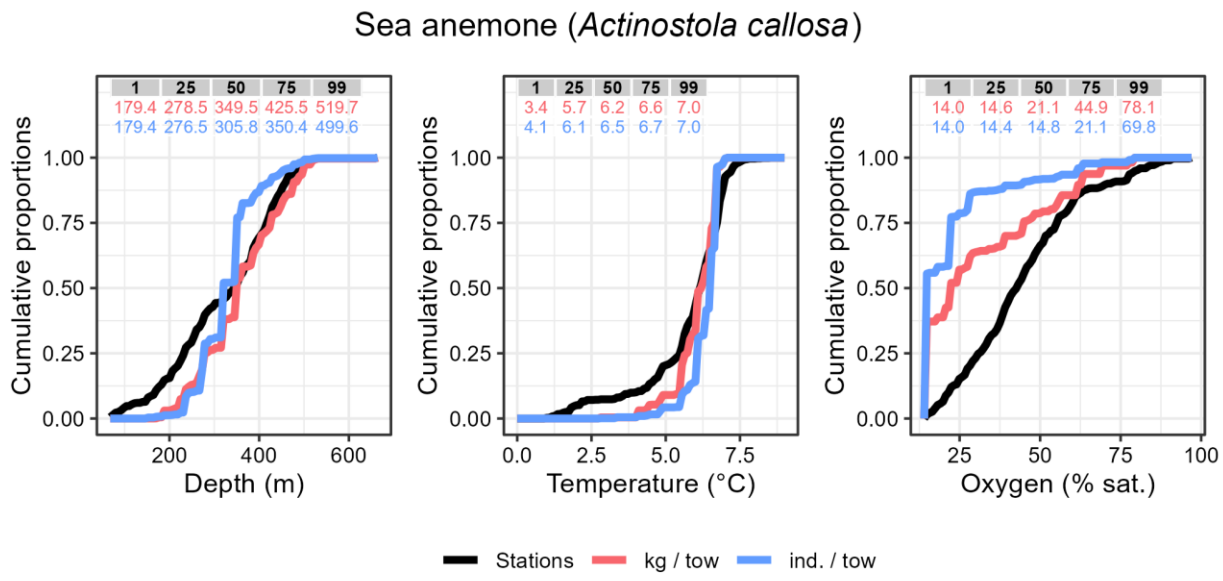


Figure 45c. Cumulative proportions of available values of depth, temperature and dissolved oxygen and standardized catches per tow for the sea anemone *Actinostola callosa* in the winter survey in 2022, 2023 and 2024.

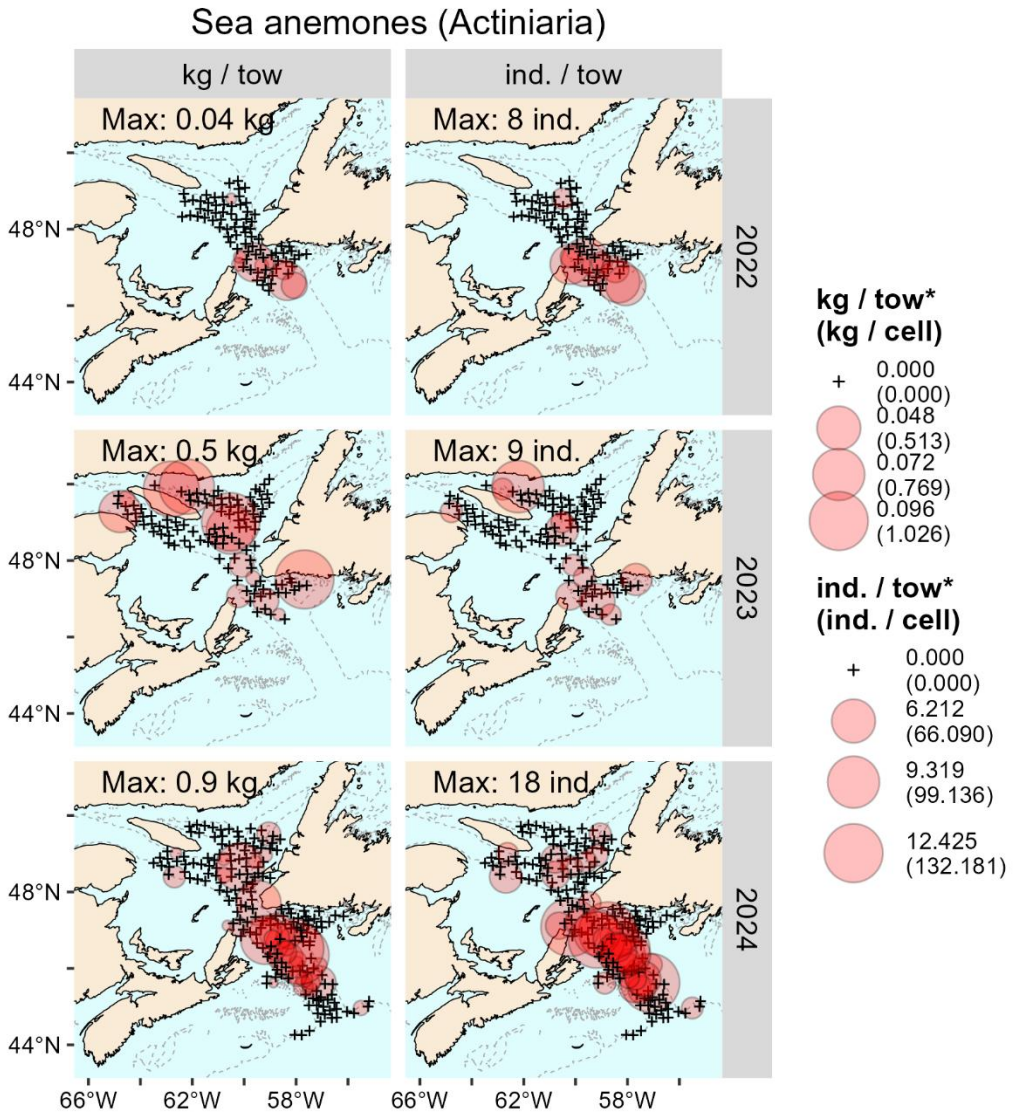


Figure 46a. Standardized catches by weight and/or number (colored bubbles) and cases of absence (black crosses) for specimens whose identification could not be more precise than the order Actiniaria (may include taxa 2150, 2158, 2159, 2162, 2165, 2167, 2171, 2173, 2182 and 2207) in the winter surveys of 2022, 2023, and 2024.

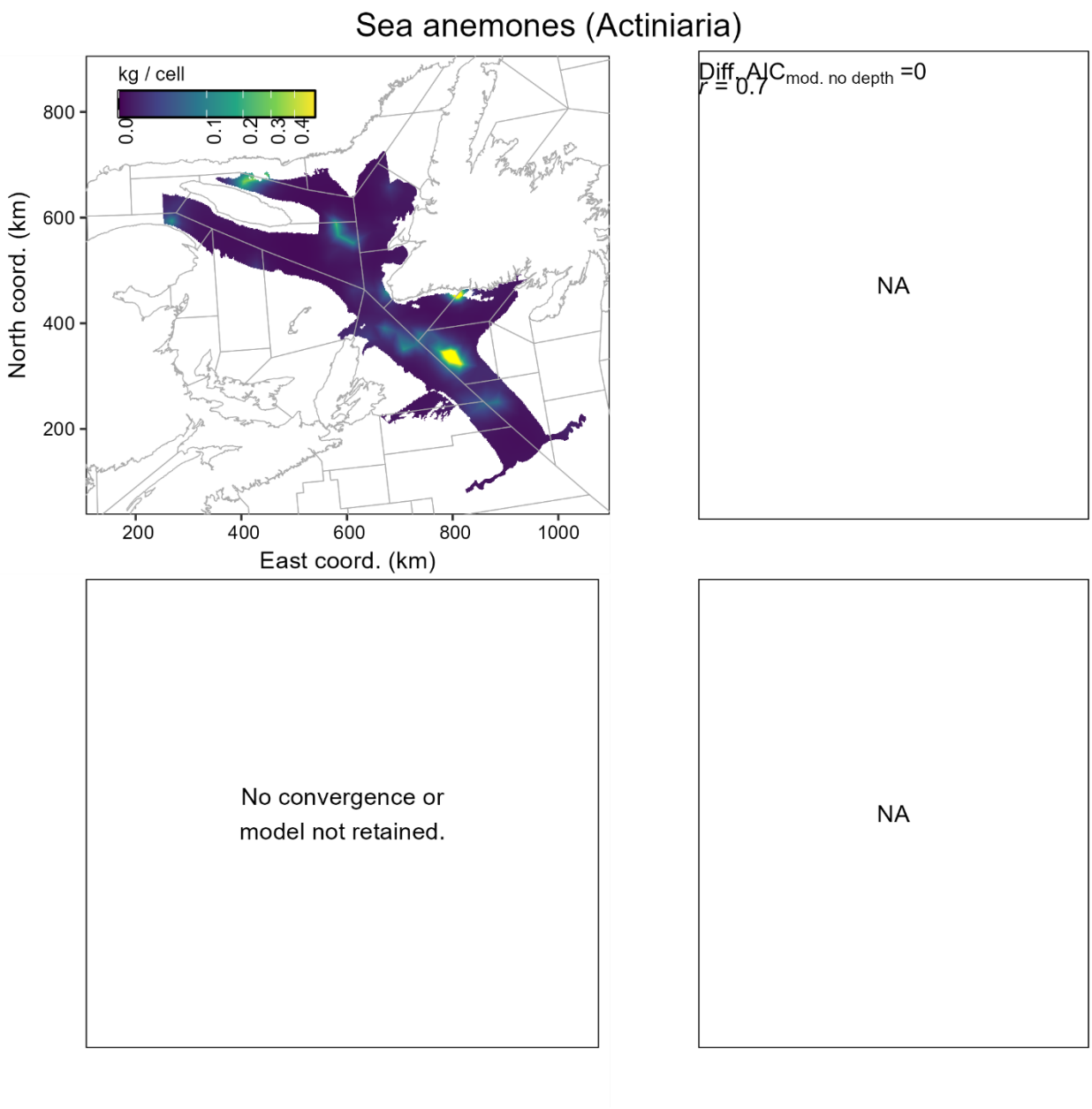


Figure 46b. Predicted weight (upper panels) and number (lower panels) values per 0.25 km^2 cell according to the selected spatial interpolation models for specimens whose identification could not be more precise than the order Actiniaria (may include taxa 2150, 2158, 2159, 2162, 2165, 2167, 2171, 2173, 2182 and 2207) in the 2022, 2023, and 2024 winter survey.

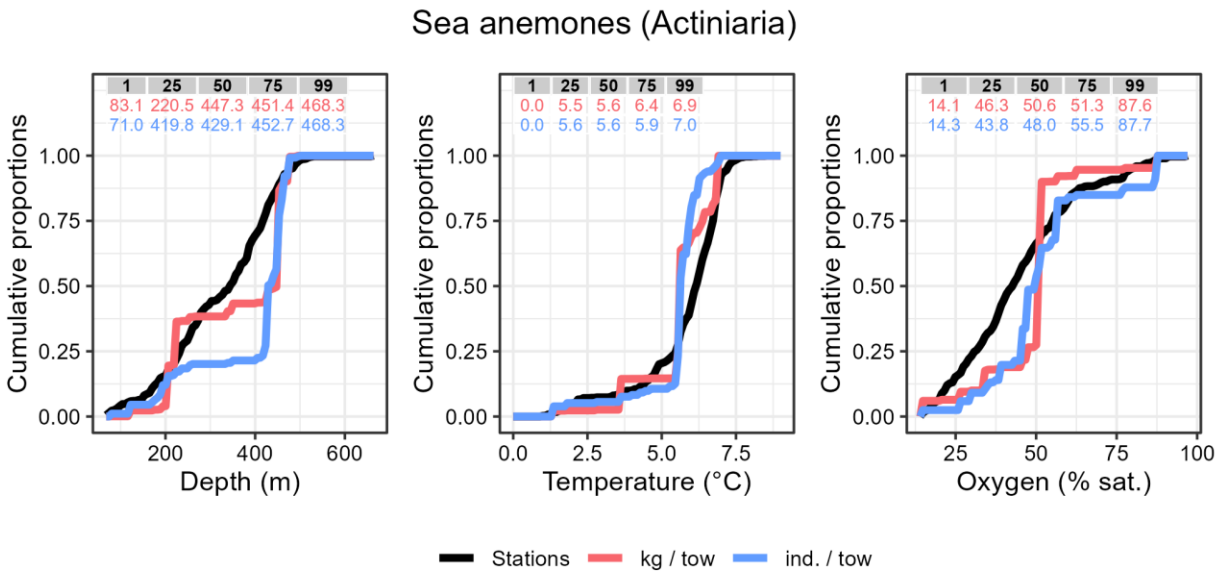


Figure 46c. Cumulative proportions of available values of depth, temperature and dissolved oxygen and standardized catches per tow for specimens whose identification could not be more precise than the order Actiniaria (may include taxa 2150, 2158, 2159, 2162, 2165, 2167, 2171, 2173, 2182 and 2207) in the winter survey in 2022, 2023 and 2024.

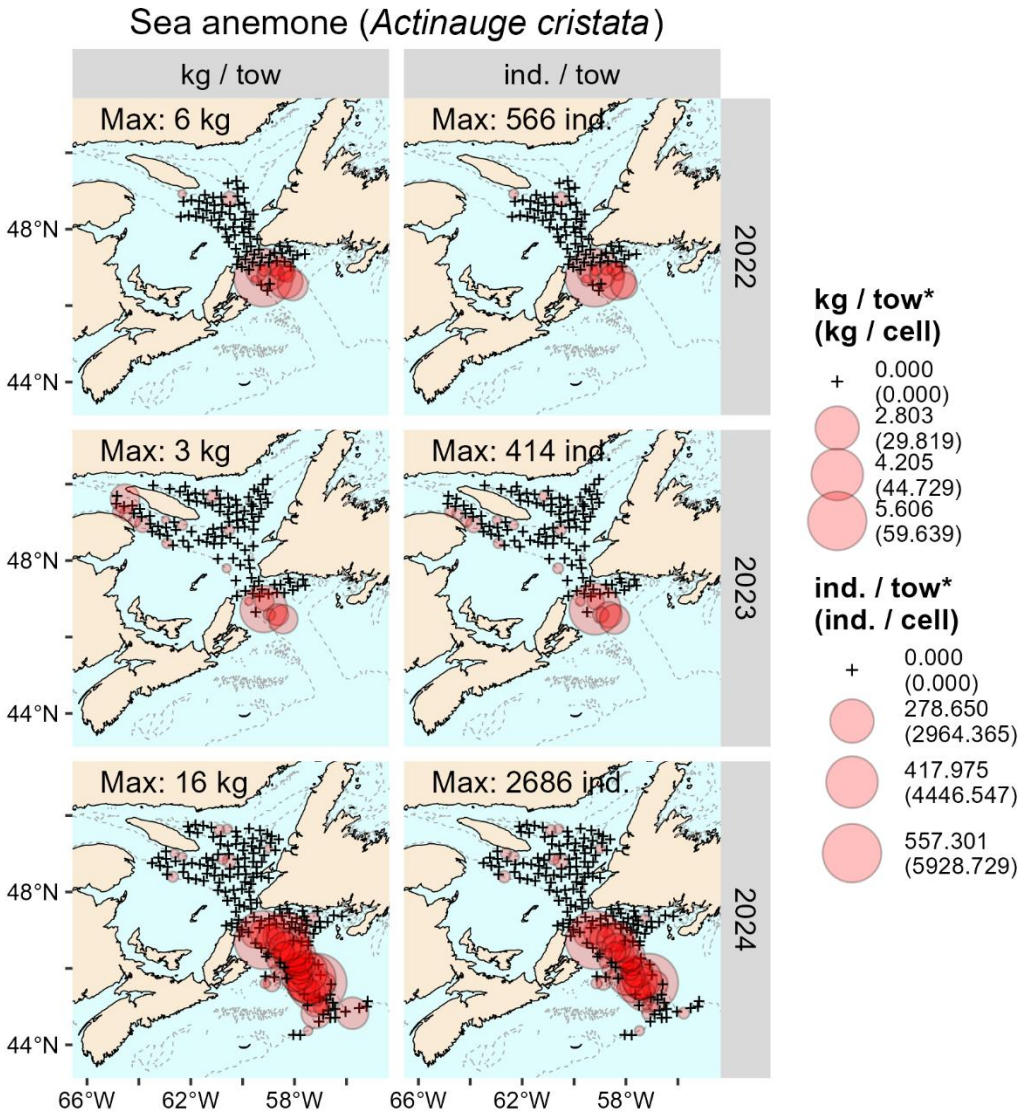


Figure 47a. Standardized catches by weight and/or number (colored bubbles) and cases of absence (black crosses) for the sea anemone *Actinauge cristata* in the winter surveys of 2022, 2023, and 2024.

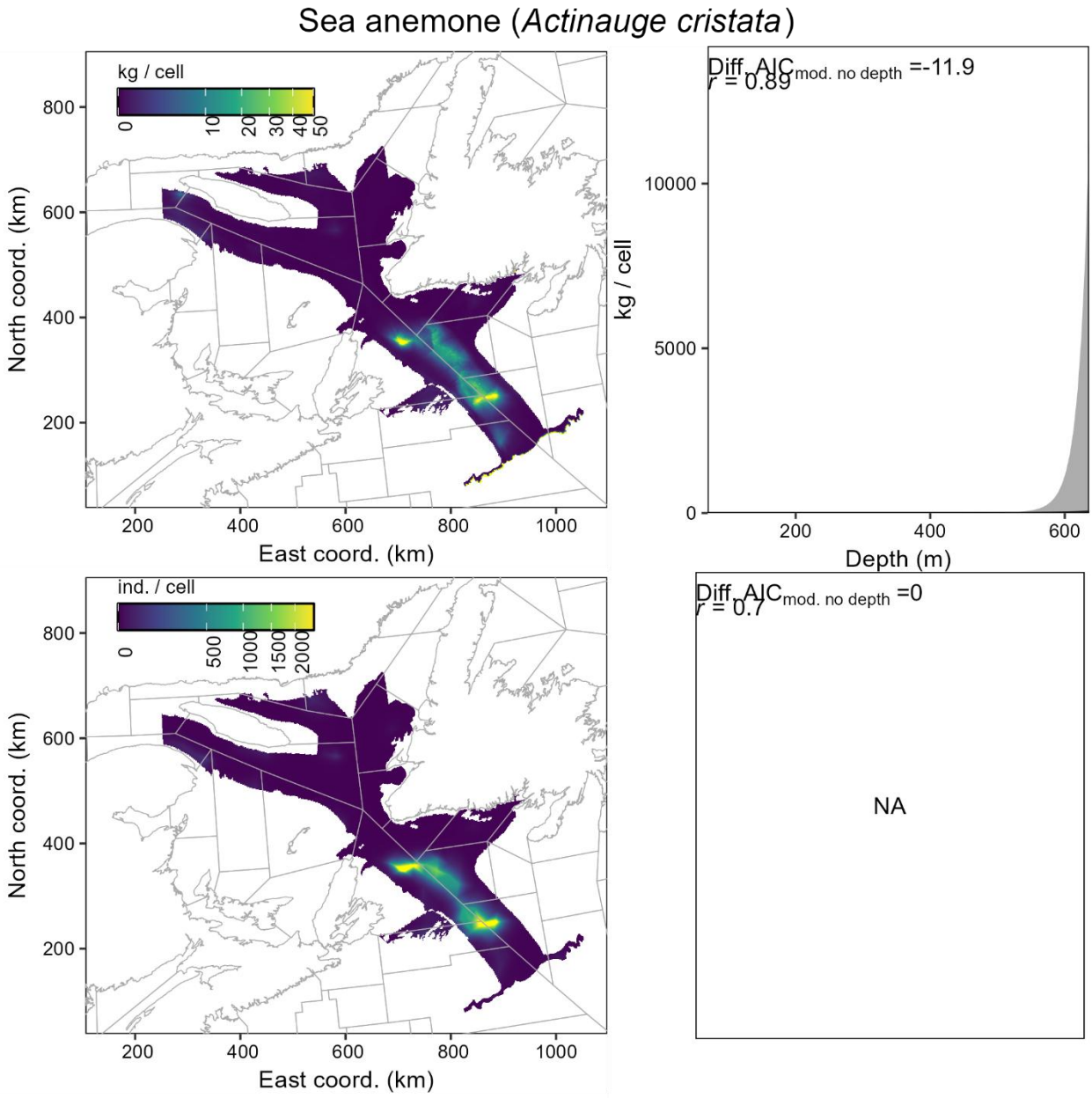


Figure 47b. Predicted weight (upper panels) and number (lower panels) values per 0.25 km^2 cell according to the selected spatial interpolation models for the sea anemone *Actinauge cristata* in the 2022, 2023, and 2024 winter survey.

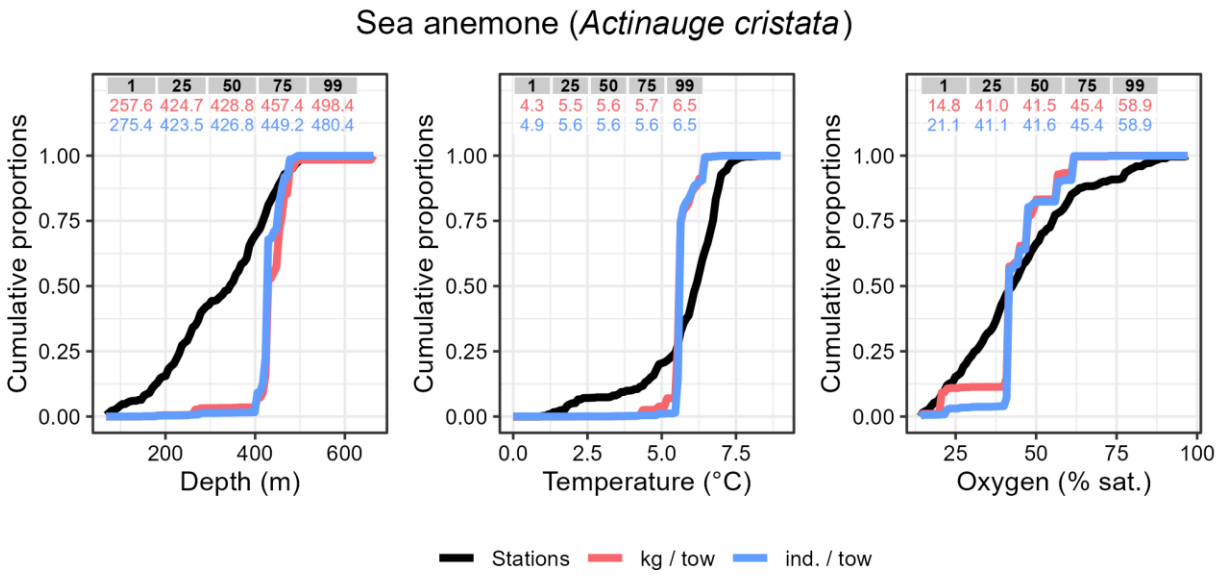


Figure 47c. Cumulative proportions of available values of depth, temperature and dissolved oxygen and standardized catches per tow for the sea anemone *Actinauge cristata* in the winter survey in 2022, 2023 and 2024.

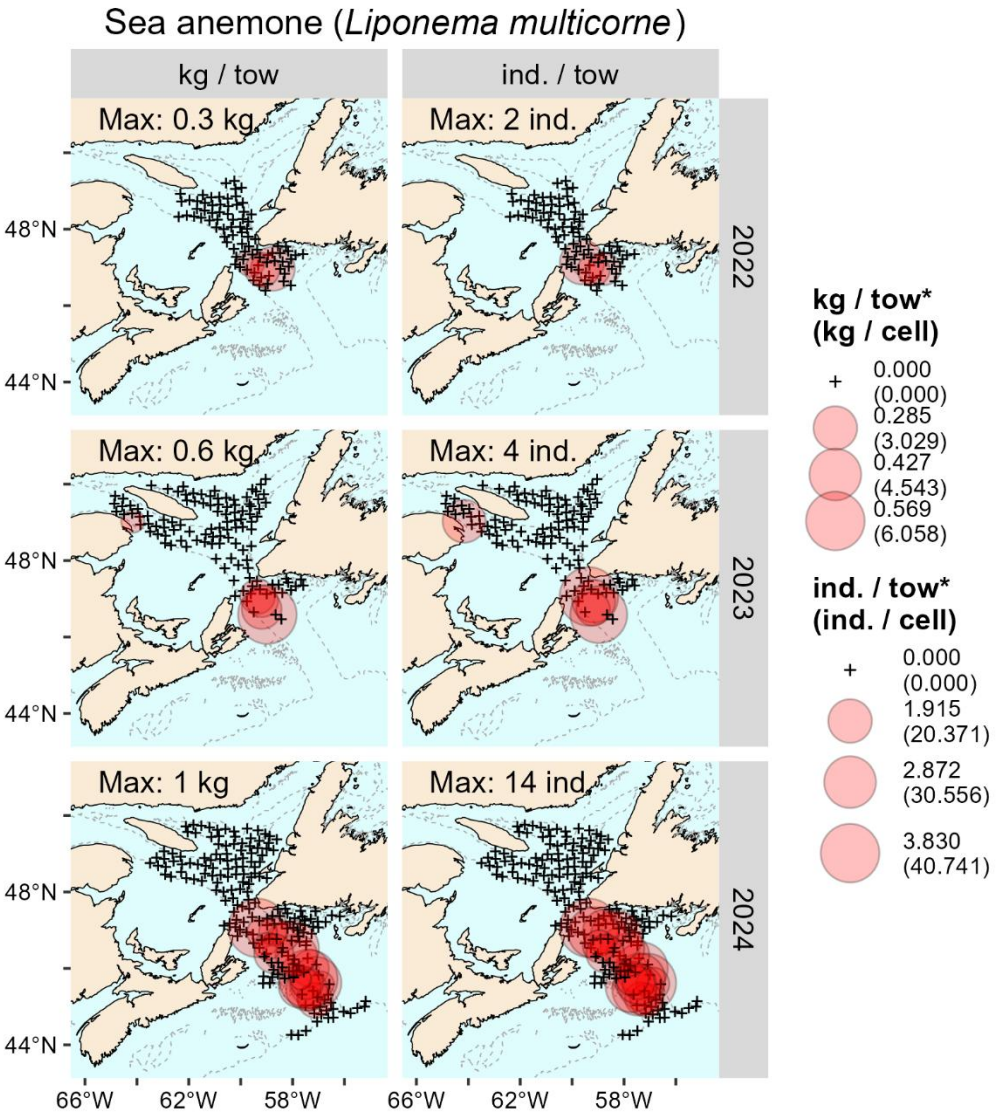


Figure 48a. Standardized catches by weight and/or number (colored bubbles) and cases of absence (black crosses) for the sea anemone *Liponema multicorne* in the winter surveys of 2022, 2023, and 2024.

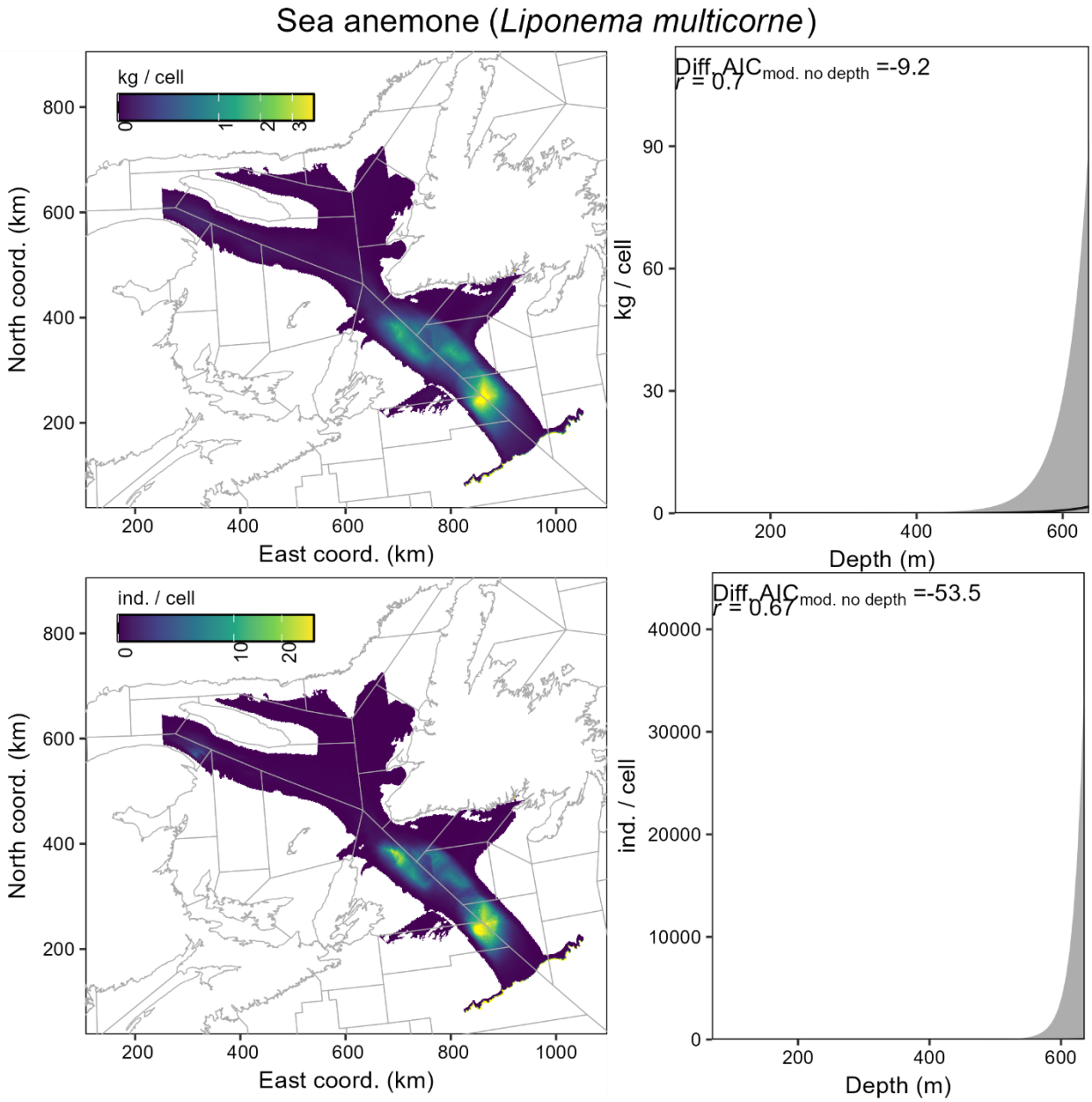


Figure 48b. Predicted weight (upper panels) and number (lower panels) values per 0.25 km^2 cell according to the selected spatial interpolation models for the sea anemone *Liponema multicorne* in the 2022, 2023, and 2024 winter survey.

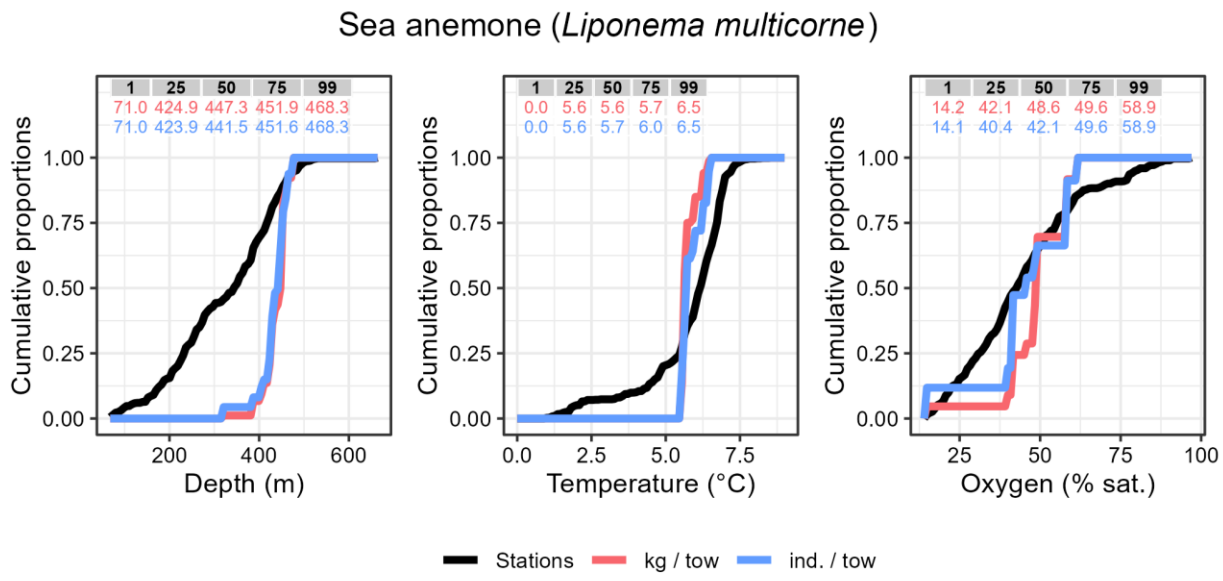


Figure 48c. Cumulative proportions of available values of depth, temperature and dissolved oxygen and standardized catches per tow for the sea anemone *Liponema multicorne* in the winter survey in 2022, 2023 and 2024.

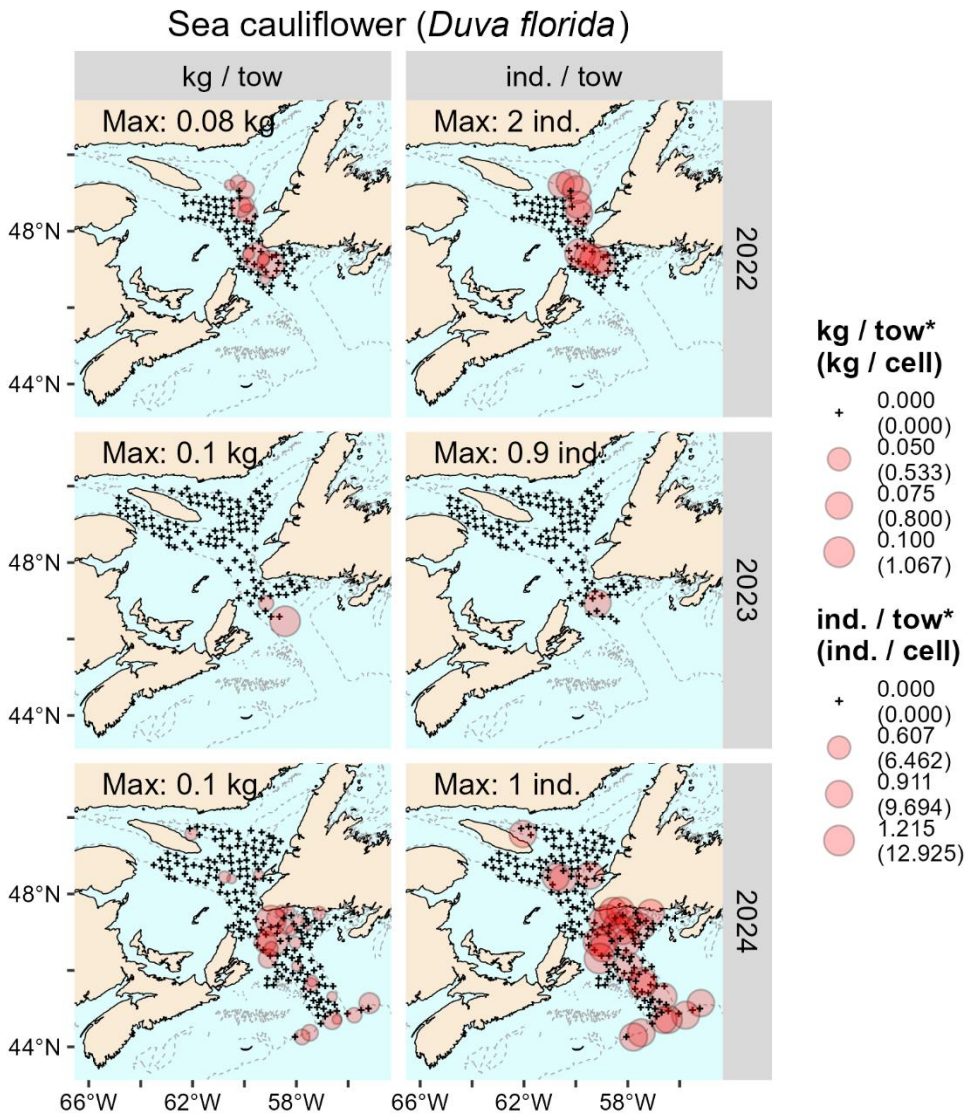


Figure 49a. Standardized catches by weight and/or number (colored bubbles) and cases of absence (black crosses) for the sea cauliflower in the winter surveys of 2022, 2023, and 2024.

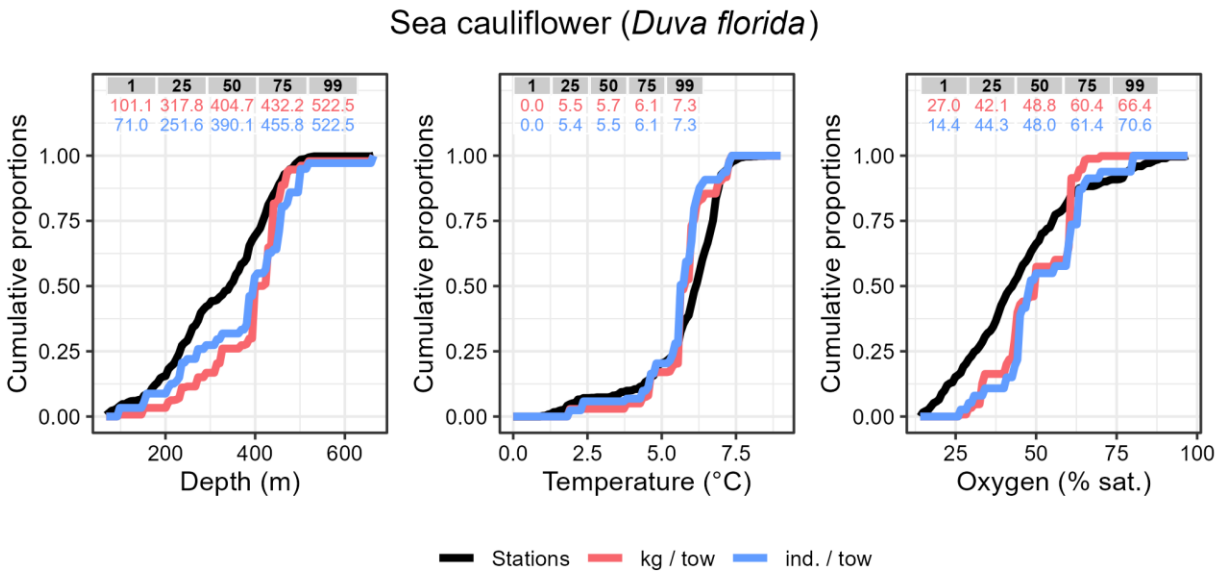


Figure 49b. Cumulative proportions of available values of depth, temperature and dissolved oxygen and standardized catches per tow for the sea cauliflower in the winter survey in 2022, 2023 and 2024.

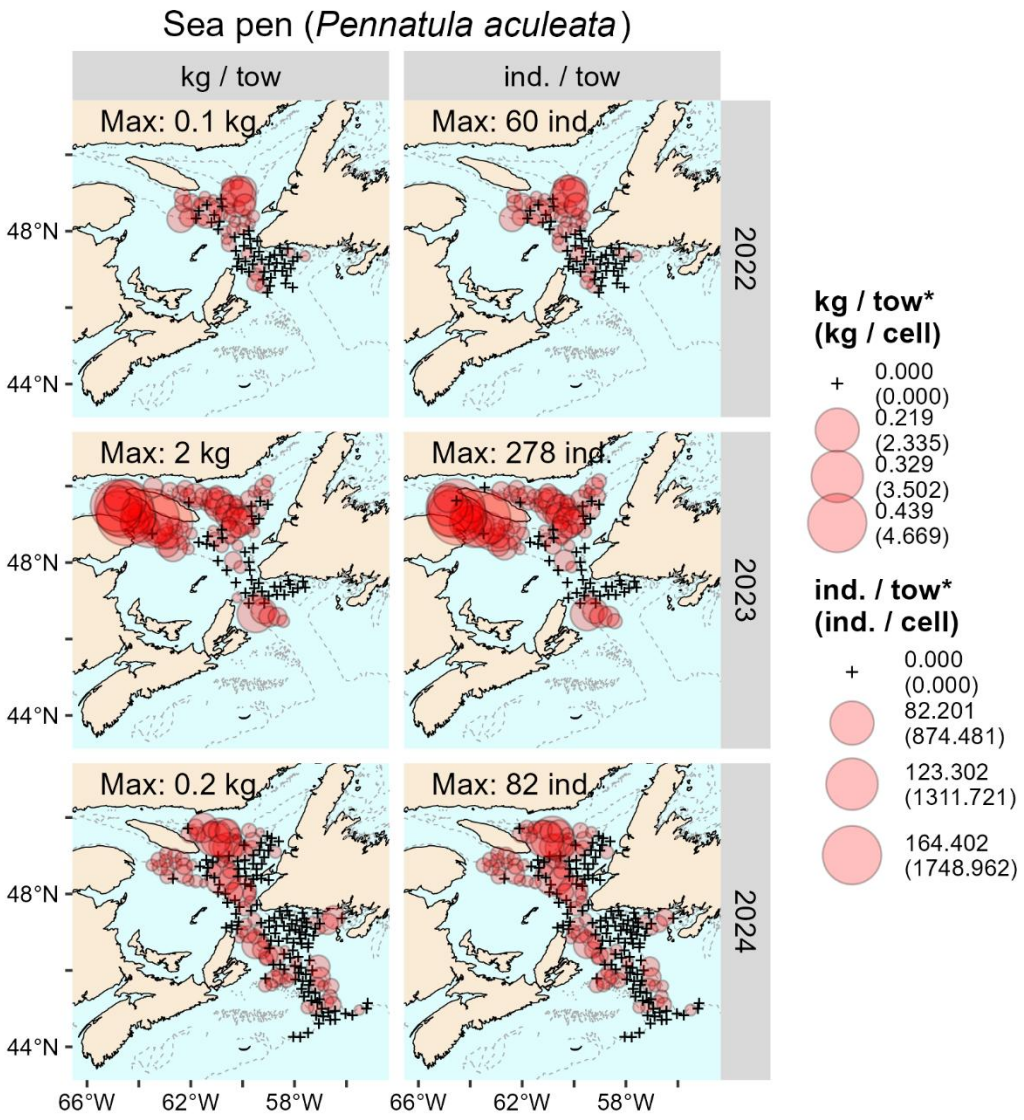


Figure 50a. Standardized catches by weight and/or number (colored bubbles) and cases of absence (black crosses) for the sea pen *Pennatula aculeata* in the winter surveys of 2022, 2023, and 2024.

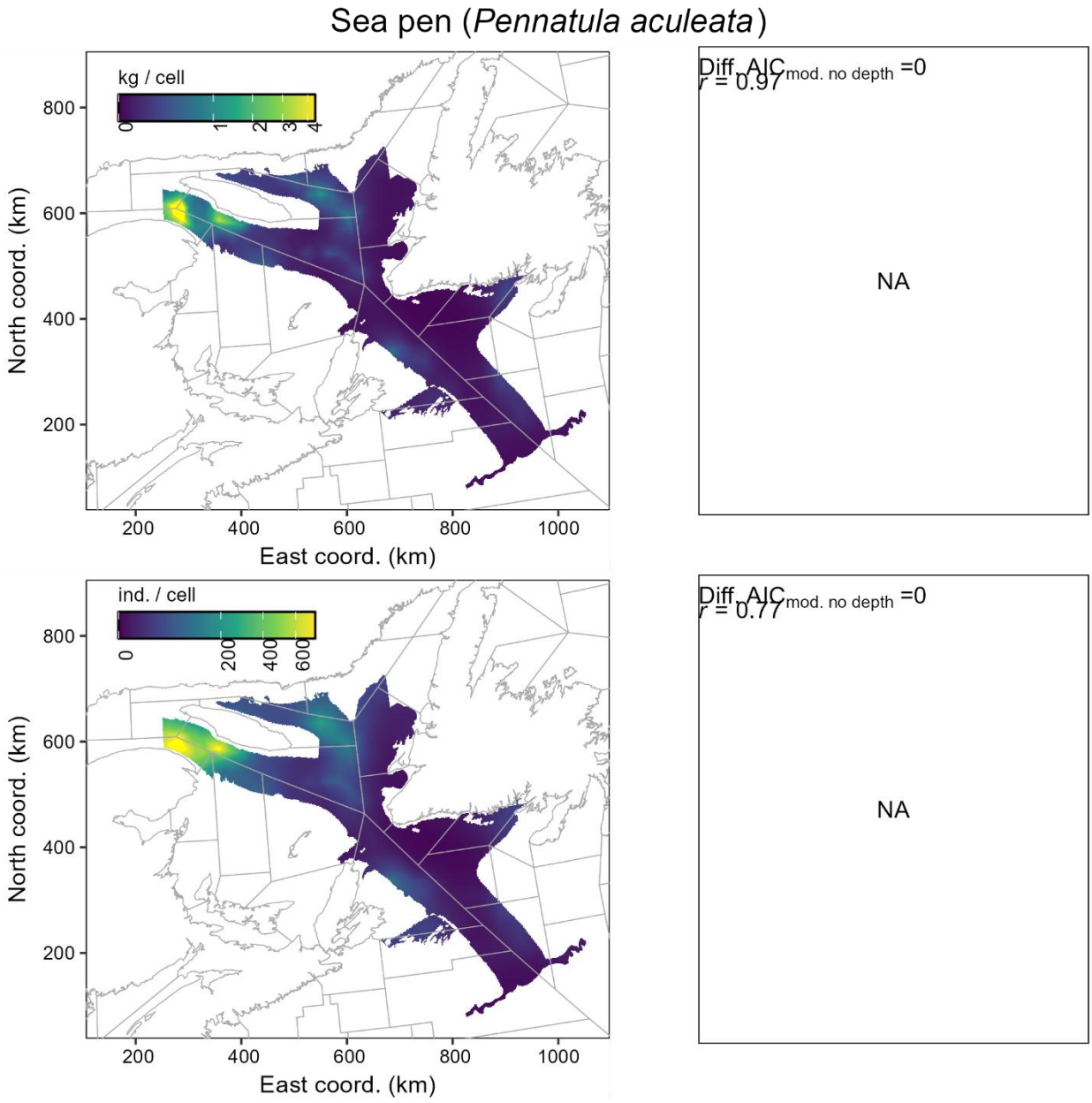


Figure 50b. Predicted weight (upper panels) and number (lower panels) values per 0.25 km^2 cell according to the selected spatial interpolation models for the sea pen *Pennatula aculeata* in the 2022, 2023, and 2024 winter survey.

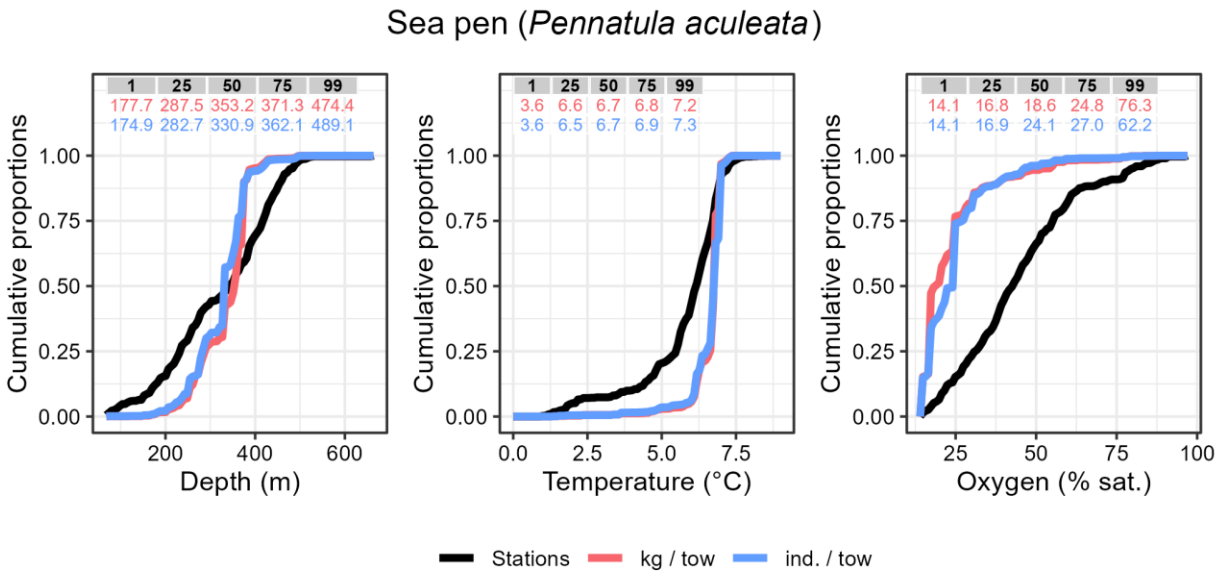


Figure 50c. Cumulative proportions of available values of depth, temperature and dissolved oxygen and standardized catches per tow for the sea pen *Pennatula aculeata* in the winter survey in 2022, 2023 and 2024.

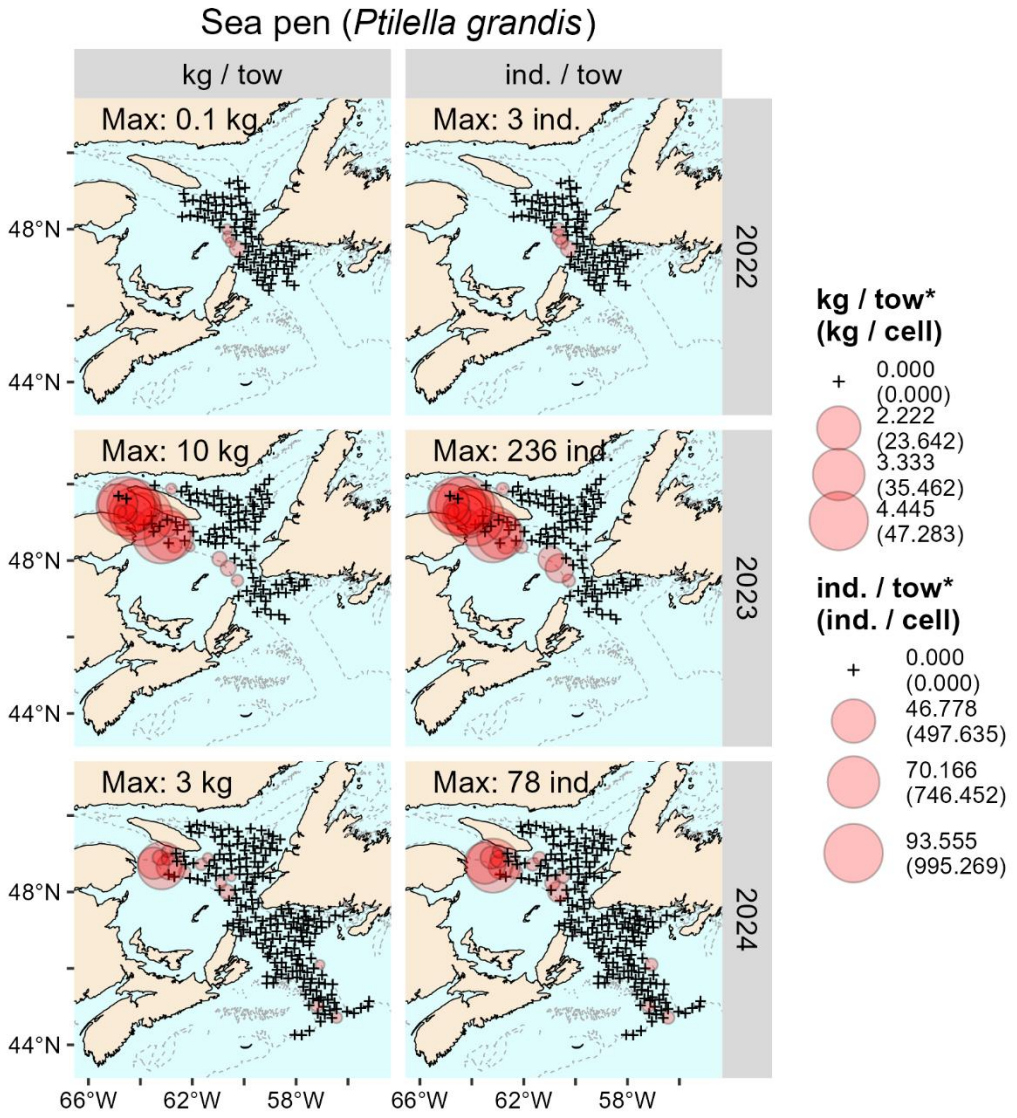


Figure 51a. Standardized catches by weight and/or number (colored bubbles) and cases of absence (black crosses) for the sea pen *Ptilella grandis* in the winter surveys of 2022, 2023, and 2024.

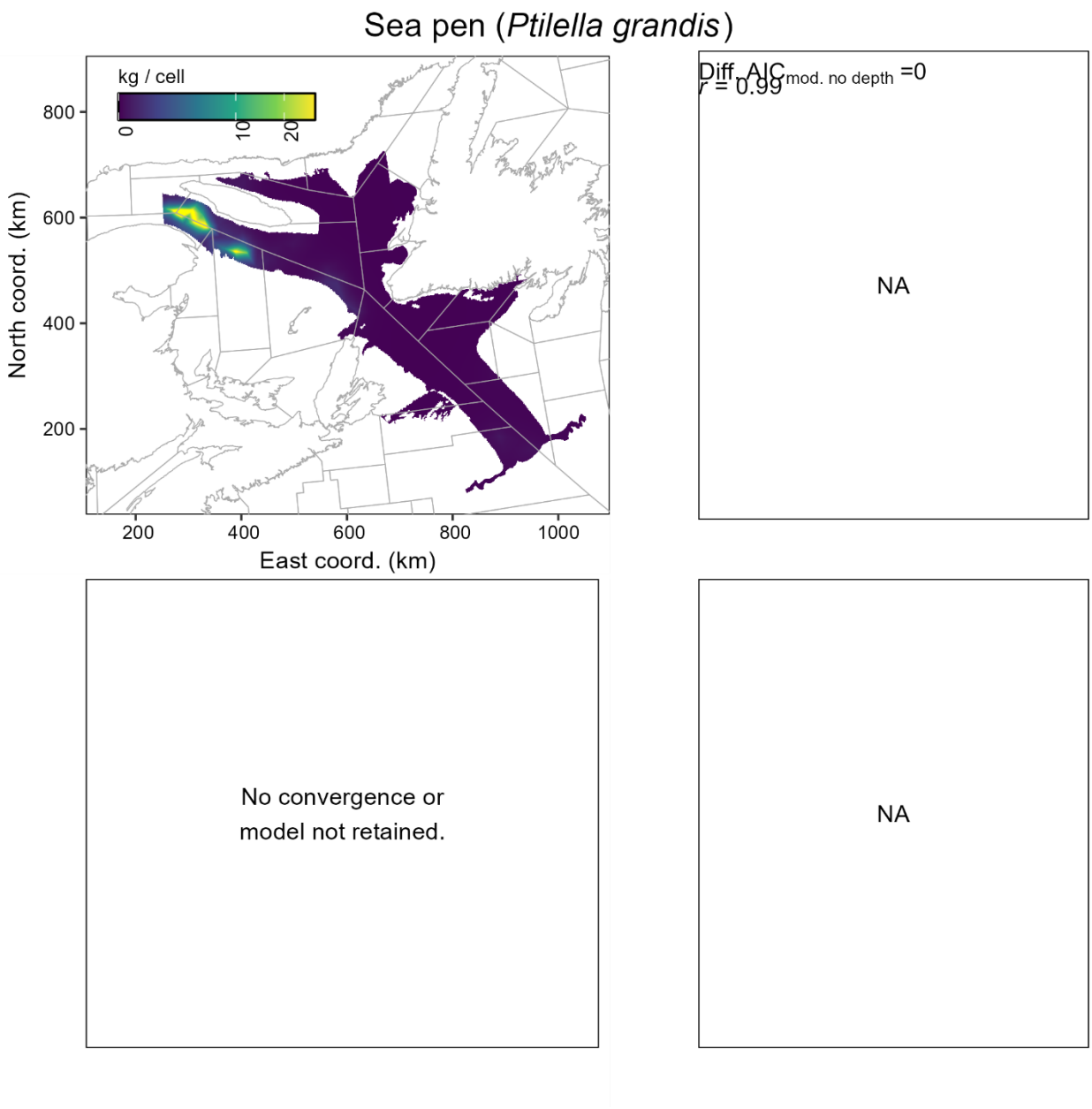


Figure 51b. Predicted weight (upper panels) and number (lower panels) values per 0.25 km^2 cell according to the selected spatial interpolation models for the sea pen *Ptilella grandis* in the 2022, 2023, and 2024 winter survey.

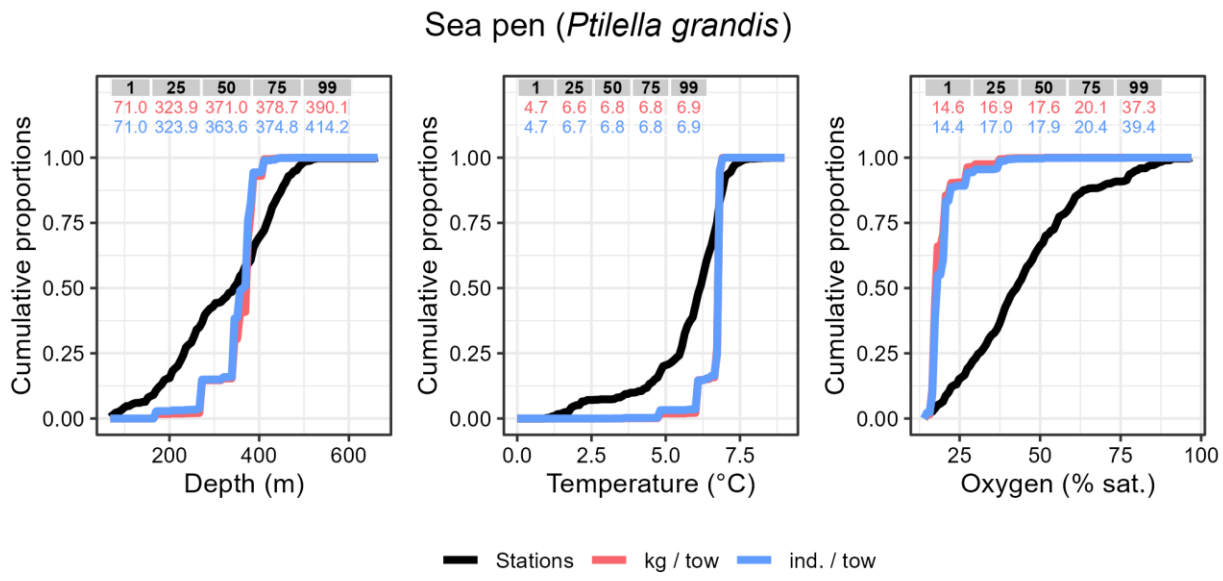


Figure 51c. Cumulative proportions of available values of depth, temperature and dissolved oxygen and standardized catches per tow for the sea pen *Ptilella grandis* in the winter survey in 2022, 2023 and 2024.

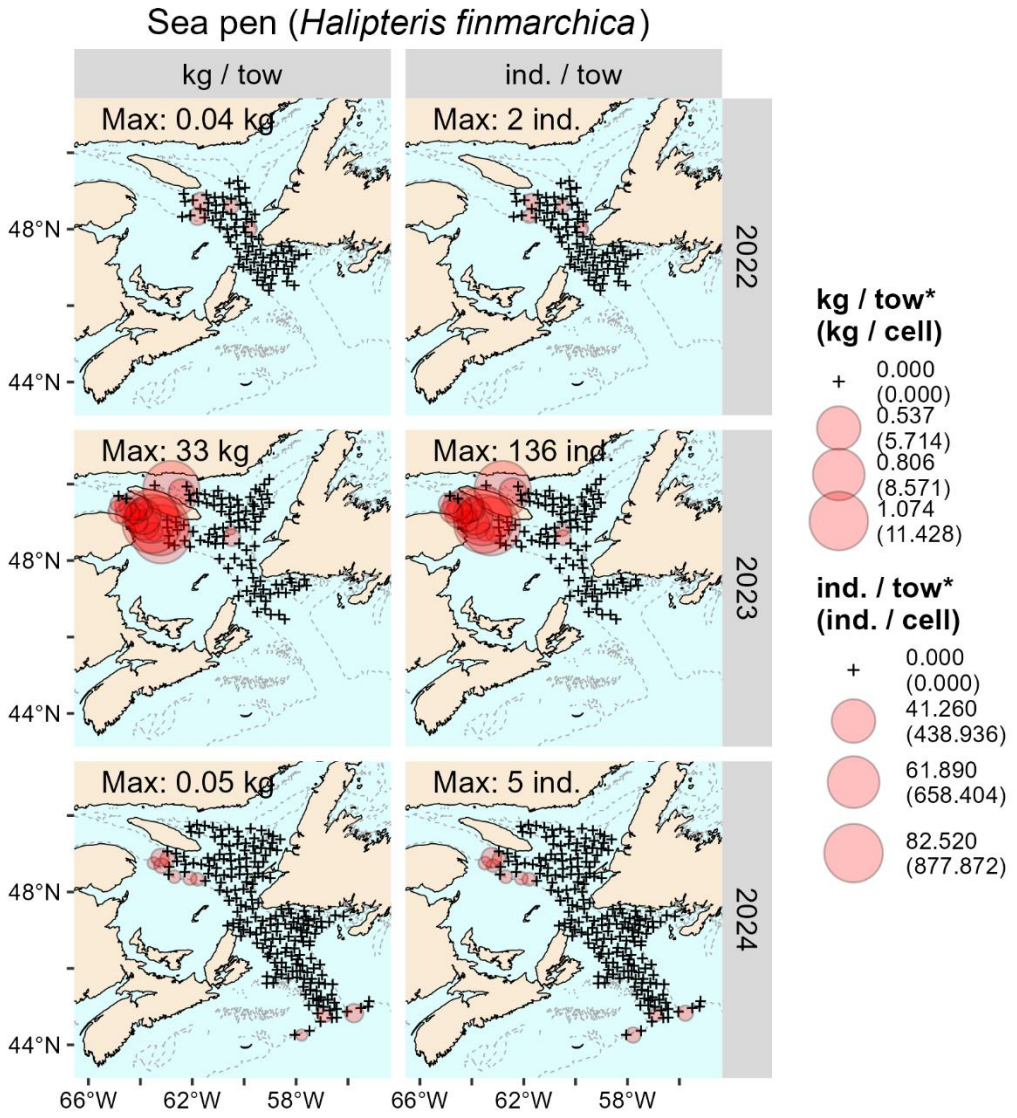


Figure 52a. Standardized catches by weight and/or number (colored bubbles) and cases of absence (black crosses) for the sea pen *Halipteris finmarchica* in the winter surveys of 2022, 2023, and 2024.

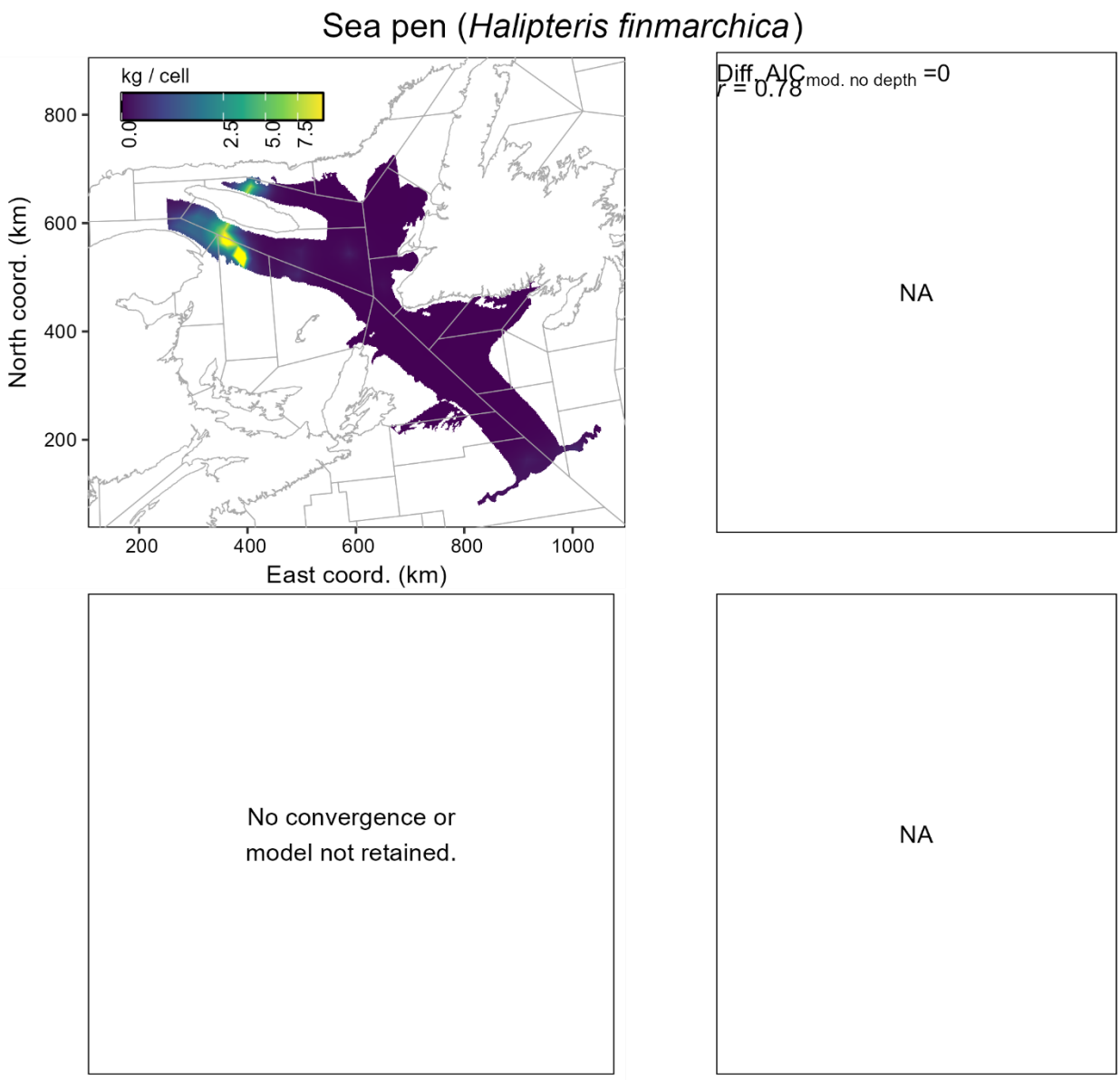


Figure 52b. Predicted weight (upper panels) and number (lower panels) values per 0.25 km^2 cell according to the selected spatial interpolation models for the sea pen *Halipteris finmarchica* in the 2022, 2023, and 2024 winter survey.

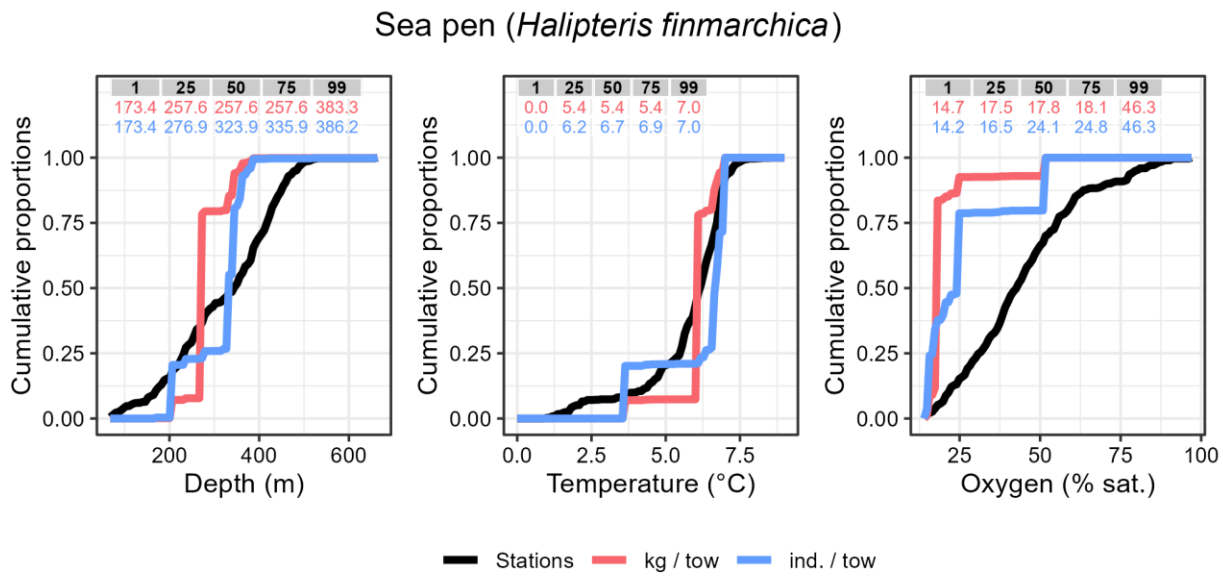


Figure 52c. Cumulative proportions of available values of depth, temperature and dissolved oxygen and standardized catches per tow for the sea pen *Halipteris finmarchica* in the winter survey in 2022, 2023 and 2024.

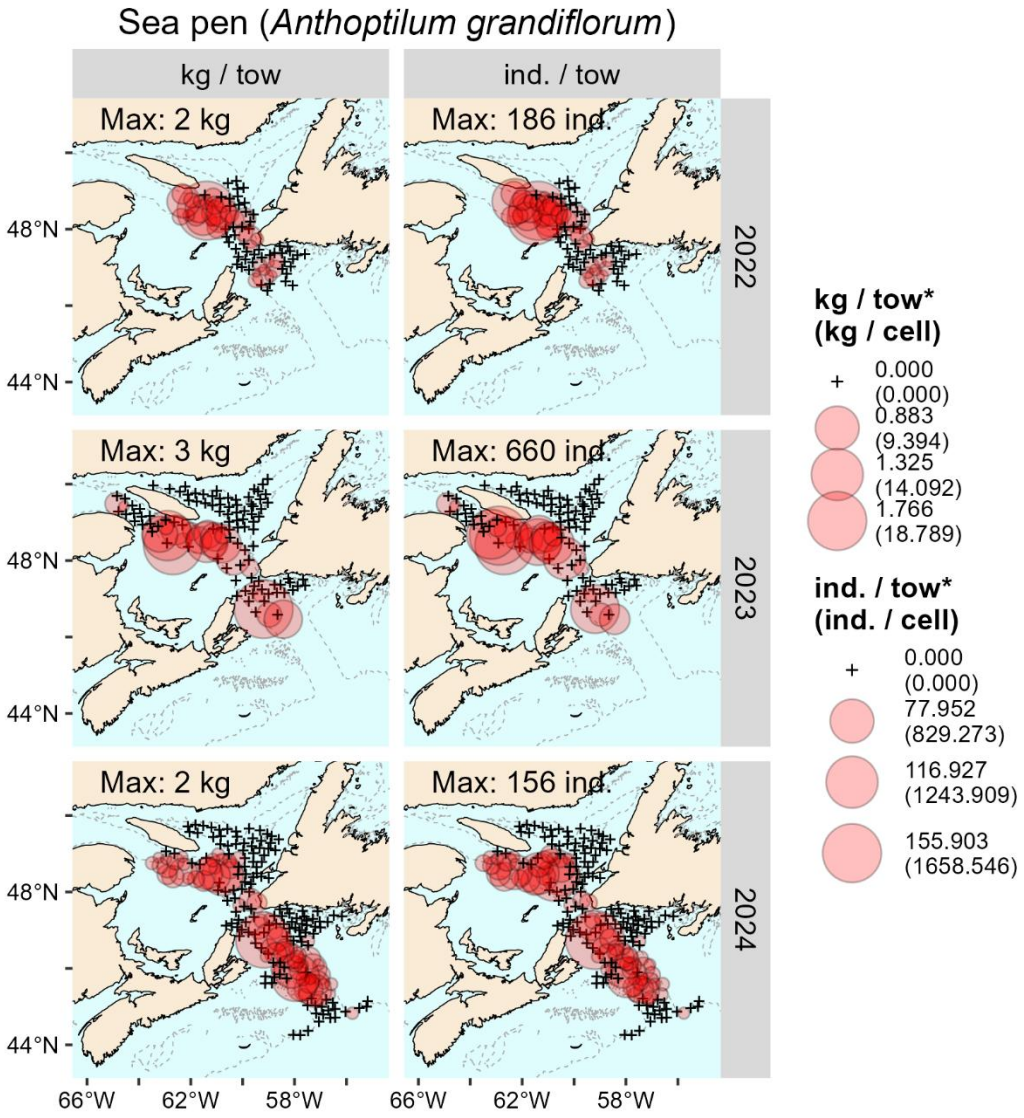


Figure 53a. Standardized catches by weight and/or number (colored bubbles) and cases of absence (black crosses) for the sea pen *Anthoptilum grandiflorum* in the winter surveys of 2022, 2023, and 2024.

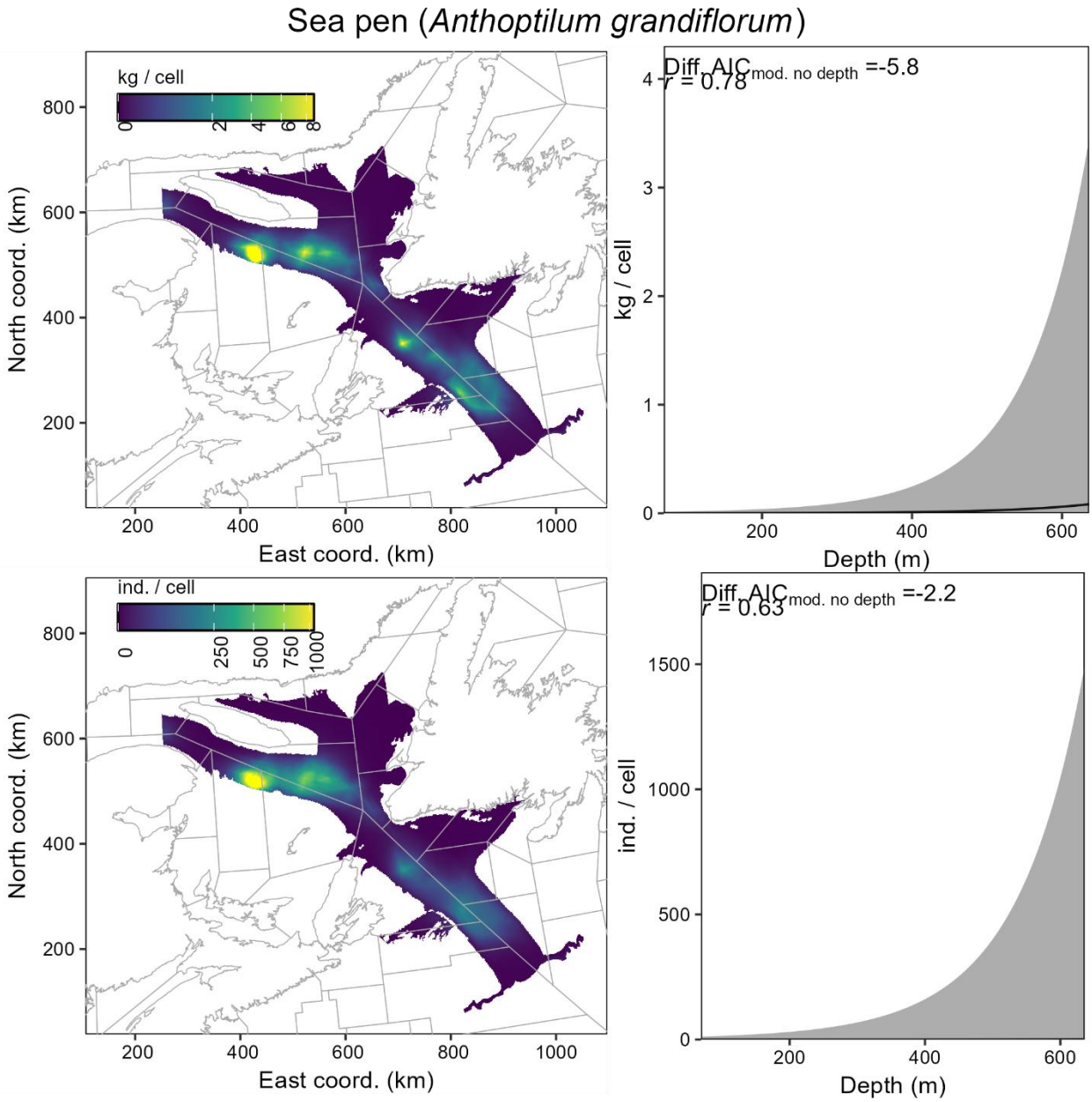


Figure 53b. Predicted weight (upper panels) and number (lower panels) values per 0.25 km^2 cell according to the selected spatial interpolation models for the sea pen *Anthoptilum grandiflorum* in the 2022, 2023, and 2024 winter survey.

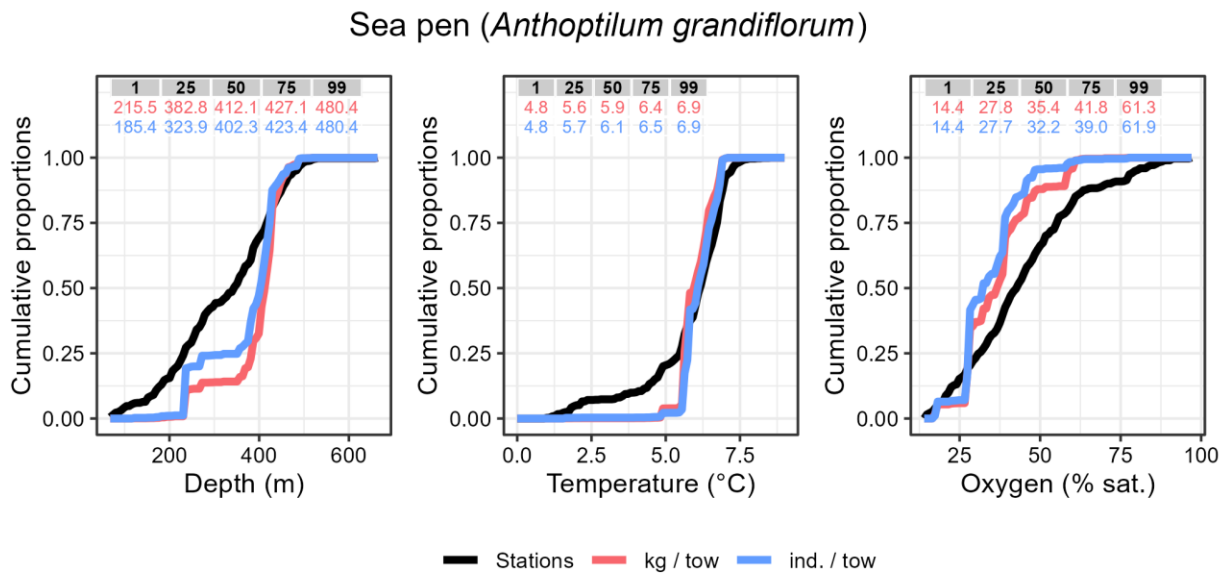


Figure 53c. Cumulative proportions of available values of depth, temperature and dissolved oxygen and standardized catches per tow for the sea pen *Anthoptilum grandiflorum* in the winter survey in 2022, 2023 and 2024.

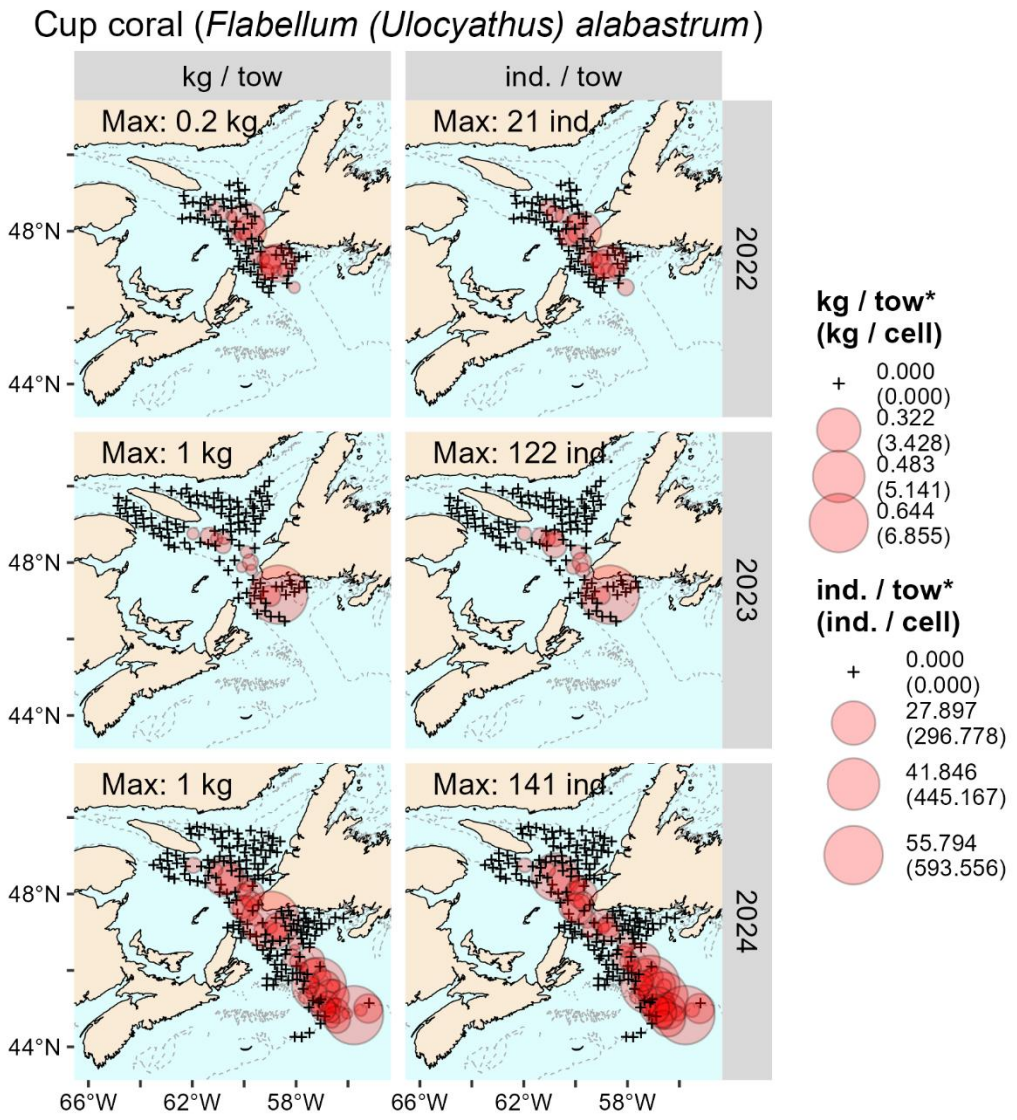


Figure 54a. Standardized catches by weight and/or number (colored bubbles) and cases of absence (black crosses) for the cup coral in the winter surveys of 2022, 2023, and 2024.

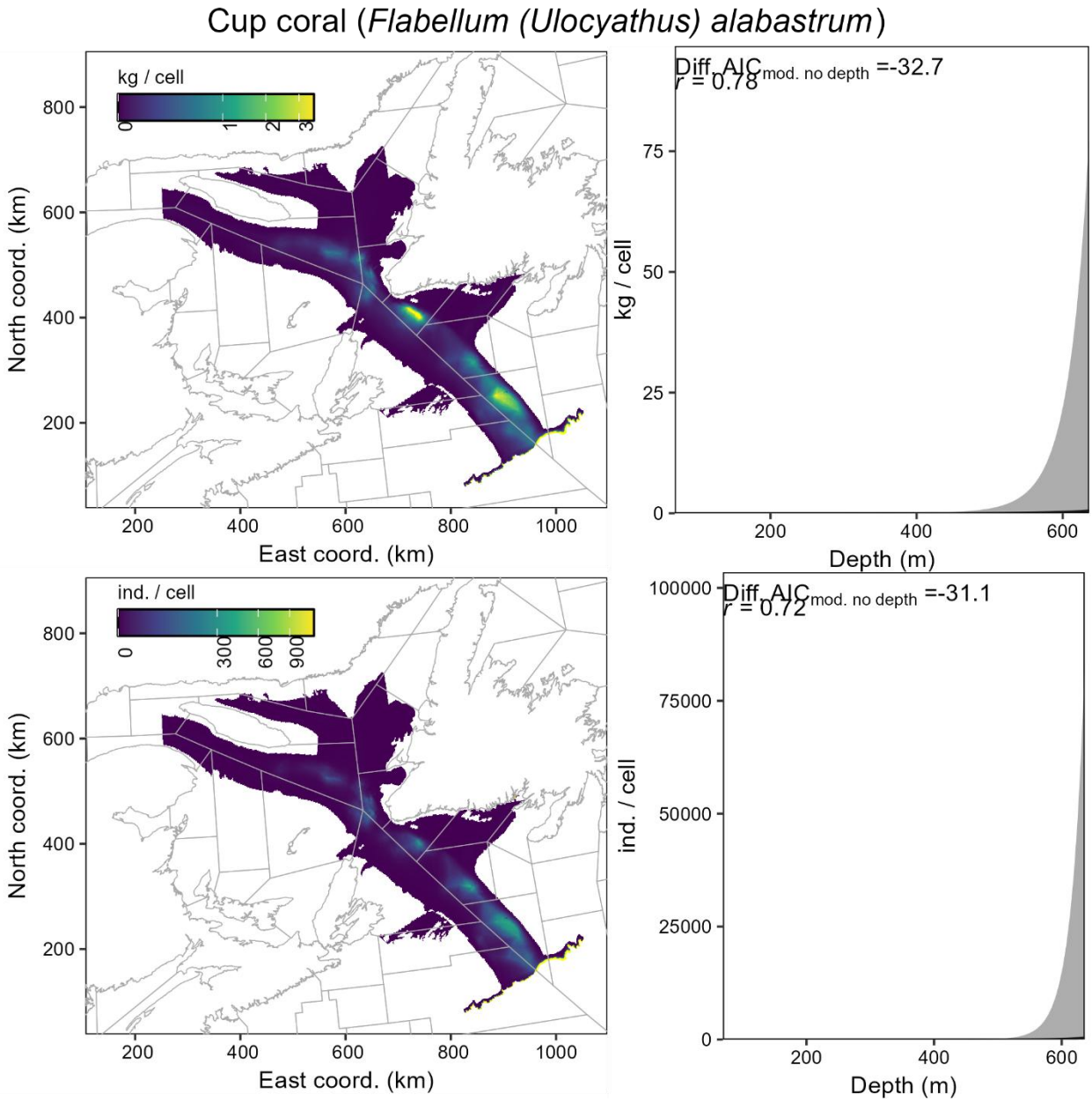


Figure 54b. Predicted weight (upper panels) and number (lower panels) values per 0.25 km^2 cell according to the selected spatial interpolation models for the cup coral in the 2022, 2023, and 2024 winter survey.

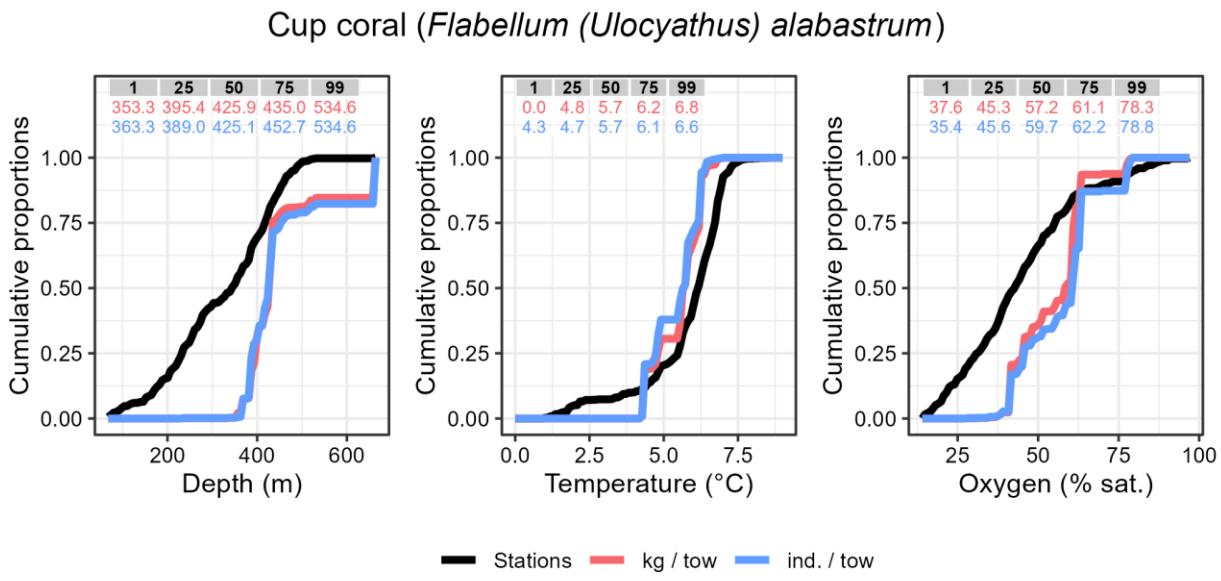


Figure 54c. Cumulative proportions of available values of depth, temperature and dissolved oxygen and standardized catches per tow for the cup coral in the winter survey in 2022, 2023 and 2024.

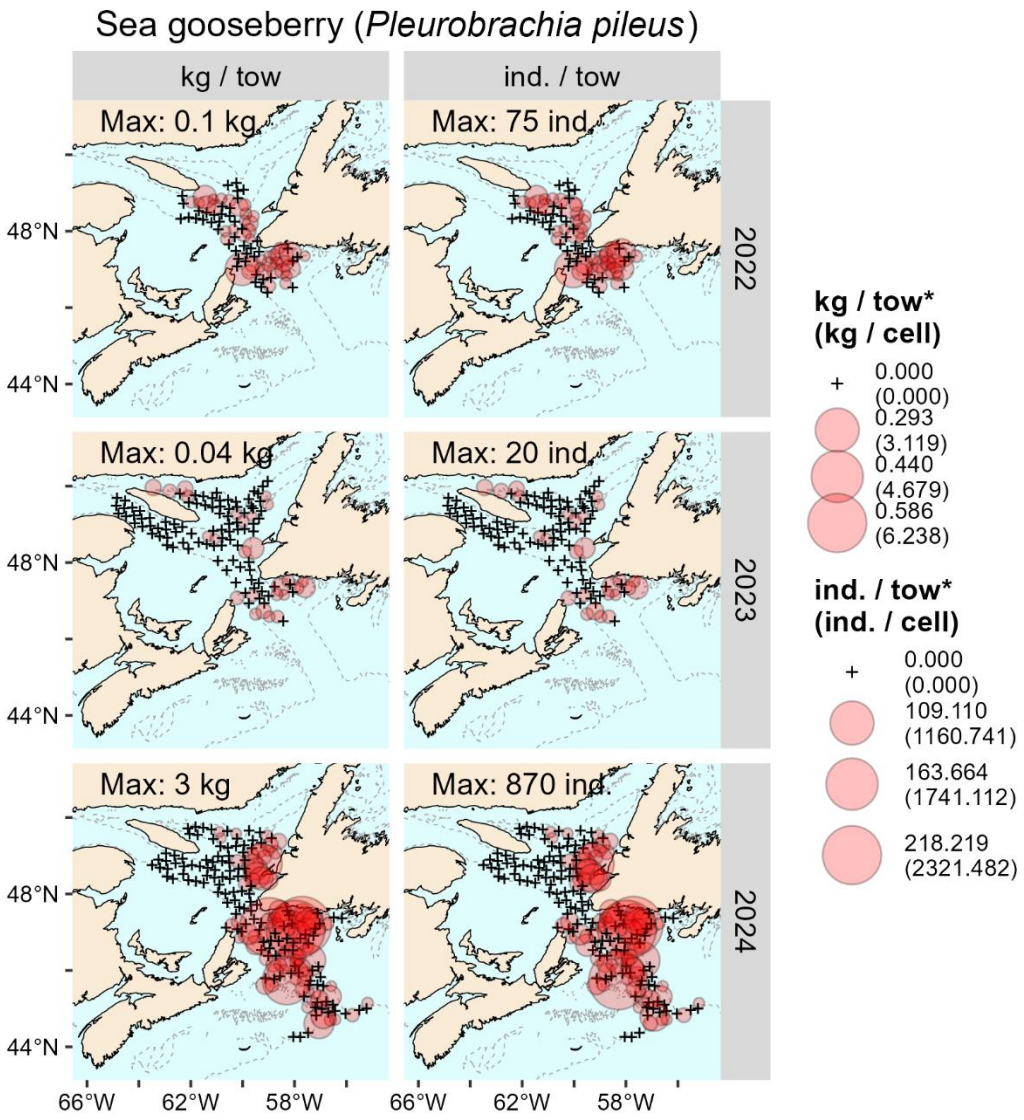


Figure 55a. Standardized catches by weight and/or number (colored bubbles) and cases of absence (black crosses) for the lion's mane in the winter surveys of 2022, 2023, and 2024.

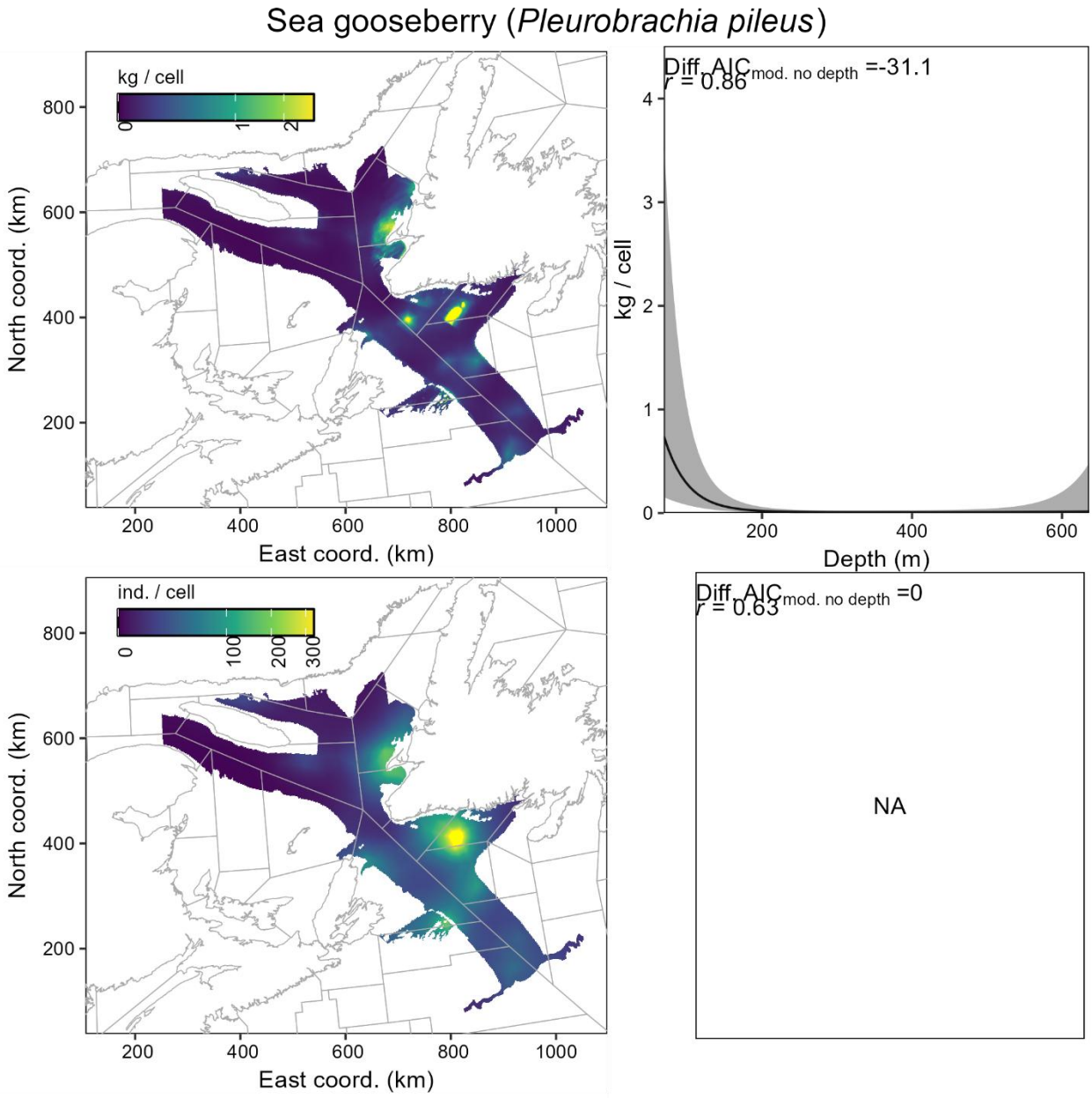


Figure 55b. Predicted weight (upper panels) and number (lower panels) values per 0.25 km^2 cell according to the selected spatial interpolation models for the sea gooseberry in the 2022, 2023, and 2024 winter survey.

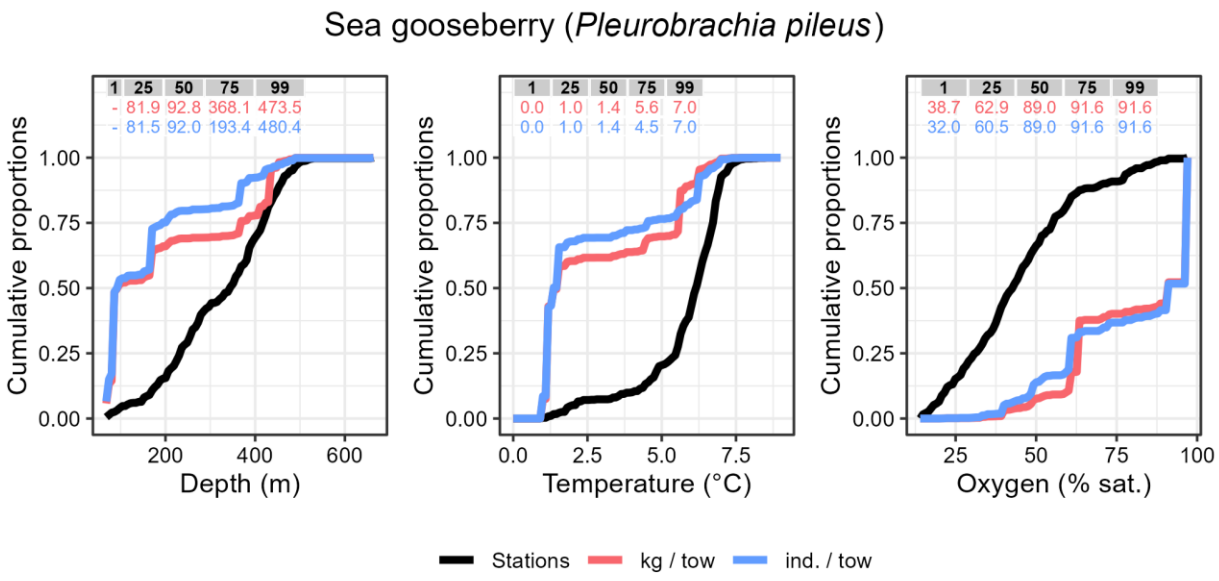


Figure 55c. Cumulative proportions of available values of depth, temperature and dissolved oxygen and standardized catches per tow for the sea gooseberry in the winter survey in 2022, 2023 and 2024.

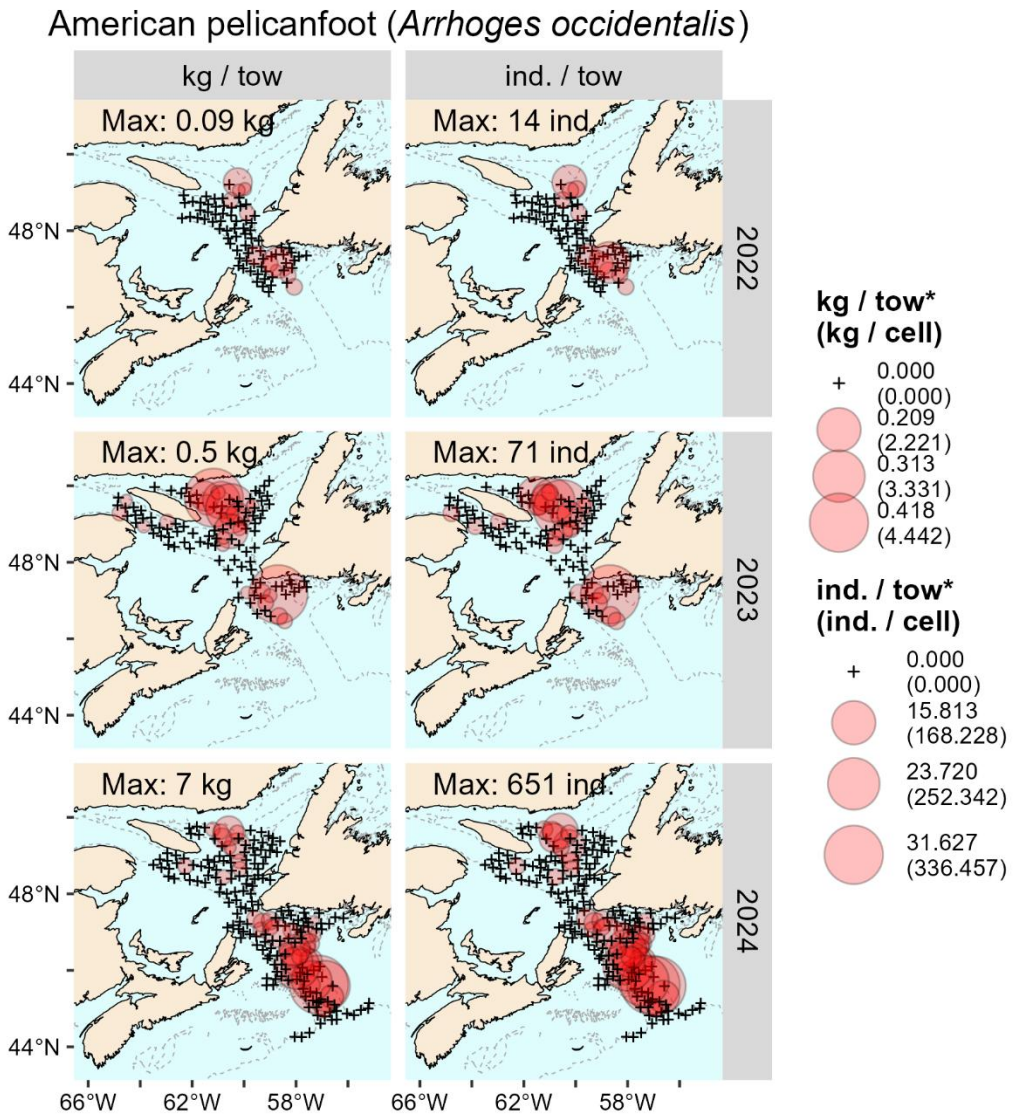


Figure 56a. Standardized catches by weight and/or number (colored bubbles) and cases of absence (black crosses) for the American pelicanfoot in the winter surveys of 2022, 2023, and 2024.

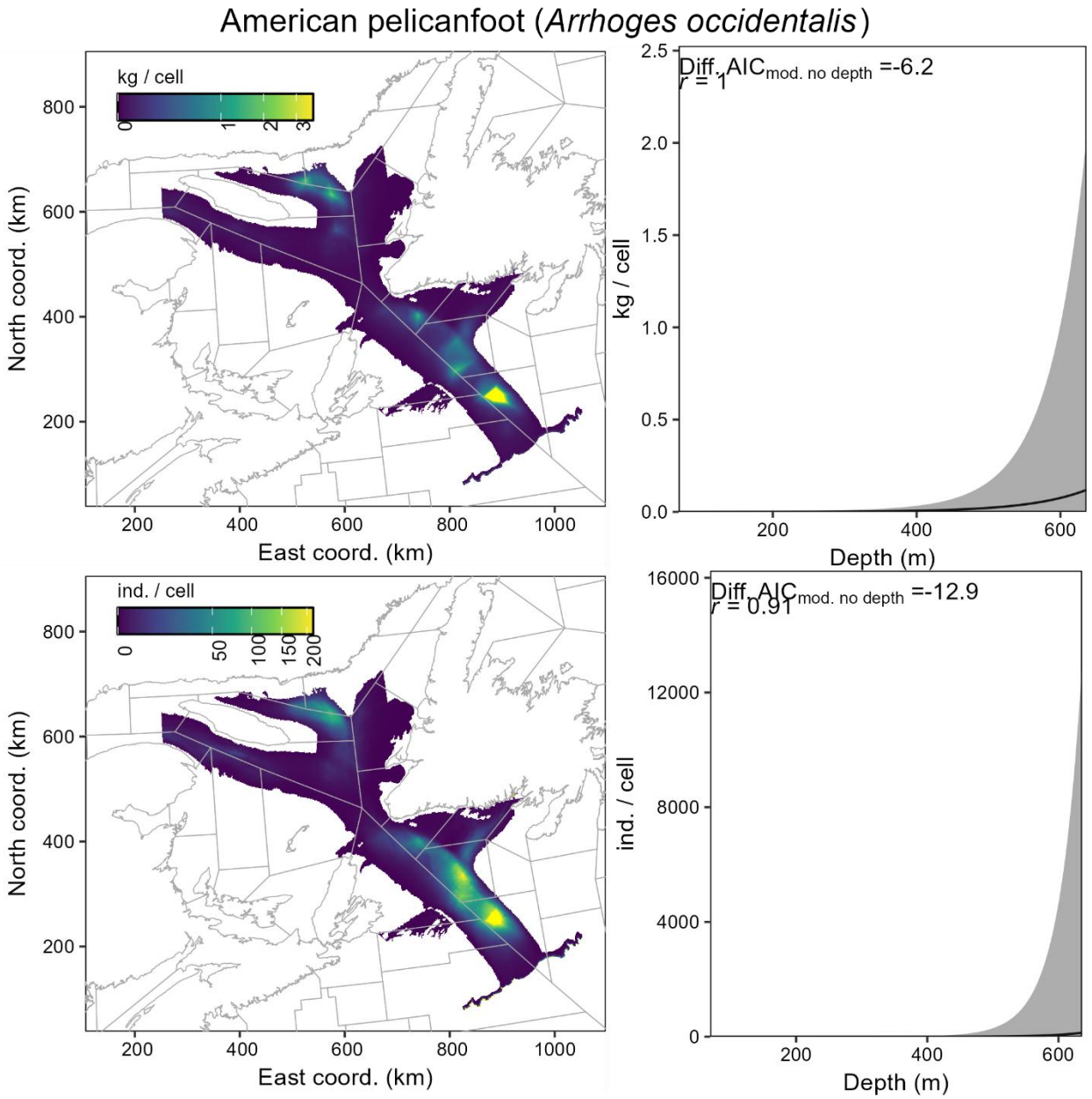


Figure 56b. Predicted weight (upper panels) and number (lower panels) values per 0.25 km^2 cell according to the selected spatial interpolation models for the American pelicanfoot in the 2022, 2023, and 2024 winter survey.

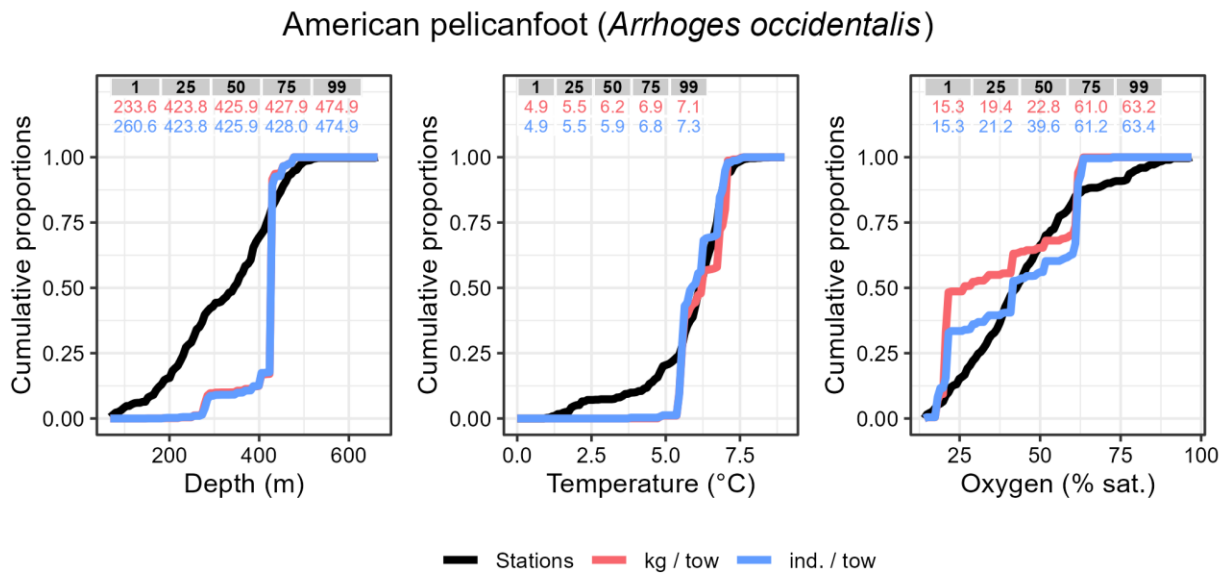


Figure 56c. Cumulative proportions of available values of depth, temperature and dissolved oxygen and standardized catches per tow for the American pelicanfoot in the winter survey in 2022, 2023 and 2024.

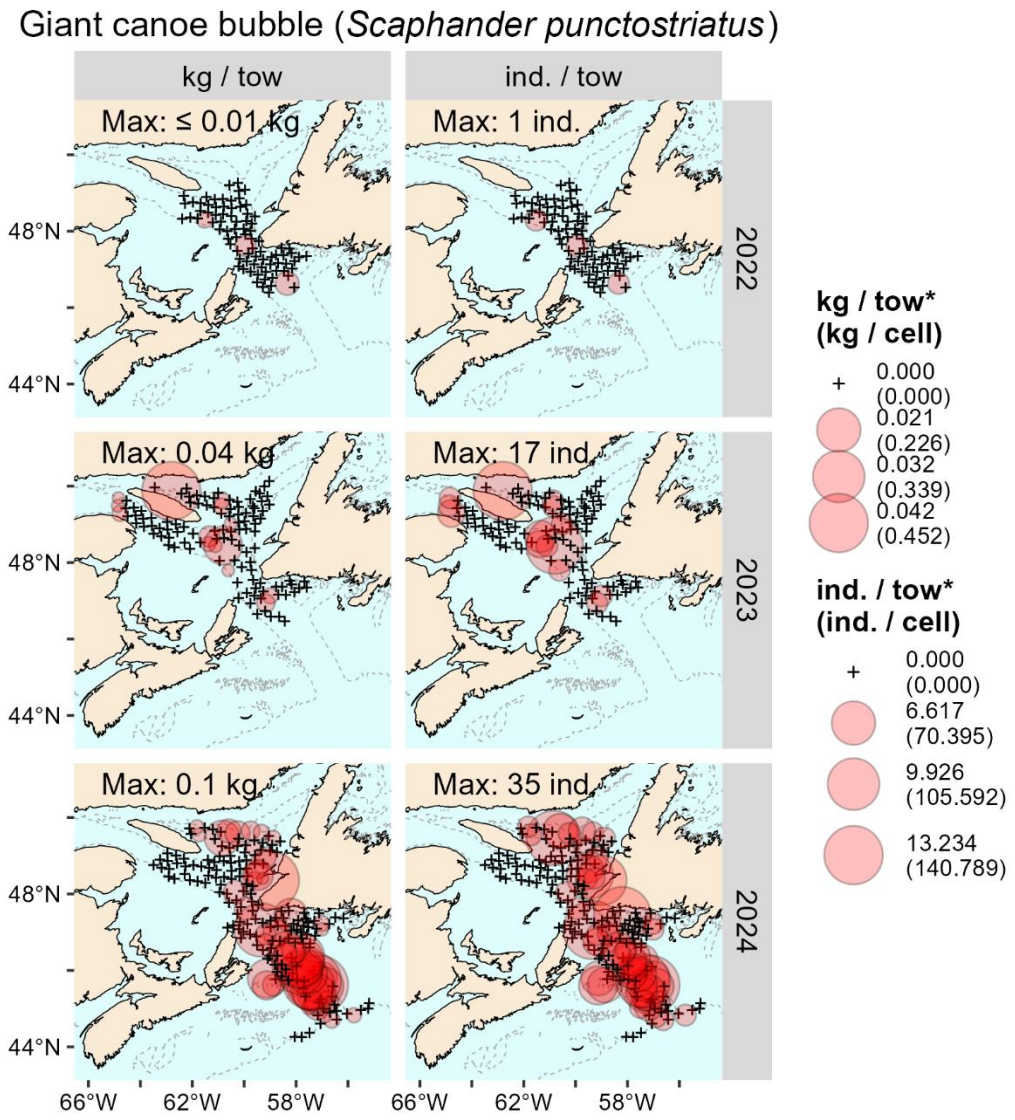


Figure 57a. Standardized catches by weight and/or number (colored bubbles) and cases of absence (black crosses) for the giant canoe bubble in the winter surveys of 2022, 2023, and 2024.

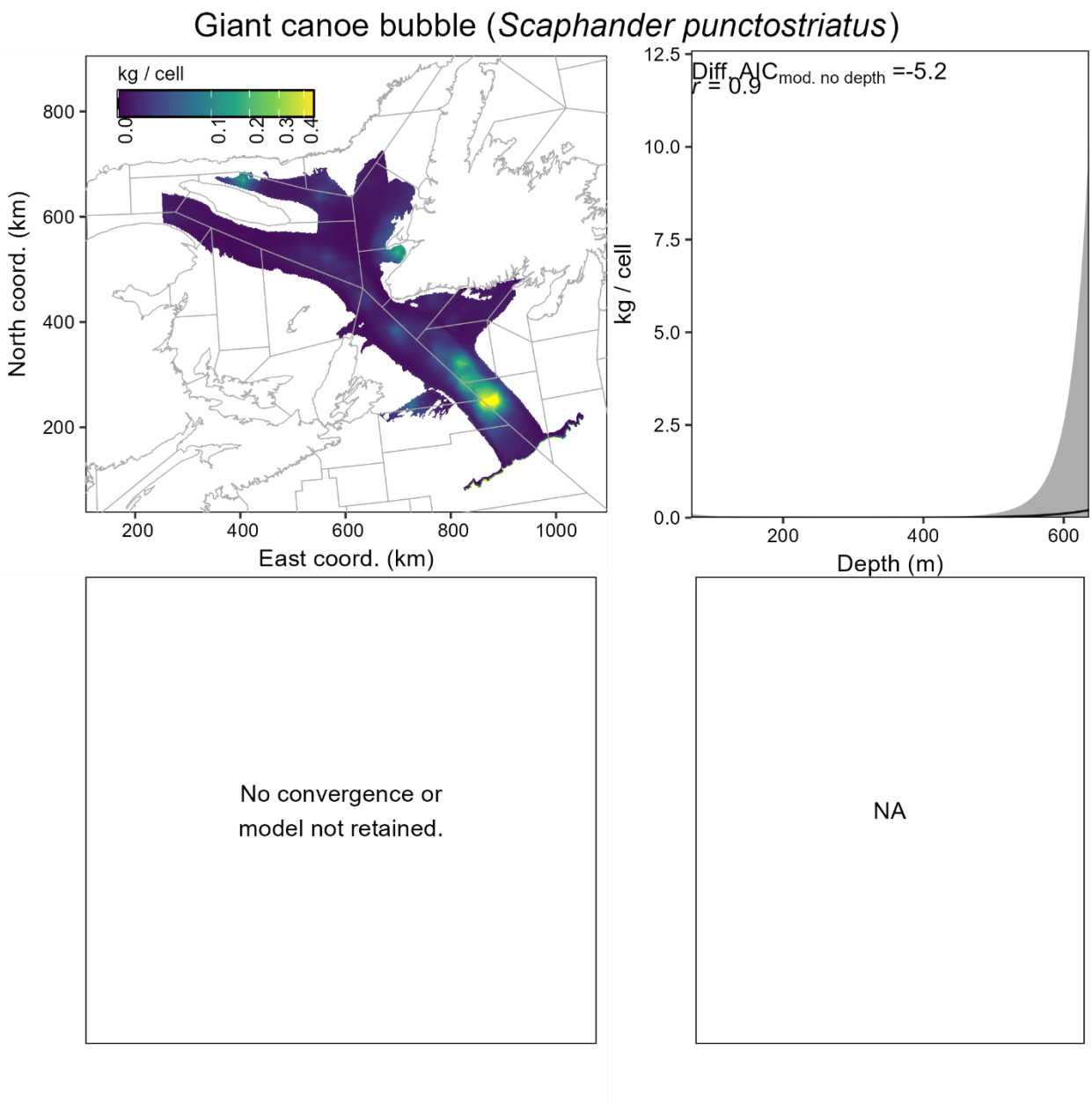


Figure 57b. Predicted weight (upper panels) and number (lower panels) values per 0.25 km^2 cell according to the selected spatial interpolation models for the giant canoe bubble in the 2022, 2023, and 2024 winter survey.

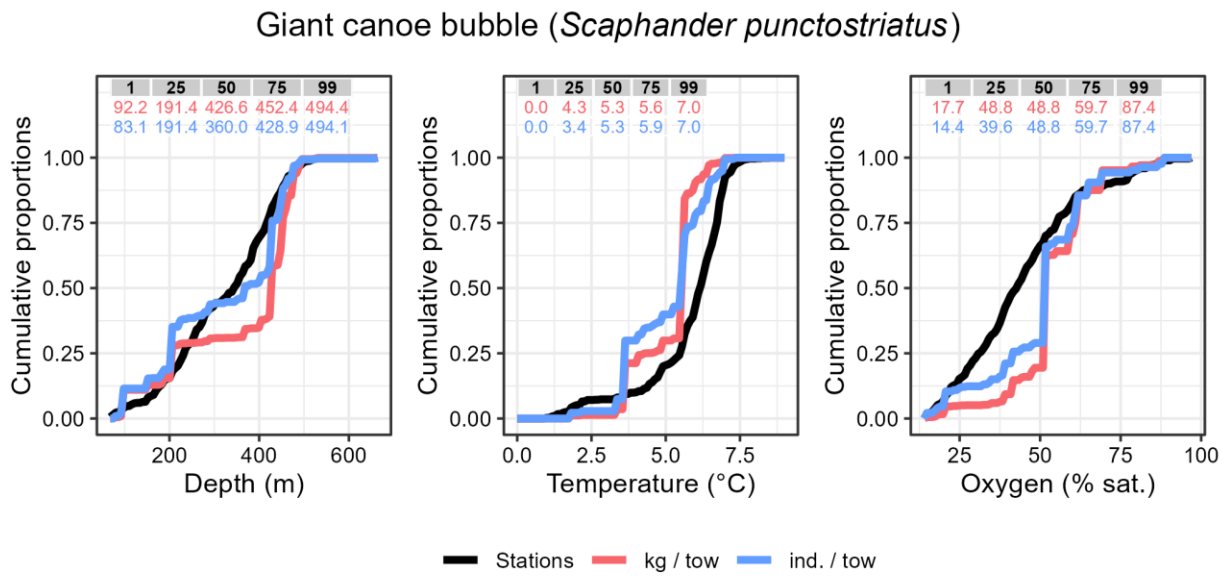


Figure 57c. Cumulative proportions of available values of depth, temperature and dissolved oxygen and standardized catches per tow for the giant canoe bubble in the winter survey in 2022, 2023 and 2024.

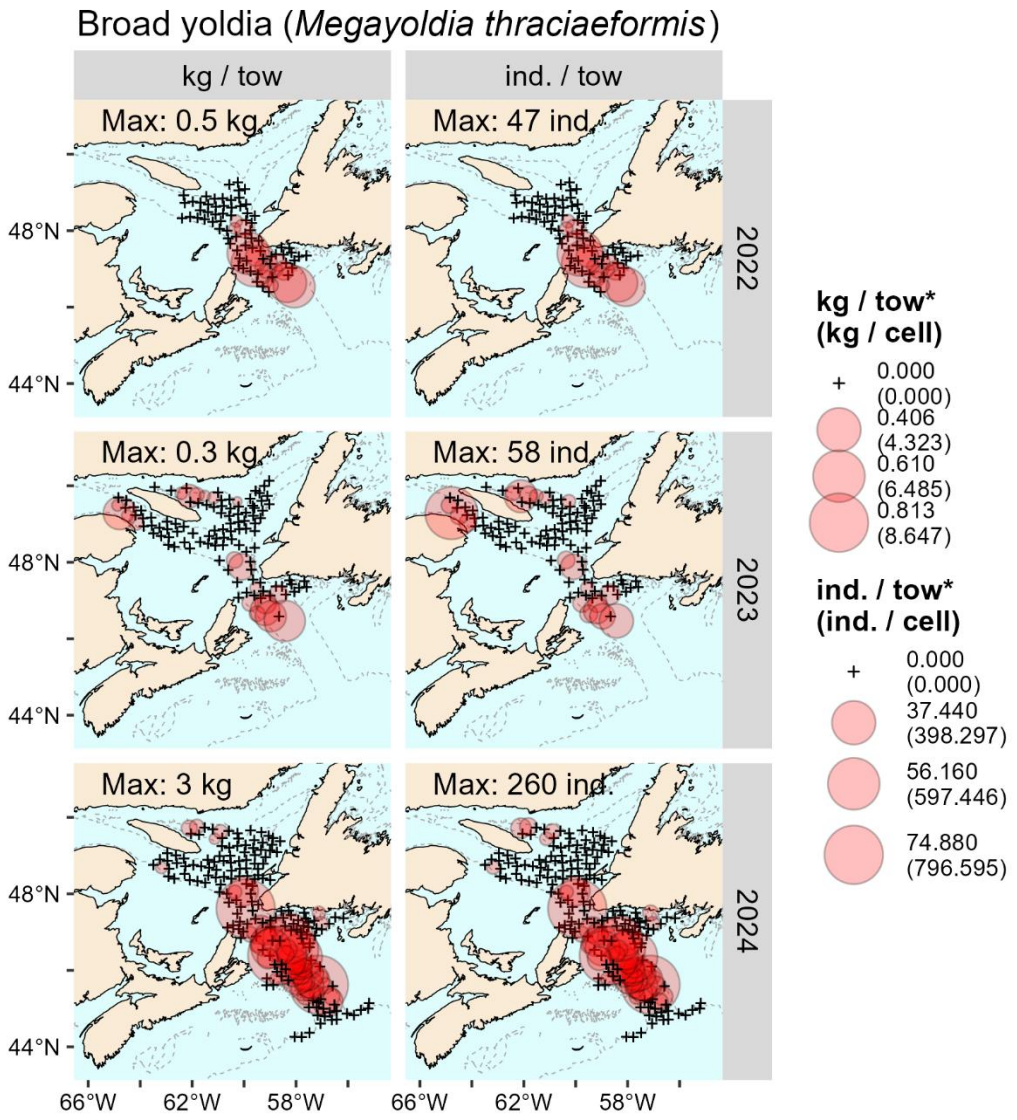


Figure 58a. Standardized catches by weight and/or number (colored bubbles) and cases of absence (black crosses) for the broad yoldia in the winter surveys of 2022, 2023, and 2024.

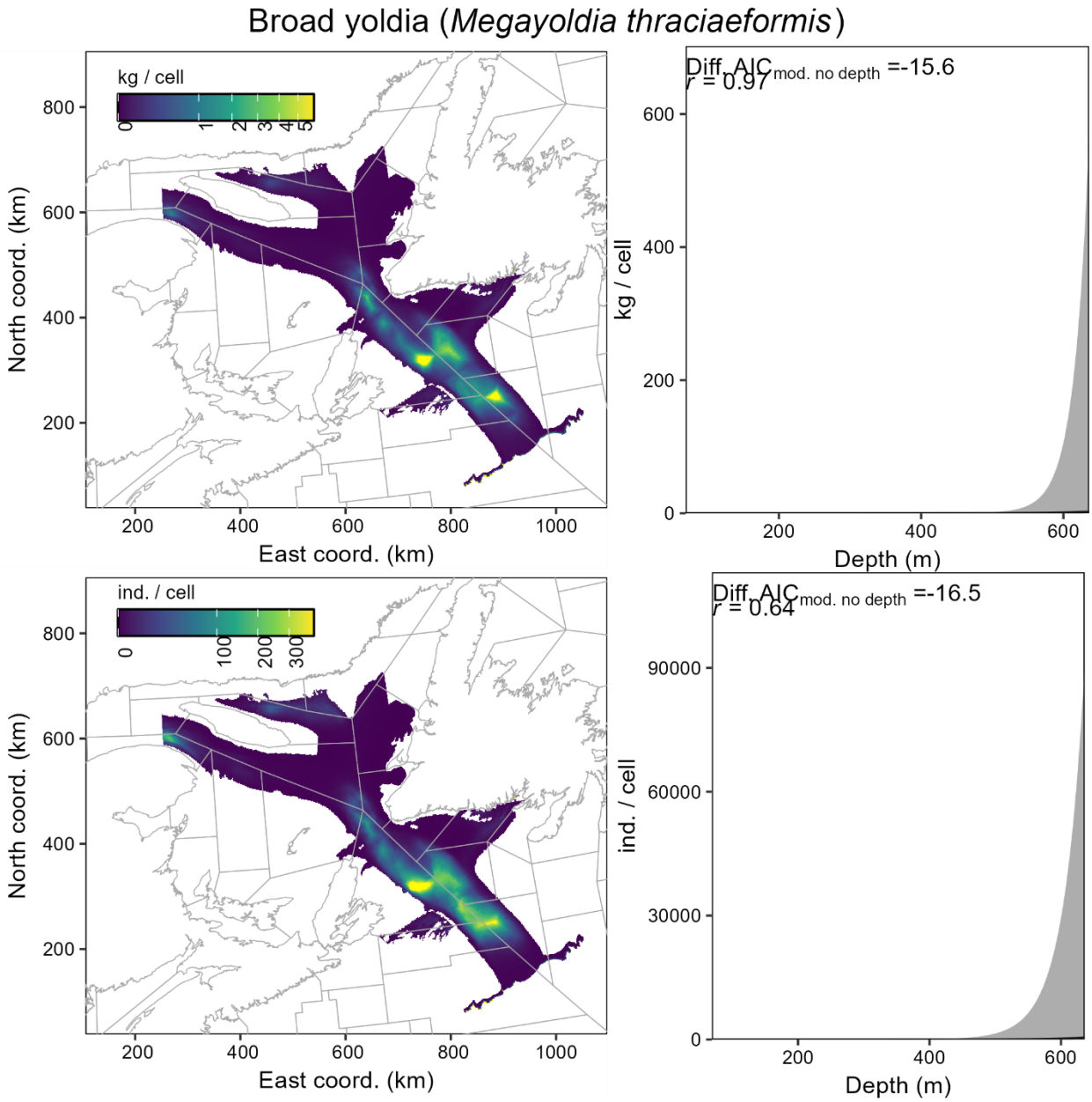


Figure 58b. Predicted weight (upper panels) and number (lower panels) values per 0.25 km^2 cell according to the selected spatial interpolation models for the broad yoldia in the 2022, 2023, and 2024 winter survey.

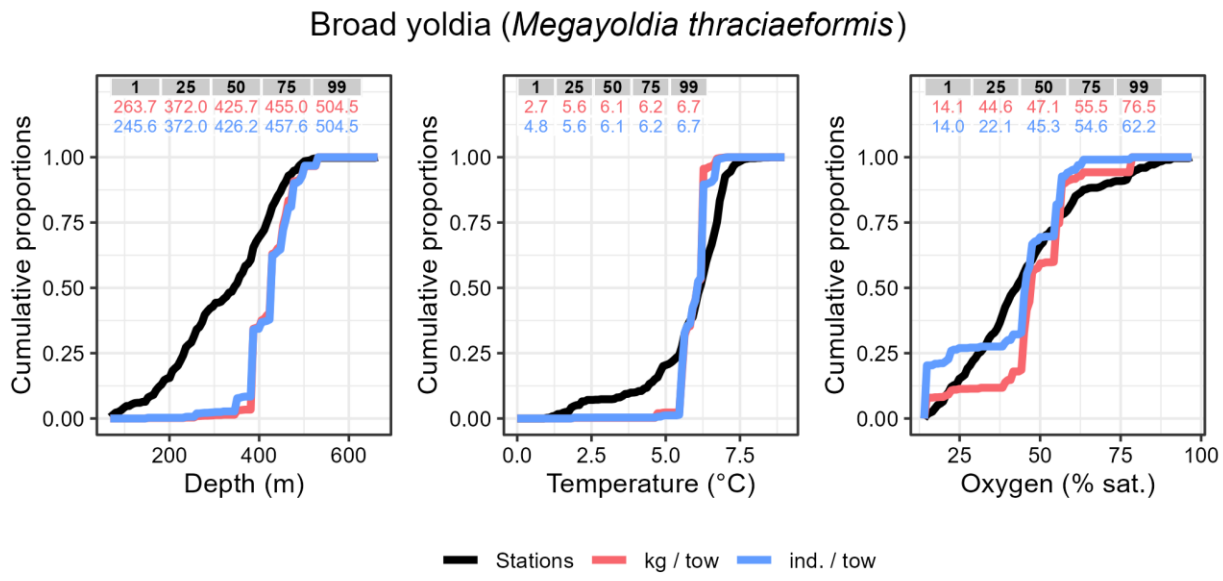


Figure 58c. Cumulative proportions of available values of depth, temperature and dissolved oxygen and standardized catches per tow for the broad yoldia in the winter survey in 2022, 2023 and 2024.

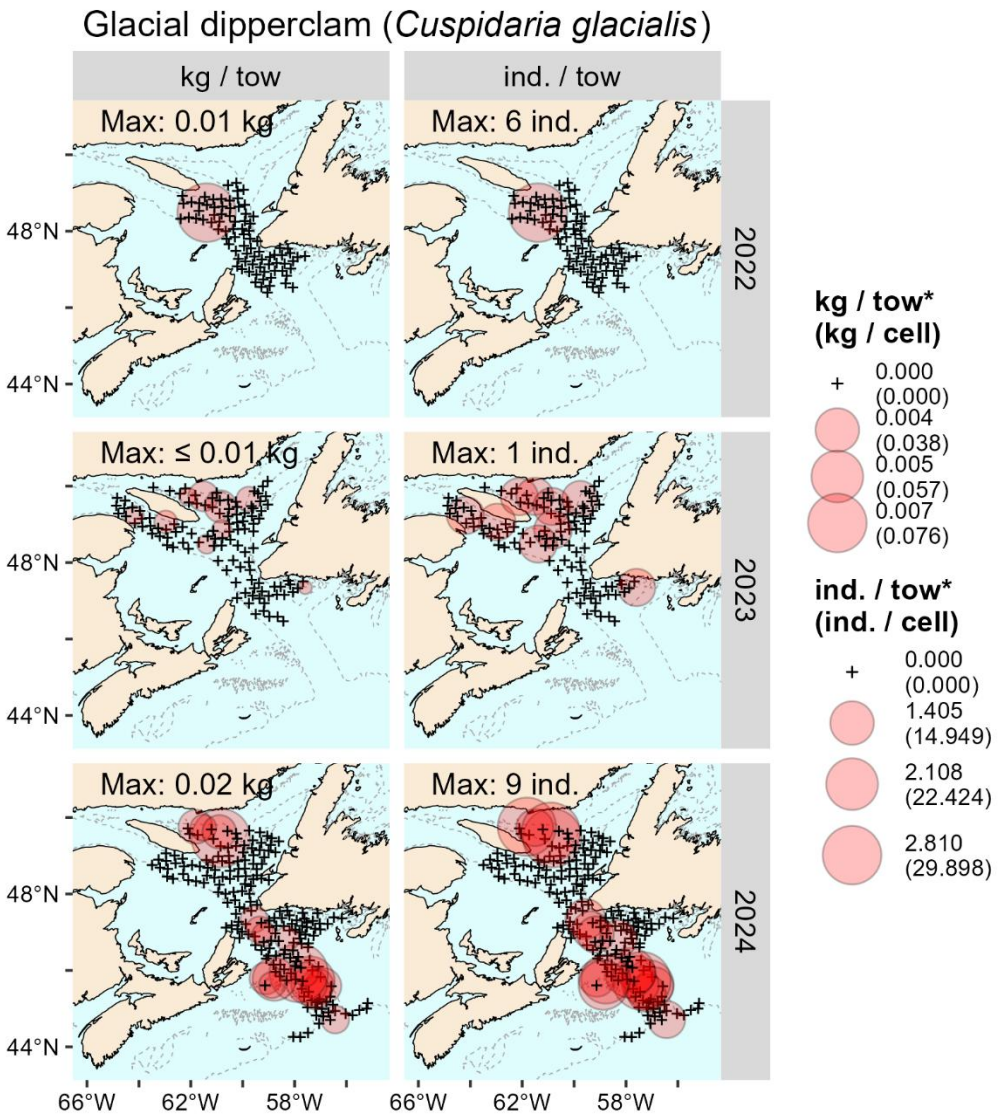


Figure 59a. Standardized catches by weight and/or number (colored bubbles) and cases of absence (black crosses) for the glacial dipperclam in the winter surveys of 2022, 2023, and 2024.

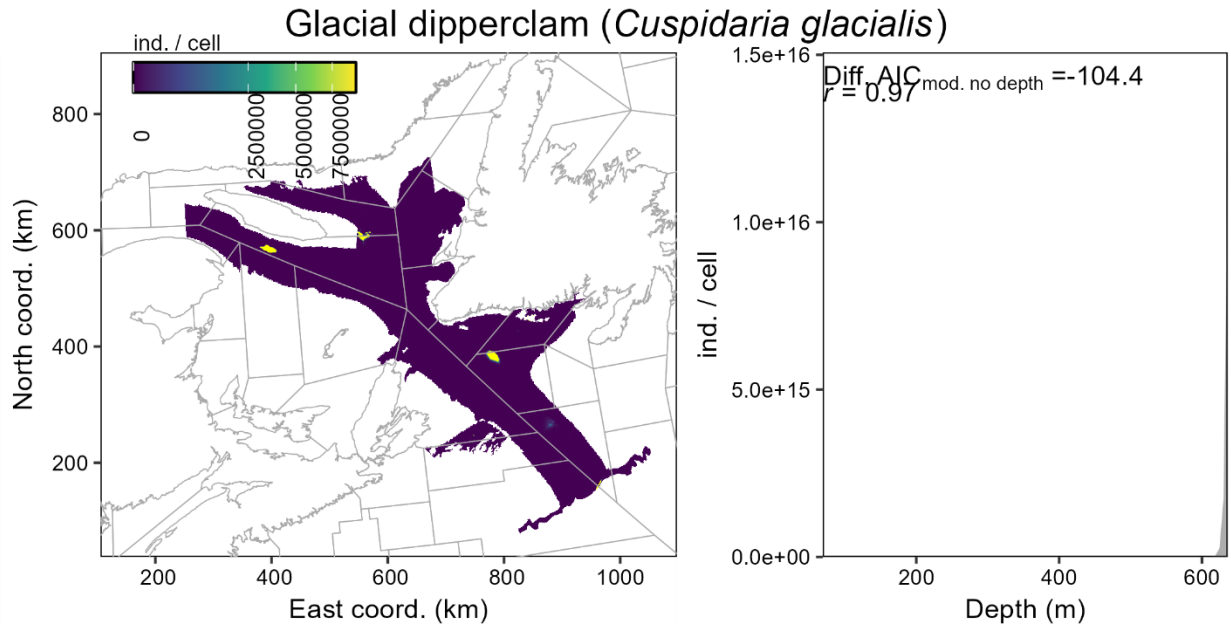


Figure 59b. Predicted number values per 0.25 km^2 cell according to the selected spatial interpolation model for the glacial dipperclam in the 2022, 2023, and 2024 winter survey.

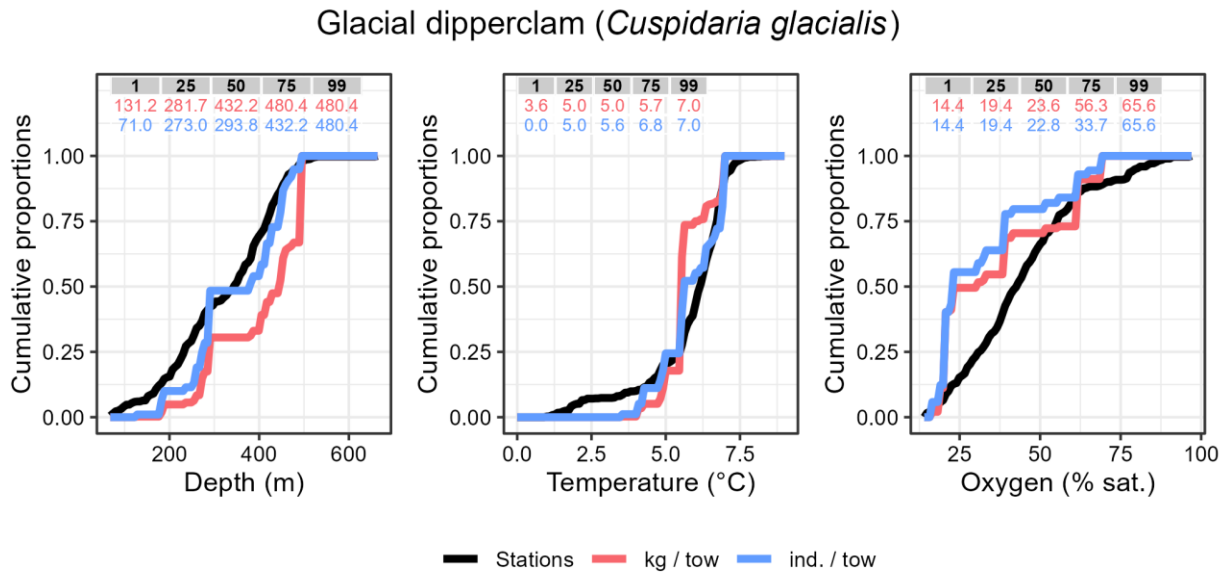


Figure 59c. Cumulative proportions of available values of depth, temperature and dissolved oxygen and standardized catches per tow for the glacial dipperclam in the winter survey in 2022, 2023 and 2024.

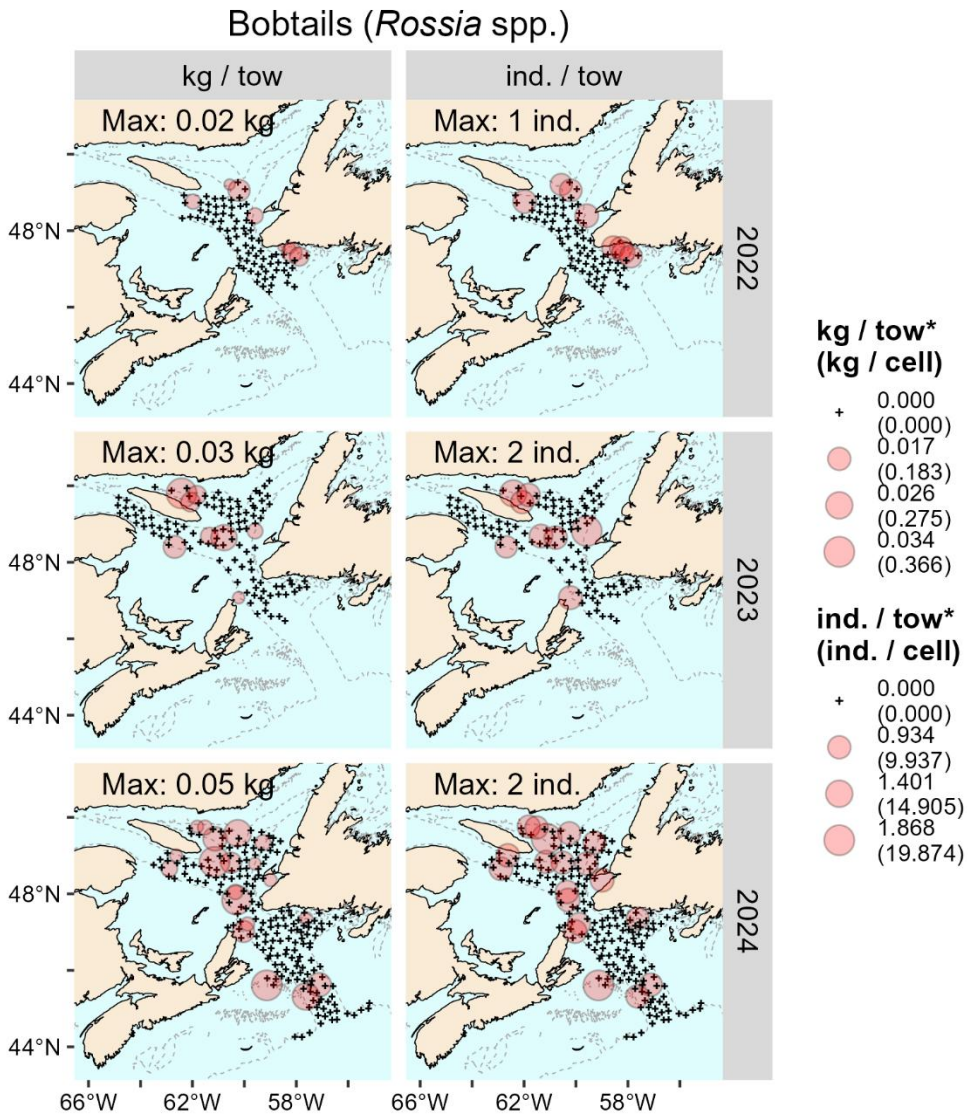


Figure 60a. Standardized catches by weight and/or number (colored bubbles) and cases of absence (black crosses) for bobtails of the genus *Rossia* in the winter surveys of 2022, 2023, and 2024.

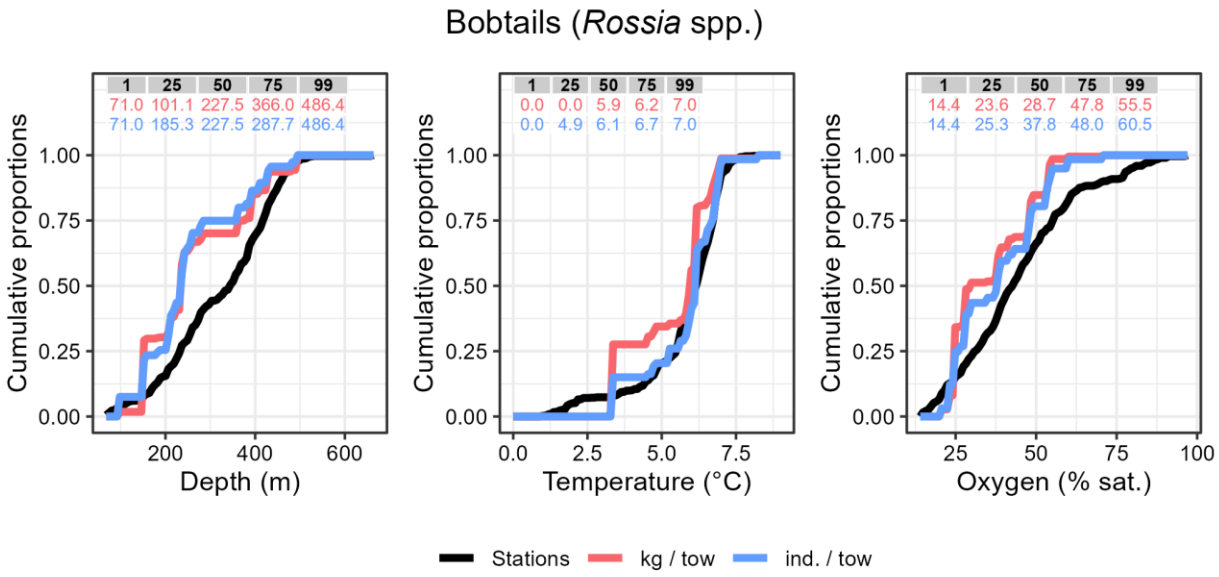


Figure 60b. Cumulative proportions of available values of depth, temperature and dissolved oxygen and standardized catches per tow for bobtails of the genus *Rossia* in the winter survey in 2022, 2023 and 2024.

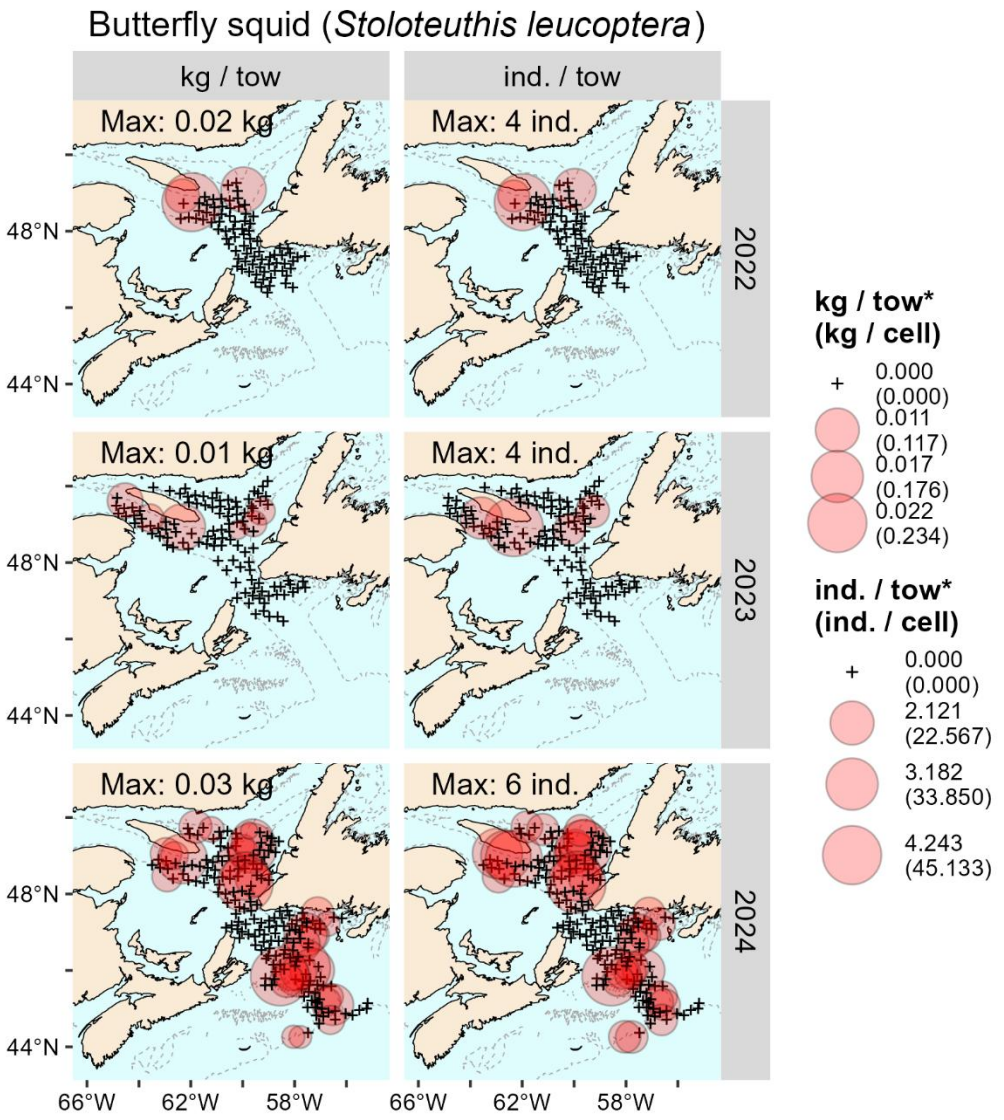


Figure 61a. Standardized catches by weight and/or number (colored bubbles) and cases of absence (black crosses) for the butterfly squid *Stoloteuthis leucoptera* in the winter survey in 2022, 2023 and 2024.

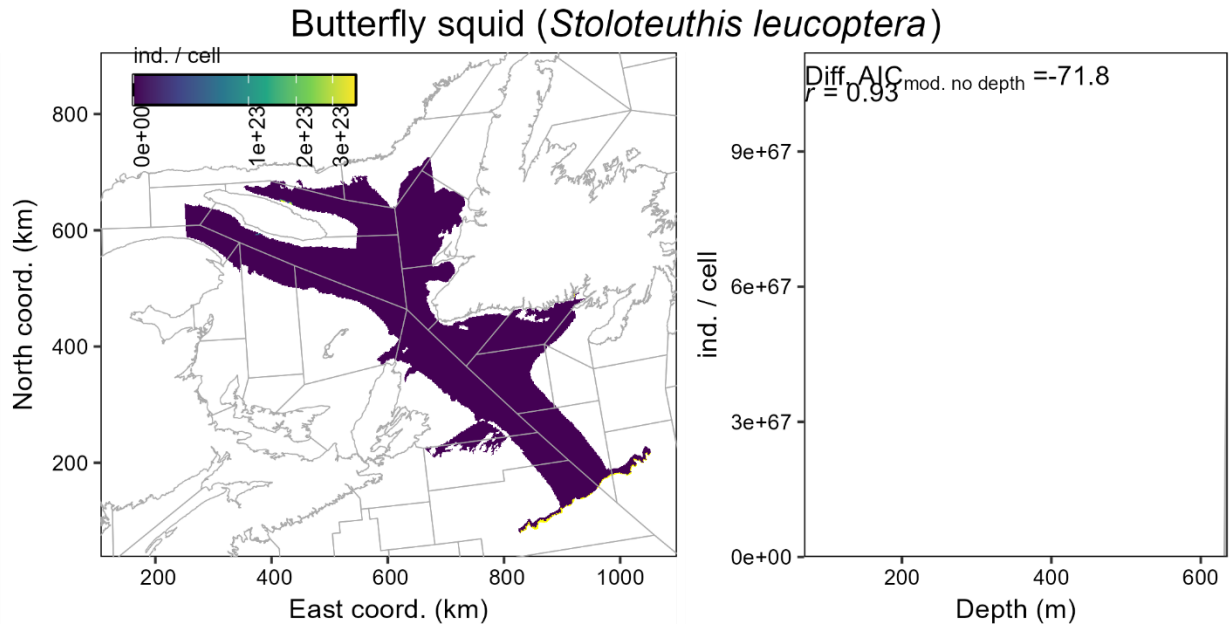


Figure 61b. Predicted number values per 0.25 km^2 cell according to the selected spatial interpolation model for the butterfly squid *Stoloteuthis leucoptera* in the 2022, 2023, and 2024 winter survey.

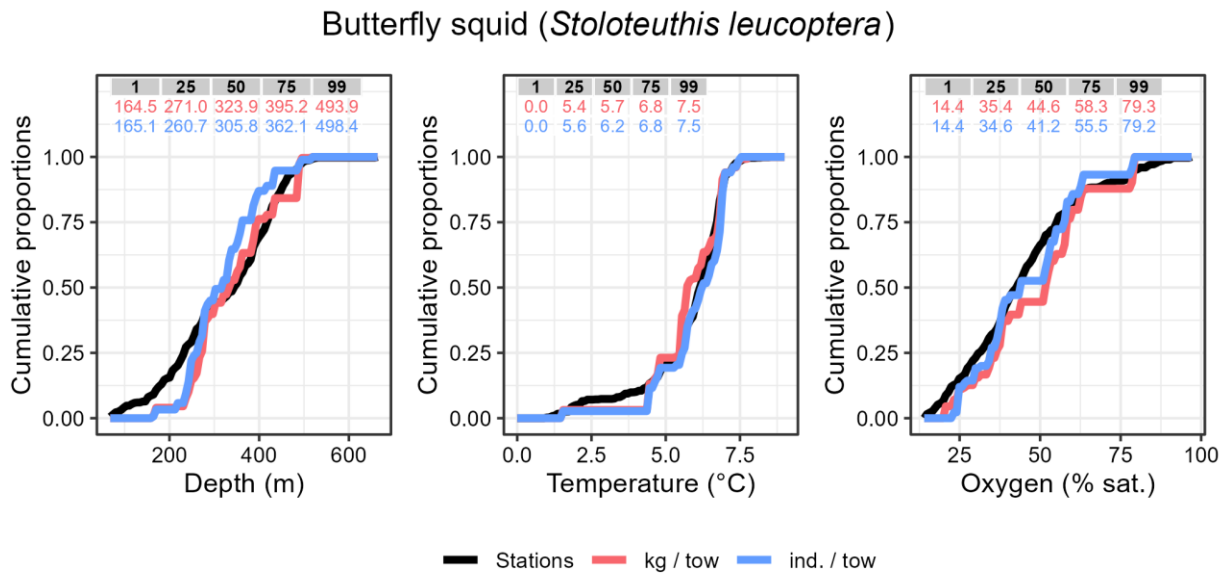


Figure 61c. Cumulative proportions of available values of depth, temperature and dissolved oxygen and standardized catches per tow for the butterfly squid *Stoloteuthis leucoptera* in the winter survey in 2022, 2023 and 2024.

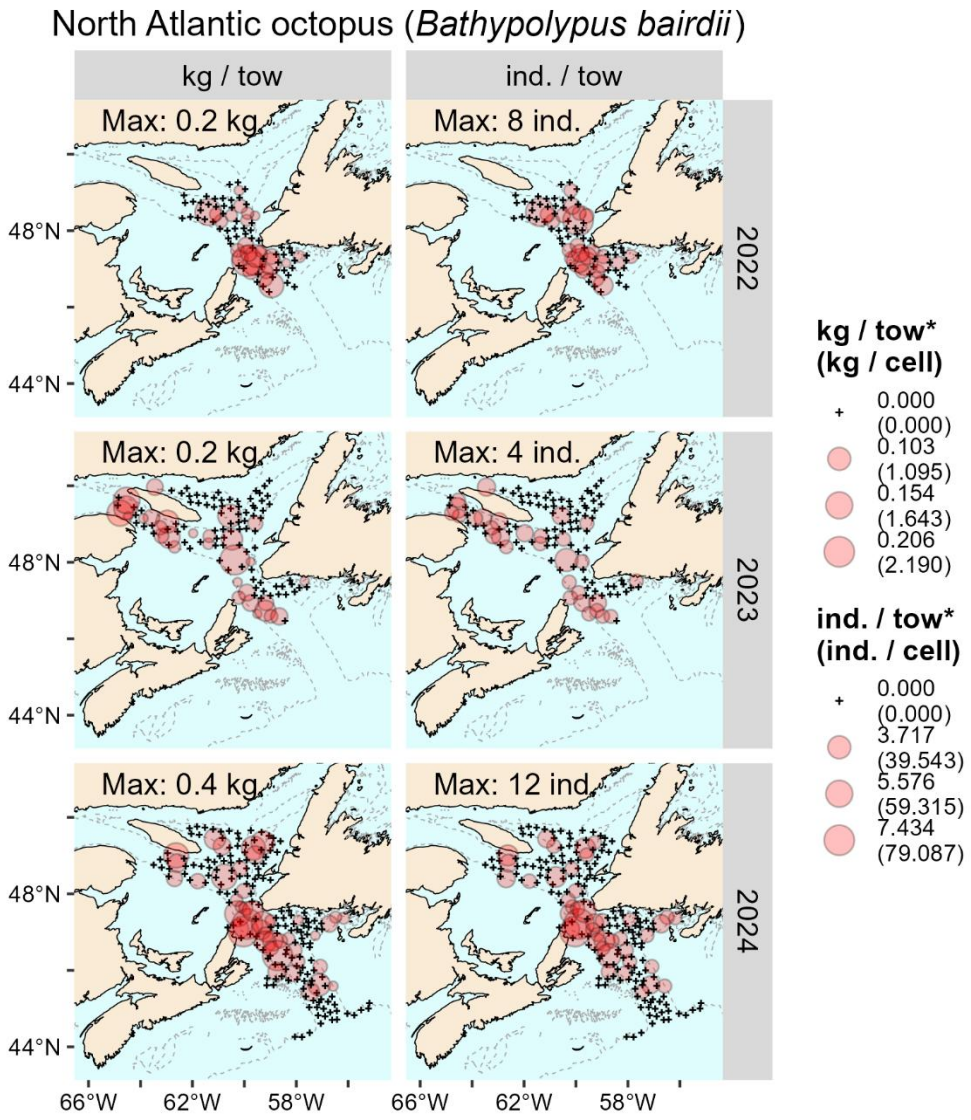


Figure 62a. Standardized catches by weight and/or number (colored bubbles) and cases of absence (black crosses) for the North Atlantic octopus in the winter survey in 2022, 2023 and 2024.

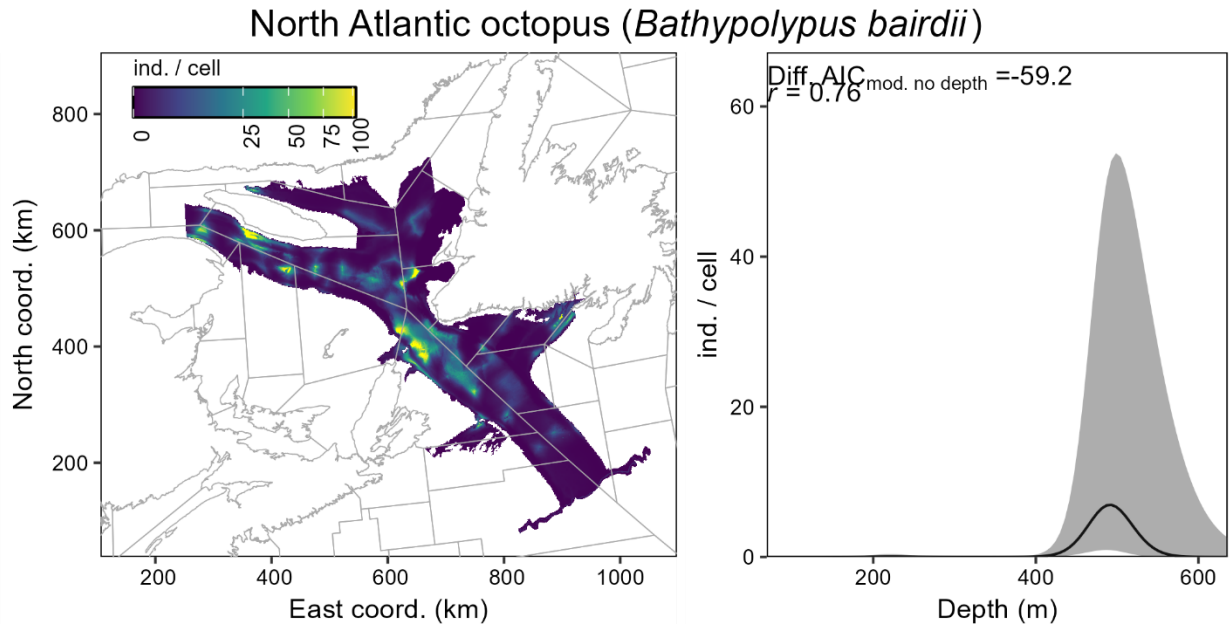


Figure 62b. Predicted weight (upper panels) and number (lower panels) values per 0.25 km^2 cell according to the selected spatial interpolation models for the North Atlantic octopus in the 2022, 2023, and 2024 winter survey.

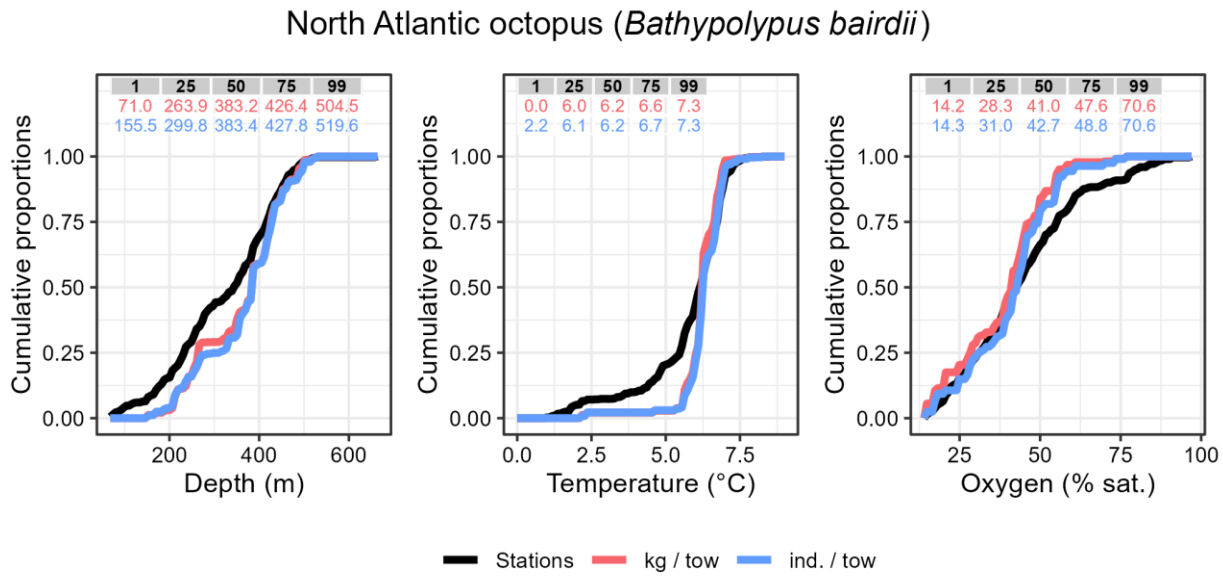


Figure 62c. Cumulative proportions of available values of depth, temperature and dissolved oxygen and standardized catches per tow for the North Atlantic octopus in the winter survey in 2022, 2023 and 2024.

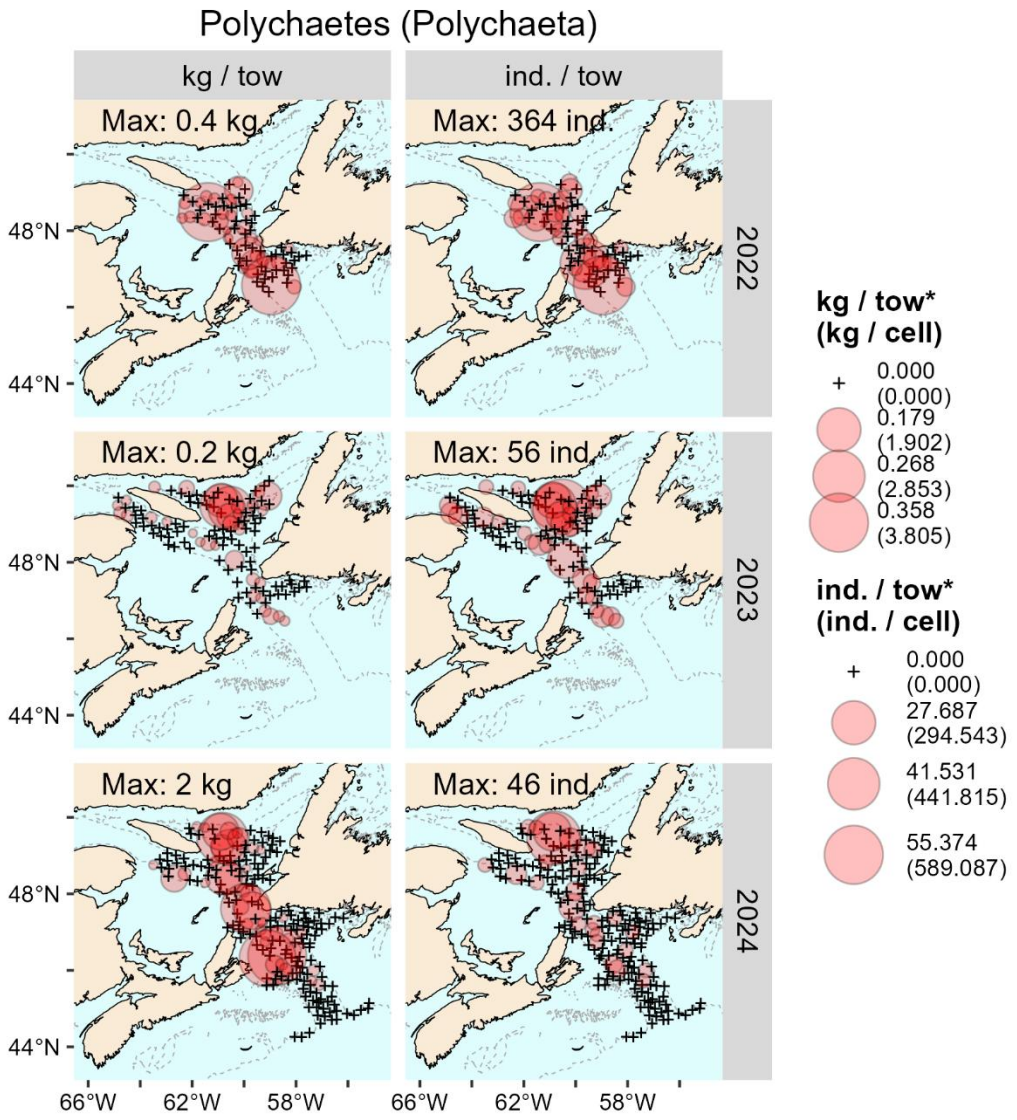


Figure 63a. Standardized catches by weight and/or number (colored bubbles) and cases of absence (black crosses) for specimens whose identification could not be more precise than the class Polychaeta in the winter survey in 2022, 2023 and 2024.

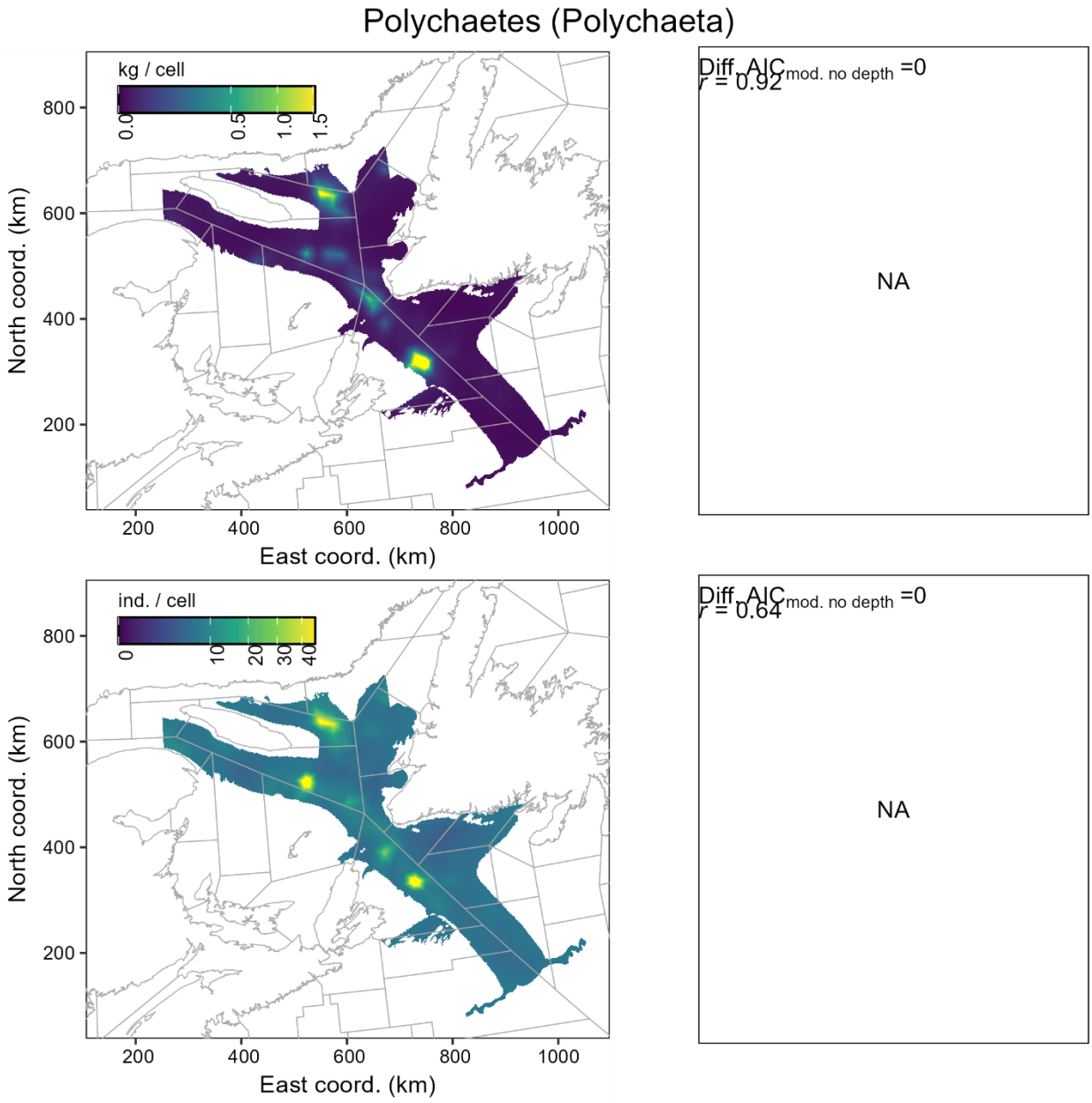


Figure 63b. Predicted weight (upper panels) and number (lower panels) values per 0.25 km^2 cell according to the selected spatial interpolation models for specimens whose identification could not be more precise than the class Polychaeta in the 2022, 2023, and 2024 winter survey.

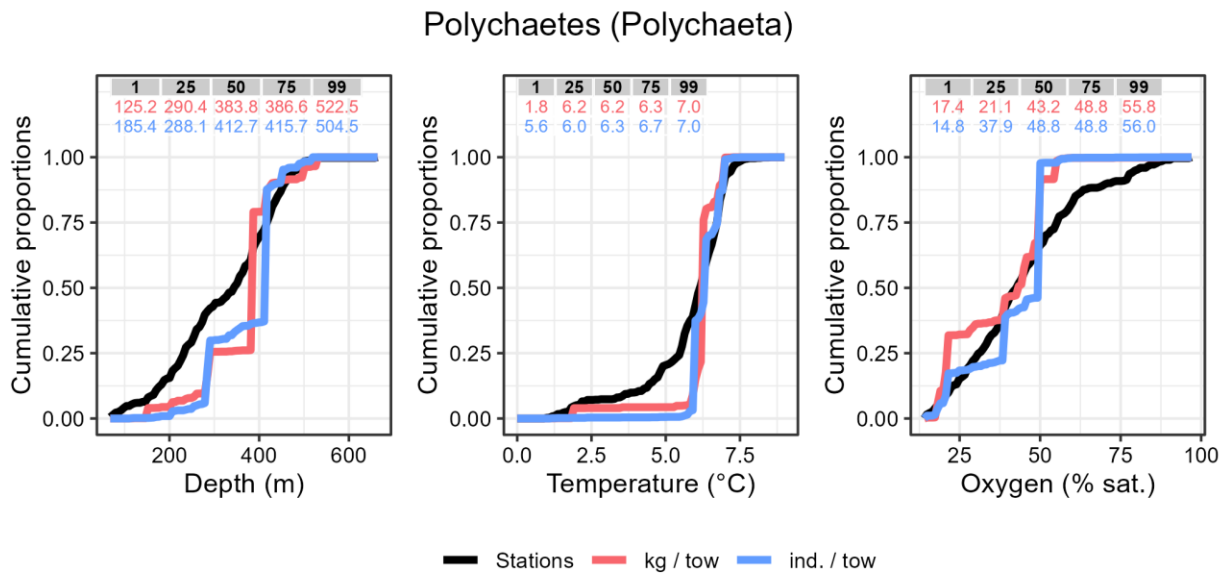


Figure 63c. Cumulative proportions of available values of depth, temperature and dissolved oxygen and standardized catches per tow for specimens whose identification could not be more precise than the class Polychaeta in the winter survey in 2022, 2023 and 2024.

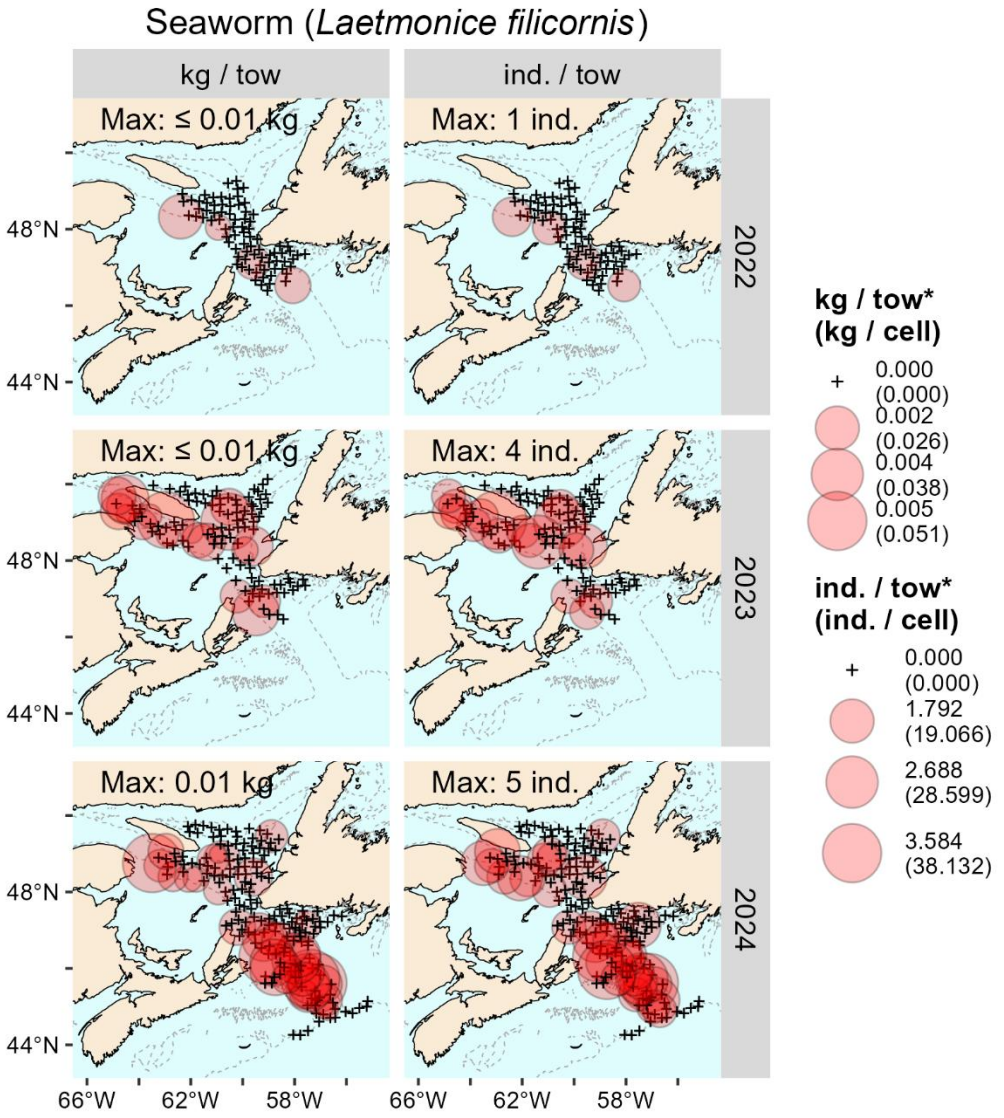


Figure 64a. Standardized catches by weight and/or number (colored bubbles) and cases of absence (black crosses) for the seaworm *Laetmonice filicornis* in the winter survey in 2022, 2023 and 2024.

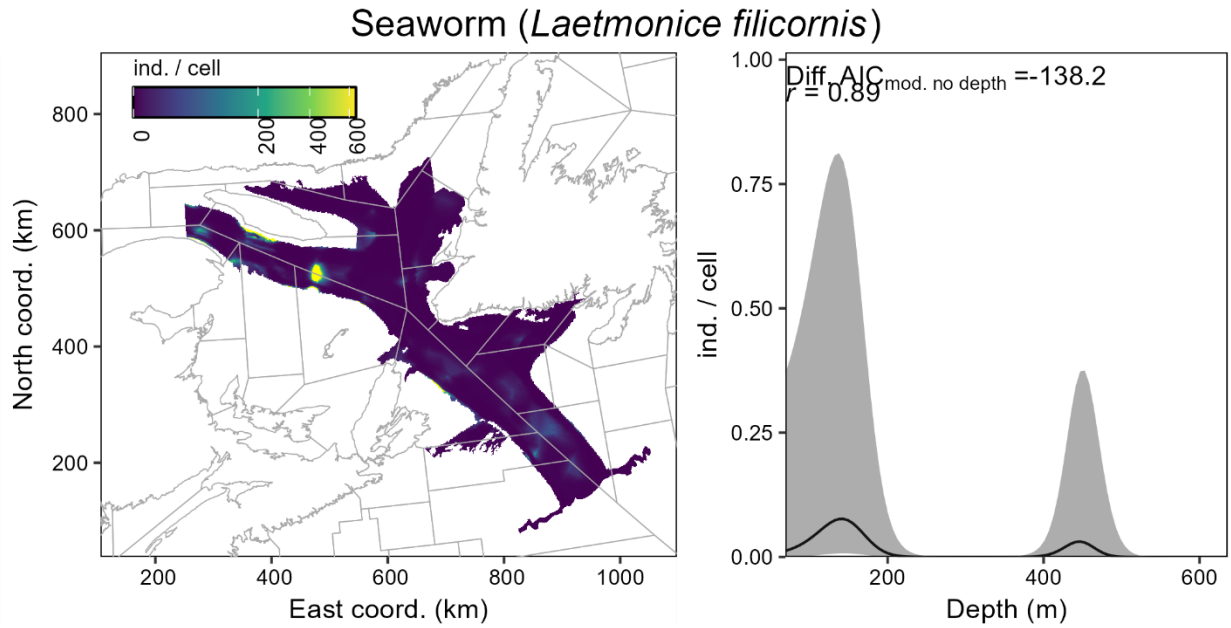


Figure 64b. Predicted number values per 0.25 km^2 cell according to the selected spatial interpolation model for the seaworm *Laetmonice filicornis* in the 2022, 2023, and 2024 winter survey.

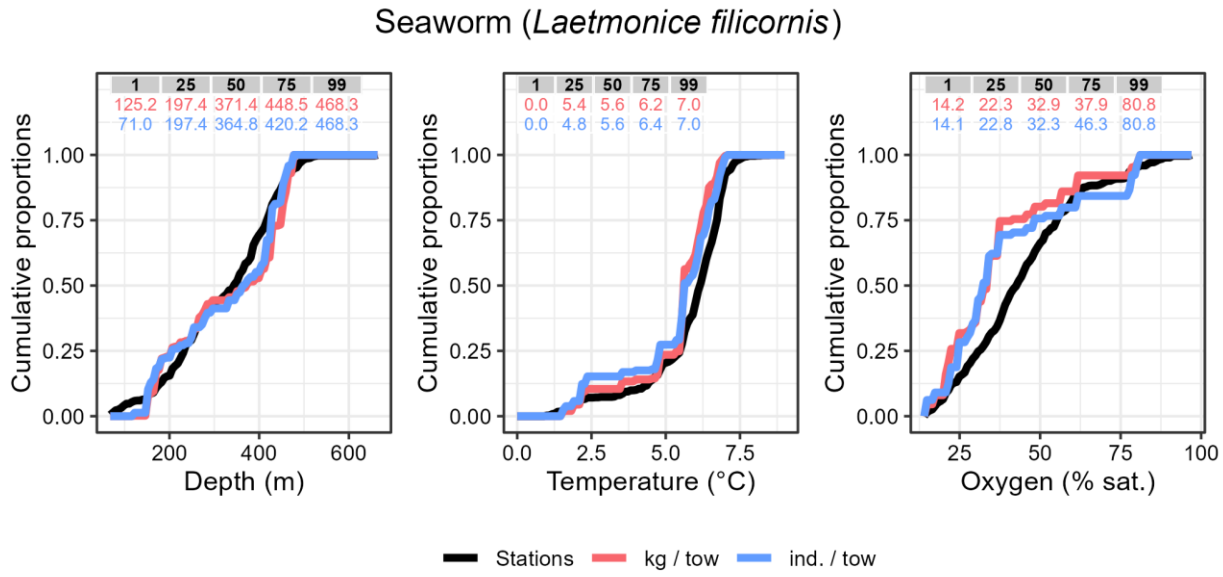


Figure 64c. Cumulative proportions of available values of depth, temperature and dissolved oxygen and standardized catches per tow for the seaworm *Laetmonice filicornis* in the winter survey in 2022, 2023 and 2024.

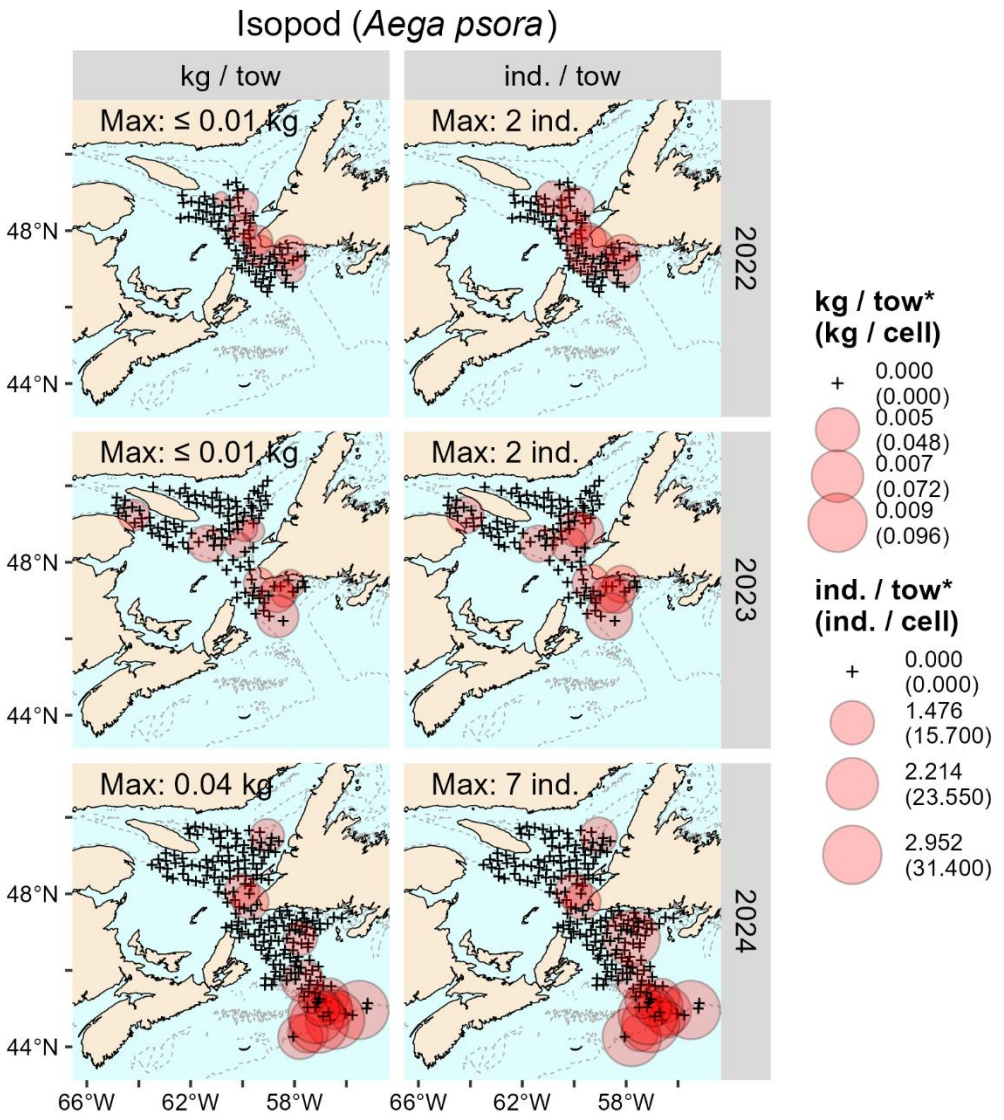


Figure 65a. Standardized catches by weight and/or number (colored bubbles) and cases of absence (black crosses) for the isopod *Aega psora* in the winter survey in 2022, 2023 and 2024.

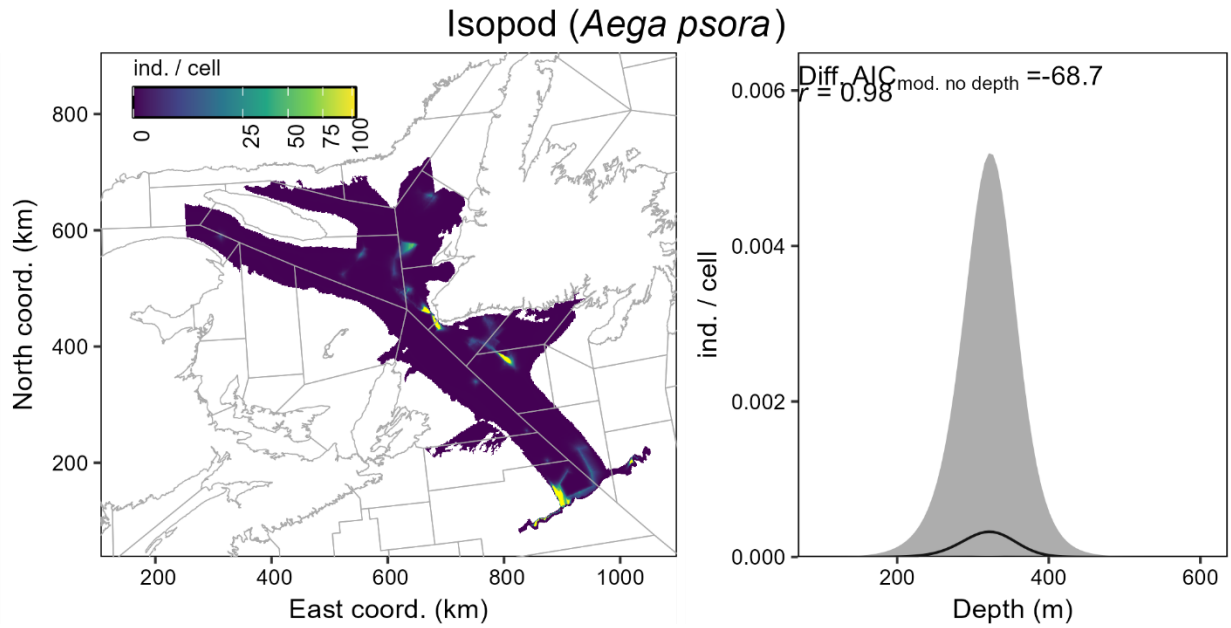


Figure 65b. Predicted number values per 0.25 km^2 cell according to the selected spatial interpolation model for the isopod *Aega psora* in the 2022, 2023, and 2024 winter survey.

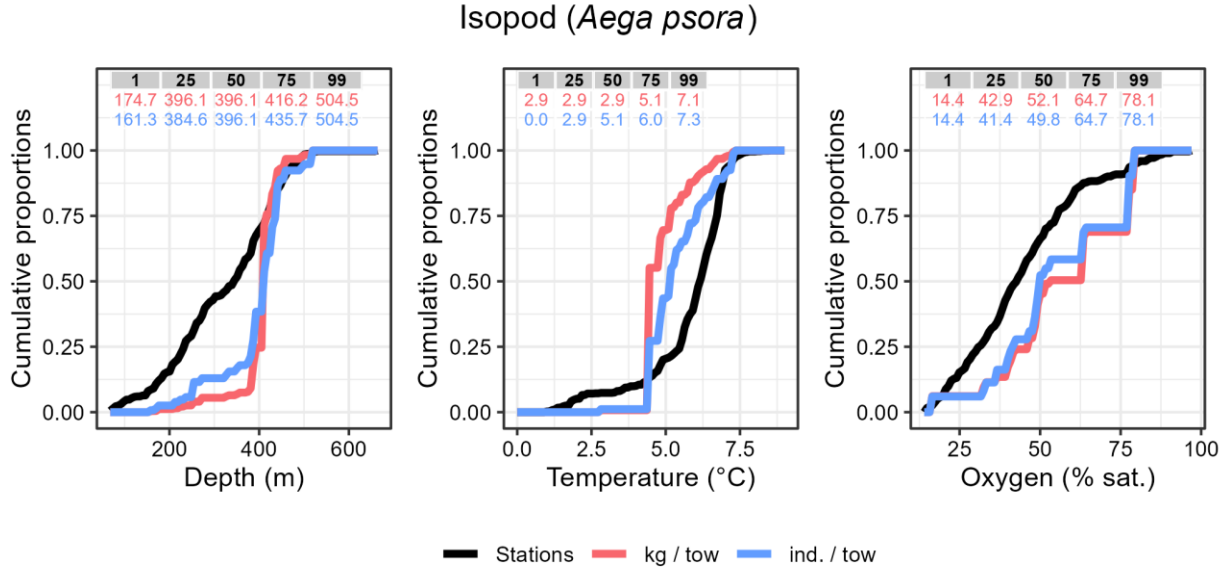


Figure 65c. Cumulative proportions of available values of depth, temperature and dissolved oxygen and standardized catches per tow for the isopod *Aega psora* in the winter survey in 2022, 2023 and 2024.

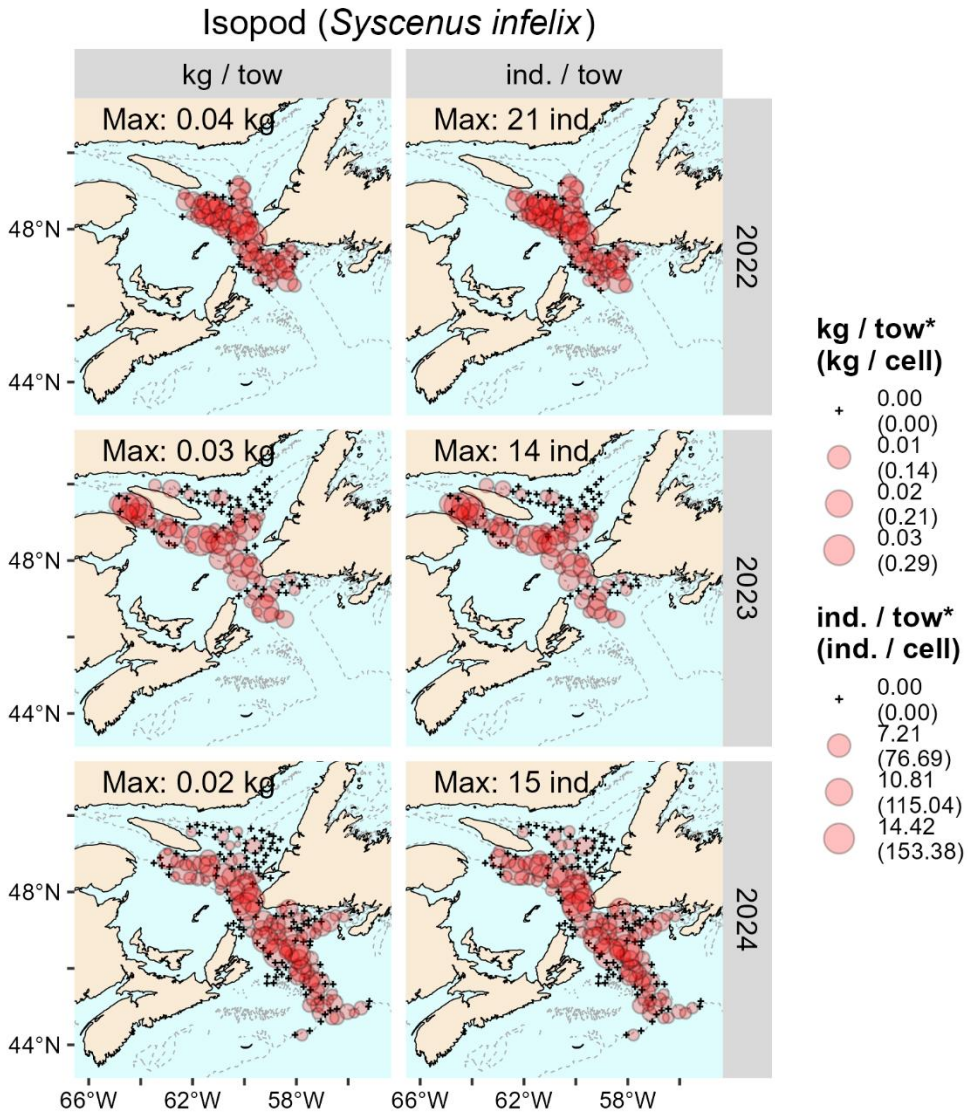


Figure 66a. Standardized catches by weight and/or number (colored bubbles) and cases of absence (black crosses) for the isopod *Syscenus infelix* in the winter survey in 2022, 2023 and 2024.

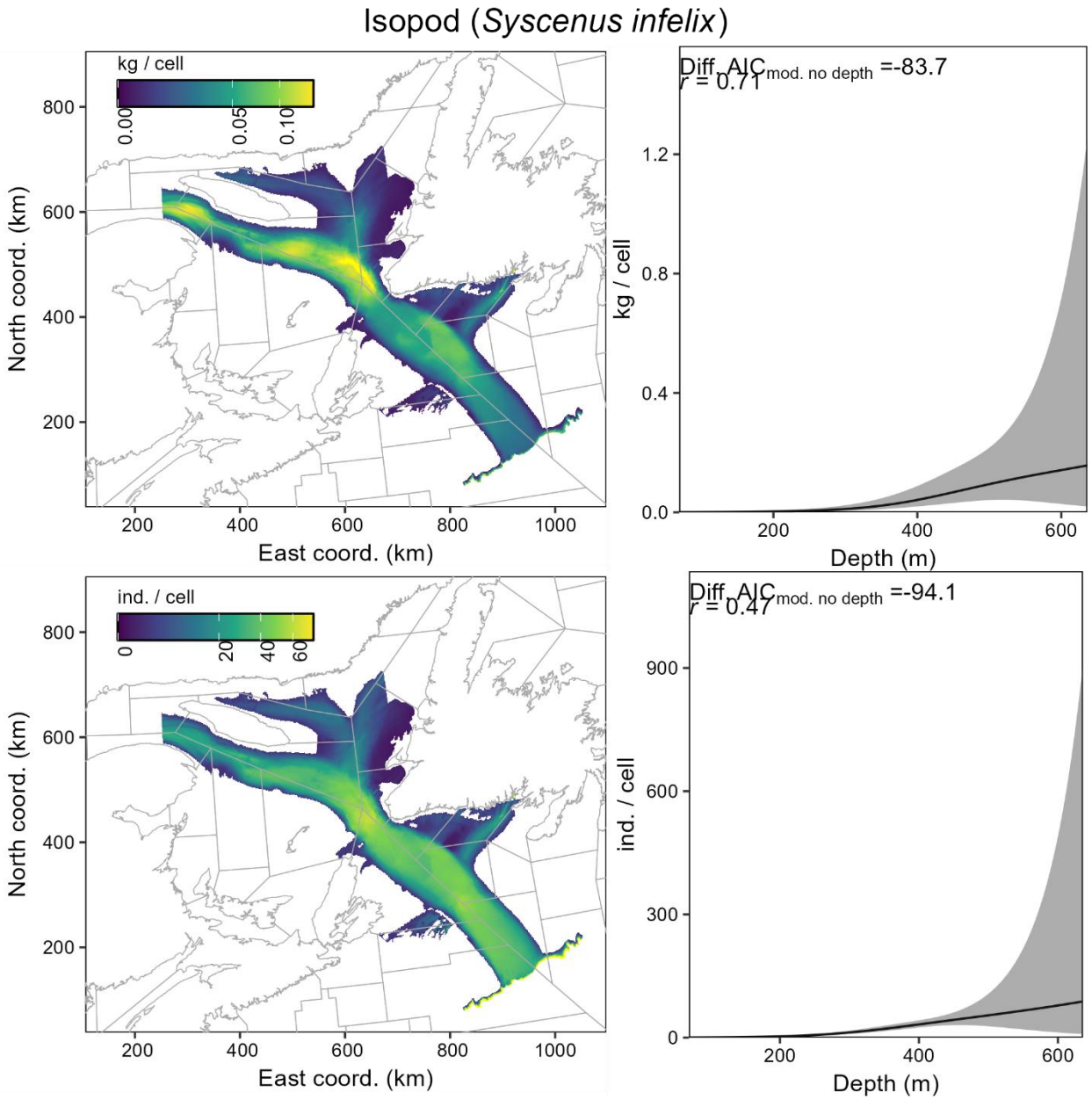


Figure 66b. Predicted weight (upper panels) and number (lower panels) values per 0.25 km^2 cell according to the selected spatial interpolation models for the isopod *Syscenus infelix* in the 2022, 2023, and 2024 winter survey.

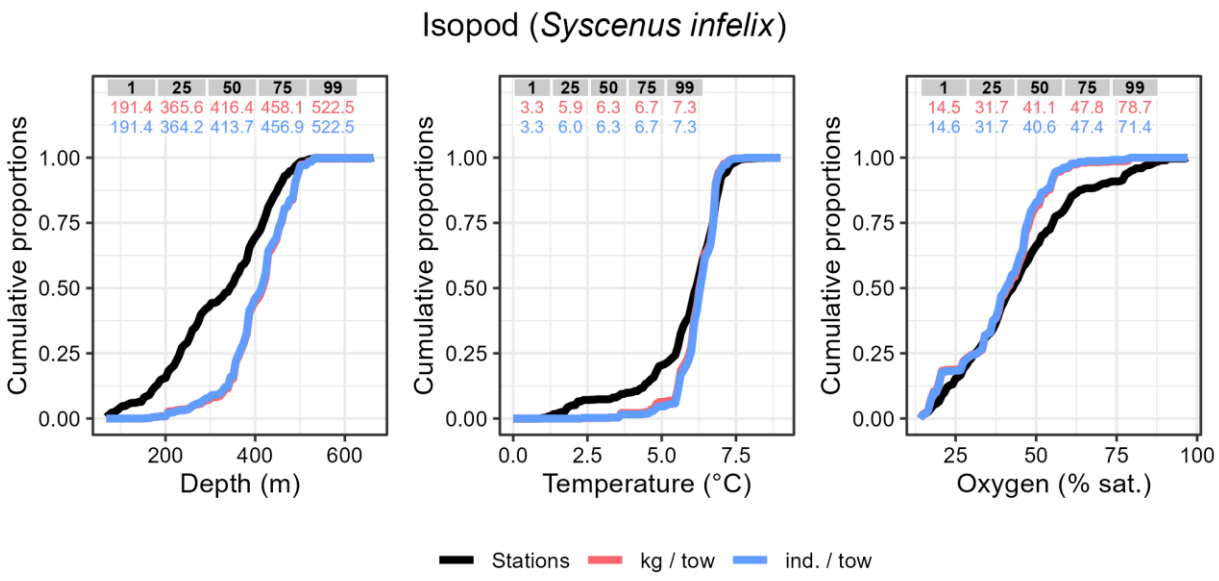


Figure 66c. Cumulative proportions of available values of depth, temperature and dissolved oxygen and standardized catches per tow for the isopod *Syscenus infelix* in the winter survey in 2022, 2023 and 2024.

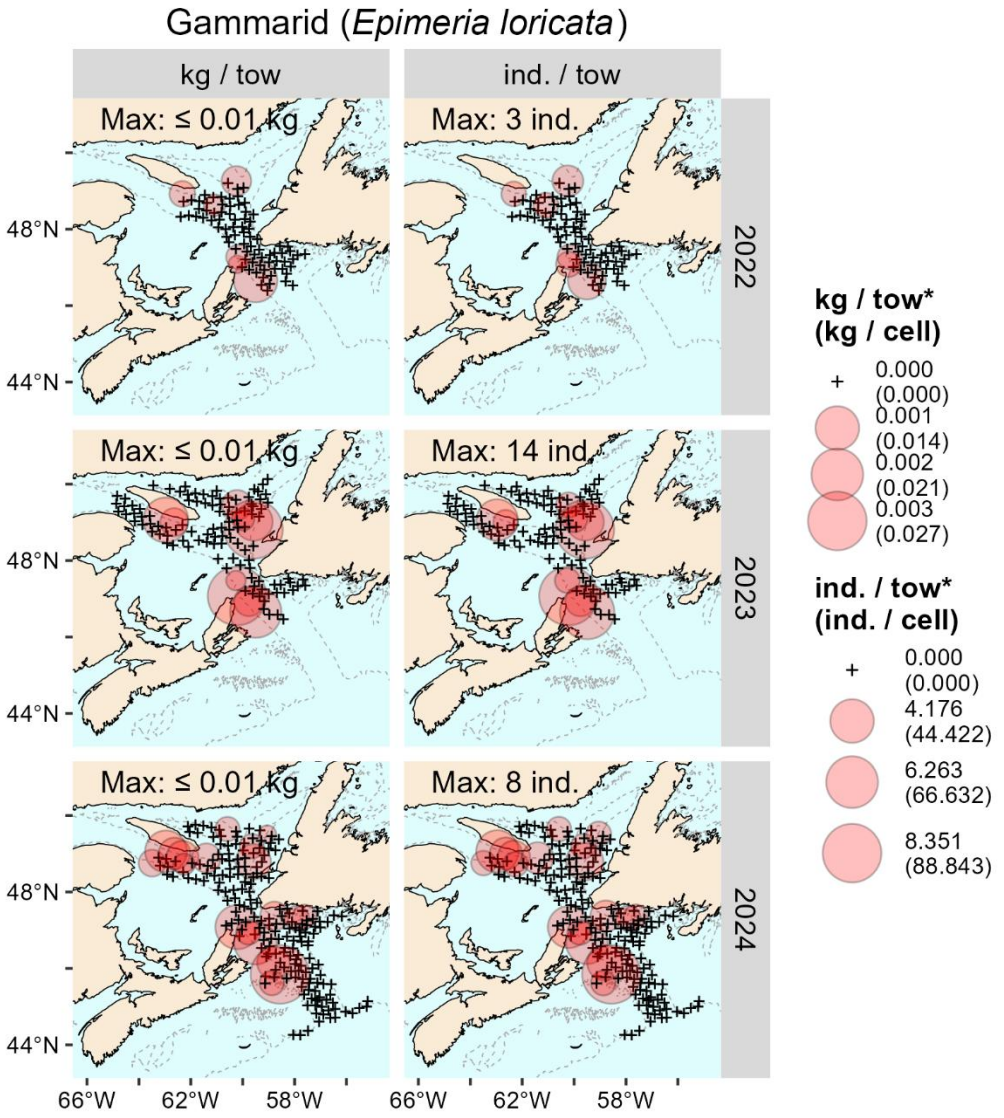


Figure 67a. Standardized catches by weight and/or number (colored bubbles) and cases of absence (black crosses) for the gammarid *Epimeria loricata* in the winter survey in 2022, 2023 and 2024.

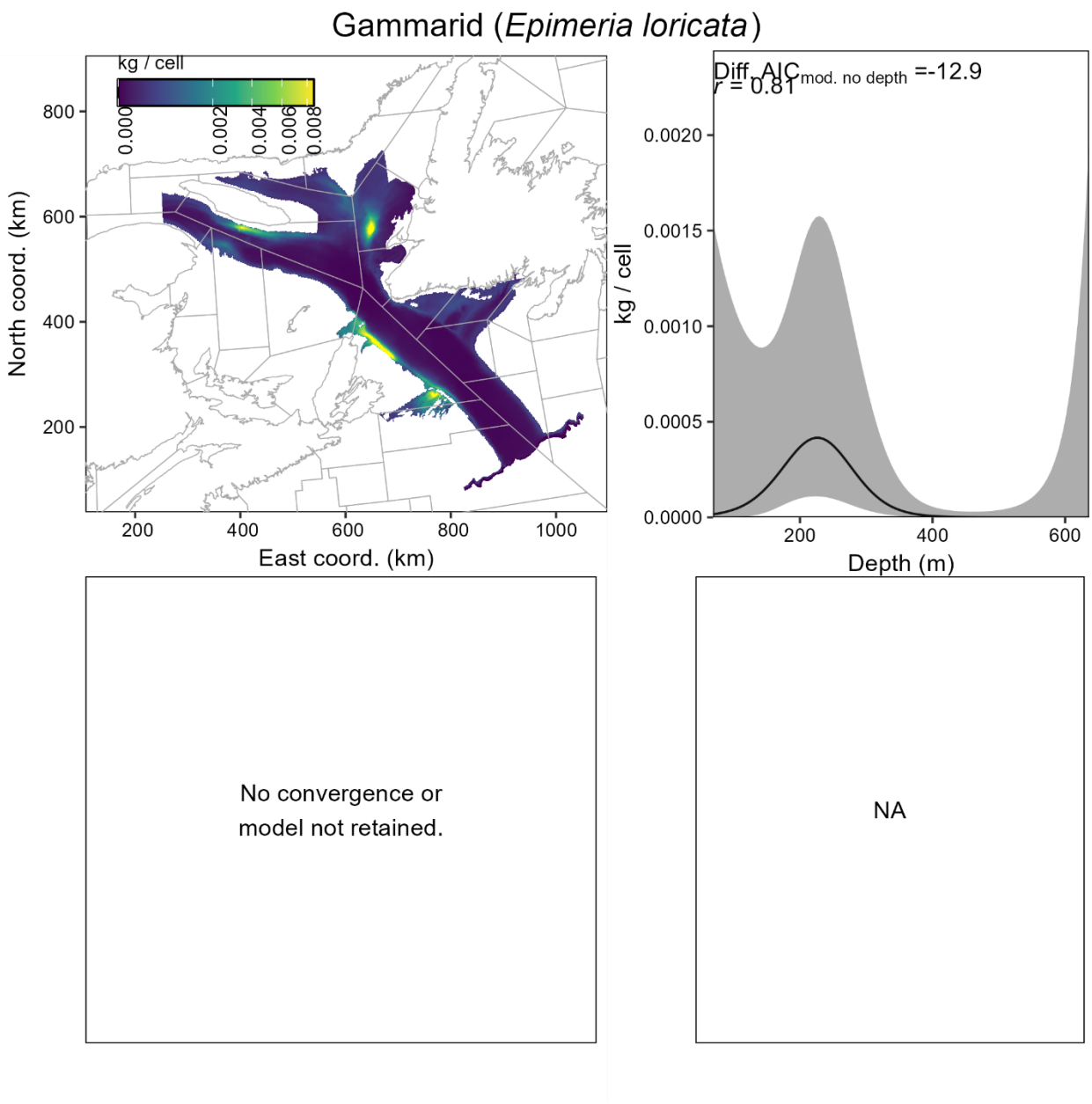


Figure 67b. Predicted weight (upper panels) and number (lower panels) values per 0.25 km^2 cell according to the selected spatial interpolation models for the gammarid *Epimeria loricata* in the 2022, 2023, and 2024 winter survey.

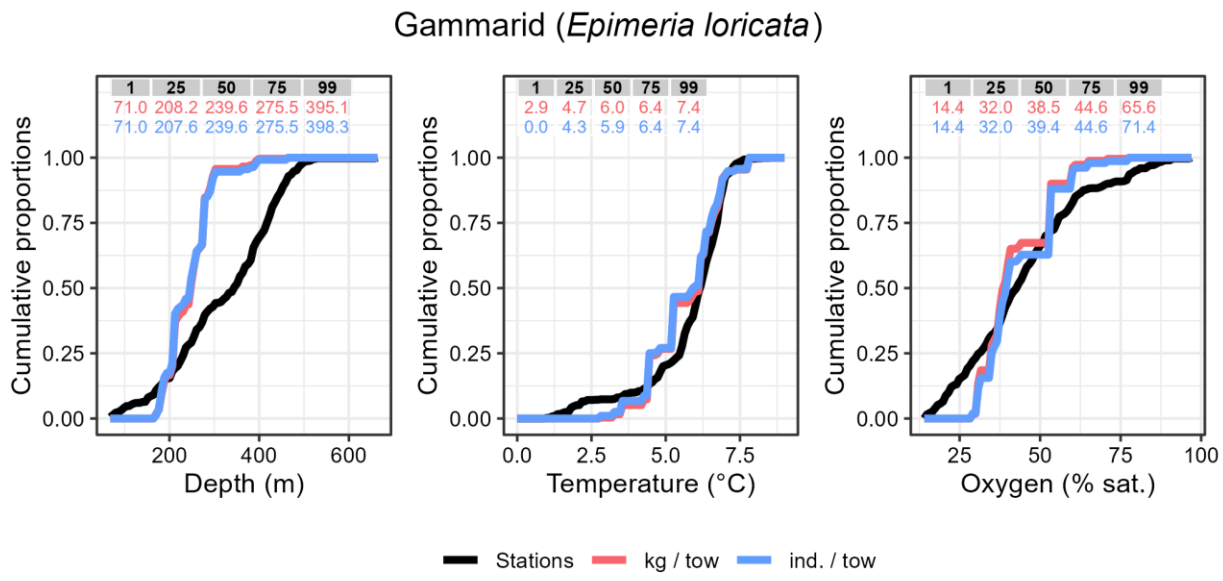


Figure 67c. Cumulative proportions of available values of depth, temperature and dissolved oxygen and standardized catches per tow for the gammarid *Epimeria loricata* in the winter survey in 2022, 2023 and 2024.

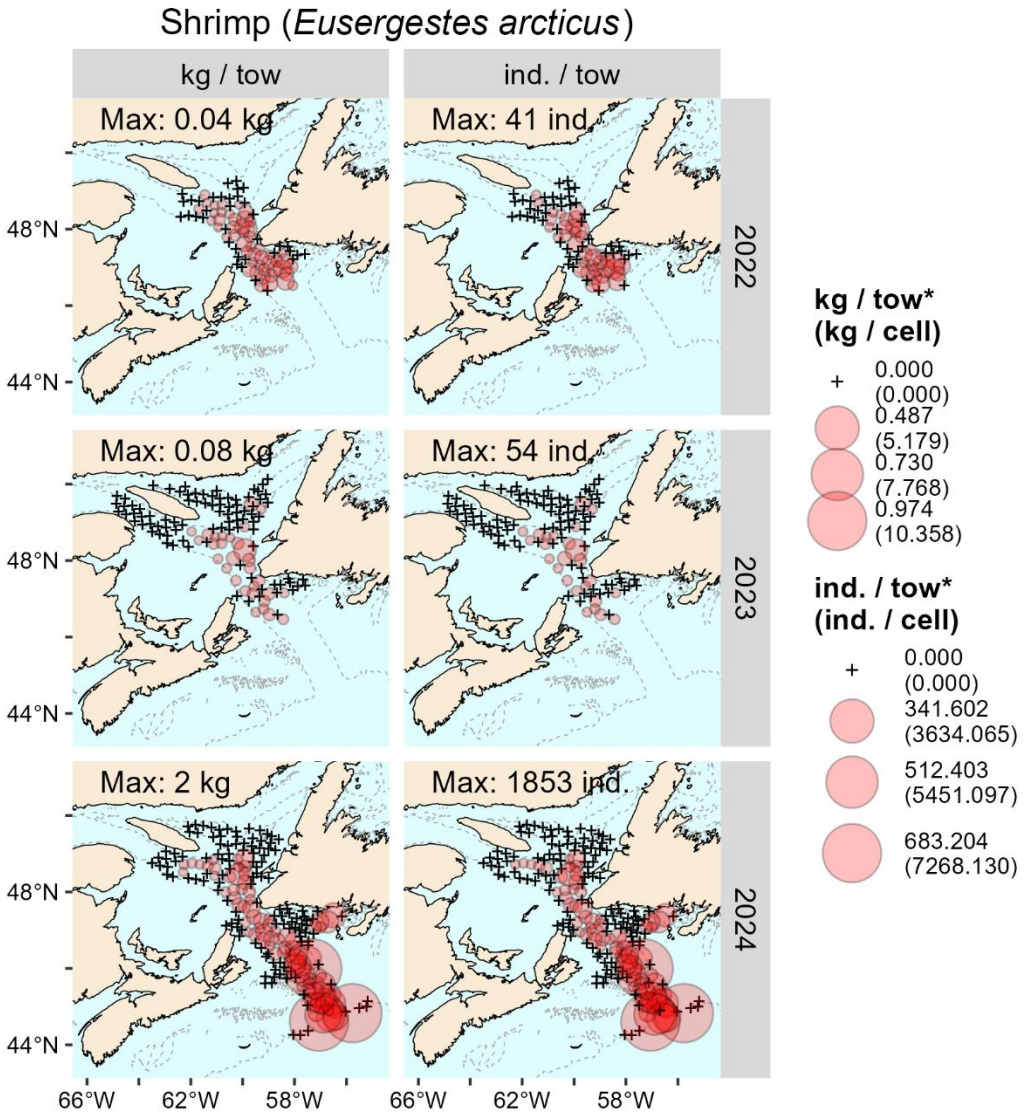


Figure 68a. Standardized catches by weight and/or number (colored bubbles) and cases of absence (black crosses) for the shrimp *Eusergestes arcticus* in the winter survey in 2022, 2023 and 2024.

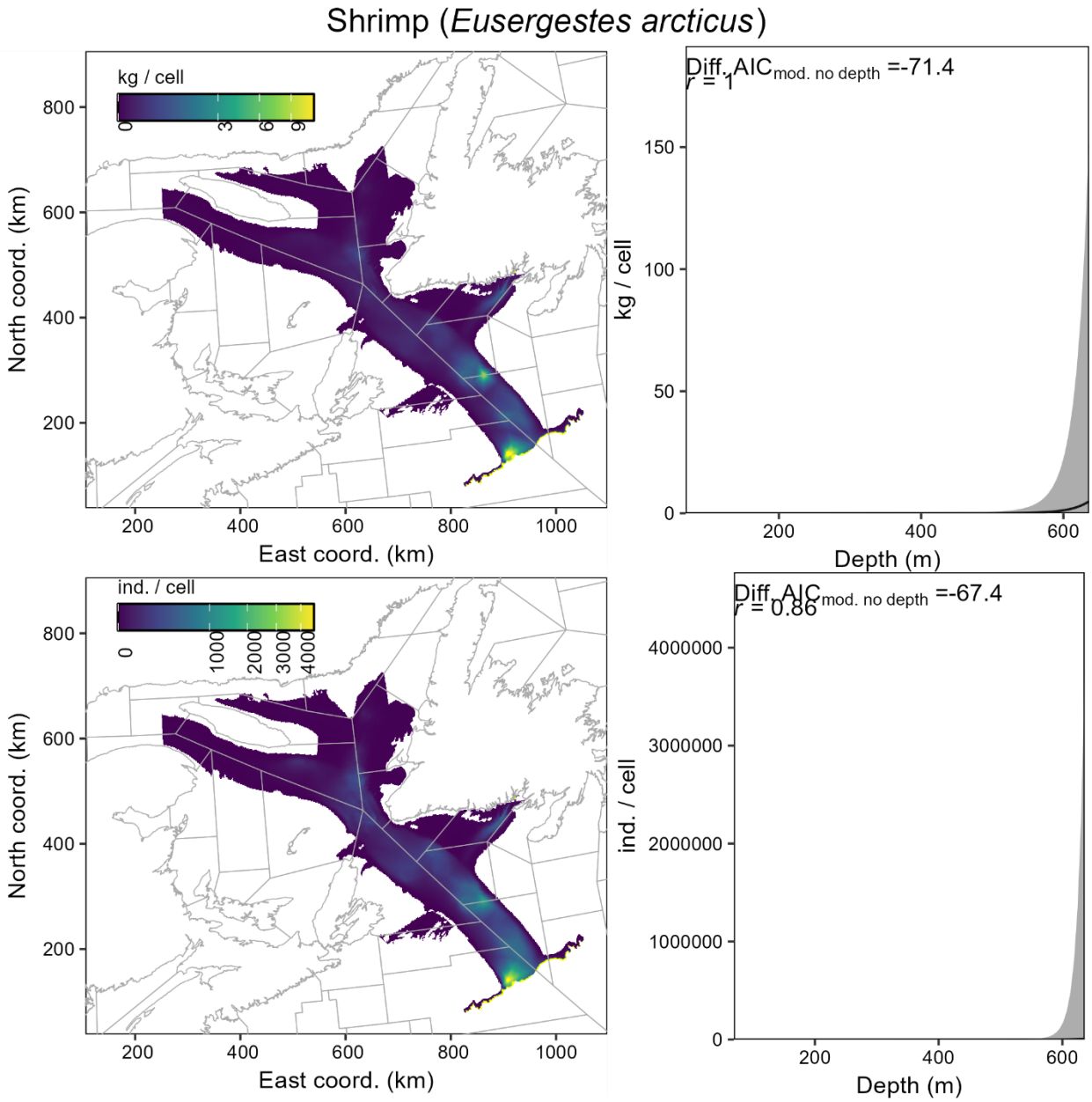


Figure 68b. Predicted weight (upper panels) and number (lower panels) values per 0.25 km^2 cell according to the selected spatial interpolation models for the shrimp *Eusergestes arcticus* in the 2022, 2023, and 2024 winter survey.

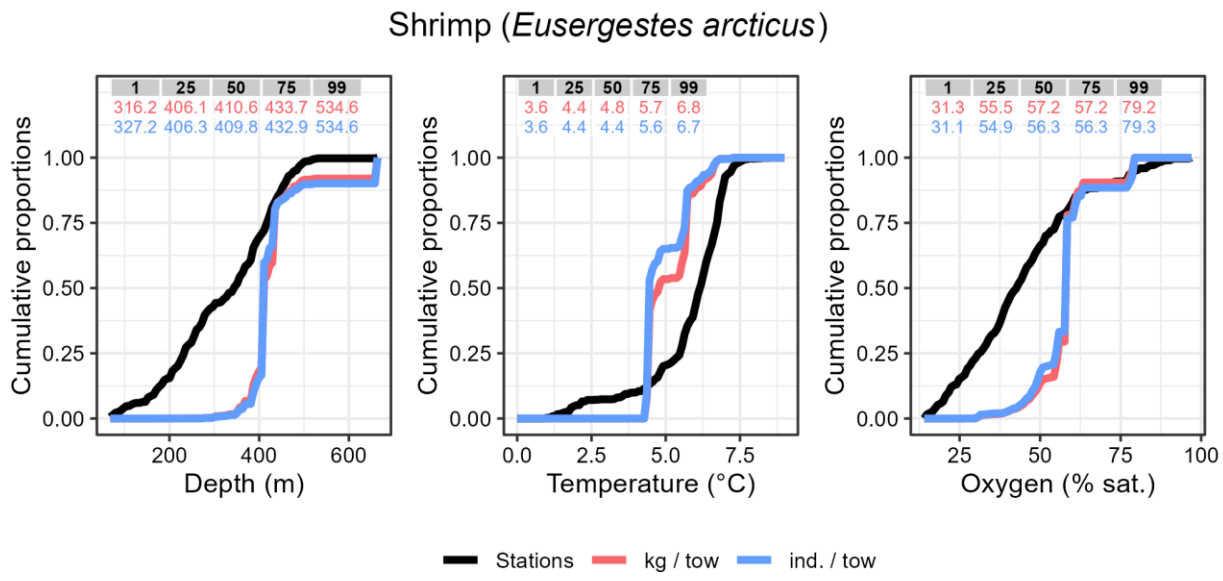


Figure 68c. Cumulative proportions of available values of depth, temperature and dissolved oxygen and standardized catches per tow for the shrimp *Eusergestes arcticus* in the winter survey in 2022, 2023 and 2024.

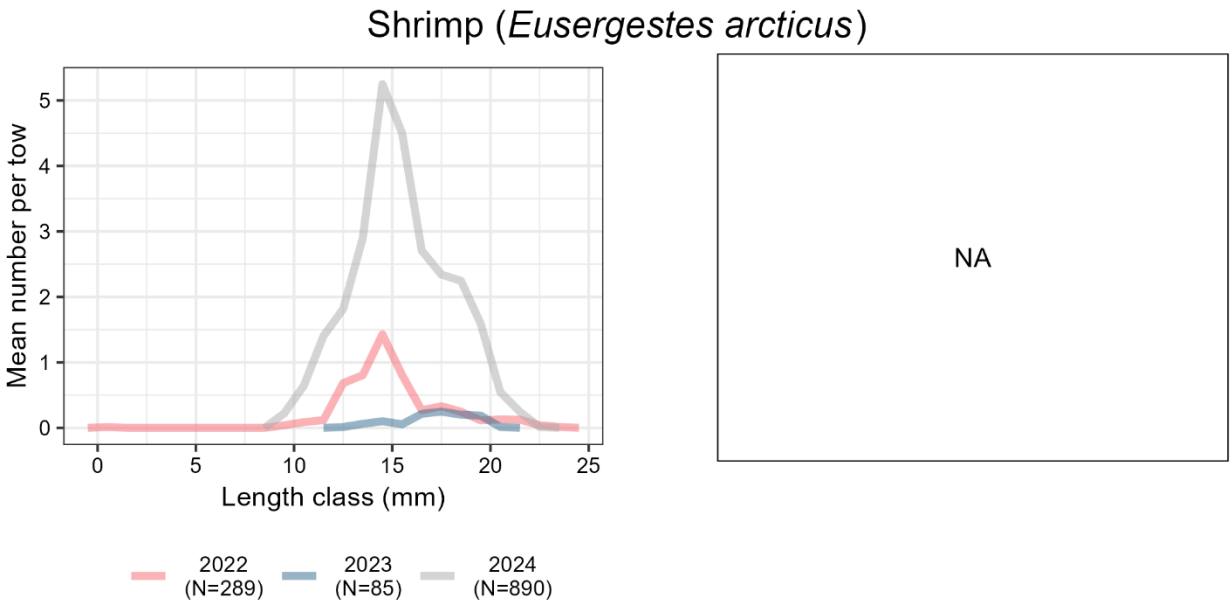


Figure 68d. Annual length frequencies (left panel) and length-weight observations with the global relationship prediction (right panel) for the shrimp *Eusergestes arcticus* in the winter survey in 2022, 2023 and 2024.

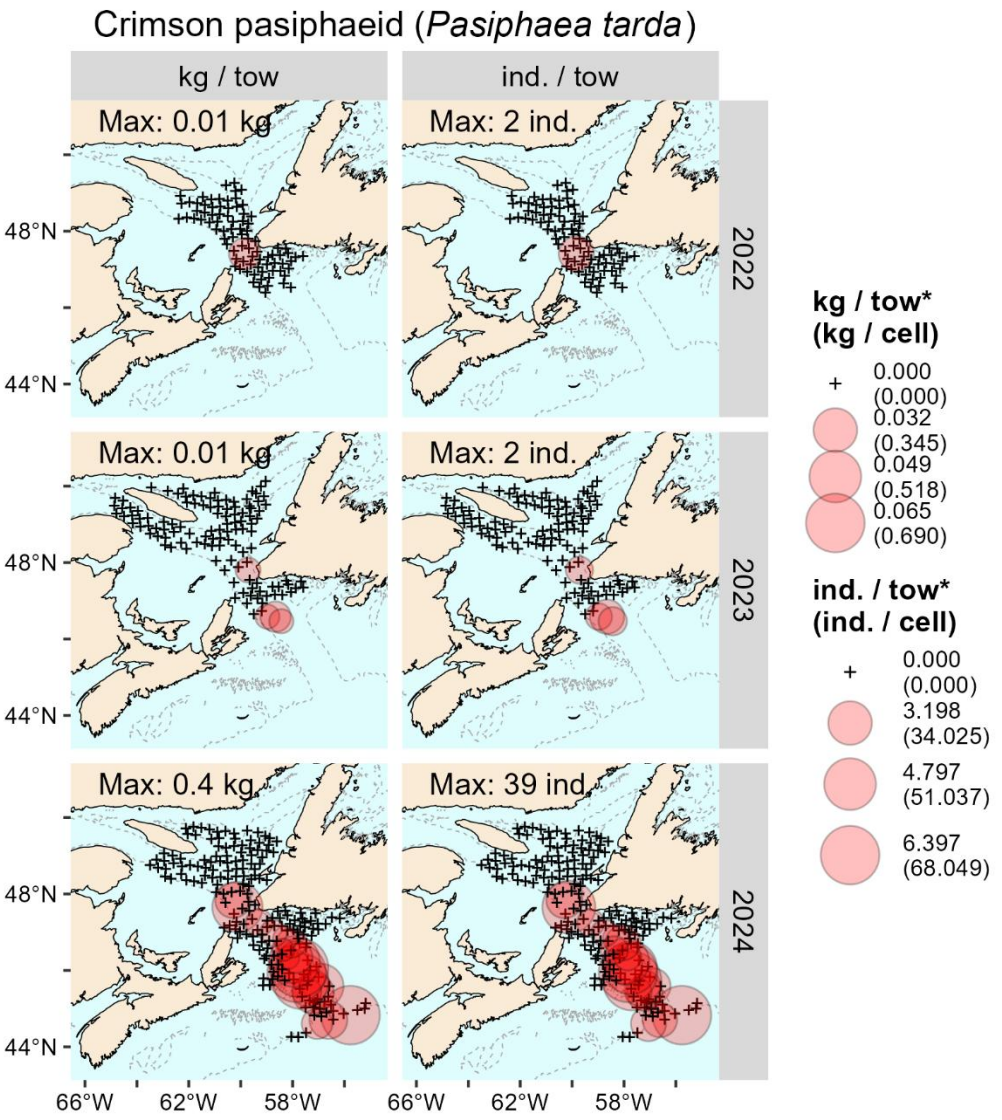


Figure 69a. Standardized catches by weight and/or number (colored bubbles) and cases of absence (black crosses) for the crimson pasiphaeid *Pasiphaea tarda* in the winter survey in 2022, 2023 and 2024.

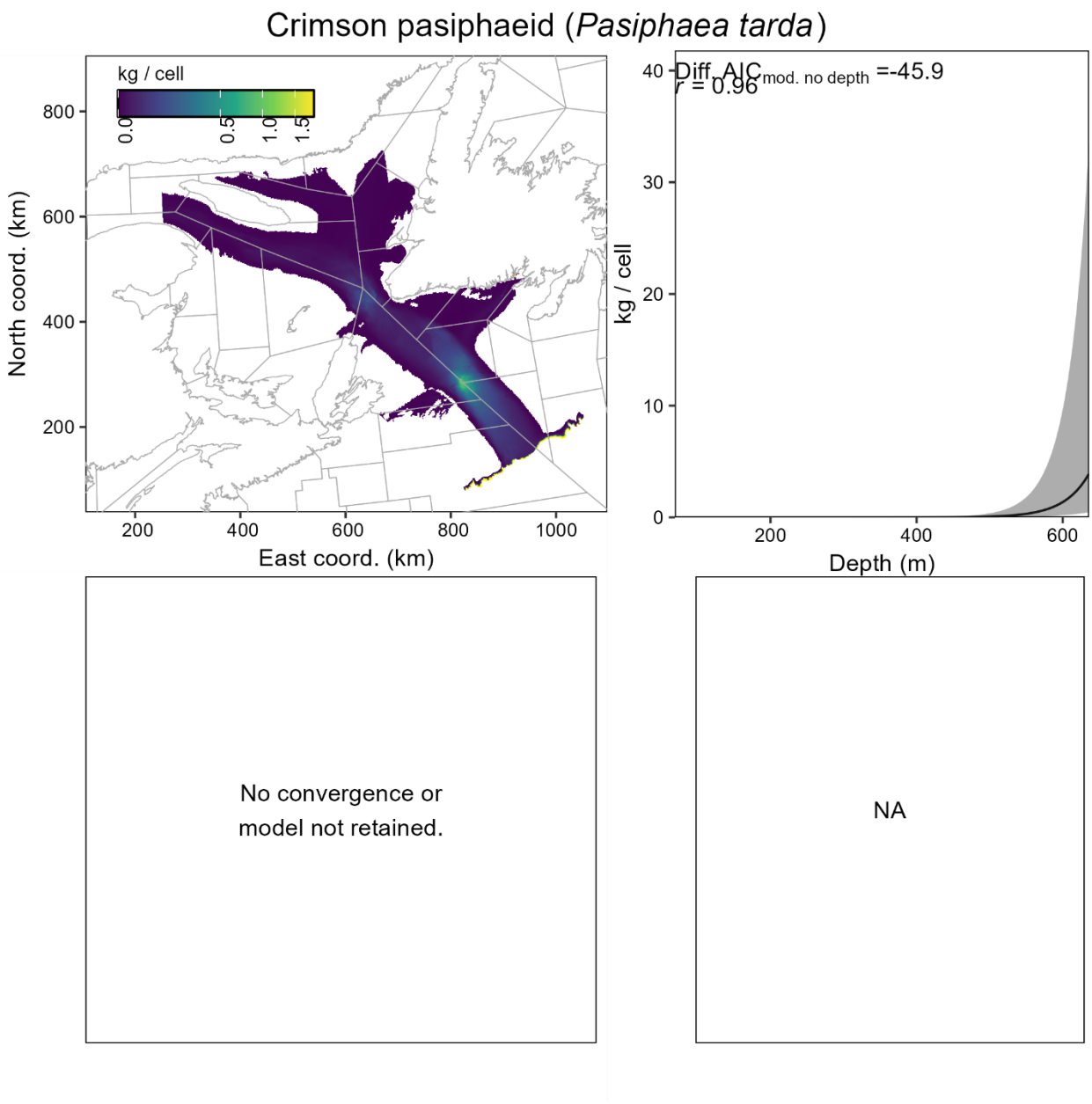


Figure 69b. Predicted weight (upper panels) and number (lower panels) values per 0.25 km^2 cell according to the selected spatial interpolation models for the crimson pasiphaeid *Pasiphaea tarda* in the 2022, 2023, and 2024 winter survey.

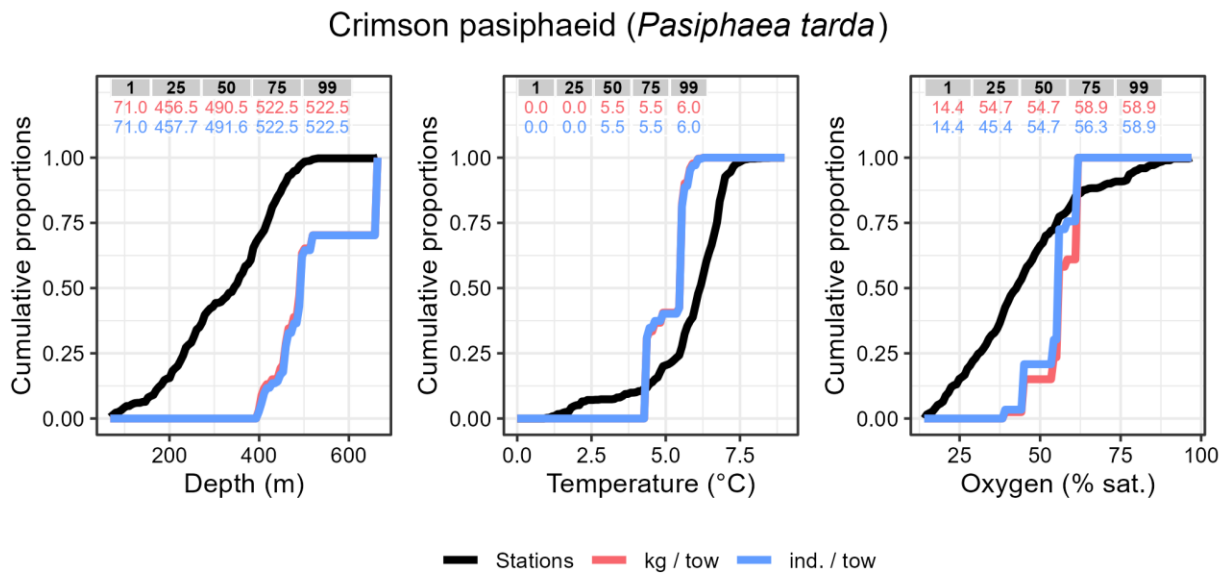


Figure 69c. Cumulative proportions of available values of depth, temperature and dissolved oxygen and standardized catches per tow for the crimson pasiphaeid *Pasiphaea tarda* in the winter survey in 2022, 2023 and 2024.

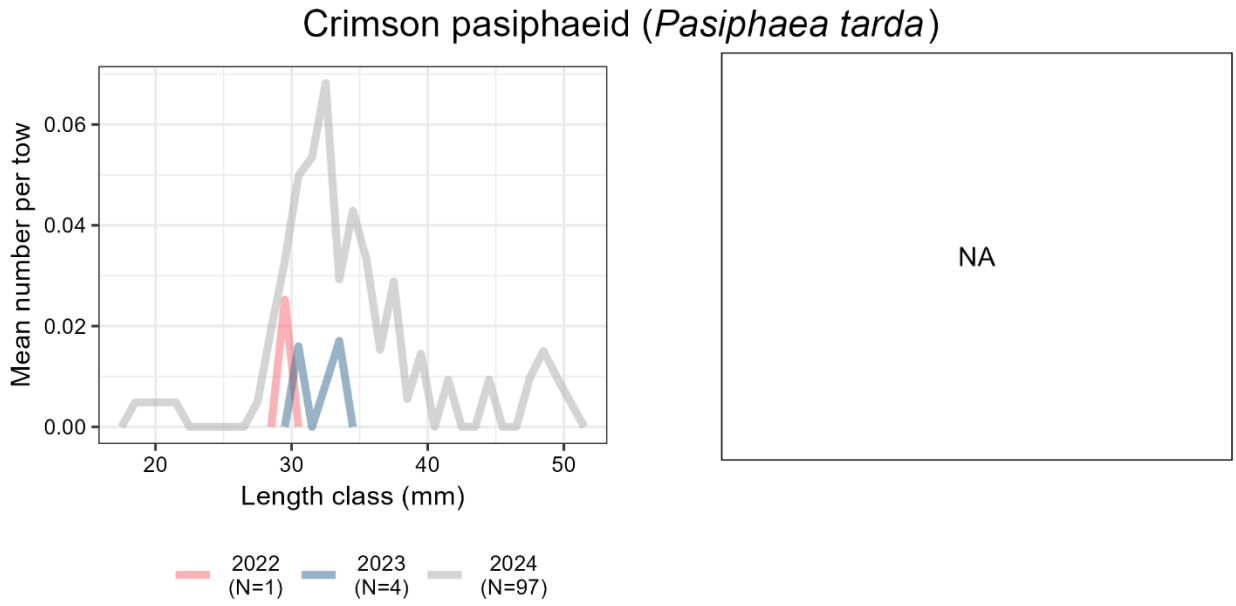


Figure 69d. Annual length frequencies (left panel) and length-weight observations with the global relationship prediction (right panel) for the crimson pasiphaeid *Pasiphaea tarda* in the winter survey in 2022, 2023 and 2024.

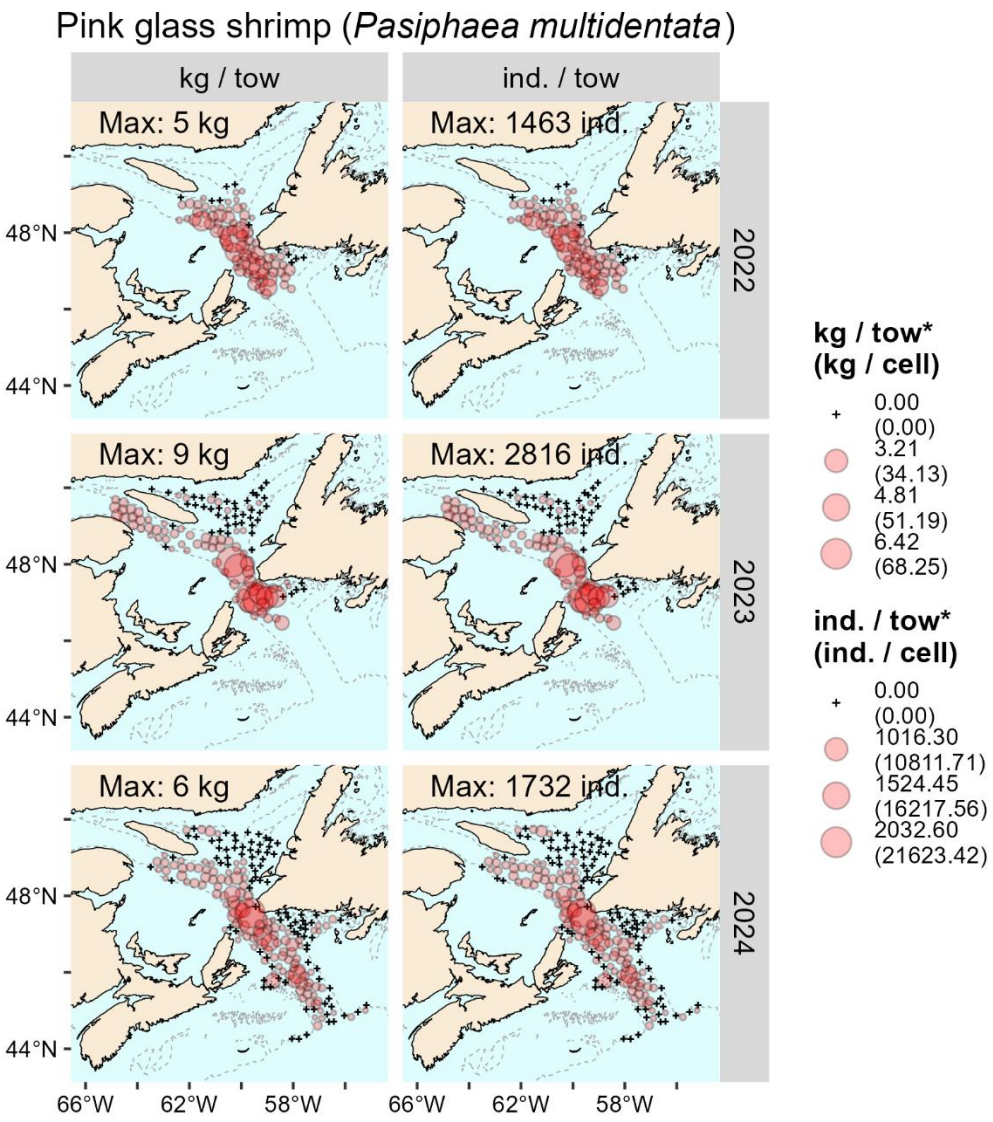


Figure 70a. Standardized catches by weight and/or number (colored bubbles) and cases of absence (black crosses) for the pink glass shrimp in the winter survey in 2022, 2023 and 2024.

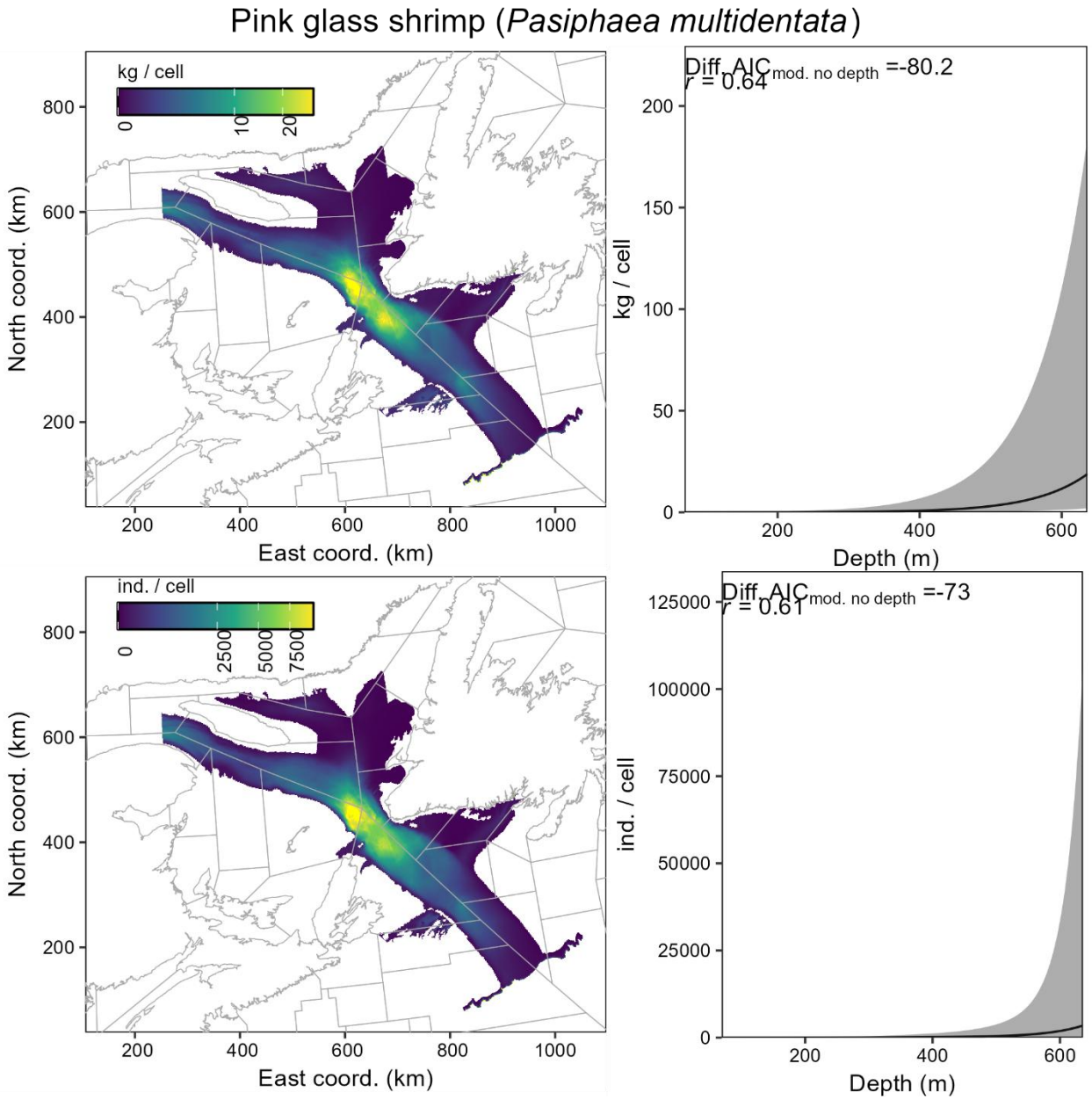


Figure 70b. Predicted weight (upper panels) and number (lower panels) values per 0.25 km^2 cell according to the selected spatial interpolation models for the pink glass shrimp in the 2022, 2023, and 2024 winter survey.

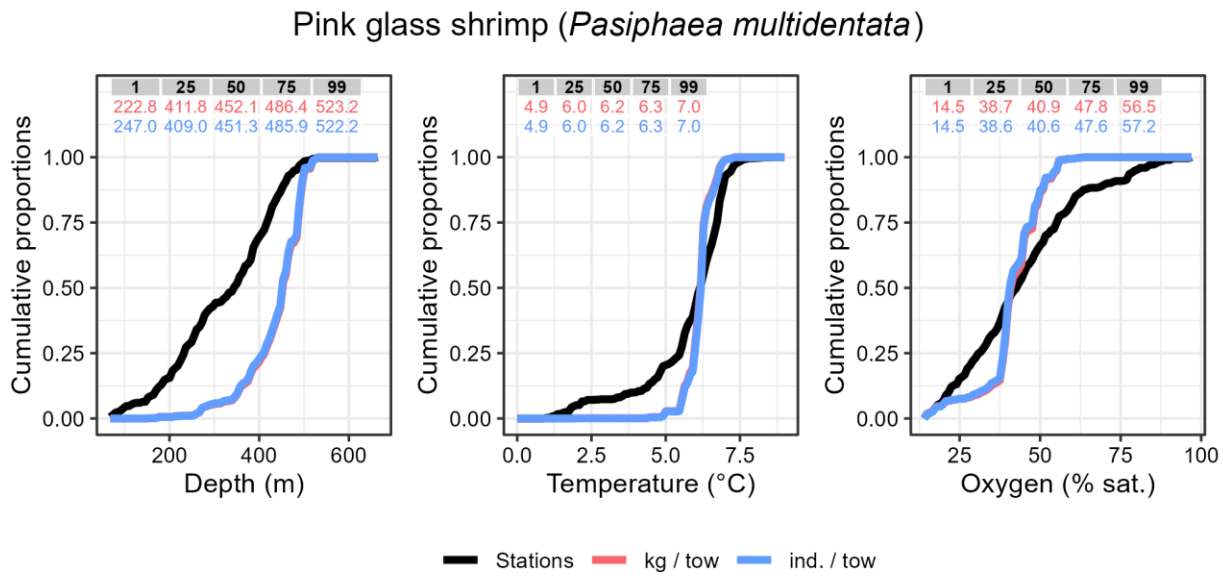


Figure 70c. Cumulative proportions of available values of depth, temperature and dissolved oxygen and standardized catches per tow for the pink glass shrimp in the winter survey in 2022, 2023 and 2024.

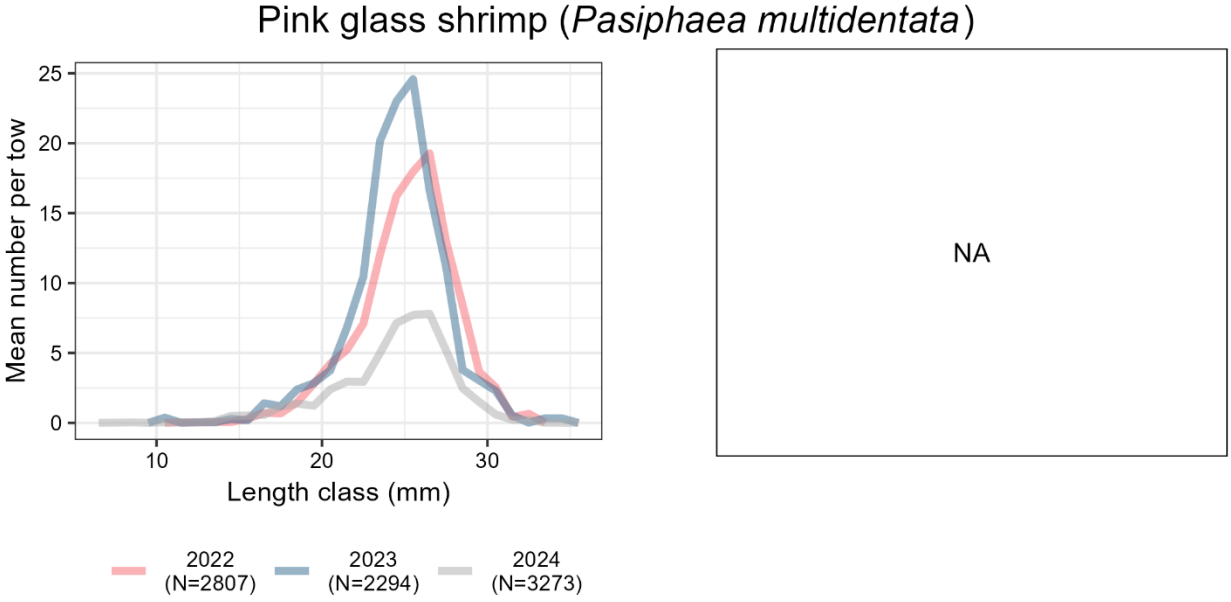


Figure 70d. Annual length frequencies (left panel) and length-weight observations with the global relationship prediction (right panel) for the pink glass shrimp in the winter survey in 2022, 2023 and 2024.

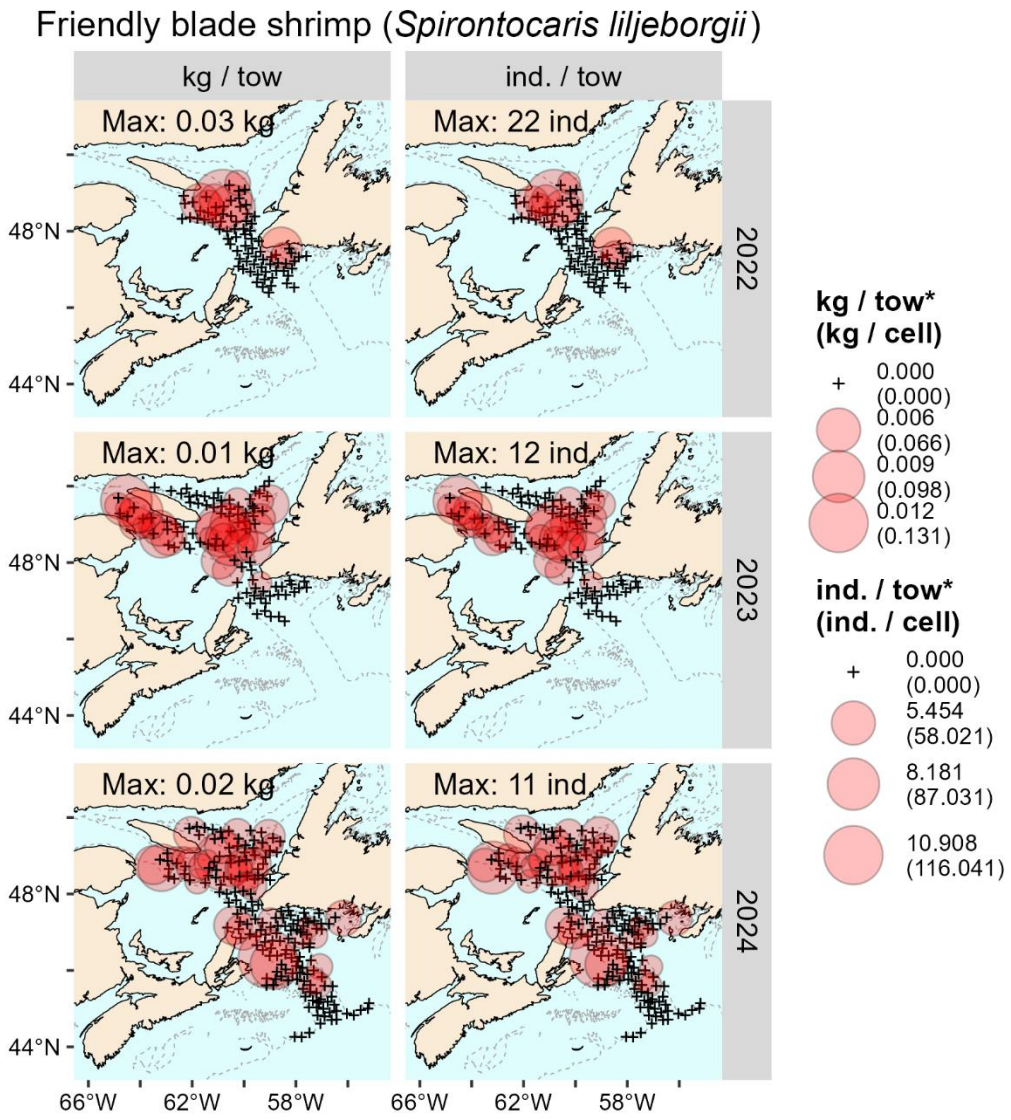


Figure 71a. Standardized catches by weight and/or number (colored bubbles) and cases of absence (black crosses) for the friendly blade shrimp *Spirontocaris liljeborgii* in the winter survey in 2022, 2023 and 2024.

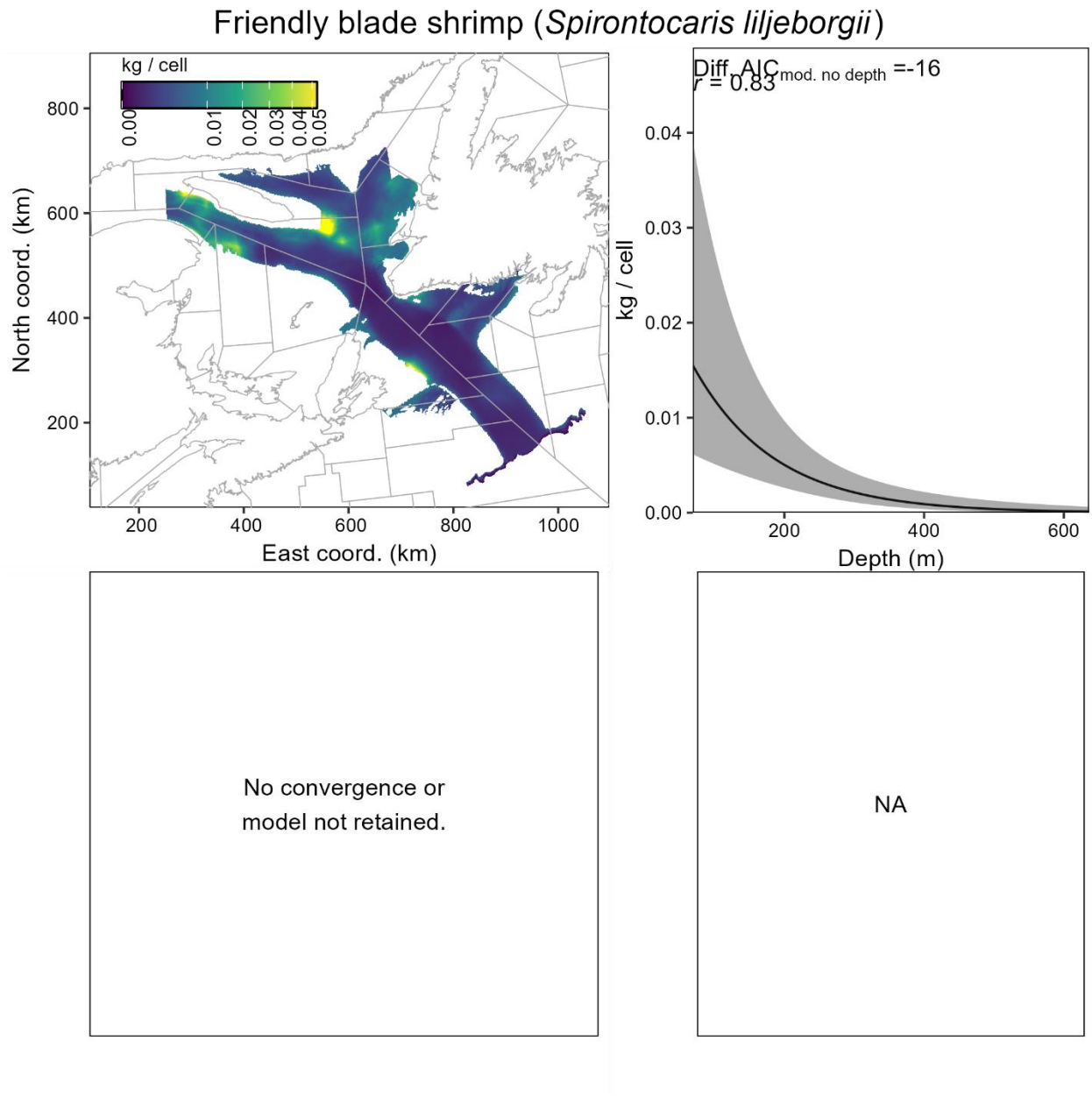


Figure 71b. Predicted weight (upper panels) and number (lower panels) values per 0.25 km^2 cell according to the selected spatial interpolation models for the friendly blade shrimp *Spirontocaris liljeborgii* in the 2022, 2023, and 2024 winter survey.

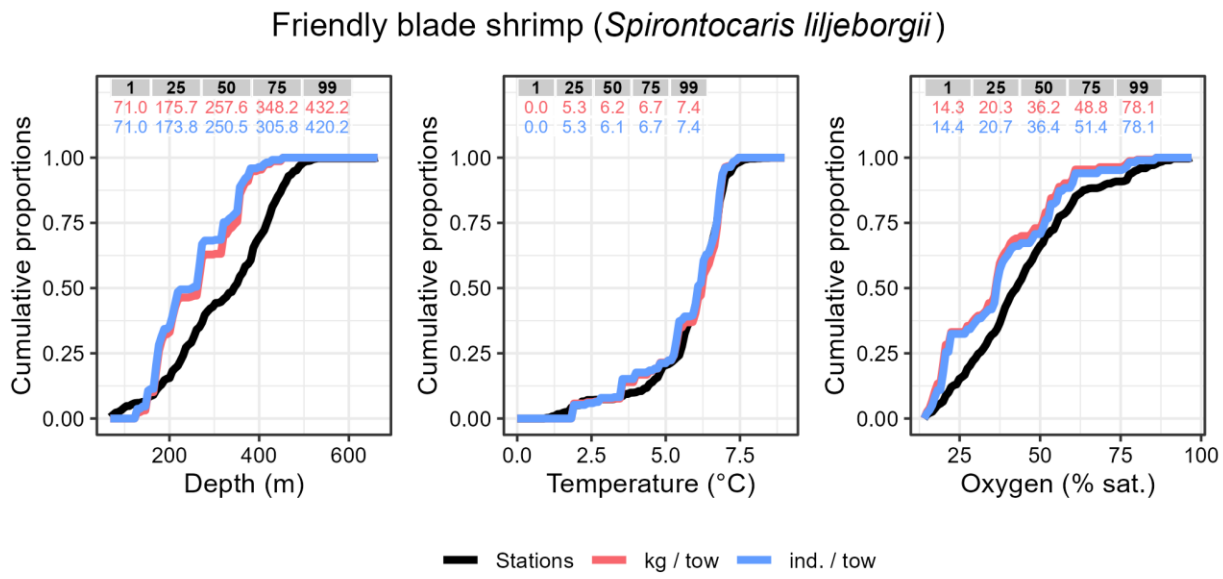


Figure 71c. Cumulative proportions of available values of depth, temperature and dissolved oxygen and standardized catches per tow for the friendly blade shrimp *Spirontocaris liljeborgii* in the winter survey in 2022, 2023 and 2024.

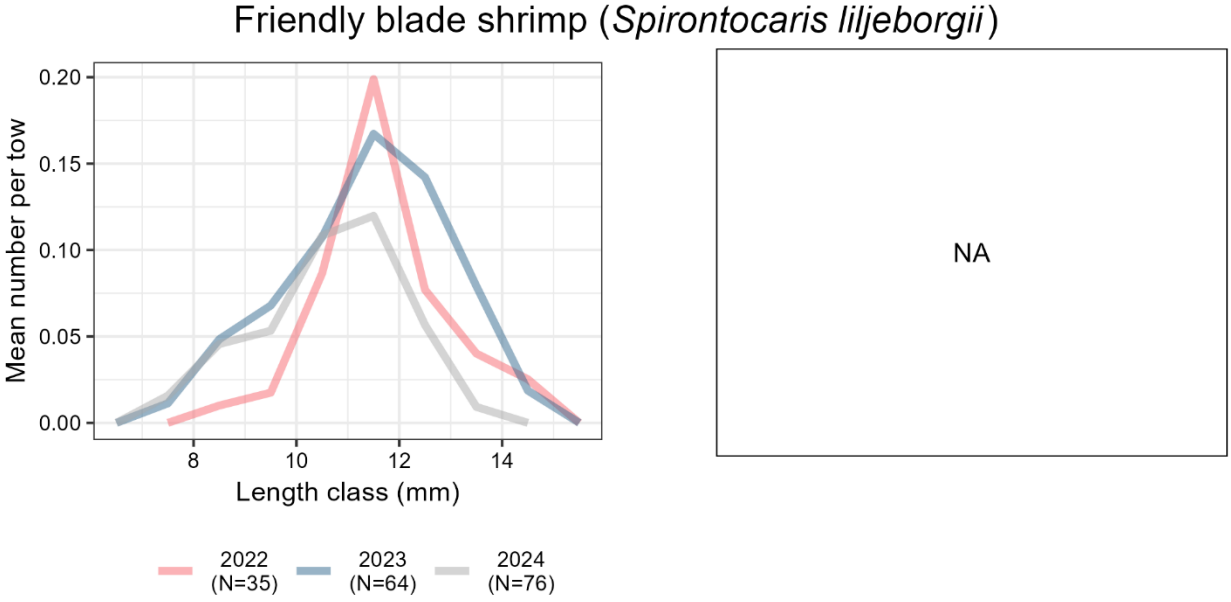


Figure 71d. Annual length frequencies (left panel) and length-weight observations with the global relationship prediction (right panel) for the friendly blade shrimp *Spirontocaris liljeborgii* in the winter survey in 2022, 2023 and 2024.

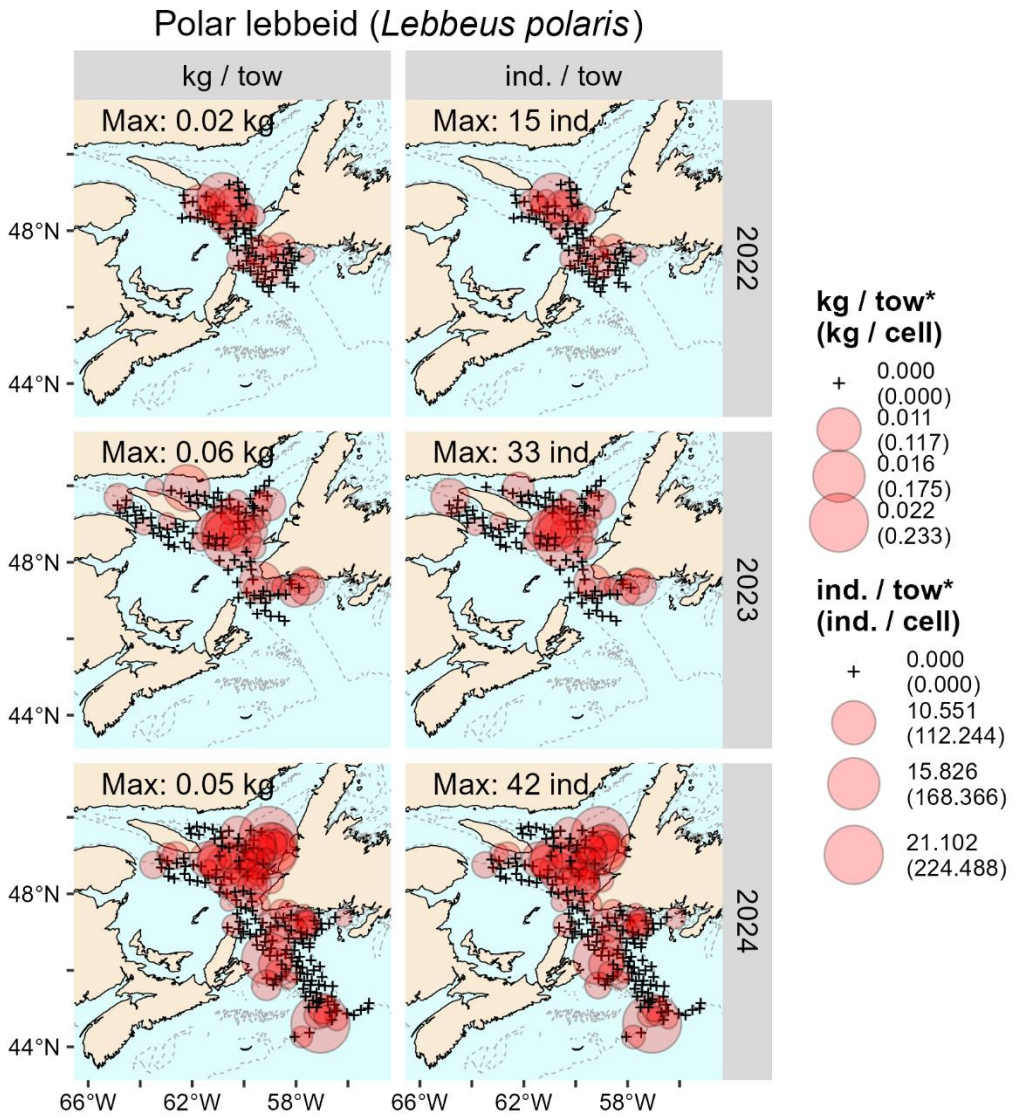


Figure 72a. Standardized catches by weight and/or number (colored bubbles) and cases of absence (black crosses) for the polar lebbeid *Lebbeus polaris* in the winter survey in 2022, 2023 and 2024.

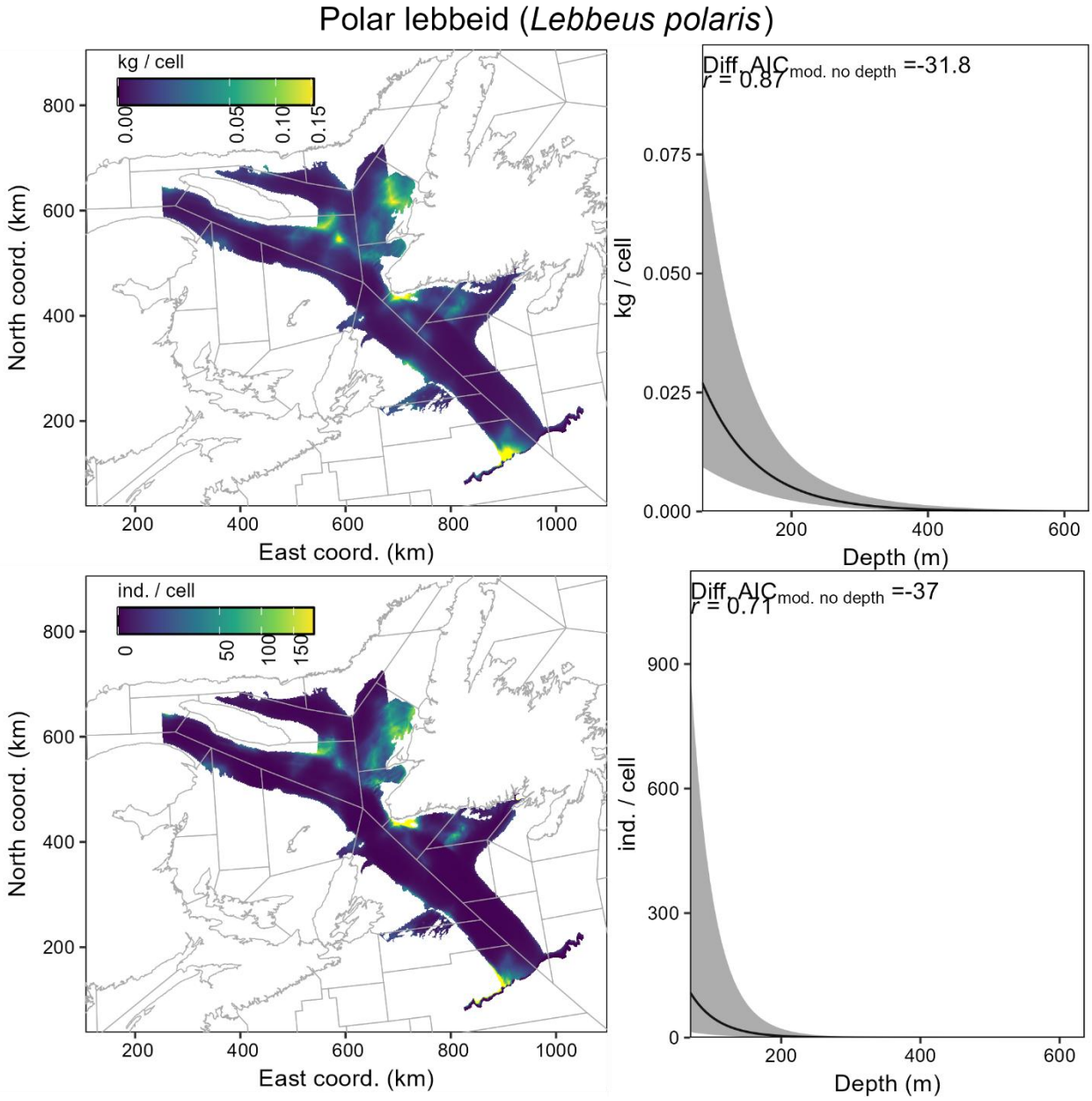


Figure 72b. Predicted weight (upper panels) and number (lower panels) values per 0.25 km^2 cell according to the selected spatial interpolation models for the polar lebbeid *Lebbeus polaris* in the 2022, 2023, and 2024 winter survey.

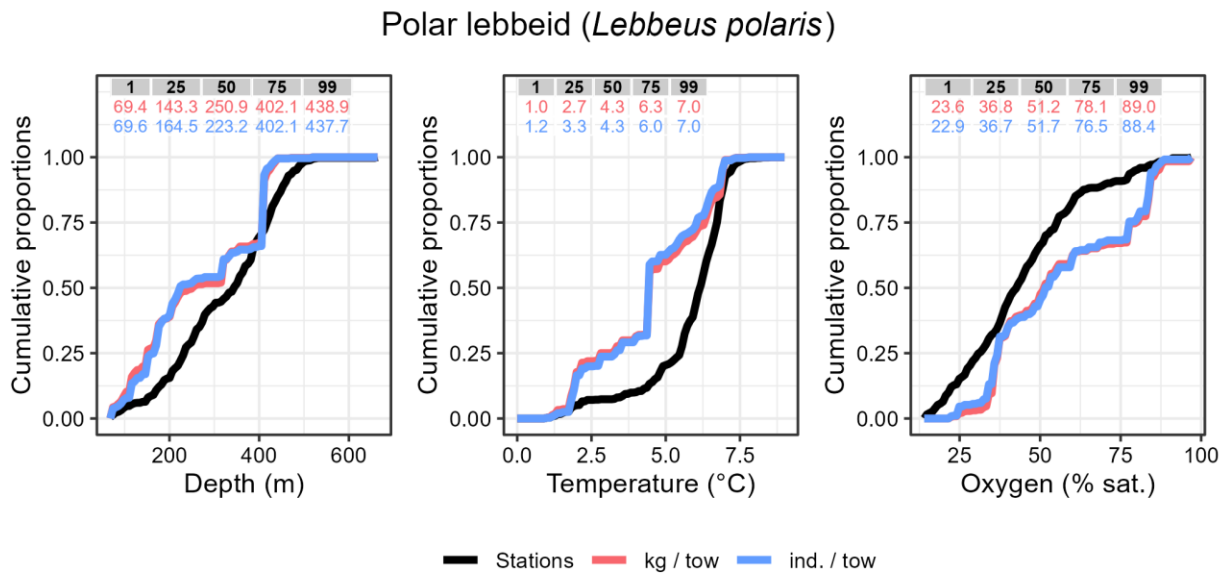


Figure 72c. Cumulative proportions of available values of depth, temperature and dissolved oxygen and standardized catches per tow for the polar lebbeid *Lebbeus polaris* in the winter survey in 2022, 2023 and 2024.

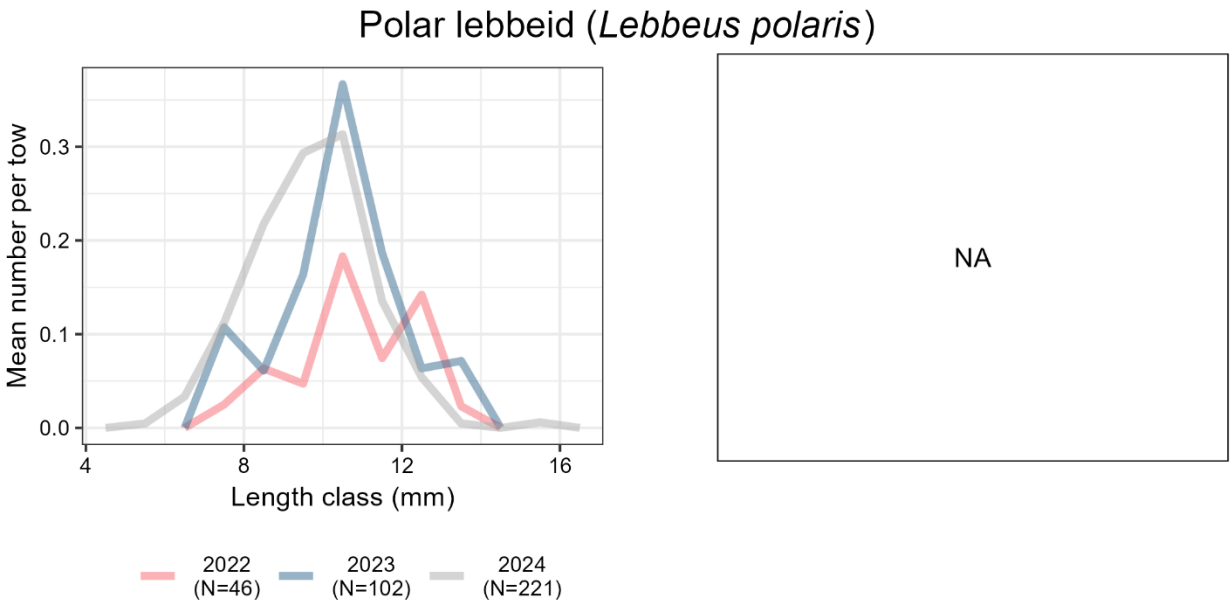


Figure 72d. Annual length frequencies (left panel) and length-weight observations with the global relationship prediction (right panel) for the polar lebbeid *Lebbeus polaris* in the winter survey in 2022, 2023 and 2024.

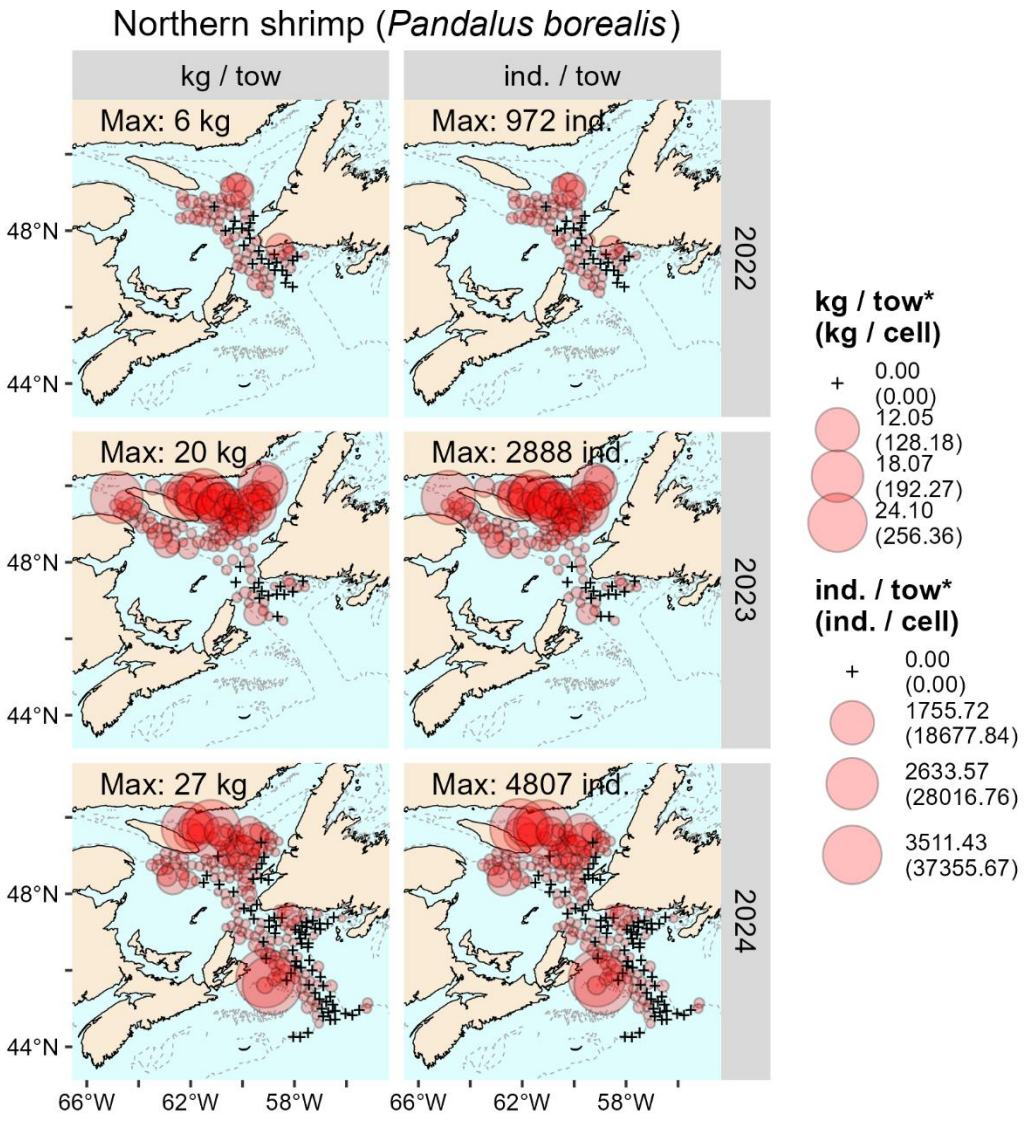


Figure 73a. Standardized catches by weight and/or number (colored bubbles) and cases of absence (black crosses) for the northern shrimp in the winter survey in 2022, 2023 and 2024.

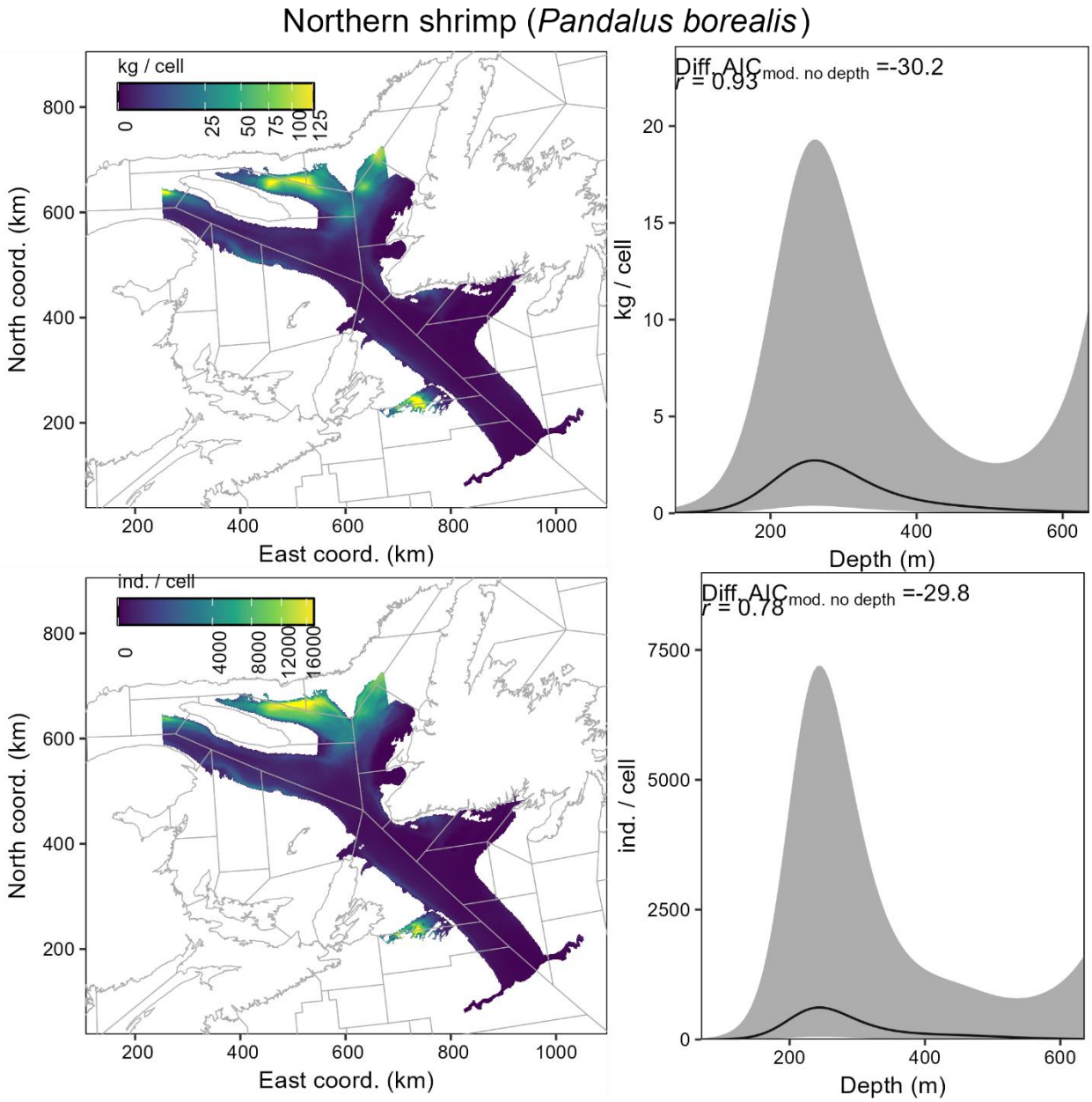


Figure 73b. Predicted weight (upper panels) and number (lower panels) values per 0.25 km^2 cell according to the selected spatial interpolation models for the northern shrimp in the 2022, 2023, and 2024 winter survey.

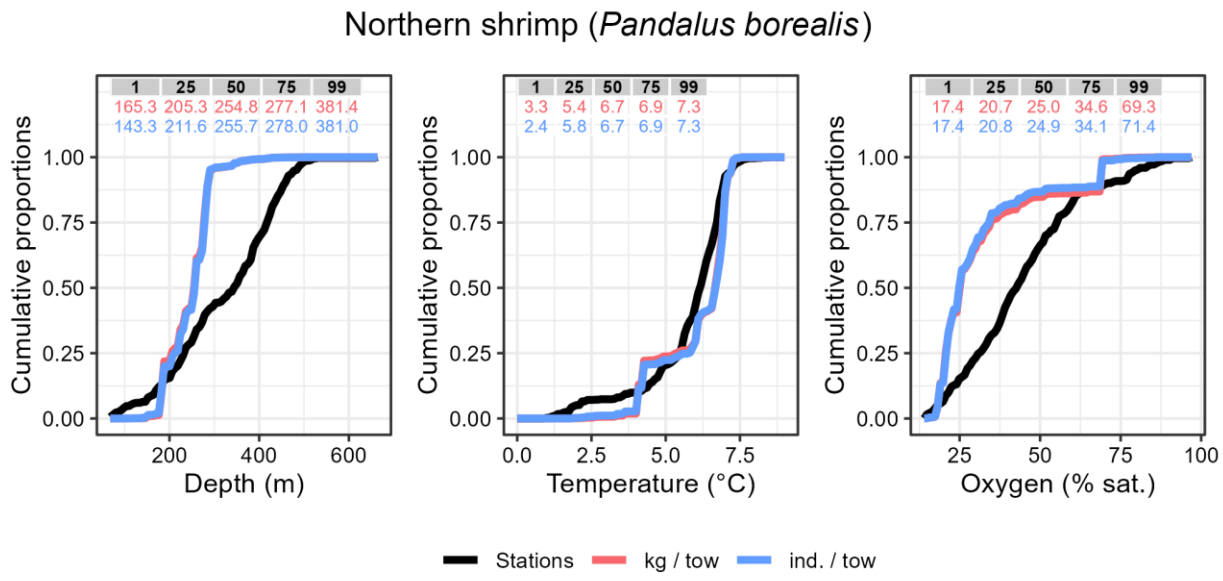


Figure 73c. Cumulative proportions of available values of depth, temperature and dissolved oxygen and standardized catches per tow for the northern shrimp in the winter survey in 2022, 2023 and 2024.

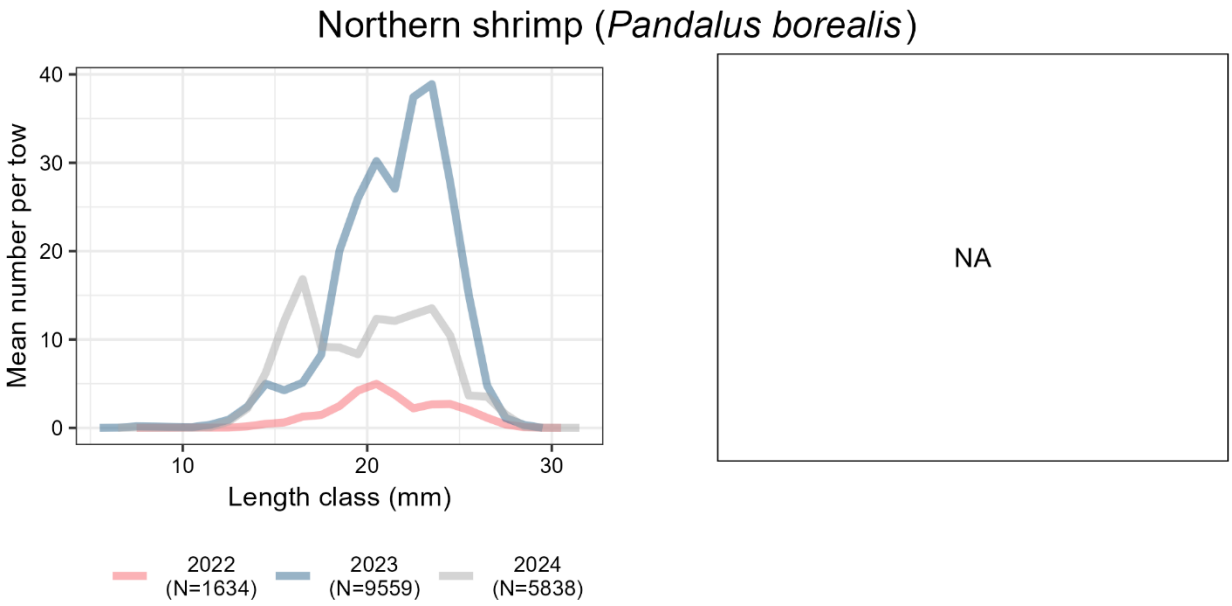


Figure 73d. Annual length frequencies (left panel) and length-weight observations with the global relationship prediction (right panel) for the northern shrimp in the winter survey in 2022, 2023 and 2024.

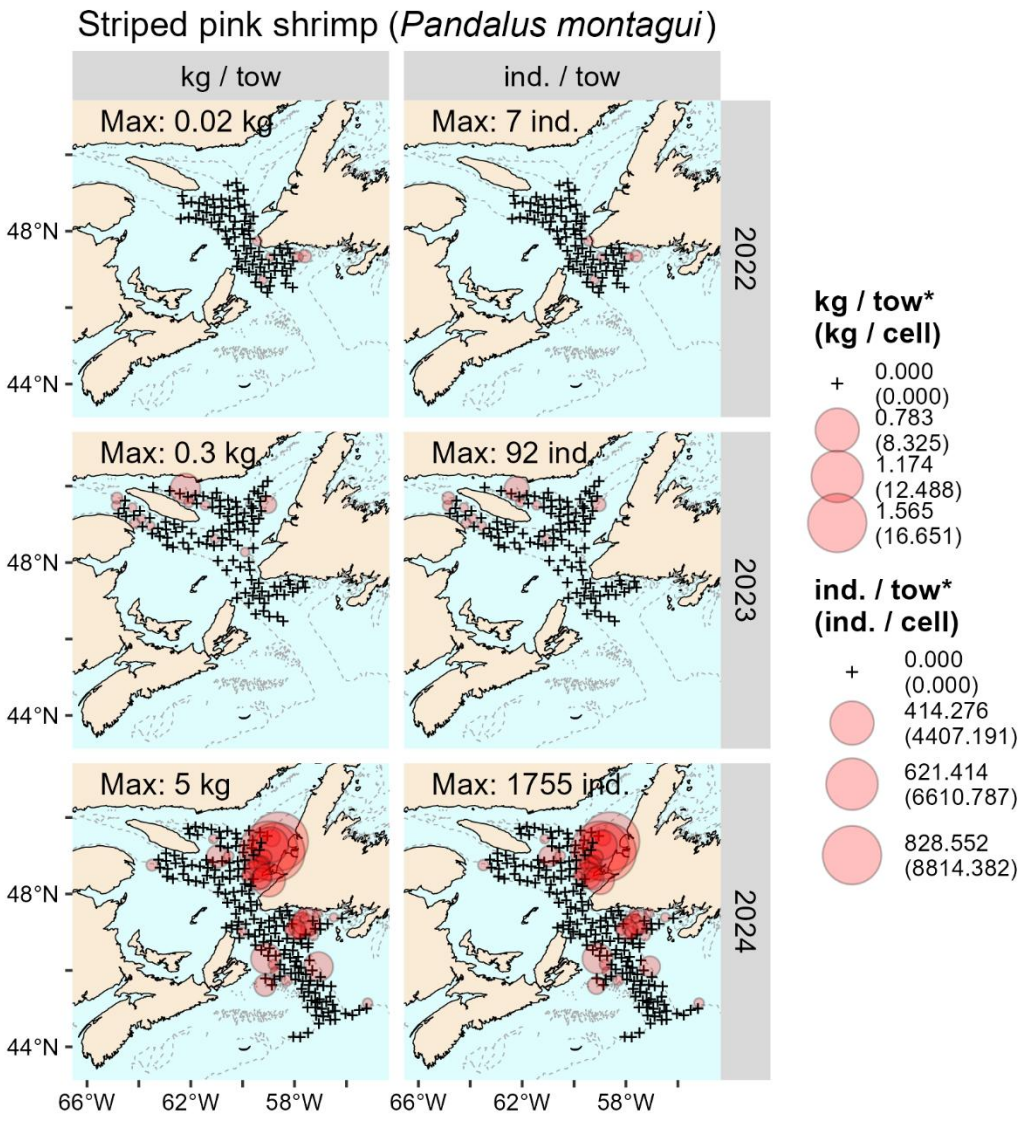


Figure 74a. Standardized catches by weight and/or number (colored bubbles) and cases of absence (black crosses) for the striped pink shrimp *Pandalus montagui* in the winter survey in 2022, 2023 and 2024.

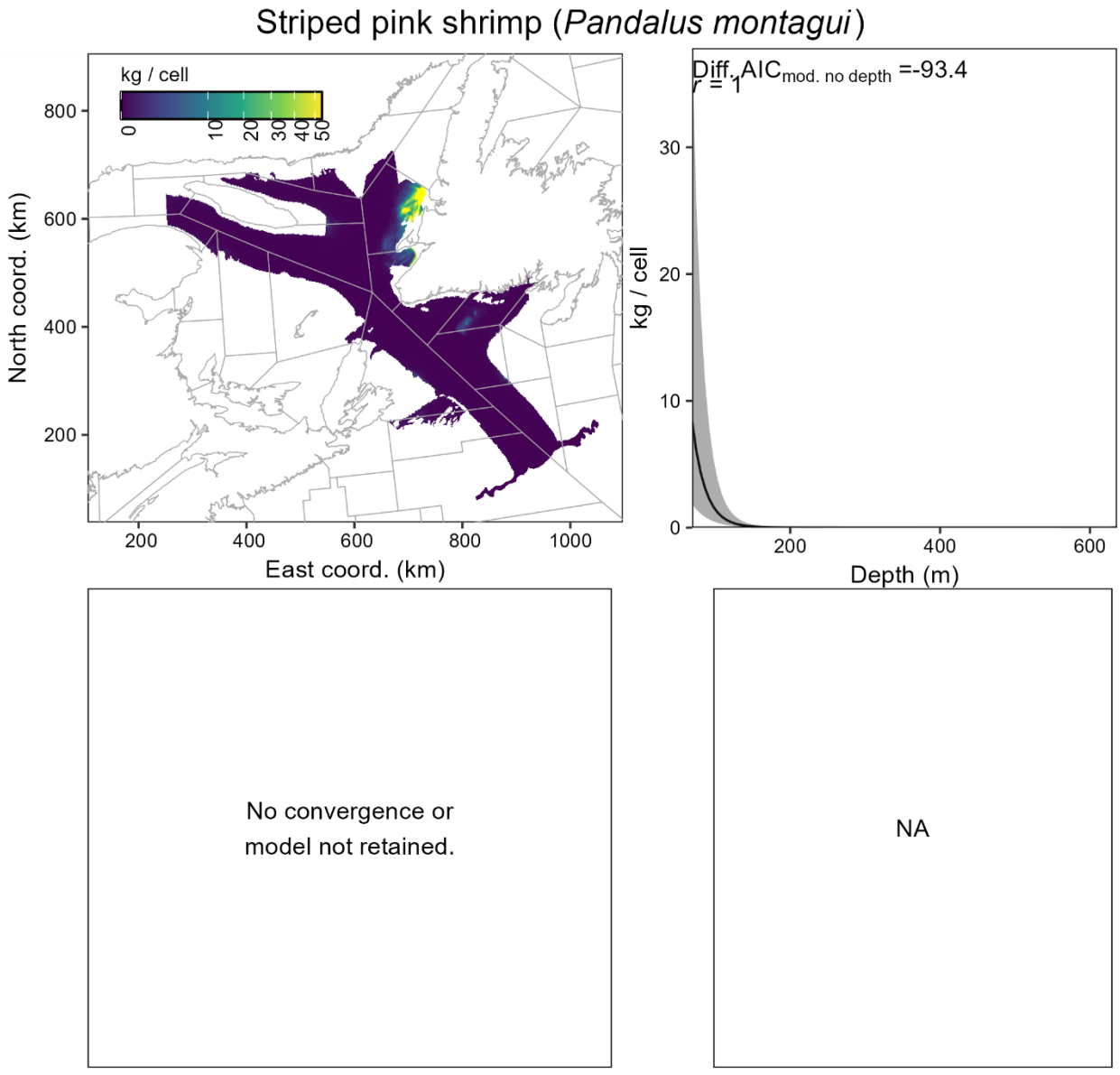


Figure 74b. Predicted weight (upper panels) and number (lower panels) values per 0.25 km^2 cell according to the selected spatial interpolation models for the striped pink shrimp *Pandalus montagui* in the 2022, 2023, and 2024 winter survey.

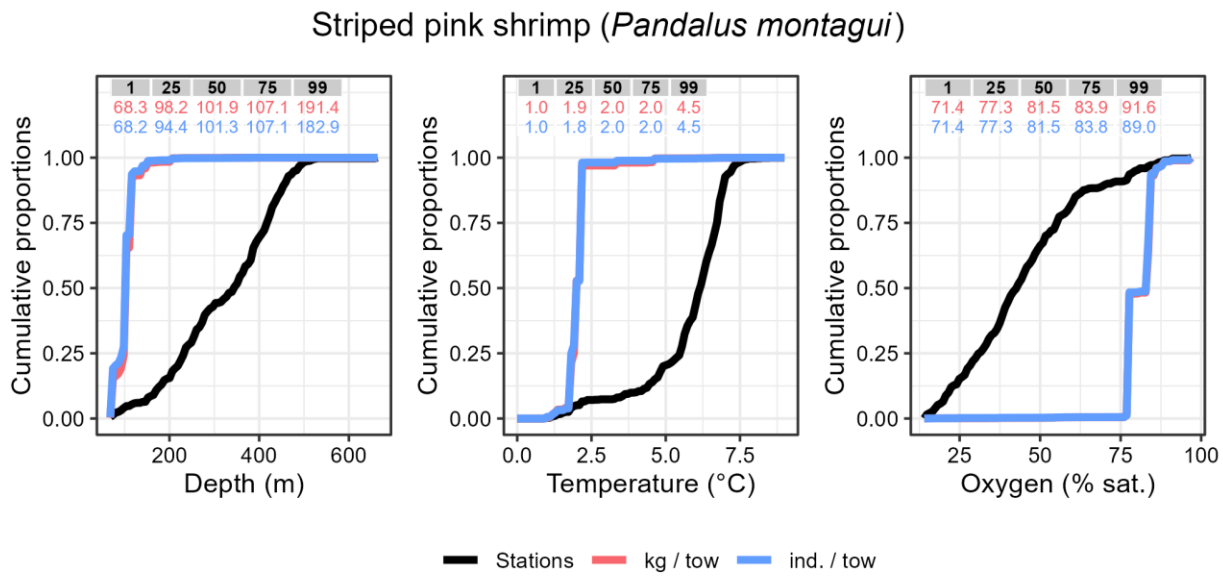


Figure 74c. Cumulative proportions of available values of depth, temperature and dissolved oxygen and standardized catches per tow for the striped pink shrimp *Pandalus montagui* in the winter survey in 2022, 2023 and 2024.

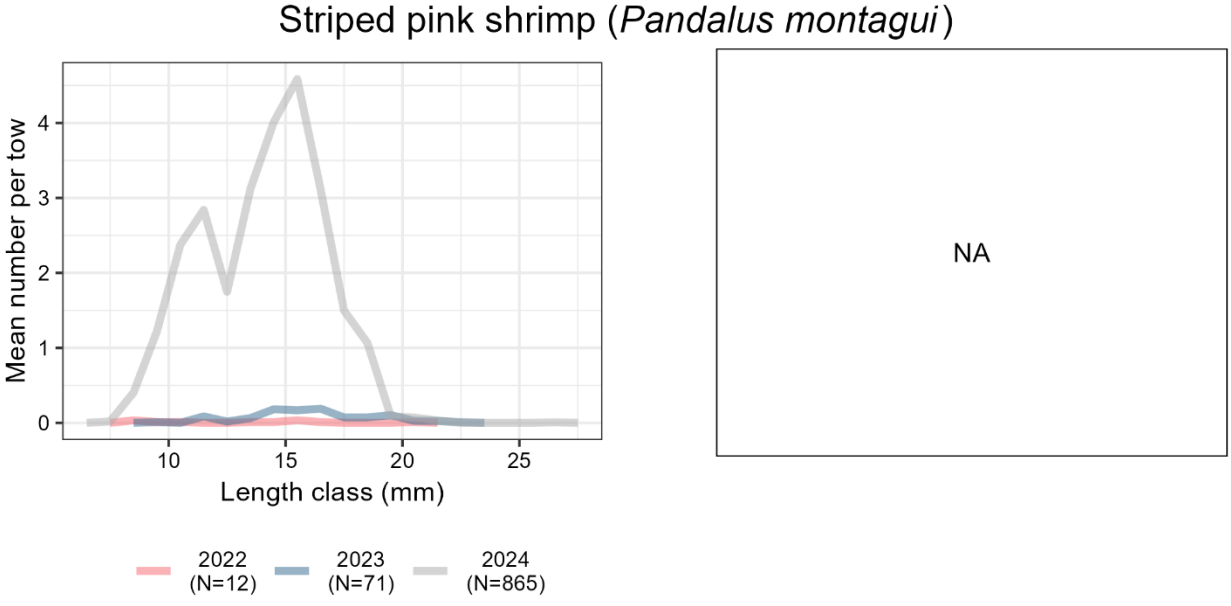


Figure 74d. Annual length frequencies (left panel) and length-weight observations with the global relationship prediction (right panel) for the striped pink shrimp *Pandalus montagui* in the winter survey in 2022, 2023 and 2024.

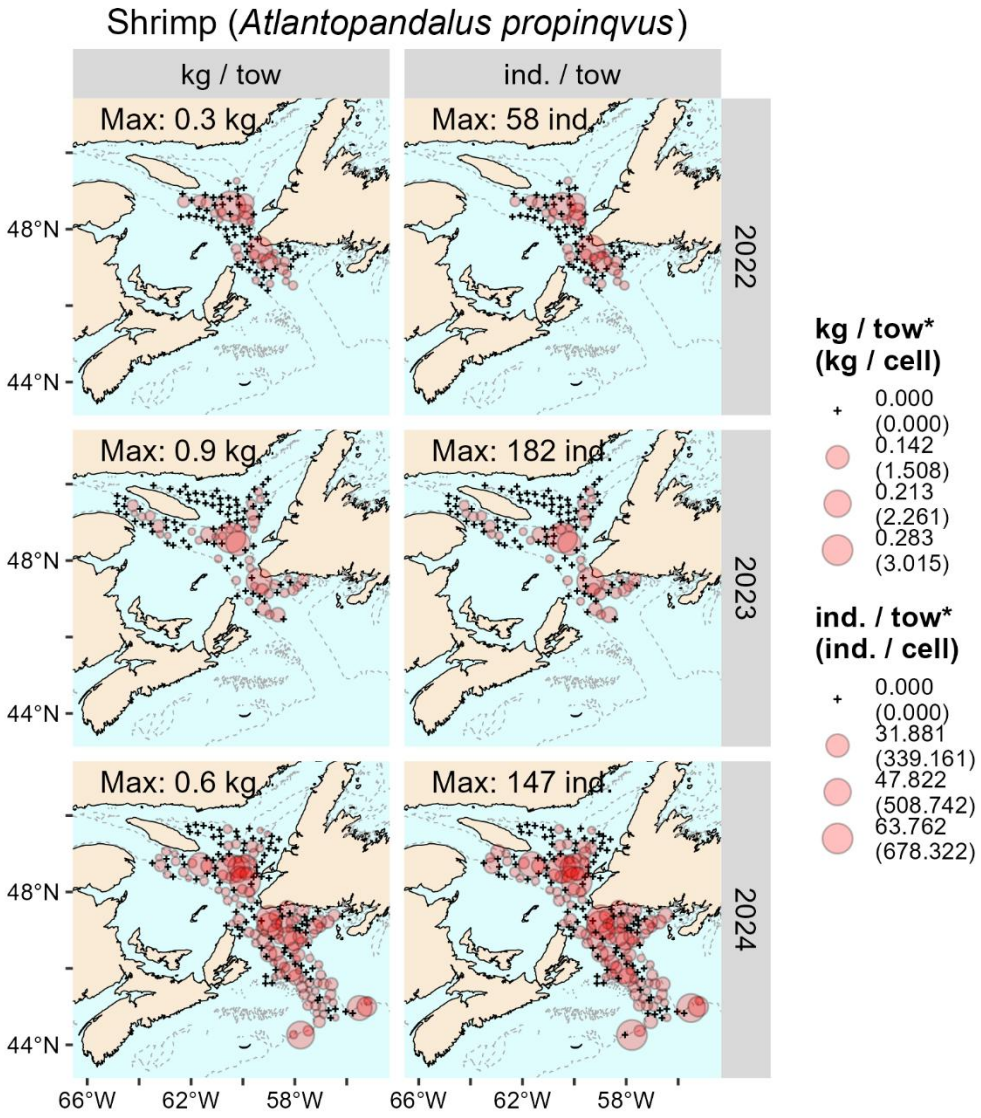


Figure 75a. Standardized catches by weight and/or number (colored bubbles) and cases of absence (black crosses) for the shrimp *Atlantopandalus propinqvus* in the winter survey in 2022, 2023 and 2024.

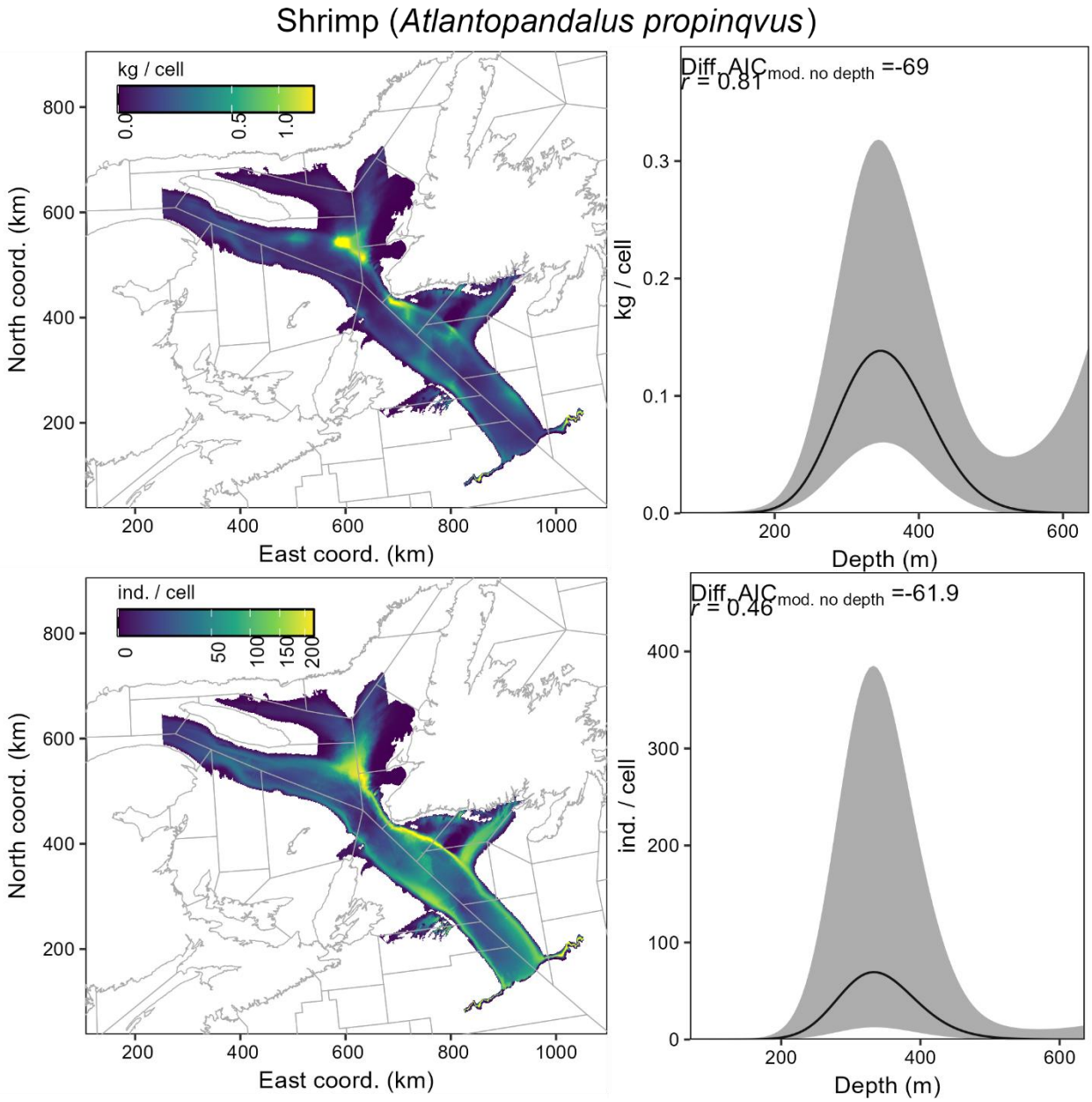


Figure 75b. Predicted weight (upper panels) and number (lower panels) values per 0.25 km^2 cell according to the selected spatial interpolation models for the shrimp *Atlantopandalus propinqvus* in the 2022, 2023, and 2024 winter survey.

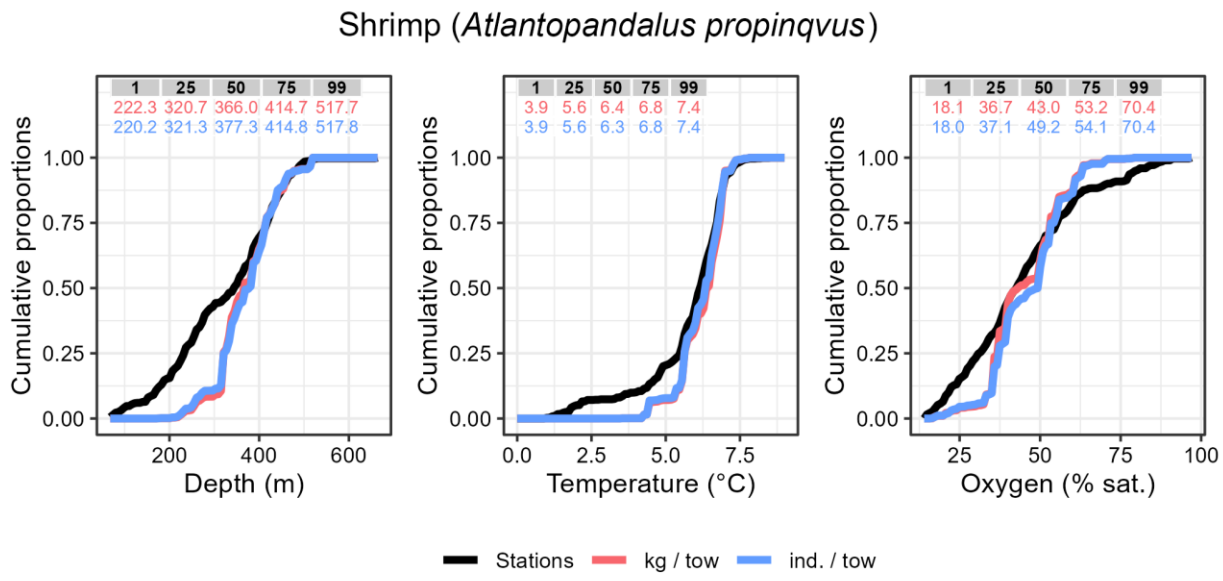


Figure 75c. Cumulative proportions of available values of depth, temperature and dissolved oxygen and standardized catches per tow for the shrimp *Atlantopandalus propinqvus* in the winter survey in 2022, 2023 and 2024.

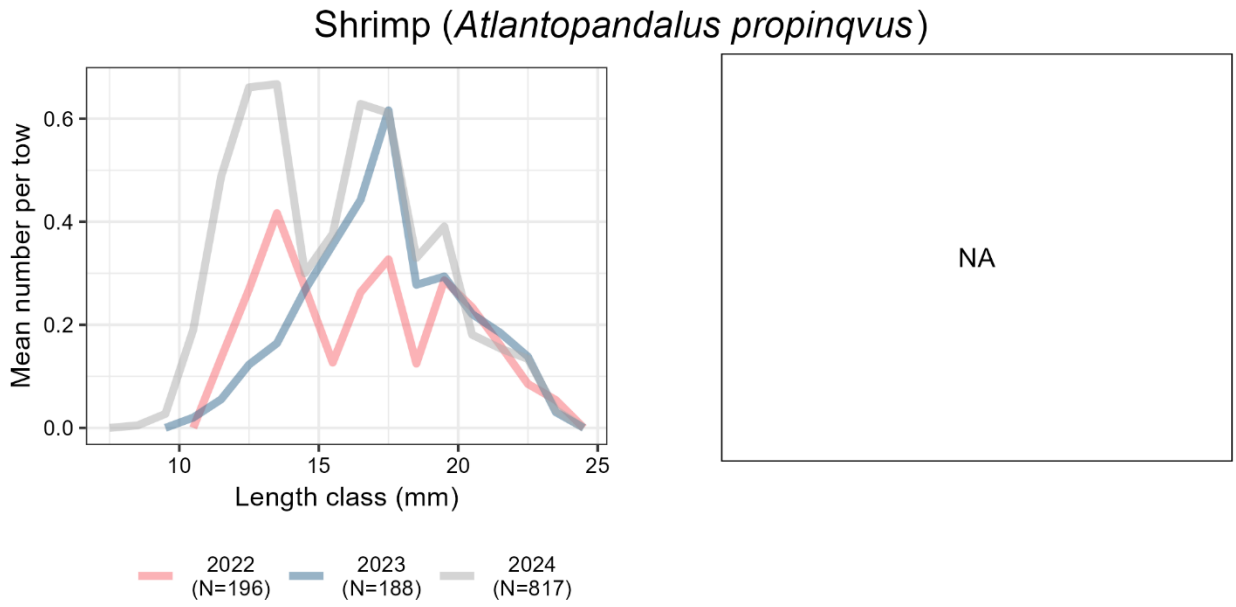


Figure 75d. Annual length frequencies (left panel) and length-weight observations with the global relationship prediction (right panel) for the shrimp *Atlantopandalus propinqvus* in the winter survey in 2022, 2023 and 2024.

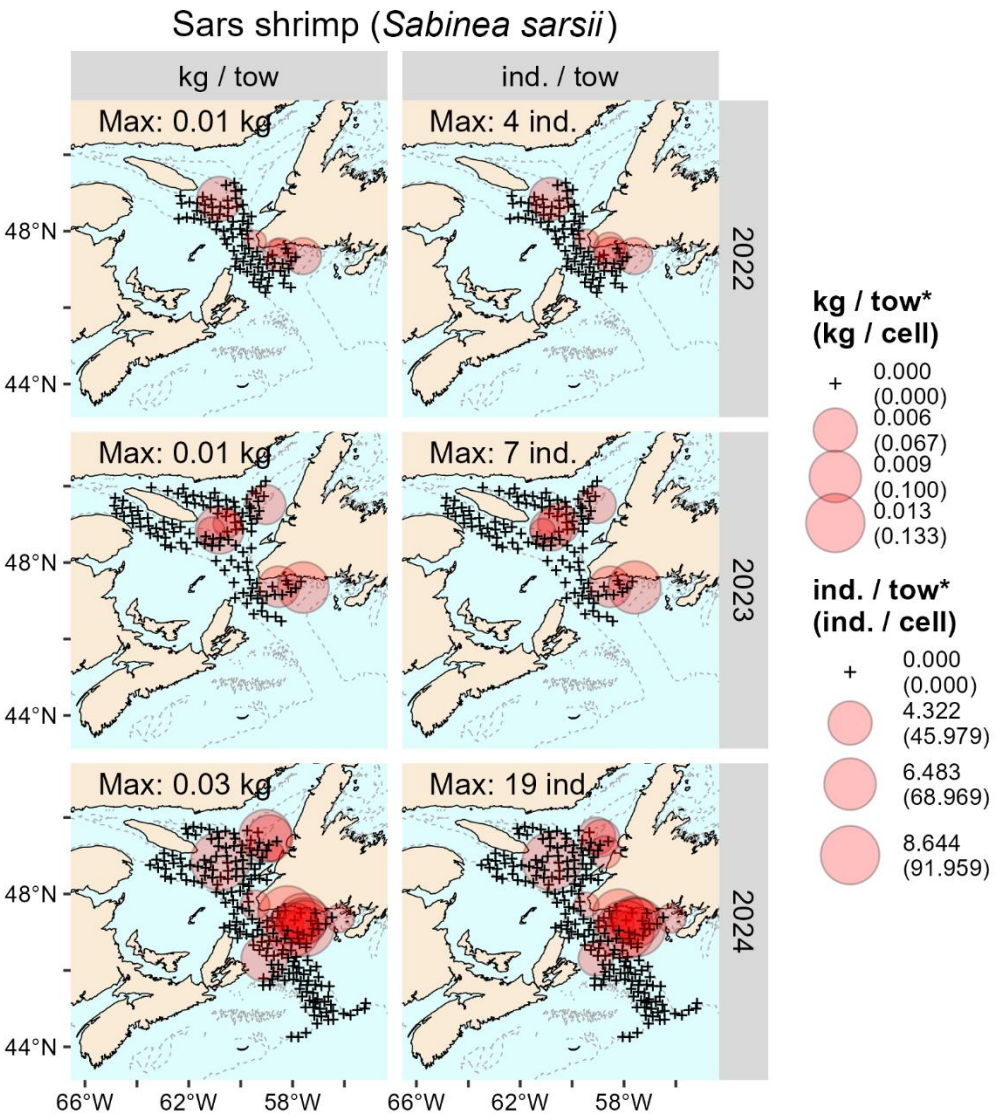


Figure 76a. Standardized catches by weight and/or number (colored bubbles) and cases of absence (black crosses) for the sars shrimp *Sabinea sarsii* in the winter survey in 2022, 2023 and 2024.

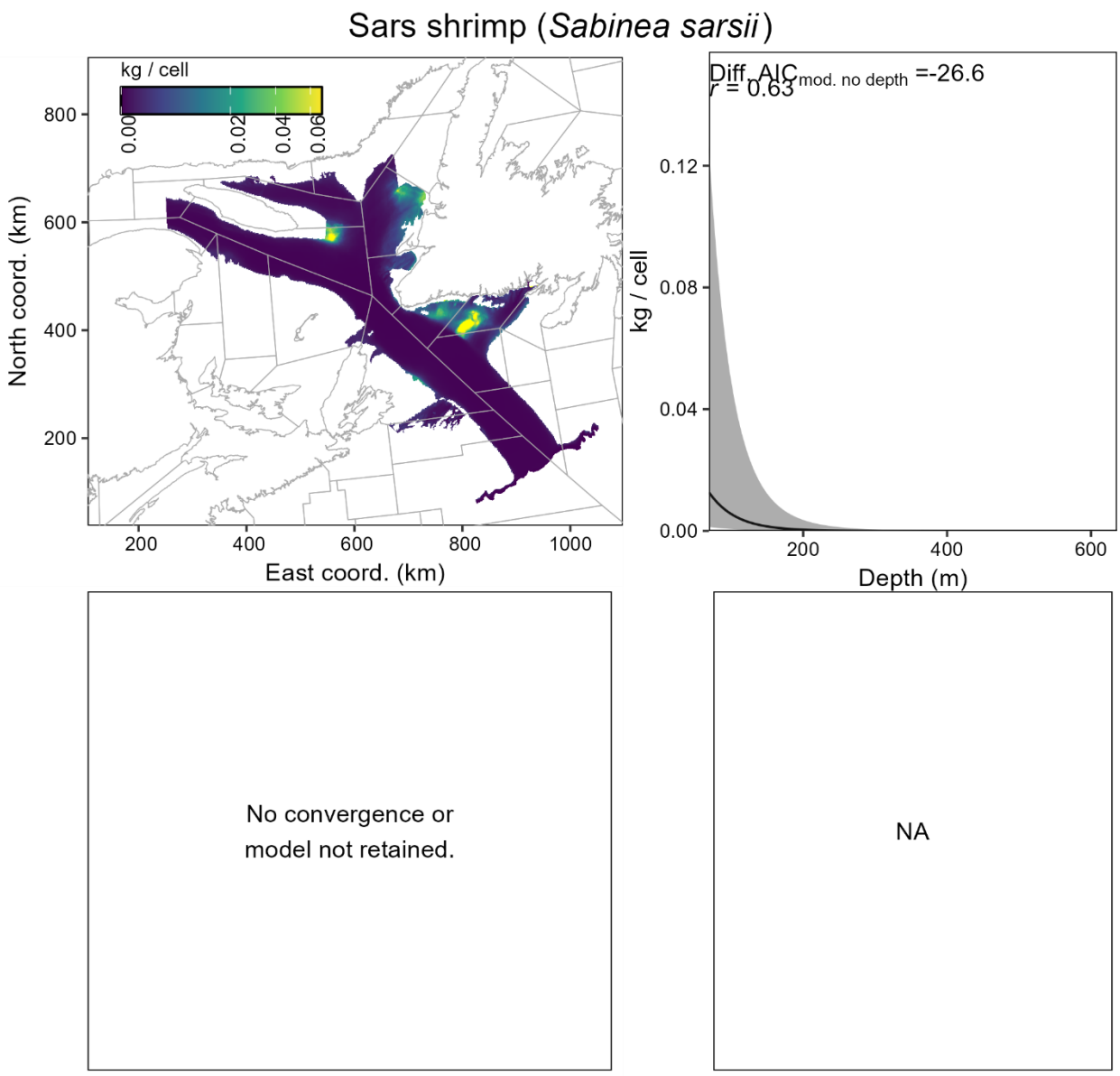


Figure 76b. Predicted weight (upper panels) and number (lower panels) values per 0.25 km^2 cell according to the selected spatial interpolation models for the sars shrimp *Sabinea sarsii* in the 2022, 2023, and 2024 winter survey.

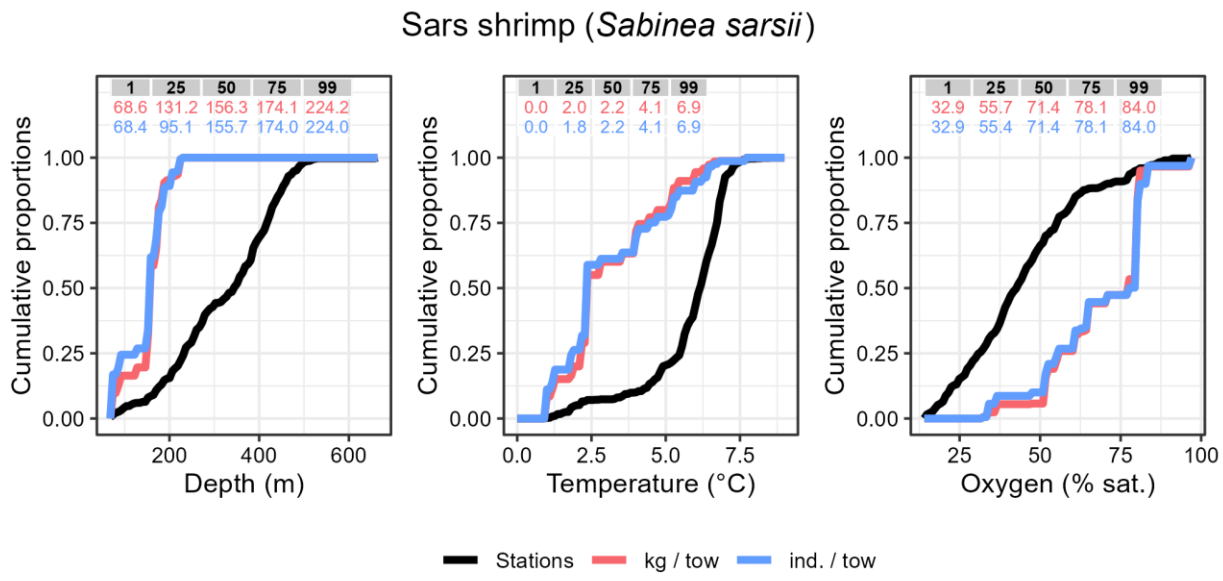


Figure 76c. Cumulative proportions of available values of depth, temperature and dissolved oxygen and standardized catches per tow for the sars shrimp *Sabinea sarsii* in the winter survey in 2022, 2023 and 2024.

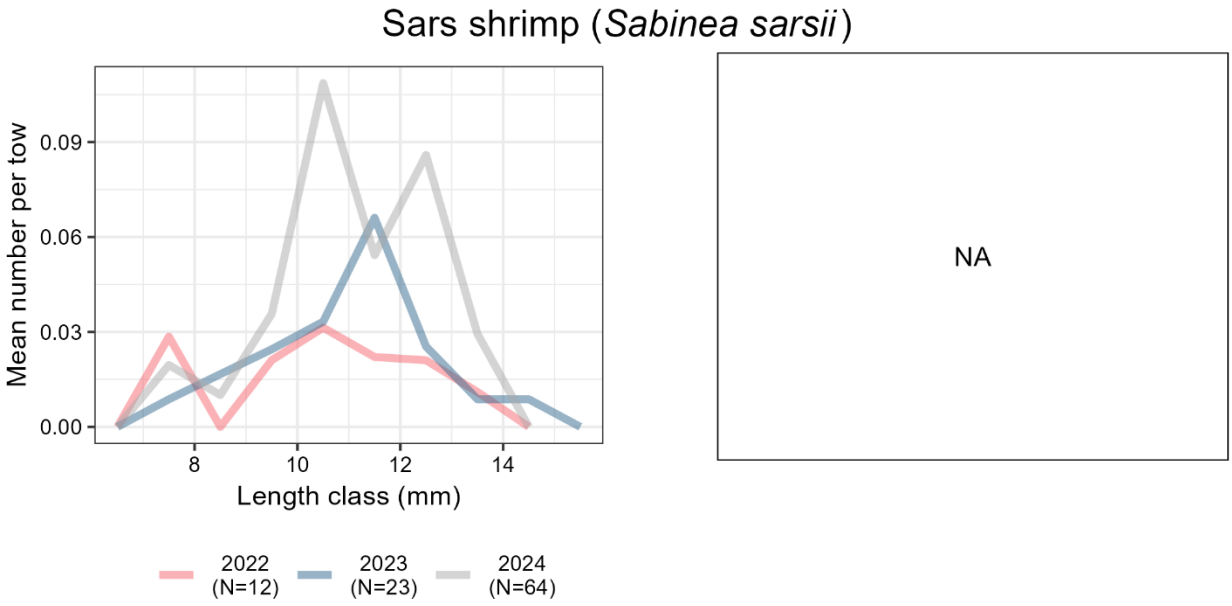


Figure 76d. Annual length frequencies (left panel) and length-weight observations with the global relationship prediction (right panel) for the sars shrimp *Sabinea sarsii* in the winter survey in 2022, 2023 and 2024.

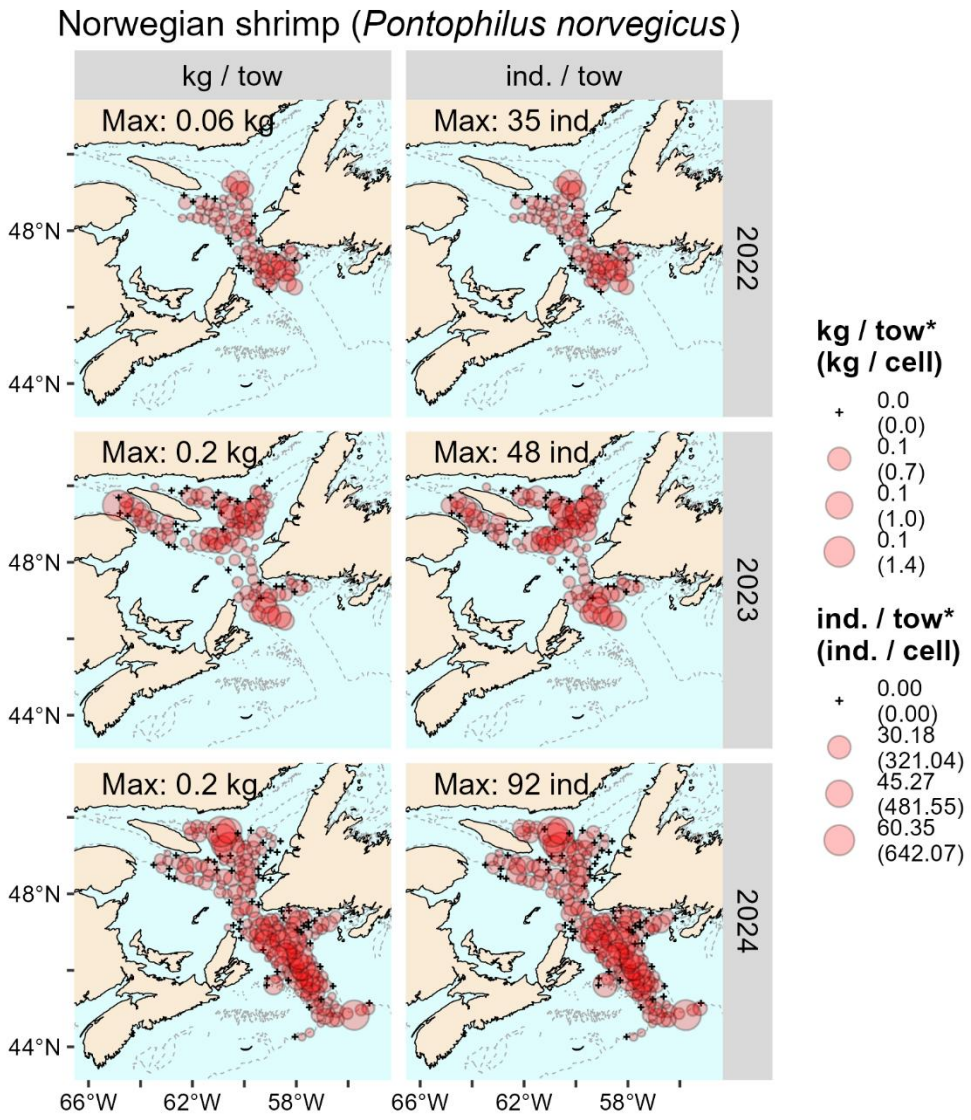


Figure 77a. Standardized catches by weight and/or number (colored bubbles) and cases of absence (black crosses) for the Norwegian shrimp *Pontophilus norvegicus* in the winter survey in 2022, 2023 and 2024.

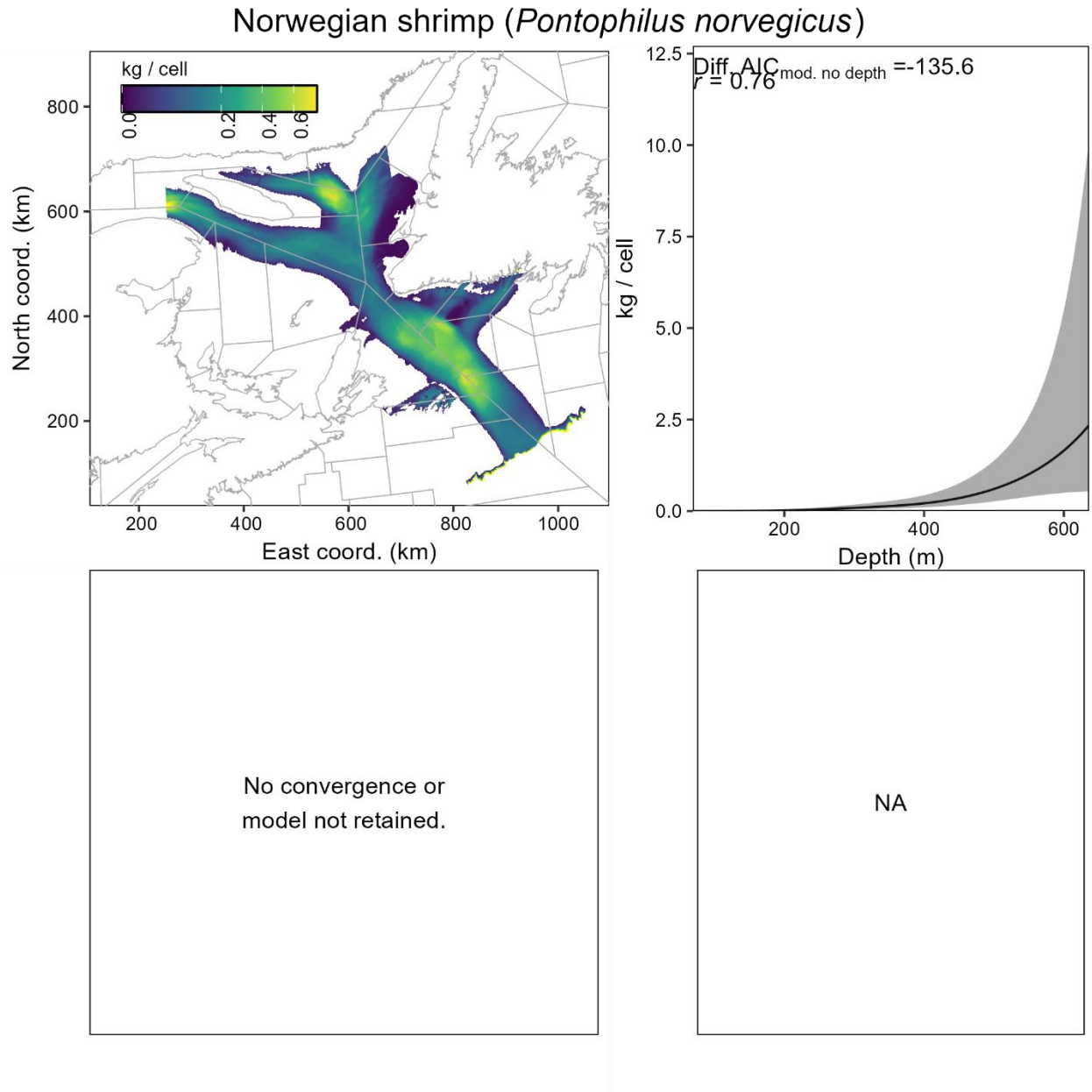


Figure 77b. Predicted weight (upper panels) and number (lower panels) values per 0.25 km^2 cell according to the selected spatial interpolation models for the Norwegian shrimp *Pontophilus norvegicus* in the 2022, 2023, and 2024 winter survey.

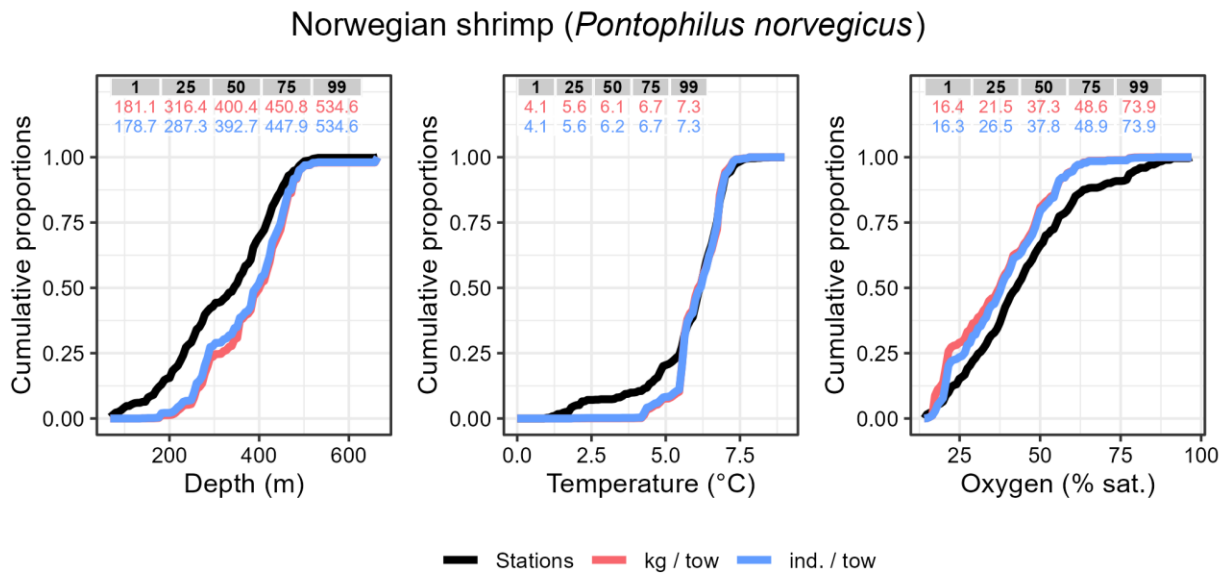


Figure 77c. Cumulative proportions of available values of depth, temperature and dissolved oxygen and standardized catches per tow for the Norwegian shrimp *Pontophilus norvegicus* in the winter survey in 2022, 2023 and 2024.

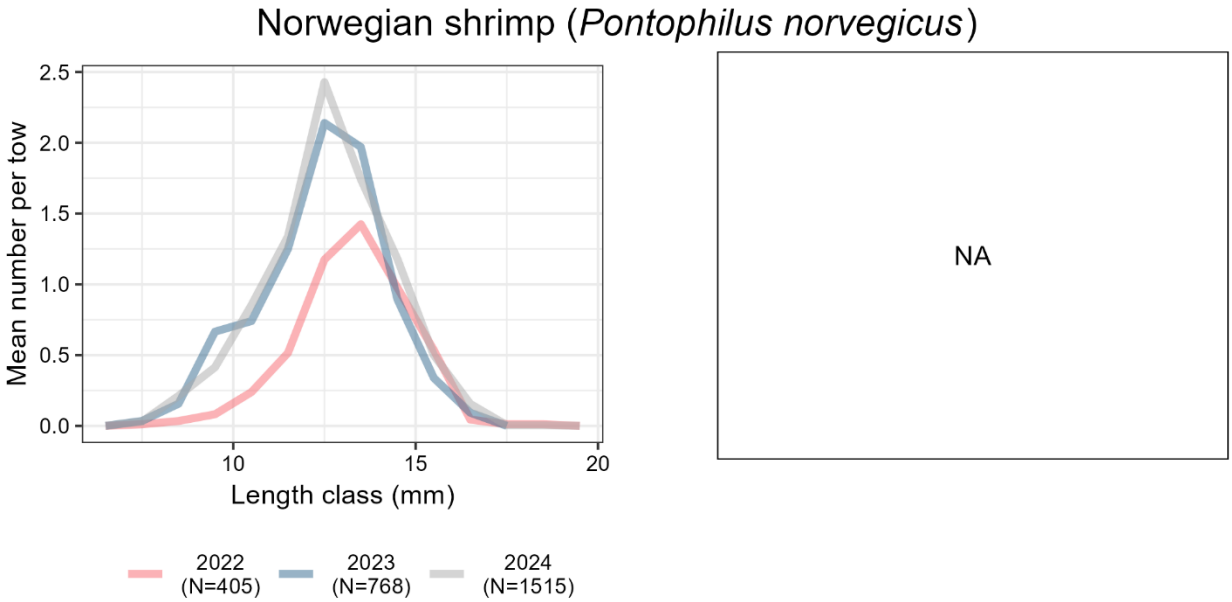


Figure 77d. Annual length frequencies (left panel) and length-weight observations with the global relationship prediction (right panel) for the Norwegian shrimp *Pontophilus norvegicus* in the winter survey in 2022, 2023 and 2024.

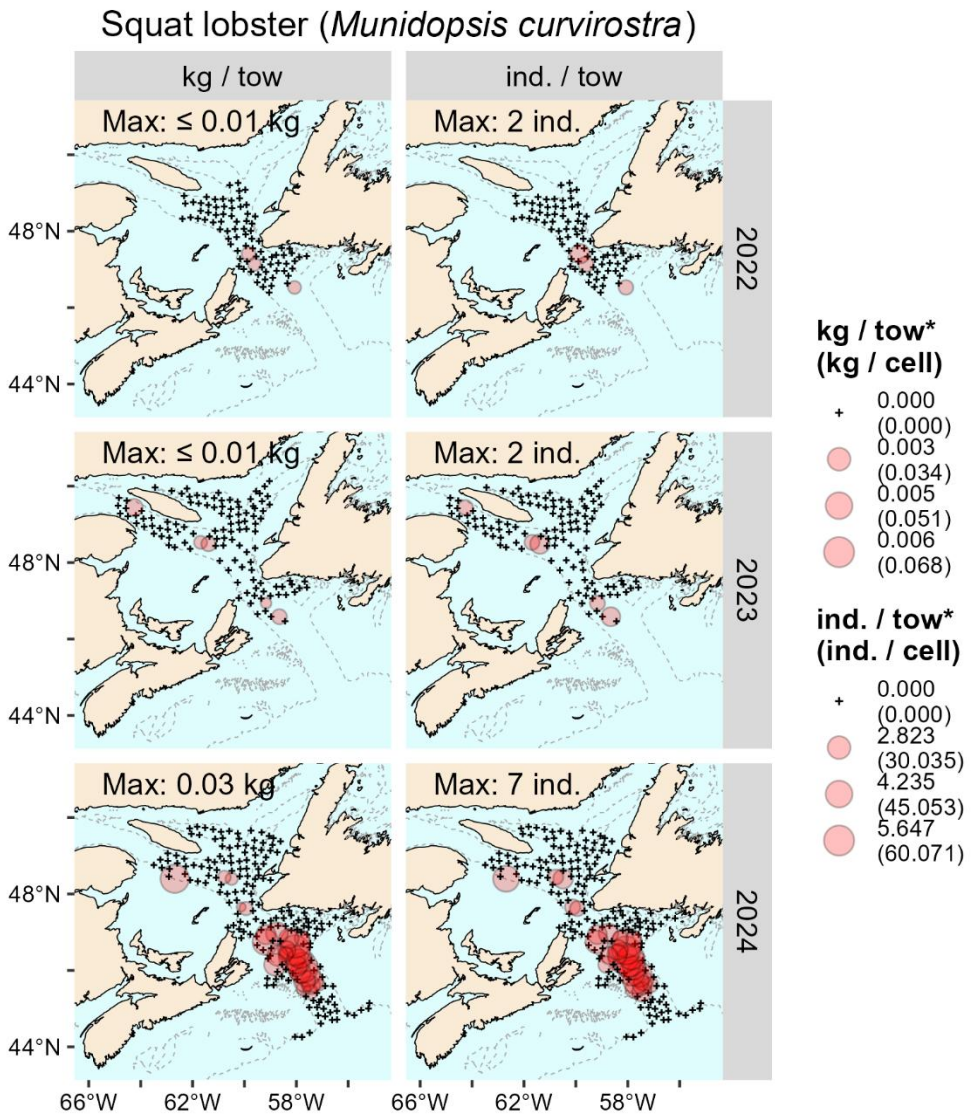


Figure 78a. Standardized catches by weight and/or number (colored bubbles) and cases of absence (black crosses) for the squat lobster in the winter survey in 2022, 2023 and 2024.

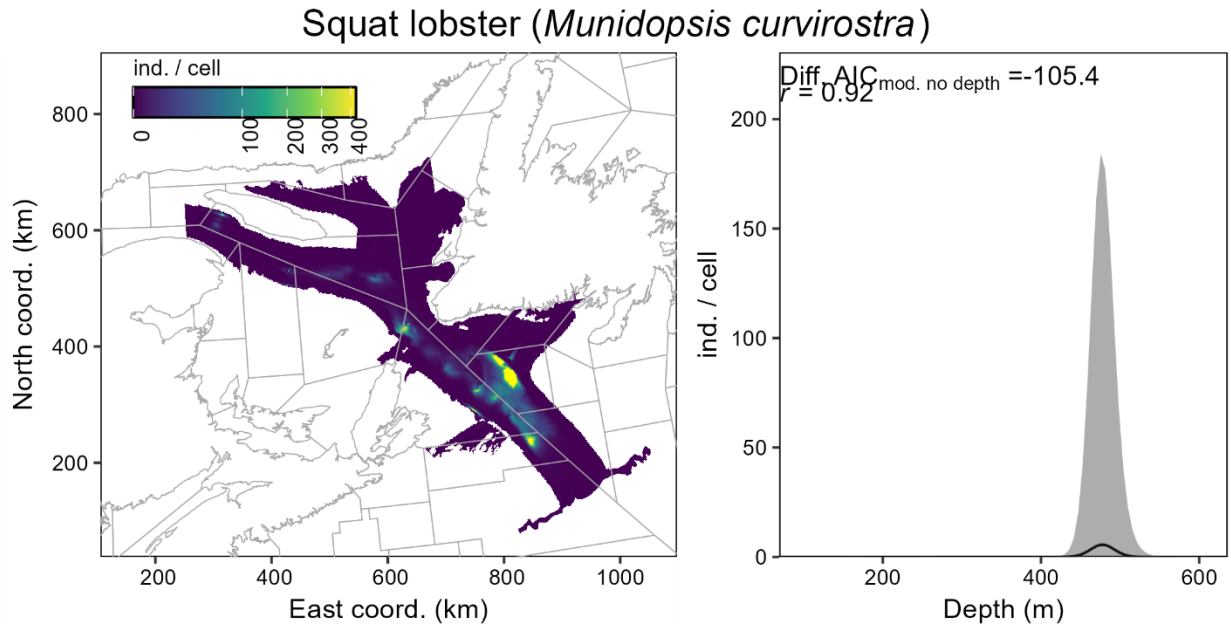


Figure 78b. Predicted number values per 0.25 km^2 cell according to the selected spatial interpolation model for the squat lobster in the 2022, 2023, and 2024 winter survey.

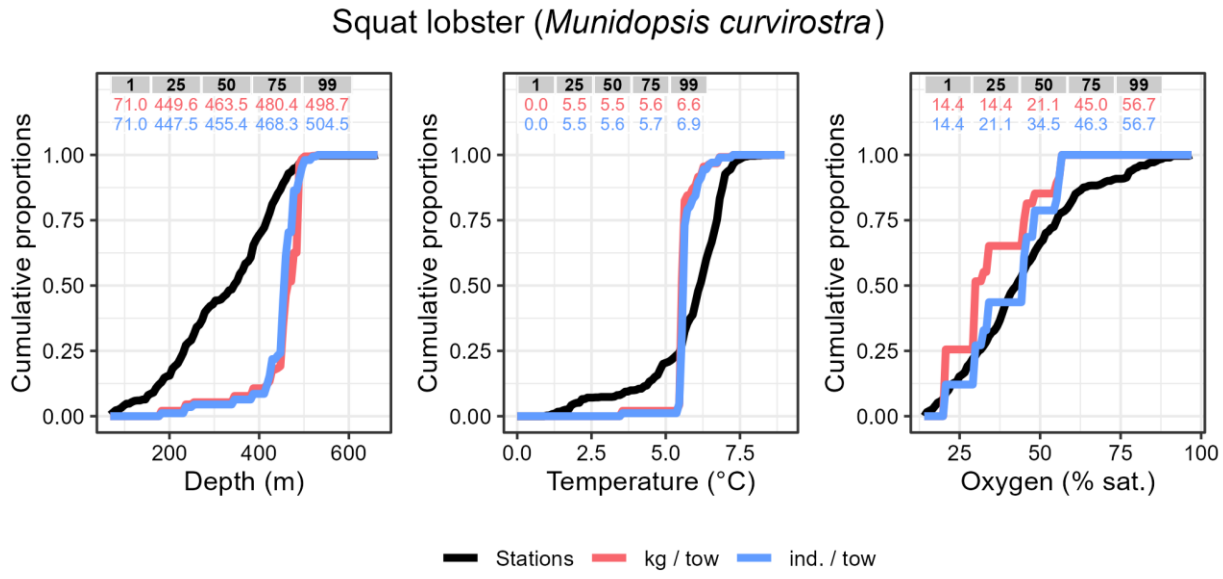


Figure 78c. Cumulative proportions of available values of depth, temperature and dissolved oxygen and standardized catches per tow for the squat lobster in the winter survey in 2022, 2023 and 2024.

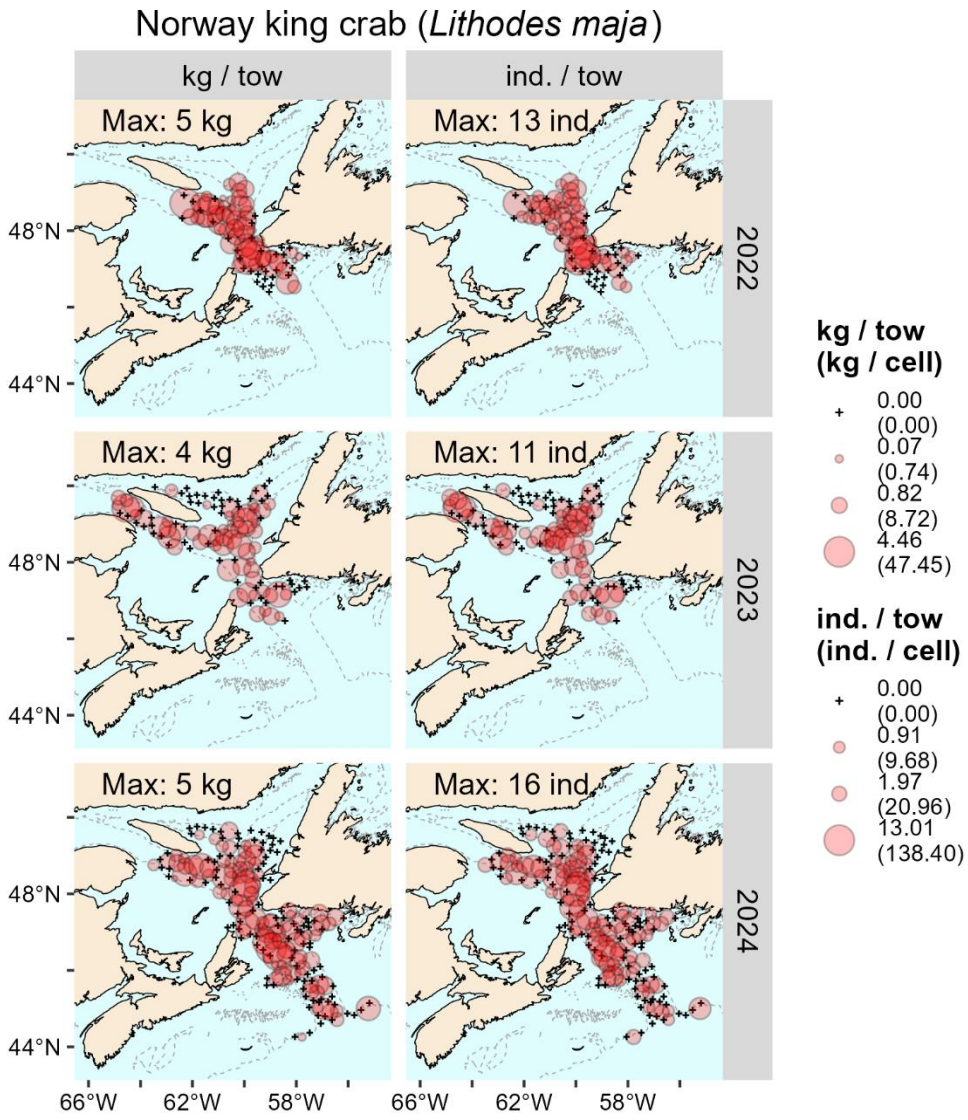


Figure 79a. Standardized catches by weight and/or number (colored bubbles) and cases of absence (black crosses) for the Norway king crab in the winter survey in 2022, 2023 and 2024.

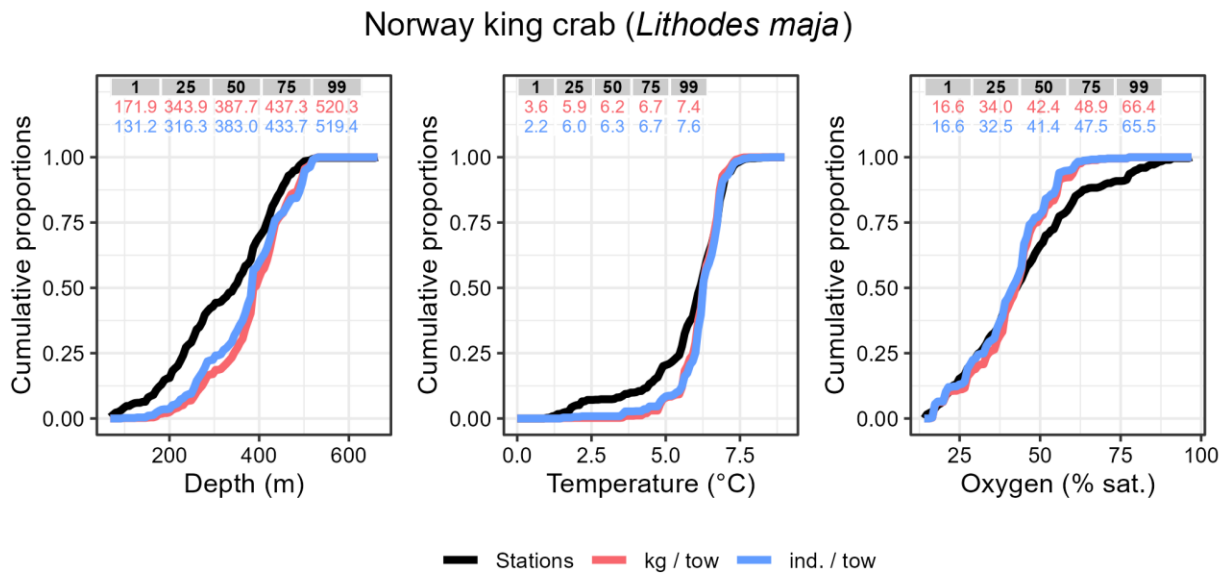


Figure 79b. Cumulative proportions of available values of depth, temperature and dissolved oxygen and standardized catches per tow for the Norway king crab in the winter survey in 2022, 2023 and 2024.

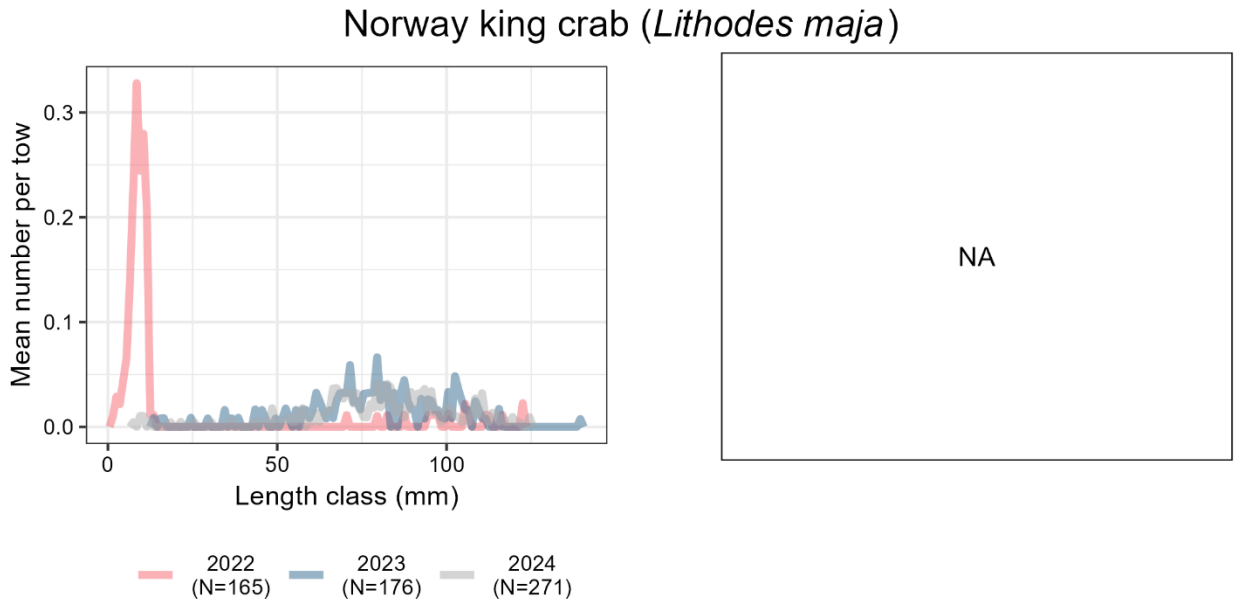


Figure 79c. Annual length frequencies (left panel) and length-weight observations with the global relationship prediction (right panel) for the Norway king crab in the winter survey in 2022, 2023 and 2024.

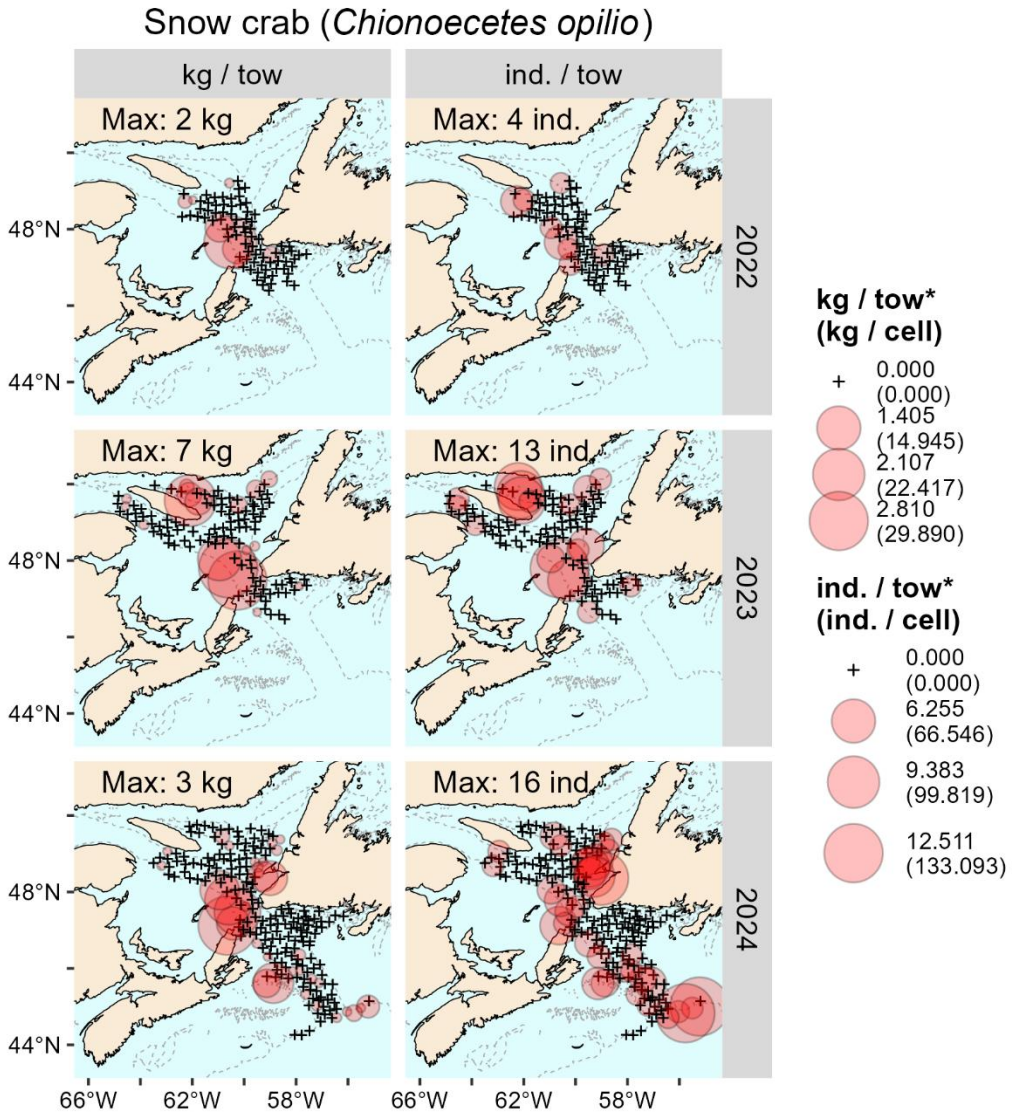


Figure 80a. Standardized catches by weight and/or number (colored bubbles) and cases of absence (black crosses) for the snow crab in the winter survey in 2022, 2023 and 2024.

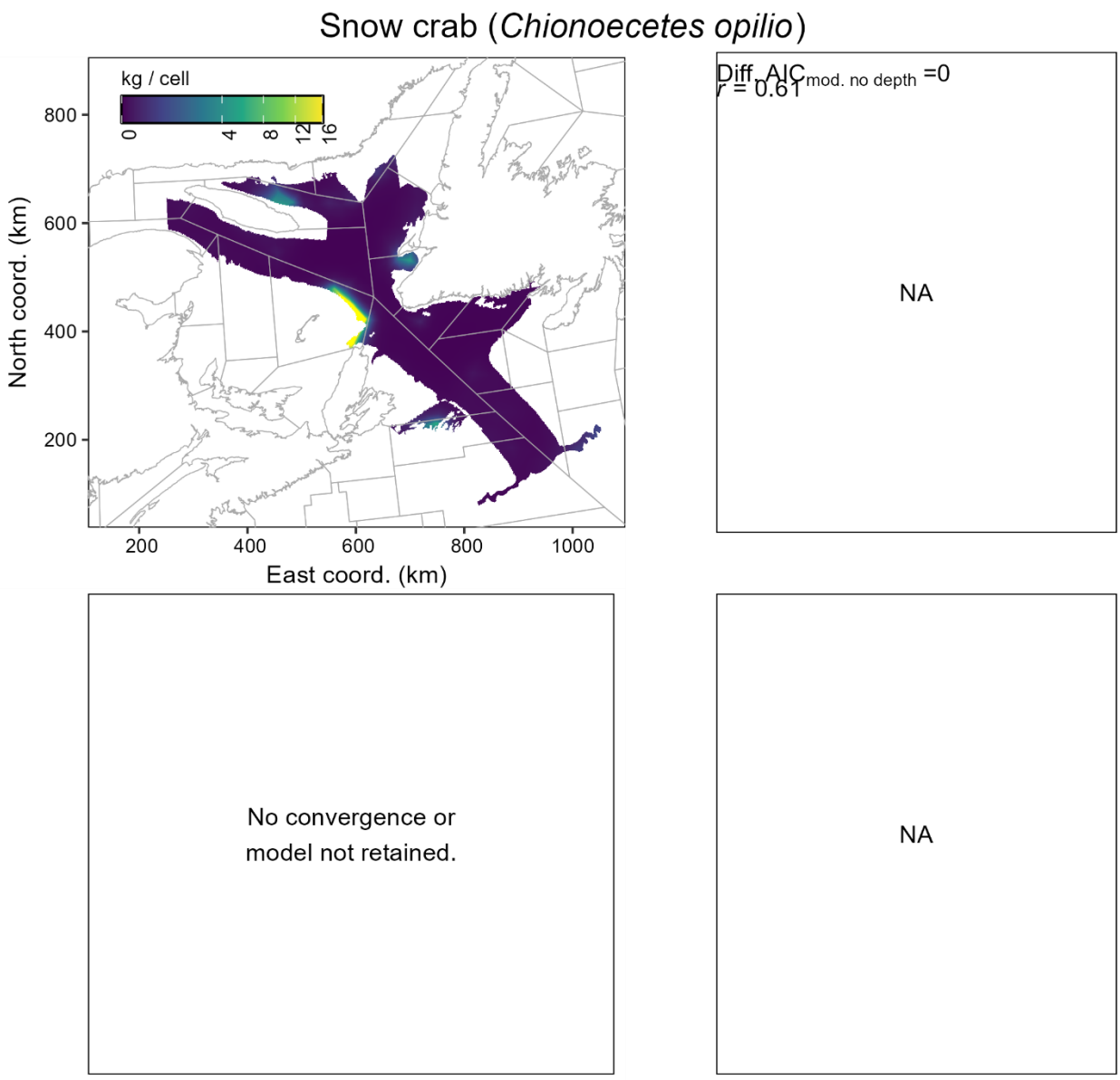


Figure 80b. Predicted weight (upper panels) and number (lower panels) values per 0.25 km^2 cell according to the selected spatial interpolation models for the snow crab in the 2022, 2023, and 2024 winter survey.

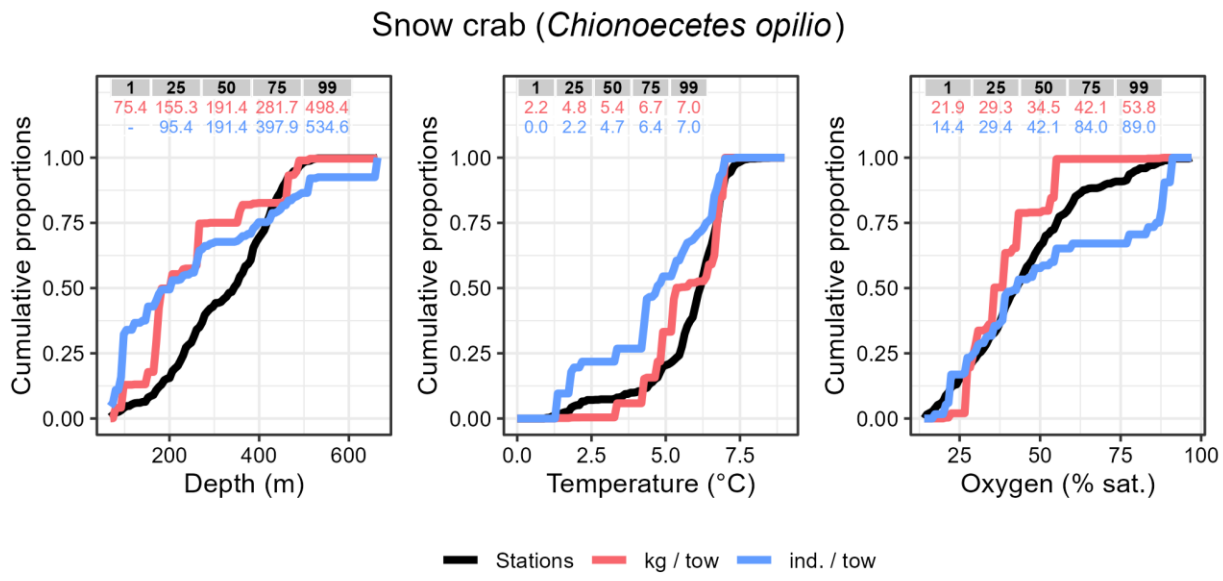


Figure 80c. Cumulative proportions of available values of depth, temperature and dissolved oxygen and standardized catches per tow for the snow crab in the winter survey in 2022, 2023 and 2024.

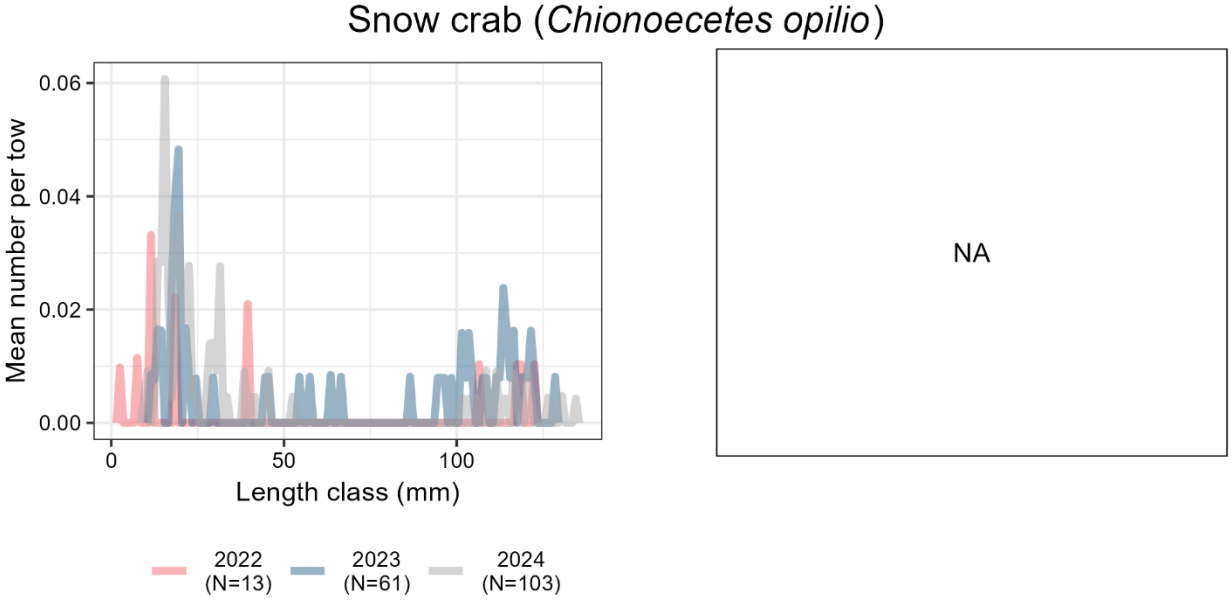


Figure 80d. Annual length frequencies (left panel) and length-weight observations with the global relationship prediction (right panel) for the snow crab in the winter survey in 2022, 2023 and 2024.

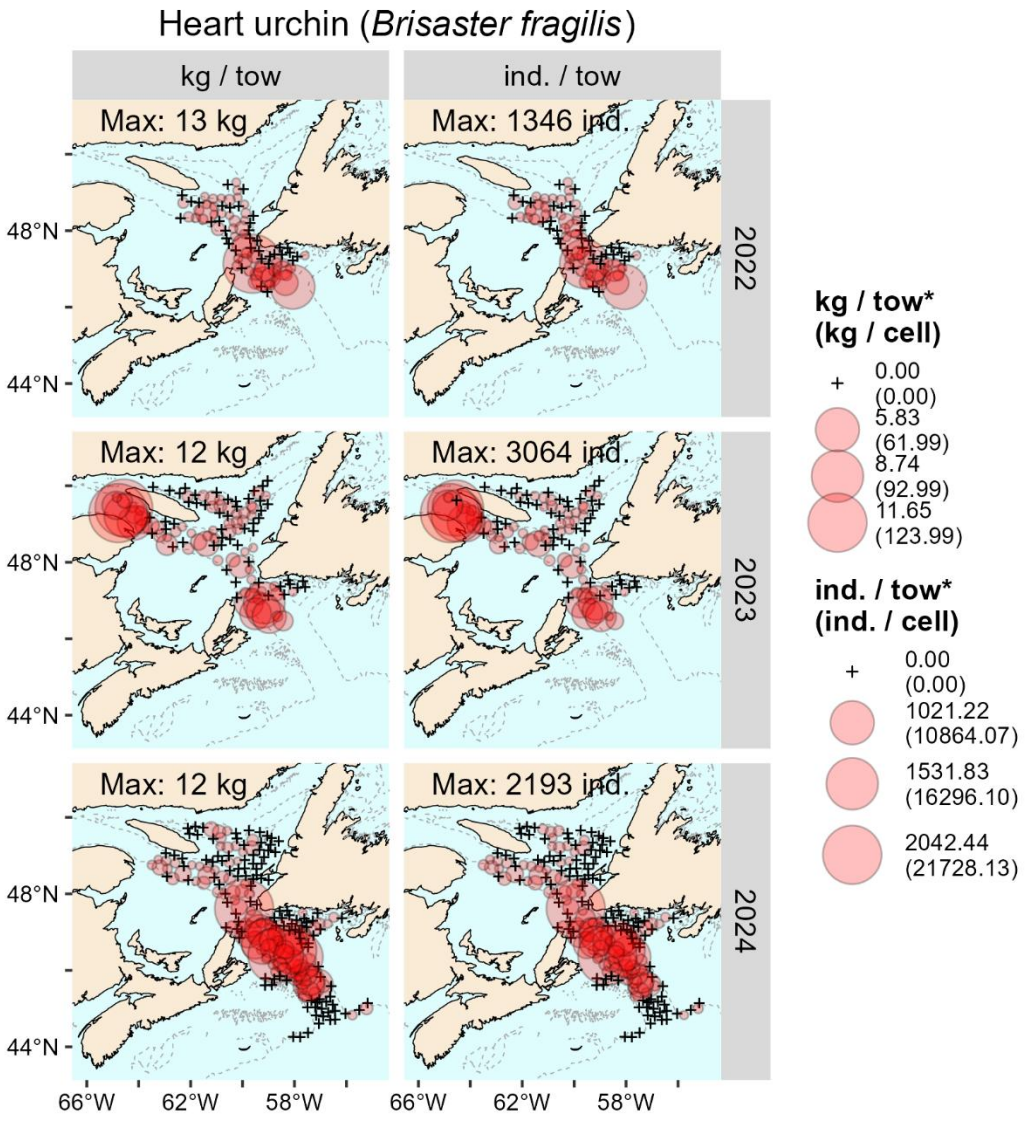


Figure 81a. Standardized catches by weight and/or number (colored bubbles) and cases of absence (black crosses) for the heart urchin in the winter survey in 2022, 2023 and 2024.

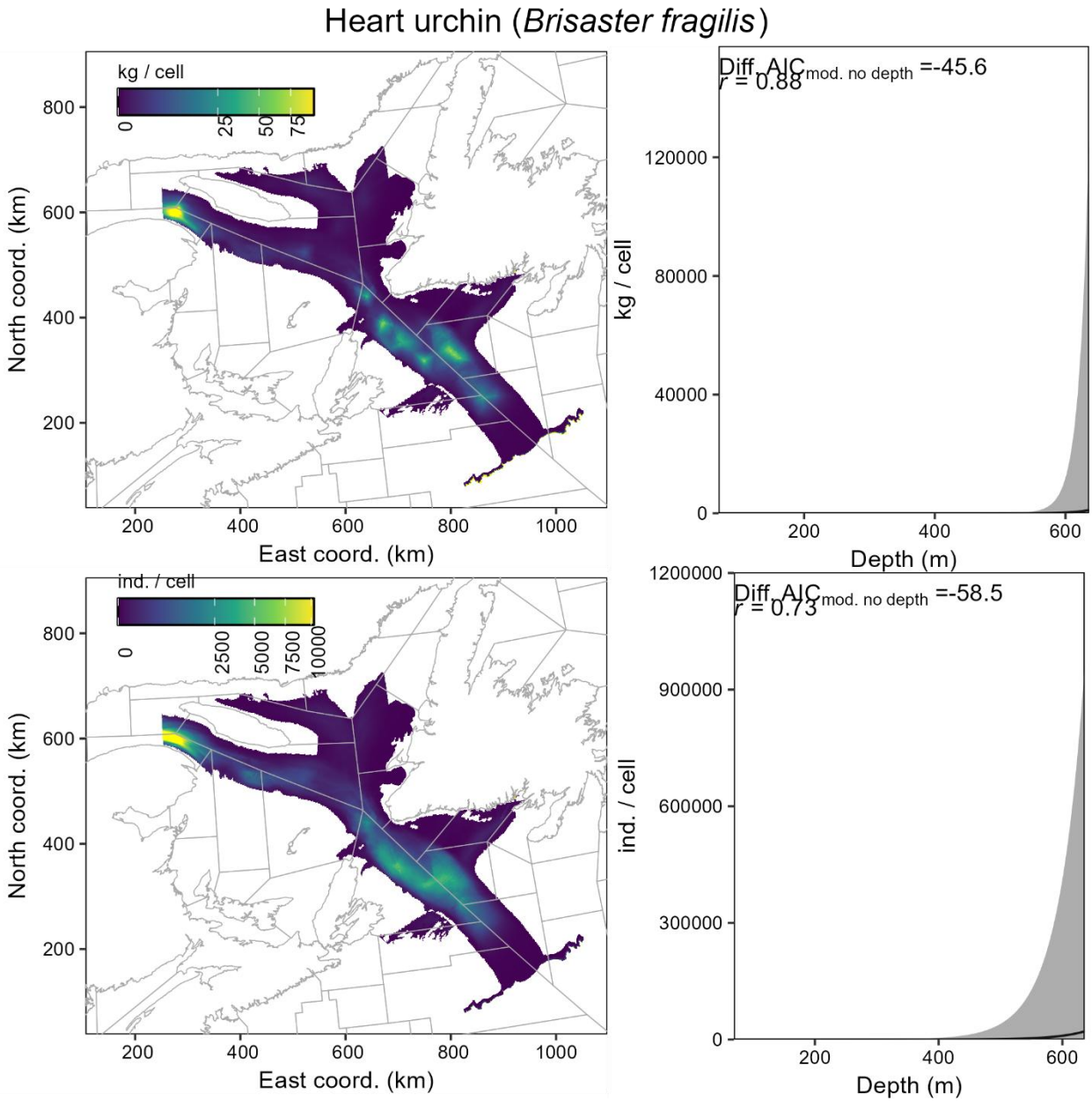


Figure 81b. Predicted weight (upper panels) and number (lower panels) values per 0.25 km^2 cell according to the selected spatial interpolation models for the heart urchin in the 2022, 2023, and 2024 winter survey.

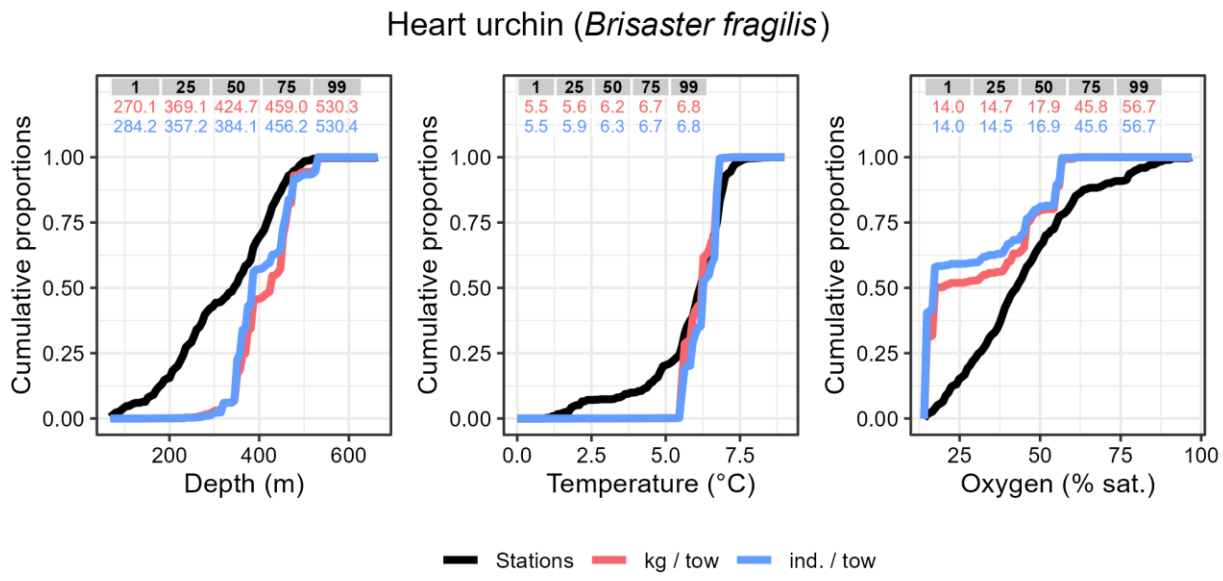


Figure 81c. Cumulative proportions of available values of depth, temperature and dissolved oxygen and standardized catches per tow for the heart urchin in the winter survey in 2022, 2023 and 2024.

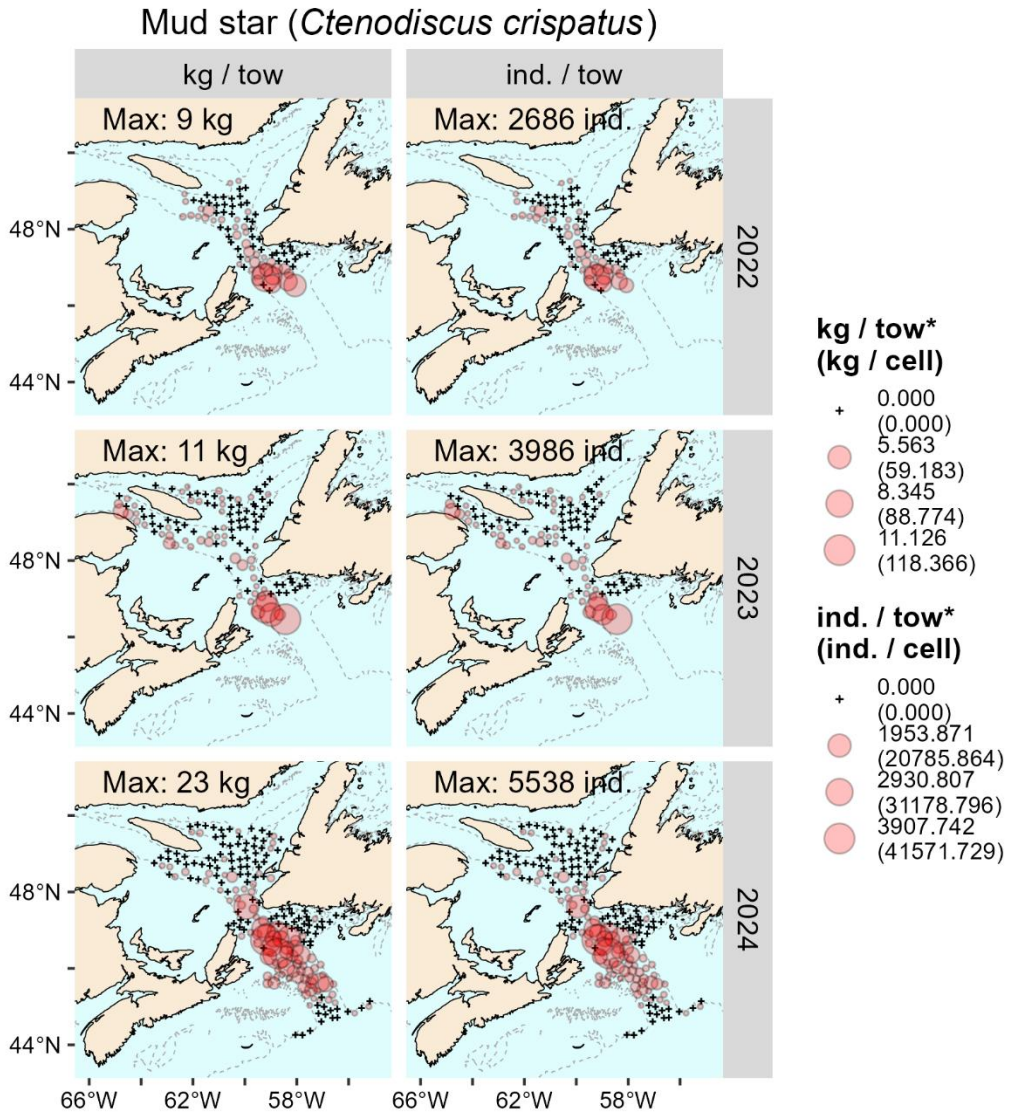


Figure 82a. Standardized catches by weight and/or number (colored bubbles) and cases of absence (black crosses) for the mud star in the winter survey in 2022, 2023 and 2024.

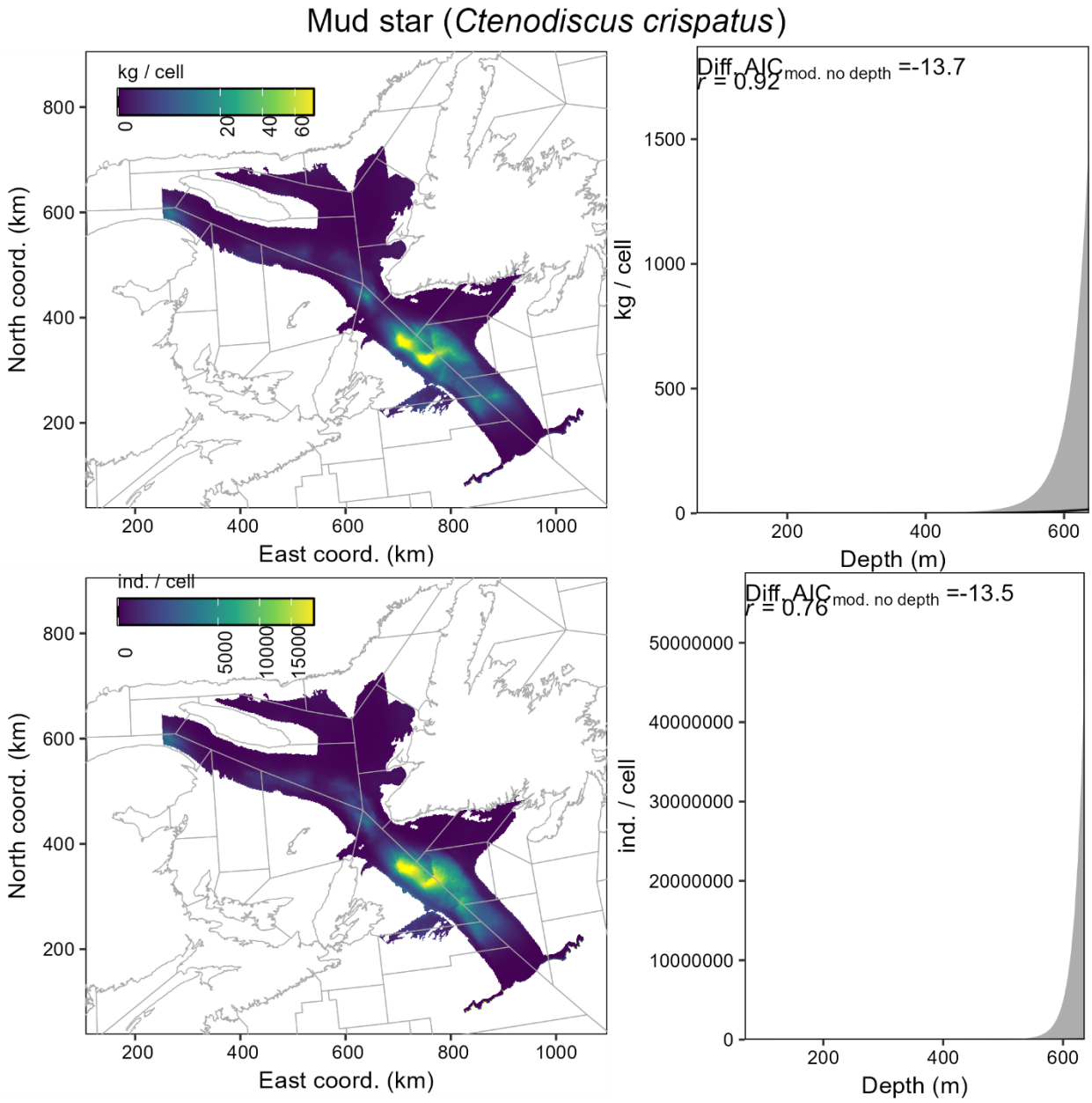


Figure 82b. Predicted weight (upper panels) and number (lower panels) values per 0.25 km^2 cell according to the selected spatial interpolation models for the mud star in the 2022, 2023, and 2024 winter survey.

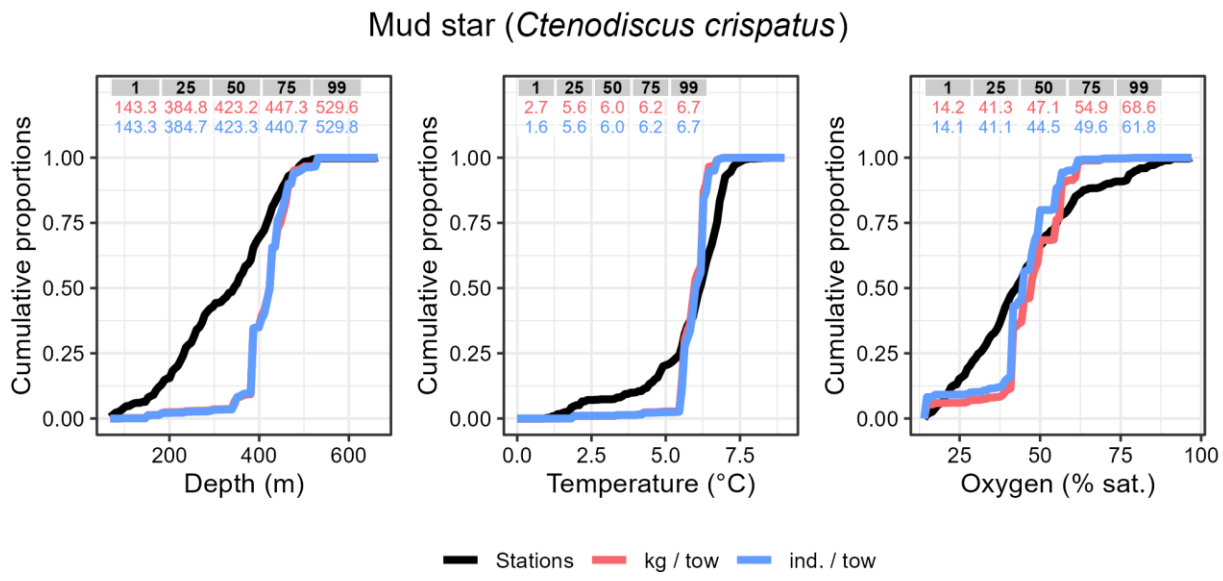


Figure 82c. Cumulative proportions of available values of depth, temperature and dissolved oxygen and standardized catches per tow for the mud star in the winter survey in 2022, 2023 and 2024.

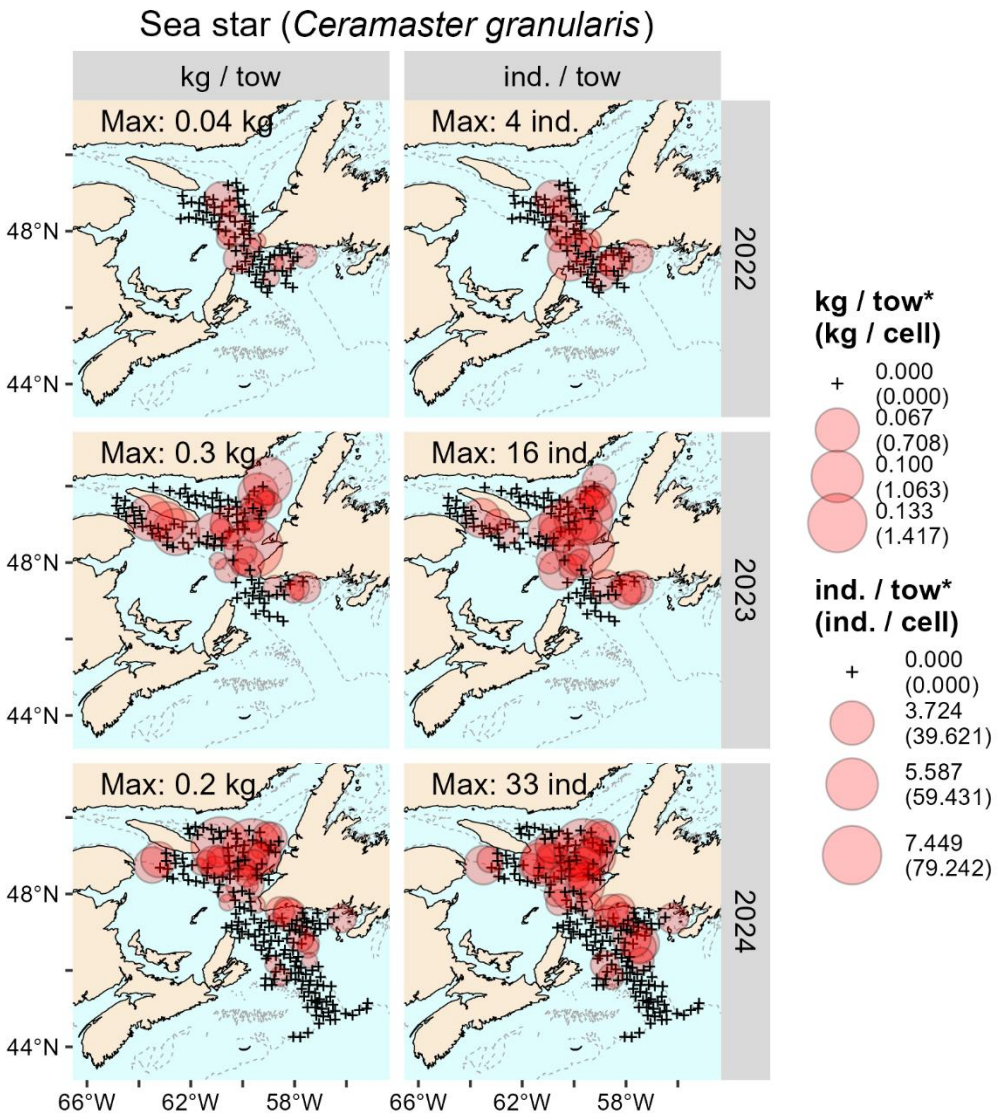


Figure 83a. Standardized catches by weight and/or number (colored bubbles) and cases of absence (black crosses) for the sea star *Ceramaster granularis* in the winter survey in 2022, 2023 and 2024.

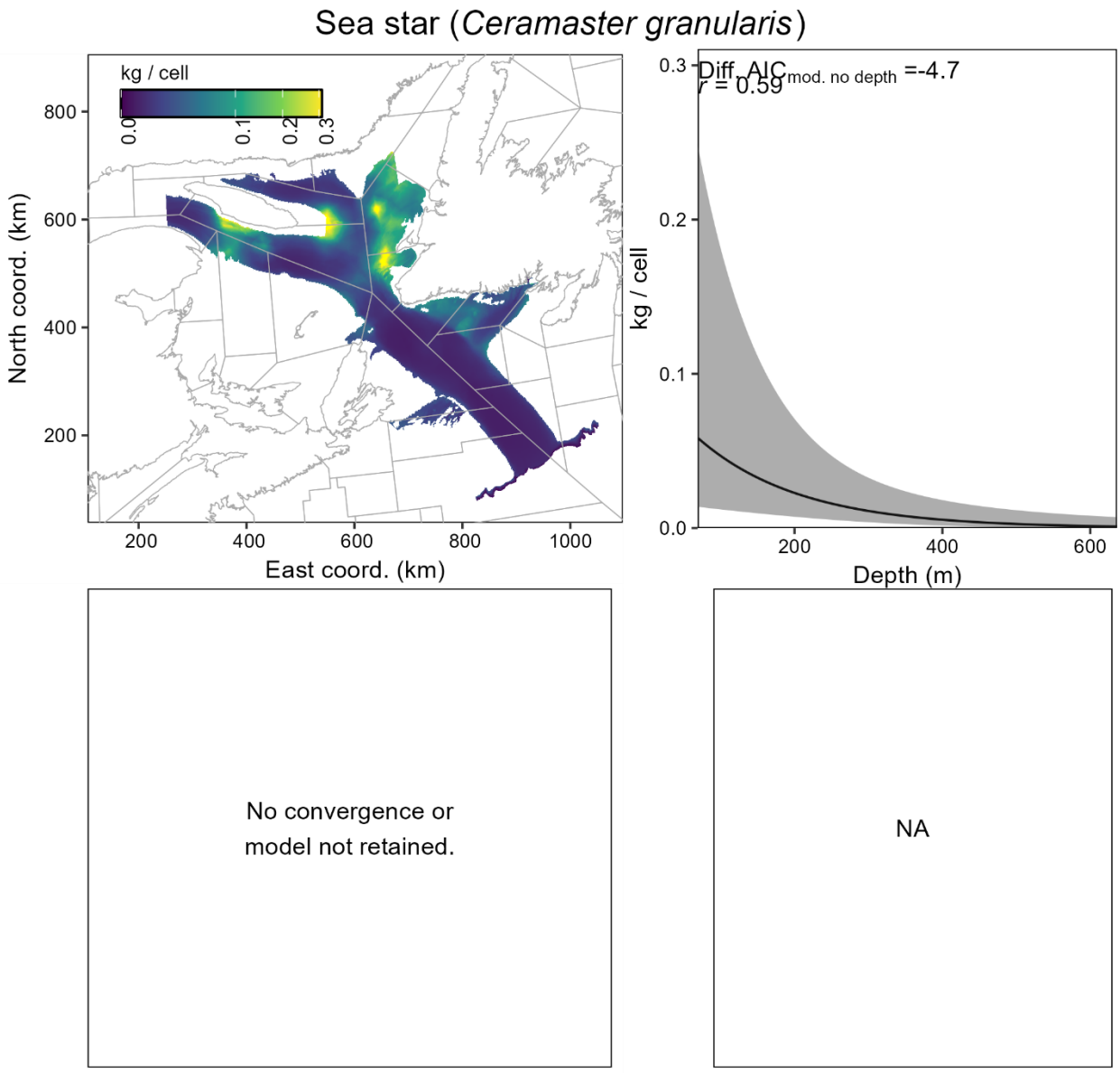


Figure 83b. Predicted weight (upper panels) and number (lower panels) values per 0.25 km^2 cell according to the selected spatial interpolation models for the sea star *Ceramaster granularis* in the 2022, 2023, and 2024 winter survey.

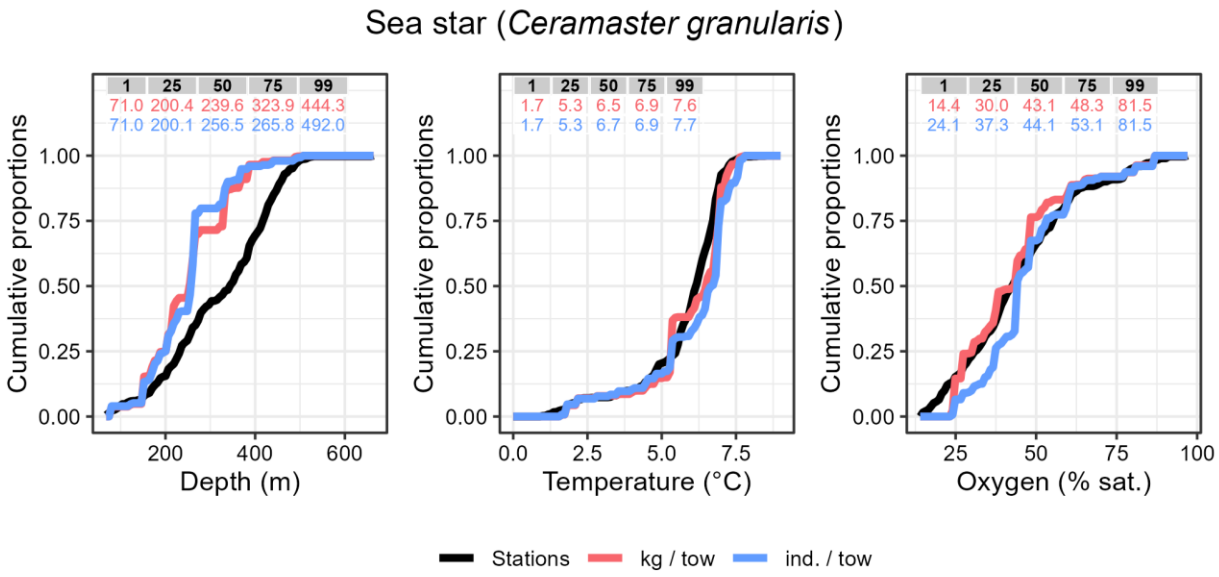


Figure 83c. Cumulative proportions of available values of depth, temperature and dissolved oxygen and standardized catches per tow for the sea star *Ceramaster granularis* in the winter survey in 2022, 2023 and 2024.

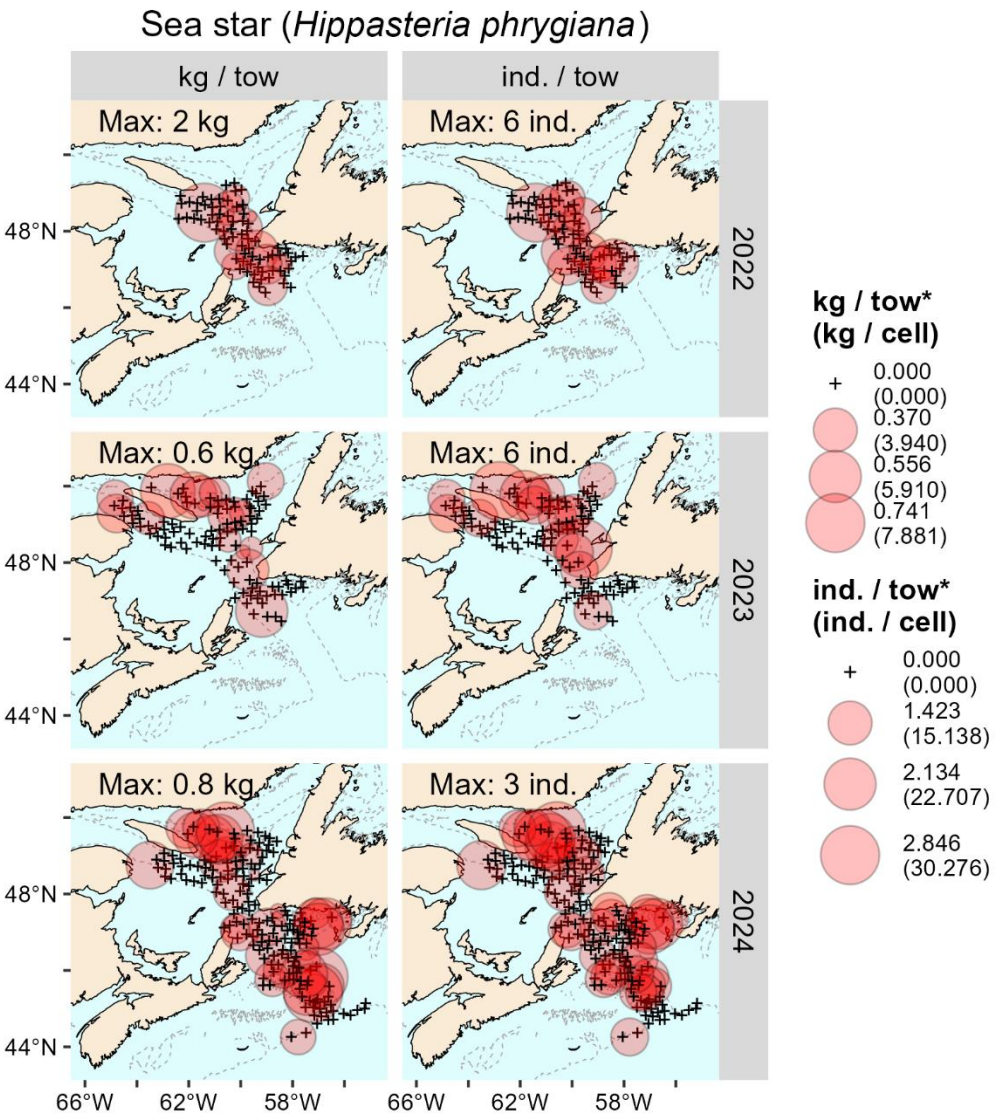


Figure 84a. Standardized catches by weight and/or number (colored bubbles) and cases of absence (black crosses) for the sea star *Hippasteria phrygiana* in the winter survey in 2022, 2023 and 2024.

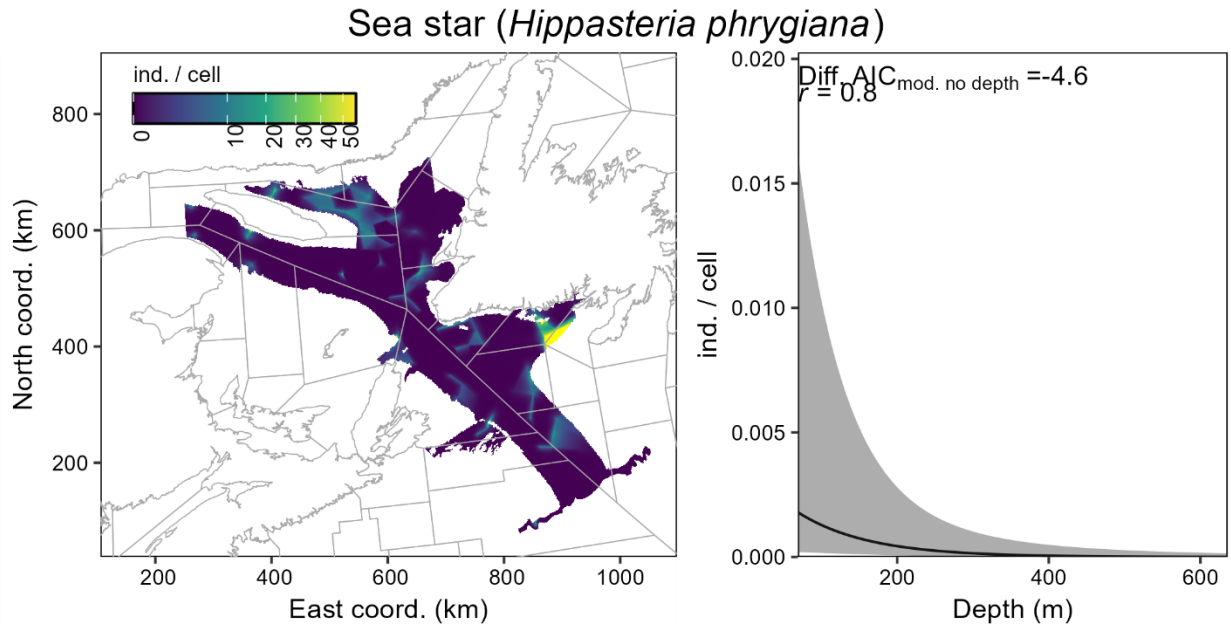


Figure 84b. Predicted number values per 0.25 km^2 cell according to the selected spatial interpolation model for the sea star *Hippasteria phrygiana* in the 2022, 2023, and 2024 winter survey.

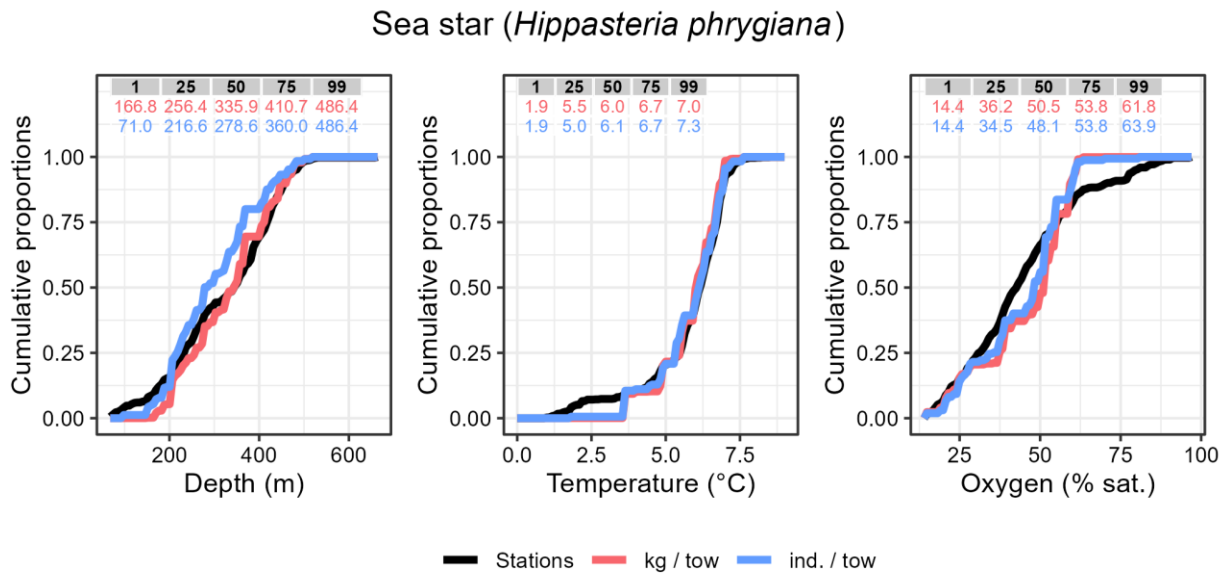


Figure 84c. Cumulative proportions of available values of depth, temperature and dissolved oxygen and standardized catches per tow for the sea star *Hippasteria phrygiana* in the winter survey in 2022, 2023 and 2024.

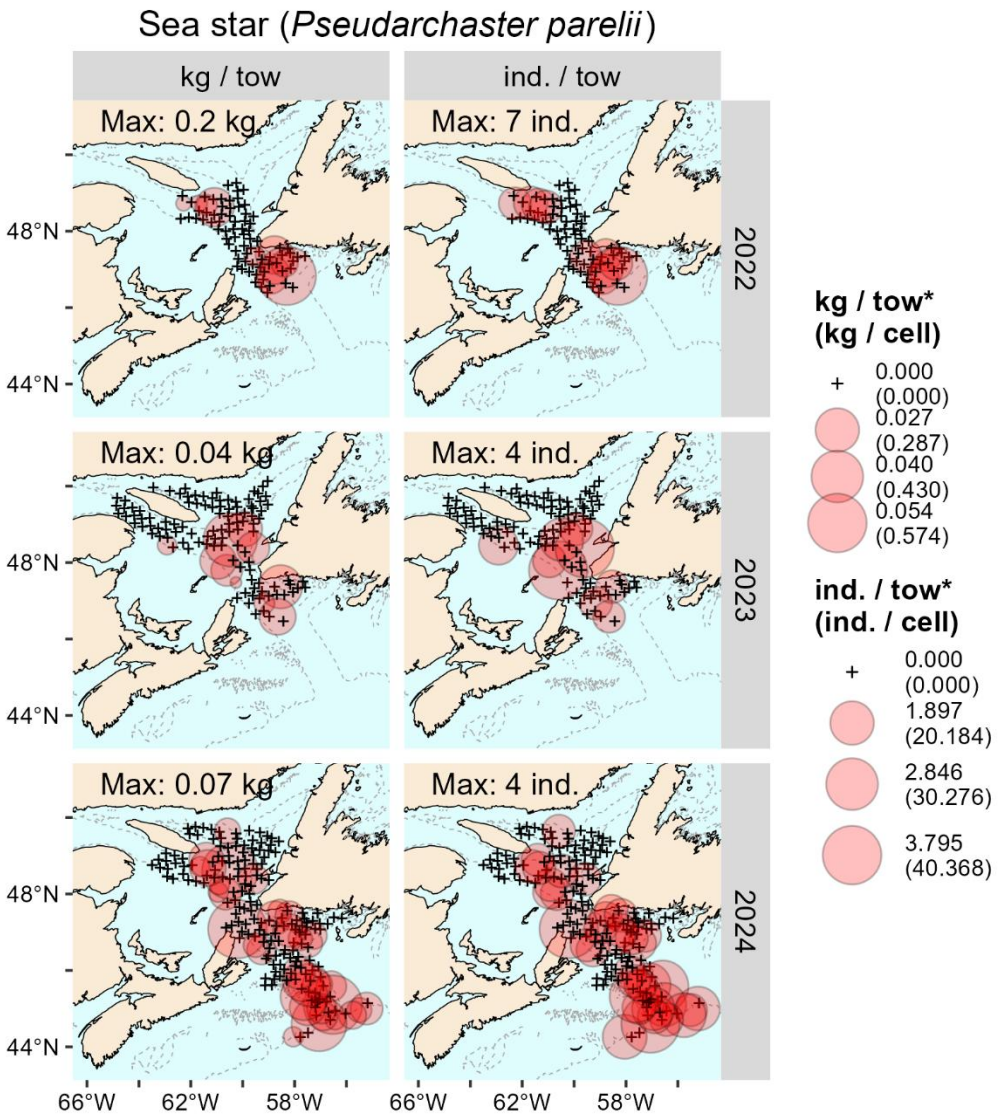


Figure 85a. Standardized catches by weight and/or number (colored bubbles) and cases of absence (black crosses) for the sea star *Pseudarchaster parelii* in the winter survey in 2022, 2023 and 2024.

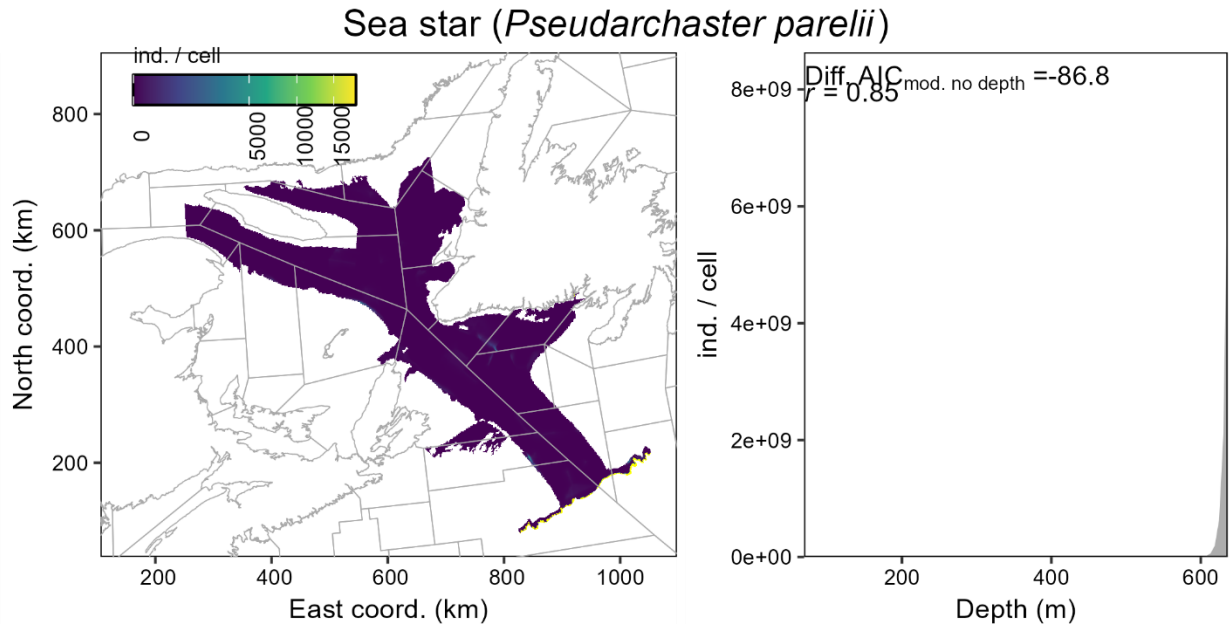


Figure 85b. Predicted number values per 0.25 km^2 cell according to the selected spatial interpolation model for the sea star *Pseudarchaster parelii* in the 2022, 2023, and 2024 winter survey.

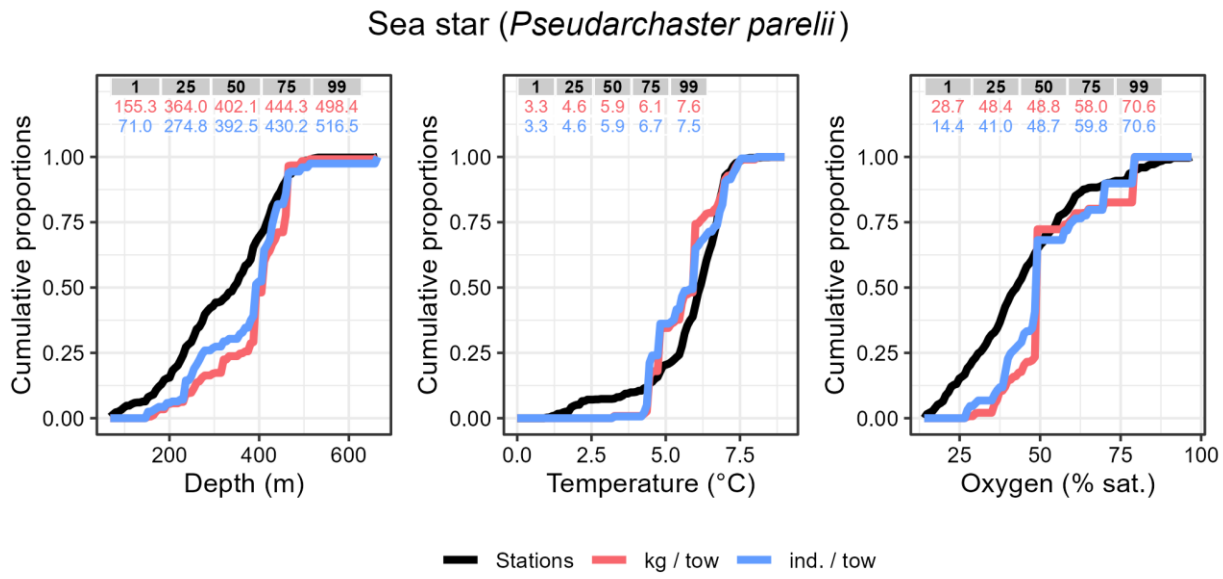


Figure 85c. Cumulative proportions of available values of depth, temperature and dissolved oxygen and standardized catches per tow for the sea star *Pseudarchaster parelii* in the winter survey in 2022, 2023 and 2024.

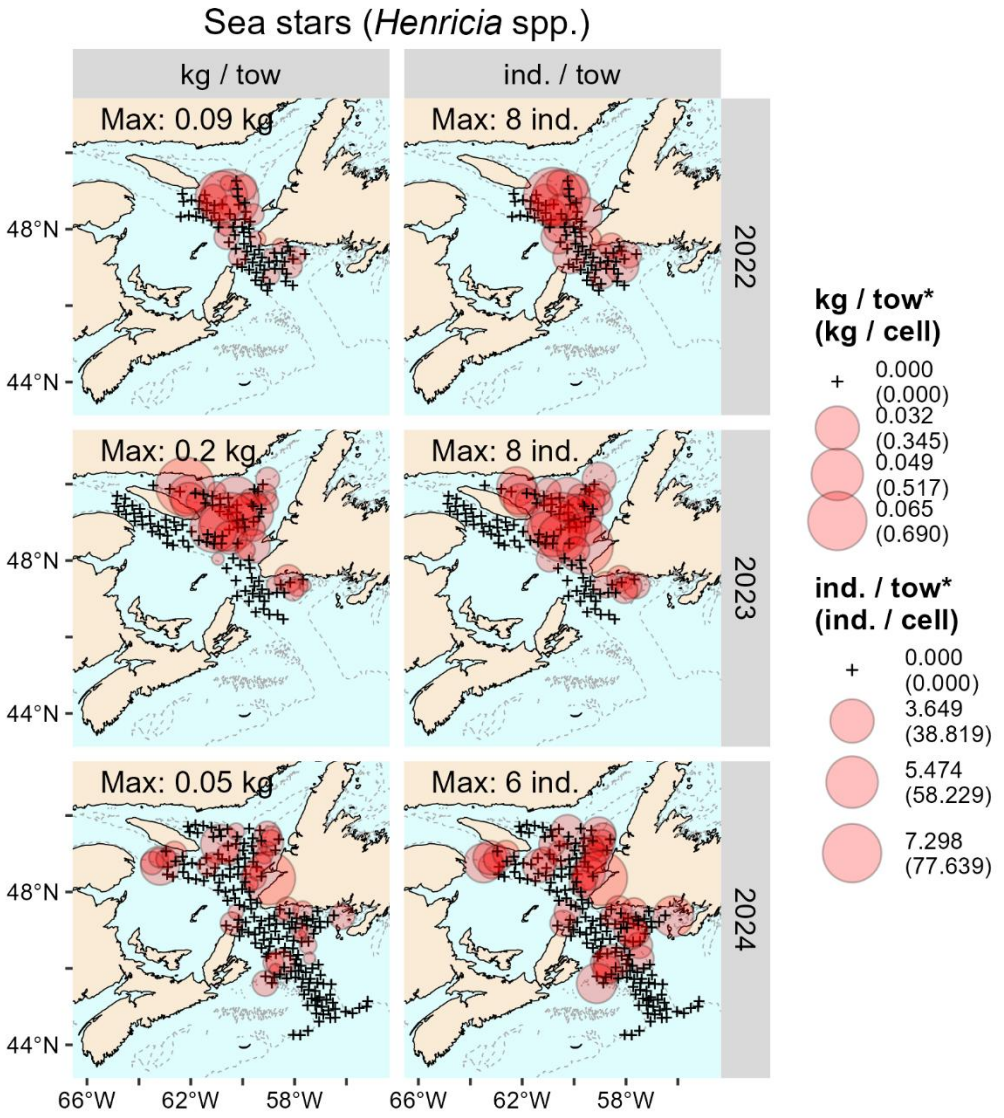


Figure 86a. Standardized catches by weight and/or number (colored bubbles) and cases of absence (black crosses) for sea stars of the genus *Henricia* in the winter survey in 2022, 2023 and 2024.

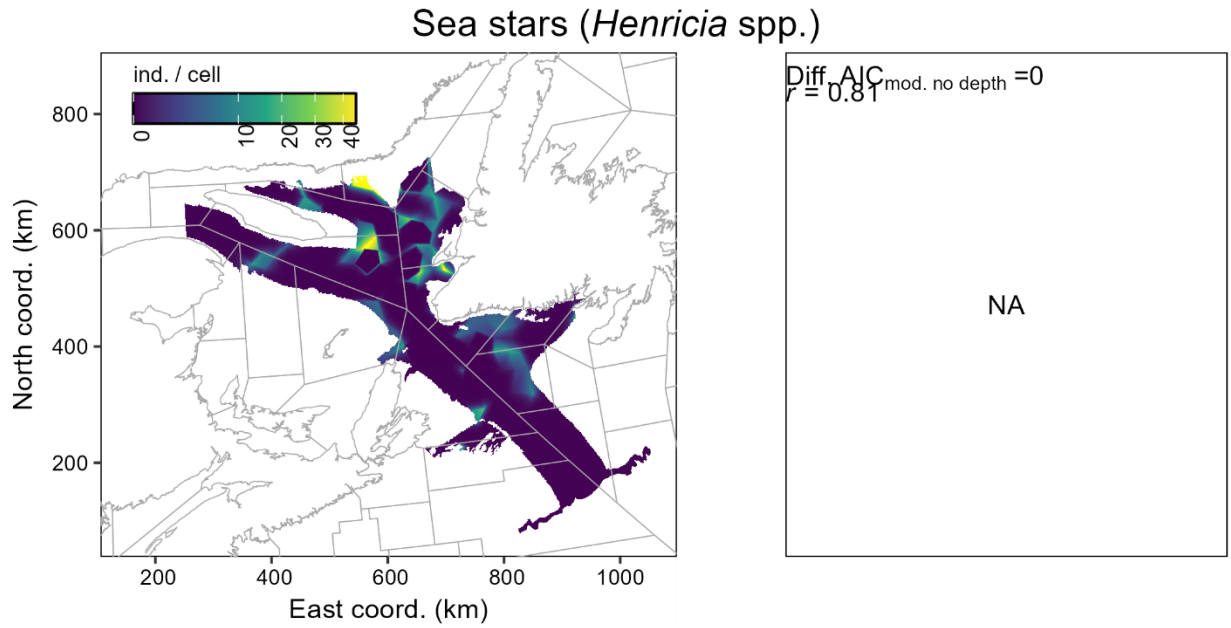


Figure 86b. Predicted number values per 0.25 km^2 cell according to the selected spatial interpolation model for the sea stars of the genus *Henricia* in the 2022, 2023, and 2024 winter survey.

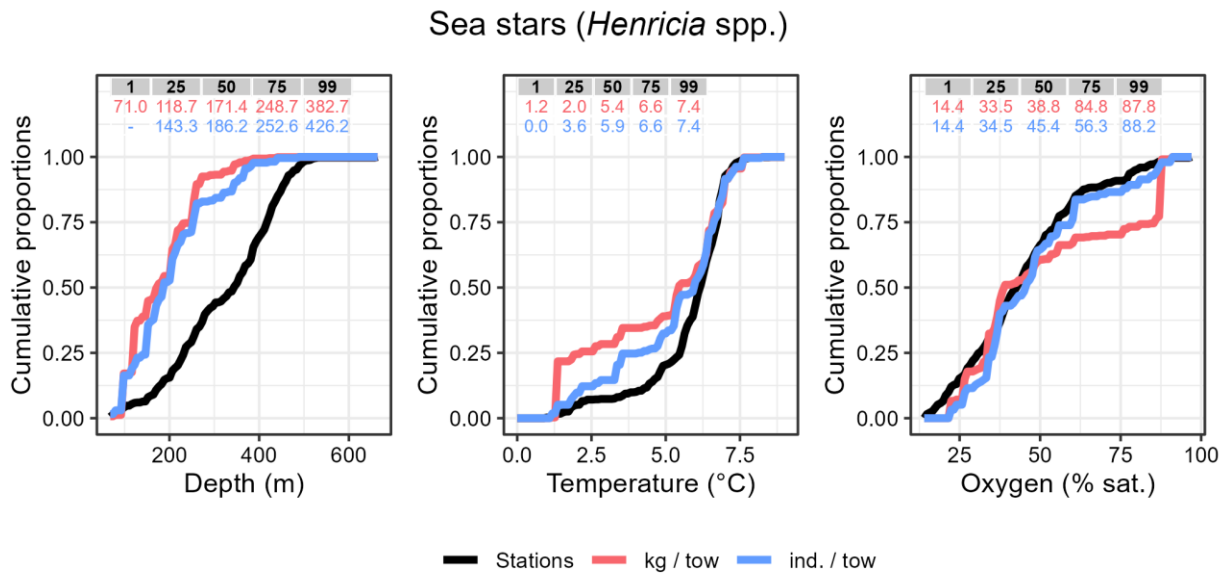


Figure 86c. Cumulative proportions of available values of depth, temperature and dissolved oxygen and standardized catches per tow for sea stars of the genus *Henricia* in the winter survey in 2022, 2023 and 2024.

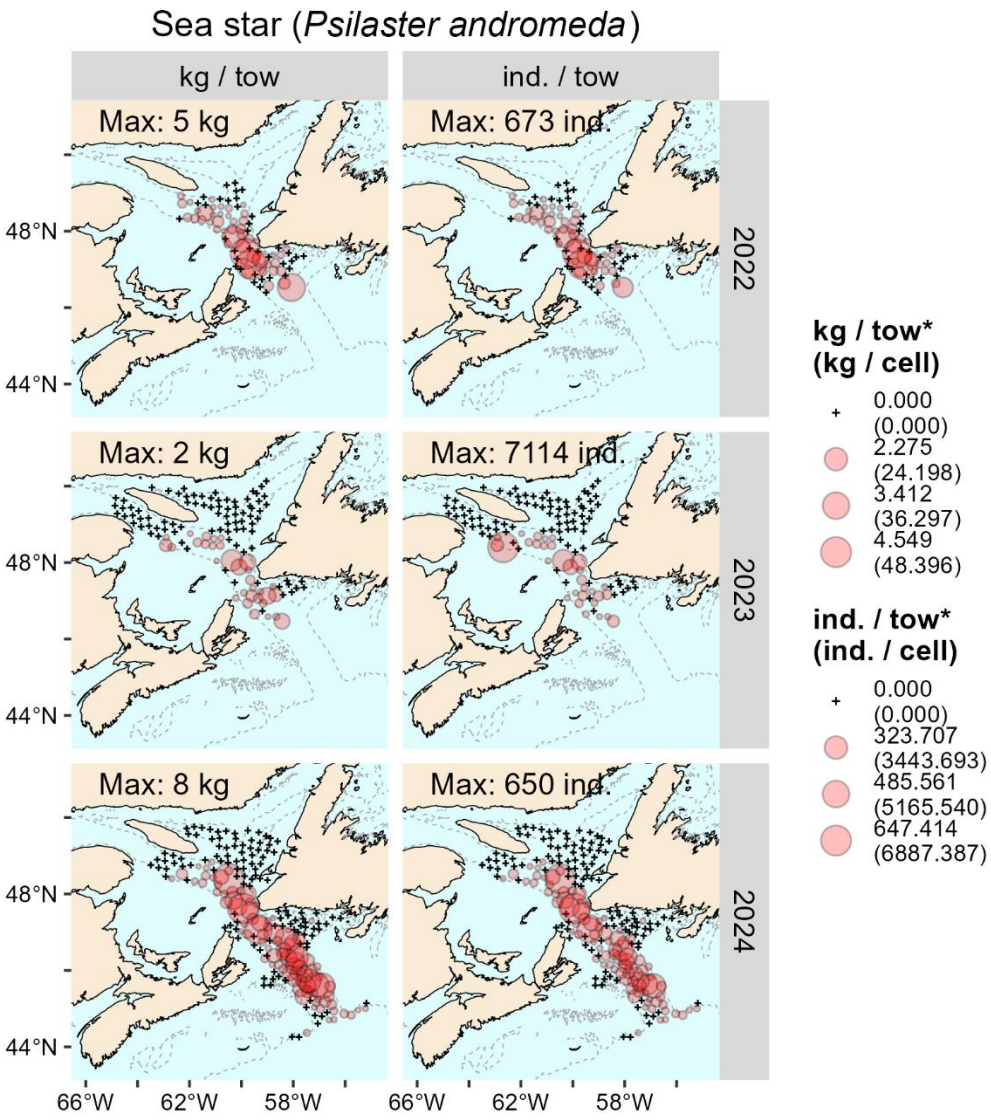


Figure 87a. Standardized catches by weight and/or number (colored bubbles) and cases of absence (black crosses) for the sea star *Psilaster andromeda* in the winter survey in 2022, 2023 and 2024.

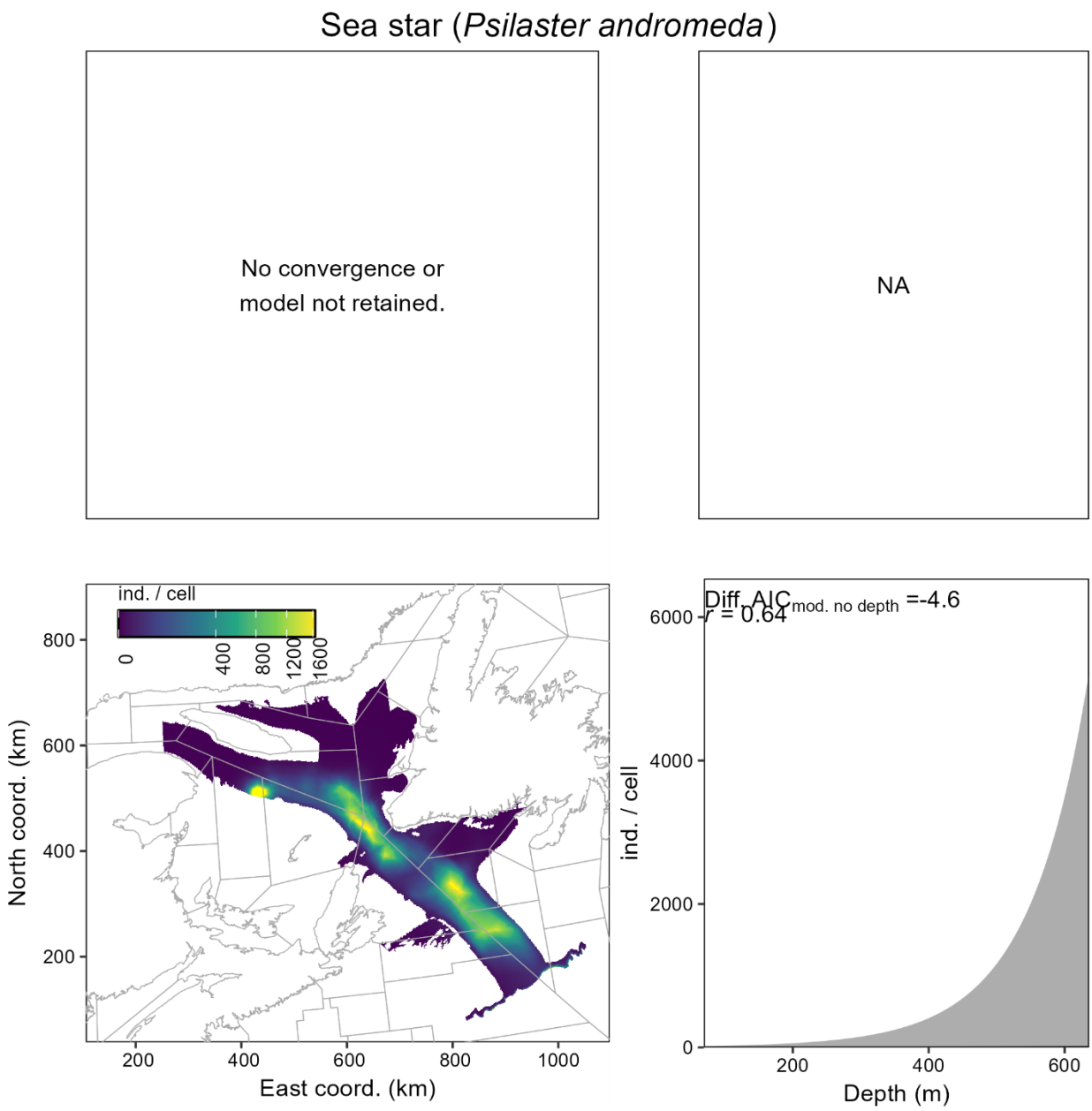


Figure 87b. Predicted weight (upper panels) and number (lower panels) values per 0.25 km^2 cell according to the selected spatial interpolation models for the sea star *Psilaster andromeda* in the 2022, 2023, and 2024 winter survey.

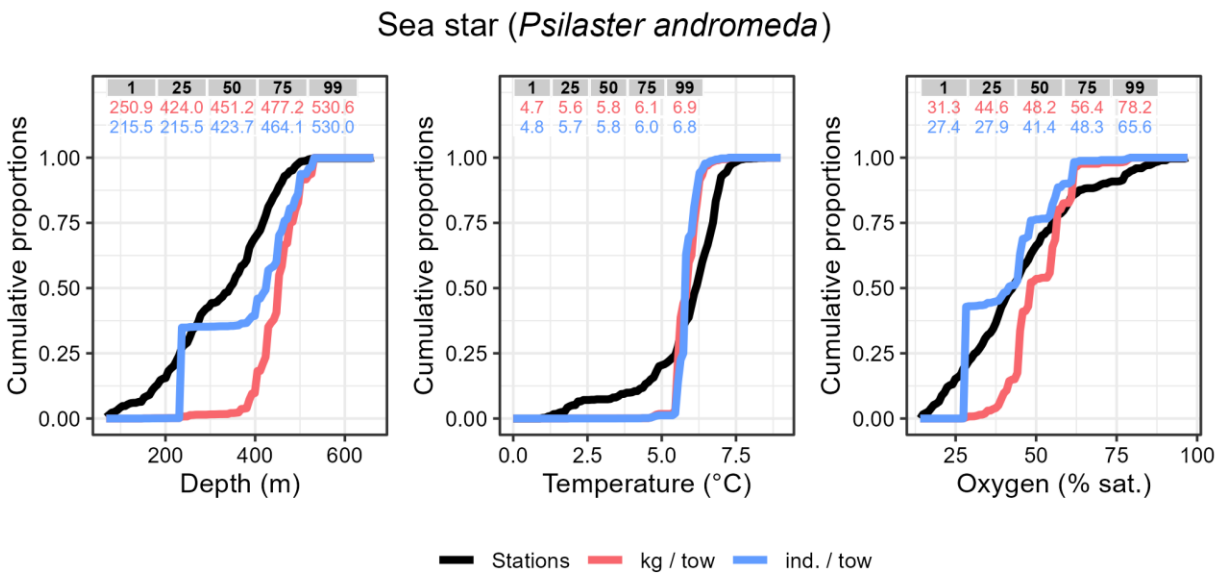


Figure 87c. Cumulative proportions of available values of depth, temperature and dissolved oxygen and standardized catches per tow for the sea star *Psilaster andromeda* in the winter survey in 2022, 2023 and 2024.

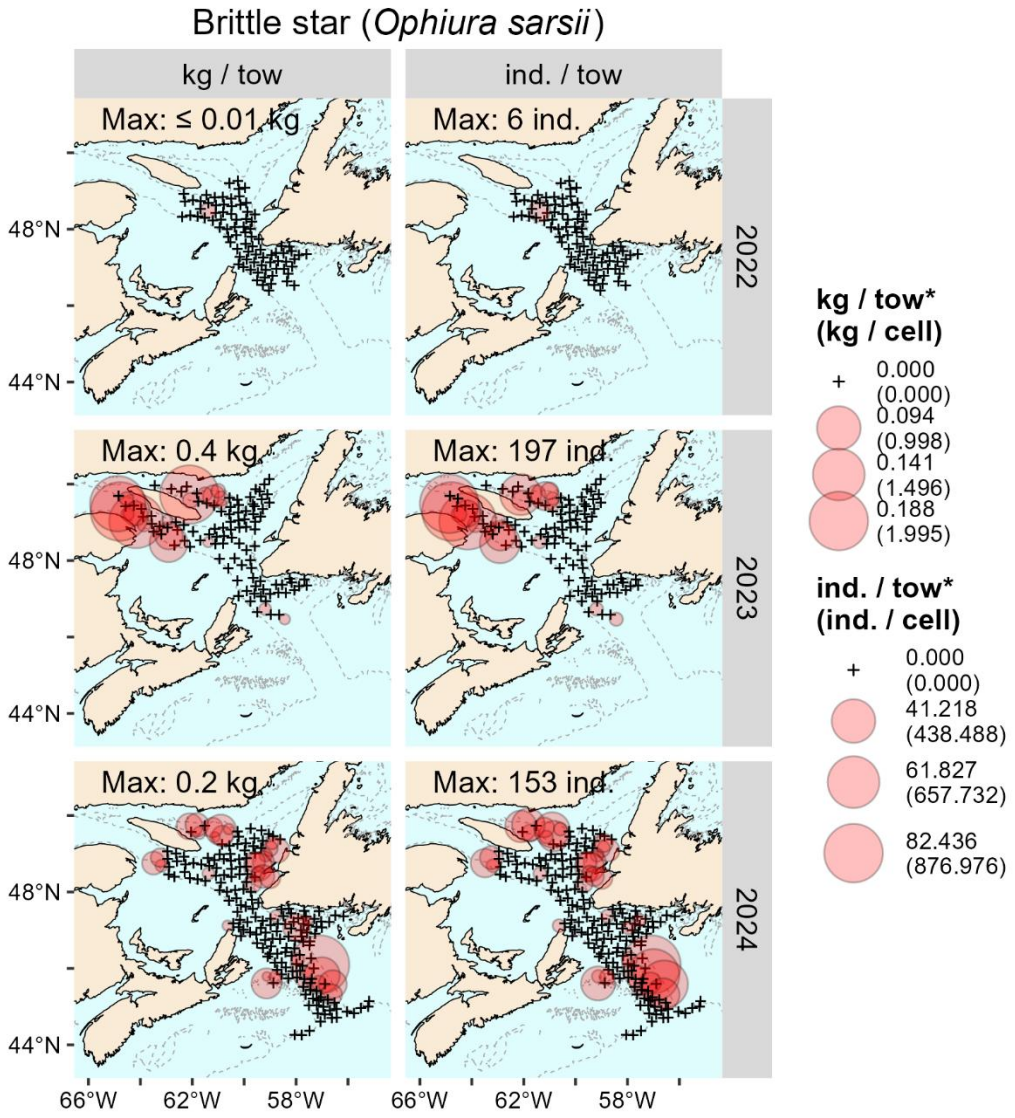


Figure 88a. Standardized catches by weight and/or number (colored bubbles) and cases of absence (black crosses) for the brittle star *Ophiura sarsii* in the winter survey in 2022, 2023 and 2024.

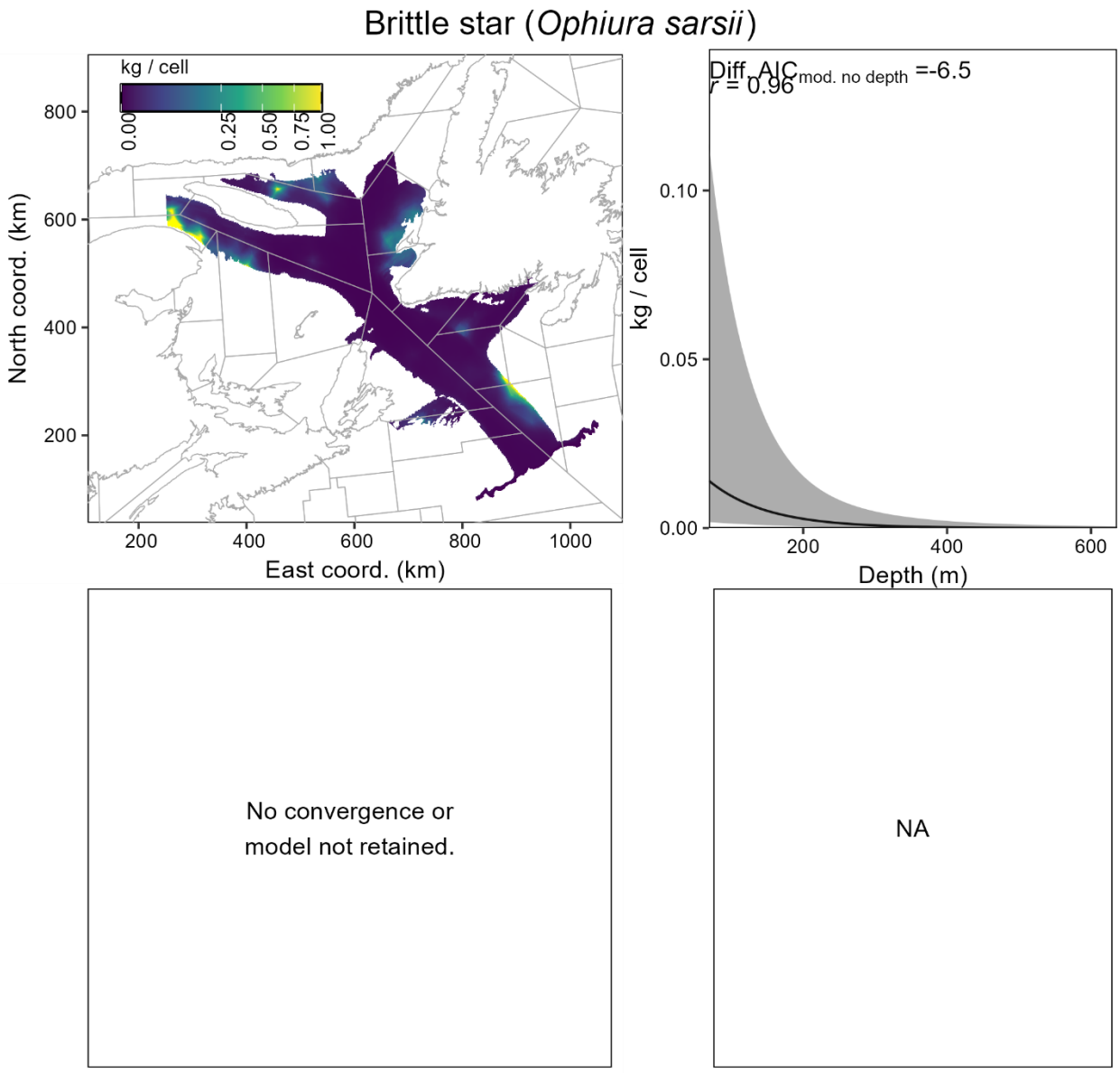


Figure 88b. Predicted weight (upper panels) and number (lower panels) values per 0.25 km^2 cell according to the selected spatial interpolation models for the brittle star *Ophiura sarsii* in the 2022, 2023, and 2024 winter survey.

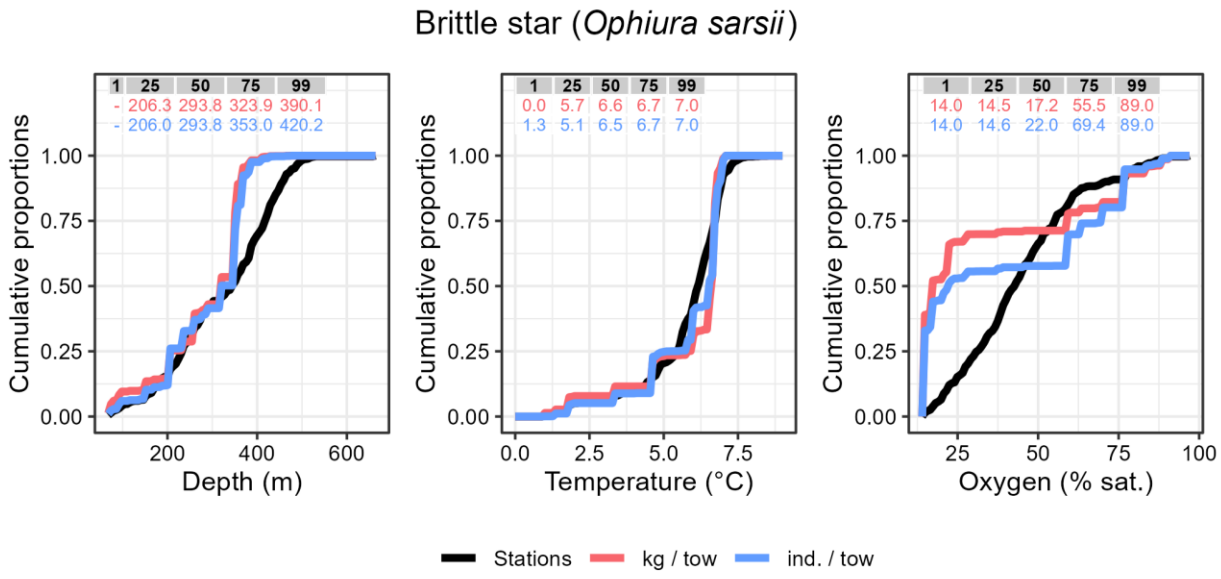


Figure 88c. Cumulative proportions of available values of depth, temperature and dissolved oxygen and standardized catches per tow for the brittle star *Ophiura sarsii* in the winter survey in 2022, 2023 and 2024.

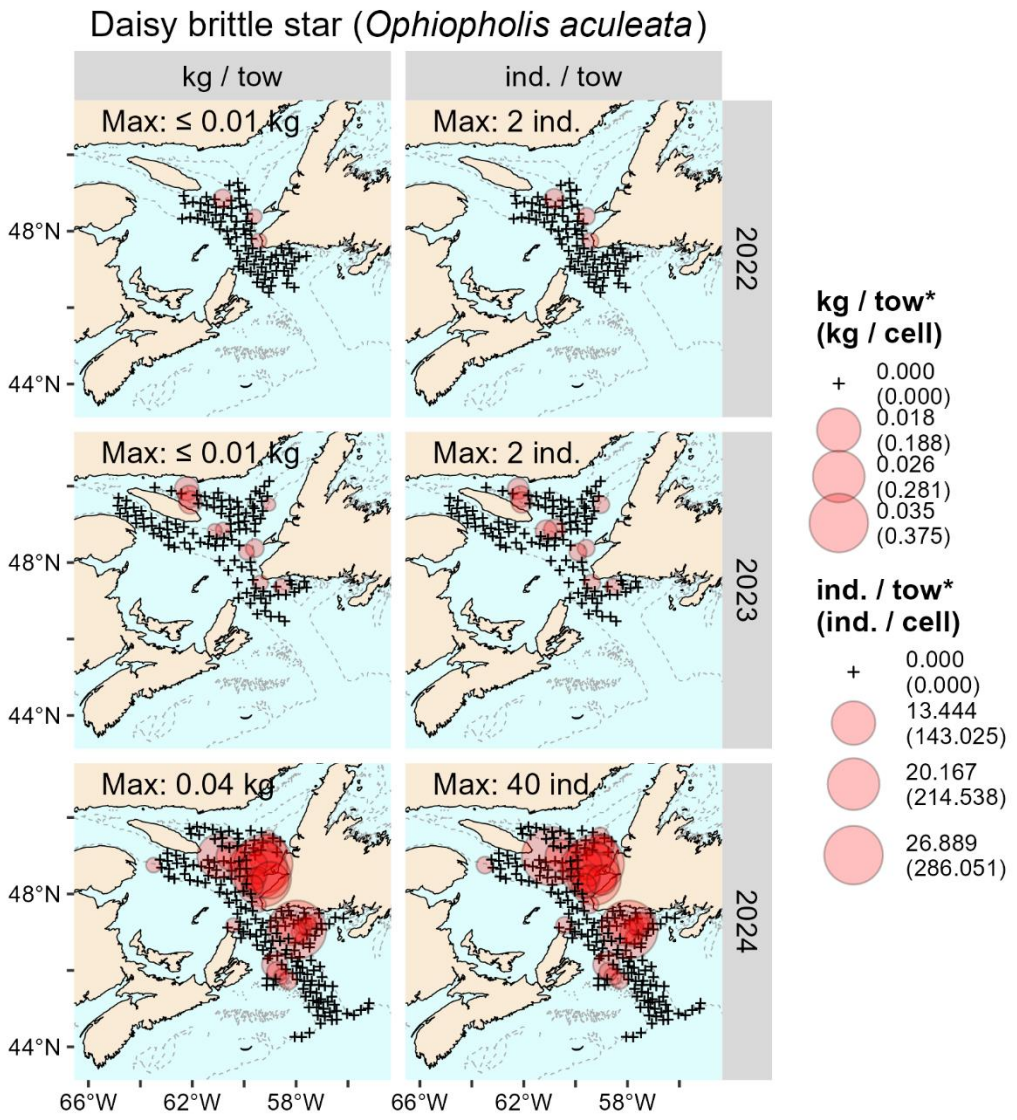


Figure 89a. Standardized catches by weight and/or number (colored bubbles) and cases of absence (black crosses) for the daisy brittle star in the winter survey in 2022, 2023 and 2024.

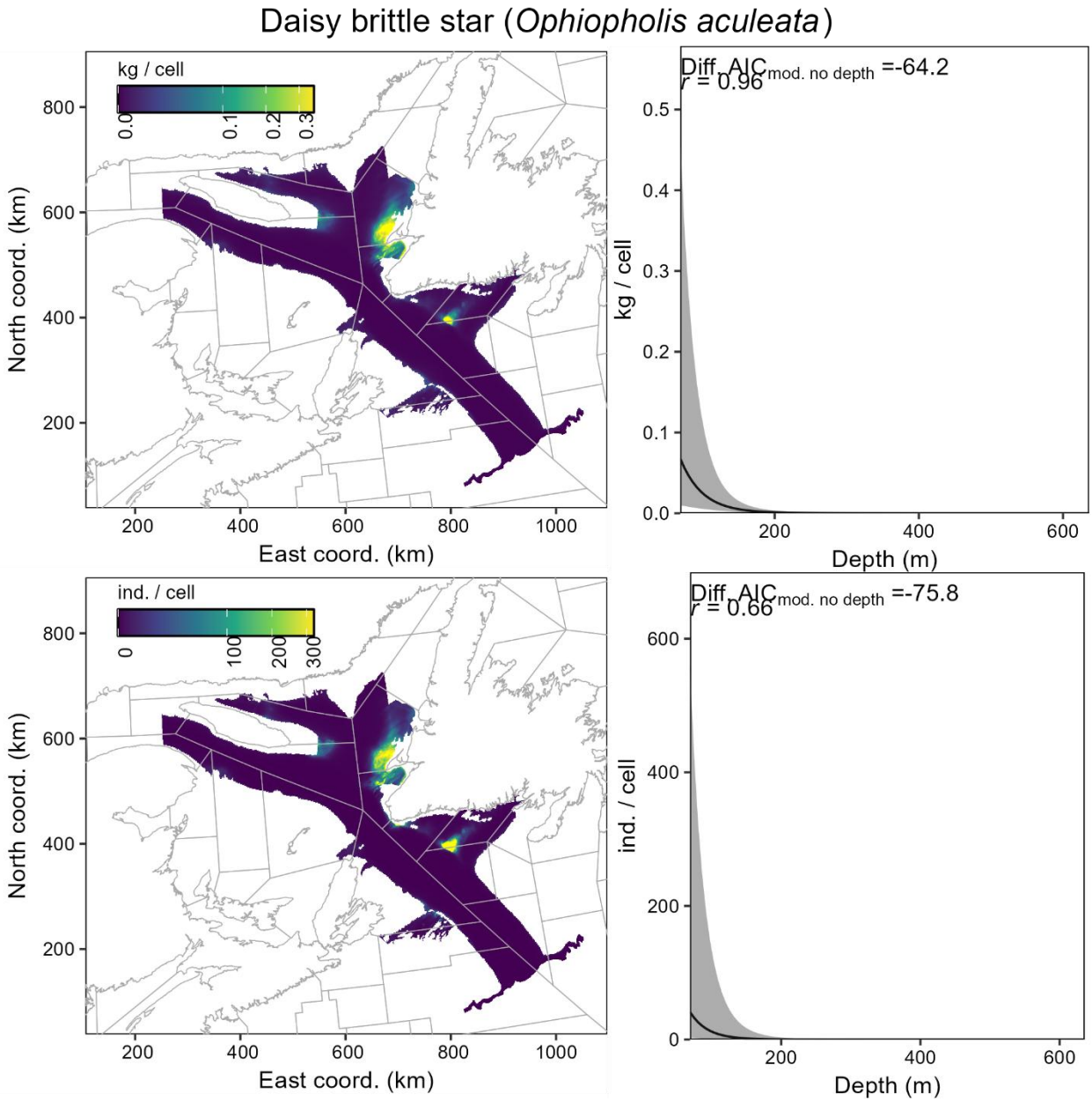


Figure 89b. Predicted weight (upper panels) and number (lower panels) values per 0.25 km^2 cell according to the selected spatial interpolation models for the daisy brittle star in the 2022, 2023, and 2024 winter survey.

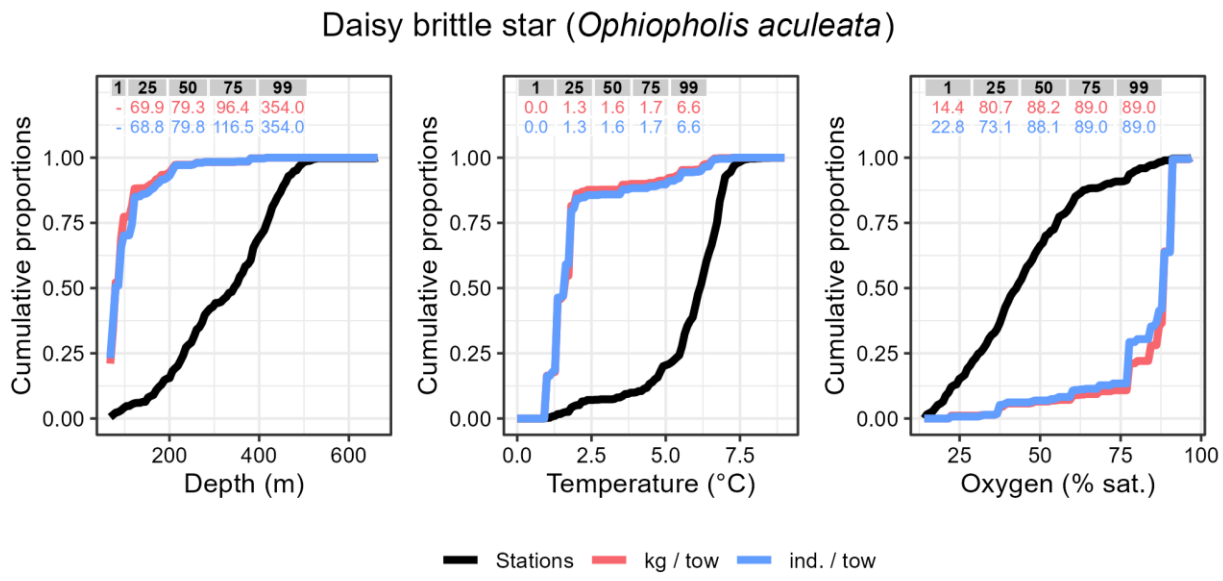


Figure 89c. Cumulative proportions of available values of depth, temperature and dissolved oxygen and standardized catches per tow for the daisy brittle star in the winter survey in 2022, 2023 and 2024.

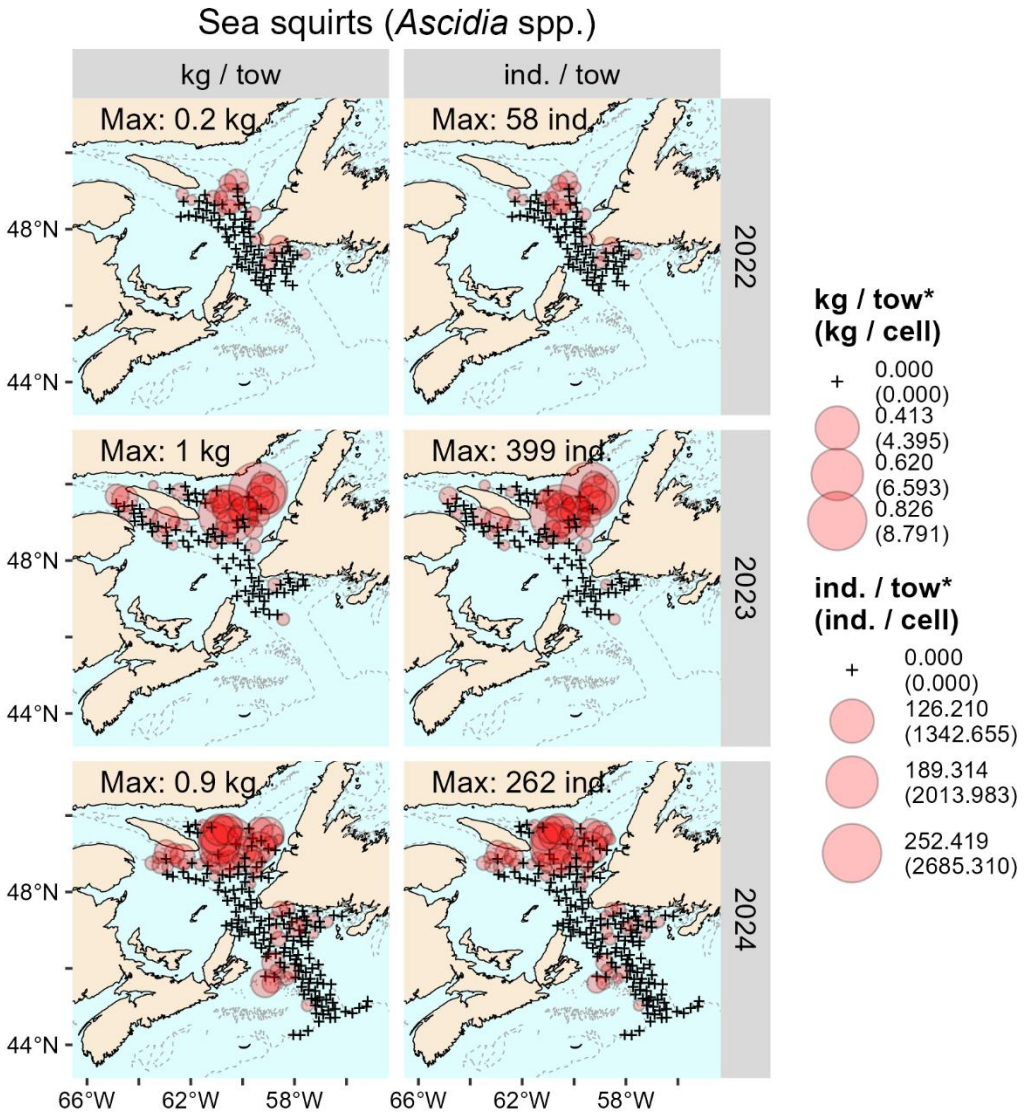


Figure 90a. Standardized catches by weight and/or number (colored bubbles) and cases of absence (black crosses) for sea squirts of the genus *Ascidia* in the winter survey in 2022, 2023 and 2024.

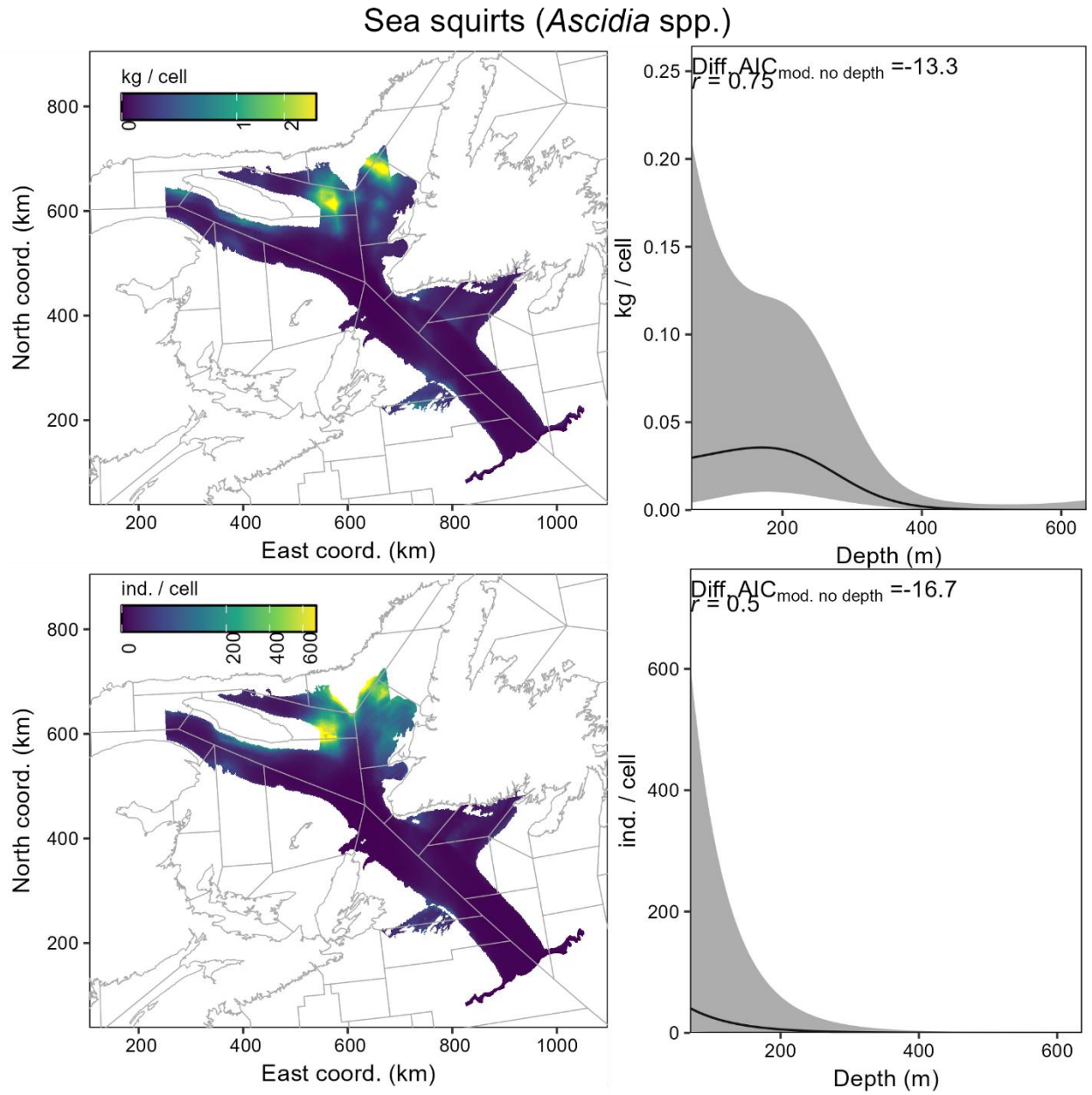


Figure 90b. Predicted weight (upper panels) and number (lower panels) values per 0.25 km^2 cell according to the selected spatial interpolation models for sea squirts of the genus *Ascidia* in the 2022, 2023, and 2024 winter survey.

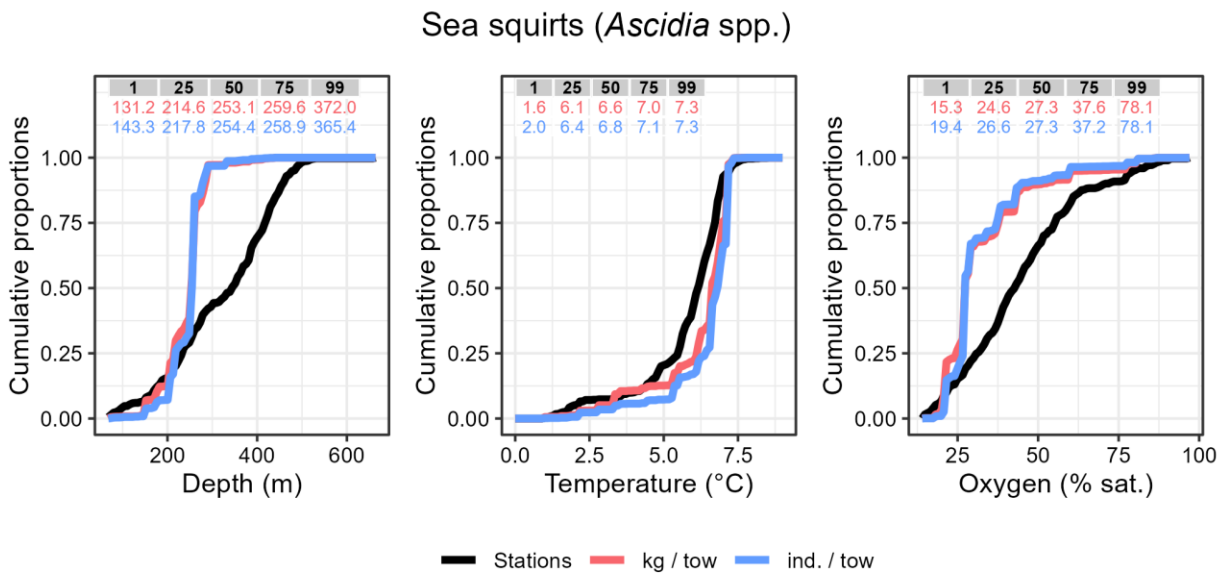


Figure 90c. Cumulative proportions of available values of depth, temperature and dissolved oxygen and standardized catches per tow for sea squirts of the genus *Ascidia* in the winter survey in 2022, 2023 and 2024.

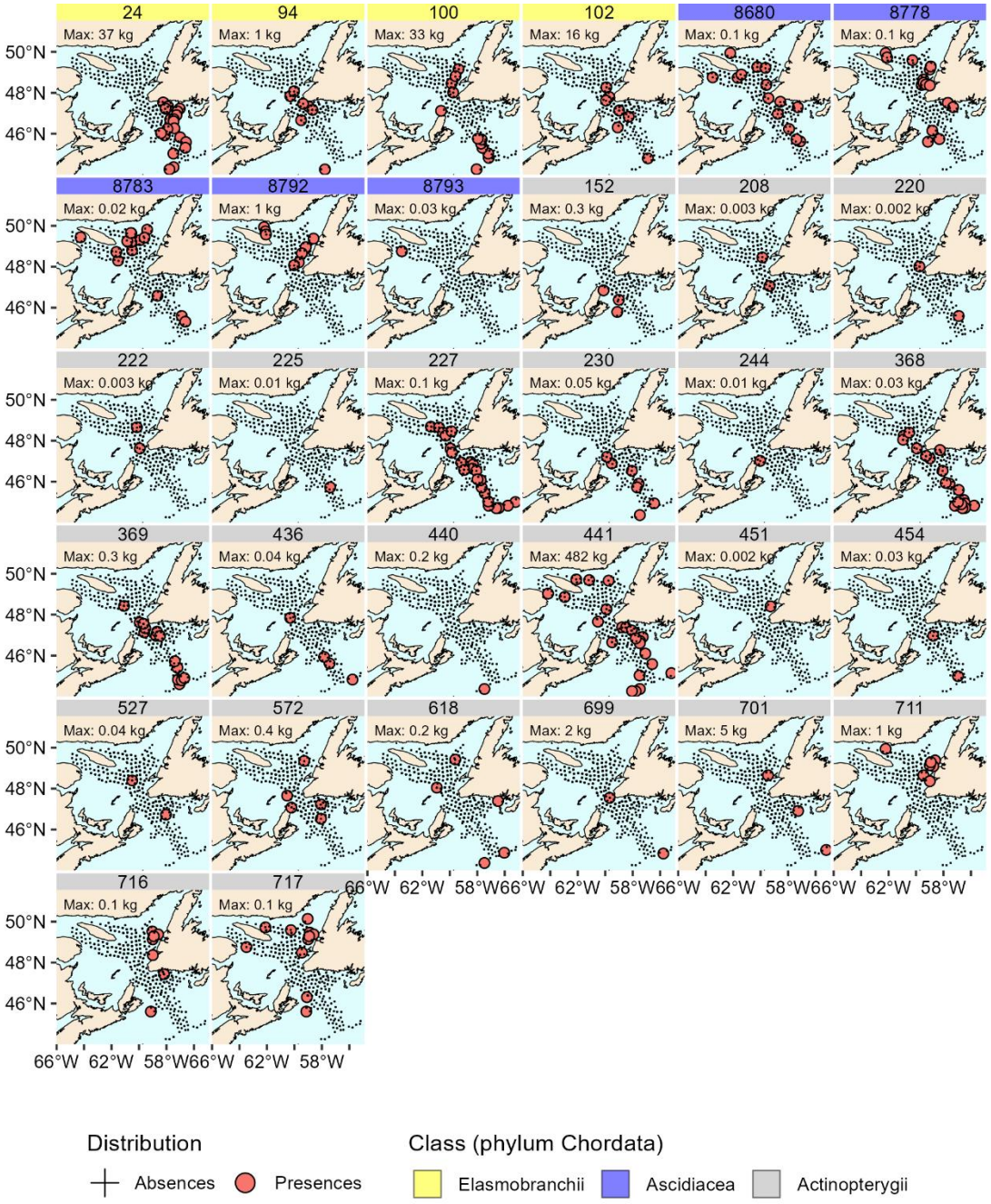


Figure 91. Geographic location of the presence (red circles) and absence (black crosses) of rare taxa within different classes of the phylum Chordata during the winter survey on board the MV Mersey Venture in 2022, 2023, and 2024 (combined). Panels are identified by the STRAP code of the taxon represented and by a colored band reflecting the taxon's phylogenetic class. The values in the upper left corner of each panel indicate the maximum catch in standardized weight per tow.

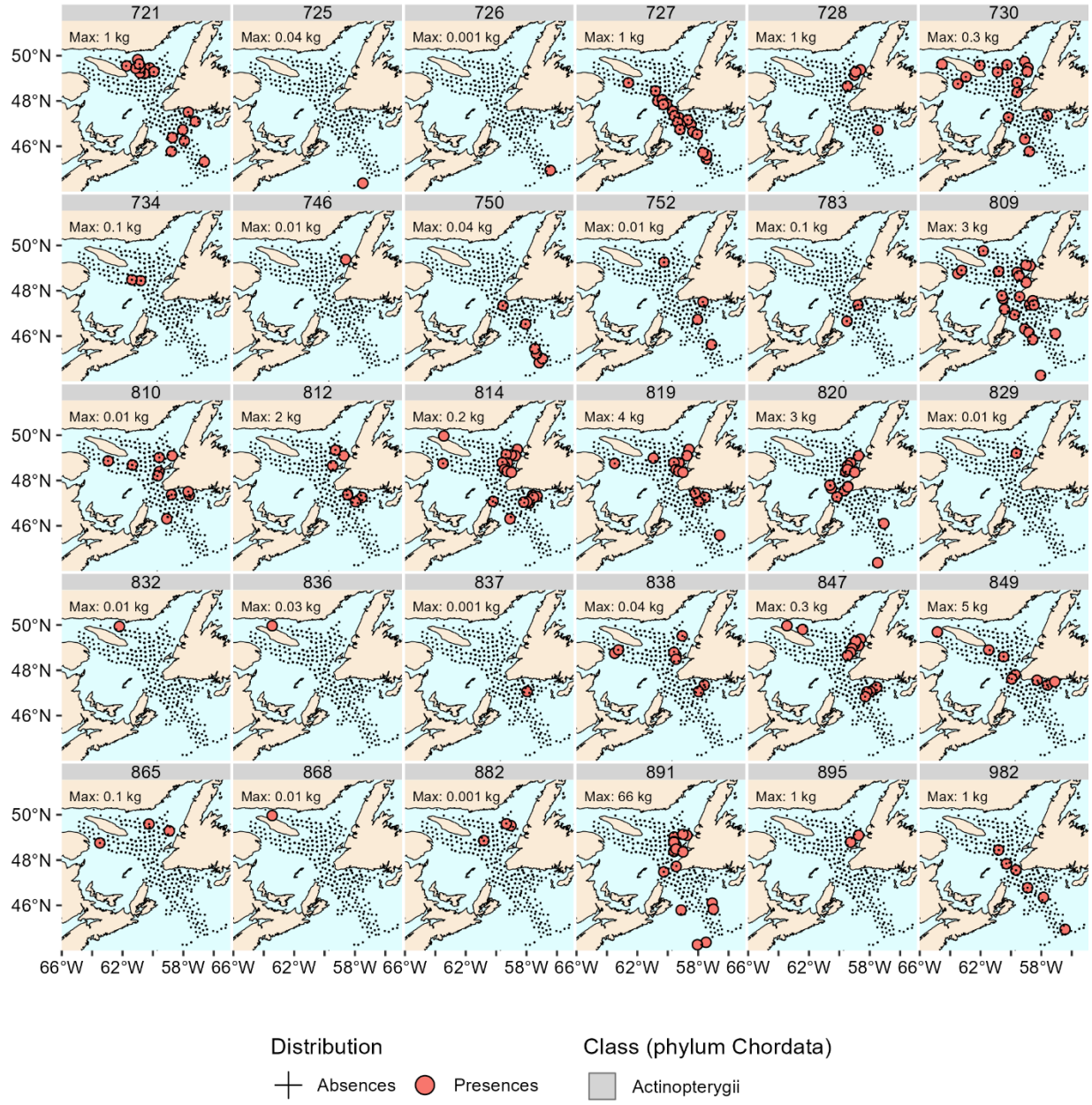


Figure 91 (continued).

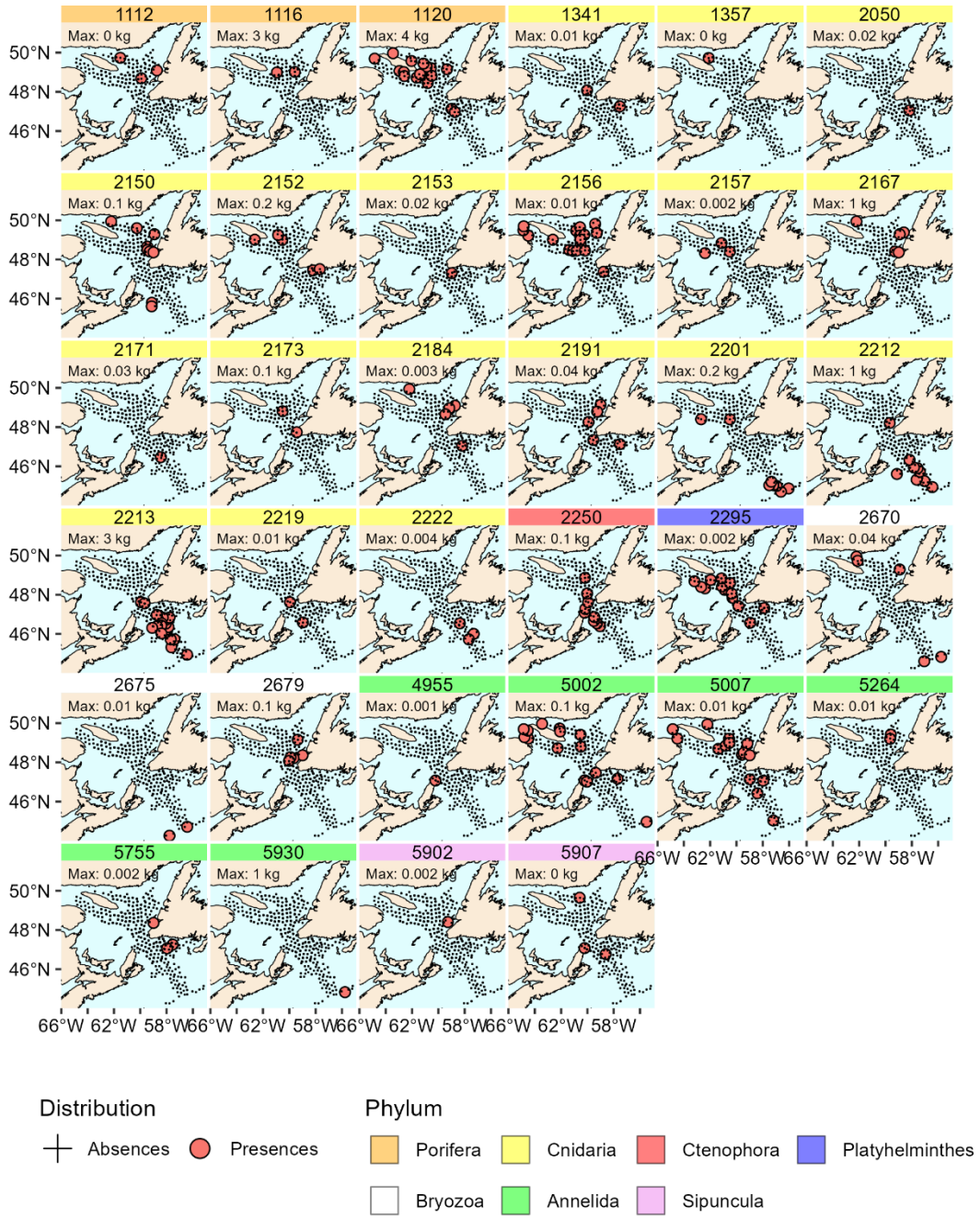


Figure 92. Geographic location of the presence (red circles) and absence (black crosses) of rare taxa within seven different phyla during the winter survey on board the MV Mersey Venture in 2022, 2023, and 2024 (combined). Panels are identified by the STRAP code of the taxon represented and by a color reflecting the taxon's phylogenetic membership. The values in the upper left corner of each panel indicate the maximum catch in standardized weight per tow.

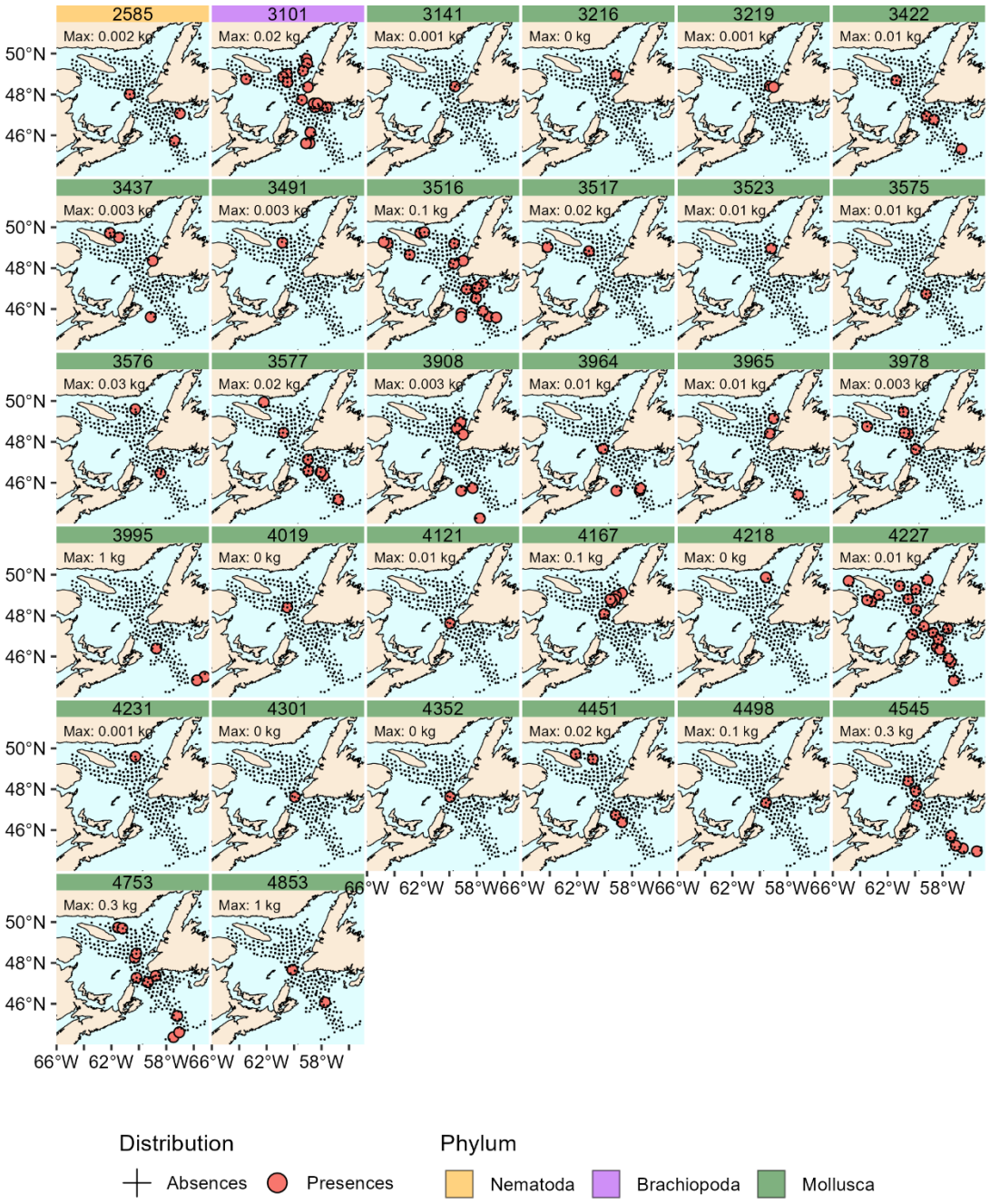


Figure 93. Geographic location of the presence (red circles) and absence (black crosses) of rare taxa within three different phyla during the winter survey on board the MV Mersey Venture in 2022, 2023, and 2024 (combined). Panels are identified by the STRAP code of the taxon represented and by a color reflecting the taxon's phylogenetic membership. The values in the upper left corner of each panel indicate the maximum catch in standardized weight per tow.

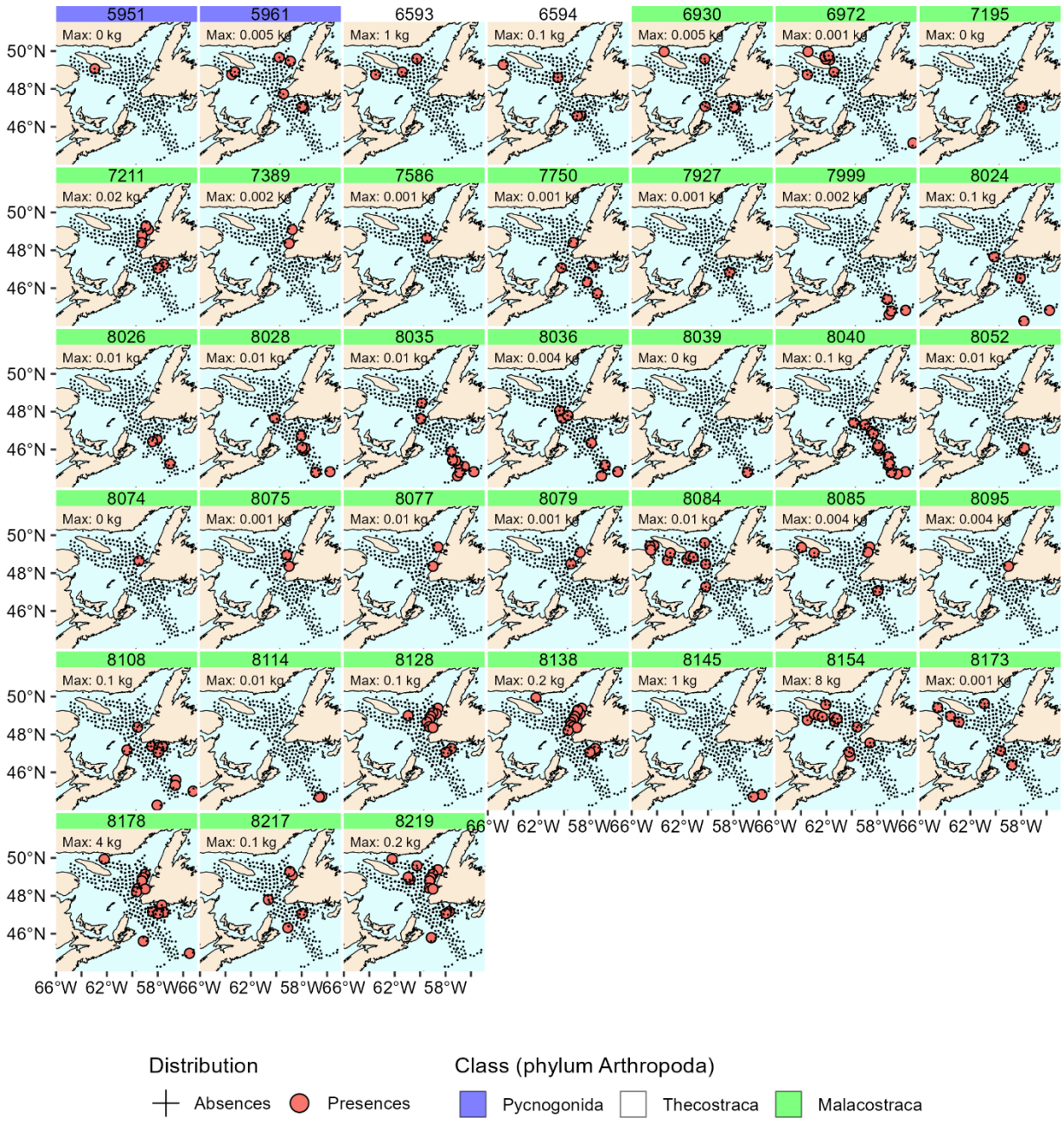


Figure 94. Geographic location of the presence (red circles) and absence (black crosses) of rare taxa within different classes of the phylum Arthropoda during the winter survey on board the MV Mersey Venture in 2022, 2023, and 2024 (combined). Panels are identified by the STRAP code of the taxon represented and by a color reflecting the taxon's phylogenetic class. The values in the upper left corner of each panel indicate the maximum catch in standardized weight per tow.

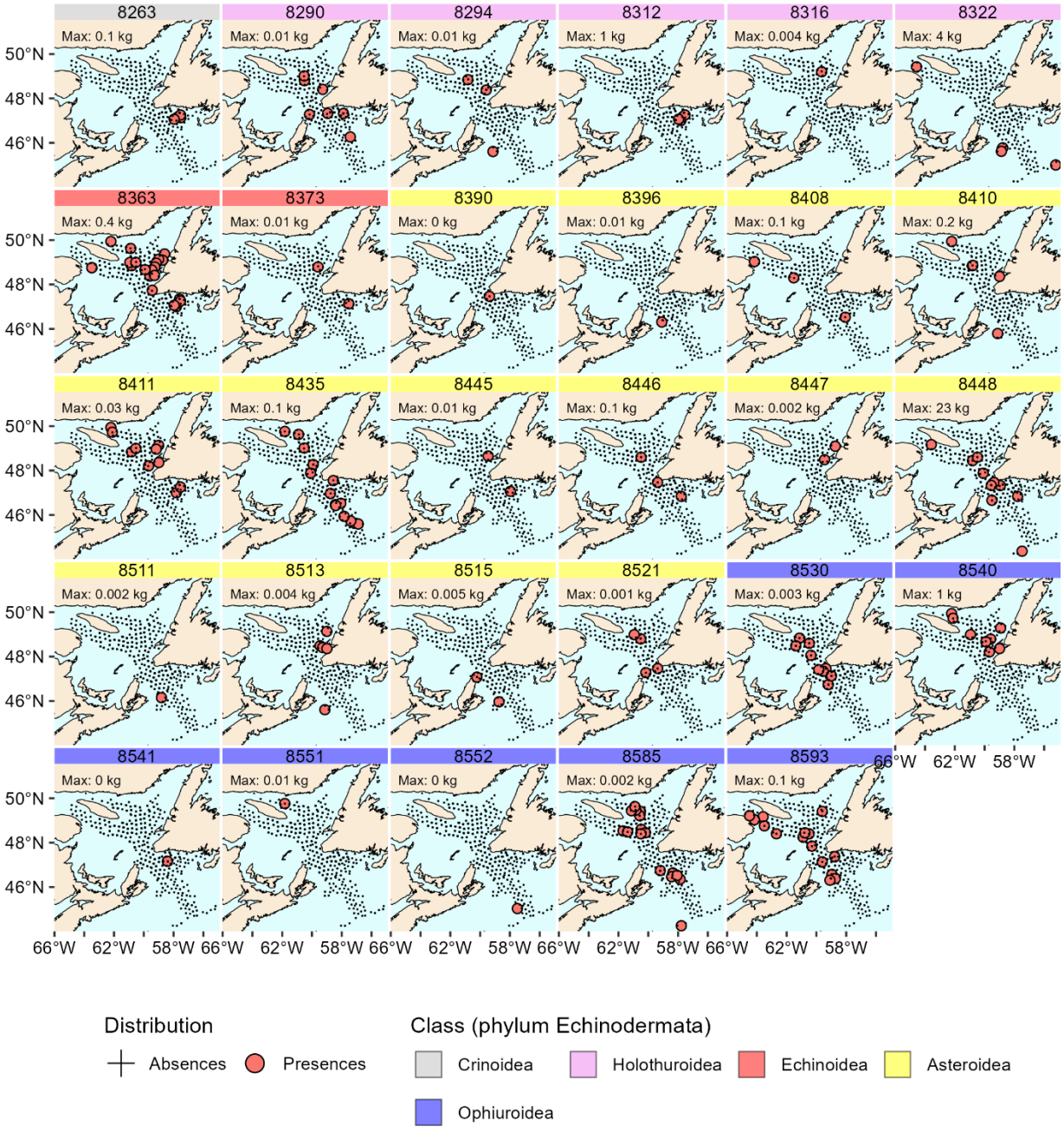


Figure 95. Geographic location of the presence (red circles) and absence (black crosses) of rare taxa within different classes of the phylum Echinodermata during the winter survey on board the MV Mersey Venture in 2022, 2023, and 2024 (combined). Panels are identified by the STRAP code of the taxon represented and by a color reflecting the taxon's phylogenetic class. The values in the upper left corner of each panel indicate the maximum catch in standardized weight per tow.

APPENDICES

Appendix A. Supplemental information on the survey and analyzes

Table A1. Description, number of occurrences and total catches in weight (kg) and in number (ind.) for taxonomic codes excluded from this report.

STRAP code	Description	Number of occurrences	Total catch weight in kg (total catch number)
999	Unidentified fish species	16	0,332 (30)
1100	Invertebrates	15	0,134 (3)
2296	Fecampiidae egg capsule	9	0,00965 (7)
9801	First unidentified invertebrate species per set	1	0,0011 (1)
9810	First unidentified fish species per set	4	0,0462 (4)
9965	Smooth skate egg capsule	1	0,0063 (1)
9966	Thorny skate egg capsule	1	0,0235 (0)
9970	Skates eggs	11	0,194 (15)
9995	Trash (shrimp sorting)	410	92,7 (1)
9999	Unknown	1	0,135 (0)

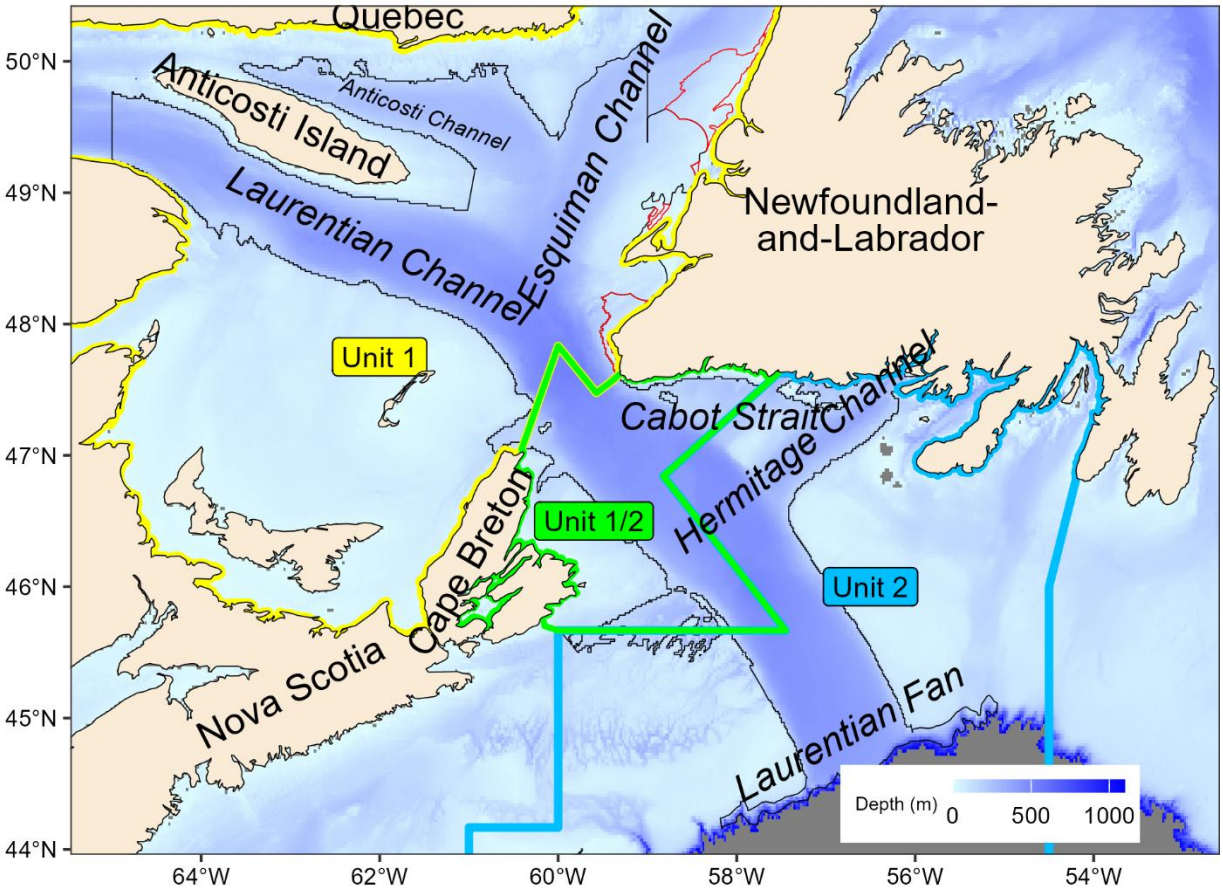


Figure A1. Location of provinces, channels, and other points of interest during the winter survey on board the MV Mersey Venture in 2022, 2023, and 2024. Shades of blue reflect bathymetry according to GEBCO (excluding depths less than 0 m and greater than 1100 m), and the black and red lines delineate the boundaries of the completed and excluded study areas, respectively, from the area initially planned for analysis. The yellow and blue polygons delineate the NAFO Divisions and Subdivisions exclusively associated with Units 1 (4RST) and 2 (3Ps4Vs and 4Wfgj) for redfish management, while the green polygon around 3Pn4Vn corresponds to Unit 1 from January to May and Unit 2 from June to December.

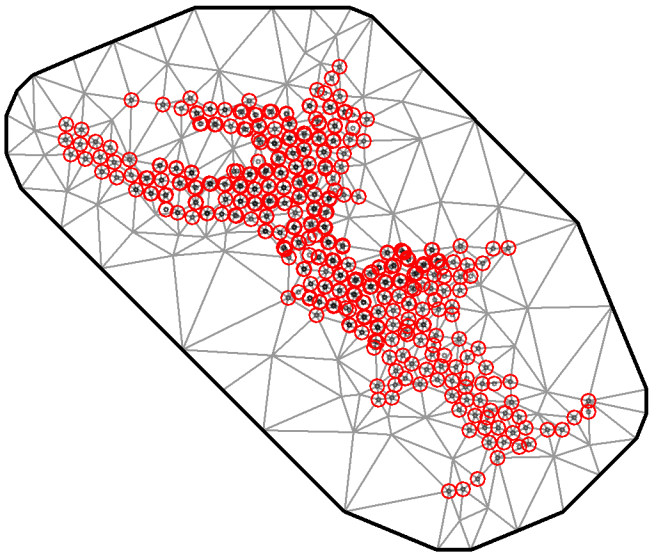


Figure A2. Delaunay triangulation scheme (*sdmTMBmesh* object) used for spatial interpolation models of densities in weight and number per 0.25 km^2 cell (black and gray lines), with the location of sampling stations shown as red circles.

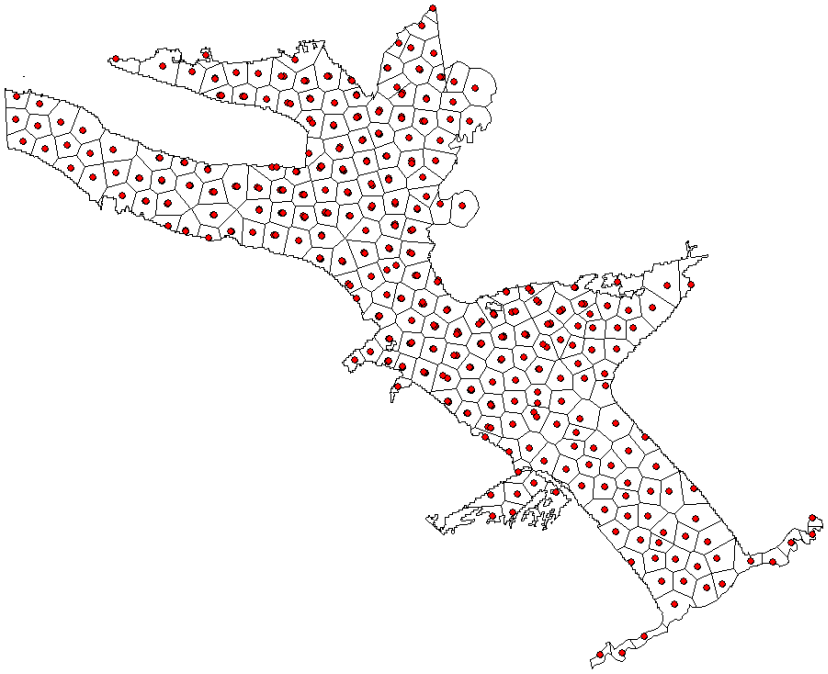


Figure A3. Illustration of Voronoi polygons (black lines) and associated sampling stations (red circles) from the winter survey on board the MV Mersey Venture in 2022, 2023 and 2024.

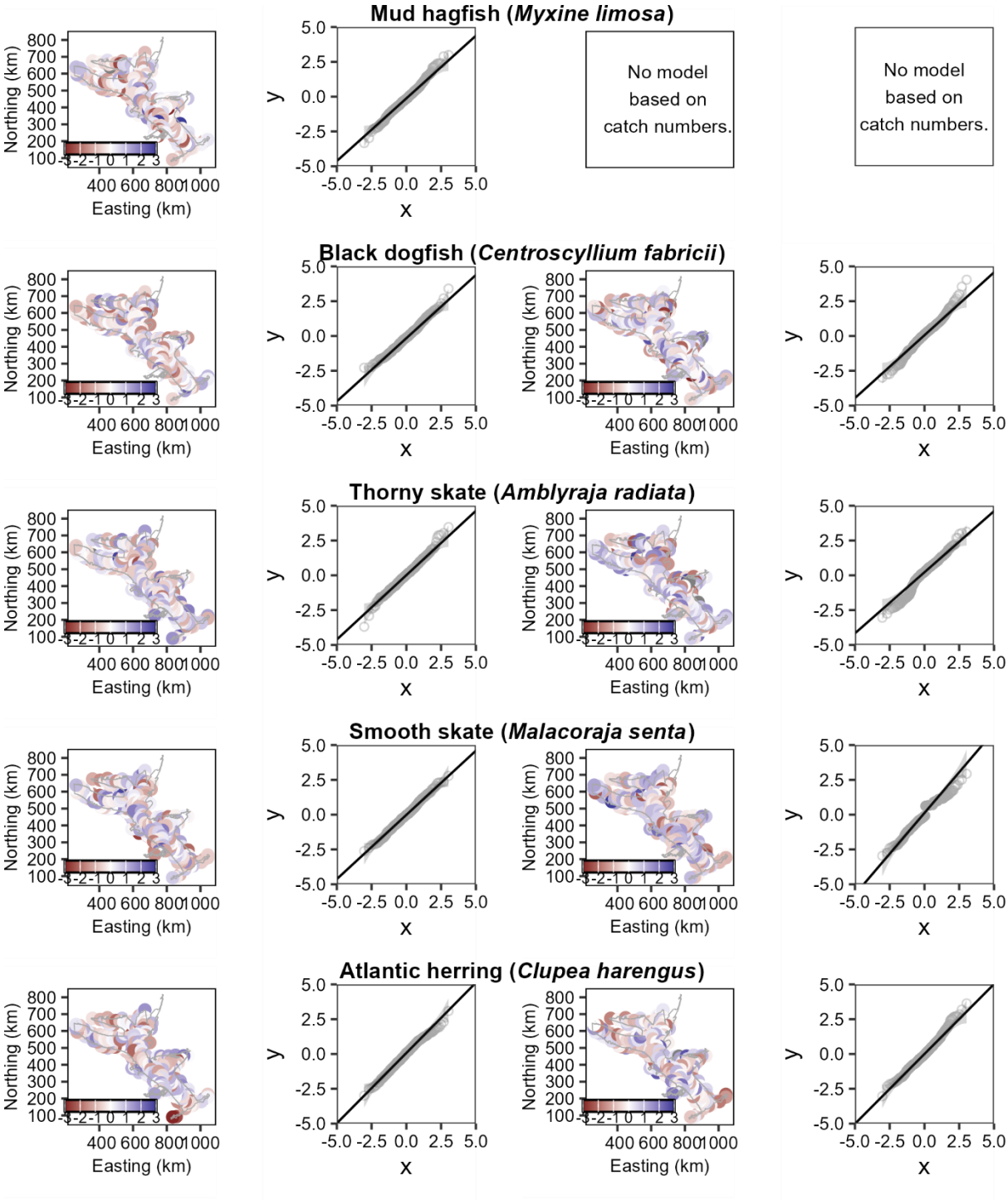


Figure B1. Illustration of the 'mle-mvn' residuals of the selected spatial interpolation models in the weight analysis (columns 1 and 2) and/or the number analysis (columns 3 and 4) per cell, for five of the taxa considered common. Columns 1 and 3 give the residuals in space within the study area, while columns 2 and 4 give the Q-Q normal diagrams for these residuals compared with a 1:1 ratio.

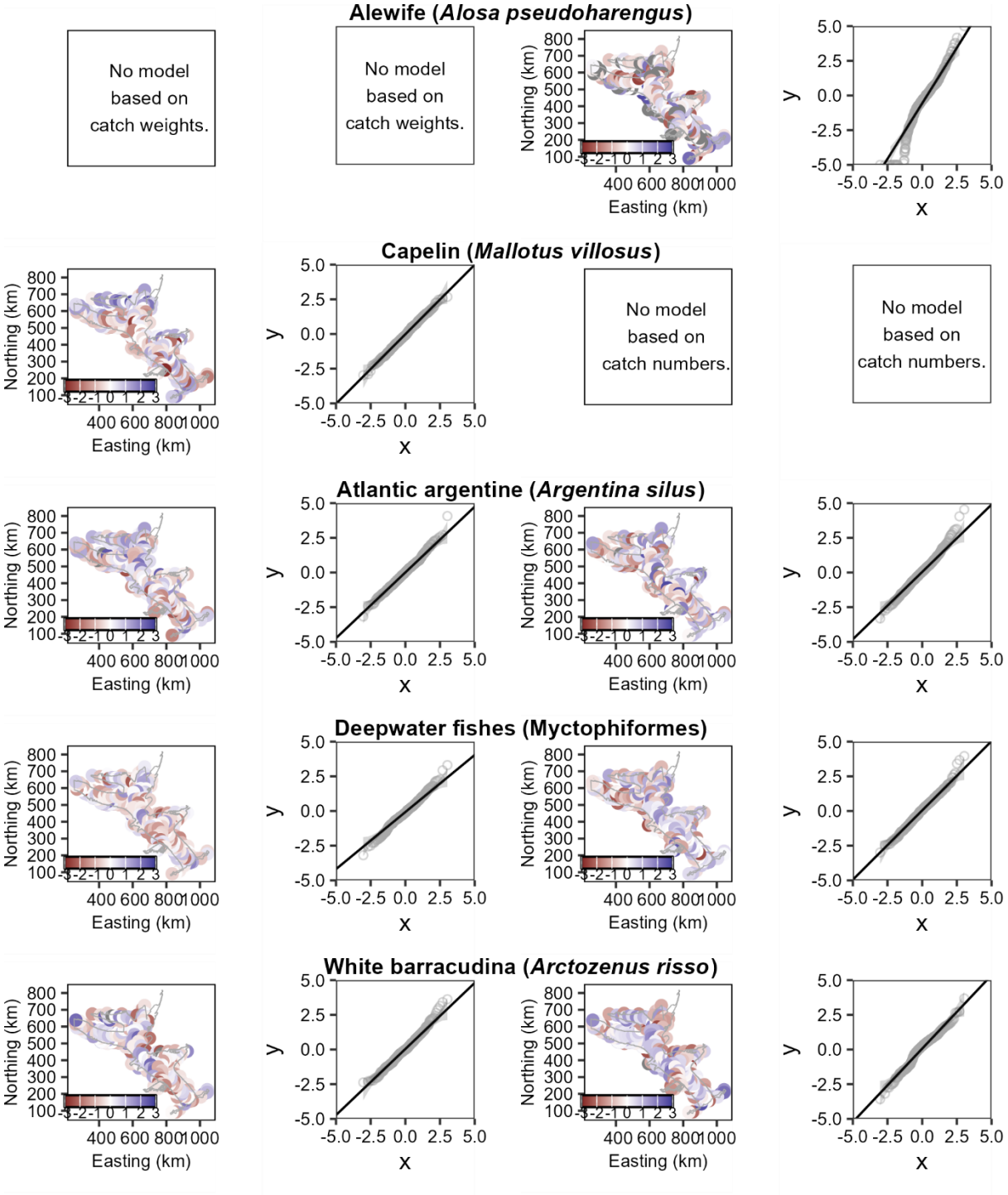


Figure B2. Illustration of the 'mle-mvn' residuals of the selected spatial interpolation models in the weight analysis (columns 1 and 2) and/or the number analysis (columns 3 and 4) per cell, for five of the taxa considered common. Columns 1 and 3 give the residuals in space within the study area, while columns 2 and 4 give the Q-Q normal diagrams for these residuals compared with a 1:1 ratio.

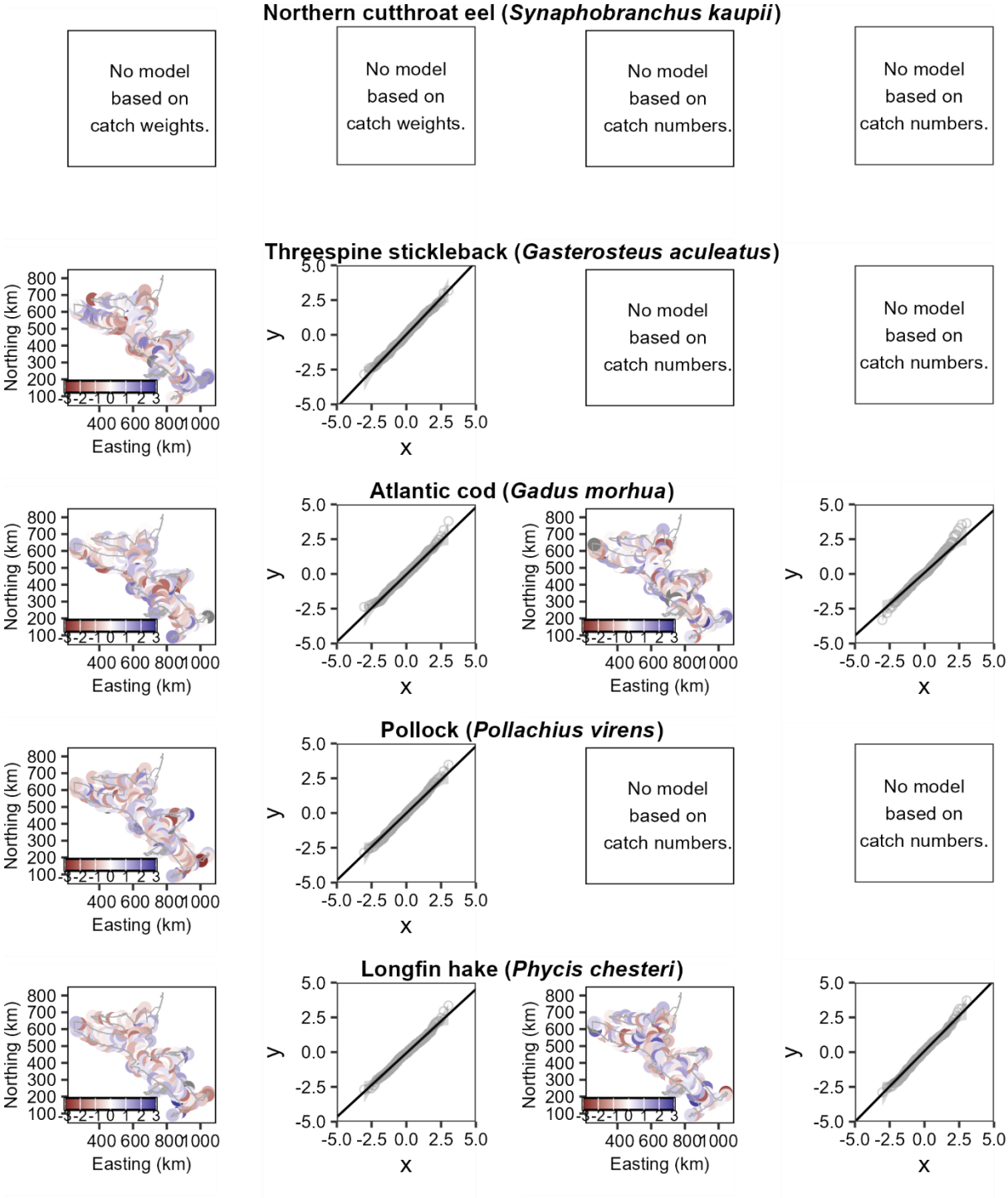


Figure B3. Illustration of the 'mle-mvn' residuals of the selected spatial interpolation models in the weight analysis (columns 1 and 2) and/or the number analysis (columns 3 and 4) per cell, for five of the taxa considered common. Columns 1 and 3 give the residuals in space within the study area, while columns 2 and 4 give the Q-Q normal diagrams for these residuals compared with a 1:1 ratio.

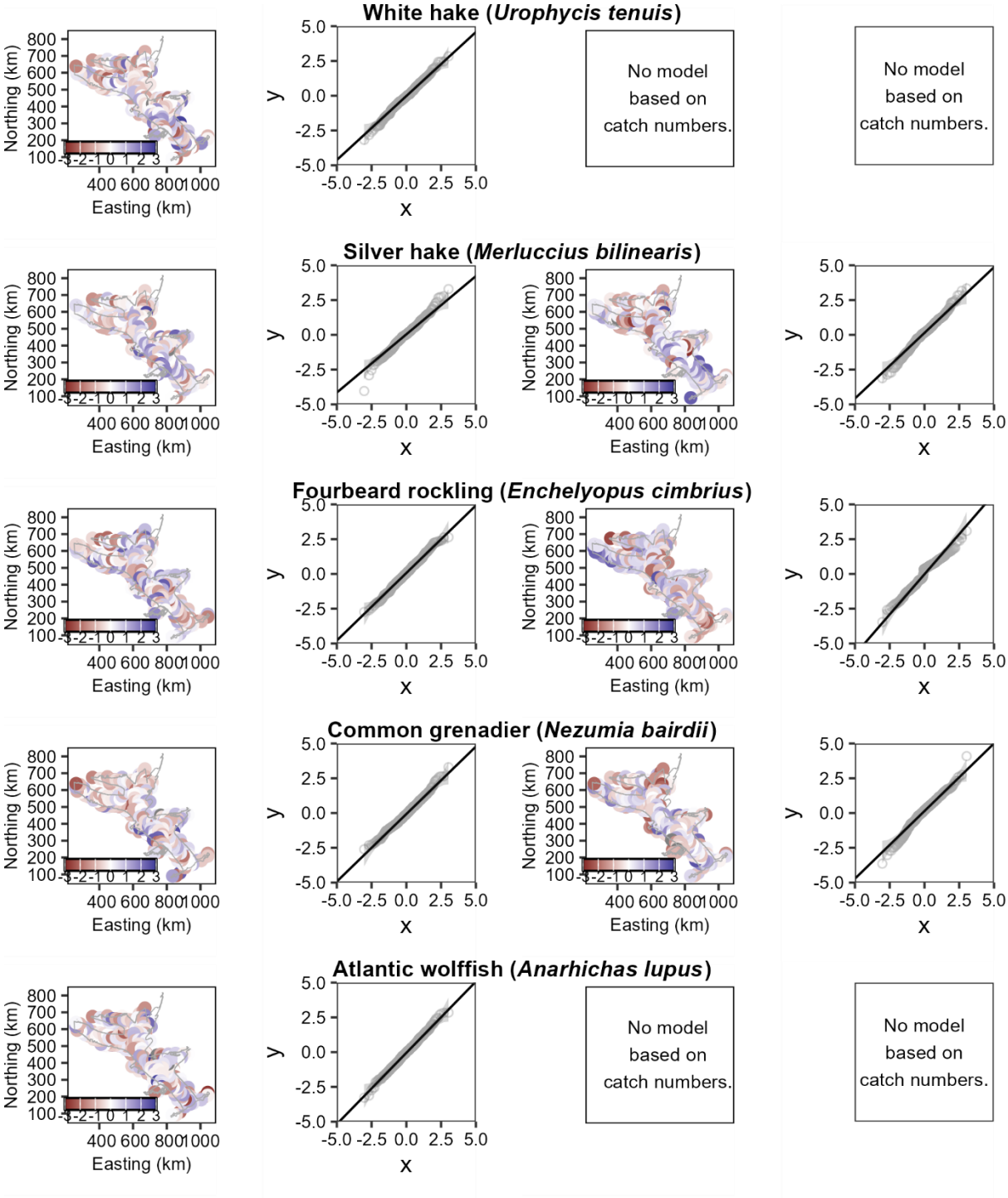


Figure B4. Illustration of the 'mle-mvn' residuals of the selected spatial interpolation models in the weight analysis (columns 1 and 2) and/or the number analysis (columns 3 and 4) per cell, for five of the taxa considered common. Columns 1 and 3 give the residuals in space within the study area, while columns 2 and 4 give the Q-Q normal diagrams for these residuals compared with a 1:1 ratio.

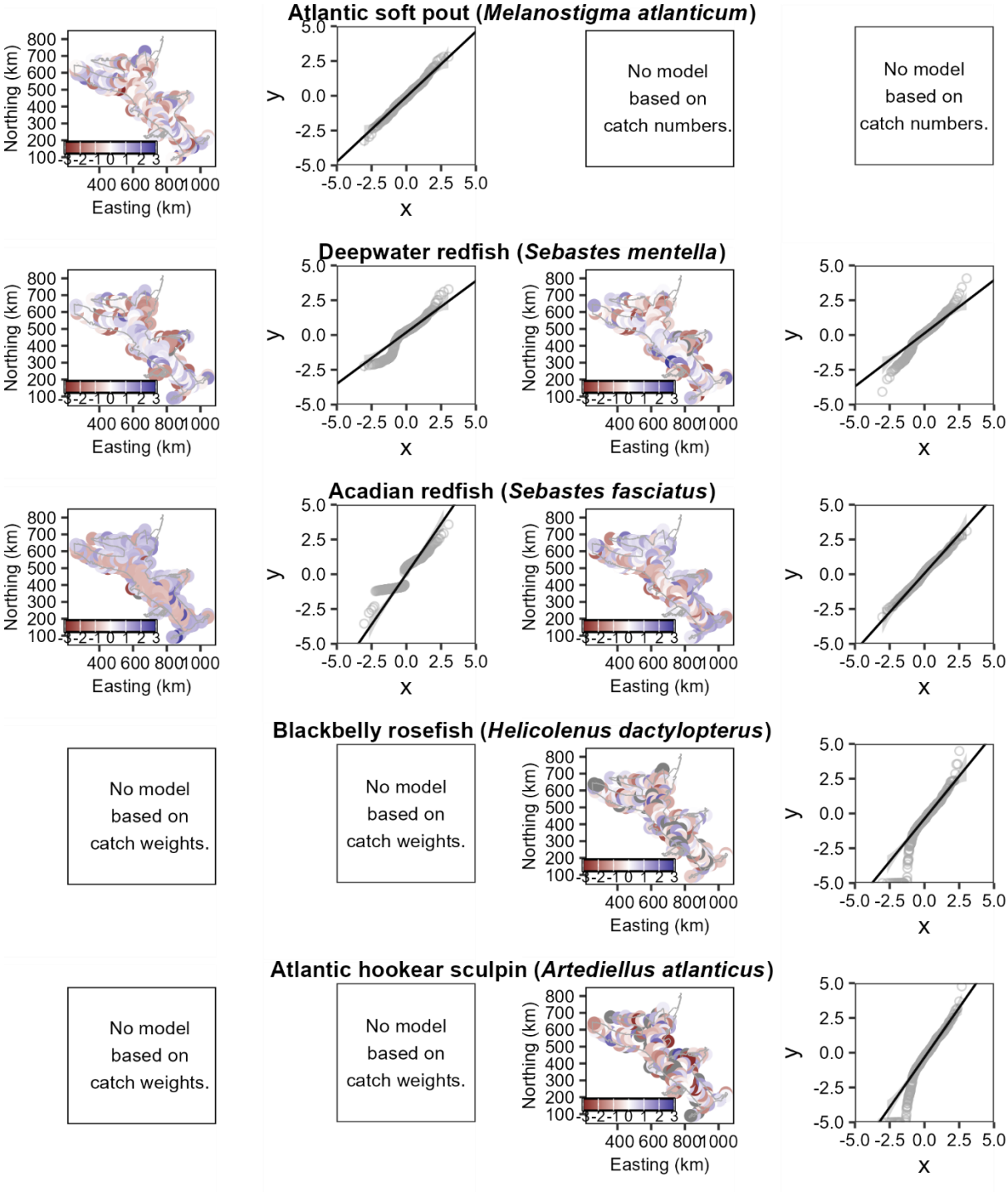


Figure B5. Illustration of the 'mle-mvn' residuals of the selected spatial interpolation models in the weight analysis (columns 1 and 2) and/or the number analysis (columns 3 and 4) per cell, for five of the taxa considered common. Columns 1 and 3 give the residuals in space within the study area, while columns 2 and 4 give the Q-Q normal diagrams for these residuals compared with a 1:1 ratio.

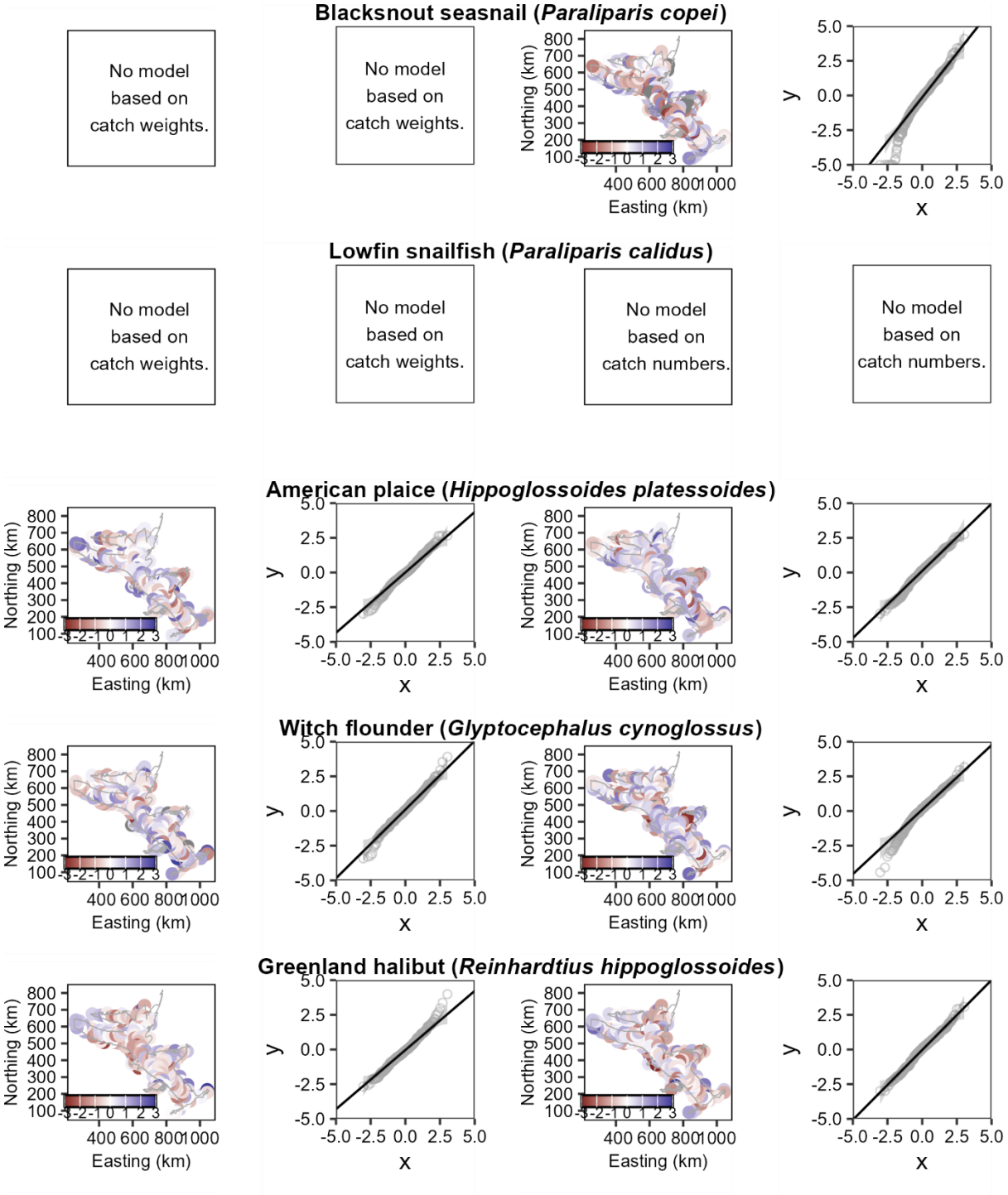


Figure B6. Illustration of the 'mle-mvn' residuals of the selected spatial interpolation models in the weight analysis (columns 1 and 2) and/or the number analysis (columns 3 and 4) per cell, for five of the taxa considered common. Columns 1 and 3 give the residuals in space within the study area, while columns 2 and 4 give the Q-Q normal diagrams for these residuals compared with a 1:1 ratio.

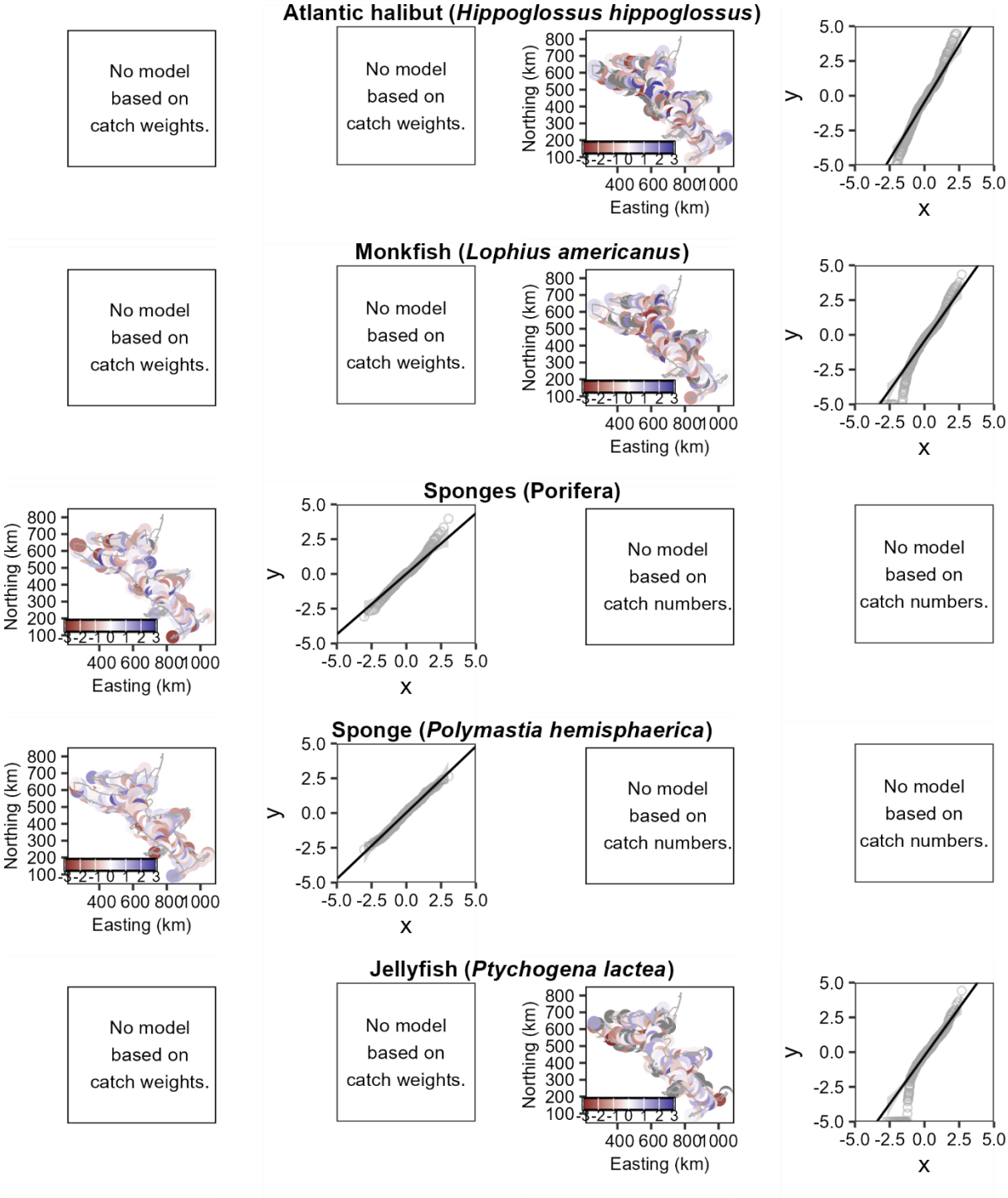


Figure B7. Illustration of the 'mle-mvn' residuals of the selected spatial interpolation models in the weight analysis (columns 1 and 2) and/or the number analysis (columns 3 and 4) per cell, for five of the taxa considered common. Columns 1 and 3 give the residuals in space within the study area, while columns 2 and 4 give the Q-Q normal diagrams for these residuals compared with a 1:1 ratio.

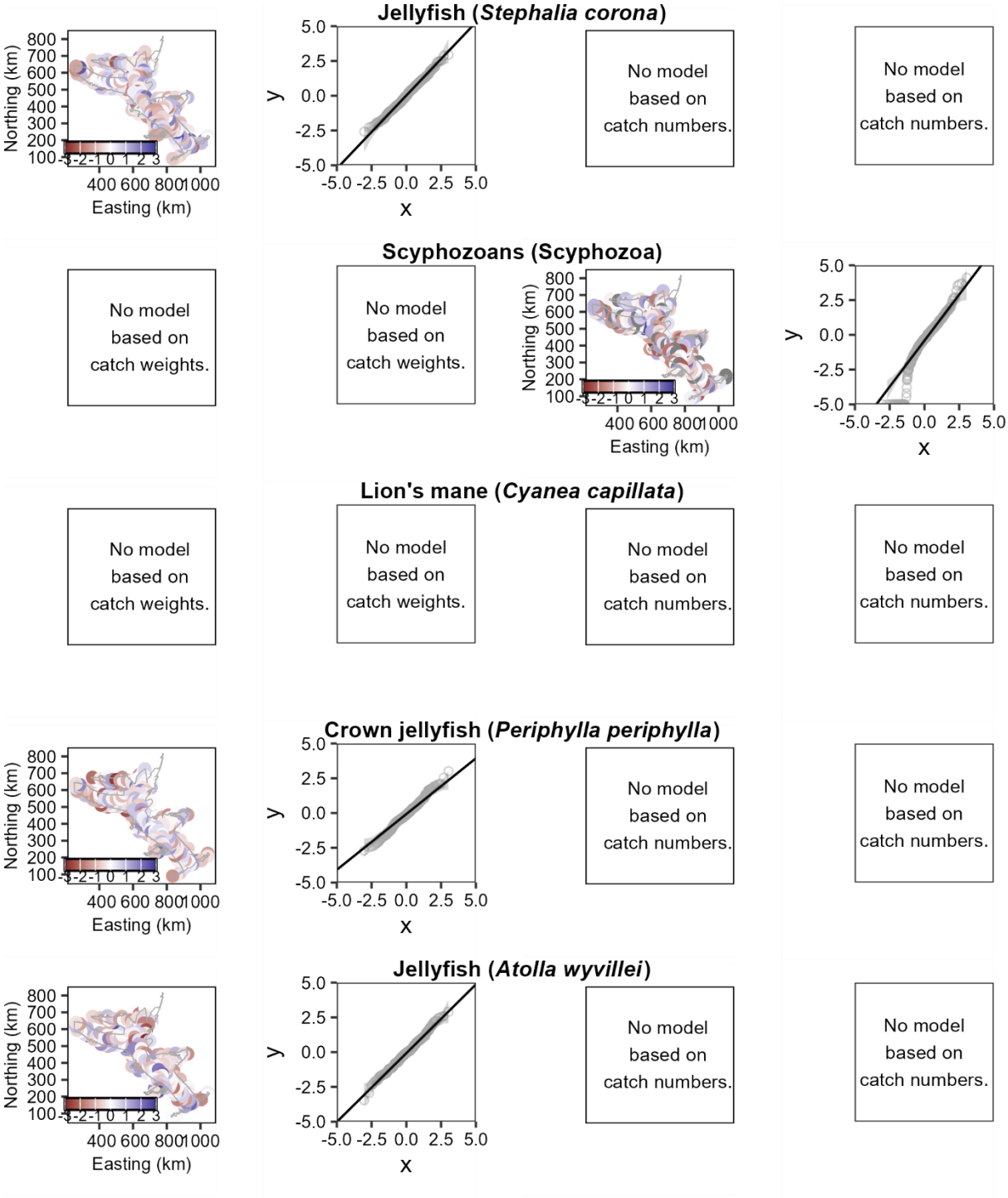


Figure B8. Illustration of the 'mle-mvn' residuals of the selected spatial interpolation models in the weight analysis (columns 1 and 2) and/or the number analysis (columns 3 and 4) per cell, for five of the taxa considered common. Columns 1 and 3 give the residuals in space within the study area, while columns 2 and 4 give the Q-Q normal diagrams for these residuals compared with a 1:1 ratio.

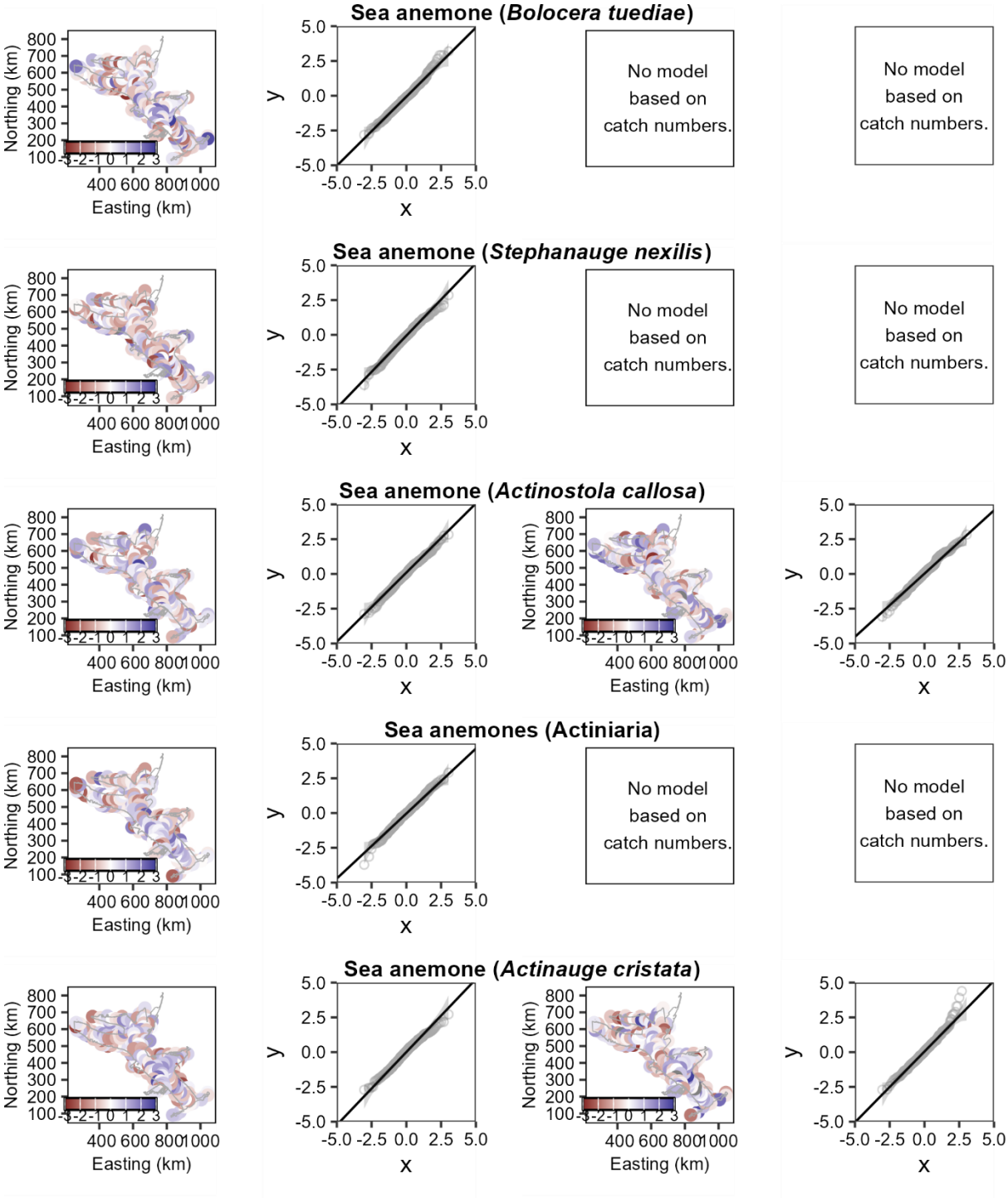


Figure B9. Illustration of the 'mle-mvn' residuals of the selected spatial interpolation models in the weight analysis (columns 1 and 2) and/or the number analysis (columns 3 and 4) per cell, for five of the taxa considered common. Columns 1 and 3 give the residuals in space within the study area, while columns 2 and 4 give the Q-Q normal diagrams for these residuals compared with a 1:1 ratio.

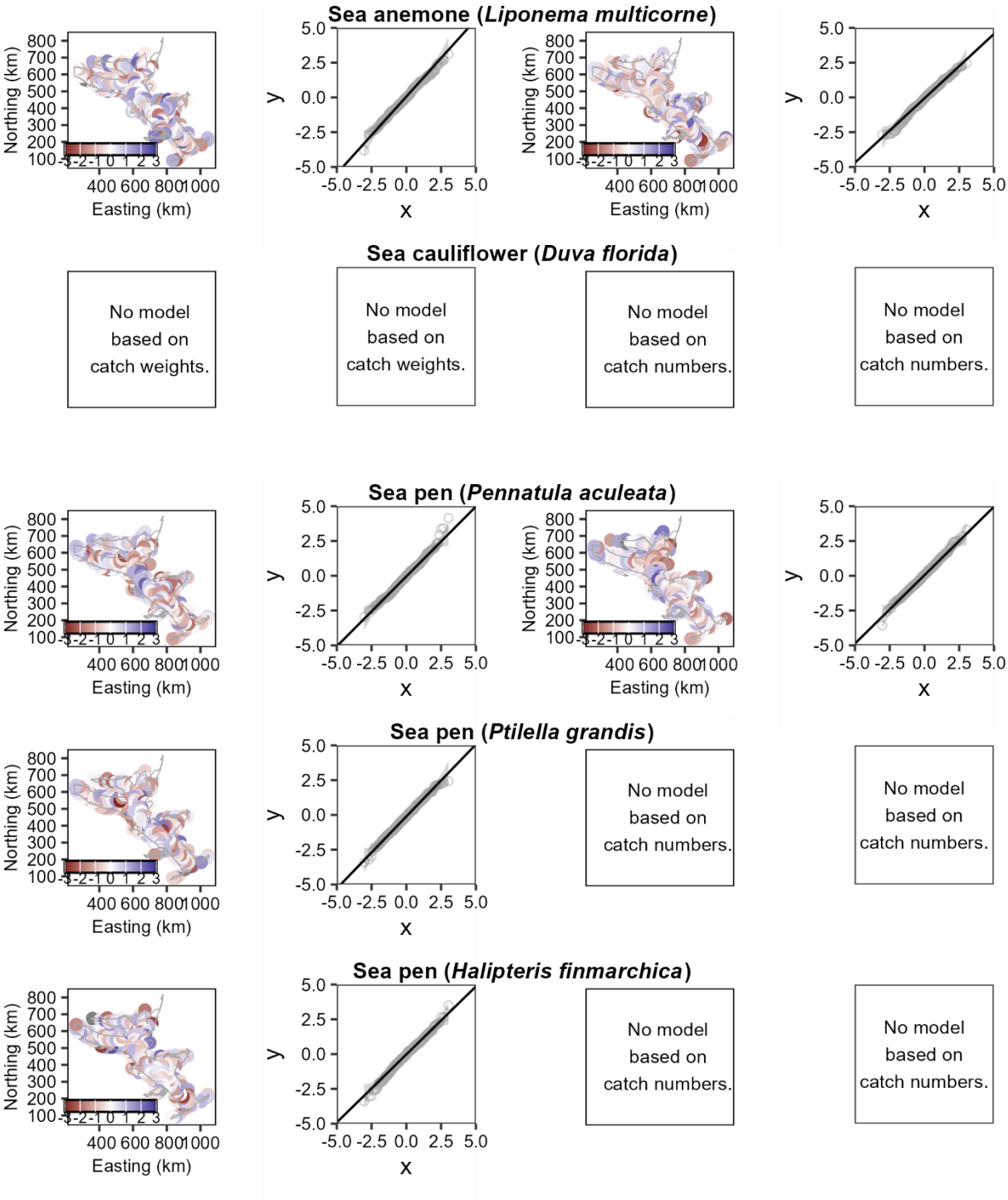


Figure B10. Illustration of the 'mle-mvn' residuals of the selected spatial interpolation models in the weight analysis (columns 1 and 2) and/or the number analysis (columns 3 and 4) per cell, for five of the taxa considered common. Columns 1 and 3 give the residuals in space within the study area, while columns 2 and 4 give the Q-Q normal diagrams for these residuals compared with a 1:1 ratio.

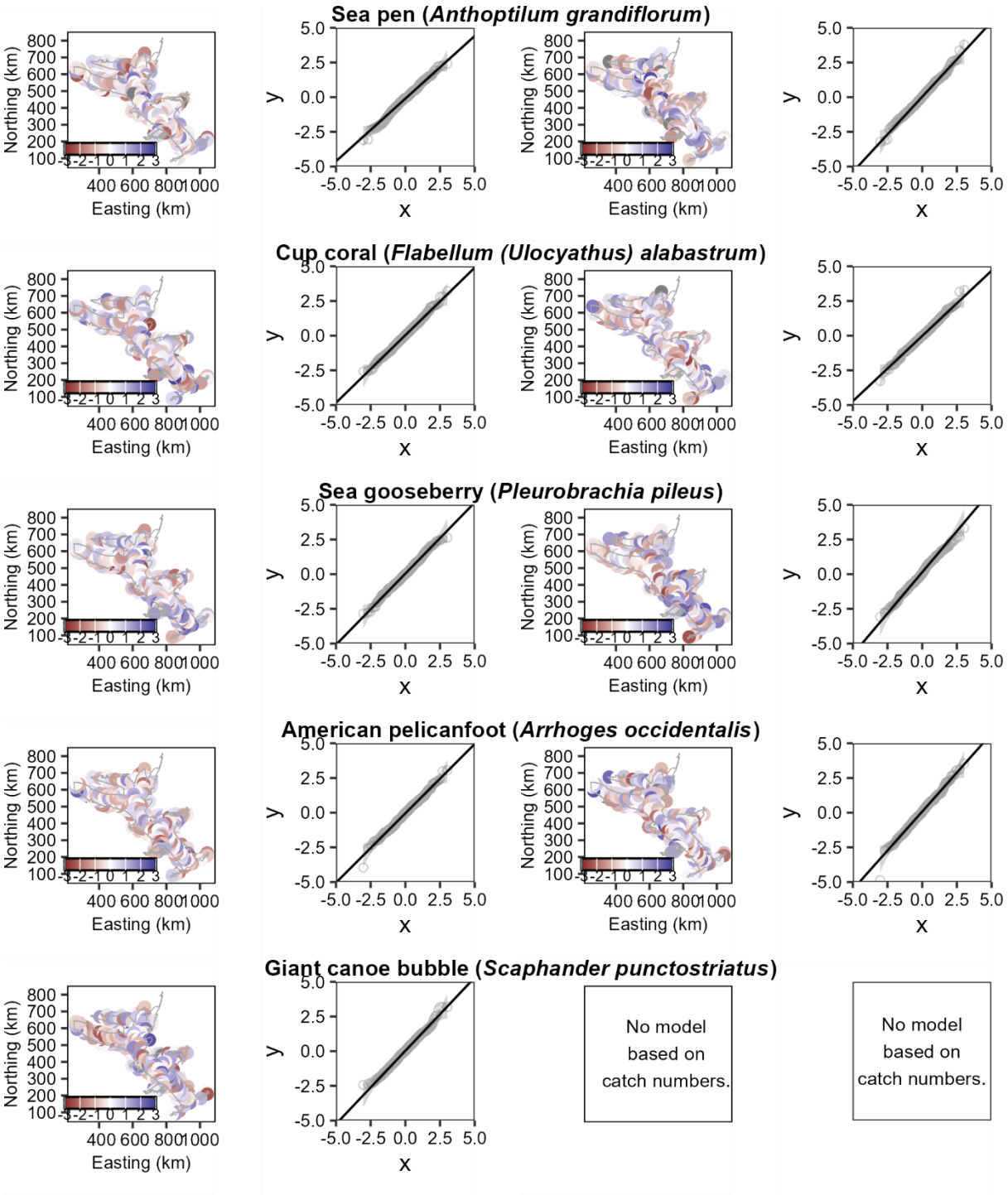


Figure B11. Illustration of the 'mle-mvn' residuals of the selected spatial interpolation models in the weight analysis (columns 1 and 2) and/or the number analysis (columns 3 and 4) per cell, for five of the taxa considered common. Columns 1 and 3 give the residuals in space within the study area, while columns 2 and 4 give the Q-Q normal diagrams for these residuals compared with a 1:1 ratio.

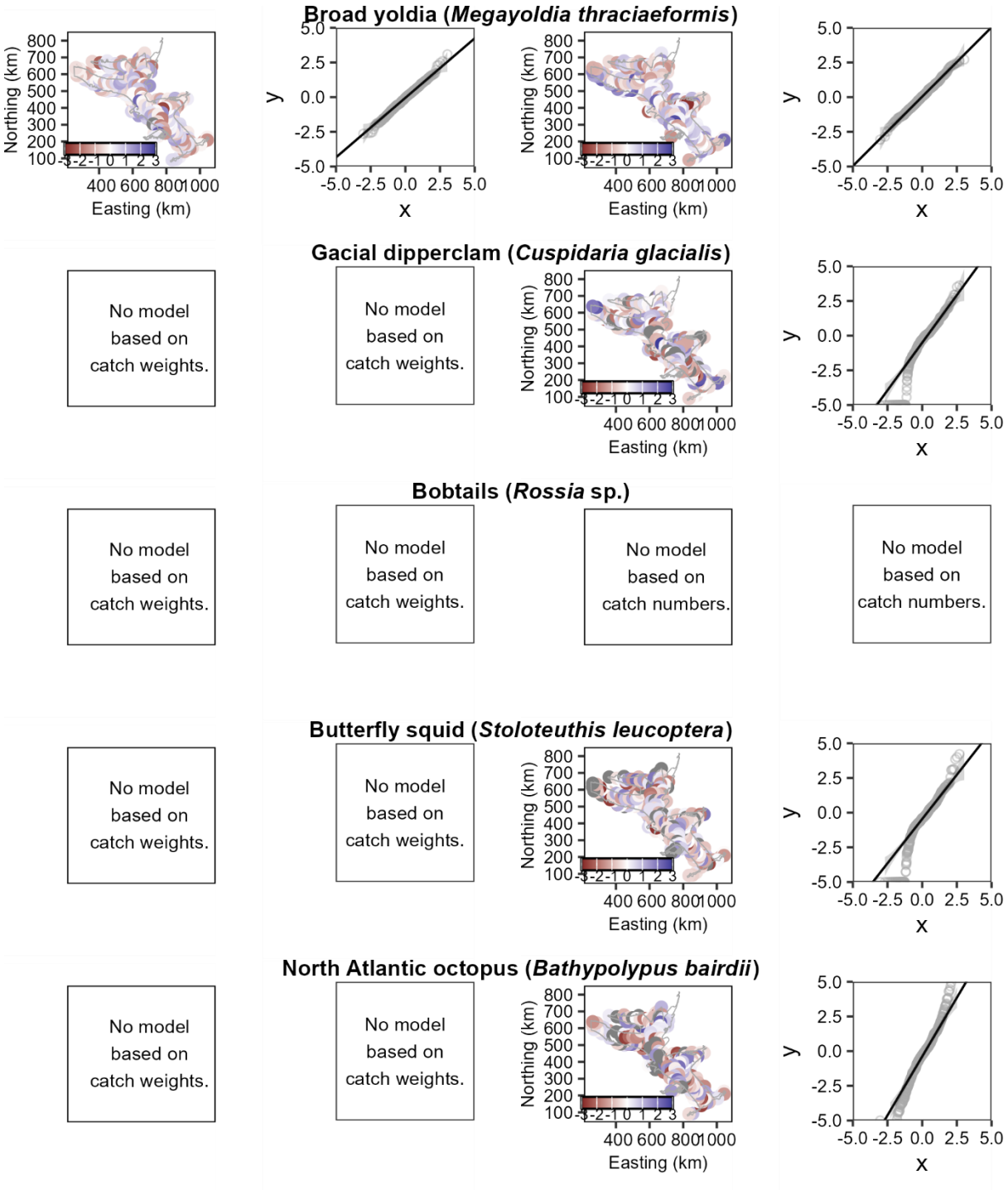


Figure B12. Illustration of the 'mle-mvn' residuals of the selected spatial interpolation models in the weight analysis (columns 1 and 2) and/or the number analysis (columns 3 and 4) per cell, for five of the taxa considered common. Columns 1 and 3 give the residuals in space within the study area, while columns 2 and 4 give the Q-Q normal diagrams for these residuals compared with a 1:1 ratio.

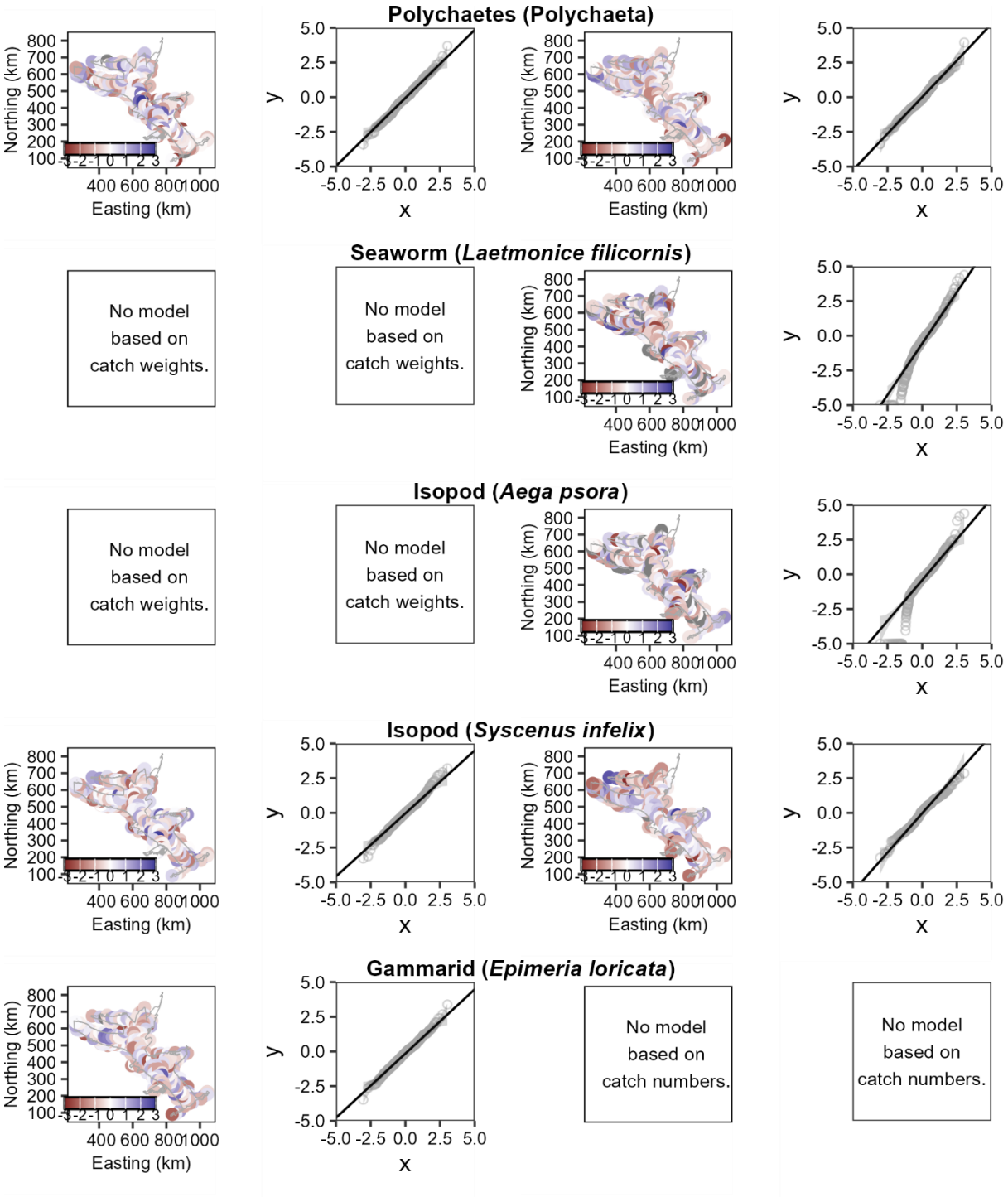


Figure B13. Illustration of the 'mle-mvn' residuals of the selected spatial interpolation models in the weight analysis (columns 1 and 2) and/or the number analysis (columns 3 and 4) per cell, for five of the taxa considered common. Columns 1 and 3 give the residuals in space within the study area, while columns 2 and 4 give the Q-Q normal diagrams for these residuals compared with a 1:1 ratio.

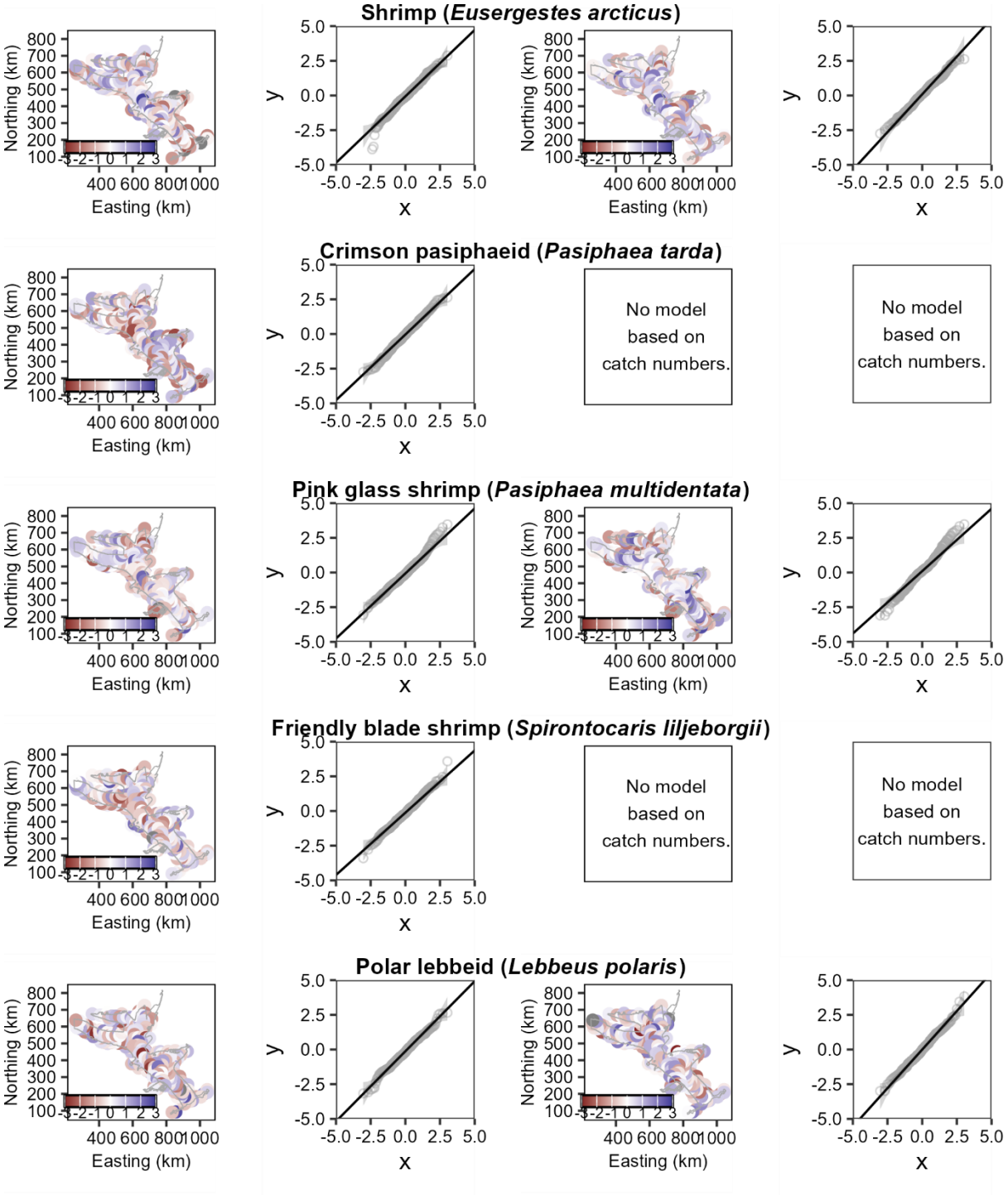


Figure B14. Illustration of the 'mle-mvn' residuals of the selected spatial interpolation models in the weight analysis (columns 1 and 2) and/or the number analysis (columns 3 and 4) per cell, for five of the taxa considered common. Columns 1 and 3 give the residuals in space within the study area, while columns 2 and 4 give the Q-Q normal diagrams for these residuals compared with a 1:1 ratio.

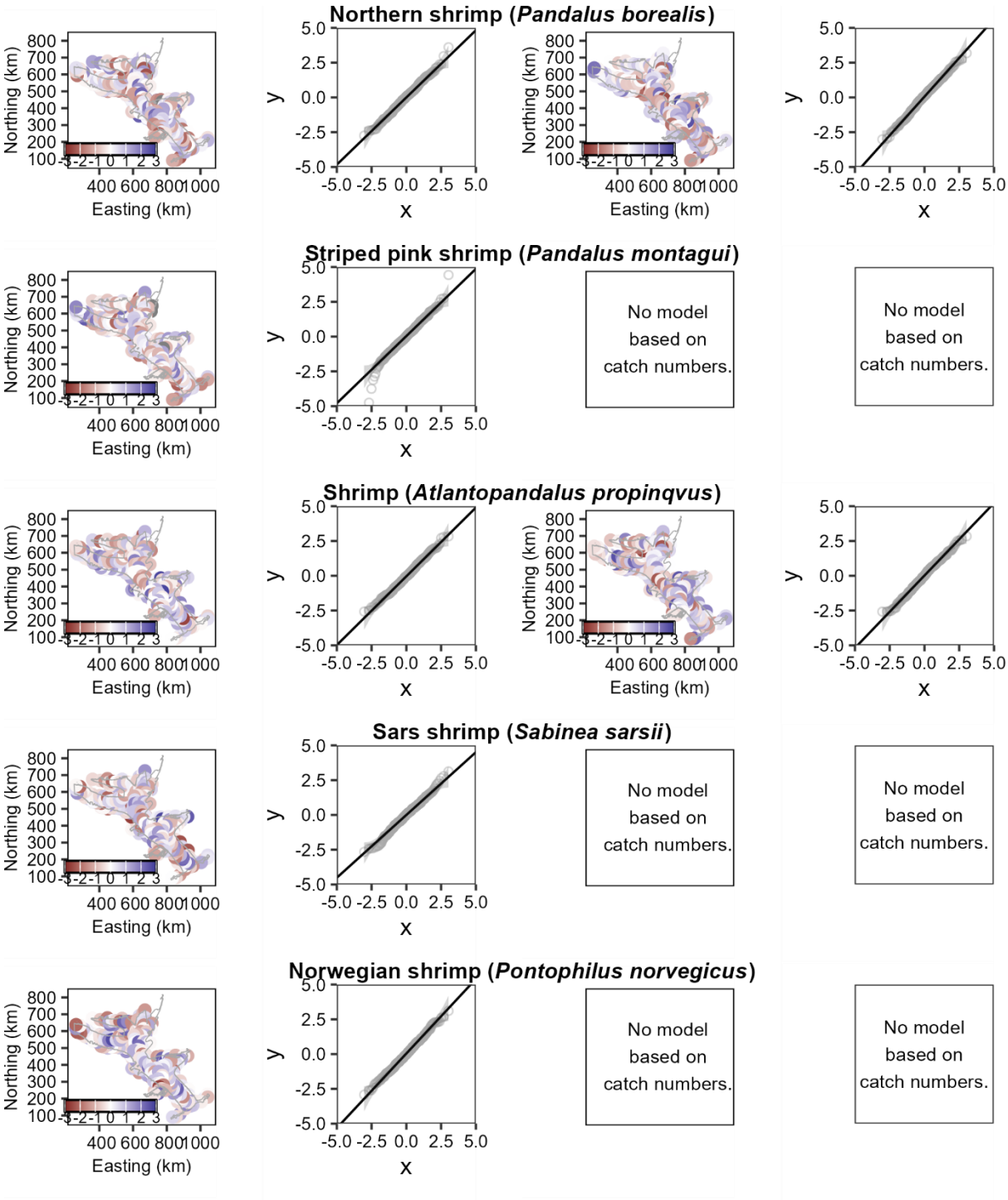


Figure B15. Illustration of the 'mle-mvn' residuals of the selected spatial interpolation models in the weight analysis (columns 1 and 2) and/or the number analysis (columns 3 and 4) per cell, for five of the taxa considered common. Columns 1 and 3 give the residuals in space within the study area, while columns 2 and 4 give the Q-Q normal diagrams for these residuals compared with a 1:1 ratio.

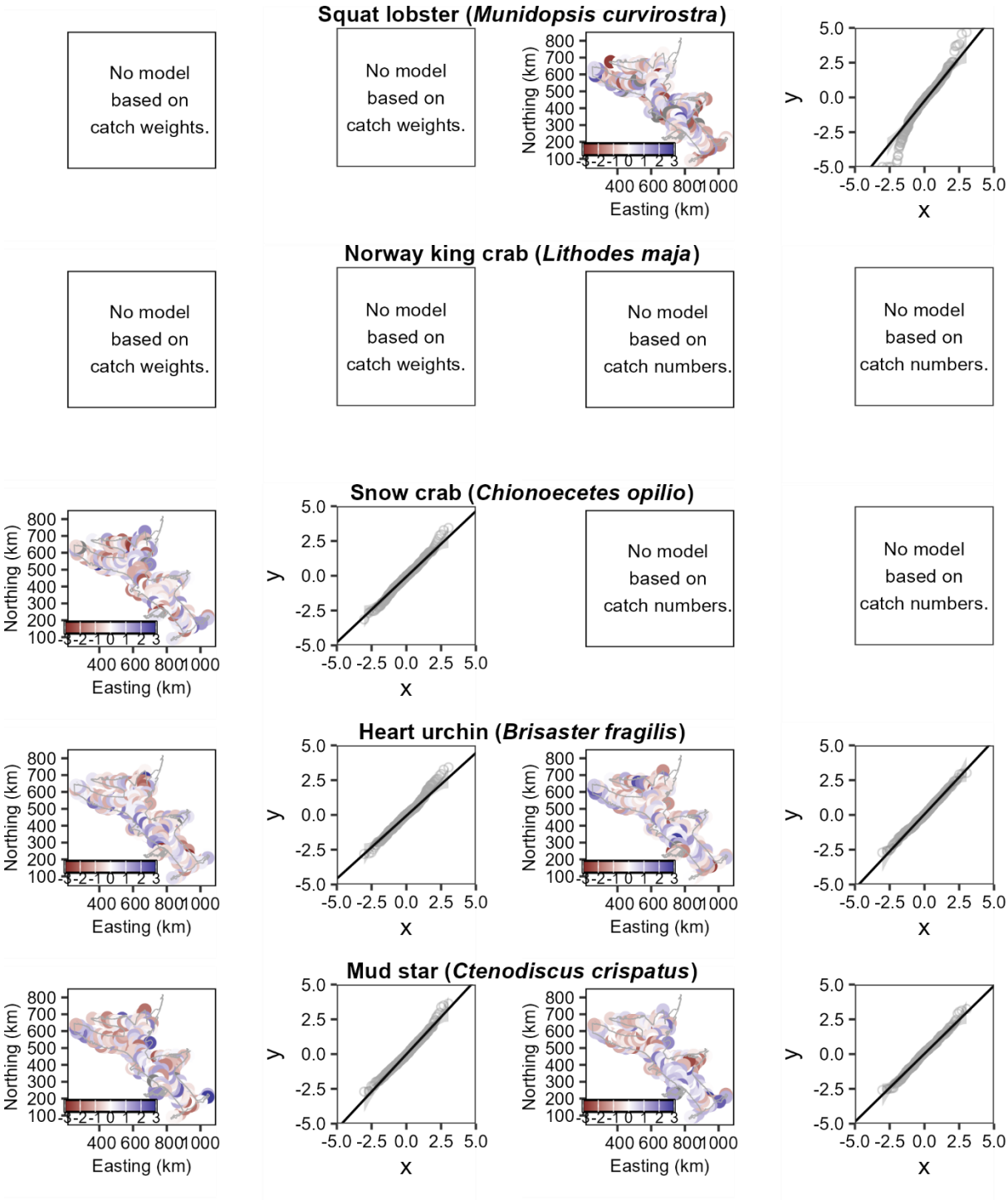


Figure B16. Illustration of the 'mle-mvn' residuals of the selected spatial interpolation models in the weight analysis (columns 1 and 2) and/or the number analysis (columns 3 and 4) per cell, for five of the taxa considered common. Columns 1 and 3 give the residuals in space within the study area, while columns 2 and 4 give the Q-Q normal diagrams for these residuals compared with a 1:1 ratio.

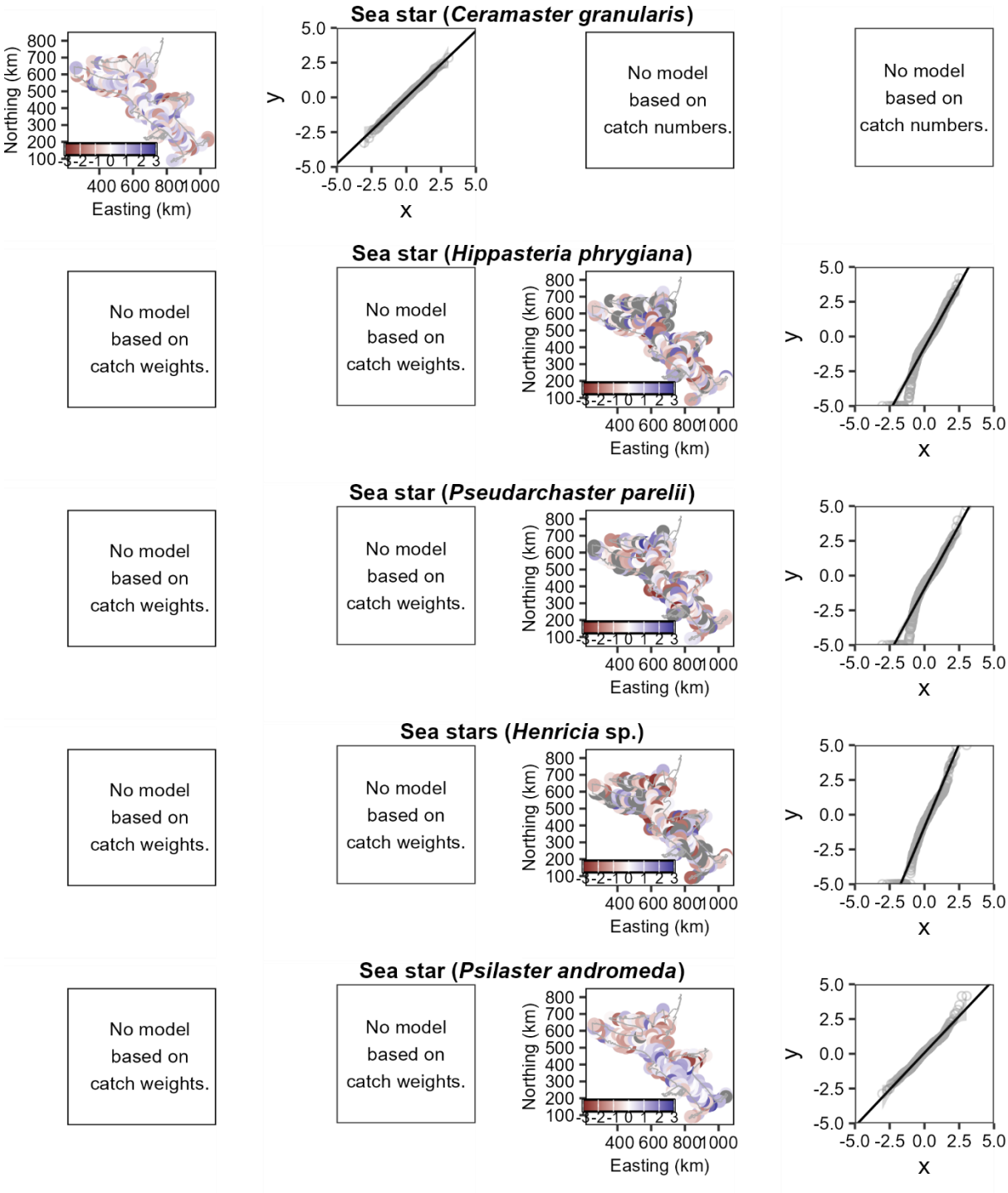


Figure B17. Illustration of the 'mle-mvn' residuals of the selected spatial interpolation models in the weight analysis (columns 1 and 2) and/or the number analysis (columns 3 and 4) per cell, for five of the taxa considered common. Columns 1 and 3 give the residuals in space within the study area, while columns 2 and 4 give the Q-Q normal diagrams for these residuals compared with a 1:1 ratio.

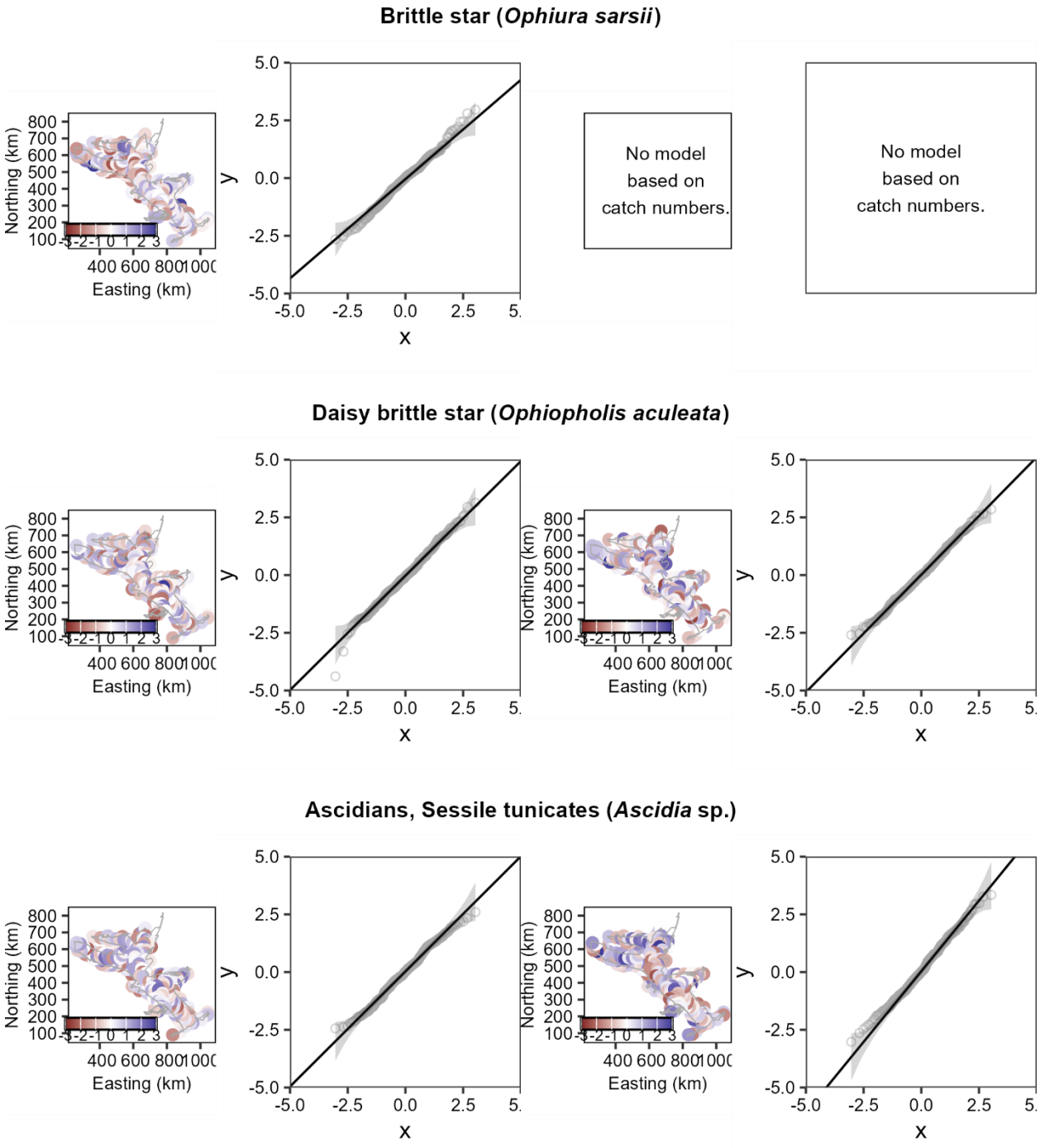


Figure B18. Illustration of the 'mle-mvn' residuals of the selected spatial interpolation models in the weight analysis (columns 1 and 2) and/or the number analysis (columns 3 and 4) per cell, for three of the taxa considered common. Columns 1 and 3 give the residuals in space within the study area, while columns 2 and 4 give the Q-Q normal diagrams for these residuals compared with a 1:1 ratio.



Figure B19. Diagnostics of the sdmTMB models selected in the analysis of catch weights that converged and for which at least one of the diagnostic tests failed. The x-axis shows the tests as presented by the *sanity* function and the y-axis gives the STRAP code of the taxon concerned with the selected model (mod1 = with an effect of depth; mod2 = without an effect of depth).

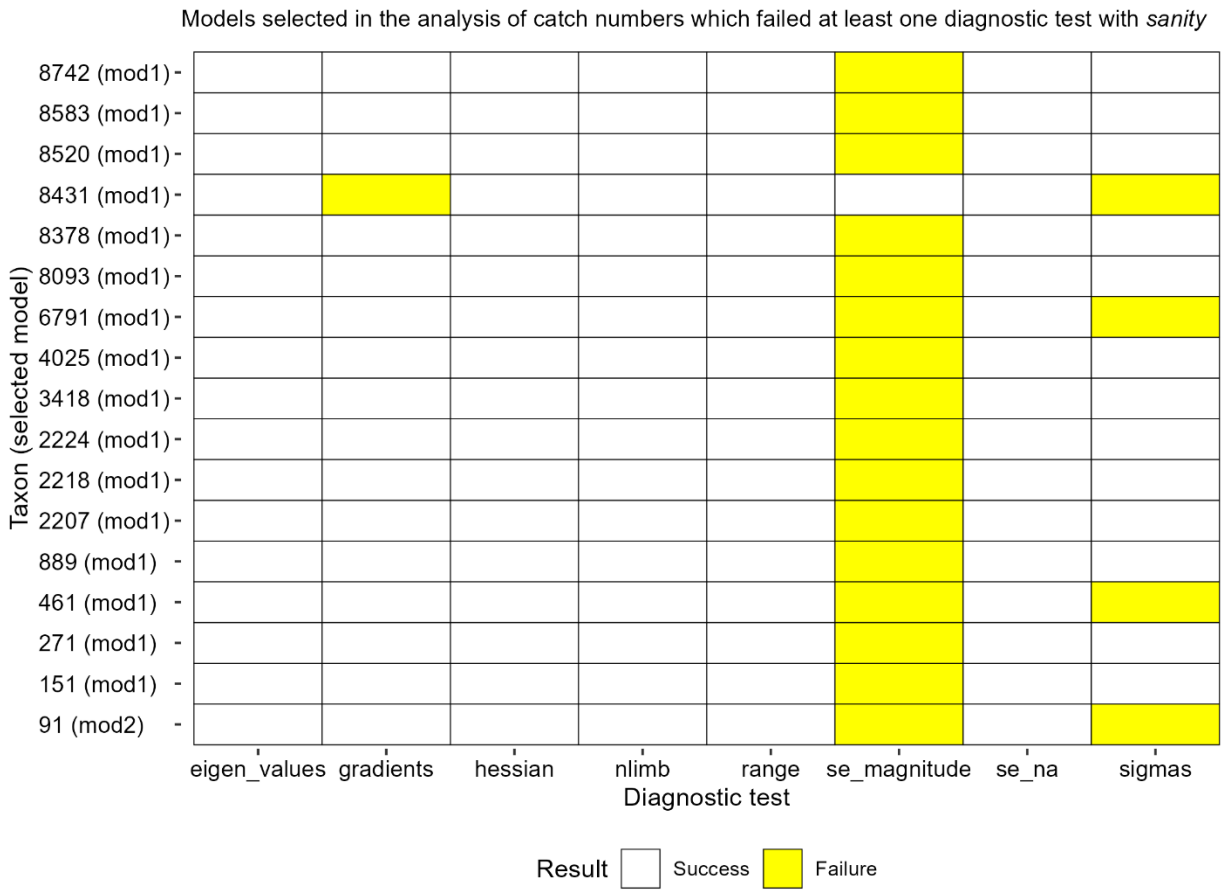


Figure B20. Diagnostics of the sdmTMB models selected in the analysis of catch numbers that converged and for which at least one of the diagnostic tests failed. The x-axis shows the tests as presented by the *sanity* function and the y-axis gives the STRAP code of the taxon concerned with the selected model (mod1 = with an effect of depth; mod2 = without an effect of depth).

Appendix C. Tagging of Atlantic halibut

The spatial distribution of Atlantic halibut extends over a large portion of Atlantic Canada. It is believed that in winter, Atlantic halibut from the GSL stock migrate to the depths of the Laurentian Channel for the spawning season, and the two populations of Atlantic halibut (the GSL and the Scotian Shelf and southern Grand Banks, SSSGB) overlap at the entrance to the GSL. To determine whether Atlantic halibut belonged to the GSL or SSSGB population, satellite tags were deployed in 2024 on a total of 12 Atlantic halibut ranging from 89 to 190 cm in length, two in the GSL and ten in the SSSGB. A portion of the pelvic fin was collected from these individuals and other samples from the survey for genetic analysis.

Seven tags detached and began transmitting their position on the predetermined date of June 15, 2024, corresponding to times at sea ranging from 101 to 126 days. Four tags detached before the predetermined date, between March 5, 2024, and April 23, 2024, for times at sea of 5, 20, 44, and 55 days. One tag did not transmit any data.

Table C1 and **Figure C1** show the tag attachment locations and the point at which each tag detached. In all cases, the capture locations and the corresponding tag detachment points are within the area covered by the same stock.

Table C1. Details of Atlantic halibut marked with a satellite tag. Note that size refers to fork length for this species.

Station	Size (cm)	Tag attachment			Tag release		
		Date	Latitude	Longitude	Date	Latitude	Longitude
16	160	2024-02-10	48.0514	-60.9538	2024-06-15	48.7997	-63.2560
104	89	2024-02-19	47.8014	-59.7170	2024-06-15	47.7666	-59.7053
158	100	2024-02-28	44.9658	-55.4945	2024-04-23	45.4557	-57.2315
158	100	2024-02-28	44.9658	-55.4945	-	-	-
160	117	2024-02-28	44.9894	-55.2252	2024-06-15	44.9242	-55.4606
164	190	2024-02-29	44.3653	-57.4891	2024-03-05	46.1284	-57.5193
165	144	2024-02-29	44.2504	-57.7832	2024-06-15	44.2611	-57.7224
165	121	2024-02-29	44.2504	-57.7832	2024-06-15	44.2592	-57.7992
189	135	2024-03-04	46.1258	-57.9800	2024-06-15	46.8426	-58.4775
207	156	2024-03-06	46.5675	-58.9512	2024-06-15	46.2120	-58.7193
207	95	2024-03-06	46.5675	-58.9512	2024-03-26	46.5460	-58.9353
209	100	2024-03-07	46.5390	-58.3814	2024-04-18	43.5093	-56.2154

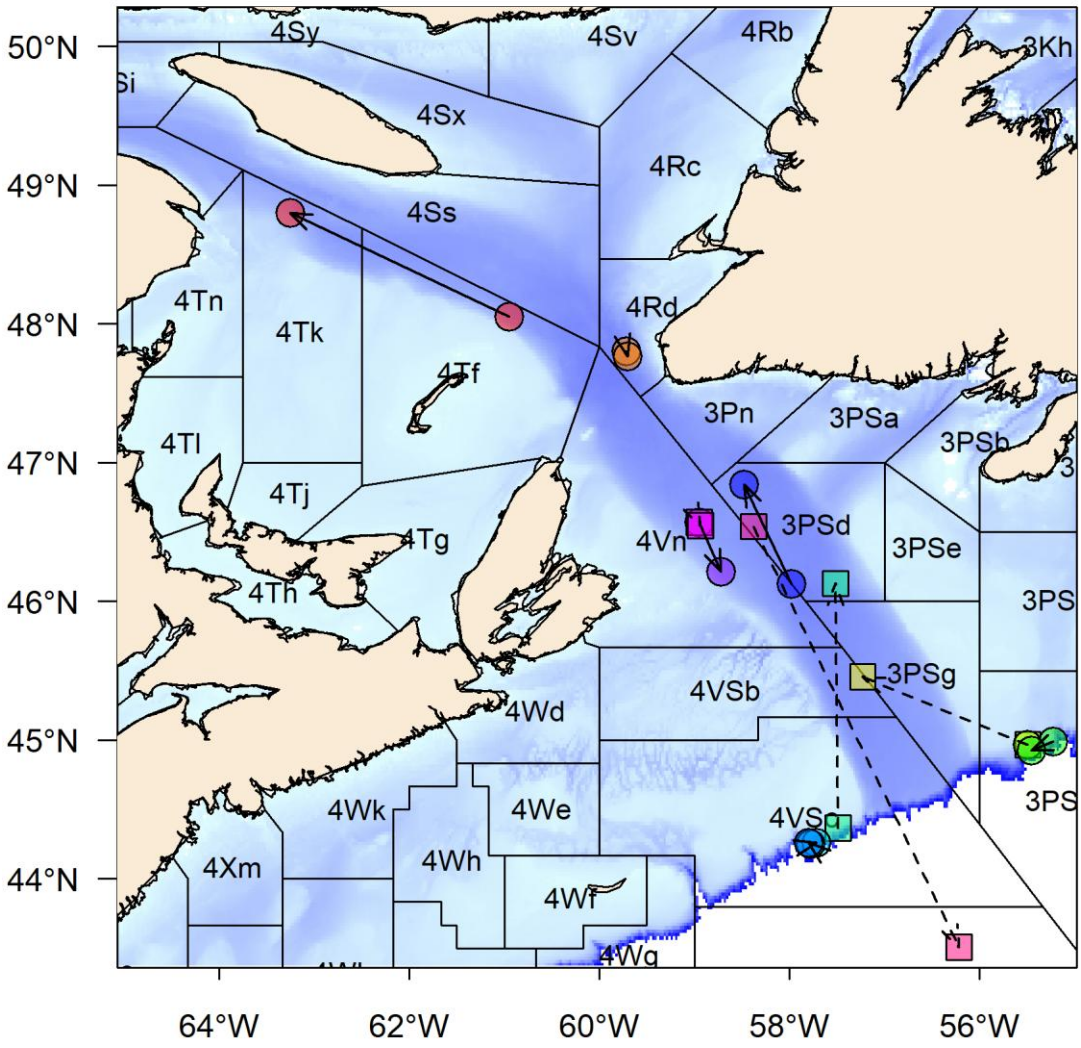


Figure C1. Locations of tag attachments and releases for tagged Atlantic halibut. Tags released prematurely are indicated by a square symbol and a dotted arrow.

Appendix D. Other research projects

Fish stomach samples for ecosystem modelling

Stomach samples were collected each year of the winter survey (2022–2024). The objective was to improve and maintain up-to-date knowledge of the diets of fish targeted by a commercial fishery. The target species were Atlantic cod, Greenland halibut, both redfish species, Atlantic halibut, haddock, pollock, white hake, American plaice, winter flounder, and witch flounder. For Atlantic cod, Greenland halibut, and redfish, stomach collection was stratified by length to account for ontogenetic variations in their diet. Stomach samples of white hake, American plaice, winter flounder, and witch flounder were collected at the request of the DFO Gulf Region (Moncton, New Brunswick).

Genetics of groundfish populations

Several genetic projects were conducted during the three years of the survey. The objective was to better understand the winter migrations of different species as well as the membership of captured individuals in their respective stocks.

White hake

In 2022, portions of the pelvic fin were collected from a sample of 30 white hake individuals when the catch of a tow exceeded 25 kg. As part of a more in-depth microbiome study and at the request of DFO Gulf Region in 2023, a maximum of 15 individuals per tow were harvested whole. A portion of the pelvic fin was collected from an additional 15 individuals per tow when possible. In 2024, pelvic fin fragments were collected from a maximum of 5 individuals per tow.

Atlantic cod

In 2022, samples of the pelvic fin were taken from 30 Atlantic cod individuals from tows with catches of 50 kg and over. In 2023 and 2024, samples were taken from 5 individuals on each tow.

Atlantic halibut

In 2023 and 2024, pelvic fin samples were taken from all Atlantic halibut individuals captured.

Greenland halibut

The 2022 and 2024 surveys involved the collection of genetic samples on Greenland halibut larger than 20 cm in different areas of the survey. No samples for genetic analysis were collected for this species in 2023.

Redfish

In 2023 and 2024, genetic material was collected by brushing the inside of the mouths of sampled redfish individuals with a sterile swab. This protocol aimed to develop a species identification method (distinction between *S. mentella* and *S. fasciatus*) applicable on a large scale in surveys and commercial fisheries. In 2024, pelvic fin samples were also collected for further analysis.

Groundfish – Atlas project

The Atlas project aimed to enhance knowledge of ecosystems of interest to DFO using specimens from targeted taxa. In 2022 and 2023, the targeted species were the northern shortfin squid, Atlantic argentine, common grenadier, various hookear sculpins, fourbeard rockling, Newfoundland spiny lumpsucker and the Arctic cod. In 2024, the collection focused on the northern shortfin squid, fourbeard rockling, white barracudina, Esmark's eelpout and Atlantic eelpout. Targeted analyzes for these species included stomach content analysis, intraspecific

relationships, interactions between species and their environment, and analysis of their productivity traits.

Groundfish maturity stages

Gonads were collected to update maturity ogives and visual maturity staging charts for Atlantic halibut, Greenland halibut, and American plaice. For Atlantic halibut, gonads were collected from all individuals over 50 cm caught in 2022 and 2023. Photographs of the whole gonads were also taken. In 2023, gonads were collected and photographed using a size- and sex-stratified approach for Greenland halibut, and a size-stratified approach for American plaice. The sampling of American plaice was conducted at the request of DFO Gulf Region.

Atlantic herring stock assessment

As part of the DFO's assessment of Atlantic herring stocks in the Gulf and Quebec regions, specimens of this species were collected in NAFO Divisions 4RS and 4TVn. Sampling was conducted randomly in Divisions 4RS, while length stratification was applied in 4TVn. The number of individuals sought per tow was 55.

Gorgonocephalian taxonomy

Portions of the central disc of gorgonocephalians were taken to determine the species present in the Northwest Atlantic.

Cnidarian identification

At the request of the DFO Newfoundland Region’s Marine Protected Areas Management Team, samples of sea pens, soft corals and hard corals were preserved in 2024.

Sea pens and hard coral

In order to carry out contaminant analyzes and to preserve collection specimens, 10 specimens of different species of sea pens (*Anthoptilum grandiflorum*, *Pennatula aculeata, Ptilella grandis*, *Balticina finmarchica*, *Kophobelemnon stelliferum*, white pens) and hard corals (*Flabellum (Ulocyathus) alabastrum*) were preserved for these purposes during the winter 2024 survey.

Environmental DNA

During the winter survey of 2022, water samples were taken using an experimental device attached directly to the trawl, in order to validate the link between the presence of species according to environmental DNA and those present in the trawl.

Appendix E. List of participants to the survey

Table E1. List of scientific staff who participated in the winter survey, by year.

Year	Team (alphabetical order)
2022	Bruno Comeau, Caroline Chavarria, François Turcotte, Jean-François Lussier, Jean-Patrick Bourbonnière, Jordan Ouellette-Plante, Marie-Claude Marquis, Marie-France Robichaud, Marie-Maude Rondeau, Pierre-Marc Scallon-Chouinard and Émilie Simard
2023	Bruno Comeau, Caroline Chavarria, Caroline Senay, Jean-François Lussier, Jean-Patrick Bourbonnière, Joeleen Savoie, Marie-Claude Marquis, Marie-France Robichaud, Marie-Maude Rondeau, Pierre-Marc Scallon-Chouinard and Émilie Simard
2024	Andrew Darcy, Brian Boivin, Bruno Comeau, Carly Weber, Caroline Chavarria, David Poissant, Éric Parent, Jean-François Lussier, Jean-Patrick Bourbonnière, Joeleen Savoie, Jordan Ouellette-Plante, Marie-Claude Marquis, Marie-France Robichaud, Marie-Maude Rondeau, Pierre-Marc Scallon-Chouinard, Sarah Brown-Vuillemin, Tom Bermingham and Émilie Simard